



*Advances in*  
**CHEMISTRY**  
**RESEARCH**

VOLUME 26

**James C. Taylor**  
Editor

NOVA

Complimentary Contributor Copy

Complimentary Contributor Copy



ADVANCES IN CHEMISTRY RESEARCH

# ADVANCES IN CHEMISTRY RESEARCH

VOLUME 26

No part of this digital document may be reproduced, stored in a retrieval system or transmitted in any form or by any means. The publisher has taken reasonable care in the preparation of this digital document, but makes no expressed or implied warranty of any kind and assumes no responsibility for any errors or omissions. No liability is assumed for incidental or consequential damages in connection with or arising out of information contained herein. This digital document is sold with the clear understanding that the publisher is not engaged in rendering legal, medical, or any other professional services.

Complimentary Contributor Copy

# **ADVANCES IN CHEMISTRY RESEARCH**

Additional books in this series can be found on Nova's website under the Series tab.

Additional e-books in this series can be found on Nova's website under the e-book tab.

Complimentary Contributor Copy

ADVANCES IN CHEMISTRY RESEARCH

**ADVANCES IN CHEMISTRY RESEARCH**

**VOLUME 26**

**JAMES C. TAYLOR**  
**EDITOR**



Complimentary Contributor Copy



*Chapter 9*

**EVALUATION OF THE POSSIBILITY OF USING  
NORMALIZATION WITH COBALT IN DETECTION  
OF ANTHROPOGENIC HEAVY METALS IN SEDIMENTS**

*Sanja M. Sakan<sup>1\*</sup>, Nenad M. Sakan<sup>2</sup>  
and Dragana S. Đorđević<sup>1</sup>*

<sup>1</sup>ICTM, Chemistry Centre, University of Belgrade, Belgrade, Serbia

<sup>2</sup>Institute of Physics, University of Belgrade, Belgrade, Serbia

**ABSTRACT**

Geochemical normalization with conservative elements has been effectively used for assessing the enrichment of metal pollutants and distinguishing their natural and anthropogenic sources. Without correcting for textural and mineralogical variability, a comparison of heavy metal data with regional background is complicated because of large variability due to irregular grain size and sediment composition. The normalization with cobalt in the enrichment factor calculation presents a new approach in detection of anthropogenic elements in sediments. In present study, the heavy metal concentrations (Cd, Cu, Fe, Mn, Cr, Ni, Pb, V and Zn) were determined in the river sediments of 35 rivers in Serbia.

The enrichment factor (EF) was used to estimate the anthropogenic heavy metals input as well as to make a quantification of the metal enrichment degree. Different research sources recommend the use of Fe, Li, Al and Si as conservative elements. Within the scope of this research the cobalt was selected as the element for the normalization.

It was observed that the cobalt concentration is not higher than the regional background concentration, which is similar to the average concentration of this element in the continental crust.

The positive correlation between Cd, Cr, Fe, Ni, Pb, V, Mn and Zn with Co suggests that it could therefore be a suitable normalizing element in EF calculations for the studied river sediments.

The anthropogenic influence of heavy metal pollution could be traced by the use of such EF values, and the values for the studied river systems are presented.

**Complimentary Contributor Copy**

## 1. INTRODUCTION

Sediments in surface water are most vulnerable to various pollution including heavy metals due to their ease of access for the disposal of urban and industrial wastewater (Chabukdhara et al. 2012). In fact, the sediment acts as an accumulation reservoir and could bound or release heavy metals from the water column (Comero et al. 2014). Through the hydrological cycle, over 99% of pollutants are stored in sediments, while far less than 1% remains dissolved in water. Therefore the sediments are the major sinks and carriers for contaminants in aquatic environments (Bartolli et al. 2012). Trace elements, especially heavy metals, were among the most common and significant environmental pollutants (Davutoglu et al. 2011; Relić et al. 2013; Sakan et al. 2012a; Sakan et al. 2012b; Sakan et al. 2013). Due to the heavy metal non biodegradable nature, and their long-biological half-lives for elimination from the water body, significant effect on human health is expected because of their long term accumulation in the food chain (Chabukdhara et al. 2012). The main routes of heavy metal entering the aquatic systems are mainly through the natural inputs such as weathering and erosion of rocks as well as the anthropogenic sources, including urban, industrial and agricultural activities, terrestrial runoff and sewage disposal (Çevik et al. 2009). In the last few decades, human input of these elements to hydrogeoenvironment has exceeded their natural inputs in the majority of regions around the world (Iqbal et al. 2013).

It is difficult to determine what proportion of the sedimentary metal load is natural and what proportion is anthropogenic. The comparison of trace metal data is not possible without correcting for textural and mineralogical variability, e.g., the grain size and sediment composition reflects on regional background. In order to overcome this problem, a normalization procedure should be used to compensate for granulometric and mineralogical effects on metal contents and enable differentiation between inputs derived from anthropogenic activities and those from natural (bio) geochemical processes (Ho et al. 2012). Generally, there are two types of normalization techniques when studying metal contamination in river-mouth and coastal sediments, namely (1) methods based on granulometric approaches and (2) methods using geochemical approaches. However, granulometric normalization cannot fully compensate for metal variability, because natural metal contents and their variability in sediments are determined not only by grain size distribution, but also by the composition of primary and secondary minerals (Ho et al. 2012). To overcome this drawback, the geochemical approach is more commonly used. This implies the normalization of metal data by the contents of a conservative element such as Al, Fe, Li, Rb, Sc, and organic carbon (Sarkar et al. 2011, Chabukdhara et al. 2012, Ho et al. 2012, Sakan et al. 2012a, Sakan et al. 2014, Sakan et al. 2015a). Aluminum, the most important constituents of the aluminosilicate mineral fraction, is often used as a normalizer. Besides Al, Fe and Li are also common normalizers used in many studies. It is recommended that cobalt should be considered as an element for normalization in future studies (Sakan et al. 2015b). Also, in Matthai et al. (2001) is shown that Co may be used as a normalizing element for determining contaminant sources in the marine environment. Förstner and Wittman (1981) also concluded that Co is generally associated with silicate and clay minerals. Because of that cobalt should be considered as a suitable normalizing element in areas where there is no substantial anthropogenic contributions of this trace metal to surficial sediments.

The aim of our study was to assess metal contamination along the Serbian river courses and to describe a new approach in detection of anthropogenic elements in sediments using normalization with cobalt. Quantification of the metal enrichment was estimated by the means of calculating enrichment factor with cobalt as element for normalization.

## 2. EXPERIMENTAL

### 2.1. Study Area

Surface river sediments were collected from 35 points in Serbia. All rivers in Serbia belong to the drainage basins of three seas: the Black Sea, the Adriatic or the Aegean Sea. The largest in area is the Black Sea drainage basins, covers an area of 81,261 km<sup>2</sup> or 92% of the territory of Serbia. The entire basin is drained by only one river, the Danube, which flows into the Black Sea. All major rivers, like Tisa, Sava and the Great Morava belong to it.

The Danube is the second longest river in Europe, flowing for 2857 km from Germany's Black Forest to its delta on the Black Sea (Comero et al. 2014). This river is flowing through nine countries. The rock types outcropping along the river basin are very different both for lithogenic composition and for age. Drainage basins of most tributaries are dominated by the same lithologies affecting the Danube course, probably with a greater contribution from sedimentary lithologies.

The river Tisa (966 km and 157,220 km<sup>2</sup>) is the largest Danube tributary with respect to its length and catchment area.

The Tisa catchment area is bordered by the Carpathians in the north-west to south-east, while the divide is low to the west and south-west. A small part of the Tisa watershed area lies within Serbia territory, and covers only 6% or 8,994 km<sup>2</sup>. It is predominantly lowland, and part of the Pannonian Basin, which is the largest of the sediment-filled, postorogenic basins of the Alpine region (Adriano et al. 2003).

The Sava river (945 km) is the biggest tributary to the Danube river. The 95,551 km<sup>2</sup> large catchment is extended over Slovenia, Croatia, Bosnia and Herzegovina and Serbia.

### 2.2. Sampling Locations

Sediment samples (Figure 1, Table 1) were taken from 15 rivers during the year 2008. Sampling profiles are given in Figure 1: for the Danube: Bezdán (10-12), Bogojevo (13) and Tekija (14,15); for Sava: Ostružnica (16), Sremska Mitrovica (17), Šabac (18) and Jamena (19); for Tisa: Martonoš (1, 5-9) and Titel (2-4); for Great Morava: Ljubičevski most (22) and Bagrdan (23); for West Morava: Kratovska stena (24) and Maskare (25); for Ibar: Raška (20) and Kraljevo (21); for Nišava: Niš (27) and Dimitrovgrad (28); for DTD canal: Vrbas (30); for Tamiš: Pančevo (29); for Topčiderska river: Rakovica (31); for Kolubara: Draževac (33); for South Morava: Mojsinje (26); for Toplica: Doljevac (35); for Pek: Kusiće (34) and for Porečka river: Mosna (32). The granulometric fraction (< 63 μm) of the bottom sediment samples ("grab" – the sample) were used to determinate the element contents after air drying for 8 days (Sakan et al. 2011). The sampling was conducted using Van Veen grab sampler.



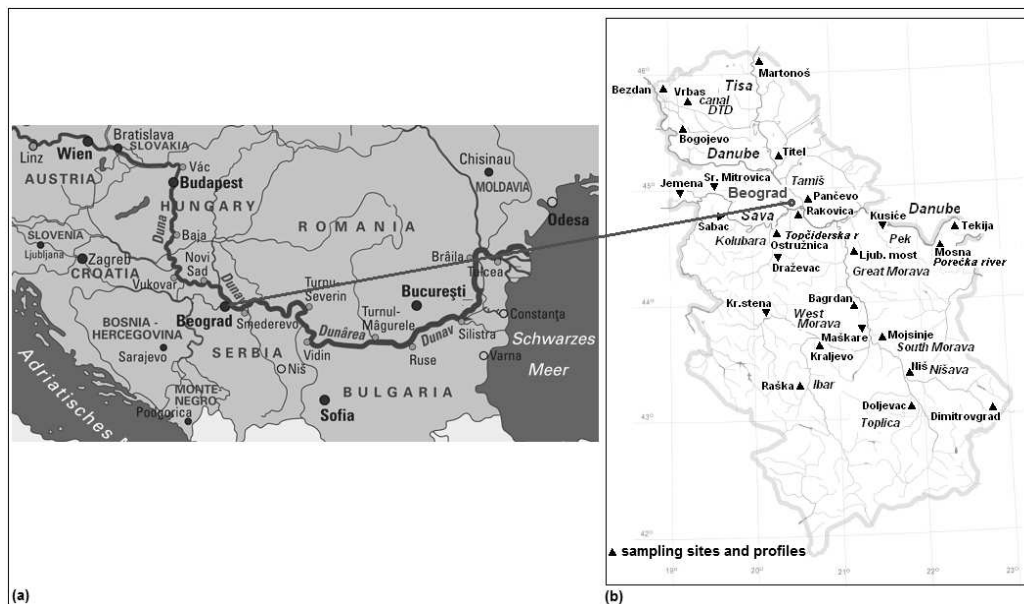


Figure 1. Danube watershed (a) and Profiles and sampling sites in Serbian rivers (b).

**Table 1. Sampling locations with sampling sites**

| Number of sample | Sampling sites and profiles (rivers) | Watershade  |
|------------------|--------------------------------------|-------------|
| 1                | Tisa, Martonoš                       | Danube      |
| 2                | Tisa, Titel                          | Danube      |
| 3                | Tisa, Titel                          | Danube      |
| 4                | Tisa, Titel                          | Danube      |
| 5                | Tisa, Martonoš                       | Danube      |
| 6                | Tisa, Martonoš                       | Danube      |
| 7                | Tisa, Martonoš                       | Danube      |
| 8                | Tisa, Martonoš                       | Danube      |
| 9                | Tisa, Martonoš                       | Danube      |
| 10               | Danube, Bezdán                       | Black Sea   |
| 11               | Danube, Bezdán                       | Black Sea   |
| 12               | Danube, Bezdán                       | Black Sea   |
| 13               | Danube, Bogojovo                     | Black Sea   |
| 14               | Danube, Gruja                        | Black Sea   |
| 15               | Danube, Gruja                        | Black Sea   |
| 16               | Sava, Ostružnica                     | Danube      |
| 17               | Sava, SremskaMitrovica               | Danube      |
| 18               | Sava, Šabac                          | Danube      |
| 19               | Sava, Jamena                         | Danube      |
| 20               | Ibar, Raška                          | West Morava |
| 21               | Ibar, Kraljevo                       | West Morava |
| 22               | Great Morava, Ljubičevski most       | Danube      |

| Number of sample | Sampling sites and profiles (rivers) | Watershade   |
|------------------|--------------------------------------|--------------|
| 23               | Great MoravaMorava, Bagrdan          | Danube       |
| 24               | West Morava, Kratovskastena          | Great Morava |
| 25               | West Morava, Maskare                 | Great Morava |
| 26               | South Morava, Mojsinje               | Great Morava |
| 27               | Niš, Nišava                          | South Morava |
| 28               | Nišava, Dimitrovgrad                 | South Morava |
| 29               | Tamiš                                | Danube       |
| 30               | Vrbas, Begej                         | Danube       |
| 31               | TopčiderskaRiver, Rakovica           | Sava         |
| 32               | PorečkaRiver, Mosna                  | Danube       |
| 33               | Kolubara, Draževac                   | Sava         |
| 34               | Pek, Kusiće                          | Danube       |
| 35               | Toplica, Doljevac                    | South Morava |

### 2.3. Analysis of Element Content

Analysis of metals was carried out using the atomic emission spectrometer with an inductively coupled plasma iCAP-6500 Duo (Thermo Scientific, United Kingdom), after triacid total digestion (HCl, HNO<sub>3</sub> and HF). A 0.5 g sediment sample was placed in a Teflon vessel. Then 9 mL HCl (37%), 3 mL HNO<sub>3</sub> (70%) and 3 mL HF (48%) were added to the vessel. One Teflon vessel only contains the acid mixture for a blank. A microwave digestion system brings the sample to 165°C in 10 minutes (holding time 0 s), then 175°C in three minutes, where held for 10 minutes (max power was 1200 W) (Rönkkömäki et al. 2008). Microwave digestion was performed in a pressurized microwave oven (Ethos 1, Advanced Microwave Digestion System, Milestone, Italy) equipped with a rotor holding 10 microwave vessels (PTFE).

After cooling the digestion system, 10 mL H<sub>3</sub>BO<sub>3</sub> (5g/100mL water) is added. Again, the microwave digestion system brings the sample to 175°C in 10 minutes at 1420W and holds the temperature at 170°C for three minutes. The digestate is then diluted to a final volume of 100 mL (Nam et al. 2001). The solutions were stored in polyethylene flasks for later determination of metals using ICP OES.

All reagents used in the analytical procedure were of analytical grade. Deionized water was used throughout the study. Analytical blanks were run in the same way as the samples, and concentrations determined using standard solutions prepared in the same acid matrix. The metal standards were prepared from a stock solution of 1,000 mg L<sup>-1</sup> by successive dilutions. The instrumental calibration was checked every 10–12 samples; if deviated by more than 2.5%, the machine was recalibrated before analysis continued.

For each digestion were obtained reagent blanks. They were prepared in the same way as the samples without the sediments and CRMs. Blank samples, reflecting blank values for the sampling bottles, reagents, digestion vessels, filtration and any contamination during the whole procedure were prepared and digested in parallel with the batch of samples, using the same procedure, the same quantities of all reagents, but omitting the test portion. The concentrations obtained for all metals in the blanks were close to the detection limit of the method, indicating a zero contamination effect in digestion method.

The accuracy and precision of our results were checked by analyzing sediment reference materials (BCR standards, 143R and 146R). Accuracy was determined by comparing the measured concentration with the certified value, and then expressed in percentage. The percentage recovery of each element was determined as: [measured concentration in  $\text{mg kg}^{-1}$ /mean certified value for BCR 143 in  $\text{mg kg}^{-1}$ ] and [measured concentration in  $\text{mg kg}^{-1}$ /mean certified value for BCR 146 in  $\text{mg kg}^{-1}$ ]. Accuracy was assessed as percentage relative standard deviation (RSD), with  $\text{RSD} < 20\%$  being deemed acceptable (Chen and Ma, 1998; Chand and Prasad, 2013). Calculation results for the accuracy and precision of applied method are given in Table 2. Obtained results indicate a good concordance of the certified and analytical values for BCR 143 and BCR 146 reference materials; the accuracy ranged from 80.9 to 118% and precision was less than 10 % (from 0.03 to 3.80 %).

Results are expressed in  $\text{mg kg}^{-1}$  of dry sediment.

#### 2.4. Metal Pair Ratio (M/Co) for Elements in Sediments

The relative proportion of heavy metals and the normalizers in a natural sediment source are fairly constant. Therefore, the simplest approach in the geochemical normalization of heavy metals in sediments is to express the ratio of the content of a given heavy metal to that of the normalizer.

**Table 2. Total contents of heavy metals in Certified Reference Materials (146R and 143R)**

| Element | Certified 146R          | Found | Accuracy (%) | Certified 143R          | Found | Accuracy (%) |
|---------|-------------------------|-------|--------------|-------------------------|-------|--------------|
|         | ( $\text{mg kg}^{-1}$ ) |       |              | ( $\text{mg kg}^{-1}$ ) |       |              |
| Cd      | 18.8                    | 18.3  | 97.3         | 71.8                    | 70.5  | 98.2         |
| Co      | 7.39                    | 7.62  | 103          | 12.3                    | 12.0  | 102          |
| Cu      | 838                     | 678   | 80.9         | 130.6                   | 111.4 | 85.3         |
| Pb      | 609                     | 532   | 87.4         | 179.7                   | 212.9 | 118          |
| Mn      | 323                     | 347   | 108          | 904                     | 834   | 92.2         |
| Ni      | 70                      | 60    | 85.4         | 299                     | 248   | 82.9         |
| Zn      | 3060                    | 2749  | 89.8         | 1055                    | 1116  | 106          |
| Cr      | 196                     | 167   | 85.2         |                         |       |              |

#### 2.5. Enrichment Factor (EF)

Metal enrichment in the sediments is broadly evaluated by enrichment factor (EF) defined as:

$$\text{EF} = (\text{M}/\text{Y})_{\text{sample}}/(\text{M}/\text{Y})_{\text{background}}$$

where M is the concentration of the potentially enriched element and Y is the concentration of the proxy element (Sakan et al. 2009). Most researchers have used as background for



interpreting results the average shale as suggested in early work of Turekian and Wedepohl (1961). However, some critical aspects are noted in the literature for this approach. EF based on average shale values does not compensate for lithological peculiarities of the respective catchment area; natural geochemical differences due to different underlying lithologies, especially in large areas, can easily alter the EF by a factor of 100 (e.g., limestone vs shale areas). In this paper, the EF values were calculated with regional background and interpreted as suggested by Acevedo-Figueroa et al. (2006), where:  $EF < 1$  indicates no enrichment;  $EF < 3$  is minor; 3-5 is moderate; 5-10 is moderately severe; 10-25 is severe; 25-50 is very severe; and  $> 50$  is extremely severe.

## 2.6. Statistics

The correlations were determined using the simple Pearson correlation coefficient.

# 3. RESULTS AND DISCUSSION

## 3.1. Metal Content

Concentrations of studied elements in river sediments and summary statistics are presented in Table 3 and Table 4. The data for studied elements, extracted from sediments show that:

- Mn concentrations ranged from 648 to 3688 mg kg<sup>-1</sup> with an average 1399 mg kg<sup>-1</sup>;
- Cd content fluctuated between 1.28 to 10.5 mg kg<sup>-1</sup> with an average 4.82 mg kg<sup>-1</sup>. High Cd values observed in all samples suggest an anthropogenic contribution to Cd mean concentrations;
- Co concentrations ranged from 8.22 to 36.2 mg kg<sup>-1</sup> with an average 22.0 mg kg<sup>-1</sup>;
- Cr exhibited a significant concentrations varying between 59.8 to 230 mg kg<sup>-1</sup>, mean 113 mg kg<sup>-1</sup>;
- Fe is the major element in all sediment samples, ranging from 24556 to 62800 mg kg<sup>-1</sup>, with an average 44178 mg kg<sup>-1</sup>;
- Ni concentration ranged from 33.2 to 274 mg kg<sup>-1</sup> with an average 77.8 mg kg<sup>-1</sup>;
- Pb concentrations varied from 57.8 to 318 mg kg<sup>-1</sup> with an average 132 mg kg<sup>-1</sup>;
- V content fluctuated between 60.4 to 149 mg kg<sup>-1</sup> with an average 111 mg kg<sup>-1</sup>;
- Zn concentrations ranged from 66.6 to 1095 mg kg<sup>-1</sup> with an average 353 mg kg<sup>-1</sup>;
- Cu concentrations ranged from 11.5 to 870 mg kg<sup>-1</sup>, with an average 78.5 mg kg<sup>-1</sup>.

Mean elemental concentrations in the Danube, Sava and Tisa do not vary significantly. However, a wider spread in the majority of concentration data is observed for the tributaries dataset. This could reflect a higher degree of variation in the sediment chemical composition, in the context of different sub-basins areas for tributaries, as well as may suggest anthropogenic source for elements origin.

**Table 3. Content of studied elements in sediments, expressed in [mg kg<sup>-1</sup>]**

| Sample           | V    | Fe    | Cd   | Co   | Cr    | Cu   | Mn   | Ni   | Pb   | Zn   |
|------------------|------|-------|------|------|-------|------|------|------|------|------|
| 1                | 87.2 | 33105 | 5.05 | 10.0 | 59.8  | 47.8 | 1276 | 39.2 | 95.7 | 330  |
| 2                | 131  | 49098 | 4.23 | 20.5 | 103.3 | 64.5 | 1234 | 46.2 | 118  | 335  |
| 3                | 122  | 46711 | 4.97 | 21.2 | 95.8  | 74.1 | 1324 | 45.0 | 124  | 391  |
| 4                | 109  | 42246 | 4.41 | 19.1 | 90.2  | 63.8 | 1399 | 39.2 | 124  | 338  |
| 5                | 122  | 46480 | 6.37 | 22.6 | 106   | 88.3 | 1722 | 47.7 | 112  | 360  |
| 6                | 131  | 50118 | 6.89 | 21.3 | 99.8  | 90.5 | 2108 | 42.4 | 142  | 420  |
| 7                | 115  | 43445 | 6.23 | 19.8 | 92.8  | 74.0 | 1870 | 42.8 | 90.3 | 346  |
| 8                | 114  | 43281 | 6.09 | 19.3 | 89.5  | 71.1 | 1683 | 41.5 | 119  | 337  |
| 9                | 123  | 46932 | 7.00 | 21.5 | 96.3  | 87.1 | 1816 | 46.3 | 140  | 411  |
| 10               | 95.5 | 40134 | 2.25 | 16.2 | 73.4  | 28.0 | 1387 | 33.2 | 90.0 | 168  |
| 11               | 106  | 39637 | 2.12 | 16.3 | 75.0  | 23.8 | 1036 | 36.0 | 114  | 157  |
| 12               | 107  | 40922 | 2.49 | 16.8 | 79.9  | 31.4 | 979  | 35.8 | 104  | 208  |
| 13               | 95.5 | 37534 | 2.35 | 15.4 | 76.1  | 28.9 | 896  | 35.0 | 132  | 220  |
| 14               | 97.7 | 40389 | 2.78 | 19.0 | 78.4  | 40.7 | 1352 | 37.9 | 80.3 | 221  |
| 15               | 113  | 44697 | 5.31 | 21.5 | 123   | 41.9 | 1185 | 70.8 | 136  | 228  |
| 16               | 87.5 | 36506 | 3.46 | 21.7 | 112   | 32.0 | 1025 | 93.6 | 89.0 | 270  |
| 17               | 108  | 46480 | 3.02 | 28.5 | 154   | 36.4 | 1759 | 126  | 115  | 213  |
| 18               | 104  | 43872 | 3.74 | 26.4 | 140   | 36.4 | 1660 | 119  | 113  | 272  |
| 19               | 113  | 45780 | 4.69 | 27.3 | 145   | 31.3 | 1819 | 119  | 110  | 213  |
| 20               | 72.1 | 36863 | 10.5 | 13.6 | 102   | 29.0 | 904  | 142  | 318  | 947  |
| 21               | 101  | 47630 | 8.32 | 36.2 | 230   | 39.4 | 1352 | 274  | 263  | 1095 |
| 22               | 129  | 55319 | 7.91 | 32.3 | 170   | 65.6 | 1734 | 42.6 | 182  | 499  |
| 23               | 110  | 46593 | 6.82 | 27.7 | 152   | 53.0 | 1226 | 156  | 182  | 449  |
| 24               | 94.5 | 33860 | 3.60 | 12.2 | 85.6  | 155  | 808  | 84.2 | 77.2 | 250  |
| 25               | 110  | 46461 | 7.50 | 31.8 | 222   | 52.6 | 1032 | 236  | 213  | 660  |
| 26               | 124  | 50105 | 3.88 | 23.4 | 106   | 47.9 | 3688 | 55.1 | 150  | 238  |
| 27               | 112  | 38745 | 2.65 | 16.3 | 86.3  | 85.0 | 731  | 35.9 | 138  | 411  |
| 28               | 101  | 34881 | 5.53 | 16.2 | 70.7  | 22.1 | 770  | 34.6 | 84.1 | 114  |
| 29               | 149  | 62800 | 3.12 | 26.5 | 112   | 51.9 | 1413 | 50.4 | 137  | 191  |
| 30               | 60.4 | 24556 | 1.28 | 8.2  | 62.1  | 11.5 | 648  | 34.7 | 57.8 | 66.7 |
| 31               | 128  | 50739 | 3.91 | 27.9 | 161   | 40.9 | 1226 | 133  | 144  | 338  |
| 32               | 138  | 51266 | 3.13 | 23.8 | 118   | 137  | 868  | 59.0 | 119  | 155  |
| 33               | 114  | 47245 | 5.45 | 28.7 | 146   | 39.4 | 1352 | 132  | 126  | 417  |
| 34               | 127  | 50977 | 6.26 | 30.5 | 88.7  | 870  | 1997 | 41.6 | 157  | 922  |
| 35               | 137  | 50808 | 5.23 | 29.5 | 148   | 55.6 | 1685 | 115  | 135  | 167  |
| MAQ <sup>a</sup> | /    | /     | 2    | /    | 100   | 100  | /    | 50   | 100  | 300  |

<sup>a</sup> Republic of Serbia (1990): MAQ-Maximum Allowed Quantity.

**Table 4. Summary statistics for studies elements [mg kg<sup>-1</sup>]**

|              | Mn   | Cd   | Co   | Cr   | Fe    | Ni   | Pb   | V    | Zn   | Cu   |
|--------------|------|------|------|------|-------|------|------|------|------|------|
| Mean         | 1399 | 4.82 | 22.0 | 113  | 44178 | 77.8 | 132  | 111  | 353  | 78.5 |
| Median       | 1352 | 4.69 | 21.5 | 102  | 45780 | 46.3 | 124  | 112  | 330  | 47.9 |
| Minimum      | 648  | 1.28 | 8.22 | 59.8 | 24556 | 33.2 | 57.8 | 60.4 | 66.6 | 11.5 |
| Maximum      | 3688 | 10.5 | 36.2 | 230  | 62800 | 274  | 318  | 149  | 1095 | 870  |
| Harmonic M.  | 1235 | 3.91 | 19.7 | 101  | 42896 | 54.3 | 118  | 108  | 252  | 42.8 |
| Geometric M. | 1311 | 4.37 | 20.9 | 107  | 43566 | 63.2 | 125  | 109  | 298  | 52.2 |

Complimentary Contributor Copy

The majority of the tributaries are influenced by antropogenic sources. Their metals content in sediments could be influenced by mining activities in the catchment area (Comero et al. 2014).

If compared to the Serbian standards (Republic of Serbia, 1990), Cd, Cr, Ni, Pb and Zn level exceeded the MAQ limit on some localities. These results indicate serious antropogenic pollution at some stations and that heavy metals concentrations in sediments pose a potential risk to aquatic life.

### 3.2. Metal Pair Ratio (M/Co) for Elements in Sediments

Figure 2 shows metal to cobalt ratios in different sampling sites selected for this study. The ratios are shown in the form of the logarithm. The metal pair ratios clearly reflect enrichment: for Fe, sites 20 and 24 (Ibar and West Morava); for Mn: 1 and 26 (Tisa and South Morava); for Zn: 20, 27 and 34 (Ibar, Nišava and Pek); for Pb: 13, 20, 27 and 34 (Danube, Ibar, Nišava and Pek); for V: 24 and 32 (West Morava and Porečka river); for Cr: 20 (Ibar); for Cu: 24, 27, 32 and 34 (West Morava, Nišava, Porečka river, and Pek); for Ni: 20 to 25 (Ibar, Great Morava and West Morava) and for Cd: 1, 6-9, 20, 24 and 28 (Tisa, Ibar, West Morava and Nišava).

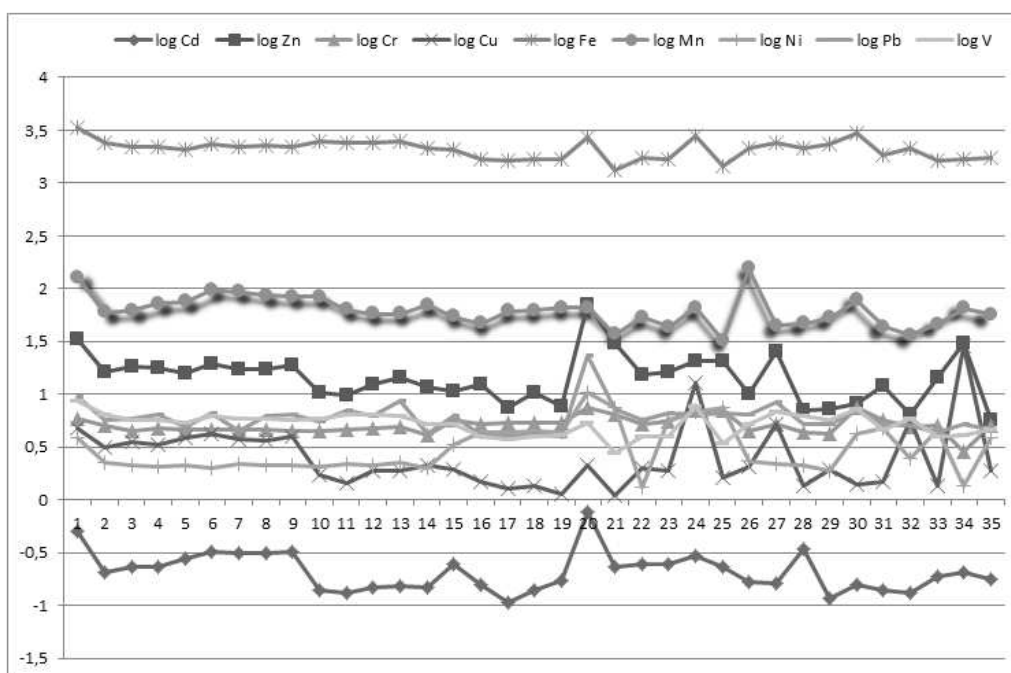


Figure 2. Ratio M/Co, represented as logarithm.

Figure 3 shows a variation of M/Co in the studied sediments using the Box plot. Outlier and extreme values of M/Co observed were found at localities: 20 (Ibar, for Cd), 20 (Ibar, for Zn), 34 (Pek, for Cu), 26 (South Morava, for Mn), and 20 (Ibar, for Pb). This can be attributed to the antropogenic activities in the catchments of these rivers.



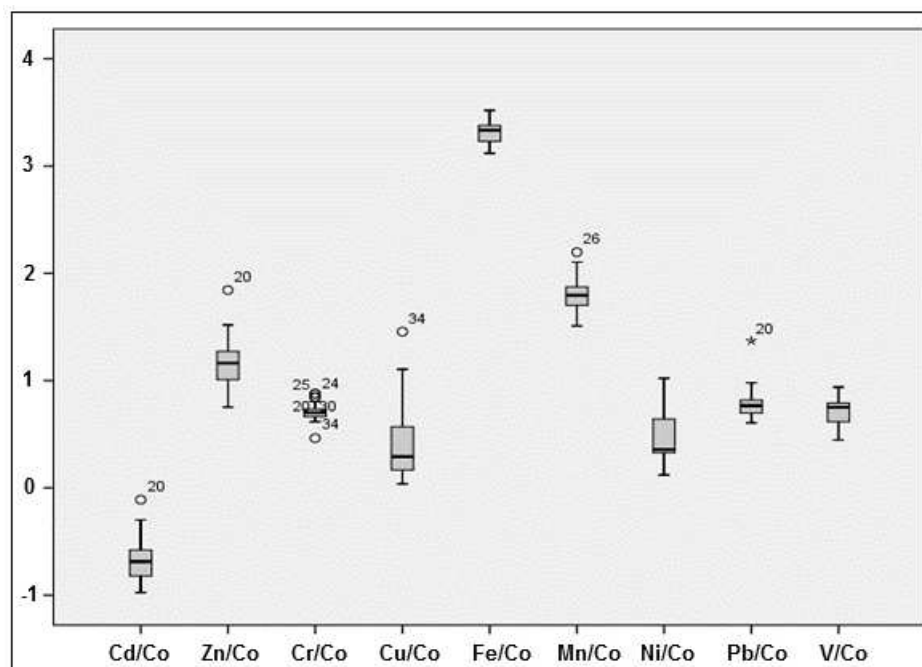


Figure 3. Box-plot for M/Co, represented as logarithm.

### 3.3. Correlation Matrix

Pearson's correlation coefficient gives an idea about the possible relationships between metals: common origin, uniform distribution, similar behaviors and relationships amongst metals (Diop et al. 2015).

Table 5 reports the values of Pearson's correlation coefficient (N=35) for pairs of studied elements. Figure 4 presents correlation diagrams between Co and other elements.

Co is positive correlated with Cr, Cd, Fe, Ni, Pb, V, Zn, and Mn, and no correlated with Cu. Cd is positive correlated with Cr, Ni, Pb, Zn; Cr with Cd, Fe, Ni, Pb, and Zn; Fe with Cr, V and Mn; Ni with Cd, Cr, Pb, Zn; Cd, Cr, Ni, Zn; V with Fe, Mn; Zn with Cd, Cr, Ni, Pb and Cu; Mn with Fe, and V and Cu is positive correlated with Zn. Correlation matrix shows significant and positive correlation among Cd, Cr, Ni, Pb and Zn. These correlations possibly reflect the same or similar source input for these metals. Non existence of the Cu correlation with all the elements (except Zn) suggests different origin or dissimilar sedimentological properties.

### 3.4. Enrichment Factor (EF)

For correct examination of the sediments pollution using the calculation of EF is most important a proper selection of element for normalization and background values. In this chapter, cobalt is selected as a normalization element.

Complimentary Contributor Copy

**Table 5. Correlation matrix for sediment samples giving values of Pearson's correlation coefficients, r, for pair of elements (N=35)**

|    |   | Cd             | Co             | Cr             | Fe             | Ni             | Pb             | V              | Zn            | Mn    | Cu |
|----|---|----------------|----------------|----------------|----------------|----------------|----------------|----------------|---------------|-------|----|
| Cd | r | 1              |                |                |                |                |                |                |               |       |    |
|    | p |                |                |                |                |                |                |                |               |       |    |
| Co | r | <b>0.387*</b>  | 1              |                |                |                |                |                |               |       |    |
|    | p | 0.022          |                |                |                |                |                |                |               |       |    |
| Cr | r | <b>0.451**</b> | <b>0.858**</b> | 1              |                |                |                |                |               |       |    |
|    | p | 0.007          | 0.000          |                |                |                |                |                |               |       |    |
| Fe | r | 0.273          | <b>0.779**</b> | <b>0.513**</b> | 1              |                |                |                |               |       |    |
|    | p | 0.113          | 0.000          | 0.002          |                |                |                |                |               |       |    |
| Ni | r | <b>0.452**</b> | <b>0.609**</b> | <b>0.869**</b> | 0.172          | 1              |                |                |               |       |    |
|    | p | 0.006          | 0.000          | 0.000          | 0.324          |                |                |                |               |       |    |
| Pb | r | <b>0.743**</b> | <b>0.427*</b>  | <b>0.571**</b> | 0.318          | <b>0.627**</b> | 1              |                |               |       |    |
|    | p | 0.000          | 0.010          | 0.000          | 0.063          | 0.000          |                |                |               |       |    |
| V  | r | 0.103          | <b>0.583**</b> | 0.272          | <b>0.903**</b> | -0.092         | 0.037          | 1              |               |       |    |
|    | p | 0.558          | 0.000          | 0.114          | 0.000          | 0.599          | 0.831          |                |               |       |    |
| Zn | r | <b>0.759**</b> | <b>0.415*</b>  | <b>0.459**</b> | 0.201          | <b>0.552**</b> | <b>0.824**</b> | -0.036         | 1             |       |    |
|    | p | 0.000          | 0.013          | 0.006          | 0.247          | 0.001          | 0.000          | 0.837          |               |       |    |
| Mn | r | 0.194          | <b>0.378*</b>  | 0.120          | <b>0.496**</b> | -0.064         | 0.063          | <b>0.432**</b> | 0.070         | 1     |    |
|    | p | 0.264          | 0.025          | 0.493          | 0.002          | 0.714          | 0.719          | 0.010          | 0.688         |       |    |
| Cu | r | 0.144          | 0.215          | -0.110         | 0.210          | -0.137         | 0.065          | 0.235          | <b>0.421*</b> | 0.191 | 1  |
|    | p | 0.410          | 0.215          | 0.530          | 0.227          | 0.432          | 0.710          | 0.174          | 0.012         | 0.272 |    |

The bold values represent significant correlated parameter.

\* Correlation is significant at the 0.05 level.

\*\* Correlation is significant at the 0.01 level.

Complimentary Contributor Copy

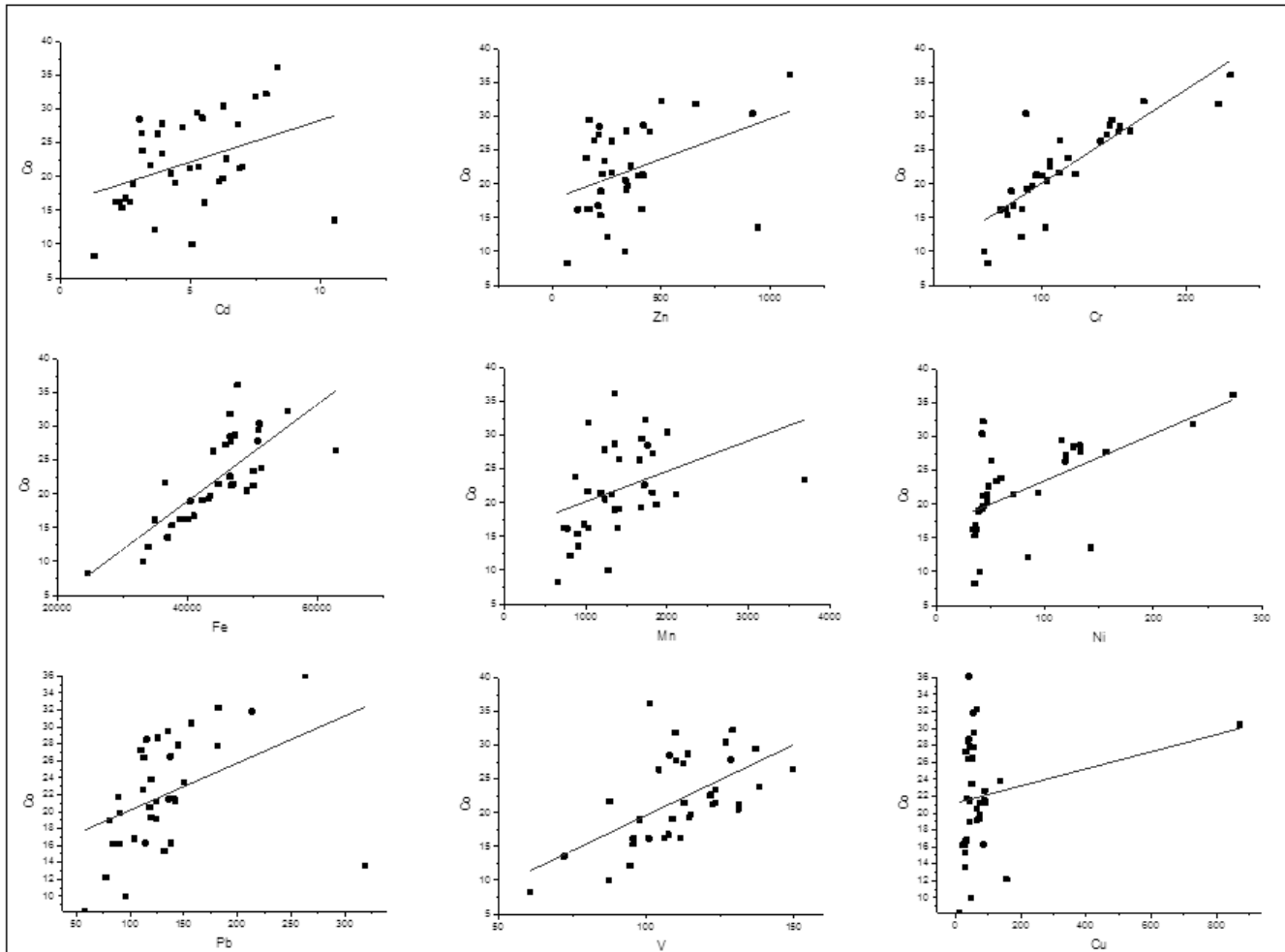


Figure 4. Correlation diagrams between Co and Cd, Zn, Cr, Fe, Mn, Ni, Pb, V, and Zn.

Complimentary Contributor Copy

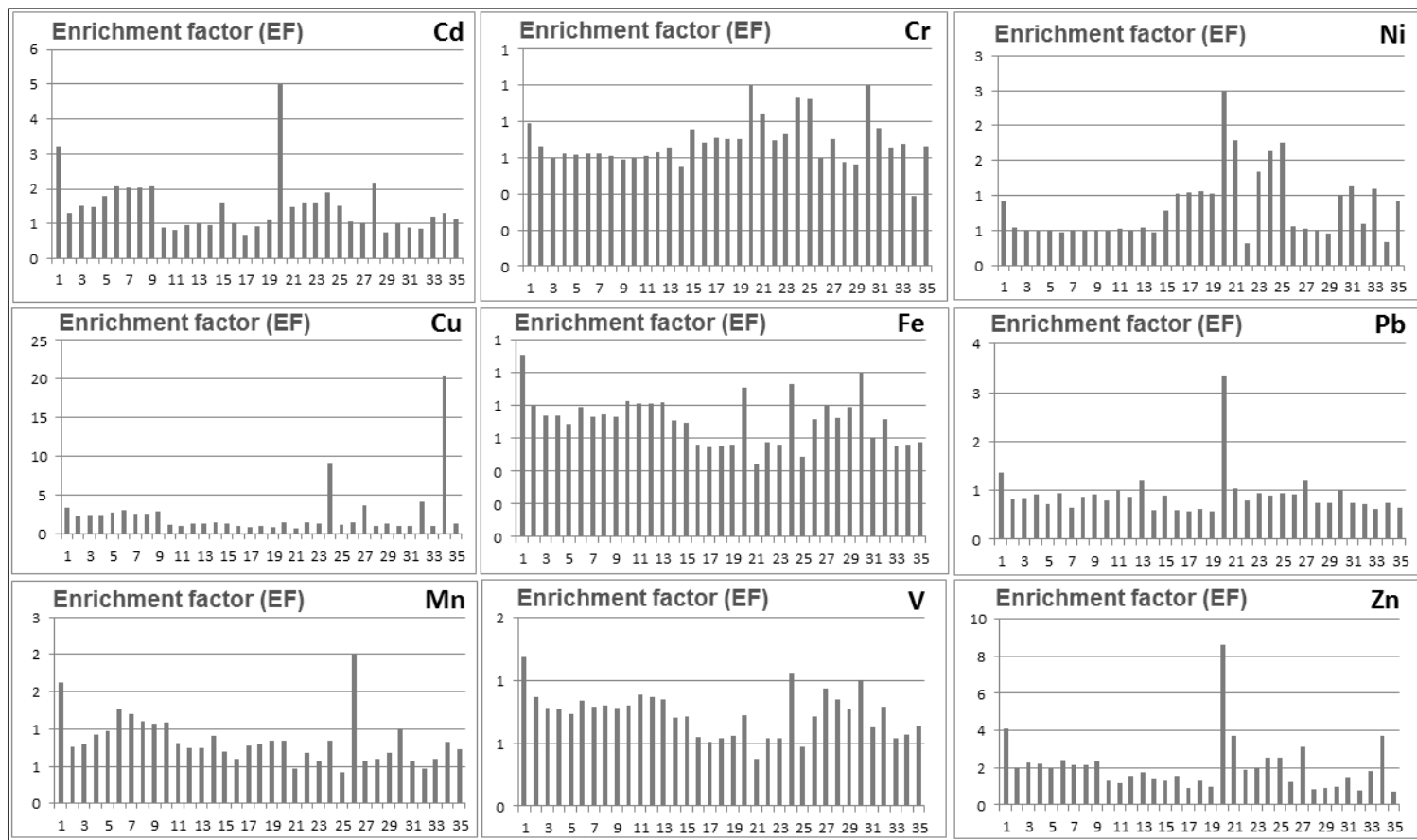


Figure 5. EF values for studied elements.

Complimentary Contributor Copy

The occurrence of cobalt in the earth's surface varies greatly (Barańkiewicz and Siepak, 1999). The occurrence of cobalt in soils is to a large extent determined by bedrock. Its content in the soil is within a fairly broad range, i.e., 0.1 to 100 mg kg<sup>-1</sup>, the lowest average values occur in sandy podsol soils 5.5 mg kg<sup>-1</sup> and organic soils 4.4 mg kg<sup>-1</sup>, and the highest for dark brown clay soils, fen soils and limestone soils 10-12 mg kg<sup>-1</sup>. The average content of cobalt in the soils of the world amounts to 8 mg kg<sup>-1</sup> (Barańkiewicz and Siepak, 1999). The median total Co content in stream sediment is 8.0 mg kg<sup>-1</sup> (Co, 2015). In continental crust, content of Co is 24 mg kg<sup>-1</sup> (Waterpohl, 1995).

The positive correlation between Cd, Cr, Fe, Ni, Pb, V, Mn and Zn with Co and its content, which is similar to the average concentration of this element in the continental crust, soil and sediment suggests the possibility of using Co as normalization element in this research. Also, this element is not substantially enriched by anthropogenic sources in studied area.

Background measurements represent the natural concentrations in unpolluted soils and sediments. It is difficult to assess if a soil is absolutely free of contaminants (Relić et al. 2011). The element content in the DTD canal (station in Vrbas) was chosen as background values for elements in this research, due to the lack of significant anthropogenic sources of toxic elements at this area, and similarity of the sediment samples to other investigated river sediments in their geochemical characteristics and composition. Background values of elements in this research are: 1.28 mg kg<sup>-1</sup> Cd; 11.5 mg kg<sup>-1</sup> Cu; 8.22 mg kg<sup>-1</sup> Co; 648 mg kg<sup>-1</sup> Mn; 62.1 mg kg<sup>-1</sup> Cr; 34.7 mg kg<sup>-1</sup> Ni; 57.8 mg kg<sup>-1</sup> Pb; 66.6 mg kg<sup>-1</sup> Zn; 24 556 mg kg<sup>-1</sup> Fe and 60,4 mg kg<sup>-1</sup> V.

As indicated in Figure 5, with respect to the calculated EF, Cd is ranked no to moderate enrichment (EF = 0.68-4.99), Cr is no enrichment (EF = 0.39-1.00), Cu is no to severe (0.78-20.43), Fe is no enrichment (0.44-1.11), Ni is no to minor (0.31-2.49), Pb is no to moderate (0.57-3.34), Mn is no to minor (0.41-2.00), V is no enrichment (0.38-1.18), and Zn is no to moderately severe enrichment (0.70-8.62). On the basis of local background values and cobalt as normalizer, the Serbian river sediments were found to be enriched in Cd, Cu, Zn and Pb and to a lesser extent in Ni and Mn. On the contrary, no significant enrichment occurs for Fe, Cr and V. Values of EF for Cr indicate a strong lithogenic origin of Cr (weathering of ophiolite complexes).

## CONCLUSION

The absence of the anthropogenic influence of cobalt in river sediments in Serbia led us to conclusion that it could be used as a normalizing element in further investigations. The use of cobalt presents not only novelty in river sediment analysis but it also possesses an impetus for the use in other regions. The use of cobalt as a normalizing element could help to determine the contamination sources more precisely and more distinctive. The presence of anthropogenic contributions of Cd, Cu, Zn and Pb, was shown by the using Co as normalizing element, and it is in consistence with the previous measurements. There is a need for further investigation on influence of background content variation on the values of enrichment factor.

## ACKNOWLEDGMENTS

This study was supported by the Ministry of Education, Science and Technological Development of Serbia, Grant Nos. 172001 and 43007. In addition, we would like to thank the Republic Hydrometeorological Service of Serbia for the sediment samples.

## REFERENCES

- Acevedo-Figueroa, D., Jiménez, B.D., Rodríguez-Sierra, C.J. (2006). Trace metals in sediments of two estuarine lagoons from Puerto Rico. *Environmental Pollution*, 141, 33-342.
- Adriano, D.C., Németh, T., & Gyóri, Z. (2003). Natural Attenuation of Metals along the Tisza River-Floodplain-Wetlands Continuum. University of Debrecen, Centre of Agricultural Sciences, Hungary.
- Barałkiewicz, D., & Siepak, J. (1999). Chromium, nickel and cobalt in environmental samples and Existing legal norms. *Polish Journal of Environmental Studies*, 8, 201-2018.
- Bartolli, G., Papa, S., Sagnella, E., & Fioreto, A. (2012). Heavy metal content in sediments along the Calore river: relationships with physical-chemical characteristics. *Journal of Environmental Management*, 95, S9-S14.
- Chabuhdhara, M., & Nema, A. (2012). Assessment of heavy metal contamination in Hindon River sediments: A chemometric and geochemical approach. *Chemosphere*, 87, 945-953.
- Chand, M., & Prasad, S. (2013). ICP-OES assessment of heavy metal contamination in tropical marine sediments: A comparative study of two digestion techniques. *Microchemical Journal*, 111, 53-61.
- Chen, M., & Ma, L.Q. (1998). Comparison of four USEPA digestion methods for trace metal analysis using certified and Florida soils. *Journal of Environmental Quality*, 27, 1294-1300.
- Co-Cobalt. 21.02.2015. Available from: [www.weppi.gtk.fi/publ/foregsatlas/text/Co.pdf](http://www.weppi.gtk.fi/publ/foregsatlas/text/Co.pdf)
- Comero, S., Vaccaro, S., Locoro, G., De Capitani, & Gawlik, B.M. (2014). Characterization of the Danube River sediments using the PMF multivariate approach. *Chemosphere*, 95, 329-335.
- Ćevik F., Goksu, M.Z.L., Derici, O.B. & Findik, O. (2009). An assessment of metal pollution in surface sediment of Seghan Dam by using enrichment factor, geoaccumulation index and statistical analysis. *Environmental Monitoring Assessment*, 152, 309 - 317.
- Davutluoglu, O.I., Seckin, G., Ersu, C.B., Yimlaz, T., & Sari, B. (2011). Heavy metal content and distribution in surface sediments of the Seyhan River, Turkey. *Journal of Environmental Management*, 92, 2250-2259.
- Diop, C., Dewaelé, D., Cazier, F., Diouf, A., Ouddane, B. (2015). Assessment of trace metals contamination level, bioavailability and toxicity in sediments from Dakar coast and saint Louis estuary in Senegal, West Africa. *Chemosphere*, <http://dx.doi.org/10.1016/j.chemosphere.2014.12.041>
- Förstner, U., & Wittmann, G.T.W. (1981). *Metal pollution in the aquatic environment*. Springer, New York, 486 pp.

- Ho, H.H., Swennen, R., Cappuyns, V., Vassilieva, E., & Tran, T.V. (2012). Necessity of normalization to aluminum to assess the contamination by heavy metals and arsenic in sediments near Haiphong Harbor, Vietnam. *Journal of Normalization to Aluminum to Assess the Contamination by Heavy Metals and Arsenic in Sediments near Haiphong Harbor, Vietnam*. *Journal of Asian Earth Sciences*, 56, 229-236.
- Iqbal, J., Tirmizi, S.A., & Shah, M.H. (2013). Statistical apportionment and risk assessment of selected metals in sediments from Rawal lake (Pakistan). *Environmental Monitoring and Assessment*, 185, 729-743.
- Matthai, C., & Birch, G. (2001). Detection of anthropogenic Cu, Pb and Zn in continental shelf sediments off Sydney, Australia – a new approach using normalization with cobalt. *Marine Pollution Bulletin*, 42, 1055-1063.
- Nam, S.H., Kim, M.J., Park, Y.I., & Lee, S.J. (2001). A study on various pretreatment and preparation for the determination of inorganic elements in sediment. *Analytical Sciences*, 17, a263-a265.
- Relić, D., Dorđević, D., Sakan, S., Anđelković, I., Miletić, S., & Đuričić, J. (2011). Aqua regia extracted metals in sediments from the industrial area and surroundings of Pančevo, Serbia. *Journal of Hazardous Materials*, 186, 1893-1901.
- Relić, D., Dorđević, D., Sakan, S., Anđelković, I., Pantelić, A., Stanković, R., & Popović, A. (2013). Conventional, microwave, and ultrasound sequential extractions for the fractionation of metals in sediments within the Petrochemical Industry, Serbia. *Environmental Monitoring Assessment*, 185, 7627-7645.
- Republic of Serbia (1990). MAQ-Official Gazete, 11/239.
- Rönkkömäki, H., Pöykiö, R., Nurmesniemi, H., Popov, K., Merisalu, E., Tuomi, T., & Välimäki, I. (2008). Particle size distribution and dissolution properties of metals in cyclone fly ash. *International Journal of Environment Science and Technology*, 5, 485-494.
- Sakan, S.M., Dorđević, D.S., Manojlović, D.D., & Polić, P.S. (2009). Assessment of heavy metal pollutants accumulation in the Tisza river sediments. *Journal of Environmental Management*. 90, 3382-3390.
- Sakan, S., Dorđević, D., Dević, G., Relić, D., Anđelković, I., & Đuričić, J. (2011). A study of trace element contamination in river sediments in Serbia using microwave-assisted aqua regia digestion and multivariate statistical analysis. *Microchemical Journal*, 99, 492-502.
- Sakan, S., & Dorđević, D. (2012a). Distinguishing between natural and anthropogenic sources of trace elements in the sediments using the methods of geochemical normalization and statistical analysis. In D.A. De Leon & P.R. Aragon (Eds.), *Trace elements: Environmental Sources, Geochemistry and Human Health* (pp. 117-134), Nova Science Publishers, Inc.
- Sakan, S., Dorđević, D., Lazić, M., & Tadić, M. (2012b). Assessment of arsenic and mercury contamination in the Tisa River sediments and industrial canal sediments (Danube alluvial formation), Serbia. *Journal of Environmental Science and Health, Part A*, 47, 109-116.
- Sakan, S., & Dorđević, D. (2013). Assessment of trace element contamination in the river and alluvial sediments using a sequential extraction technique and statistical analysis. In S. Hong-Bo (Ed.), *Metal Contamination: Sources, Detection and Environmental Impact* (pp. 119-155), Nova Science Publishers, Inc.

- Sakan, S., Dević, G., Relić, D., Anđelković, I., Sakan, N., & Đorđević, D. (2014). Risk assessment of trace element contamination in river sediments in Serbia using pollution indices and statistical methods: a pilot study. *Environmental Earth Sciences*, doi: 10.1007/s12665-014-3886-1
- Sakan, S., Dević, G., Relić, D., Anđelković, I., Sakan, N., & Đorđević, D. (2015a). Evaluation of sediment contamination with heavy metals: the importance of determining appropriate background content and suitable element for normalization. *Environmental Geochemistry and Health*, 37, 97-113.
- Sakan, S., Dević, G., Relić, D., Anđelković, I., & Sakan, N. (2015b). Environmental assessment of heavy metal pollution in freshwater sediment, Serbia. *CLEAN-Soil Air Water*, doi: 10.1002/clen.201400275
- Sarkar, S., Ghosh, P.B., Sil, A.K., & Saha, T. (2011). Heavy metal pollution assessment through comparison of different indices in sewage-fed fishery pond sediments at East Kolkata Wetland, India. *Environmental Earth Sciences*, 63, 915-924.
- Turekian, K.K., & Wedepohl, K.H. (1961). Distribution of the elements in some major units of the earth's crust. Geological Society of America Bulletin. *Geochimica et Cosmochimica Acta*, 59, 1217-1232.
- Wedepohl, K.H. (1995). The composition of the continental crust. *Geochimica et Cosmochimica Acta*, 59, 1217-1232.





# ADVANCES IN ENVIRONMENTAL RESEARCH

VOLUME 41

Justin A. Daniels  
Editor

NOVA

Complimentary Contributor Copy



ADVANCES IN ENVIRONMENTAL RESEARCH

**ADVANCES IN  
ENVIRONMENTAL RESEARCH**

**VOLUME 41**

No part of this digital document may be reproduced, stored in a retrieval system or transmitted in any form or by any means. The publisher has taken reasonable care in the preparation of this digital document, but makes no expressed or implied warranty of any kind and assumes no responsibility for any errors or omissions. No liability is assumed for incidental or consequential damages in connection with arising out of information contained herein. This digital document is sold with the clear understanding that the publisher is not engaged in rendering legal, medical or any other professional services.

**Complimentary Contributor Copy**

# **ADVANCES IN ENVIRONMENTAL RESEARCH**

Additional books in this series can be found on Nova's website  
under the Series tab.

Additional e-books in this series can be found on Nova's website  
under the e-book tab.

Complimentary Contributor Copy

ADVANCES IN ENVIRONMENTAL RESEARCH

**ADVANCES IN  
ENVIRONMENTAL RESEARCH**

**VOLUME 41**

**JUSTIN A. DANIELS**  
**EDITOR**



Complimentary Contributor Copy

Copyright © 2015 by Nova Science Publishers, Inc.

**All rights reserved.** No part of this book may be reproduced, stored in a retrieval system or transmitted in any form or by any means: electronic, electrostatic, magnetic, tape, mechanical photocopying, recording or otherwise without the written permission of the Publisher.

We have partnered with Copyright Clearance Center to make it easy for you to obtain permissions to reuse content from this publication. Simply navigate to this publication's page on Nova's website and locate the "Get Permission" button below the title description. This button is linked directly to the title's permission page on [copyright.com](http://copyright.com). Alternatively, you can visit [copyright.com](http://copyright.com) and search by title, ISBN, or ISSN.

For further questions about using the service on [copyright.com](http://copyright.com), please contact:

Copyright Clearance Center

Phone: +1-(978) 750-8400 Fax: +1-(978) 750-4470 E-mail: [info@copyright.com](mailto:info@copyright.com).

#### **NOTICE TO THE READER**

The Publisher has taken reasonable care in the preparation of this book, but makes no expressed or implied warranty of any kind and assumes no responsibility for any errors or omissions. No liability is assumed for incidental or consequential damages in connection with or arising out of information contained in this book. The Publisher shall not be liable for any special, consequential, or exemplary damages resulting, in whole or in part, from the readers' use of, or reliance upon, this material. Any parts of this book based on government reports are so indicated and copyright is claimed for those parts to the extent applicable to compilations of such works.

Independent verification should be sought for any data, advice or recommendations contained in this book. In addition, no responsibility is assumed by the publisher for any injury and/or damage to persons or property arising from any methods, products, instructions, ideas or otherwise contained in this publication.

This publication is designed to provide accurate and authoritative information with regard to the subject matter covered herein. It is sold with the clear understanding that the Publisher is not engaged in rendering legal or any other professional services. If legal or any other expert assistance is required, the services of a competent person should be sought. FROM A DECLARATION OF PARTICIPANTS JOINTLY ADOPTED BY A COMMITTEE OF THE AMERICAN BAR ASSOCIATION AND A COMMITTEE OF PUBLISHERS.

Additional color graphics may be available in the e-book version of this book.

#### **Library of Congress Cataloging-in-Publication Data**

ISSN: 2158-5717

ISBN:

# CONTENTS

|                  |  |            |
|------------------|--|------------|
| <b>Preface</b>   |  | <b>vii</b> |
| <b>Chapter 1</b> | The Impact of Forest Canopy Structure on Simulations of Atmosphere-Biosphere NO <sub>x</sub> Exchange<br><i>Ana Firanj, Branislava Lalic, Laurens Ganzeveld and Zorica Podrascanin</i>                           | <b>1</b>   |
| <b>Chapter 2</b> | Numerical Simulation of CO <sub>2</sub> Sequestration in Saline Aquifer Influenced by Heterogeneous Capillary Pressure and Wettability<br><i>Sung Soo Park and Kun Sang Lee</i>                                  | <b>17</b>  |
| <b>Chapter 3</b> | Estimation of Riverine Nutrient Fluxes from an Urban Watershed in New Jersey<br><i>Yunfang Li, David Colombini, Yu Qian, Benjamin B. Witherell and Huan Feng</i>   | <b>35</b>  |
| <b>Chapter 4</b> | Residual Environmental Impacts in Post-Mining Site: A Field Survey on the Iberian Peninsula<br><i>Ryunosuke Kikuchi and Romeu Gerardo</i>  | <b>49</b>  |
| <b>Chapter 5</b> | Pollution Characteristics and Potential Ecological Risk Assessment of Heavy Metals in River Sediments Based on Calculation of Pollution Indices<br><i>Sanja M. Sakan, Nenad M. Sakan and Dragana S. Đorđević</i> | <b>63</b>  |
| <b>Chapter 6</b> | Rainfall Patterns and the Relation to Atmospheric Circulation in Northern Patagonia (Argentina)<br><i>M. H. González, E. M. Garbarini and P. E. Romero</i>   | <b>85</b>  |
| <b>Chapter 7</b> | Forest Management to Prevent Crown Fires: A Case Study of a Dry Deciduous Forest in Kratie, Cambodia<br><i>Koji Tamai</i>  | <b>101</b> |
| <b>Chapter 8</b> | Stakeholder Inclusion in Design and Planning - A Case Study on Wastewater Management in Nepal<br><i>Martina Maria Keitsch and Udhab Nepal</i>  | <b>111</b> |
| <b>Chapter 9</b> | Methane Interactions with an Atmospheric Moisture<br><i>Alexander Y. Galashev</i>  | <b>127</b> |

Complimentary Contributor Copy

---

|                   |  |            |
|-------------------|--|------------|
| <b>Chapter 10</b> | Lanthanides and Actinides in Soils of Khibiny-Lovozero Province<br><i>Yu. N. Vodyanitskii, A. T. Savichev and N. V. Kosareva</i> | <b>157</b> |
| <b>Chapter 11</b> | Safer Irrigation Technology Adoption under Uncertainty Perception<br>in Ghana<br><i>Victor Owusu</i>                             | <b>175</b> |
| <b>Chapter 12</b> | Nano Biomaterial for Decontamination of Carcinogenic Metal<br>from Waste Water<br><i>Pritee Goyal and Dhanraj T. Masram</i>      | <b>191</b> |
| <b>Index</b>      |  | <b>203</b> |



*Chapter 5*

**POLLUTION CHARACTERISTICS AND POTENTIAL  
ECOLOGICAL RISK ASSESSMENT OF HEAVY METALS  
IN RIVER SEDIMENTS BASED ON CALCULATION OF  
POLLUTION INDICES**

*Sanja M. Sakan<sup>1</sup>, Nenad M. Sakan<sup>2</sup> and Dragana S. Đorđević<sup>1</sup>*

<sup>1</sup>ICTM, Chemistry Centre, University of Belgrade, Belgrade, Serbia

<sup>2</sup>Institute of Physics, University of Belgrade, Belgrade, Serbia

**ABSTRACT**

The presented study was carried out in order to evaluate risk assessment of selected heavy metals (Cd, Cu, Mn, Cr, Ni, Pb, Zn, Co and V) in river sediments in Serbia. The purpose of this chapter is to describe a new approach in ecological geochemistry assessment of heavy metal pollution using different pollution indices for estimation the anthropogenic input of elements, quantifying the degree of metal enriched in sediments, assessment the pollution status of the area and estimation of the potential acute toxicity of studied contaminants. Concentrations of heavy metals were determined at 35 river sediments. The metal concentrations (in mg kg<sup>-1</sup>) ranged: Mn, 648-3688; Cd, 1.28-10.5; Co, 8.22-36.2; Cr, 59.8-230; Ni, 33.2-274; Pb, 57.8-318; V, 60.4-149; Zn, 66.6-1095, and Cu, 11.5-870. Pollution indices were calculated separately for all sampling sites, to evaluate the extent of metal enrichment at each site. Based on calculated indices, the studied river sediments were found to be significantly contaminated by Cd, Cu and Zn. The most contaminated river systems in Serbia are the Ibar, Pek, and West Morava.

**1. INTRODUCTION**

Growing human population and related human activities have intensified emission of various pollutants into the environment. In order to prevent environmental pollution and to protect natural resources, the ecological status of the Earth's ecosystems is intensively investigated. One of the most important natural reservoirs is water (Milačić et al. 2010).

Complimentary Contributor Copy

To protect water resources, detailed and accurate information on the occurrence of polluting substances in aqueous environment is needed. River sediments are reservoirs of materials derived from both anthropogenic and natural weathering processes. Sediments have been used as an important tool to assess the health status of aquatic ecosystems and are an integral component for functioning of ecological integrity (Zahra et al. 2014). Sediments act as a sink of organic as well as inorganic pollutants (heavy metals) and provide a history of anthropogenic pollutant input (Zahra et al. 2014). Sediment contamination by heavy metals may cause direct harm to benthic organisms and indirect harm to water column ecosystems through remobilization.

In order to identify pollution problems, the anthropogenic contributions should be distinguished from the natural sources. Various procedures reported in the literature for the assessment of the anthropogenic contributions (Pekey et al. 2004; Mediolla et al. 2008; Harikumar et al. 2009; Milačić et al. 2010; Kabir et al. 2011; Relić et al. 2011; Sakan et al. 2012a; Sakan et al. 2012b; Gao et al. 2013; Relić et al. 2013; Sakan et al. 2013). Geochemical approaches such as the enrichment factor (EF) and geochemical index methods have been successfully used to estimate the impact of the activities of civilisation on sediments (Chabukdhara and Nema, 2012). Many scientists have studied metal contamination in sediments using geochemical approaches (Abraham and Parker, 2008; Harikumar et al. 2009; Sakan et al. 2009; Hu et al. 2011; Kabir et al. 2011; Hui-na et al. 2012; Gao et al. 2013; Sakan et al. 2014; Sakan et al. 2015a, Sakan et al. 2015b).

In this study, the evaluation of the metal pollution level and possible sources compared to background pollution is performed for river sediments in Serbia. The main objectives were to determine the total content of Cd, Co, Cr, Cu, Mn, Ni, Pb, V and Zn and the calculation of the contamination factor, enrichment factor, index of geoaccumulation, ecological risk factor, pollution load index, combined pollution index, and ecological risk index to estimate the anthropogenic input of the elements and to assess the pollution status of the area. In this research was also determined Al content, since this element was used as normalizing element.

## 2. EXPERIMENTAL

### 2.1. Study Area

Cross border pollution indicates a need to determine the pollutants in the water and sediment in all the countries along the river's flow. Because of that, for this investigation sediment was selected from the main rivers in Serbia.

The Danube is the most important and the second largest river in Europe, which flows through more countries than any other river in the world - Germany, Austria, Slovakia, Hungary, Croatia, Serbia, Romania, Bulgaria, Ukraine, and Moldova. On its way from the Black Forest (Germany) to its mouth in the Black Sea (Romania and Ukraine), the Danube River passes by or through ten riparian states, which makes it the most international river in the world. The major tributaries of the Danube river are: the Drava, Sava and Drina in the west, the Morava in the south, the Tisa, Tamiš, Moriš and Timok rivers in the north and east were the most important lines of communications.

The Sava river is the biggest tributary to the Danube river. Along its total length of 944 km and total catchment area of 97,713 km<sup>2</sup>, the Sava River connects four countries and more than 8 million people who live in and from its catchment area. River Tisa is considered the largest tributary of Danube River by its total length of 977 kilometers. Tisa River's source is in Ukraine in the Western Carpathians where the Black Tisa at the altitude of 960 meters and White Tisa at the altitude of 1700 meters join. Tisa River flows through Ukraine, Slovakia, Romania, Hungary and Serbia.

## 2.2. Sampling Locations

Sampling was performed during the year 2008. 35 samples of river sediment were taken from 15 rivers in Serbia: the Danube – samples D1 to D6 (Black Sea watershed), the Sava – S1 to S4 (Danube watershed), the Tisa – T1 to T9 (Danube watershed), the Ibar – I1 and I2 (West Morava watershed), the Great Morava – V1 and V2 (Danube watershed), the West Morava – Z1 and Z2 (Great Morava watershed), the South Morava – JM (Great Morava watershed), the Nišava – N1 and N2 (South Morava watershed), the Tamiš – Ta (Danube watershed), the DTD canal – DT (Danube watershed), the Topčiderska River – Tr (Sava watershed), the Porečka River – Pr (Danube watershed), the Kolubara – Ko (Sava watershed), the Pek – Pe (Danube watershed) and the Toplica – To (South Morava watershed). For the larger rivers, sampling was conducted at several locations (Figure 1). The sediment samples were stored at 4°C in order to prevent changes in the chemical composition of the sediments. The contents of the micro and macro-elements were determined in the granulometric fraction < 63 µm of the bottom sediment samples (“grab”- the sample) after air drying for 8 days (Sakan et al. 2011).

## 2.3. Analysis of Element Content

In this paper, the total content of elements in the sediments was determined by digestion with very strong acids: HNO<sub>3</sub>+HCl+HF. A 0.5 g sediment sample was placed in a Teflon vessel. Then 9 mL HCl (37%), 3 ml HNO<sub>3</sub> (70%) and 3 mL HF (48%) were added to the vessel. One Teflon vessel only contains the acid mixture for a blank. A microwave digestion system brings the sample to 165°C in 10 minutes (holding time 0 s), then 175°C in three minutes, where it was kept for 10 minutes (max power was 1200 W) (Rönkkömäki et al. 2008). Microwave digestion was performed in a pressurised microwave oven (Ethos 1, Advanced Microwave Digestion System, Milestone, Italy) equipped with a rotor holding 10 microwave vessels (PTFE).

After cooling the digestion system, 10 ml H<sub>3</sub>BO<sub>3</sub> (5g/100mL water) are added. Again, the microwave digestion system brings the sample to 175°C in 10 minutes at 1420W and holds the temperature at 170°C for three minutes. The digestate is then diluted to a final volume of 100 mL (Nam et al. 2001).

In this research, the following elements were determined in each sample: Cd, Co, Cr, Cu, Mn, Ni, Pb, V, Al and Zn. The results are expressed in mg kg<sup>-1</sup> dry sediment. The analytical determination of the studied elements was realised with an atomic emission spectrometer with an inductively coupled plasma iCAP-6500 Duo (Thermo Scientific, United Kingdom). The

Complimentary Contributor Copy

detector was a RACID86 Charge injector device (CID). Analytical grade chemicals were used throughout the study without any further purification. The metal standards were prepared from a stock solution of  $1,000 \text{ mg L}^{-1}$  by successive dilutions. The concentrations obtained for all the elements in the blanks were close to the detection limit of the method, indicating that contamination was not a problem in the digestion.

## 2.4. Quality Control

The accuracy and precision of the obtained results were checked by analyzing sediment reference material (BCR standards, 143R and 146R).

## 2.5. Quantification of Sediment Contamination

Various calculation methods for quantifying the degree of metal enriched in sediments have been put forward. In this paper, different indices were used to assess the degree of trace element contamination in river sediments in Serbia: Contamination factor (CF), Enrichment factor (EF), Index of geoaccumulation (Igeo), Ecological risk factor ( $Er^i$ ), Potential ecological risk index (RI), Pollution load index (PLI), and Combined pollution index (CPI).

### *Contamination Factor (CF)*

The contamination factor is calculated as the ratio between the metal content in the sediment at a given station and the normal concentration levels (background concentration), reflecting the metal enriched in the sediment:

$$CF = C_s/C_b.$$

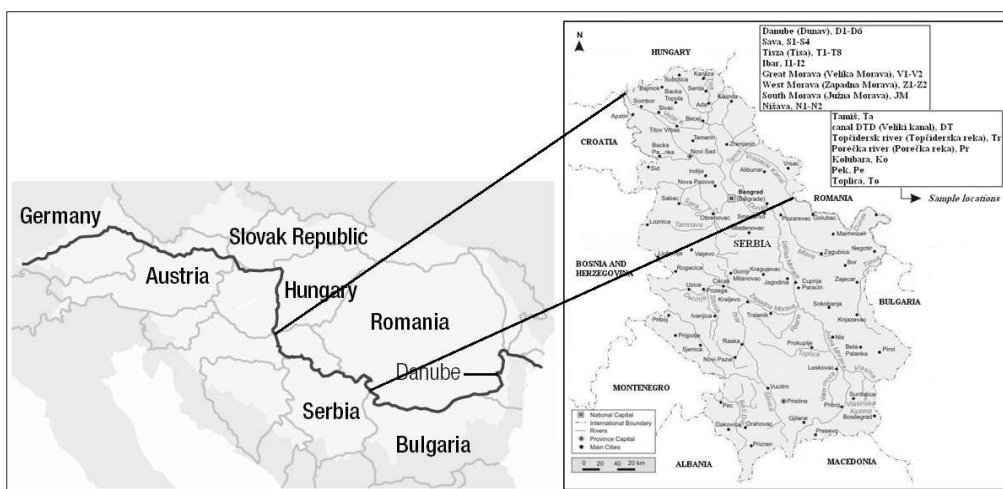


Figure 1. The Danube river basin and map of sampling locations.

CF classified into four groups in Pekey et al. (2004) and Hakanson (1980).

**Enrichment Factor (EF)**

A common approach to estimating how much the sediment is impacted (naturally and anthropogenically) with heavy metal is to calculate the Enrichment Factor (EF) for metal concentrations above the un-contaminated background levels. The EF of a heavy metal in sediment can be calculated using the following formula:

$$EF = (M/Y)_{\text{sample}} / (M/Y)_{\text{background}},$$

where M is the concentration of the potentially enriched element and Y is the concentration of the proxy element.

Although EF is not a function of time in its mathematical expression, it reflects the status and degree of sediment pollution (Ruzhong et al. 2010).

**Index of Geoaccumulation (Igeo)**

Index of geoaccumulation (Igeo), introduced by Müller (Müller, 1979), has been used widely to evaluate the degree of metal contamination or pollution in terrestrial, aquatic and marine environments.

The Igeo of an element in sediment can be calculated with the formula (Asaah and Abimbola, 2006; Mediola et al. 2008):

$$I_{\text{geo}} = \log_2 [C_{\text{metal}} / 1.5 C_{\text{metal (control)}}],$$

where  $C_{\text{metal}}$  is the concentration of the heavy metal in the enriched sample and  $C_{\text{metal (control)}}$  is the concentration of the metal in the unpolluted sample or control. The factor 1.5 is introduced to minimise the effect of the possible variations in the background or control values, which may be attributed to lithogenic variations in the sediment (Mediola et al. 2008).

**Ecological Risk Factor**

An ecological risk factor ( $Er^i$ ) to quantitatively express the potential ecological risk of a given contaminant also suggested by Hakanson (1980) is:

$$Er^i = Tr^i \cdot Cf^i,$$

where  $Tr^i$  is the toxic–response factor for a given substance (for Hg, Cd, As, Cr and Zn, they are 40, 30, 10, 2 and 1 respectively; and 5 for Pb, Cu and Ni (Yang et al. 2009), and  $Cf^i$  is the contamination factor.

**Ecological Risk Index**

The potential ecological risk index (RI) (Hakanson 1980; Yang et al. 2009) is defined as the summation of the change occurred in metals with respect to the background values considering the toxicological factor. The mathematical relation of RI can be shown as:

$$RI = \sum (T_i \times C_i/C_o),$$

where  $n$  is the number of heavy metals,  $T_i$  is the toxic–response factor for a given substance,  $C_i$  represents the metal content in the sediment and  $C_0$  is the regional background value of heavy metals.

### ***Pollution Load Index (PLI)***

Tomlinson et al. (1980) introduced the concept of the PLI to assess metal pollution in sediment. The PLI for a single site is the  $n$ th root of the number ( $n$ ) of multiple contamination factors (CF) multiplied together (Mohiuddin et al. 2012):

$$PLI = (CF_1 \times CF_2 \times CF_3 \times \dots \times CF_n)^{1/n}.$$

This empirical index provides a simple, comparative means for assessing the level of heavy metal pollution.

### ***Combined Pollution Index***

The combined pollution index (CPI) was used to evaluate the pollution level of heavy metal. There are two steps in this assessment process.

First step: the contamination coefficient of heavy metal is obtained by:

$$C_f^i = C^i / C_n^i.$$

Second step: the combined pollution index is obtained by:  $CPI = \sum C_f^i / m$ , where  $C_f^i$  is the contamination coefficient of heavy metal,  $C^i$  is the concentration of heavy metal in the sediment,  $C_n^i$  is the background values,  $m$  is number of heavy metals and CPI is the combined pollution index.

## **2.6. Statistical Analysis**

To better illustrate the changes in the metal contents in the sediments, it was used the box-plot method. A correlation matrix of pollution indices was performed to recognize relationships among the different contamination factors. The statistical analyses were conducted using SPSS 21.0.

## **3. RESULTS AND DISCUSSION**

### **3.1. The Accuracy Check**

The accuracy of analytical procedures applied were checked by the analysis of certified reference materials (BCR standards, 143R and 146R). The percentage recovery of each element was obtained as: [(measured concentration in  $\text{mg kg}^{-1}$ ) / mean certified value for CRM in  $\text{mg kg}^{-1}$ ]  $\times 100$ . The obtained results indicate a good agreement between the certified and analytical values. The recovery of elements being practically complete for most of them and the values were in the acceptable range (recovery: 80-120%) (Chang et al. 2009).

Complimentary Contributor Copy

The precision is expressed as relative standard deviations. The relative standard deviations of the means of duplicate measurement were less than 4% (from 0.03 to 3.80%) for all the measured elements.

### 3.2. Heavy Metals in River Sediments

The basic statistics for the Cd, Co, Cr, Cu, Mn, Ni, Pb, Zn, and V concentration measured at 35 stations are summarized in Table 1. In general, the heavy metal concentrations of the sediments were found to decrease in the sequence Mn > Zn > Cu > Pb > Ni > Cr > V > Co > Cd. Some of heavy metals showed significant spatial variations, suggesting a non uniform distribution of those heavy metals.

### 3.3. Discussion about Pollution Indices

Contamination of the investigated river sediments with the studied heavy metals was assessed using: CF, EF, Igeo, Er, RI, PLI, and CPI.

**Table 1. Mean and median of heavy metals content [ $\text{mg kg}^{-1}$ ] in studied sediments**

|          | Cd   | Co   | Cr   | Cu   | Mn   | Ni   | Pb   | V    | Zn   |
|----------|------|------|------|------|------|------|------|------|------|
| Mean     | 4.82 | 22.0 | 113  | 78.5 | 1399 | 77.8 | 132  | 111  | 353  |
| St. Dev. | 2.08 | 6.63 | 41.0 | 141  | 556  | 58.5 | 51.0 | 18.5 | 232  |
| Median   | 4.69 | 21.5 | 102  | 47.9 | 1352 | 46.3 | 124  | 112  | 330  |
| Minimum  | 1.28 | 8.22 | 59.8 | 11.5 | 648  | 33.2 | 57.8 | 60.4 | 66.6 |
| Maximum  | 10.5 | 36.2 | 230  | 870  | 3688 | 274  | 318  | 149  | 1095 |

**Table 2. Grades of Enrichment factor and Index of geoaccumulation**

| Enrichment factor (EF) |                    | Index of geoaccumulation (Igeo) |                                 |
|------------------------|--------------------|---------------------------------|---------------------------------|
| Value                  | Pollution category | Value                           | Pollution category              |
| EF < 1                 | No enrichment      | Igeo < 0                        | unpolluted (class 0)            |
| 1 ≤ EF ≤ 3             | Minor              | 0 ≤ Igeo < 1                    | unpolluted/moderately (class 1) |
| 3 ≤ EF ≤ 5             | Moderate           | 1 ≤ Igeo < 2                    | moderately (class 2)            |
| 5 ≤ EF ≤ 10            | Moderately severe  | 2 ≤ Igeo < 3                    | moderately/heavily (class 3)    |
| 10 ≤ EF ≤ 25           | Severe             | 3 ≤ Igeo < 4                    | heavily (class 4)               |
| 25 ≤ EF ≤ 50           | Very severe        | 4 ≤ Igeo < 5                    | heavily/extremely (class 5)     |
| EF > 50                | Extremely severe   | Igeo ≥ 5                        | extremely (class 6)             |

**Table 3. Grades of Ecological risk factor, Contamination factor, and Ecological risk index**

| Ecological risk factor ( <b>Er</b> ) |               | Contamination factor ( <b>CF</b> ) |                            | Ecological risk index ( <b>RI</b> ) |               |
|--------------------------------------|---------------|------------------------------------|----------------------------|-------------------------------------|---------------|
| Value                                | Risk category | Value                              | Pollution category         | Value                               | Risk category |
| $Er < 40$                            | Low           | $CF < 1$                           | No metal enrichment        | $RI < 150$                          | Low risk      |
| $40 \leq Er < 80$                    | Moderate      | $1 \leq CF \leq 3$                 | Moderately contamination   | $150 \leq RI < 300$                 | Moderate      |
| $80 \leq Er < 160$                   | Considerable  | $3 \leq CF \leq 6$                 | Considerable contamination | $300 \leq RI < 600$                 | Considerable  |
| $160 \leq Er < 320$                  | High          | $CF > 6$                           | Very high contamination    | $RI \geq 600$                       | Very high     |
| $Er \geq 320$                        | Very high     | / <sup>a</sup>                     | /                          | /                                   | /             |

<sup>a</sup> no data.

Tables 2 and 3 show the predicted severity of contamination determined by these indices and ecological risk based on the calculated factors. On the base of the pollution load index, contamination of sediment can be classified as pollution exists, when the PLI > 1, and no metal pollution, if the PLI < 1 (Varol 2011). When CPI < 1, the sediment is unpolluted; when the CPI ≥ 1, the sediment is contaminated by heavy metals (Jian-Min et al. 2007; Hui-na et al. 2012). In Tables 4-7 are shown values of CF, EF, Igeo, Er, RI, CPI and PLI in sediment samples. In Table 8 is shown results of statistical analysis of pollution indices. Figures 2-6 show a variation of calculated pollution indices using the Box plot. On the figures, open circle represents outlying points, while (\*) represents extreme points.

The values of PLI ranged from 1.4 to 4.27 and CPI values ranged from 1.65 to 10.02, indicating that the concentration levels of studied elements in most of the stations exceeded the background values. Values of RI ranged from 87.3 to 575, indicating ecological risk from low risk to considerable. Outlier and extreme values of PLI, RI and CPI (Figure 2) were observed at locations: 21 – Ibar and 33 – Pek (PLI); 20 – Ibar, 21 – Ibar and 33 – Pek (RI) and 20 – Ibar, 21 – Ibar, 25 – West Morava and 33 – Pek (CPI). Obtained results indicate that Ibar, Pek, and Great Morava are the rivers with high level of heavy metal pollution. The high value of RI for Ibar and Pek indicated ecological risk for the studied elements in investigated rivers. The results of risk index were synchronous with results of the degree of contamination.

**EF** In this paper, EF was calculated for each of studied heavy metal. The calculation of this factor was based on the background value determined for the studied area (Sakan et al. 2015b). The element content of elements in the DTD canal (station in Vrbas) was chosen as background values for elements in this research, due to the lack of significant anthropogenic sources of toxic elements at this area.

Background values of elements in this research are (in mg kg<sup>-1</sup>): 1.28 (Cd), 11.5 (Cu), 8.22 (Co), 648 (Mn), 62.1 (Cr), 34.7 (Ni), 57.8 (Pb), 66.6 (Zn), 60.4 (V) and 360323 (Al). The element used for sediment normalization is aluminum. This element was chosen because Al is a conservative element and a major constituent of clay minerals, and has been successfully used in previous investigations (Rubio et al. 2000).



**Table 4. CF values of elements in sediment samples**

| SL <sup>a</sup> | NS <sup>b</sup> | Cd   | Co   | Cr   | Cu   | Mn   | Ni   | Pb   | V    | Zn   |
|-----------------|-----------------|------|------|------|------|------|------|------|------|------|
| T1              | 1               | 3.95 | 1.22 | 0.96 | 4.16 | 1.97 | 1.13 | 1.66 | 1.44 | 4.95 |
| T2              | 2               | 3.30 | 2.50 | 1.66 | 5.60 | 1.90 | 1.33 | 2.04 | 2.17 | 5.03 |
| T3              | 3               | 3.88 | 2.58 | 1.54 | 6.45 | 2.04 | 1.30 | 2.15 | 2.03 | 5.87 |
| T4              | 4               | 3.45 | 2.33 | 1.45 | 5.55 | 2.16 | 1.13 | 2.15 | 1.80 | 5.07 |
| T5              | 5               | 4.98 | 2.75 | 1.70 | 7.68 | 2.66 | 1.37 | 1.94 | 2.01 | 5.39 |
| T6              | 6               | 5.38 | 2.59 | 1.61 | 7.87 | 3.25 | 1.22 | 2.45 | 2.17 | 6.30 |
| T7              | 7               | 4.87 | 2.41 | 1.49 | 6.43 | 2.89 | 1.23 | 1.56 | 1.90 | 5.20 |
| T8              | 8               | 4.76 | 2.35 | 1.44 | 6.18 | 2.60 | 1.20 | 2.06 | 1.89 | 5.06 |
| T9              | 9               | 5.47 | 2.62 | 1.55 | 7.57 | 2.80 | 1.33 | 2.42 | 2.04 | 6.17 |
| D1              | 10              | 1.76 | 1.97 | 1.18 | 2.44 | 2.14 | 0.96 | 1.56 | 1.58 | 2.53 |
| D2              | 11              | 1.66 | 1.98 | 1.21 | 2.07 | 1.60 | 1.04 | 1.97 | 1.76 | 2.36 |
| D3              | 12              | 1.95 | 2.04 | 1.29 | 2.73 | 1.51 | 1.03 | 1.79 | 1.78 | 3.12 |
| D4              | 13              | 1.84 | 1.87 | 1.22 | 2.51 | 1.38 | 1.01 | 2.27 | 1.58 | 3.30 |
| D5              | 14              | 2.17 | 2.31 | 1.26 | 3.54 | 2.09 | 1.09 | 1.39 | 1.62 | 3.31 |
| D6              | 15              | 4.15 | 2.61 | 1.98 | 3.64 | 1.83 | 2.04 | 2.35 | 1.86 | 3.43 |
| S1              | 16              | 2.70 | 2.64 | 1.80 | 2.78 | 1.58 | 2.70 | 1.54 | 1.45 | 4.06 |
| S2              | 17              | 2.36 | 3.47 | 2.47 | 3.17 | 2.71 | 3.63 | 1.99 | 1.78 | 3.20 |
| S3              | 18              | 2.92 | 3.21 | 2.26 | 3.16 | 2.56 | 3.42 | 1.95 | 1.72 | 4.07 |
| S4              | 19              | 3.66 | 3.32 | 2.33 | 2.73 | 2.81 | 3.43 | 1.90 | 1.86 | 3.19 |
| I1              | 20              | 8.23 | 1.65 | 1.65 | 2.52 | 1.39 | 4.10 | 5.51 | 1.19 | 14.2 |
| I2              | 21              | 6.50 | 4.40 | 3.71 | 3.43 | 2.09 | 7.89 | 4.55 | 1.67 | 16.4 |
| V1              | 22              | 6.18 | 3.92 | 2.74 | 5.70 | 2.68 | 1.23 | 3.15 | 2.14 | 7.49 |
| V2              | 23              | 5.33 | 3.37 | 2.46 | 4.61 | 1.89 | 4.50 | 3.14 | 1.82 | 6.74 |
| Z1              | 24              | 2.81 | 1.48 | 1.38 | 13.5 | 1.25 | 2.43 | 1.34 | 1.56 | 3.75 |
| Z2              | 25              | 5.86 | 3.87 | 3.57 | 4.57 | 1.59 | 6.81 | 3.69 | 1.82 | 9.90 |
| JM              | 26              | 3.03 | 2.85 | 1.70 | 4.17 | 5.69 | 1.59 | 2.60 | 2.04 | 3.57 |
| N1              | 27              | 2.07 | 1.98 | 1.39 | 7.39 | 1.13 | 1.03 | 2.39 | 1.84 | 6.16 |
| N2              | 28              | 4.32 | 1.97 | 1.14 | 1.92 | 1.19 | 1.00 | 1.46 | 1.67 | 1.71 |
| Ta              | 29              | 2.44 | 3.22 | 1.81 | 4.51 | 2.18 | 1.45 | 2.37 | 2.47 | 2.86 |
| Tr              | 30              | 3.05 | 3.39 | 2.59 | 3.55 | 1.89 | 3.82 | 2.50 | 2.13 | 5.06 |
| Pr              | 31              | 2.45 | 2.90 | 1.90 | 11.9 | 1.34 | 1.70 | 2.07 | 2.29 | 2.32 |
| Ko              | 32              | 4.26 | 3.49 | 2.36 | 3.42 | 2.09 | 3.81 | 2.17 | 1.89 | 6.26 |
| Pe              | 33              | 4.89 | 3.70 | 1.43 | 75.7 | 3.08 | 1.20 | 2.72 | 2.10 | 13.8 |
| To              | 34              | 4.09 | 3.58 | 2.39 | 4.83 | 2.60 | 3.31 | 2.33 | 2.27 | 2.50 |

<sup>a</sup> Sample labels.<sup>b</sup> Number of sample.

The results of the calculation of EF of metals in sediments are presented in Table 5 and Figure 3. The analysis demonstrate that values of EF were for: Cd: 0.68-8.18 (no enrichment to moderately severe); Co: 0.81-4.49 (no enrichment to moderate); Cr: 0.49-3.35 (no enrichment to moderate); Cu: 0.84-35.03 (no enrichment to very severe); Mn: 0.65-3.99 (no enrichment to moderate); Ni: 0.42-4.84 (no enrichment to moderate); Pb: 0.80-5.48 (no enrichment to moderately severe); V: 0.72-2.63 (no enrichment to minor) and Zn: 0.96-14.13 (no enrichment to severe). These results suggesting various degrees of metal enrichment in studied rivers. Outlier and extreme values were observed for: Cd, localities: 7 – Tisa, 20 –

Ibar and 22 – Great Morava; Co, 22 - Great Morava and 34 – Toplica; Cr, 22 – Great Morava; Cu, 7 – Tisa and 24 – West Morava; Mn, 14 – Danube, 22 – Great Morava and 7 - Tisa; Ni, 21 - Ibar; Pb, 22 – Great Morava and 20 – Ibar; V, 5 – Tisa, 34 – Toplica, 14 – Danube, 22 – Great Morava and 7 – Tisa; Zn, 7 – Tisa, 22 – Great Morava, 20 and 21 – Ibar.

*Er* The potential ecological risk factors for studied metals were estimated for all stations (Table 7, Figure 4).

**Table 5. EF values of elements in sediments**

| SL <sup>a</sup> | Cd   | Co   | Cr   | Cu    | Mn   | Ni   | Pb   | V    | Zn   |
|-----------------|------|------|------|-------|------|------|------|------|------|
| T1              | 2.64 | 0.82 | 0.64 | 2.78  | 1.32 | 0.76 | 1.11 | 0.97 | 3.31 |
| T2              | 1.88 | 1.42 | 0.94 | 3.18  | 1.08 | 0.76 | 1.16 | 1.24 | 2.86 |
| T3              | 1.94 | 1.29 | 0.77 | 3.21  | 1.02 | 0.65 | 1.07 | 1.01 | 2.93 |
| T4              | 1.65 | 1.12 | 0.70 | 2.66  | 1.04 | 0.54 | 1.03 | 0.87 | 2.43 |
| T5              | 4.60 | 2.54 | 1.57 | 7.09  | 2.45 | 1.27 | 1.79 | 1.86 | 4.98 |
| T6              | 2.88 | 1.38 | 0.86 | 4.21  | 1.74 | 0.65 | 1.31 | 1.16 | 3.37 |
| T7              | 6.72 | 3.32 | 2.06 | 8.88  | 3.99 | 1.70 | 2.16 | 2.63 | 7.18 |
| T8              | 2.41 | 1.19 | 0.73 | 3.13  | 1.31 | 0.61 | 1.05 | 0.96 | 2.56 |
| T9              | 2.37 | 1.14 | 0.67 | 3.28  | 1.22 | 0.58 | 1.05 | 0.89 | 2.68 |
| D1              | 1.44 | 1.62 | 0.97 | 2.00  | 1.75 | 0.78 | 1.28 | 1.30 | 2.07 |
| D2              | 0.68 | 0.81 | 0.49 | 0.84  | 0.65 | 0.42 | 0.80 | 0.72 | 0.96 |
| D3              | 1.29 | 1.35 | 0.85 | 1.80  | 1.00 | 0.68 | 1.19 | 1.18 | 2.07 |
| D4              | 1.07 | 1.09 | 0.72 | 1.47  | 0.81 | 0.59 | 1.33 | 0.92 | 1.93 |
| D5              | 3.36 | 3.57 | 1.95 | 5.47  | 3.23 | 1.69 | 2.15 | 2.51 | 5.12 |
| D6              | 2.79 | 1.76 | 1.33 | 2.45  | 1.23 | 1.37 | 1.58 | 1.26 | 2.30 |
| S1              | 2.21 | 2.16 | 1.47 | 2.28  | 1.30 | 2.21 | 1.26 | 1.19 | 3.32 |
| S2              | 1.48 | 2.17 | 1.55 | 1.98  | 1.70 | 2.28 | 1.25 | 1.12 | 2.01 |
| S3              | 1.84 | 2.02 | 1.42 | 1.99  | 1.61 | 2.15 | 1.23 | 1.09 | 2.56 |
| S4              | 2.43 | 2.20 | 1.55 | 1.81  | 1.86 | 2.28 | 1.26 | 1.24 | 2.12 |
| I1              | 8.18 | 1.64 | 1.64 | 2.51  | 1.39 | 4.08 | 5.48 | 1.19 | 14.1 |
| I2              | 3.99 | 2.70 | 2.28 | 2.10  | 1.28 | 4.84 | 2.79 | 1.03 | 10.1 |
| V1              | 7.54 | 4.79 | 3.35 | 6.96  | 3.27 | 1.50 | 3.85 | 2.61 | 9.15 |
| V2              | 3.16 | 2.00 | 1.46 | 2.73  | 1.12 | 2.67 | 1.86 | 1.08 | 4.00 |
| Z1              | 2.16 | 1.14 | 1.06 | 10.4  | 0.96 | 1.86 | 1.03 | 1.20 | 2.88 |
| Z2              | 3.71 | 2.45 | 2.26 | 2.89  | 1.01 | 4.31 | 2.34 | 1.15 | 6.27 |
| JM              | 1.49 | 1.40 | 0.83 | 2.04  | 2.79 | 0.78 | 1.27 | 1.01 | 1.75 |
| N1              | 1.27 | 1.21 | 0.85 | 4.53  | 0.69 | 0.63 | 1.46 | 1.13 | 3.77 |
| N2              | 3.66 | 1.67 | 0.97 | 1.63  | 1.01 | 0.85 | 1.24 | 1.42 | 1.45 |
| Ta              | 0.92 | 1.22 | 0.69 | 1.71  | 0.83 | 0.55 | 0.90 | 0.94 | 1.08 |
| Tr              | 2.12 | 2.35 | 1.80 | 2.46  | 1.31 | 2.65 | 1.73 | 1.48 | 3.51 |
| Pr              | 1.22 | 1.45 | 0.95 | 5.94  | 0.67 | 0.85 | 1.03 | 1.14 | 1.16 |
| Ko              | 2.50 | 2.05 | 1.38 | 2.01  | 1.22 | 2.23 | 1.27 | 1.11 | 3.67 |
| Pe              | 2.26 | 1.72 | 0.66 | 35.03 | 1.43 | 0.56 | 1.26 | 0.97 | 6.40 |
| To              | 4.30 | 3.78 | 2.51 | 5.09  | 2.74 | 3.49 | 2.46 | 2.39 | 2.63 |

<sup>a</sup> Sample labels.

**Table 6. Index of geoaccumulation ( $I_{geo}$ ) values of elements in sediments**

| SL <sup>a</sup> | Cd   | Co   | Cr   | Cu   | Mn   | Ni   | Pb   | V    | Zn   |
|-----------------|------|------|------|------|------|------|------|------|------|
| T1              | 0.97 | < 0  | < 0  | 1.02 | 0.27 | < 0  | 0.10 | < 0  | 1.19 |
| T2              | 0.79 | 0.51 | < 0  | 1.32 | 0.24 | < 0  | 0.31 | 0.37 | 1.21 |
| T3              | 0.95 | 0.54 | < 0  | 1.46 | 0.31 | < 0  | 0.36 | 0.30 | 1.36 |
| T4              | 0.83 | 0.44 | < 0  | 1.31 | 0.36 | < 0  | 0.36 | 0.18 | 1.22 |
| T5              | 1.20 | 0.61 | < 0  | 1.63 | 0.57 | < 0  | 0.26 | 0.29 | 1.28 |
| T6              | 1.28 | 0.54 | < 0  | 1.66 | 0.77 | < 0  | 0.49 | 0.37 | 1.43 |
| T7              | 1.18 | 0.47 | < 0  | 1.46 | 0.65 | < 0  | 0.04 | 0.24 | 1.24 |
| T8              | 1.15 | 0.45 | < 0  | 1.42 | 0.55 | < 0  | 0.32 | 0.23 | 1.22 |
| T9              | 1.29 | 0.56 | < 0  | 1.62 | 0.63 | < 0  | 0.48 | 0.31 | 1.41 |
| D1              | 0.16 | 0.27 | < 0  | 0.49 | 0.36 | < 0  | 0.04 | 0.05 | 0.52 |
| D2              | 0.10 | 0.28 | < 0  | 0.32 | 0.06 | < 0  | 0.27 | 0.16 | 0.45 |
| D3              | 0.26 | 0.31 | < 0  | 0.60 | 0.01 | < 0  | 0.18 | 0.17 | 0.73 |
| D4              | 0.20 | 0.22 | < 0  | 0.52 | < 0  | < 0  | 0.42 | 0.05 | 0.79 |
| D5              | 0.37 | 0.43 | < 0  | 0.86 | 0.33 | < 0  | < 0  | 0.07 | 0.79 |
| D6              | 1.02 | 0.55 | < 0  | 0.89 | 0.20 | 0.31 | 0.45 | 0.22 | 0.83 |
| S1              | 0.59 | 0.57 | < 0  | 0.62 | 0.05 | 0.59 | 0.03 | < 0  | 0.99 |
| S2              | 0.45 | 0.84 | < 0  | 0.75 | 0.59 | 0.88 | 0.28 | 0.17 | 0.76 |
| S3              | 0.67 | 0.76 | < 0  | 0.75 | 0.54 | 0.82 | 0.26 | 0.14 | 1.00 |
| S4              | 0.89 | 0.79 | < 0  | 0.60 | 0.63 | 0.83 | 0.24 | 0.22 | 0.75 |
| I1              | 1.70 | 0.10 | < 0  | 0.52 | < 0  | 1.01 | 1.30 | < 0  | 2.25 |
| I2              | 1.47 | 1.08 | 0.20 | 0.83 | 0.33 | 1.66 | 1.11 | 0.11 | 2.39 |
| V1              | 1.42 | 0.96 | < 0  | 1.34 | 0.58 | < 0  | 0.74 | 0.35 | 1.61 |
| V2              | 1.27 | 0.81 | < 0  | 1.12 | 0.23 | 1.10 | 0.74 | 0.19 | 1.50 |
| Z1              | 0.63 | < 0  | < 0  | 2.20 | < 0  | 0.48 | < 0  | 0.04 | 0.92 |
| Z2              | 1.36 | 0.95 | 0.16 | 1.11 | 0.06 | 1.51 | 0.90 | 0.19 | 1.89 |
| JM              | 0.70 | 0.64 | < 0  | 1.02 | 1.33 | 0.06 | 0.55 | 0.31 | 0.87 |
| N1              | 0.32 | 0.28 | < 0  | 1.60 | < 0  | < 0  | 0.46 | 0.21 | 1.41 |
| N2              | 1.06 | 0.27 | < 0  | 0.25 | < 0  | < 0  | < 0  | 0.11 | 0.13 |
| Ta              | 0.49 | 0.77 | < 0  | 1.10 | 0.37 | < 0  | 0.46 | 0.50 | 0.65 |
| Tr              | 0.71 | 0.82 | < 0  | 0.86 | 0.23 | 0.94 | 0.51 | 0.35 | 1.22 |
| Pr              | 0.49 | 0.66 | < 0  | 2.07 | < 0  | 0.13 | 0.32 | 0.42 | 0.44 |
| Ko              | 1.04 | 0.85 | < 0  | 0.83 | 0.33 | 0.93 | 0.37 | 0.23 | 1.43 |
| Pe              | 1.18 | 0.90 | < 0  | 3.92 | 0.72 | < 0  | 0.59 | 0.34 | 2.22 |
| To              | 1.00 | 0.87 | < 0  | 1.17 | 0.55 | 0.79 | 0.44 | 0.41 | 0.51 |

<sup>a</sup> Sample labels.

The values of  $I_{geo}$  were for: Cd: 49.80-247 (moderate to high); Cr: 1.92-7.42 (low); Cu: 9.60-378 (low to very high); Ni: 4.80-39.45 (low to moderate); Pb: 6.70-27.55 (low); and Zn: 0.96-14.13 (low risk). Outlier and extreme values were observed for: Cu, localities: 31 – Porečka river, 24 – West Morava, and 33 – Pek; Ni, 21 – Ibar; Pb, 20 and 21 – Ibar, and 25 – West Morava; Zn, 21 – Ibar and 33 – Pek.

$I_{geo}$  The  $I_{geo}$  values for selected metals at each sampling site are listed in Table 6 and Figure 5.

Complimentary Contributor Copy

**Table 7. Er (for Cd, Cr, Cu, Ni, Pb, and Zn), RI, CPI and PLI values of elements in sediments**

| SL <sup>a</sup> | Cd   | Cr   | Cu   | Ni   | Pb   | Zn    | RI   | CPI   | PLI  |
|-----------------|------|------|------|------|------|-------|------|-------|------|
| T1              | 118  | 1.92 | 20.8 | 5.65 | 8.30 | 4.95  | 190  | 2.34  | 2.00 |
| T2              | 99   | 3.32 | 28   | 6.65 | 10.2 | 5.03  | 156  | 2.54  | 2.11 |
| T3              | 116  | 3.08 | 32.2 | 6.5  | 108  | 5.87  | 187  | 2.82  | 2.41 |
| T4              | 104  | 2.9  | 27.8 | 5.65 | 10.8 | 5.07  | 163  | 2.50  | 2.12 |
| T5              | 149  | 3.4  | 38.4 | 6.85 | 9.70 | 5.39  | 217  | 2.98  | 2.30 |
| T6              | 161  | 3.22 | 39.4 | 6.10 | 12.2 | 6.3   | 237  | 3.25  | 2.62 |
| T7              | 146  | 2.98 | 32.2 | 6.15 | 7.80 | 5.2   | 205  | 2.75  | 2.17 |
| T8              | 143  | 2.88 | 30.9 | 6.00 | 10.3 | 5.06  | 205  | 2.73  | 2.27 |
| T9              | 164  | 3.1  | 37.8 | 6.65 | 12.1 | 6.17  | 243  | 3.20  | 2.67 |
| D1              | 52.8 | 2.36 | 12.2 | 4.80 | 7.80 | 2.53  | 87.3 | 1.66  | 1.52 |
| D2              | 49.8 | 2.42 | 10.4 | 5.20 | 9.85 | 2.36  | 114  | 1.88  | 1.79 |
| D3              | 58.5 | 2.58 | 13.6 | 5.15 | 8.95 | 3.12  | 97   | 1.76  | 1.60 |
| D4              | 55.2 | 2.44 | 12.6 | 5.05 | 11.4 | 3.3   | 94   | 1.72  | 1.52 |
| D5              | 65.1 | 2.52 | 17.7 | 5.45 | 6.95 | 3.31  | 104  | 1.88  | 1.59 |
| D6              | 124  | 3.96 | 18.2 | 10.2 | 11.8 | 3.43  | 179  | 2.40  | 2.18 |
| S1              | 81   | 3.6  | 13.9 | 13.5 | 7.70 | 4.06  | 128  | 2.11  | 1.86 |
| S2              | 70.8 | 4.94 | 15.8 | 18.2 | 9.95 | 3.2   | 128  | 2.47  | 2.24 |
| S3              | 87.6 | 4.52 | 15.8 | 17.1 | 9.75 | 4.07  | 143  | 2.50  | 2.22 |
| S4              | 110  | 4.66 | 13.6 | 17.2 | 9.50 | 3.19  | 164  | 2.52  | 2.29 |
| I1              | 247  | 3.3  | 12.6 | 20.5 | 27.6 | 14.21 | 406  | 4.55  | 3.20 |
| I2              | 195  | 7.42 | 17.2 | 39.4 | 22.8 | 16.43 | 358  | 5.33  | 4.27 |
| V1              | 185  | 5.48 | 28.5 | 6.15 | 15.8 | 7.49  | 256  | 3.47  | 2.86 |
| V2              | 160  | 4.92 | 23.0 | 22.5 | 15.7 | 6.74  | 247  | 3.38  | 3.33 |
| Z1              | 84.3 | 2.76 | 67.6 | 12.2 | 6.70 | 3.75  | 197  | 2.99  | 2.17 |
| Z2              | 176  | 7.14 | 22.8 | 34.0 | 18.4 | 9.9   | 287  | 4.13  | 3.49 |
| JM              | 90.9 | 3.4  | 20.8 | 7.95 | 13.0 | 3.57  | 150  | 2.75  | 2.48 |
| N1              | 62.1 | 2.78 | 37.0 | 5.15 | 12.0 | 6.16  | 129  | 2.49  | 1.86 |
| N2              | 130  | 2.28 | 9.6  | 5.00 | 7.30 | 1.71  | 159  | 1.65  | 1.40 |
| Ta              | 73.2 | 3.62 | 22.6 | 7.25 | 11.8 | 2.86  | 132  | 2.45  | 2.29 |
| Tr              | 91.5 | 5.18 | 17.8 | 19.1 | 12.5 | 5.06  | 158  | 2.80  | 2.54 |
| Pr              | 73.5 | 3.8  | 59.5 | 8.50 | 10.4 | 2.32  | 167  | 2.90  | 2.25 |
| Ko              | 128  | 4.72 | 17.1 | 19.0 | 10.8 | 6.26  | 196  | 2.97  | 2.67 |
| Pe              | 147  | 2.86 | 378  | 6.00 | 13.6 | 13.83 | 575  | 10.18 | 3.66 |
| To              | 123  | 4.78 | 24.2 | 16.6 | 11.6 | 2.5   | 188  | 2.78  | 2.49 |

<sup>a</sup> Sample labels.

The results of the geo-accumulation index showed that values for studied elements in sediments were for: Cd: 0.10-1.70 (uncontaminated to moderately); Co: < 0-1.08 (no enrichment to moderately); Cr: < 0-0.90 (uncontaminated to unpolluted/moderately); Cu: 0.25-3.92 (unpolluted/moderately to heavily); Mn: < 0-1.33 (uncontaminated to moderately); Ni: < 0-1.66 (uncontaminated to moderately); Pb: < 0-1.30 (uncontaminated to moderately);

Complimentary Contributor Copy

V: < 0-0.50 (uncontaminated to unpolluted/moderately) and Zn: 0.13-2.39 (uncontaminated to moderately/heavily).

**Table 8. Statistical analysis of pollution indices**

|                    | Mean | St. Dev. | Min   | Max  | Median |
|--------------------|------|----------|-------|------|--------|
| Cd <sub>EF</sub>   | 2.77 | 1.78     | 0.68  | 8.18 | 2.32   |
| Co <sub>EF</sub>   | 1.90 | 0.90     | 0.81  | 4.79 | 1.66   |
| Cr <sub>EF</sub>   | 1.29 | 0.65     | 0.49  | 3.35 | 1.01   |
| Cu <sub>EF</sub>   | 4.37 | 5.84     | 0.84  | 35.0 | 2.70   |
| Mn <sub>EF</sub>   | 1.53 | 0.82     | 0.65  | 3.99 | 1.29   |
| Ni <sub>EF</sub>   | 1.58 | 1.20     | 0.42  | 4.84 | 1.06   |
| Pb <sub>EF</sub>   | 1.62 | 0.93     | 0.80  | 5.48 | 1.26   |
| V <sub>EF</sub>    | 1.29 | 0.50     | 0.72  | 2.63 | 1.15   |
| Zn <sub>EF</sub>   | 3.78 | 2.82     | 0.96  | 14.1 | 2.87   |
| Cd <sub>ER</sub>   | 115  | 47.2     | 49.8  | 247  | 113    |
| Co <sub>ER</sub>   | nd*  | nd       | nd    | nd   | nd     |
| Cr <sub>ER</sub>   | 3.68 | 1.31     | 1.92  | 7.42 | 3.31   |
| Cu <sub>ER</sub>   | 35.0 | 62.1     | 9.60  | 378  | 21.7   |
| Mn <sub>ER</sub>   | nd   | nd       | nd    | nd   | nd     |
| Ni <sub>ER</sub>   | 11.4 | 8.49     | 4.80  | 39.4 | 6.75   |
| Pb <sub>ER</sub>   | 11.6 | 4.33     | 6.70  | 27.6 | 10.8   |
| V <sub>ER</sub>    | nd   | nd       | nd    | nd   | nd     |
| Zn <sub>ER</sub>   | 5.42 | 3.45     | 1.71  | 16.4 | 4.99   |
| Cd <sub>Igeo</sub> | 0.85 | 0.42     | 0.10  | 1.70 | 0.92   |
| Co <sub>Igeo</sub> | 0.55 | 0.30     | -0.21 | 1.08 | 0.56   |
| Cr <sub>Igeo</sub> | 0.15 | 0.32     | -0.44 | 0.90 | 0.10   |
| Cu <sub>Igeo</sub> | 1.15 | 0.68     | 0.25  | 3.92 | 1.06   |
| Mn <sub>Igeo</sub> | 0.32 | 0.34     | -0.28 | 1.33 | 0.33   |
| Ni <sub>Igeo</sub> | 0.21 | 0.61     | -0.45 | 1.66 | -0.10  |
| Pb <sub>Igeo</sub> | 0.39 | 0.31     | -0.12 | 1.30 | 0.36   |
| V <sub>Igeo</sub>  | 0.21 | 0.15     | -0.23 | 0.50 | 0.22   |
| Zn <sub>Igeo</sub> | 1.14 | 0.53     | 0.13  | 2.39 | 1.20   |
| Cd <sub>CF</sub>   | 3.84 | 1.57     | 1.66  | 8.23 | 3.77   |
| Co <sub>CF</sub>   | 2.72 | 0.76     | 1.22  | 4.40 | 2.62   |
| Cr <sub>CF</sub>   | 1.84 | 0.65     | 0.96  | 3.71 | 1.66   |
| Cu <sub>CF</sub>   | 7.00 | 12.4     | 1.92  | 75.7 | 4.34   |
| Mn <sub>CF</sub>   | 2.19 | 0.85     | 1.13  | 5.69 | 2.09   |
| Ni <sub>CF</sub>   | 2.28 | 1.70     | 0.96  | 7.89 | 1.35   |
| Pb <sub>CF</sub>   | 2.33 | 0.86     | 1.34  | 5.51 | 2.15   |
| V <sub>CF</sub>    | 1.86 | 0.27     | 1.19  | 2.47 | 1.85   |
| Zn <sub>CF</sub>   | 5.42 | 3.45     | 1.71  | 16.4 | 4.99   |
| PLI                | 2.37 | 0.64     | 1.40  | 4.27 | 2.26   |
| RI                 | 196  | 97.0     | 87.3  | 575  | 173    |
| CPI                | 2.96 | 1.50     | 1.65  | 10.2 | 2.74   |

nd\* - no data.

Complimentary Contributor Copy

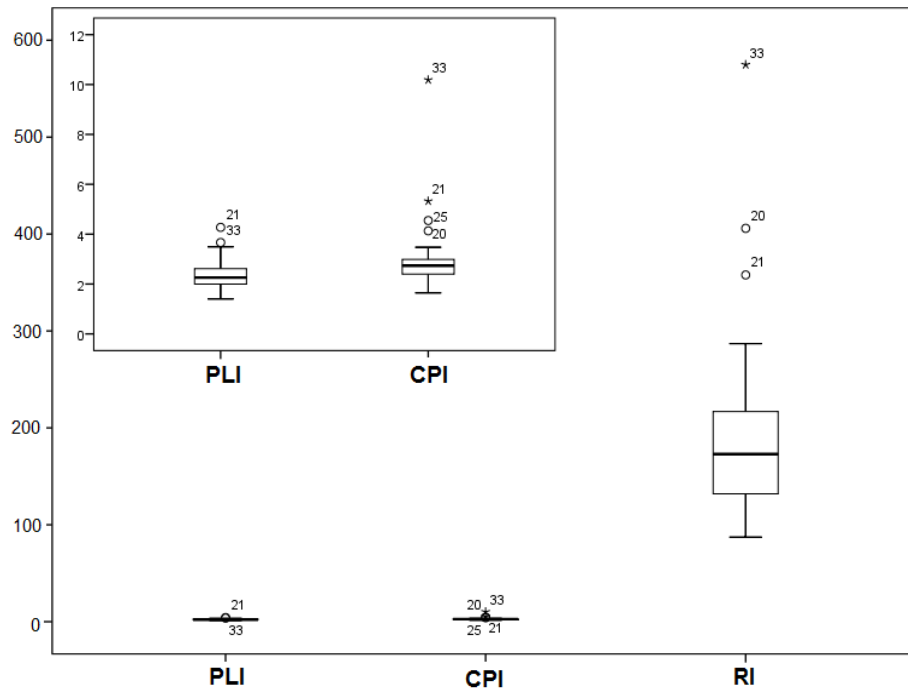


Figure 2. Box-plot for PLI, CPI and RI in sediments.

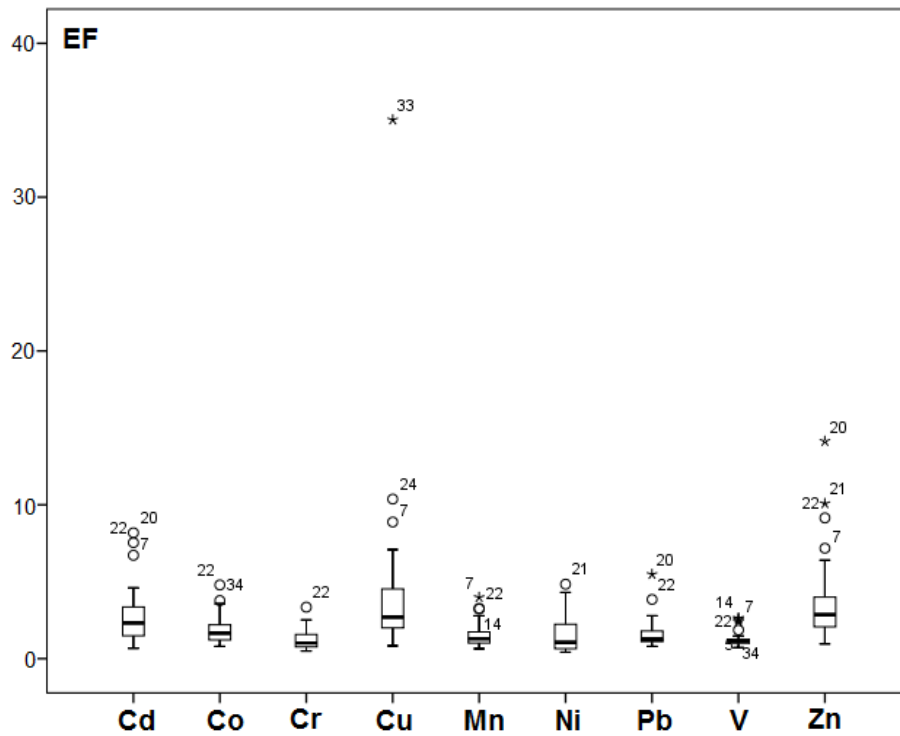


Figure 3. Box-plot of EF in sediments.

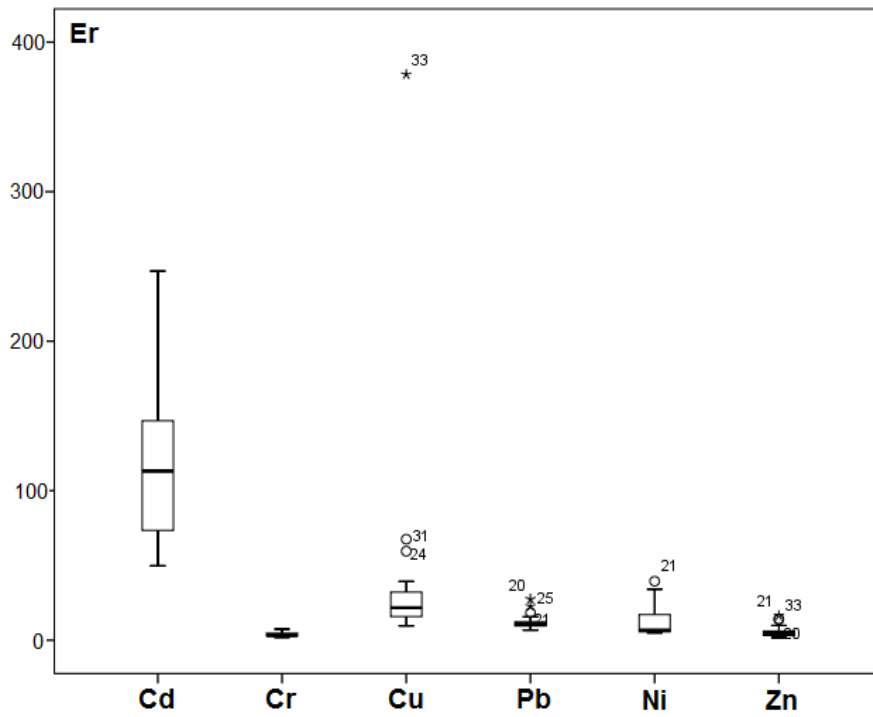


Figure 4. Box-plot of Er in sediments.

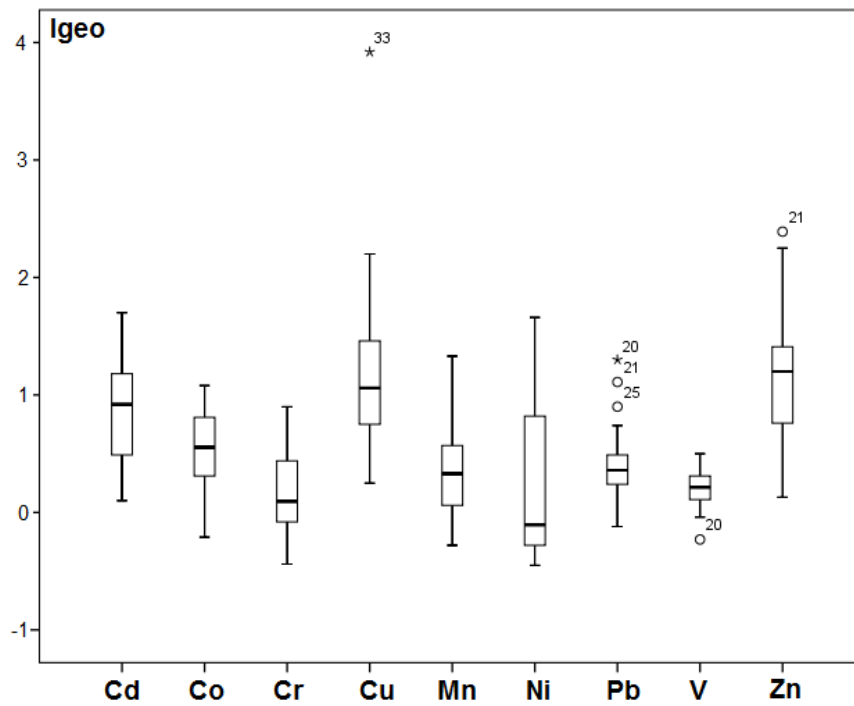


Figure 5. Box-plot of Igeo in sediments.

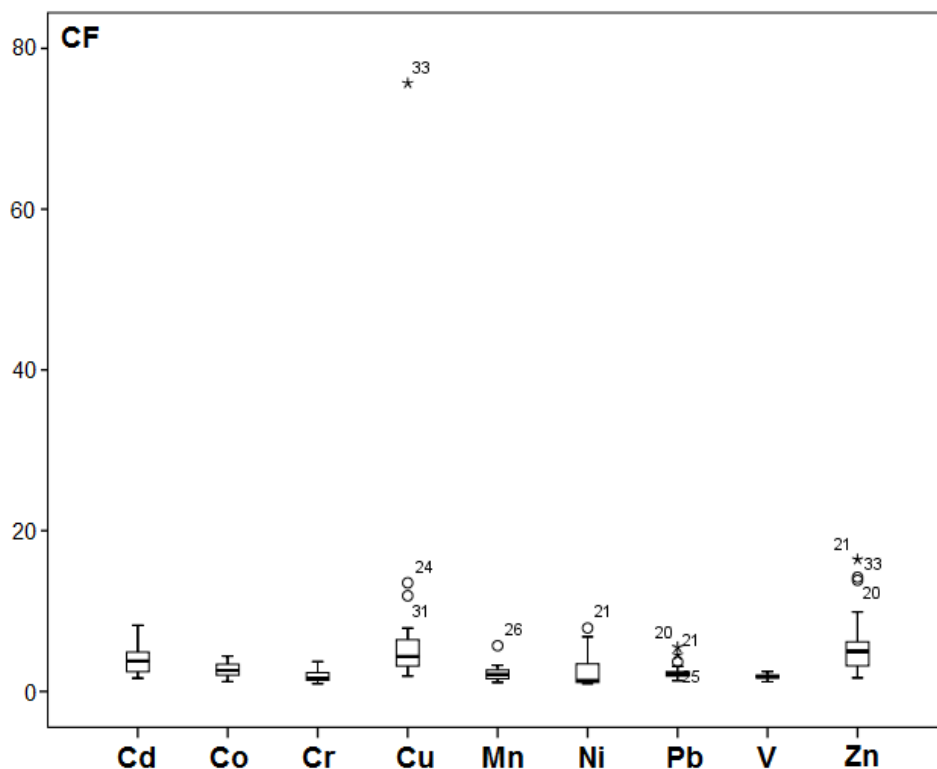


Figure 6. Box-plot of CF in sediments.

These results indicate that the sediments were contaminated with studied element, mainly with Cd, Cu and Zn.

Outlier and extreme values were observed for: Cu, localities: 33 - Pek; Pb, 25 - West Morava, 20 and 21 - Ibar; V, 20 - Ibar; and Zn, 21 - Ibar.

**CF** The results of the analysis of the contamination factor for the studied metals were shown in Table 4 and Figure 6. The values of CF demonstrated for: Cd: 1.66-8.23 (no enrichment to moderately severe); Co: 1.22-4.40 (moderately to considerable contamination); Cr: 0.96-3.71 (no metal enrichment to considerable contamination); Cu: 1.92-75.7 (moderately to very high contamination); Mn: 1.13-5.69 (moderately to considerable contamination); Ni: 0.96-7.89 (no enrichment to very high contamination); Pb: 1.34-5.51 (moderately to considerable contamination); V: 1.19-2.47 (moderately contamination) and Zn: 1.71-16.43 (moderately to very high contamination).

Outlier and extreme values were observed for: Cu, 24 - West Morava, 31 - Porečka river, and 33 - Pek; Mn, 26 - South Morava; Ni, 21 - Ibar; Pb, 20 and 21 - Ibar; and Zn, 20 and 21 - Ibar, and 33 - Pek.

### 3.4. Correlations

Pearson's correlation analysis was applied to test the relationships among the pollution indices.

Complimentary Contributor Copy



**Table 9. Tables with correlations among pollution indices (Cd, Cr, Cu, and Ni)**

|                    |   |         |         |         |                  |                  |                    |                  |
|--------------------|---|---------|---------|---------|------------------|------------------|--------------------|------------------|
|                    |   | PLI     | RI      | CPI     | Cd <sub>EF</sub> | Cd <sub>Er</sub> | Cd <sub>Igeo</sub> | Cd <sub>CF</sub> |
| PLI                | r | 1       |         |         |                  |                  |                    |                  |
|                    | p |         |         |         |                  |                  |                    |                  |
| RI                 | r | 0.823** | 1       |         |                  |                  |                    |                  |
|                    | p | 0.000   |         |         |                  |                  |                    |                  |
| CPI                | r | 0.772** | 0.941** | 1       |                  |                  |                    |                  |
|                    | p | 0.000   | 0.000   |         |                  |                  |                    |                  |
| Cd <sub>EF</sub>   | r | 0.390*  | 0.479** | 0.242   | 1                |                  |                    |                  |
|                    | p | 0.022   | 0.004   | 0.167   |                  |                  |                    |                  |
| Cd <sub>Er</sub>   | r | 0.744** | 0.762** | 0.523** | 0.784**          | 1                |                    |                  |
|                    | p | 0.000   | 0.000   | 0.002   | 0.000            |                  |                    |                  |
| Cd <sub>Igeo</sub> | r | 0.730** | 0.738** | 0.515** | 0.733**          | 0.976**          | 1                  |                  |
|                    | p | 0.000   | 0.000   | 0.002   | 0.000            | 0.000            |                    |                  |
| Cd <sub>CF</sub>   | r | 0.744** | 0.762** | 0.523** | 0.784**          | 1.000**          | 0.976**            | 1                |
|                    | p | 0.000   | 0.000   | 0.002   | 0.000            | 0.000            | 0.000              |                  |
|                    |   | PLI     | RI      | CPI     | Cr <sub>EF</sub> | Cr <sub>Er</sub> | Cr <sub>Igeo</sub> | Cr <sub>CF</sub> |
| Cr <sub>EF</sub>   | r | 0.390** | 0.189   | 0.101   | 1                |                  |                    |                  |
|                    | p | 0.023   | 0.284   | 0.570   |                  |                  |                    |                  |
| Cr <sub>Er</sub>   | r | 0.703** | 0.282   | 0.264   | 0.697**          | 1                |                    |                  |
|                    | p | 0.000   | 0.106   | 0.131   | 0.000            |                  |                    |                  |
| Cr <sub>Igeo</sub> | r | 0.681** | 0.260   | 0.251   | 0.687**          | 0.982**          | 1                  |                  |
|                    | p | 0.000   | 0.137   | 0.152   | 0.000            | 0.000            |                    |                  |
| Cr <sub>CF</sub>   | r | 0.703** | 0.282   | 0.264   | 0.697**          | 1.000**          | 0.982**            | 1                |
|                    | p | 0.000   | 0.106   | 0.131   | 0.000            | 0.000            | 0.000              |                  |
|                    |   | PLI     | RI      | CPI     | Cu <sub>EF</sub> | Cu <sub>Er</sub> | Cu <sub>Igeo</sub> | Cu <sub>CF</sub> |
| Cu <sub>EF</sub>   | r | 0.338   | 0.688** | 0.822** | 1                |                  |                    |                  |
|                    | p | 0.050   | 0.000   | 0.000   |                  |                  |                    |                  |
| Cu <sub>Er</sub>   | r | 0.367*  | 0.699** | 0.856** | 0.967**          | 1                |                    |                  |
|                    | p | 0.033   | 0.000   | 0.000   | 0.000            |                  |                    |                  |
| Cu <sub>Igeo</sub> | r | 0.378*  | 0.599** | 0.715** | 0.860**          | 0.842**          | 1                  |                  |
|                    | p | 0.027   | 0.000   | 0.000   | 0.000            | 0.000            |                    |                  |
| Cu <sub>CF</sub>   | r | 0.367*  | 0.699** | 0.856** | 0.967**          | 1.000**          | 0.842**            | 1                |
|                    | p | 0.033   | 0.000   | 0.000   | 0.000            | 0.000            | 0.000              |                  |
|                    |   | PLI     | RI      | CPI     | Ni <sub>EF</sub> | Ni <sub>Er</sub> | Ni <sub>Igeo</sub> | Ni <sub>CF</sub> |
| Ni <sub>EF</sub>   | r | 0.609** | 0.346*  | 0.234   | 1                |                  |                    |                  |
|                    | p | 0.000   | 0.045   | 0.184   |                  |                  |                    |                  |
| Ni <sub>Er</sub>   | r | 0.700** | 0.344*  | 0.282   | 0.922**          | 1                |                    |                  |
|                    | p | 0.000   | 0.046   | 0.106   | 0.000            |                  |                    |                  |
| Ni <sub>Igeo</sub> | r | 0.647** | 0.298   | 0.240   | 0.908**          | 0.959**          | 1                  |                  |
|                    | p | 0.000   | 0.086   | 0.172   | 0.000            | 0.000            |                    |                  |
| Ni <sub>CF</sub>   | r | 0.700** | 0.344*  | 0.282   | 0.922**          | 1.000**          | 0.959**            | 1                |
|                    | p | 0.000   | 0.046   | 0.106   | 0.000            | 0.000            | 0.000              |                  |

\*\* Correlation is significant at the 0.01 level; \* Correlation is significant at the 0.05 level.

Complimentary Contributor Copy

**Table 10. Tables with correlations among pollution indices (Pb, Zn)**

|                    |   | PLI     | RI      | CPI     | PbEF    | PbEr    | PbIgeo  | PbCF |
|--------------------|---|---------|---------|---------|---------|---------|---------|------|
| Pb <sub>EF</sub>   | r | 0.466** | 0.467** | 0.270   | 1       |         |         |      |
|                    | p | 0.005   | 0.005   | 0.122   |         |         |         |      |
| Pb <sub>Er</sub>   | r | 0.782** | 0.645** | 0.507** | 0.757** | 1       |         |      |
|                    | p | 0.000   | 0.000   | 0.002   | 0.000   |         |         |      |
| Pb <sub>Igeo</sub> | r | 0.806** | 0.623** | 0.521** | 0.654** | 0.973** | 1       |      |
|                    | p | 0.000   | 0.000   | 0.002   | 0.000   | 0.000   |         |      |
| Pb <sub>CF</sub>   | r | 0.782** | 0.645** | 0.507** | 0.757** | 1.000** | 0.973** | 1    |
|                    | p | 0.000   | 0.000   | 0.002   | 0.000   | 0.000   | 0.000   |      |
|                    |   | PLI     | RI      | CPI     | ZnEF    | ZnEr    | ZnIgeo  | ZnCF |
| Zn <sub>EF</sub>   | r | 0.631** | 0.687** | 0.526** | 1       |         |         |      |
|                    | p | 0.000   | 0.000   | 0.001   |         |         |         |      |
| Zn <sub>Er</sub>   | r | 0.851** | 0.868** | 0.868** | 0.833** | 1       |         |      |
|                    | p | 0.000   | 0.000   | 0.000   | 0.000   |         |         |      |
| Zn <sub>Igeo</sub> | r | 0.822** | 0.802** | 0.802** | 0.792** | 0.947** | 1       |      |
|                    | p | 0.000   | 0.000   | 0.000   | 0.000   | 0.000   |         |      |
| Zn <sub>CF</sub>   | r | 0.851** | 0.868** | 0.868** | 0.833** | 1.000** | 0.947** | 1    |
|                    | p | 0.000   | 0.000   | 0.000   | 0.000   | 0.000   | 0.000   |      |

**Table 11. Tables with correlations among pollution indices (Co, Mn, and V)**

|                    |   | PLI     | RI     | CPI     | Co <sub>EF</sub> | Co <sub>Igeo</sub> | Co <sub>CF</sub> |
|--------------------|---|---------|--------|---------|------------------|--------------------|------------------|
| Co <sub>EF</sub>   | r | 0.258   | 0.142  | 0.108   | 1                |                    |                  |
|                    | p | 0.141   | 0.422  | 0.543   |                  |                    |                  |
| Co <sub>Igeo</sub> | r | 0.611** | 0.297  | 0.394*  | 0.543**          | 1                  |                  |
|                    | p | 0.000   | 0.088  | 0.021   | 0.001            |                    |                  |
| Co <sub>CF</sub>   | r | 0.683** | 0.365* | 0.451** | 0.563**          | 0.985**            | 1                |
|                    | p | 0.000   | 0.034  | 0.007   | 0.001            | 0.000              |                  |
|                    |   | PLI     | RI     | CPI     | Mn <sub>EF</sub> | Mn <sub>Igeo</sub> | Mn <sub>CF</sub> |
| Mn <sub>EF</sub>   | r | 0.021   | 0.037  | 0.005   | 1                |                    |                  |
|                    | p | 0.906   | 0.834  | 0.980   |                  |                    |                  |
| Mn <sub>Igeo</sub> | r | 0.272   | 0.181  | 0.238   | 0.615**          | 1                  |                  |
|                    | p | 0.119   | 0.304  | 0.176   | 0.000            |                    |                  |
| Mn <sub>CF</sub>   | r | 0.223   | 0.142  | 0.205   | 0.582**          | 0.960**            | 1                |
|                    | p | 0.205   | 0.423  | 0.244   | 0.000            | 0.000              |                  |
|                    |   | PLI     | RI     | CPI     | V <sub>EF</sub>  | V <sub>Igeo</sub>  | V <sub>CF</sub>  |
| V <sub>EF</sub>    | r | -0.085  | -0.041 | -0.097  | 1                |                    |                  |
|                    | p | 0.632   | 0.818  | 0.587   |                  |                    |                  |
| V <sub>Igeo</sub>  | r | 0.151   | 0.000  | 0.132   | 0.139            | 1                  |                  |
|                    | p | 0.393   | 0.998  | 0.456   | 0.434            |                    |                  |
| V <sub>CF</sub>    | r | 0.165   | 0.022  | 0.143   | 0.148            | 0.994**            | 1                |
|                    | p | 0.351   | 0.900  | 0.419   | 0.403            | 0.000              |                  |

\*\* Correlation is significant at the 0.01 level; \* Correlation is significant at the 0.05 level.

Complimentary Contributor Copy

Table 9, 10 and 11 shows the correlation matrix among PLI, RI, CPI, as well as EF, Er, Igeo and CF calculated for studied elements. PLI is positive correlated with RI and CPI, RI with PLI, CPI and CPI with PLI and RI. Since that PLI and CPI reflect the level of heavy metal pollution and RI reflect the ecological risk for the investigated elements, it can be concluded that the elements with the most anthropogenic influence also evidence the highest risk of contamination. A significantly high correlation was observed for Cd, Cu, Pb and Zn and their pollution indices. These positive correlations points to anthropogenic contributions in the studied sediments. Because of high Er values for Cd (all locations) and Cu (Z1, Pr and Pe sampling sites), these elements are relatively harmful environment contaminants.

Mn, V and Cr contamination factors are not correlated with RI and CPI, indicating that these elements are not significant contaminant on these localities. The existence of significant positive correlations among individual pollution indices for Cr, Ni, Co and Mn indicates the existence of local sources of contamination in some locations.

## CONCLUSION

Heavy metals are of considerable environmental concern due to their toxicity, wide sources, and accumulation behaviors. Data from sediments provide important information about environmental pollution, as well as indicating a stress on the ecological status of rivers.

In this paper, distribution and accumulation of heavy metal in river sediments were investigated and compared. Obtained results suggest various degrees of metal enrichment in studied rivers. The calculated values of pollution indices indicating that the concentration levels of studied elements in most of the stations exceeded the background values. The sediments were contaminated with studied elements, mainly with Cd, Cu and Zn. The elements with the most anthropogenic influence also evidence the highest risk of contamination. Values of potential ecological risk indexes indicating ecological risk from low risk to considerable for river sediments. The high value of this index for Ibar and Pek indicated high ecological risk for the studied elements in these rivers.

In general, the results of risk index were synchronous with results of the degree of contamination. The obtained results confirmed the use of applied factors for describing the pollution status of the river and river sediments.

## ACKNOWLEDGMENT

This study was supported by the Ministry of Education, Science and Technological Development of Serbia, Grant Nos. 172001 and 43007. In addition, we would like to thank the Republic Hydrometeorological Service of Serbia for the sediment samples.

Complimentary Contributor Copy

## REFERENCES

- Abraham, G. M. S., and Parker P. J. (2008). Assessment of heavy metal enrichment factors and the degree of contamination in marine sediment from Tamaki Estuary, Auckland, New Zealand. *Environmental Monitoring Assessment*, 136, 227–238.
- Asaah, A. V., and Abimbola, A. F. (2006). Heavy metal concentrations and distribution in surface soils of the Bassa Industrial Zone 1, Doula, Cameroon. *The Arabian Journal for Science and Engineering*, 31, 147–158.
- Chabuhdhara, M., and Nema, A. (2012). Assessment of heavy metal contamination in Hindon River sediments: A chemometric and geochemical approach. *Chemosphere*, 87, 945-953.
- Chang, C. Y., Wang, C. F., Mui, D. T., and Chiang, H. L. (2009). Application of methods (sequential extraction procedures and high-pressure digestion method) to fly ash particles to determine the element constituents: a case study for BCR 176. *Journal of Hazardous Materials*, 163, 578–587.
- Gao, H., Bai, J., Xiao, R., Liu, P., Jiang, W., and Wang, J. (2013). Levels, sources and risk assessment of trace elements in wetland soils of a typical shallow freshwater lake, China. *Stochastic Environmental Research and Risk Assessment*, 27, 275–284.
- Hakanson, L. (1980). Ecological risk index for aquatic pollution control, a sedimentological approach. *Water Research*, 14, 975-1001.
- Harikumar, P. S., Nasir, U. P., and Mujeebu Rahman, M. P. (2009). Distribution of heavy metals in the core sediments of a tropical wetland system. *International Journal of Environmental Science and Technology*, 6, 225-232.
- Hu, X., Wang, C., and Zou, L. (2011). Characteristic of heavy metals and Pb isotopic signatures in sediments cores collected from typical urban shallow lakes in Nanjing, China. *Journal of Environmental Management*, 92, 742-748.
- Hui-na, Z., Xing-zhong, Y., Guang-ming, Z., Min, J., Jie, L., Chang, Z., Juan, Y., Hua-jun, H., Zhi-feng, L., and Hong-wei, J. (2012). Ecological risk assessment of heavy metals in sediments of Xiawan Port based on modified potential ecological risk index. *Transactions of Nonferrous Metals Society of China*, 22, 1470-1477.
- Jian-Min, Z., Zhi, D., Mei-Fang, C., and Cong-Qiang, L. (2007). Soil heavy metal pollution around the Dabaoshan mine, Guangdong Province, China. *Pedosphere*, 17, 588-594.
- Kabir, I., Lee, H., Kim, G., and Jun, T. (2011). Correlation assessment and monitoring of the potential pollutants in the surface sediments of Pyeongchang River. *International Journal of Sediment Research*, 26, 152-162.
- Mediolla, L. L., Domingues, M. C. D., and Sandoval, M. R. G. (2008). Environmental Assessment of and Active Tailings Pile in the State of Mexico (Central Mexico). *Research Journal of Environmental Sciences*, 2, 197–208.
- Milačić, R., Ščančar, J., Murko, S., Kocman, D., and Horvat, M. (2010). A complex investigation of the extent of pollution in sediments of the Sava River. Part 1: selected elements. *Environmental Monitoring and Assessment*, 163, 263–75.
- Mohiuddin, K. M., Otomo, K., Ogawa, Y., and Shikazono, N. (2012). Seasonal and spatial distribution of trace elements in the water and sediments of the Tsurumi river in Japan. *Environmental Monitoring and Assessment*, 184, 265-279.
- Müller, G. (1979). Schwermetalle in den Sedimenten des Rheins-Veränderungen seit 1971. *Umschau*, 79, 778–783.

- Nam, S. H., Kim, M. J., Park, Y. I., and Lee, S. J. (2001). A study on various pretreatment and preparation for the determination of inorganic elements in sediment. *Analytical Sciences*, 17, a263-a265.
- Pekey, H., Karakaş, D., Ayberk, S., Tolun, L., and Bakoğlu, M. (2004). Ecological risk assessment using trace elements from surface sediments of Izmit Bay (Northeastern Marmara Sea) Turkey. *Marine Pollution Bulletin*, 48, 946-953.
- Relić, D., Đorđević, D., Sakan, S., Anđelković, I., Miletić, S., and Đuričić, J. (2011). Aqua regia extracted metals in sediments from the industrial area and surroundings of Pančevo, Serbia. *Journal of Hazardous Materials*, 186, 1893-1901.
- Relić, D., Đorđević, D., Sakan, S., Anđelković, I., Pantelić, A., Stanković, R., and Popović, A. (2013). Conventional, microwave, and ultrasound sequential extractions for the fractionation of metals in sediments within the Petrochemical Industry, Serbia. *Environmental Monitoring Assessment*, 185, 7627-7645.
- Rubio, B., Nombela, M. A., and Vilas, F. (2000). Geochemistry of major and trace elements in sediments of the Ria de Vigo (NW Spain): an assessment of metal pollution. *Marine Pollution Bulletin*, 40, 968-980.
- Ruzhong, L., Kun, S., Yueying, L., and Yong, S. (2010). Assessment of heavy metal pollution in estuarine surface sediments of Tangxi river in Chaohu Lake basin. *Chinese Geographical Science*, 20, 9-17.
- Rönkkömäki, H., Pöykiö, R., Nurmesniemi, H., Popov, K., Merisalu, E., Tuomi, T., and Välimäki, I. (2008). Particle size distribution and dissolution properties of metals in cyclone fly ash. *International Journal of Environment Science and Technology*, 5, 485-494.
- Sakan, S. M., Đorđević, D. S., Manojlović, D. D., and Polić, P. S. (2009). Assessment of heavy metal pollutants accumulation in the Tisza river sediments. *Journal of Environmental Management*, 90, 3382-3390.
- Sakan S. M., Đorđević D. S., Dević G., Relić D., Anđelković I., Đuričić J. (2011) A study of trace element contamination in river sediments in Serbia using microwave-assisted aqua regia digestion and multivariate statistical analysis. *Microchem. J.*, 99:492-502.
- Sakan, S., and Đorđević, D. (2012a). Distinguishing between natural and anthropogenic sources of trace elements in the sediments using the methods of geochemical normalization and statistical analysis. In D. A. De Leon and P. R. Aragon (Eds.), *Trace elements: Environmental Sources, Geochemistry and Human Health* (pp. 117-134), Nova Science Publishers, Inc.
- Sakan, S., Đorđević, D., Lazić, M., and Tadić, M. (2012b). Assessment of arsenic and mercury contamination in the Tisa River sediments and industrial canal sediments (Danube alluvial formation), Serbia. *Journal of Environmental Science and Health, Part A*, 47, 109-116.
- Sakan, S., and Đorđević, D. (2013). Assessment of trace element contamination in the river and alluvial sediments using a sequential extraction technique and statistical analysis. In S. Hong-Bo (Ed.), *Metal Contamination: Sources, Detection and Environmental Impact* (pp. 119-155), Nova Science Publishers, Inc.
- Sakan, S., Dević, G., Relić, D., Anđelković, I., Sakan, N., and Đorđević, D. (2014). Risk assessment of trace element contamination in river sediments in Serbia using pollution indices and statistical methods: a pilot study. *Environmental Earth Sciences*, doi: 10.1007/s12665-014-3886-1

- Sakan, S., Dević, G., Relić, D., Anđelković, I., Sakan N, and Đorđević D. (2015a). Evaluation of sediment contamination with heavy metals: the importance of determining appropriate background content and suitable element for normalization. *Environmental Geochemistry and Health*, 37, 97-113.
- Sakan, S., Dević, G., Relić, D., Anđelković, I., and Sakan, N. (2015b). Environmental assessment of heavy metal pollution in freshwater sediment, Serbia. *CLEAN-Soil Air Water*, doi: 10.1002/clen.201400275
- Tomlinson, D. C., Wilson, J. G., Harris, C. R., and Jeffrey, D. W. (1980). Problems in the assessment of heavy-metal levels in estuaries and the formation of a pollution index. *Helgoländer Meeresunters*, 33, 566-575.
- Varol, M. (2011). Assessment of heavy metal contamination in the sediments of the Tigris river (Turkey) using pollution indices and multivariate statistical techniques. *Journal of Hazardous Materials*, 195, 355-364.
- Yang, Z., Wang, Y., Shen, Z., Niu, J., and Tang, Z. (2009). Distribution and speciation of heavy metals in sediments from the mainstream, tributaries, and lakes of the Yangtze River catchment of Wuhan, China. *Journal of Hazardous Materials*, 166, 1186-1194.
- Zahra, A., Hashmi, M. Z., Malik, R. N., and Ahmed, Z. (2014). Enrichment and geo-accumulation of heavy metals and risk assessment of sediments of the Kurang Nallah—Feeding tributary of the Rawal Lake Reservoir, Pakistan. *Science of the Total Environment*, 470-471, 925-933.

CHEMISTRY RESEARCH AND APPLICATIONS

# Biogeochemistry of Trace Elements

Oleg S. Pokrovsky  
Jerome Viers  
Editors



NOVA

Complimentary Contributor Copy





**CHEMISTRY RESEARCH AND APPLICATIONS**

**BIOGEOCHEMISTRY OF  
TRACE ELEMENTS**

No part of this digital document may be reproduced, stored in a retrieval system or transmitted in any form or by any means. The publisher has taken reasonable care in the preparation of this digital document, but makes no expressed or implied warranty of any kind and assumes no responsibility for any errors or omissions. No liability is assumed for incidental or consequential damages in connection with or arising out of information contained herein. This digital document is sold with the clear understanding that the publisher is not engaged in rendering legal, medical or any other professional services.

**Complimentary Contributor Copy**

# **CHEMISTRY RESEARCH AND APPLICATIONS**

Additional books and e-books in this series can be found  
on Nova's website under the Series tab.

Complimentary Contributor Copy

CHEMISTRY RESEARCH AND APPLICATIONS

**BIOGEOCHEMISTRY OF  
TRACE ELEMENTS**

**OLEG S. POKROVSKY**

**AND**

**JEROME VIERS**

**EDITORS**



Complimentary Contributor Copy

Copyright © 2018 by Nova Science Publishers, Inc.

**All rights reserved.** No part of this book may be reproduced, stored in a retrieval system or transmitted in any form or by any means: electronic, electrostatic, magnetic, tape, mechanical photocopying, recording or otherwise without the written permission of the Publisher.

We have partnered with Copyright Clearance Center to make it easy for you to obtain permissions to reuse content from this publication. Simply navigate to this publication's page on Nova's website and locate the "Get Permission" button below the title description. This button is linked directly to the title's permission page on [copyright.com](http://copyright.com). Alternatively, you can visit [copyright.com](http://copyright.com) and search by title, ISBN, or ISSN.

For further questions about using the service on [copyright.com](http://copyright.com), please contact:

Copyright Clearance Center

Phone: +1-(978) 750-8400 Fax: +1-(978) 750-4470 E-mail: [info@copyright.com](mailto:info@copyright.com).

#### **NOTICE TO THE READER**

The Publisher has taken reasonable care in the preparation of this book, but makes no expressed or implied warranty of any kind and assumes no responsibility for any errors or omissions. No liability is assumed for incidental or consequential damages in connection with or arising out of information contained in this book. The Publisher shall not be liable for any special, consequential, or exemplary damages resulting, in whole or in part, from the readers' use of, or reliance upon, this material. Any parts of this book based on government reports are so indicated and copyright is claimed for those parts to the extent applicable to compilations of such works.

Independent verification should be sought for any data, advice or recommendations contained in this book. In addition, no responsibility is assumed by the publisher for any injury and/or damage to persons or property arising from any methods, products, instructions, ideas or otherwise contained in this publication.

This publication is designed to provide accurate and authoritative information with regard to the subject matter covered herein. It is sold with the clear understanding that the Publisher is not engaged in rendering legal or any other professional services. If legal or any other expert assistance is required, the services of a competent person should be sought. FROM A DECLARATION OF PARTICIPANTS JOINTLY ADOPTED BY A COMMITTEE OF THE AMERICAN BAR ASSOCIATION AND A COMMITTEE OF PUBLISHERS.

Additional color graphics may be available in the e-book version of this book.

#### **Library of Congress Cataloging-in-Publication Data**

ISBN: ; 9: /3/75836/467/9" \*gDqqm#

*Published by Nova Science Publishers, Inc. † New York*

**Complimentary Contributor Copy**

# CONTENTS

|                     |   |            |
|---------------------|---|------------|
| <b>Introduction</b> |   | <b>vii</b> |
| <b>Chapter 1</b>    | Trace Metal Exposure in Different Livestock Production Systems<br><i>I. Orjales, R. Rodríguez-Bermúdez, M. Miranda, M. López-Alonso and M. Garcia-Vaquero</i>   | <b>1</b>   |
| <b>Chapter 2</b>    | Lithological Distribution of Rare Earth Elements in Soil and Atmospheric Precipitates in the Bregalnica River Basin<br><i>Trajče Stafilov, Biljana Balabanova and Robert Šajn</i>   | <b>23</b>  |
| <b>Chapter 3</b>    | Identification, Evaluation, and Estimation of the Levels of Potentially Harmful Trace Elements in Sediments Based on the Application of Different Methods<br><i>Sanja M. Sakan, Nenad M. Sakan and Dragana S. Đorđević</i>  | <b>55</b>  |
| <b>Chapter 4</b>    | Accumulation of Trace Elements in Sediments and Macrophytes of Thermokarst Lakes in Western Siberia<br><i>R. M. Manasyrov, O. S. Pokrovsky, L. S. Shirokova, S. N. Kirpotin and N. S. Zinner</i>  | <b>81</b>  |
| <b>Chapter 5</b>    | Trace Elements in Snow Cover of Western Siberia: Impact of Snow Deposition on Surface Water Chemistry<br><i>V. P. Shevchenko, S. N. Vorobyev, I. V. Krickov, R. M. Manasyrov, N. V. Politova, S. G. Kopysov, O. M. Dara, Y. Auda, L. S. Shirokova, L. G. Kolesnichenko, V. A. Zemtsov, S. N. Kirpotin and O. S. Pokrovsky</i> | <b>113</b> |

|                          |   |            |
|--------------------------|---|------------|
| <b>Chapter 6</b>         | Major and Trace Elements in Peat Pore Water Found in the Permafrost Zone of Western Siberia   | <b>167</b> |
|                          | <i>T. V. Raudina, S. V. Loiko, A. Lim, I. V. Krickov, L. S. Shirokova, G. I. Istigechev, D. M. Kuzmina, S. P. Kulizhsky, S. N. Vorobyev and O. S. Pokrovsky</i> |            |
| <b>Chapter 7</b>         | Hot Spots of Permafrost Thawing Enhance Trace Metal Release into Thermokarst Waters   | <b>211</b> |
|                          | <i>S. V. Loiko, O. S. Pokrovsky, T. V. Raudina, A. G. Lim, L. G. Kolesnichenko, L. S. Shirokova, S. N. Vorobyev, S. N. Kirpotin and D. M. Kuzmina</i>           |            |
| <b>Chapter 8</b>         | Trace Elements in the Form of Organo-Mineral Colloids in the Mixing Zone of the Arctic River  | <b>245</b> |
|                          | <i>O. S. Pokrovsky, J. Viers, A. V. Chupakov, L. S. Shirokova, V. V. Gordeev and V. P. Shevchenko</i>   |            |
| <b>Chapter 9</b>         | The Distribution of Metals in Different Types of Soils of Northern Karelia  | <b>289</b> |
|                          | <i>O. Yu. Drozdova, Yu. A. Zavgorodnyaya, D. A. Bychkov, V. V. Demin and S. A. Lapitskiy</i>  |            |
| <b>Chapter 10</b>        | Trace Metals in Soil Catenas of the Arctic Islands (The Svalbard and Novaya Zemlya Archipelagos)  | <b>309</b> |
|                          | <i>Vidas V. Kriauciunas, Stanislav A. Iglovsky and Irina A. Kuznetsova</i>  |            |
| <b>Chapter 11</b>        | Trace Metal Binding Properties of the Peat: Static and Dynamic Sorption   | <b>359</b> |
|                          | <i>Irina A. Kuznetsova, Stanislav A. Iglovsky and Vidas V. Kriauciunas</i>  |            |
| <b>About the Editors</b> |   | <b>373</b> |
| <b>Index</b>             |   | <b>375</b> |

*Chapter 3*

**IDENTIFICATION, EVALUATION, AND ESTIMATION  
OF THE LEVELS OF POTENTIALLY HARMFUL TRACE  
ELEMENTS IN SEDIMENTS BASED ON  
THE APPLICATION OF DIFFERENT METHODS**

*Sanja M. Sakan<sup>1,\*</sup>, Nenad M. Sakan<sup>2</sup> and Dragana S. Đorđević<sup>1</sup>*

<sup>1</sup>Centre of Excellence in Environmental Chemistry and Engineering –  
ICTM, University of Belgrade, Belgrade, Serbia

<sup>2</sup>Institute of Physics, University of Belgrade, Zemun, Serbia

**ABSTRACT**

Potentially harmful trace elements pollution in aquatic ecosystems is a worldwide environmental problem that has received increasing attention over the last few decades because of its adverse effects. Sediments pollution by toxic elements is related to different kinds of human activities such as industrial production, agricultural operations, burning of fossil fuels, mining and metallurgical processes and waste disposal practices.

Trace elements are distributed throughout sediment components and associated with them in various ways including ion exchange, adsorption, precipitation, and complexation. They are not permanently fixed by sediment. Changes of the environment conditions, such as acidification, redox potential or organic ligand concentrations, can cause mobilization of element from solid to liquid phase and cause contamination of surrounding waters.

Proper assessment of the implication of sediment contamination with trace element normally requires more than one method to be used. This paper describes methods for

---

\* Corresponding author: ssakan@chem.bg.ac.rs.

identification, evaluation, and estimation of the levels of potentially harmful trace elements in sediments using the different methods: sequential extraction, pollution indices and statistical analyses. Obtained results indicate that heavy metal contamination should be taken into account during development of management strategies to protect the aquatic environment in the Serbia.

**Keywords:** Serbia, potentially harmful, trace elements, aquatic ecosystems, sediment

## 1. INTRODUCTION

In recent years, investigations of potentially toxic inorganic pollutants have increased (Li and Thornton, 2001; Relić et al. 2005; Silveira et al. 2006; Farkas et al. 2007; Widmeyer and Bendell-Young, 2008; Daesslé et al. 2009; Egiarte et al. 2009; Mil-Homens et al. 2009; Nguyen et al. 2009; Feng et al. 2011; Wang et al. 2015; Sakan et al. 2016; Sierra et al. 2017), because they threatens the economic and ecological value of many localities. Potentially harmful trace elements are naturally occurring elements that meet the following conditions: 1) cannot be degraded or destroyed; 2) are persistent in the environment; 3) can be bioaccumulated and 4) biomagnified (higher concentrations are found in organisms higher up in the food chain) (Sierra et al. 2017).

Trace element may be introduced into the aquatic systems by both natural processes (e.g., weathering, erosion and atmospheric deposition and as a result of human activities, for which reason they can be used as a tracers of environmental pollution (Manta et al. 2002). Significant quantities of heavy metals are discharged into rivers, which can be strongly accumulated and biomagnified along water, sediment, and aquatic food chain, resulting in sublethal effects or death in local fish population (Yi et al. 2011).

The aquatic sediments are characterized by extreme complexity and diversity. Elements in sediments can be associated with several reactive components. Although total metal concentrations may indicate the overall level of metals in soils and sediments, they provide no information regarding the chemical nature or potential mobility and bioavailability of a particular element (Silveira et al. 2006).

There is a great diversity of possible associations of heavy metal elements with the various substrates. They can be adsorbed on the particle surfaces of clays, iron, and manganese oxyhydroxides or organic matter present in the lattice of secondary minerals, such as, carbonates or sulfides; occluded in amorphous iron and manganese oxyhydroxides, sulfides or remains of biological organisms and present in the lattice of primary minerals (Tessier et al., 1979). Heavy metals in sediments can be classified on the basis of the primary accumulation mechanism, as the adsorptive and the exchangeable one, as well as on the bonding substrate, the carbonate phase, the Mn-oxide, as well as organic matter or sulfides, and finally detrital or lattice metals (Salomons and Förstner, 1980). A number of studies on metal distribution and fractionation in river sediments,



suspended particles, soils and on fractionations of metals have been performed (Davidson et al. 1998; Egiarte et al. 2010; Yobouet et al. 2010; Relić et al. 2013).

Sequential fractionation is a frequently used approach to evaluate metal distribution into different chemical forms present in a solid phase. Conceptually, sequential fractionation categorizes metal associated with chemically homogenous fractions that, ultimately affect metal variability. The reactivity or mobility of toxic elements in sediments, and thus their potential toxicity depends on phase in which they occur in, and to which chemical and physical processes these phases are subject to (Rao et al. 2010). These phases are also referred to as fractions, and they include the following wide-range categories: water-soluble, exchangeable, specifically adsorbed, carbonate, Fe and Mn oxides, organic matter, sulfides, and silicates. All of these fractions may occur in a variety of structural forms (Sakan et al. 2016).

Prlica et al. (2008) emphasized that sequential extraction procedure must be used an additional tool for assessing the potential bioavailability and toxicity of metals in sediment. Despite the potential limitations of sequential extraction procedures, particularly relating to the potential for reagents to be non-selective and for metal-ions to be re-adsorb to different sediment phases, this method remains a powerful technique in the assessment the significance of heavy metal pollution of the environment (Farkas et al. 2007). Bacon and Davidson (2008) concluded that this method will have a healthy future in the 21<sup>st</sup> century.

To evaluate the potential biological adverse effect, hazard quotient (HQ) is one kind of single value estimate and is also the simplest method to estimate toxicity potential of the selected pollutants in the sediment (Qian et al. 2015).

In this research, 32 samples of river sediment from 15 rivers in Serbia were studied to estimate their environmental pollution levels of potentially toxic elements. The five-step sequential extraction procedure was used to determine the respective distribution and to assess the environmental mobility of toxic elements. The hazard quotient has been calculated to estimate toxicity potential of the selected pollutants in the sediments. To identify the relationship among heavy metal in river sediments and their possible sources, multivariate statistical analysis (hierarchical cluster analysis) was performed in this research.

## **2. EXPERIMENTAL**

### **2.1. Sampling Location**

The largest and most important rivers that flow through Serbia are: the Danube, Sava, Great Morava, West Morava, South Morava, Tisa, Ibar, Drina, Timok, Nišava, Tamiš and Begej. The Danube is the largest river in the country, flowing for 588 km inside Serbia,

while forming the border with Romania, and the second largest river in Europe. The basin drains parts of 19 countries. Some major tributaries of the Danube are still heavily polluted. Water quality in the Middle and Lower Danube remained relatively high (class II) between 1950 and the 1970s, but deteriorated afterwards due to rapid industrial development, poor pollution control and inputs from heavily polluted tributaries (Tockner et al. 2009).

The 945-km long Sava River is the largest tributary of the Danube by volume (average discharge: 1572 m<sup>3</sup>/s) and the second largest, after the Tisza, by catchment area (95,793 km<sup>2</sup>). In Serbia, it remains a typical lowland river. Until the 1990s, the Sava was affected by heavy pollution from the metallurgical, chemical, leather, textile, food, cellulose and paper industries, as well as from agricultural activities. The Sava is the main recipient of wastewater from many cities and is impacted by the polluted water of the tributaries (Tockner et al. 2009).

The River Tisza (966km; 157,220 km<sup>2</sup>) is the largest Danube tributary in its length and catchment area. A small part of the Tisza watershed area lies within Serbian territory, and covers only 6% or 8,994 km<sup>2</sup>. It is predominantly lowland and part of the Pannonian basin, which is the largest of the sediment-filled, postorogenic basins of the Alpine region (Adriano et al. 2003). Ecological accidents that took place in 2000 in the superior watershed and their effects on the rivers upstream with resulting transboundary influences proved the necessity of a regional approach to environmental protection and the active involvement of riverside countries in establishing common strategies and programs for preventing and reducing the risk of accidental pollution (Adriano et al. 2003).

The 308 km long West Morava drains south-western Serbia (catchment area: 15,567 km<sup>2</sup>). The largest tributary is the Ibar.

## **2.2. Description of the Sampling Site and Sampling**

Cross border pollution indicates a need to determine the pollutants in the water and sediment in all the countries along the river's flow.

Because of that, for this investigation sediment was selected from the main rivers in Serbia. 32 samples of river sediment from 15 rivers in Serbia were collected for this research (Table 1, Figure 1): the Danube (Black Sea watershed), the Sava (Danube watershed), the Tisa (Danube watershed), the Ibar (West Morava watershed), the Great Morava (Danube watershed), the West Morava (Great Morava watershed), the South Morava (Great Morava watershed), the Nišava (South Morava watershed), the Tamiš (Danube watershed), the DTD canal-Vrbaš (Danube watershed), the Topčiderska River

(Sava watershed), the Porečka River (Danube watershed), the Kolubara (Sava watershed), the Pek (Danube watershed) and the Toplica (South Morava watershed). For the larger rivers, sampling was conducted at several locations (Figure 1).

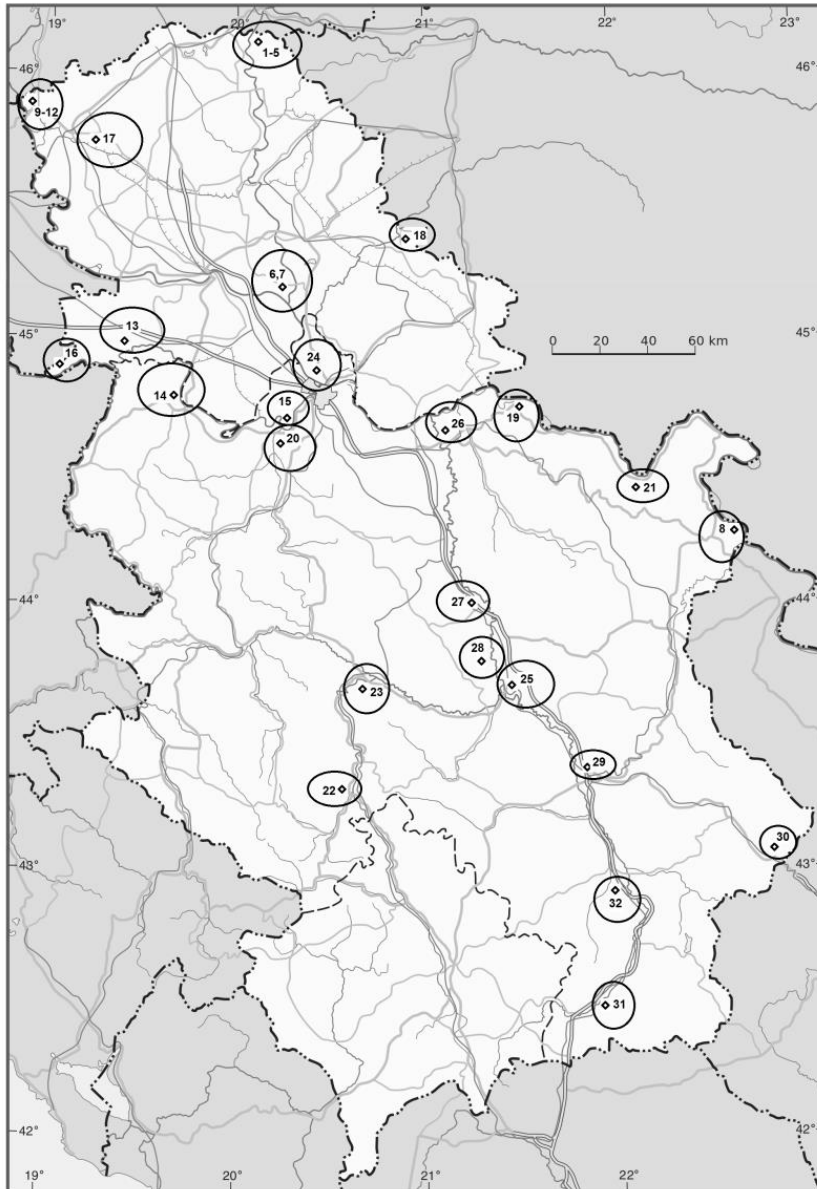


Figure 1. Sampling locations, rivers in Serbia. Explanation: 1-5/Tisa (Martonoš); 6,7/Tisa (Titel); 8/Danube (Gruja); 9-12/Danube (Bezdan); 13/Sava (Sremka Mitrovica); 14/Sava (Šabac); 15/Sava (Ostružnica); 16/Sava (Jamena); 17/DTD canal (Begej, Vrbas); 18/Tamiš; 19/Pek (Kisiće); 20/Kolubara (Draževac); 21/Porečka river (Mosna); 22/Ibar (Raška); 23/Ibar (Kraljevo); 24/Topčiderska river (Rakovica); 25/South Morava (Mojsinje); 26/Great Morava (Ljubicevski bridge); 27/Great Morava (Bagrdan); 28/West Morava (Maskare); 29/Nišava (Niš); 30/Nišava (Dimitrovgrad); 31/South Morava (Vladičin Han); 32/Toplica (Doljevac).

**Table 1. Number of sediment sample, river name and sampling site**

| Sample | River             | Sampling site     |
|--------|-------------------|-------------------|
| 1      | Tisa              | Martonoš          |
| 2      | Tisa              | Martonoš          |
| 3      | Tisa              | Martonoš          |
| 4      | Tisa              | Martonoš          |
| 5      | Tisa              | Martonoš          |
| 6      | Tisa              | Titel             |
| 7      | Tisa              | Titel             |
| 8      | Danube            | Gruja             |
| 9      | Danube            | Bezdan            |
| 10     | Danube            | Bezdan            |
| 11     | Danube            | Bezdan            |
| 12     | Danube            | Bezdan            |
| 13     | Sava              | Sremska Mitrovica |
| 14     | Sava              | Šabac             |
| 15     | Sava              | Ostružnica        |
| 16     | Sava              | Jemena            |
| 17     | DTD canal         | Begej, Vrbas      |
| 18     | Tamiš             | Jaša Tomić        |
| 19     | Pek               | Kusiće            |
| 20     | Kolubara          | Draževac          |
| 21     | Porečka river     | Mosna             |
| 22     | Ibar              | Raška             |
| 23     | Ibar              | Kraljevo          |
| 24     | Topčiderska river | Rakovica          |
| 25     | South Morava      | Mojsinje          |
| 26     | Great Morava      | Ljubičevski most  |
| 27     | Great Morava      | Bagrdan           |
| 28     | West Morava       | Maskare           |
| 29     | Nišava            | Niš               |
| 30     | Nišava            | Dimitrovgrad      |
| 31     | South Morava      | Vladičin Han      |
| 32     | Toplica           | Doljevac          |

The sediment samples were stored at 4°C in order to prevent changes in the chemical composition of the sediments. The contents of the micro and macro-elements were determined in the granulometric fraction < 63 µm of the bottom sediment samples (“grab”- the samples) after air drying for 8 days (Sakan et al. 2011).

### 2.3. Sequential Extraction of Studied Elements

The sediment samples were analyzed by modified version of a sequential extraction procedure described in the manuscripts (Polić and Pfendt, 1992; Relić et al. 2005; Sakan et al. 2007).

The extractants and operationally defined chemical fractions applied in this research were as follows:

*The first step (exchangeable fraction, F1):* Each 1 g of sediment sample was added 40 ml of a 1 M  $\text{CH}_3\text{COO}(\text{NH}_4)$ , with agitation for 2 hours at 22°C. The extract was separated from the solid phase by centrifugation at 3000 rpm for 20 min, and the supernatant stored for later analysis. The elements adsorbed on the sediments were exchangeable and are in equilibrium with the water's ionic composition, which was typical for sorption-desorption processes (Mingbiao et al. 2008).

*The second step (easily reducible fraction, F2):* Residue from stage 1 was added 40 ml of a 0.5 M  $\text{NH}_2\text{OH}\cdot\text{HCl}$  (pH 1.5). The suspension was then agitated for 16 hours at 22°C. The extract was separated from the solid phase by centrifugation, as described for stage 1.

*The third step (metals bound to moderately reducible phases, F3):* Residue from stage 2 was added 40 ml mixture of 0.2 M  $\text{H}_2\text{C}_2\text{O}_4$  / 0.2 M  $(\text{NH}_4)_2\text{C}_2\text{O}_4$ . The suspension was then agitated for 10 hours at 22°C. The extract was separated from the solid phase by centrifugation, as described for stage 1.

*The fourth step (oxidizable fractions-elements associated with organic matter and sulfides, F4):* Residue from stage 3 was added 10 ml 8.8 mol l<sup>-1</sup>  $\text{H}_2\text{O}_2$  solution, and the mixture left at room temperature for 1h. It was then heated to 85°C for 1h in a water bath, and then the volume was reduced to 2-3 ml by the further heating in a water bath. Another 10 ml portion of 8.8 mol l<sup>-1</sup>  $\text{H}_2\text{O}_2$  solution was added, and the mixture heated to dryness at 85°C for 1h. After cooling, 50 ml of a 1.0 mol l<sup>-1</sup> solution of ammonium acetate (pH 2) was added to residue, followed by agitation for 16 h at 22°C. The addition of ammonium acetate was designed to prevent adsorption of the extracted metals onto the oxidized sediment (Mingbiao et al. 2008). The extract was separated from the solid phase by centrifugation, as above.

After the first four extraction steps, extract was separated from solid residue by centrifugation at 3000×g for 20 min, decant supernatant, diluted to 50 ml with 1M  $\text{HNO}_3$  and stored in a polyethylene bottle at 4°C until metal analysis. The residue was washed with 20 ml deionized water and shaken 15 min, followed by centrifugation for 20 min at 3000×g. The supernatant was decanted and discarded, acting cautiously not to discard any solid residues. In this way, the residue was prepared for the next BCR step (Sutherland 2010; Relić et al. 2013).

*The fifth step (residual fraction–metals strongly associated with the crystalline structure of minerals, F5):* The Stage 4 residue was digested using a mixture of the acids (8 ml aqua regia, 3:1, v/v,  $\text{HCl}$  to  $\text{HNO}_3$ ) on water bath for 1 h at 85°C, until the volume was reduced to 2–3 ml. Another 8 ml portion of aqua regia was added, and the mixture heated to dryness at 85°C for 1 h. The final residue was dissolved in 1M  $\text{HNO}_3$  and diluted to 50 ml and stored in a polyethylene bottle at 4°C until metal analysis.

## **2.4. Determination of Element Concentrations**

In this research, the following elements were determined in each sample: Ba, Ca, Cd, Co, Cr, Cu, Fe, K, Li, Mg, Mn, Na, Ni, Pb, V and Zn. Element concentrations in solutions obtained at each step were determined using an atomic emission spectrometer with an inductively coupled plasma iCAP-6500 Duo (Thermo Scientific, United Kingdom). The detector was a RACID86 Charge injector device (CID). Analytical grade chemicals were used throughout the study without any further purification. The metal standards were prepared from a stock solution of 1,000 mg l<sup>-1</sup> by successive dilutions. The concentrations obtained for all the elements in the blanks were close to the detection limit of the method, indicating that contamination was not a problem in the analyses.

The analytical data quality was controlled by using laboratory quality assurance and quality control methods, including the use of calibration with standards, and analysis of both, reagent blanks and replicates. The blank solutions were prepared in the same way as samples during the extraction procedure.

Duplicate samples are used to measure the precision of the method. In this research, duplicate analysis was performed for seven sediment samples for fifth-step sequential extraction. The precision is expressed as the relative standard deviations. The relative standard deviations of the means of duplicate measurement were less than 10% (from 0.6 to 7.2%).

The total amounts of elements in this paper are defined as the sum of the five binding fractions (Facchinelli et al. 2001; Sakan et al. 2007). This method results in concentrations normally referred to as “pseudo-total,” “total extractable amount” and “sequentially extractable amount,” as the silicates are not completely destroyed (Facchinelli et al. 2001).

All concentrations values below the detection limit were replaced by half of the DL, as suggested by Relić et al. (2005).

The moisture content of each sample was determined by drying a separate 1 g sample in an oven (105 ± 2°C) to constant weight. From this, a correction to dry mass was obtained, which was applied to all reported metal concentrations. Sediment data in this study are reported on a dry weight mg kg<sup>-1</sup> basis.

## **2.5. The Hazard Quotients (HQ)**

The potential toxic risk to aquatic ecosystems was evaluated by calculating the hazard quotients (HQ) of the chemical contaminants using the equation (Wang et al. 2015):  $HQ = SCC/SQG$ , where SCC is the concentration of metals in sediments in µg/g, and SQG is the sediment quality guideline in µg/g. SQG values were determined at ERL

levels according to Long et al. (1995): Cd = 1.2; Cr = 81; Cu = 34; Ni = 20.9; Pb = 46.7; and Zn = 150, in  $\mu\text{g/g}$ . According to Long et al. (1995), ERL is defined based on the concentration when 10<sup>th</sup> percentiles of organisms are influenced by the toxicity of a specific contaminant, while ERM value is decided when 50<sup>th</sup> percentiles are influenced by the toxicity of contaminant in that concentration. For toxicity characterization, HQ values were used to express the potential risk to ecological receptors; at  $\text{HQ} < 0.1$  no adverse effects were expected; at  $0.1 < \text{HQ} < 1$  potential hazard were expected to be low, but in the range of  $1.0 < \text{HQ} < 10$ , some adverse effects or moderate hazard are probable; and, finally, if  $\text{HQ} > 10$ , high hazard potential is anticipated (Feng et al. 2011).

## **2.6. Statistical Methods**

Descriptive data analyses were performed in this research. The statistical analyses done in this study include also Cluster analysis (CA). The purpose of cluster analysis is to identify groups or clusters of similar sites on the basis of similarities within a class and dissimilarities between different classes (Chabuhdhara and Nema, 2012). Cluster analysis can be run in the Q-mode, when clusters of samples are sought, or in the R-mode, when clusters of variables are desired. The hierarchical clustering joining of the most similar observations, and successively of the next most similar observations, was employed in the presented research. The statistical analyses were performed using IBM SPSS Statistics-Statistical Package for the Social Sciences (SPSS) (version 21.0).

## **3. RESULTS AND DISCUSSION**

### **3.1. Metal Fractionation**

Using the method of sequential extraction, a metal fractionation was performed, i.e., an assessment of the distribution of the content metals in the different fraction was carried out. The results are given in Table 2 as the mean, median, maximum and minimum values, as well as the standard deviation for each metal and fraction. The percentage element distribution by fractions was calculated as the average content of the extracted element in each fraction with respect to the total content of the extracted element (Figures 2-6).

**Table 2. Summary statistics of element content in sediment (mg kg<sup>-1</sup>) in five fractions**

|        | Ba 1* | Ba 2 | Ba 3  | Ba 4  | Ba 5  | Ba s  | Ca 1  | Ca 2  | Ca 3  | Ca 4  | Ca 5  | Ca s  |
|--------|-------|------|-------|-------|-------|-------|-------|-------|-------|-------|-------|-------|
| Mean   | 60.1  | 24.8 | 3.11  | 6.26  | 24.1  | 118   | 11320 | 22787 | 42    | 1606  | 1960  | 37715 |
| Median | 56.7  | 22.6 | 2.60  | 5.55  | 21.9  | 114   | 11671 | 19961 | 38    | 944   | 583   | 33316 |
| SD     | 17.0  | 10.7 | 3.15  | 3.09  | 9.57  | 29.2  | 1829  | 15269 | 25    | 2095  | 3330  | 19797 |
| Min    | 32.8  | 8.20 | 0.57  | 1.80  | 11.6  | 58.6  | 3383  | 1697  | 2     | 83    | 199   | 5925  |
| Max    | 97.0  | 62.7 | 18.2  | 16.80 | 71.4  | 199   | 13745 | 62942 | 99    | 6423  | 14005 | 79607 |
|        | Cd1   | Cd2  | Cd3   | Cd4   | Cd5   | Cds   | Cr1   | Cr2   | Cr3   | Cr4   | Cr5   | Crs   |
| Mean   | 0.74  | 1.03 | 0.22  | 0.47  | 2.25  | 4.70  | 0.02  | 2.67  | .56   | 11.0  | 42.3  | 62.5  |
| Median | 0.62  | 0.77 | 0.21  | 0.30  | 2.15  | 4.40  | 0.02  | 1.21  | .00   | 7.80  | 32.0  | 52.5  |
| SD     | 0.54  | 1.15 | 0.12  | 0.56  | 0.50  | 1.69  | 0.02  | 2.70  | .10   | 13.8  | 23.0  | 30.2  |
| Min    | 0.05  | 0.08 | 0.07  | 0.15  | 1.10  | 2.57  | <DL   | 0.11  | .60   | 2.00  | 14.0  | 26.7  |
| Max    | 1.80  | 6.00 | 0.67  | 3.10  | 3.10  | 10.6  | 0.08  | 7.60  | 6.7   | 80.0  | 98.8  | 134   |
|        | Cu1   | Cu2  | Cu3   | Cu4   | Cu5   | Cus   | Fe1   | Fe2   | Fe3   | Fe4   | Fe5   | Fes   |
| Mean   | 4.98  | 10.7 | 24.8  | 13.3  | 24.8  | 78.6  | 2.48  | 2936  | 4534  | 1229  | 19121 | 27822 |
| Median | 2.00  | 0.92 | 18.1  | 4.40  | 25.0  | 51.7  | 1.75  | 3119  | 028   | 1185  | 18831 | 28897 |
| SD     | 14.1  | 28.6 | 29.9  | 44.4  | 12.0  | 125   | 2.54  | 1730  | 2186  | 365   | 3790  | 4328  |
| Min    | 0.38  | <DL  | 7.00  | 1.00  | 9.00  | 26.0  | 0.94  | 337   | 2156  | 620   | 9856  | 13453 |
| Max    | 82.0  | 162  | 179   | 254   | 78.1  | 755   | 14.8  | 6164  | 12003 | 2402  | 25590 | 34139 |
|        | K1    | K2   | K3    | K4    | K5    | Ks    | Li1   | Li2   | Li3   | Li4   | Li5   | Lis   |
| Mean   | 242   | 41.6 | 19.5  | 11.7  | 1568  | 1883  | 0.17  | 2.71  | 0.47  | 1.29  | 18.6  | 23.2  |
| Median | 249   | 42.6 | 12.6  | 10.0  | 1569  | 1846  | 0.17  | 2.35  | 0.44  | 1.15  | 19.8  | 23.8  |
| SD     | 69    | 17.9 | 19.6  | 6.43  | 322   | 375   | 0.04  | 1.26  | 0.25  | 0.42  | 3.97  | 4.33  |
| Min    | 156   | 18.1 | <DL*  | 3.40  | 1018  | 1248  | 0.10  | 0.85  | 0.12  | 0.67  | 9.80  | 13.9  |
| Max    | 446   | 78.2 | 96.7  | 31.4  | 2306  | 2794  | 0.31  | 6.10  | 1.10  | 2.20  | 24.8  | 30.0  |
|        | Mg1   | Mg2  | Mg3   | Mg4   | Mg5   | Mgs   | Mn1   | Mn2   | Mn3   | Mn4   | Mn5   | Mns   |
| Mean   | 719   | 1940 | 1574  | 807   | 5581  | 10621 | 173   | 401   | 46.48 | 31.15 | 119   | 771   |
| Median | 546   | 1549 | 369   | 687   | 5369  | 9681  | 119   | 384   | 42.60 | 26.25 | 125   | 741   |
| SD     | 419   | 1456 | 2869  | 482   | 1861  | 4748  | 121   | 202   | 27.21 | 15.59 | 22.9  | 317   |
| Min    | 384   | 335  | 115   | 217   | 2138  | 3424  | 51    | 95    | 13.70 | 8.00  | 64.0  | 240   |
| Max    | 2403  | 5177 | 10057 | 2407  | 11063 | 22522 | 581   | 1184  | 146   | 78.9  | 153   | 2009  |
|        | Na1   | Na2  | Na3   | Na4   | Na5   | Nas   | Ni1   | Ni2   | Ni3   | Ni4   | Ni5   | Nis   |
| Mean   | 106   | 26.5 | 9.03  | <DL   | 101   | 243   | 1.24  | 12.6  | 10.9  | 13.3  | 45.2  | 83.2  |
| Median | 96.0  | 24.2 | 7.05  | <DL   | 67.2  | 228   | 0.71  | 8.85  | 7.45  | 7.40  | 26.2  | 48.7  |
| SD     | 56.6  | 13.2 | 7.84  | <DL   | 128   | 140   | 1.16  | 12.5  | 9.81  | 13.5  | 33.2  | 59.6  |
| Min    | 34.5  | 12.9 | <DL   | <DL   | 27.7  | 123   | 0.28  | 1.00  | 2.10  | 1.90  | 10.8  | 25.2  |
| Max    | 257   | 89.4 | 29.0  | <DL   | 745   | 888   | 5.80  | 53.8  | 41.7  | 72.4  | 136   | 260   |
|        | Pb1   | Pb2  | Pb3   | Pb4   | Pb5   | Pbs   | V1    | V2    | V3    | V4    | V5    | Vs    |
| Mean   | 0.74  | 32.6 | 0.75  | 13.0  | 0.90  | 48.0  | 0.10  | 3.43  | 4.73  | 1.52  | 21.8  | 30.3  |
| Median | 0.20  | 24.0 | <DL   | 7.00  | <DL   | 35.7  | 0.09  | 3.50  | 4.40  | 1.50  | 21.2  | 30.7  |
| SD     | 1.88  | 40.6 | 2.44  | 13.90 | 5.11  | 47.0  | 0.09  | 1.98  | 2.05  | 0.57  | 4.59  | 7.33  |
| Min    | <DL   | 0.23 | <DL   | <DL   | <DL   | 4.44  | <DL   | 0.68  | 2.00  | 0.36  | 9.20  | 9.51  |
| Max    | 10.5  | 197  | 10.9  | 48.8  | 28.9  | 249   | 0.44  | 7.90  | 12.0  | 3.60  | 30.5  | 45.3  |
|        | Zn1   | Zn2  | Zn3   | Zn4   | Zn5   | Zns   | Co1   | Co2   | Co3   | Co4   | Co5   | Cos   |
| Mean   | 16.9  | 148  | 31.7  | 20.0  | 60.1  | 277   | 0.15  | 4.35  | 2.15  | 0.94  | 5.84  | 13.4  |
| Median | 6.80  | 98.0 | 27.0  | 15.8  | 58.2  | 242   | 0.11  | 4.90  | 1.80  | 0.88  | 5.60  | 13.1  |
| SD     | 27.4  | 158  | 21.0  | 13.1  | 17.2  | 213   | 0.15  | 3.00  | 1.29  | 0.84  | 1.61  | 3.89  |
| Min    | 1.10  | 8.57 | 6.10  | 5.50  | 19.6  | 46.4  | 0.03  | <DL   | 0.70  | <DL   | 2.40  | 3.67  |
| Max    | 123   | 675  | 97.7  | 50.3  | 95.2  | 1003  | 0.87  | 10.5  | 5.80  | 3.30  | 9.00  | 20.4  |

\* Explanation: 1-exchangeable fraction; 2-easily reducible fraction; 3-moderately reducible fraction; 4-oxidizable fraction; 5-residual fraction, s-sum extracted elements from 1 to 5 fractions.



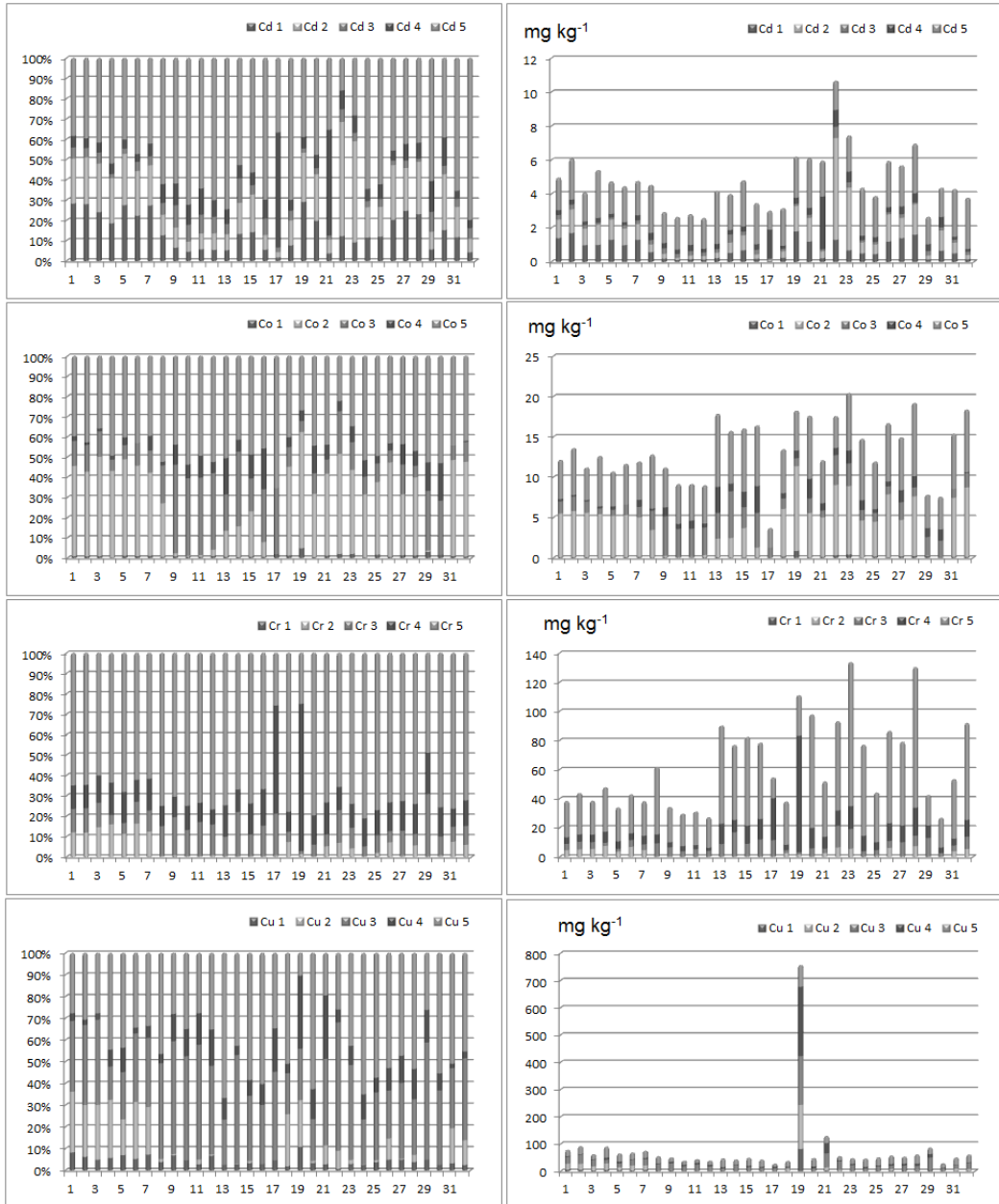


Figure 2. Distribution of Cd, Co, Cr, and Cu by fractions and by localities, shown as a percentage and content in  $\text{mg kg}^{-1}$ .

The mobility and immobility of heavy metals along with their availability in soil and sediment largely depend on their types of binding forms. The mobility and availability of the metals decrease in the order of acid soluble forms > reducible forms > oxidisable forms > residual forms. In such a situation, the first two fractions (acid soluble and reducible) constitute a more available form of the metals. Similarly, the last two fractions (oxidisable and residual) form a less available pool.

### 3.1.1. Copper

Copper is a very important element, which could influence the metabolism of the human body and it is also a nutritional element for living beings (Mingbiao et al. 2008). In the studied sediments, copper was in range 26.0 to 755 mg kg<sup>-1</sup>, with a mean content of 78.6 mg kg<sup>-1</sup>. The total content of extracted copper was the highest in the sediments from Pek river (above 700 mg kg<sup>-1</sup>). High content of Cu was also observed in Porečka river (above 100 mg kg<sup>-1</sup>). For other sediments, copper not shows significant variation in content. Average distribution by fractions of copper was: V ≈ III > IV ≈ II > I. The highest content of copper was extracted in the fifth and third fractions, indicating significance of iron oxides in bounding of this element. This suggests that Cu in the selected sediments is associated mainly with primary minerals (residual and crystalline fractions) and their weather products (poorly crystalline Fe oxides and easily reducible Mn oxide fractions) (Silveira et al. 2006). Some of copper was also bounded to organic matter, which is consistent with the results (Li et al. 2001). The mean percentage of the exchangeable, the most available fraction was only 6%. This result is in agreement with observations of Mingbiao et al. (2008). In samples from river Tisa it can be observed the significance of mobile fractions of Mn and Fe oxides in Cu bounding, as well as for sediments from Tamiš and Pek (18 and 19 samples). Elevated levels of copper in Tamiš river are shown in Lujčić et al. (2013). The source of the Pek River is near to Majdanpek, and since there is a Cu mine in Majdanpek, it is justifiable to assume that the origin of the Cu is associated with the existence of this mine (Sakan et al. 2011).

### 3.1.2. Cadmium

Cadmium levels in the sediment vary widely, from 2.57 to 10.6 mg kg<sup>-1</sup> and average value of 4.70 mg kg<sup>-1</sup>. The highest value was observed at the Ibar river (samples 22 and 23). Cadmium probably has the largest number of possible anthropogenic inputs of metals investigated, such as following: industry, transport, agriculture, waste management and electricity production (Kastratović et al. 2016). Average distribution by fractions of cadmium was: V > II > I > IV > III. In general, percent of extracted cadmium in more mobile fractions (I and II) was about 40, but in some sediments, percent of extracted Cd was about 60 (river Ibar, samples 22 and 23). The mean percentage of Cd in the stable, residual fraction (V) was, in general about 50%. Cadmium bound to residual fraction is “unreactive,” but cadmium bound to reducible Mn and amorphous/crystalline Fe oxides can eventually become available under redox conditions.

### 3.1.3. Cobalt

The minimum and maximum values of cobalt were 3.67-20.4 mg kg<sup>-1</sup> in the sediments, with an average content of 13.4 mg kg<sup>-1</sup>. The content of cobalt was higher than 15 mg kg<sup>-1</sup> in sediments from Sava, PEK, Kolubara, Ibar, Great and West Morava

and Toplica. As shown in Baralkiewicz and Siepak (1999), the occurrence of cobalt in soils is to a large extent determined by bedrock.

The average distribution by fractions of cobalt in the studied sediments was: V > II > III > IV > I. This result is in accordance with the result of Baralkiewicz and Siepak (1999) that cobalt is combines with the hydroxides of iron and manganese as well as silty minerals. The amount of cobalt bound to residual and Fe-Mn oxides was relatively high. For most of the river it was observed higher content of cobalt which is bounded to mobile fraction of Fe-Mn oxides (II fraction). Only for sediments from Danube and Nišava it was observed higher content of cobalt bounded to amorphous and partially crystalline Fe-oxide (III fraction) with respect to II fraction. Only 1% of cobalt was extracted in the first step, indicating low mobility of this element. Some of cobalt was extracted in the organic matter–sulfides fraction.

#### **3.1.4. Lead**

The range for the content of lead was between 4.44 to 249 mg kg<sup>-1</sup>, with a mean value of 48.0 mg kg<sup>-1</sup>. The highest total content of lead was recorded at the locations of the river Ibar. These results revealed the existence of local anthropogenic sources that contribute to the enrichment of lead in the quoted river sediments. Average distribution by fractions of lead in the studied sediments was: II > IV > III ≈ V ≈ I. In accordance with the distribution by fractions, it is possible to conclude that the most significant fraction binding of lead in the studied sediments is easily reducible fraction. This result is consistent with results of the other authors (Li et al. 2001; Ip et al. 2007; Mingbiao et al. 2008) that lead which is reducible in non-resident factions often dominates in sediments, due to the fact that lead can form stable complexes with iron (III, IV) and manganese (IV) oxides. Organic fraction is also significant in lead bounding in some of sediment samples (Danube, Sava, etc). Similar percent of bounded lead in organic fraction is also shown in results Yobouet et al. (2010) and Kastratović et al. (2016). Content of lead extracted in III, IV and I fractions was very low.

#### **3.1.5. Nickel**

The range for the content of nickel was between 25.2 and 260 mg kg<sup>-1</sup>. The mean total content of nickel was 83.2 mg kg<sup>-1</sup>. In some localities, significantly higher contents of nickel were found in comparison to other sites: Ibar, Sava, Kolubara, Topčiderska river, Great and West Morava, Toplica and one sample from Danube. Average distribution by fractions of nickel in the studied sediments was: V > IV ≈ II ≈ III > I. Obtained results is similar to those found in Relić et al. (2005), that the highest proportion of nickel is in residual fraction. Similar percent of extracted nickel is noticed in oxidizable, reducible and moderately reducible fraction. Content of nickel extracted in I fractions was very low. The same distribution by fraction has been demonstrated in the

Mingbiao et al. (2008) for the branch sediments of Poyang Lake. As shown in Mingbiao et al. (2008), the low percentage active fraction was an advantage, to control the pollution in studied area.

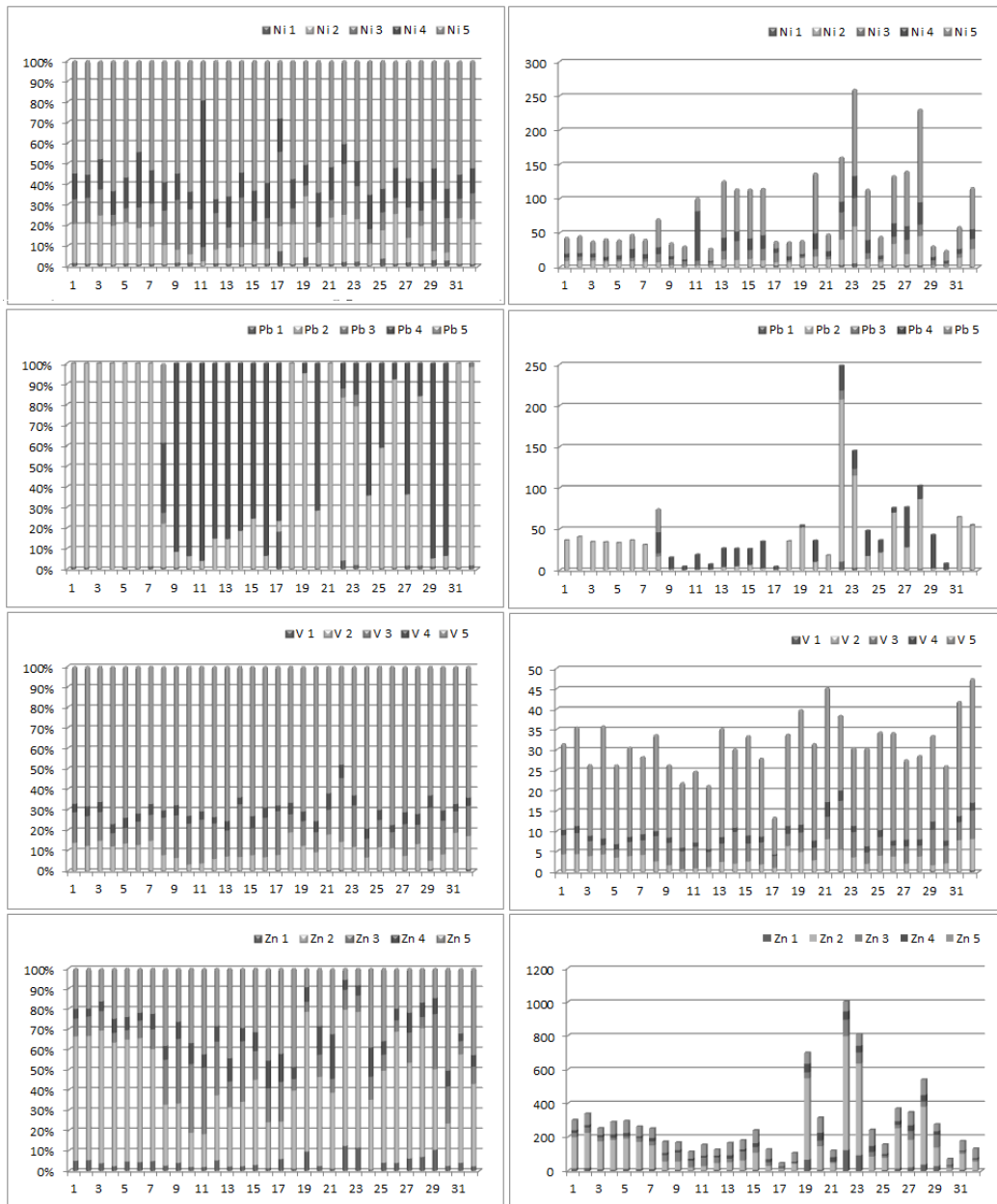


Figure 3. Distribution of Ni, Pb, V, and Zn by fractions and by localities, shown as a percentage and content in  $\text{mg kg}^{-1}$ .

### 3.1.6. Chromium

The variable total Cr content were found in the sediments (ranging from 26.7 to 134 mg kg<sup>-1</sup>, mean 62.5 mg kg<sup>-1</sup>). Average distribution by fractions of chromium in the studied sediments was: V > IV > III > II > I. Chromium content in easily available fraction at all locations was either not recorded or only an insignificant amount of bioavailable chromium was recorded. The residual fraction (associated with Fe oxides and residual pools) was generally most important in retaining this element.

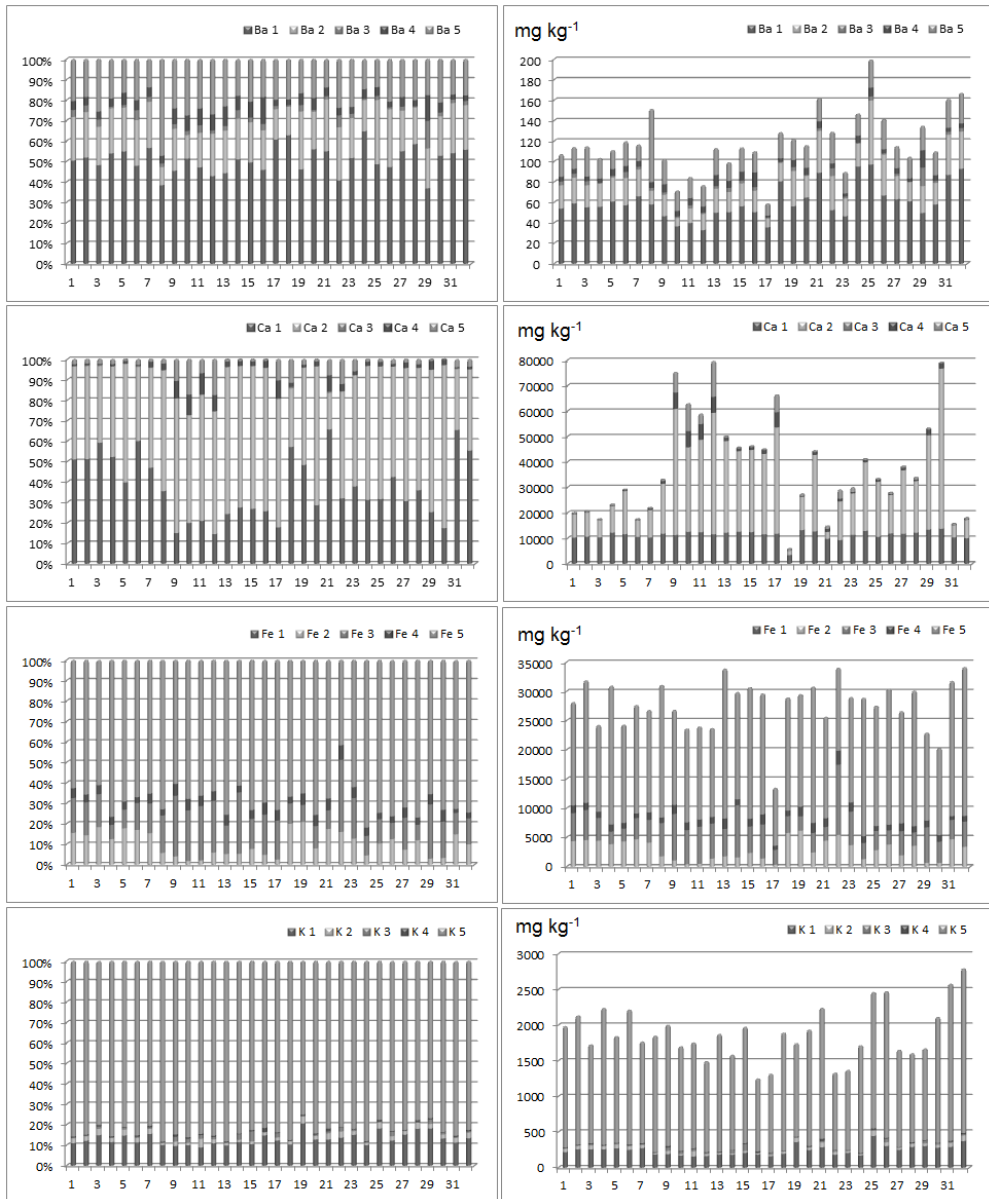


Figure 4. Distribution of Ba, Ca, Fe, and K by fractions and by localities, shown as a percentage and content in mg kg<sup>-1</sup>.

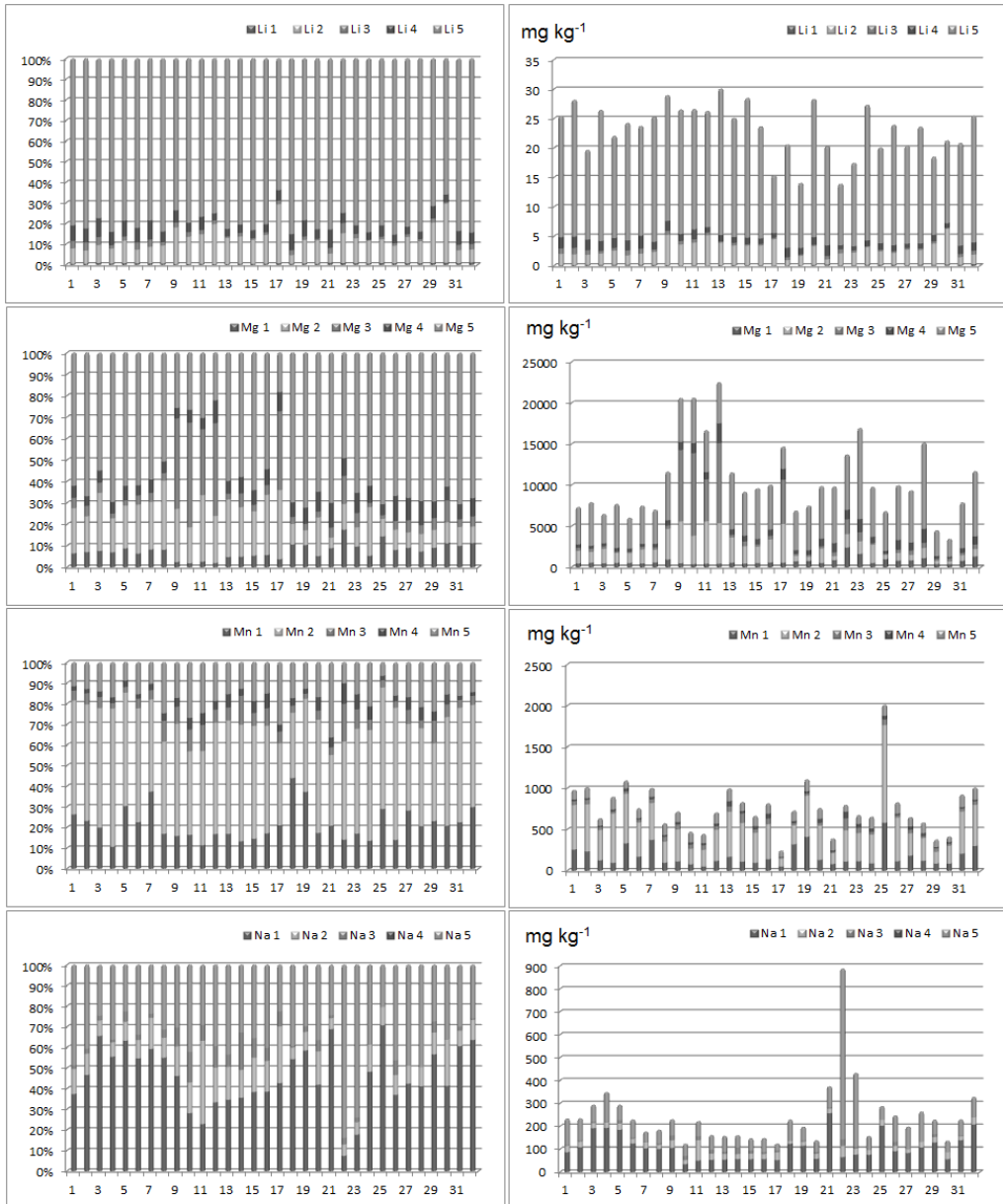


Figure 5. Distribution of Li, Mg, Mn, and Na by fractions and by localities, shown as a percentage and content in  $\text{mg kg}^{-1}$ .

Chromium bound to residual fraction is often considered “unreactive” and not affected by environmental changes. The high content of chromium is also bound in the oxidizable fraction, which is result of the stronger adsorption ability of chromium to organic matter than to the iron and manganese oxyhydroxides. A similar distribution of chromium by fractions was also observed in the manuscript *Kastratović et al. (2016)* and *Davison et al. (1998)*. The highest content of chromium is extracted from samples 23

(Ibar) and 28 (West Morava). The high concentrations of chromium in the sediments are often of geological origin and are not related to anthropogenic pollution.

### **3.1.7. Vanadium**

The range of vanadium in the studied river sediments is 9.51 to 45.3 mg kg<sup>-1</sup>, and the average value is 30.3 mg kg<sup>-1</sup>. The highest content of vanadium was found at the localities of South Morava (31) and Toplica (32), the lowest content in DTD canal (17), while in other places, its content is relatively uniform. Average distribution by fractions of vanadium in the river sediments was: V > III > II > IV > I. The highest content of vanadium was associated with the residual and oxide fraction.

### **3.1.8. Zinc**

The zinc total content in sediments was particularly variable (46.4-1003 mg kg<sup>-1</sup>, mean 277 mg kg<sup>-1</sup>). The highest content of zinc was observed in the sediment form Ibar (22 and 23), Pek (19) and West Morava (28). Average distribution by fractions of zinc in the river sediments was: II > V > IV > III > I. The highest content of zinc was extracted in easily reducible fraction, which indicates that this element is mainly associated with easily reducible Mn and Fe oxide fractions. This result is in agreement with the fact that non-residual Zn is mostly concentrated in the Fe-Mn oxides (Li et al. 2000). The Zn adsorption onto Fe-Mn oxides has higher stability constants than onto carbonates (Li et al. 2000). The exchangeable Zn was very low in studied sediments.

The highest amount of manganese (about 50%) is in reducible fraction (Figure 6), with a lower content in exchangeable and residual fractions. The largest amount of iron in the sediments is in the residual fraction (about 70%), followed by moderately and easily reducible fractions, indicating existence of Fe in surface sediments predominantly as crystalline Fe oxides. Extracted barium, sodium, lithium and potassium from studied sediments originate mainly from silicate minerals. Dominate extraction of barium in the first fraction (about 50%) indicate on existence of water-soluble and exchangeable form of Ba, i.e., available Ba as a significant form of Ba in the studied sediments. Ca is in studied river sediments represented mainly carbonates, since this element extracted dominantly in the second fraction. Magnesium is originated mainly from silicates and carbonates, since this element in higher content was extracted in the fifth and second fraction.

Heavy metals in uncontaminated soils and sediments are mainly immobile as they are bound to silicates and to primary minerals. Therefore, heavy metals in contaminated sediments are more mobile and bound to other phases (Sungur et al. 2014). Considering the extractable rates of heavy metals, it was determined that mobile fractions of Mn, Zn and Pb are higher than immobile fractions and it was concluded that human-induced effects may be a factor that can cause contamination. Since that about 20% of Cd is bound to reducible Mn and amorphous/crystalline Fe oxides, it can eventually become

available under redox conditions. It is necessary to point out that about 16% of Cd is extracted in the exchangeable, easily soluble fraction. Cu, Co, Ni, Cr and V is mainly bound to residual fraction and may be considered as “unreactive” and not affected environmental changes.

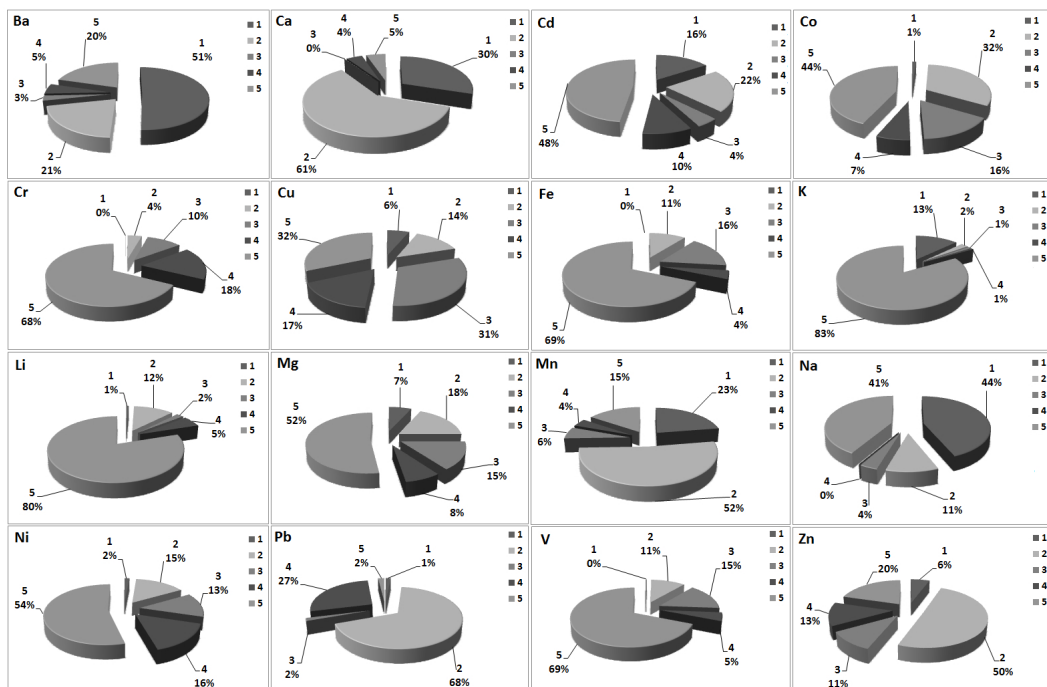


Figure 6. Average percentage distribution of studied elements by fractions.

### 3.2. Statistical Analyses

Figures 7 and 8 show the HCA results (R and Q mode) for the elements as a dendrogram in the study area.

The R mode of HCA (Figure 7) showed that the investigated elements were classified into 3 clusters: (1) Pb, Zn, and Cd; cluster (2) is consisting from two subclusters: 2a) Cr and Ni, and 2b) Fe and Co; and (3) Cu. Strong similarity between Pb, Zn, and Cd indicated strong anthropogenic input, since these elements are considered as toxic metals. Elements from cluster 2 have mixed sources, but mainly derived from natural sources, natural parent material; Cr and Ni have geological similarities, and Co and Fe also. Cr and Ni were derived from natural geological sources and generally present in the residual fractions.

At some localities, it is evident existence of anthropogenic sources of Ni. Iron is known as an Earth element in analysis. Oxides of Fe are significant substrate for cobalt in the environment (coprecipitation and adsorption on Fe and Mn oxides). Cu was isolated



from the other elements, which is indicative of lack of association with the other elements, as well as different origin of Cu, mainly from mining activities. In general, it can be concluded that heavy metal contamination originated from multiple emission sources in the studied sediments.

Cluster analysis (Q mode) was used to identify similarity between the sampling sites. The Figure 8 shows 3 clusters: (1) cluster including three subclusters: 1a) sediments from Tisa (1-7), Nišava (29), Great Morava (26 and 27), and Kolubara (20); 1b) sediments from Sava (13-16), Danube (8-12), Topčiderska river (24), Tamiš (18), Nišava (30), South Morava (25 and 31), Toplica (32), DTD canal (17) and Porečka river (21) and 1c) West Morava (28); (2) Ibar (22 and 23) and (3) Pek (19). Clusters 2 and 3 consist of sediments with higher content of toxic elements. These sediments originated from the river systems most polluted with heavy metal in Serbia: the Ibar and Pek. Another sediment sample group (Cluster 1) constitutes sediments from the major river systems: the Tisa, Sava, and Danube, along with the sediments from smaller rivers that have a higher content some of the elements as in the major rivers. The sample of Great Morava (28) makes a separate subcluster ((1c), Figure 8), as a result of large content of some elements (Ni, Zn, and Cd) in sediments.

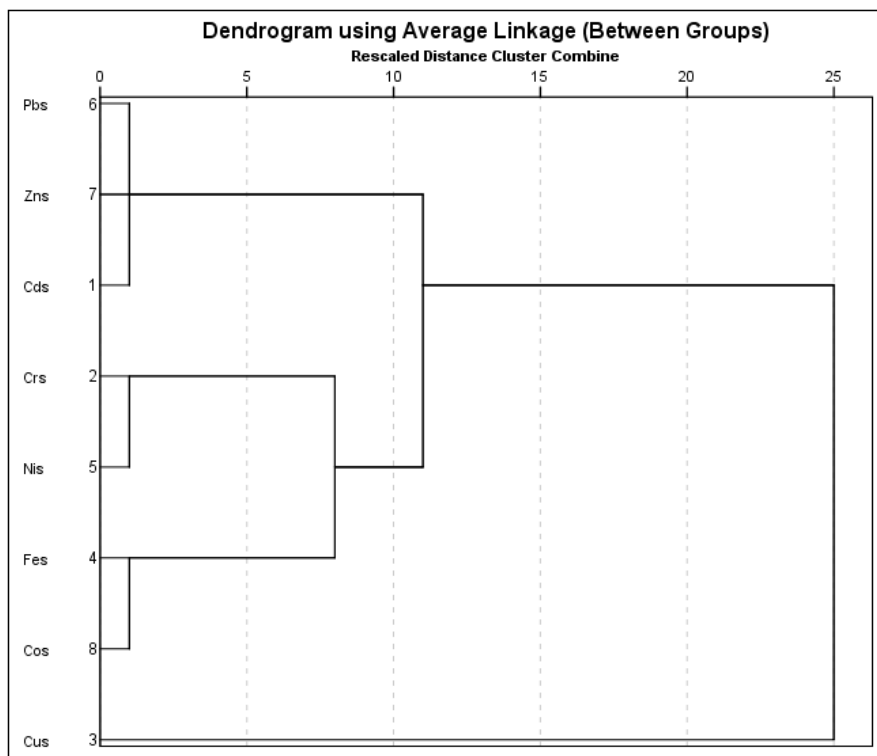


Figure 7. Dendrogram obtained by HCA (Hierarchical cluster analysis) for total sequentially extractable amount of elements in sediments (R mode).

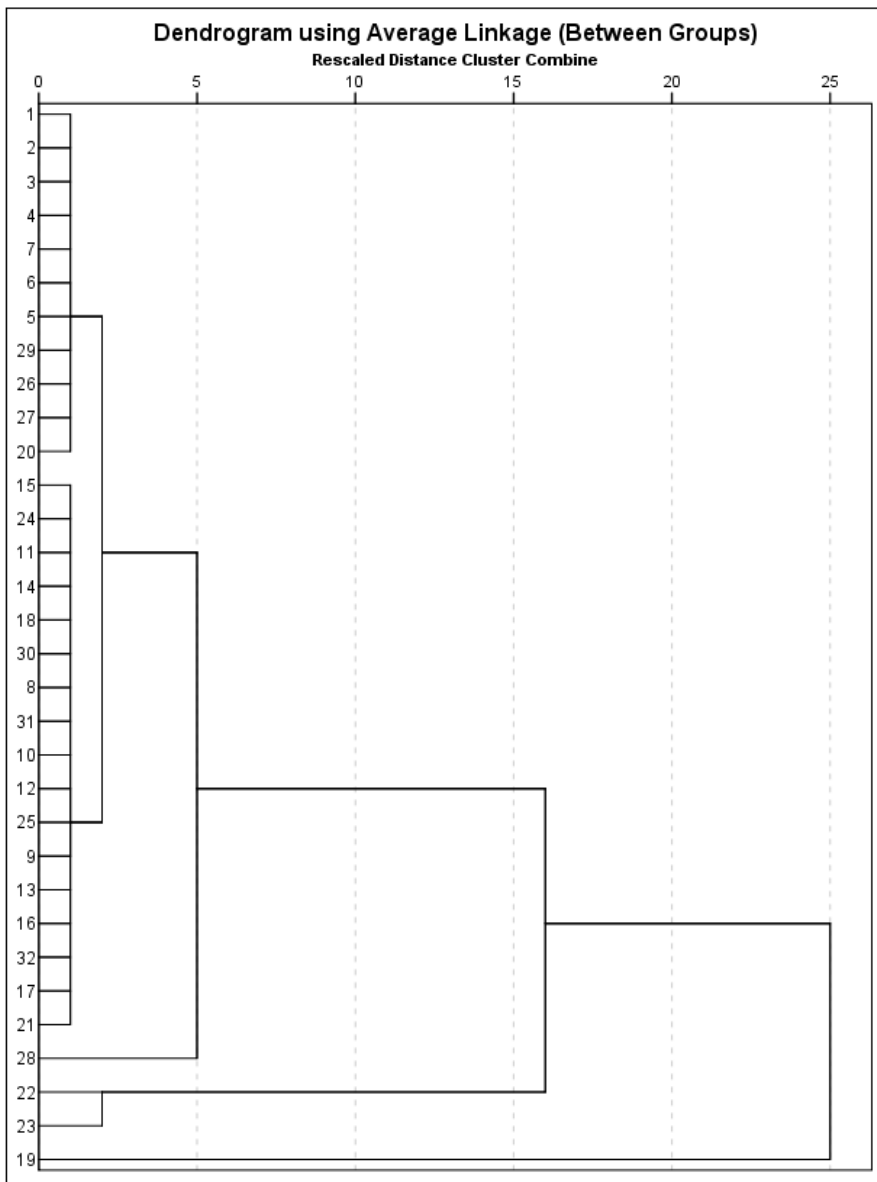


Figure 8. Dendrogram obtained by HCA (Hierarchical cluster analysis) for total sequentially extractable amount of elements in sediments (Q mode).

### 3.3. The Hazard Quotients (HQ)

HQ values calculated from the metal contents in the selected sediments range from 2.14 to 8.88 for Cd, 0.33 to 1.65 for Cr, 0.76 to 22.21 for Cu, 1.2 to 12.44 for Ni, 0.10 to 5.33 for Pb and 0.31 to 6.69 for Zn (Figure 9).

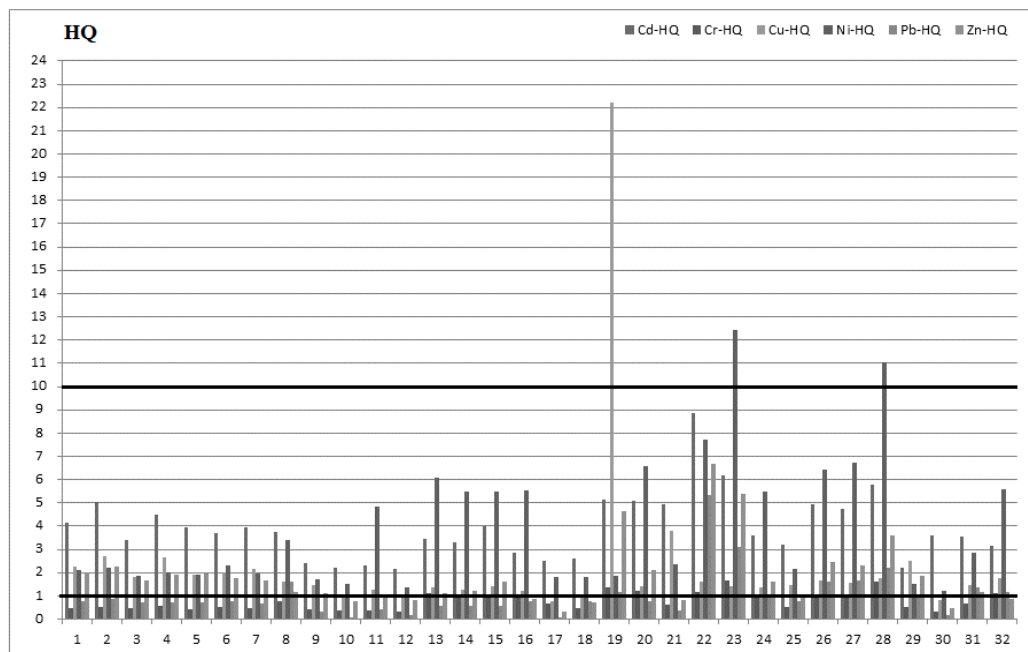


Figure 9. Hazard quotients (HQ) of the chemical contaminants (Cd, Cr, Cu, Ni, Pb, and Zn).

In general, all the heavy metals (Cd, Cr, Cu, Ni, Pb, and Zn) might cause potential hazard effects or moderate hazard effect in the present study area. For Cu and Ni, high hazard potential is anticipated. Copper and nickel were of environmental concern because the HQ values of them indicated that these two metals might result in adverse biological effects in the rivers. The rivers with high HQ values are Pek (19): Cu, Cd, and Zn; Ibar (22 and 23): Cd, Ni, Pb, and Zn; and West Morava (28): Cd, Ni, and Zn. These results suggested that the urban and industrial activities have made great contributions to heavy metal inputs.

## CONCLUSION

An overall and comparative ecological risk assessment of heavy metal pollution in surface sediments was conducted in Serbian rivers. The results show that the sediments in the studied river sediments have been polluted by toxic elements, posing certain ecological risks to the benthic community. In general, all the heavy metals (Cd, Cr, Cu, Ni, Pb, and Zn) might cause potential hazard effects or moderate hazard effect in the present river systems.

Sequential fractionation provides valuable information about the potential mobility of elements. Considering the extractable rates of heavy metals, it could be concluded that mobile fractions of Mn, Zn, Pb and Cd are higher than immobile fractions and it could be

supposed that human-induced effects may be a factor that can cause contamination. The Cu, Co, Ni, Cr and V is mainly bound to residual fraction and crystalline oxides, that indicates on dominate geochemical origin, and may be considered as “unreactive” phase and cannot be affected by the environmental changes.

This study presents the importance of applying sequential extraction, hazard quotients and Cluster analysis methods for the evaluation of sediment contamination with trace metallic and metalloid elements and the determination the origin and mobility of these contaminants in the sediments. Sequential extraction procedure can provide useful information for planning and management of polluted soils and sediments.

### ACKNOWLEDGMENTS

This chapter was supported by the Ministry of Education, Science and Technological Development of Serbia, Grant Nos. 172001 and 43007. In addition, we would like to thank the Republic Hydrometeorological Service of Serbia for the sediment samples.

### REFERENCES

- Adriano, D. C., Németh, T., Györi, Z. (2003). Assessment of heavy metal enrichment factors and the degree of contamination in marine sediment from Tamaki Estuary, Auckland, New Zeland. *Environmental Monitoring and Assessment*, 136, 227-238.
- Barańkiewicz, D., Siepak, J. (1999). Chromium, nickel and cobalt in environmental samples and existing legal norms. *Polish Journal of Environmental Studies*, 4, 201–208.
- Chabuhdhara, M., Nema, A. (2012). Assessment of heavy metal contamination in Hindon River sediments: A chemometric and geochemical approach. *Chemosphere*, 87, 945–953.
- Daesslé, L. W., Lugo-Ibarra, K. C., Tobschall, H. J., Melo, M., Gutiérrez-Galindo, E. A., García-Hernández, J., Álvarez, L. G. (2009). Accumulation of As, Pb, and Cu associated with the recent sedimentary processes in the Colorado Delta, South of the United States-Mexico boundary. *Archives of Environmental Contamination and Toxicology*, 56, 680-692.
- Davidson, C. M., Duncan, A. L., Litteljohn, D., Ure, A. M., Garden, L. M. (1998). A critical evaluation of the three stage BCR sequential extraction procedure to assess the potential mobility and toxicity of heavy metals in industriallycontaminated land. *Analytica Chimica Acta*, 363, 45–55.

- Egiarte, G., Corti, G., Pinto, M., Arostegui, J., Macías, F., Ruíz-Romero, E., Camps Arbustain, M. (2009). Fractionation of Cu, Pb, Cr, and Zn in a Soil Column Amended with an Anaerobic Municipal Sewage Sludge. *Water, Air, and Soil Pollution*, 198 (1), 133-148.
- Facchinelli, A., Sacchi, E., Mallen, L. (2001). Multivariate statistical and GIS-based approach to identify heavy metal sources in soils. *Environmental Pollution*, 114, 313-324.
- Farkas, A., Erratico, C., Viganó, L. (2007). Assessment of the environmental significance of heavy metal pollution in surficial sediments of the River Po. *Chemosphere*, 68, 761-768.
- Feng, H., Jiang, H., Gao, W., Weinstein, M. P., Zhang, Q., Zhang, W., Yu, L. Yuan, D., Tao, J. (2011). Metal contamination in sediments of the western Bohai Bay and adjacent estuaries, China. *Journal of Environmental Management*, 92, 1185-1197.
- Ip, C. C. M., Li, X. D., Zhang, G., Wai, O. W. H., Li, Y. S. (2007). Trace metal distribution in sediments of the Pearl River estuary and the surrounding coastal area, South China. *Environmental Pollution*, 147, 311-323.
- Kastratović, V., Jaćimović, Ž., Bigović, M., Đurović, D., Krivokapić, S. (2016). Environmental Status and geochemical assessment Sediments of Lake Skadar, Montenegro. *Environmental Monitoring and Assessment*, 188, 449.
- Li, X., Thornton, I. (2001). Chemical partitioning of trace and major elements in soils contaminated by mining and smelting activities. *Applied Geochemistry*, 16, 1693-1706.
- Li, X., Shen, Z., Wai, O. W. H., Li, Y. (2000). Chemical partitioning of heavy metal contaminants in sediments of the Pearl River Estuary. *Chemical Speciation & Bioavailability*, 12(1), 17-25.
- Li, X., Shen, Z. G., Wai, O. W. H., Li, Y. (2001). Chemical forms of Pb, Zn and Cu in the sediment profiles of the Pearl River estuary. *Marine Pollution Bulletin*, 42, 215-223.
- Long, E. R., MacDonald, D. D., Smith, S. L., Calder, F. D. (1995). Incidence of adverse biological effects within ranges of chemical concentrations in marine and estuarine sediments. *Environmental Management*, 19, 81-97.
- Lujčić, J., Marinović, Z., Miljanović, B. (2013). Histological analysis of fish gills as an indicator of water pollution in the Tamiš River. *Acta Agriculturae Serbica*, 18 (36), 133-1411.
- Mil-Homens, M., Branco, V., Lopez, C., Vale, C., Abrantes, F., Boer, W., Vicente, M. (2009). Using Factor Analysis to Characterise Historical Trends of Trace Metal Contamination in a Sediment Core from the Tagus Prodelta, Portugal. *Water, Air, and Soil Pollution*, 197 (1), 277-287.

- Mingbiao, L., Jianqiang, L., Weipeng, C., Maolan, W. (2008). Study of heavy metal speciation in branch sediments of Poyang Lake. *Journal of Environmental Sciences*, 20, 161-166.
- Nguyen, H. L., Braun, M., Szaloki, I., Baeyens, W., Van Grieken, R., Leermakers, M. (2009). Tracing the Metal Pollution History of the Tisza River through the Analysis of a Sediment Depth Profile. *Water, Air, and Soil Pollution*, 200 (1), 119-132.
- Polić, P., Pfenndt, P. (1992). Iron and manganese oxides as dominant nickel substrates in the Novi Beograd aquifer. *Journal of the Serbian Chemical Society*, 57, 697-703.
- Prica, M., Dalmacija, B., Rončević, S., Krčmar, D., Bečelić, M. (2008). A comparison of sediment quality results with volatile sulphide (AVS) and simultaneously extracted metals (SEM) ratio in Vojvodina (Serbia) sediments. *Science of the Total Environment*, 389, 235-244.
- Qian, Y., Zhang, W., Yu, L., Feng, H. (2015). Metal pollution in coastal sediments. *Current Pollution Reports*, 1, 203-219.
- Rao, C. R. M., Sahuquillo, A., Lopez-Sanchez, J. F. (2010). Comparison of single and sequential extraction procedures for the study of rare earth elements remobilization in different types of soils. *Analytical Chimica Acta*, 662, 128-146.
- Relić, D., Đorđević, D., Popović, A., Blagojević, T. (2005). Speciations of trace metals in the Danube alluvial sediments within an oil refinery. *Environment International*, 31, 661-669.
- Relić, D., Đorđević, D., Sakan, S., Anđelković, I., Pantelić, A., Stanković, R., Popović, A. (2013). Conventional, microwave, and ultrasound sequential extractions for the fractionation of metals in sediments within the Petrochemical Industry, Serbia. *Environmental Monitoring and Assessment*, 185, 7627-7645.
- Sakan, S., Gržetić, I., Đorđević, D. (2007). Distribution and fractionation of heavy metals in the Tisa (Tisza) river sediments. *Environmental Science and Pollution Research*, 14, 229-236.
- Sakan, S., Đorđević, D., Manojlović, D., Polić, P. (2009). Assessment of heavy metal pollutants accumulation in the Tisza river sediments. *Journal of Environmental Management*, 90, 3382-3390.
- Sakan, S., Đorđević, D., Dević, G., Relić, D., Anđelković, I., Đurićoč, J. (2011). A study of trace element contamination in river sediments in Serbia using microwave-assisted aqua regia digestion and multivariate statistical analysis. *Microchemical Journal*, 99, 492-502.
- Sakan, S., Popović, A., Anđelković, I., Đorđević, D. (2016). Aquatic sediments pollution estimate using the metal fractionation, secondary phase enrichment factor calculation, and used statistical methods. *Environmental Geochemistry and Health*, 38, 855-867.
- Salomons, W., Förstner, U. (1980). Trace metal analysis on polluted sediments. Part II: Evaluation on Environmental Impact. *Environmental Technology Letters*, 1, 506-517.

- Sierra, C., Ruíz-Barzola, O., Menéndez, M., Demey, J. R., Vicente-Villardón, J. L. (2017). Geochemical interactions study in surface river sediments at an artisanal mining area by means of Canonical (MANOVA)-Biplot. *Journal of Geochemical Exploration* 175, 72–81.
- Silveira, M. L., Alleoni, L. R. F., O'Connor, G. A., Chang, A. C. (2006). Heavy metal sequential extraction methods - A modification for tropical soils. *Chemosphere*, 64, 1929-1938.
- Sungur, A., Soyak, M., Ozcan, H. (2014). Investigation of heavy metal mobility and availability by the BCR sequential extraction procedure: relationship between soil properties and heavy metals availability. *Chemical Speciation & Bioavailability*, 26 (4), 219-230.
- Sutherland, R. A. (2010). BCR-701: A review of 10-years of sequential extraction analyses. *Analytica Chimica Acta*, 680, 10-20.
- Tessier, A., Campbell, P. G. C., Bisson, M. (1979). Sequential Extraction Procedure for the Speciation of Particulate Trace Metals. *Analytical Chemistry*, 51 (7), 844-851.
- Tockner, K., Robinson, C., Uehlinger, U. (2009). *Rivers of Europe*. = Academic Press.
- Wang, H., Wang, J., Liu, R., Yu, W., Shen, Z. (2015). Spatial variation, environmental risk and biological hazard assessment of heavy metals in surface sediments of the Yangtze River estuary. *Marine Pollution Bulletin* 93, 250–258.
- Widmeyer, J. R., Bendell-Young, L. I., (2008). Heavy metal levels in suspended sediments, Crassostrea gigas, and the risk to humans. *Archives of Environmental Contamination and Toxicology*, 55 (3), 442-450.
- Yi, Y., Yang, Y., Zhang S. (2011). Ecological risk assessment of heavy metals in sediment and human health risk assessment of heavy metals in fishes in the middle and lower reaches of the Yangtze River basin. *Environmental Pollution*, 159, 2575-2585.
- Yobouet, Y. A., Adouby, K., Trokourey, A., Yao, B. (2010). Cadmium, copper, lead and zinc speciation in contaminated soils. *International Journal of Engineering, Science and Technology*, 2, 802–812.

Ненад Сакан

**ФИЗИЧКЕ  
МЕТОДЕ  
МЈЕРЕЊА**

nubl 



Доц. др Ненад М. Сакан,  
ФИЗИЧКЕ МЕТОДЕ МЕРЕЊА

Издавач  
НУБЛ - Независни Универзитет Бања Лука

За издавача  
Горан Калинић, директор Независног Универзитета Бања Лука

Рецензенти

Др Зоран Симић  
Виши научни сарадник Астрономске Опсерваторије у Београду

Ма Немања Ракић  
Виши асистент Природно-математичког факултета  
Универзитета у Бањој Луци

Уредник  
Проф. др Милован Милутиновић

Лектор  
Доц. др Обрад Лукић

Штампарија ГРАФИД Бања Лука

За штампарију:  
Бранислав Иванковић  
Забрањено копирање у целости или по деловима без сагласности  
аутора.

Тираж: 100 примерака. Електронска верзија

ФИЗ



## ФИЗИЧКЕ МЕТОДЕ МЕРЕЊА

Ненад М. Сакан

НУБЛ  
Бања Лука 2019.

# Садржај

|   |    |
|---|----|
| Увод  | v  |
| 1 Физика и наше знање о свету око нас   | 1  |
| 1.1 Експеримент и теорија . . . . .   | 2  |
| 1.2 Математика, моћ бројева . . . . .   | 3  |
| 1.3 Теорија, физички закони . . . . .   | 4  |
| 1.4 Мерење, бројеви и теорија . . . . .   | 6  |
| 1.5 Методологија истраживања . . . . .  | 10 |
| 1.6 Типови експеримента . . . . .   | 10 |
| 1.7 Фазе експеримента . . . . .   | 11 |
| 1.8 Класификација мерења . . . . .  | 12 |
| 1.9 Калибрација мерних инструмената . . . . .   | 14 |
| 1.10 Калибрација мерне методе . . . . .   | 16 |
| 1.11 Реални мерни инструмент, особине . . . . .                                       | 17 |
| 1.12 Шум . . . . .  | 17 |
| 1.13 Амперметар и волтметар . . . . .   | 23 |
| 1.14 Особине мерних инструмената . . . . .  | 25 |
| 1.14.1 Кратак поглед на динамичке карактеристике<br>инструмента . . . . .             | 32 |
| 1.15 Грешке инструмента и методе мерења, пример ме-<br>рења струје и напона . . . . . | 36 |
| 2 Резултати мерења  | 41 |
| 2.1 Представљање резултата мерења . . . . .   | 41 |

|       |   |     |
|-------|---|-----|
| 2.2   | Зашто се јављају експерименталне грешке? . . . . .  | 43  |
| 2.3   | Врсте експерименталних грешака . . . . .            | 43  |
| 2.4   | Директно мерена величина . . . . .                  | 46  |
| 2.5   | Индиректно мерена величина . . . . .                | 55  |
| 2.6   | Графичко представљање . . . . .                     | 58  |
| 3     | Модерно доба у мерењу и обради резултата . . . . .  | 63  |
| 3.1   | Рачунар у експерименту . . . . .                    | 63  |
| 3.1.1 | Рачунар и његова веза са спољашњим светом . . . . . | 64  |
| 3.1.2 | Рачунар и мерење . . . . .                          | 64  |
| 3.2   | Рачунар у обради података . . . . .                 | 77  |
|       | Крај, или почетак? . . . . .                        | 95  |
|       | Списак слика . . . . .                              | 96  |
|       | Списак табела . . . . .                             | 102 |
|       | Библиографија . . . . .                             | 104 |

## УВОД

Свако своје  
уствајање про  
стављања резу  
шкама. Вели  
зани је био п  
"Обрада резу  
обједињује ве  
знања, тако  
зултата мере  
у [2], као и р  
ресовање за  
општу тако  
живања, [5].

Сва истра  
цес мерења.  
било да се р  
рије, о скупљ  
са циљем про  
жењу које см  
у индустрији  
само врх лед  
пљених пода  
ректно видљ  
се упознају с  
састоји од пр



## Библиографија

- [1] Иван Аничин. "Обрада резултата мерења". Физички факултет, Универзитета у Београду, 1990.
- [2] Tetsuya Saito Leslie Smith (eds.) Horst Czichos Prof. (auth.), Prof. Horst Czichos Prof. Springer Handbook of Metrology and Testing. Springer Handbooks. Springer-Verlag Berlin Heidelberg, 2 edition, 2011.
- [3] В.В.Лебедев. О.Н.Кассандрова. Обработка результатов наблюдений. Наука. Главная редакция физико-математической литературы, 1970.
- [4] Щиголев Б.М. Математическая обработка наблюдений. Гос. изд-во физ.-мат. литературы, 1962.
- [5] ASQ Measurement Quality Division and Editor Jay L. Bucher PhD. The Metrology Handbook, 2nd Edition (With CD-ROM). Pearson, nov 2019.
- [6] Третьяк. Обработка результатов наблюдений. 2004.
- [7] F. Pavese G. B. Rossi P. Ciarlini, M. G. Cox. Advanced Mathematical and Computational Tools in Metrology VI. Series on Advances in Mathematics for Applied Sciences. World Scientific Publishing Company, 2004.
- [8] Toru Yoshizawa (editor). Handbook of optical metrology: principles and applications. CRC Press, 1 edition, 2009.

- [9] An Important Question in Metrology, Based Upon Recent and Original Discoveries. Wentworth Press, mar 2019.
- [10] Rene Schodel. Modern Interferometry for Length Metrology: Exploring Limits and Novel Techniques (IPH001). IOP Publishing Ltd, mar 2019.
- [11] Momčilo Sakan. "Metodologija nauke". NUBL, Banja Luka, 2008.
- [12] Karl Popper. The Logic of Scientific Discovery (Routledge Classics). Routledge, nov 2019.
- [13] Alper Demir. Analysis and Simulation of Noise in Nonlinear Electronic Circuits and Systems (The Springer International Series in Engineering and Computer Science). Springer, nov 1997.
- [14] F. N. H Robinson. Noise Fluctuations in Electronic Devices and Circuits. Clarendon Press, nov 1974.
- [15] T. H. Wilmshurst. Signal Recovery from Noise in Electronic Instrumentation, Second Edition. Taylor & Francis, jan 1990.
- [16] Timothy C. Urdan. Statistics in Plain English, Third Edition. Routledge, may 2010.
- [17] Harry L. Van Trees. Radar-Sonar Signal Processing and Gaussian Signals in Noise (Detection, Estimation, and Modulation Theory, Part 3). Krieger Pub Co, jul 1992.
- [18] Elya B. Joffe. Grounds for Grounding: A Circuit to System Handbook. Wiley-IEEE Press, jan 2010.
- [19] Peter Wilson. The Circuit Designer's Companion. Newnes, aug 2017.

- [20] Art Ka  
Analyz
- [21] C. D.  
Wiley-
- [22] H. Mot  
data u  
curve f
- [23] A. Ch  
genera  
the ex  
Associ
- [24] Gnu r
- [25] Thom  
Intern
- [26] Lawre
- [27] M. He  
Spring
- [28] Gnupl
- [29] Philip  
Co., C
- [30] Fityk
- [31] S. Sak  
Geoch  
ecolog  
monte



- [20] Art Kay. Operational Amplifier Noise: Techniques and Tips for Analyzing and Reducing Noise. Newnes, jan 2012.
- [21] C. D. Motchenbacher. Low-Noise Electronic System Design. Wiley-Interscience, jun 1993.
- [22] H. Motulsky and A. Christopoulos. Fitting models to biological data using linear and nonlinear regression: a practical guide to curve fitting. Oxford University Press, Oxford, 2004.
- [23] A. Charnes, E. L. Frome, and P. L. Yu. The equivalence of generalized least squares and maximum likelihood estimates in the exponential family. *Journal of the American Statistical Association*, 71(353):169–171, 1976.
- [24] Gnu r home page <https://www.r-project.org/>.
- [25] Thomas Rahlf. Data Visualisation with R. Springer International Publishing, New York, 2017.
- [26] Lawrence Leemis. Learning Base R. Lightning Source, 2016.
- [27] M. Henry H. Stevens. A Primer of Ecology with R. Use R. Springer, 2009.
- [28] Gnuplot home page <http://www.gnuplot.info/>.
- [29] Philipp K. Janert. Gnuplot in Action. Manning Publications Co., Greenwich, CT, USA, 2nd edition, 2015.
- [30] Fityk home page <https://fityk.nieto.pl/>.
- [31] S. Sakan, N. Sakan, A. Popović, and D. Škrivanj, S. and Đorđević. Geochemical fractionation and assessment of probabilistic ecological risk of potential toxic elements in sediments using monte carlo simulations. *Molecules*, 24:2145, 2019.

- [32] Sanja Sakan, Gordana Dević, Dubravka Relić, Ivan Anđelković, Nenad Sakan, and Dragana Đorđević. Evaluation of sediment contamination with heavy metals: the importance of determining appropriate background content and suitable element for normalization. *Environmental Geochemistry and Health*, 37(1):97–113, Feb 2015.
- [33] Sanja M. Sakan, Gordana J. Dević, Dubravka J. Relić, Ivan B. Anđelković, Nenad M. Sakan, and Dragana S. Đorđević. Environmental assessment of heavy metal pollution in freshwater sediment, serbia. *CLEAN – Soil, Air, Water*, 43(6):838–845, 2015.
- [34] Sanja Sakan, Nenad Sakan, Ivan Anđelković, Snežana Trifunović, and Dragana Đorđević. Study of potential harmful elements (arsenic, mercury and selenium) in surface sediments from serbian rivers and artificial lakes. *Journal of Geochemical Exploration*, 180:24 – 34, 2017.



[14] Saša Šaban, Gorana Đević, Jovanka Petro, Ljiljana Čučević, Nenađ Vukobratović, and Dragana Đorđević. Evolution of environmental contamination with heavy metals: the importance of determining appropriate background values and values limits for environmental. *Environmental Geochemistry and Health*, 2019, 51:111-122, Feb 2019.

[15] Nenađ M. Šaban, Gorana J. Đević, Jovanka J. Petro, Ljiljana Čučević, Nenađ M. Vukobratović, and Dragana S. Đorđević. Environmental assessment of heavy metal pollution in freshwater systems, using CLEAN – 5.4. *Ap. Water Quality*, 2019, 2019.

[16] Saša Šaban, Nenađ Vukobratović, Jovanka Petro, Ljiljana Čučević, and Dragana Đorđević. Study of potential harmful elements (arsenic, mercury and selenium) in surface water from urban river and artificial lake. *Journal of Geographical Exploration*, 1992N = 24, 2017.

CIP - Katalogizacija u publikaciji  
 Narodna i univerzitetska biblioteka  
 Republike Srpske, Baňa Luka

53.08

САКАН, Ненад  
 Физичке методе мерења / Ненад М. Сакан. - Бања Лука :  
 Независни универзитет , 2019 (Бања Лука : Графид). - VI, 108 стр. :  
 илустр. ; 25 cm

Тираж 100. - Библиографија: стр. 105-108.

ISBN 978-99976-43-18-6

## Modeling of continuous absorption of electromagnetic radiation in dense partially ionized plasmas

To cite this article: A A Mihajlov *et al* 2011 *J. Phys. A: Math. Theor.* **44** 095502

View the [article online](#) for updates and enhancements.

### Related content

- [The Calculation of the Photo Absorption Processes in Dense Hydrogen Plasma with the Help of Cut-Off Coulomb Potential Model](#)  
Nenad M Sakan
- [CHEM-IONIZATION IN SOLAR PHOTOSPHERE: INFLUENCE ON THE HYDROGEN ATOM EXCITED STATES POPULATION](#)  
Anatolij A. Mihajlov, Ljubinko M. Ignjatovi, Vladimir A. Srekovi et al.
- [Ultrashort filaments of light in weakly ionized, optically transparent media](#)  
L Bergé, S Skupin, R Nuter et al.



**IOP | ebooks™**

Bringing you innovative digital publishing with leading voices to create your essential collection of books in STEM research.

Start exploring the collection - download the first chapter of every title for free.

# Modeling of continuous absorption of electromagnetic radiation in dense partially ionized plasmas

A A Mihajlov<sup>1</sup>, N M Sakan<sup>1</sup>, V A Srećković<sup>1</sup> and Y Vitel<sup>2</sup>

<sup>1</sup> Institute of Physics, Belgrade University, Pregrevica 118, Zemun, 11080 Belgrade, Serbia

<sup>2</sup> UPMC Univ Paris 6, Laboratoire des Plasmas Denses, 3 rue Galilee, 94200 Ivry sur Seine, France

E-mail: [mihajlov@ipb.ac.rs](mailto:mihajlov@ipb.ac.rs)

Received 3 November 2010, in final form 29 December 2010

Published 11 February 2011

Online at [stacks.iop.org/JPhysA/44/095502](http://stacks.iop.org/JPhysA/44/095502)

## Abstract

A new modeling way of describing the continuous absorption of electromagnetic (EM) radiation in a dense partially ionized hydrogen plasma is tested in this work. It is shown that the obtained results give a possibility of calculating spectral absorption coefficients which characterize the relevant absorption processes in partially ionized hydrogen plasmas with electron densities  $N_e \sim 10^{19} \text{ cm}^{-3}$  and temperatures  $T \approx 2 \times 10^4 \text{ K}$ . A key parameter of the used procedure is determined empirically. The calculation method is applied to the wavelength region  $300 \text{ nm} < \lambda < 500 \text{ nm}$ . The presented results can be of interest for dense laboratory plasmas as well as for partially ionized layers of different stellar atmospheres.

PACS numbers: 32.80.Fb, 52.25.Os, 52.27.Gr

## 1. Introduction

By now, direct methods of determination of various plasma characteristics, based on quantum or classical statistical mechanics, have been developed only for practically fully ionized plasmas [1–8]. In the case of dense partially ionized plasmas, where the density of neutral particles (atoms) is close to the density of positively charged particles (ions), such rigorous methods do not exist at present. Recently, in [9], this problem was discussed in connection with the transport properties of dense partially ionized plasmas. As for their optical characteristics, it is enough to recall that adequate calculation methods exist only for weakly and moderately ionized plasmas with electron density  $N_e \lesssim 10^{17} \text{ cm}^{-3}$ . As is well known, the influence of the neighborhood on an excited atom can be neglected in such plasmas, as for example in the Solar photosphere [10, 11], or be treated as a small perturbation and described within the framework of a perturbation theory [1, 12–19].

In this paper, we will consider the continuous absorption of electromagnetic (EM) radiation in a dense partially ionized plasma, with electron density  $N_e \sim 10^{19} \text{ cm}^{-3}$ , temperature  $T \approx 20\,000 \text{ K}$  and atom density  $N_a \approx N_e$ . Plasmas with similar parameters are of interest from both the laboratory [20, 21] and the astrophysical aspect. Here, we keep in mind the plasma of the inner layers of the solar atmosphere, as well as of partially ionized layers of other stellar atmospheres, for example the atmospheres of DA and DB white dwarfs with effective temperatures between 10 000 K and 20 000 K (see [22–24]).

Due to the exceptional simplicity of the hydrogen atom, this research is starting with the hydrogen case. Under the mentioned conditions the continuous absorption of EM radiation in hydrogen plasmas is determined by the following radiative processes:

$$\varepsilon_\lambda + \text{H}^*(n, l) \rightarrow \text{H}^+ + e_{k'}, \quad (1)$$

$$\varepsilon_\lambda + e_k + \text{H}^+ \rightarrow e_{k'} + \text{H}^+, \quad (2)$$

$$\varepsilon_\lambda + \begin{cases} e_k + \text{H}(1s), \\ \text{H}^-(1s^2), \end{cases} \rightarrow e_{k'} + \text{H}(1s), \quad (3)$$

$$\varepsilon_\lambda + \begin{cases} \text{H}^+ + \text{H}(1s), \\ \text{H}_2^+(1\Sigma_g^+), \end{cases} \rightarrow \text{H}(1s) + \text{H}^+, \quad (4)$$

where  $\varepsilon_\lambda$  is the energy of a photon with wavelength  $\lambda$ ;  $n$  and  $l$  are the principal and the orbital quantum number of hydrogen-atom excited states;  $e_k$  and  $e_{k'}$  are free electrons with energies  $E = \hbar^2 k^2 / 2m$  and  $E' = \hbar^2 k'^2 / 2m$ , respectively;  $m$  is the electron mass; and  $\hbar$  is Planck's constant.

In the considered region of  $N_e$  and  $T$ , the processes of electron– $\text{H}^+$  and electron– $\text{H}(1s)$  inverse bremsstrahlung, photo-detachment of the negative ion  $\text{H}^-(1s^2)$ ,  $\text{H}(1s)$ – $\text{H}^+$  absorption charge exchange and photo-dissociation of molecular ion  $\text{H}_2^+(1\Sigma_g^+)$ , which are described by equations (2)–(4), can be treated in the same way as in previous papers [25, 26]. Therefore, photo-ionization processes (1) will be in the focus of attention in the next section, and here let us note only that in this field methods obtained by extrapolation (with minor modifications) of the methods developed for weakly and moderately non-ideal plasmas [20, 27, 28] have been used for such processes up until now. Moreover, for the determination of absorption coefficients characterizing their influence in the region of  $N_e \gtrsim 10^{19} \text{ cm}^{-3}$ , methods based on Cramer's approximation [21, 29] have been used so far. So, developing a new modeling way of describing the continual absorption in dense partially ionized plasmas, which is the main aim of this paper, is still an actual task.

We take as the landmarks the hydrogen plasmas which were experimentally studied in [28] with  $N_e = 6.5 \times 10^{18}$  and  $1.5 \times 10^{19} \text{ cm}^{-3}$ , and  $T = 1.8 \times 10^4$  and  $2.3 \times 10^4 \text{ K}$ , respectively. The presented modeling way is tested within the optical range of photon wavelengths:  $300 \text{ nm} \leq \lambda \leq 500 \text{ nm}$ . A key parameter of the used numerical procedure is determined empirically. It is shown that this procedure already allows for the determination of the spectral absorption coefficients characterizing all the relevant absorption processes in dense partially ionized hydrogen plasmas, at least in the regions  $5 \times 10^{18} \text{ cm}^{-3} \lesssim N_e \lesssim 5 \times 10^{19} \text{ cm}^{-3}$  and  $1.6 \times 10^4 \text{ K} \lesssim T \lesssim 2.5 \times 10^4 \text{ K}$ .

The material of this paper is divided into sections 2 and 3. In section 2 the following is presented. The approximation of the cut-off Coulomb potential, together with the reasons for applying just this approximation in the considered regions of  $N_e$  and  $T$ ; the way of obtaining all the partial spectral absorption coefficients, as well as their corresponding final expressions. In section 3, the results of the calculations of the partial and the total absorption coefficients are presented and discussed.

## 2. Theory: the spectral absorption coefficients

### 2.1. The approximation of the cut-off Coulomb potential

Let us note that numerous papers dedicated to development of rather rigorous methods of ground-state and excited-atom photo-ionization processes were published over the past few decades (see for example [27, 30–36]). Although some of these methods were tested on the examples of isolated H-like and He atom systems, the main results of those papers are intended for more complex atoms and for atoms in extreme EM fields. Therefore, we will consider here that an isolated hydrogen atom  $H^*(n, l)$  should be described in the same way as in [37]. The appearance of these papers has certainly encouraged intensive investigation of the atom ionization processes in plasmas (see for example [38–45]); however, the regions of temperature and electron density which are considered here ( $N_e \sim 10^{19} \text{ cm}^{-3}$  and  $T \approx 20\,000 \text{ K}$ ) have not been examined yet. Namely, the results obtained in those papers refer to the regions of extremely large electron density and temperature, where the non-relativistic way of describing plasma becomes invalid. Besides, the models of ion screening which are used in the mentioned papers are not generally appropriate (as is being shown below) to the considered regions of plasma parameters. That is why we examine a new modeling way here, as already mentioned above.

In the considered hydrogen plasmas processes, equation (1) will present the main difficulties in describing the continuous absorption, since under the stated conditions the energy of interaction of an excited atom with its neighborhood reaches the order of the corresponding ionization potential. It means that these processes have to be considered as a result of radiative transitions in the whole system ‘electron–ion pair + the neighborhood’, namely

$$\epsilon_\lambda + (H^+ + e)_{n,l} + S_{\text{rest}} \rightarrow (H^+ + e)_E + S'_{\text{rest}}, \quad (5)$$

where  $S_{\text{rest}}$  and  $S'_{\text{rest}}$  denote the rest of the considered plasma. However, as is well known, many-body processes can sometimes be simplified by a transformation to the corresponding single-particle processes in an adequately chosen model potential.

In this context, we will introduce into the consideration the ion Wigner–Seitz radius,  $r_{s;i}$ , given by

$$r_{s;i} = \left( \frac{3}{4\pi N_i} \right)^{\frac{1}{3}}, \quad (6)$$

where  $N_i$  is the  $H^+$  ion density, and the characteristic length  $r_c$  is defined by the relation

$$U_{p;c} = -\frac{e^2}{r_c}, \quad (7)$$

where the quantity  $U_{p;c}$  has the meaning of the mean potential in which a free electron moves in the considered plasma. Then, we will take into account the fact that, according to the results of [46], the characteristic length  $r_c \cong r_{s;i}$  in the hydrogen plasmas which are considered here. It means that in these plasmas the radius of the zone where an ion and an electron can be treated as an electron–ion pair in equation (5) is just  $r_c$ .

Here, we will follow the previous paper [47], where it was noted that an adequate ion screening potential has to satisfy two main requirements:

- (a) it has to be practically equal to the Coulomb potential ( $-e^2/r$ ) in the mentioned zone, i.e. in the region  $r < r_c$ ,
- (b) outside of this zone ( $r > r_c$ ) it has to be practically equal to the mean potential  $U_{p;c}$ ,

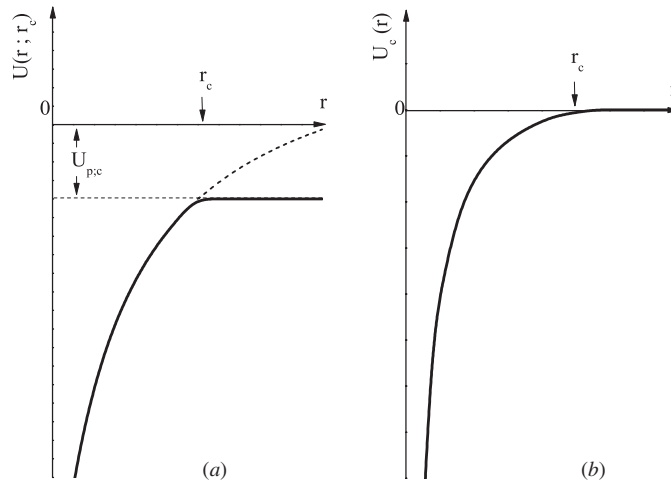


**Figure 1.** Potentials  $U(r; r_c)$  and  $U_c(r)$ , where  $r_c$  is the cut-off parameter.

where  $r$  is the distance from the considered ion, and  $e$  is the modulus of the electron charge. Condition (a) is due to the fact that the averaged potential, created by the rest of the considered plasma inside the mentioned zone, where the electron of  $(H^+ + e)$ -pair is localized, is equal to zero in the first approximation, since the rest is neutral as a whole. As for condition (b), it reflects the fact that under such a condition a realistic, physically acceptable asymptotics is realized for the electron wavefunction characterizing  $(H^+ + e)$ -pair in the considered plasma, which cannot be Coulomb-like as in an isolated electron–ion pair.

As an adequate model potential for the hydrogen plasma with  $N_e \sim 10^{19} \text{ cm}^{-3}$  we choose, as in [47], the screening cut-off Coulomb potential, which satisfies conditions (a) and (b), and can be presented in the form

$$U(r; r_c) = \begin{cases} -\frac{e^2}{r}, & 0 < r \leq r_c, \\ U_{p;c}, & r_c < r < \infty, \end{cases} \quad (8)$$

where the cut-off radius  $r_c$  is defined by relation (7), as is illustrated in figure 1(a). This potential was first introduced to the plasma physics in [48] and its properties were investigated later in [49, 50].

In connection with such a choice of the ion screening potential, let us note the following: the argumentation from [47] is taken into account here that the often used model of the Debye–Hückel (DH) potential is not adequate for the description of an electron–ion pair in a dense non-ideal plasma. It is important that we focus here only on the physical meaning of the DH potential, leaving out of the consideration all of its disadvantages, which have been noted and discussed in [46, 51]; namely, as is well known, the DH potential has the meaning of an average electrostatic potential created by the observed ion and all the charged particles from the rest of the plasma. This potential was introduced in [52] in order to describe (in accordance with its meaning) some of the thermodynamical characteristics of free-particle systems with the Coulomb interaction. From this aspect, its applications have been justified until now, if the accuracy of the calculations is not very important [46].

Let us note also that in order to reduce errors which are generated by the application of the DH potential, instead of the DH screening radius  $r_D = [kT/(8\pi N_e e^2)]^{1/2}$  for the

two-component (electron–ion) plasma, another radius  $r_e$  is often taken, given by

$$r_e = [kT/(4\pi N_e e^2)]^{1/2}, \quad (9)$$

which in principle characterizes the corresponding single-component system. In [46], it was shown that replacing  $r_D$  with  $r_e$  is really justified in weakly non-ideal plasmas, since the adequate screening radius is approaching just  $r_e$  when the non-ideality degree is approaching zero. Here, it is necessary to recall that by replacing the DH screening radius  $r_D$  with the electron screening radius  $r_e$ , the DH potential loses its physical meaning, becoming one of the numerous DH-like potentials.

However, due to its physical meaning, the DH potential could not be applied in principle to describing electron–ion scattering in dense plasmas. Namely, in such plasmas the electron in the considered electron–ion pair is itself a part of the corresponding ion’s ‘screening cloud’ and thus takes part in the creation of the DH potential. This fact is often being forgotten, but neglecting it yields an absurd situation in the case of such plasmas where the DH screening radius  $r_D$  is approaching the ion Wigner–Seitz radius  $r_{s;i}$ , given by equation (6). In such a case, the complete ion ‘screening cloud’ consists practically of one electron from the considered electron–ion pair.

Just this kind of situation is realized in a plasma of the kind treated in this paper, i.e. with  $N_e$  of the order of magnitude of  $10^{-19} \text{ cm}^{-3}$  and  $T$  of about 20 000 K, where the ion Wigner–Seitz radius  $r_{s;i}$  is close to the ion screening radius  $r_e$  given by (9), making an application of the DH potential completely unacceptable. Let us emphasize the fact that the same is valid for any other potential which has a similar meaning as DH.

For all these reasons, we consider that DH screening potentials, which were used in the above-mentioned papers [38–45] cannot be accepted for an application in any region of plasma parameters. As for DH-like potentials, one of them could be accepted in principle for an application in some regions of  $N_e$  and  $T$ , but only under the following condition:

the screening radius in the expression for the used potential guarantees that the values of the basic parameters of the considered problem (number and energies of the bound states, elastic scattering amplitude for the angle equal to zero as a function of the free-electron energy, etc) are very close to the corresponding experimental data.

This condition could probably be satisfied under the condition of the existence of reliable experimental data which could be used for the determination of the effective screening radius by means of the corresponding fitting method, and some rigorous procedure being included for describing the bound and free states of the electron in the considered DH-like potential. However, for the considered plasmas there are no such reliable experimental data in the literature.

Because of all the things mentioned, we consider that the choice of the potential  $U(r; r_c)$ , which is given by equation (8), is the best solution in the case of the considered dense partially ionized plasmas. Besides, an additional advantage of this model potential is the possibility of obtaining all the needed final results in a compact analytical form.

As in [47], we will take the value  $U_{p;c}$  as the zero of energy. After that, the potential equation (8) is transformed into the form

$$U_c(r) = \begin{cases} -\frac{e^2}{r} + \frac{e^2}{r_c}, & 0 < r \leq r_c, \\ 0, & r_c < r < \infty, \end{cases} \quad (10)$$

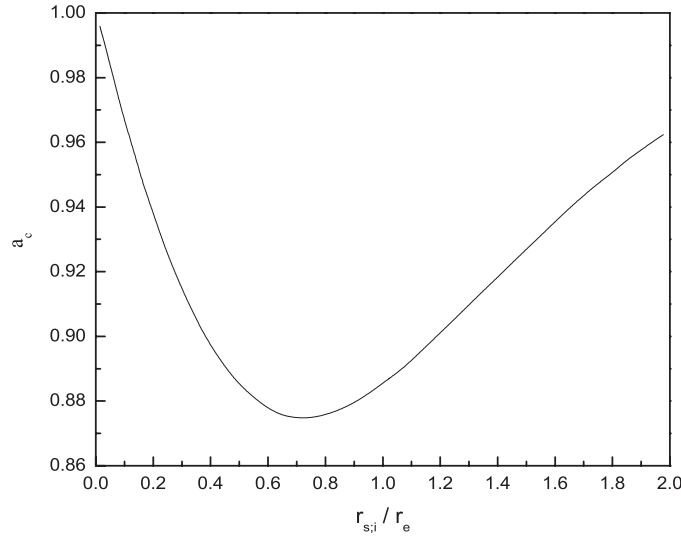


**Figure 2.** The parameter  $a_c \equiv r_c/r_e$  as the function of the ratio  $r_{s;i}/r_e$ , where  $r_{s;i}$  and  $r_e$  are given by equations (6) and (9).

which is used in further considerations, and is also illustrated in figure 1(b). It is important that, through the characteristic lengths  $r_{s;i}$  and  $r_e$  defined by equations (6) and (9), the cut-off radius  $r_c$  is determined here as a given function of  $N_e$  and  $T$ . Namely, taking that

$$r_c = a_c \cdot r_e, \tag{11}$$

we can directly determine the quantity  $a_c$  as a function of the ratio  $r_{s;i}/r_e$ , on the basis of the data from [46] about the mean potential energy of an electron in the singly ionized plasma. We recall that in [46], a quantity is determined which is equal to  $U_{p;c}/U_D = r_D/r_c$  (being just designated differently), where  $U_D = -e^2/r_D$  is the mean potential energy determined within the DH method [52]. Keeping in mind that  $r_D = r_e/2^{1/2}$ , and taking  $r_c/(\sqrt{2} \cdot r_D) = a_c$ , we obtain  $a_c = r_c/r_e$ , and then expression (11) for  $r_c$  too. As the quantity  $r_D/r_c$  is being determined among else in [46], just for the case of the singly ionized plasma, so the curve in figure 2 of this paper is obtained routinely from the curve in figure 4 in [46], which represents the quantity  $r_D/r_c$  as a function of ratio  $r_{s;i}/r_e$ . The behavior of  $a_c$  in a wide region of values of  $r_{s;i}/r_e$  is presented in figure 2.

### 2.2. Processes (I) absorption coefficients

For the sake of further considerations, it is necessary to have energies  $E_{n,l}$  of the bound states  $|n, l\rangle$  which are possible in the potential  $U_c(r)$  and the corresponding radial wavefunctions  $R_{n,l}(r)$ , as well as the radial wavefunctions  $R_{E,l}(r)$  which correspond to the free states  $|E, l\rangle$ . These quantities are determined from Schrödinger equation

$$\frac{d^2 R(r)}{dr^2} + \frac{2}{r} \frac{dR}{dr} + \left[ \frac{2m}{\hbar^2} \cdot (W - U_c(r)) - \frac{l(l+1)}{r^2} \right] = 0, \tag{12}$$

where  $W$  and  $R(r)$  denote either  $E_{n,l}$  and  $R_{n,l}(r)$  or  $E$  and  $R_{E,l}(r)$ . Here, we will find the radial wavefunctions in the form:  $R_{n,l}(r) = P_{n,l}/r$  and  $R_{E,l}(r) = P_{E,l}/r$ , where  $P_{n,l}(r)$  and  $P_{E,l}(r)$  can be expressed through the well-known analytical functions given in [53], namely



- in the region  $0 < r < r_c$ , all  $P_{n,l}(r)$  and  $P_{E,l}(r)$  with  $E < e^2/r_c$  are expressed through the corresponding Whittaker's functions, and  $P_{E,l}(r)$  with  $E > e^2/r_c$  through Coulomb-like ones which are regular at the point  $r = 0$ ;
- in the region  $r_c < r < \infty$ , all  $P_{n,l}(r)$  are expressed through modified Bessel functions, and all  $P_{E,l}(r)$  through spherical Bessel functions. Let us note that the bound-state energies (in the region  $W < 0$ ) and the free-state phase shifts (in the region  $W > 0$ ) are determined from the condition of continuity of  $R(r)$  and  $dR(r)/dr$  at the point  $r = r_c$ .

Since the considered photo-ionization processes can be described in the dipole approximation ( $r_c \ll \lambda$ ), the corresponding cross-sections, for the non-perturbed bound states in the potential  $U_c(r)$ , are given by the expressions from [54], namely

$$\sigma_{\text{ph}}(\lambda; n, l, E_{n,l}) = \frac{4\pi^2 e^2 k_{\text{ph}}}{3(2l+1)} \sum_{l'=l\pm 1} l_{\text{max}} \left( \int_0^\infty P_{n,l'} P_{E,l'} dr \right)^2, \quad (13)$$

where  $k_{\text{ph}} = \varepsilon_\lambda/\hbar c$ ,  $l_{\text{max}} \equiv \max(l, l')$ , and  $E = E_{n,l} + \varepsilon_\lambda$ .

As is well known, the spectral absorption coefficient  $\kappa_{\text{ph}}^{(0)}(\lambda; N_e, T)$ , characterizing the photo-ionization processes (1) in the case of non-perturbed energy levels in the potential  $U_c(r)$ , is given by the expression

$$\kappa_{\text{ph}}^{(0)}(\lambda; N_e, T) = \sum_{n,l} N_{n,l} \cdot \sigma_{\text{ph}}(\lambda; n, l, E_{n,l}) \cdot f_{\text{st}}(\lambda, T), \quad n \geq 2, \quad (14)$$

where  $\sigma_{\text{ph}}(\lambda; n, l, E_{n,l})$  is the partial photo-ionization cross-section defined by equation (13),  $N_{n,l}$  is the density of atoms  $\text{H}^*(n, l)$ , and factor  $f_{\text{st}}$ , given by

$$f_{\text{st}}(\lambda, T) = 1 - \exp(-2\pi\hbar c/\lambda), \quad (15)$$

describes the influence of the stimulated emission. One can see that this expression is similar to the one for the diluted hydrogen plasma (see for example [10]) and, in accordance with what was said above, it cannot model the absorption coefficients of dense non-ideal plasmas described in [28]. In order to determine the absorption coefficients  $\kappa_{\text{ph}}(\lambda; N_e, T)$  which can be applied to the mentioned modeling, we have to take into account additional details of the atom-plasma interaction, besides those which are already described by the shape of potential (10). It is known that within the usual way (i.e. as is being done in the cases of weakly non-ideal plasmas) this additional influence should be characterized by shifts and broadenings of the bound-state energy levels of the considered atoms. However, this way is generally applicable in any case, including the case of a strongly non-ideal plasma too.

This is confirmed by the approach of [55], the main feature of which is treatment of electrons in existing atoms  $\text{H}^*(n, l)$  as a Fermi gas of particles, which move in a self-consistent field created by immobile ions and other electrons. One of the results of this approach is a description of the relevant elementary event in such a gas, i.e. annihilation of an electron localized at the  $j$ th proton in the chosen  $\nu$ th state with a simultaneous creation of an electron in some free state, caused by the absorption of a photon with energy  $\varepsilon_\lambda$ . Namely, it was found that such an event can be described in terms of the corresponding probability density, which is practically equal to zero outside of a finite interval of free-state energies. This result, despite the fact that it has only qualitative significance, suggests that  $\kappa_{\text{ph}}(\lambda; N_e, T)$  can be obtained by a modification of equation (14) based on an adequately chosen probability density  $p_{n,l}(\epsilon)$  of the perturbed atom energy levels with given  $n$  and  $l$ , characterized by the corresponding shifts  $\Delta_{n,l}$  and broadenings  $\delta_{n,l}$ . It is assumed that energies  $\epsilon$  of the perturbed atomic states are dominantly grouped around energy  $\epsilon_{n,l}^{(\text{max})} = E(n, l) + \Delta_{n,l}$ , inside the interval  $(\epsilon_{n,l}^{(\text{max})} - \delta_{n,l}/2, \epsilon_{n,l}^{(\text{max})} + \delta_{n,l}/2)$ , similar to the known cases (Gaus, Lorentz, uniform, etc).

All this justifies a semi-empirical approach to the considered problem, until a corresponding strict method is developed. In this work, any  $(n, l)$ -shell (with given  $n$ ) of the perturbed hydrogen atom is characterized by only two quantities, namely an averaged shift  $\Delta_n$  and broadening  $\delta_n$ , which are treated as empirical parameters. Consequently, here it is considered that  $\Delta_{n,l} \equiv \Delta_n$ ,  $\delta_{n,l} \equiv \delta_n$  and  $p_{n,l}(\epsilon)$  describe the corresponding uniform distribution of the perturbed energy levels, i.e.

$$p_{n,l}(\epsilon) = \begin{cases} \frac{1}{\delta_n}, & |\epsilon_{n,l}^{(\max)} - \epsilon| \leq \frac{\delta_n}{2} \\ 0, & |\epsilon_{n,l}^{(\max)} - \epsilon| > \frac{\delta_n}{2}, \end{cases} \quad \epsilon_{n,l}^{(\max)} = E_{n,l} + \Delta_n. \quad (16)$$

Here, we keep in mind that the uniform distribution can approximate many other distributions well (Gaussian, cupola, etc)

Let us note that although  $\Delta_n$  is treated here as an empirical parameter, it is possible to describe its qualitative behavior as a function of  $N_e$ . Namely, for well-known physical reasons all shifts  $\Delta_{n,l}$ , and consequently  $\Delta_n$ , have to change proportionally to the density of the perturbers, the relative atom–perturber velocity and the characteristic perturbation energy. Consequently, we will have

$$\Delta_n \cong \text{const} \cdot N_e \cdot v_{ea}(T) \cdot e^2 / l(N_e, T), \quad (17)$$

where  $v_{ea}(T)$  and  $l(N_e, T)$  are the characteristic electron–atom velocity and distance. On the basis of the results of [46] in the considered cases ( $N_e \sim 1 \times 10^{19} \text{ cm}^{-3}$ ,  $T \sim 2 \times 10^4 \text{ K}$ ) any relevant characteristic length has to be close to the radius  $r_e$ , which is given by equation (9). Since  $v_{ea}(T) \sim (k_B T)^{1/2}$  and  $r_e \sim (k_B T / N_e)^{1/2}$ , from (17) the relation

$$\Delta_n \cong \text{const} \cdot N_e^{3/2} \quad (18)$$

follows, which is also in accordance with [55], and will be particularly significant in further considerations.

Here, we will describe the perturbed atomic states in the first order of the perturbation theory and, in accordance with what was said above, we will have

$$\kappa_{\text{ph}}(\lambda; N_e, T) = \left[ \sum_{n,l} N_{n,l} \cdot \frac{\varepsilon_\lambda}{\delta_n} \int_{\epsilon^-}^{\epsilon^+} \frac{\sigma_{\text{ph}}(\lambda^{(\epsilon)}; n, l, E_{n,l})}{\varepsilon_\lambda + \epsilon} \cdot d\epsilon \right] \cdot f_{\text{st}}(\lambda, T), \quad (19)$$

where  $n \geq 2$ ,  $\epsilon^- = \epsilon_{n,l}^{(\max)} - \delta_n/2$ ,  $\epsilon^+ = \epsilon_{n,l}^{(\max)} + \delta_n/2$ ,  $\epsilon_{n,l}^{(\max)} = E_{n,l} + \Delta_n$ , and  $\sigma_{\text{ph}}(\lambda^{(\epsilon)}; n, l, E_{n,l})$  is given by equation (13) for  $\lambda^{(\epsilon)} = \lambda \cdot \varepsilon_\lambda / (\varepsilon_\lambda + \epsilon)$ , i.e. for the wavelength of a photon with energy  $(\varepsilon_\lambda + \epsilon)$ .

### 2.3. Processes (2), (3) and (4) absorption coefficients

The spectral absorption coefficients characterizing the electron–ion absorption process (2), electron–atom absorption processes (3) and ion–atom absorption processes (4) are determined here as in the previous papers [25, 26, 56], dedicated to the same absorption processes in some laboratory and astrophysical plasmas.

So, the spectral absorption coefficients  $\kappa_{ei}(\lambda)$ ,  $\kappa_{ea}(\lambda)$  and  $\kappa_{ia}(\lambda)$  are defined by the expressions

$$\kappa_{ei}(\lambda) = K_{ei}(\lambda, T) \cdot N_e \cdot N_i \cdot f_{\text{st}}(\lambda, T) \cong K_{ei}(\lambda, T) \cdot N_e^2 \cdot f_{\text{st}}(\lambda, T), \quad (20)$$

$$\kappa_{ea}(\lambda) = \sigma_{\text{phd}}^- \cdot S_{ea}^{-1} \cdot N_e \cdot N_a + K_{ea}(\lambda, T) \cdot N_e \cdot N_a \cdot f_{\text{st}}(\lambda, T), \quad (21)$$

$$S_{ea} = \left( \frac{N_e \cdot N_a}{N_{\text{neg},i}} \right)_{eq} = 4 \left( \frac{mkT}{2\pi\hbar} \right)^{\frac{3}{2}} \cdot e^{-\frac{E_a^-}{kT}}, \quad (22)$$

$$\kappa_{ia}(\lambda) = K_{ia}(\lambda, T) \cdot N_i \cdot N_a \cong K_{ia}(\lambda, T) \cdot N_e \cdot N_a \cdot f_{st}(\lambda, T), \quad (23)$$

where  $N_a$ ,  $N_i$  and  $N_{neg.i}$  are the densities of H(1s) atoms, H<sup>+</sup> ions and negative H<sup>-</sup>(1s<sup>2</sup>) ions respectively, ‘eq’ denotes that the quantity  $S_{ea}$  is determined under the condition of thermodynamic equilibrium of the considered system,  $E_d^-$  is the energy of H<sup>-</sup>(1s<sup>2</sup>) ion dissociation, and the factor  $f_{st}(\lambda, T)$  is given by expression (15).

The spectral coefficient  $K_{ei}(\lambda, T)$ , given in (cm<sup>5</sup>), is calculated by means of the corresponding expressions from [54], with the Gaunt factor determined in [57]. The spectral coefficient  $K_{ea}(\lambda, T)$ , given also in (cm<sup>5</sup>), and the cross-section  $\sigma_{phd}^-$  for photo-dissociation of the ion H<sup>-</sup>(1s<sup>2</sup>) are determined on the basis of the expressions from [58] and [59]. Finally, the spectral coefficient  $K_{ia}(\lambda, T)$  is determined in the quasi-static approximation, which is described in detail in [56], and is taken in the form

$$K_{ia}(\lambda, T) = 0.62 \times 10^{-42} \frac{C(R_\lambda)(R_\lambda/a_0)^4}{1 - a_0/R_\lambda} \cdot \exp\left(-\frac{U_1(R_\lambda)}{kT}\right), \quad (24)$$

where  $U_1(R)$  is the energy of the electronic ground state  $1\Sigma_g^+$  of the molecular ion H<sub>2</sub><sup>+</sup>, as a function of internuclear distance  $R$ ,  $R_\lambda$  is the resonance internuclear distance for given  $\lambda$ ,  $a_0$  is the atomic unit of length, and  $C(R_\lambda)$  is a dimensionless coefficient which is close to 1. Parameters  $R_\lambda$ ,  $U_1(R_\lambda)$  and  $C(R_\lambda)$ , as functions of  $\lambda$ , are tabulated in [25, 56]. The relative contributions of the partial channels, i.e. H(1s)–H<sup>+</sup> absorption charge exchange and molecular ion H<sub>2</sub><sup>+</sup>(1Σ<sub>g</sub><sup>+</sup>) photo-dissociation, are obtained by multiplication of  $K_{ia}(\lambda, T)$  by factors  $X(z)$  and  $[1 - X(z)]$ , respectively. In the considered region of  $\lambda$  factor,  $X(z) = \Gamma(3/2; z)/\Gamma(3/2)$ , where  $z = -U_1(R_\lambda)/kT$ .

### 3. Results and discussion

#### 3.1. The characteristics of the cut-off Coulomb potential

In this paper, the approximation of cut-off Coulomb potential (10) is applied to modeling the spectral absorption coefficient obtained in [28] in two experiments with hydrogen plasmas, which are treated as a short and a long pulse, respectively. In the first case (short pulse), a plasma with  $N_e = 1.5 \times 10^{19}$  cm<sup>-3</sup> and  $T = 2.3 \times 10^4$  K was studied, while in the second case (long pulse), it was a plasma with  $N_e = 6.5 \times 10^{18}$  cm<sup>-3</sup> and  $T = 1.8 \times 10^4$  K. In the experiments described in [28], plasmas with electron densities up to  $\approx 10^{19}$  cm<sup>-3</sup> were created by pulse discharge in quartz capillary. Diagnostics of the plasma was carried out on the basis of optical measurements (at  $\lambda = 632.8$  nm), taking into account radial inhomogeneity of the plasma column. The temperature profile is defined from independent measurements of brightness and transparency at different distances from the center of the capillary. A detailed study is performed just for the two above-mentioned examples.

On the basis of figure 2 and equation (11) it was found that the cut-off radius  $r_c$  is equal to 44.964 au for the short pulse, and 55.052 au for the long one. For these values of  $r_c$ , the solutions of equation (12) correspond to the energies of the realized bound state, which are presented in tables 1 and 2, respectively. The corresponding partial photo-ionization cross-sections  $\sigma(\lambda; n, l, \epsilon_{n,l})$  are obtained by means of equation (13) for  $n, l$  and  $\epsilon_{n,l}$  given in tables 1 and 2. The behavior of these cross-sections is illustrated in figures 3 and 4 by the examples of photo-ionization cross-sections of all realized states with  $l = 0$ . These figures show qualitative similarity of behavior of the cross-sections in the cases  $r_c = 44.964$  au and  $r_c = 55.052$  au and domination of the cross-sections with  $n = 2$ . One can see a significant difference between the maximal values of the cross-sections with  $n = 2$  (about 2.70 and 0.75 au) which correspond to these cases. This fact reflects the tendency of a significant

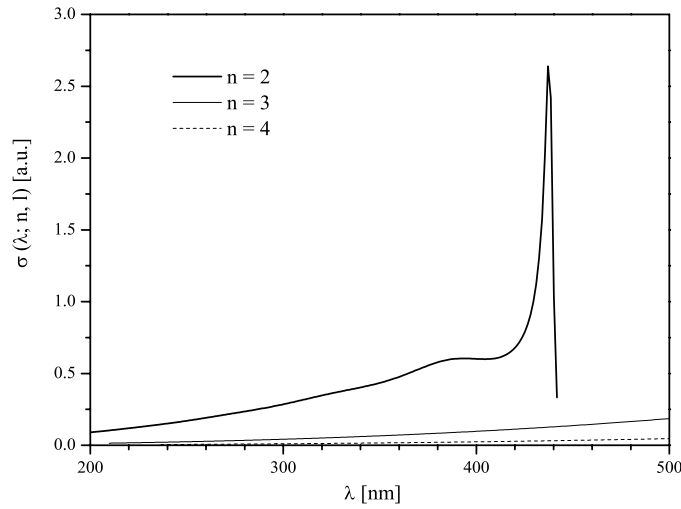


**Figure 3.** The photo-ionization cross-section for the bound state with  $l = 0$  and  $n = 2, 3$  and  $4$  in the potential  $U_c(r)$  for the short pulse ( $r_c = 44.964$  au).

**Table 1.** The energies of the bound states in the potential  $U_c(r)$  in the case of short pulse (cut-off radius  $r_c = 44.964$  au): the principal and orbital quantum numbers  $n$  and  $l$ , and the corresponding energies  $E_{n,l}$  in  $\text{cm}^{-1}$ .

| $n$ | $l$             |                |              |              |
|-----|-----------------|----------------|--------------|--------------|
|     | 0               | 1              | 2            | 3            |
| 1   | -104 856.113 87 |                |              |              |
| 2   | -22 553.198 71  | -22 553.198 71 |              |              |
| 3   | -7311.916 33    | -7311.916 33   | -7311.916 33 |              |
| 4   | -1979.099 16    | -1978.639 43   | -1978.018 38 | -1977.598 97 |

**Table 2.** The energies of the bound states in the potential  $U_c(r)$  in the case of long pulse (cut-off radius  $r_c = 55.052$  au): the principal and orbital quantum numbers  $n$  and  $l$ , and the corresponding energies  $E_{n,l}$  in  $\text{cm}^{-1}$ .

| $n$ | $l$             |                |              |              |             |
|-----|-----------------|----------------|--------------|--------------|-------------|
|     | 0               | 1              | 2            | 3            | 4           |
| 1   | -105 750.582 78 |                |              |              |             |
| 2   | -23 447.667 62  | -23 447.667 62 |              |              |             |
| 3   | -8206.369 11    | -8206.369 11   | -8206.369 11 |              |             |
| 4   | -2871.963 03    | -2871.946 89   | -2871.938 83 | -2871.930 76 |             |
| 5   | -428.407 05     | -423.274 95    | -415.402 17  | -408.2198    | -404.062 01 |

decrease of the maximal values of the cross-sections for  $n = 2$  with an increase of the cut-off radius  $r_c$ .

Let us recall that tables 1 and 2 characterize the bound states of an electron in the potential  $U_c(r)$  with the values of cut-off radius  $r_c$  given above. The energies of the corresponding ground states approach the value of  $-I_H$ , where  $I_H = 13.598$  eV is the tabulated value of the isolated hydrogen-atom ionization potential (see for an example NIST Atomic Spectra

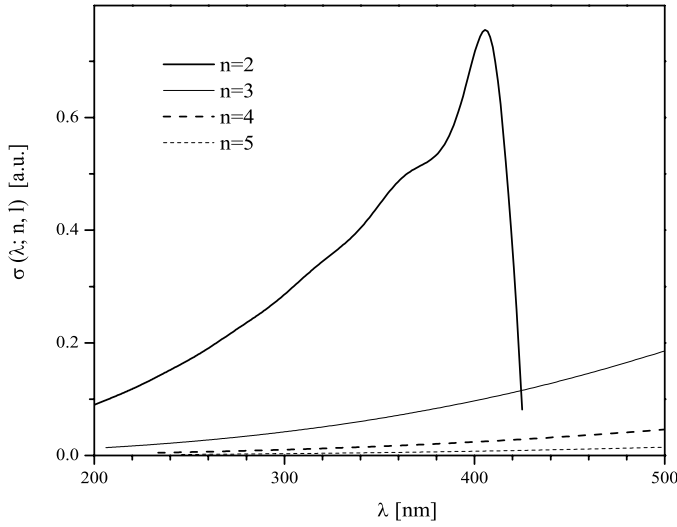


**Figure 4.** The photo-ionization cross-section for the bound state with  $l = 0$  and  $n = 2, 3, 4$  and  $5$  in the potential  $U_c(r)$  for the long pulse ( $r_c = 55.052$  au).

Database), only when  $r_c \rightarrow \infty$ , i.e. when  $N_e \rightarrow 0$  or  $T \rightarrow \infty$ . Also, the energies of the ground states (for the electron densities and the temperatures observed) would be close to  $(-I_H)$  in the case where instead of  $U_c(r)$  the potential  $U(r; r_c)$  would be used (see figure 1).

For each of the considered cut-off radii  $r_c$ , the existence is assumed here of a Boltzmann's distribution of the populations  $N_{n,l}$  of the bound states, given in table 1 or 2, which exist in equation (19). Such a distribution is determined by the corresponding values of the total density of neutral hydrogen atoms  $N_a$  and the temperature  $T$ . In accordance with [28], here it is taken that  $N_a = 1.9 \times 10^{19} \text{ cm}^{-3}$  and  $T = 22\,980 \text{ K}$  for  $r_c = 44.964 \text{ au}$ , and  $N_a = 3.4 \times 10^{19} \text{ cm}^{-3}$  and  $T = 17\,960 \text{ K}$  for  $r_c = 55.052 \text{ au}$ . As one of the consequences, we have that the total populations of groups of the states with same  $n$  are equal to  $4.4 \times 10^{17}$ ,  $3.82 \times 10^{17}$  and  $4.86 \times 10^{17} \text{ cm}^{-3}$  for  $n = 2, 3$  and  $4$  in the first case, and  $1.87 \times 10^{17}$ ,  $1.24 \times 10^{17}$ ,  $1.44 \times 10^{17}$  and  $1.85 \times 10^{17} \text{ cm}^{-3}$  for  $n = 2, 3, 4$  and  $5$  in the second case.

### 3.2. The absorption coefficient: the results of the calculations

In order to compare the obtained theoretical results with the experimental data from [28], we have to take into account all the absorption processes which cannot be neglected in the considered hydrogen plasmas, i.e. the processes described by equations (1)–(4). Therefore, when comparing our theoretical results with the experimental data from [28], we have to use the corresponding total spectral absorption coefficient  $\kappa_{\text{tot}}(\lambda)$ , namely

$$\kappa_{\text{tot}}(\lambda) = \kappa_{\text{ph}}(\lambda) + \kappa_{\text{add}}(\lambda), \tag{25}$$

where  $\kappa_{\text{ph}}(\lambda) \equiv \kappa_{\text{ph}}(\lambda; N_e, T)$  is given by equation (19), and the member  $\kappa_{\text{add}}(\lambda) \equiv \kappa_{\text{add}}(\lambda; N_e, N_a, T)$  characterizes the contribution of absorption processes (2)–(4). Consequently, we have

$$\kappa_{\text{add}}(\lambda) = \kappa_{ei}(\lambda) + \kappa_{ea}(\lambda) + \kappa_{ia}(\lambda), \tag{26}$$

where  $\kappa_{ei}(\lambda) \equiv \kappa_{ei}(\lambda; N_e, T)$ ,  $\kappa_{ea}(\lambda) \equiv \kappa_{ea}(\lambda; N_e, N_a, T)$  and  $\kappa_{ia}(\lambda) \equiv \kappa_{ia}(\lambda; N_e, N_a, T)$  are the partial spectral absorption coefficients, which are given above by equations (20)–(24).

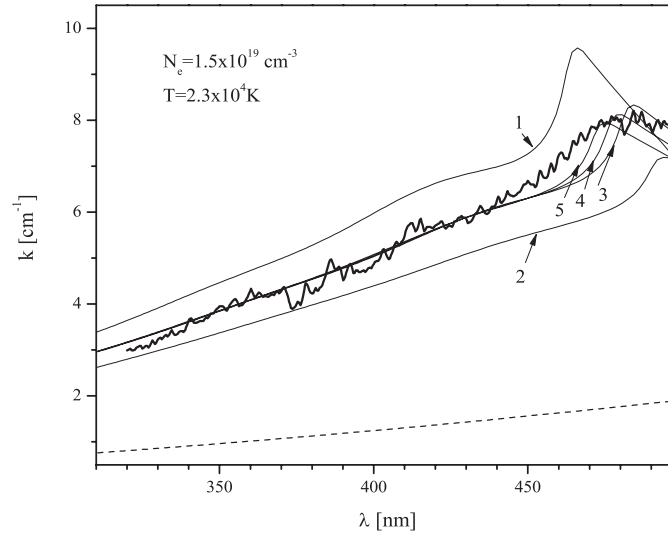


**Figure 5.** The influence of the shift and broadening to the calculated total absorption coefficient. Short pulse: 1—the absorption coefficient  $\kappa_{\text{tot}}(\lambda)$  calculated in the approximation of the constant shift with  $\Delta_n = \delta_n = 0.3$  eV; 2—the same, but with  $\Delta_n = \delta_n = 0.6$  eV; 3, 4 and 5—the same, but with  $\Delta_n = 0.45$  eV and  $\delta_n = 0.4, 0.45$  and  $0.5$  eV, respectively. Dashed curve—the absorption coefficient  $\kappa_{\text{add}}(\lambda)$  which characterizes the total contribution of absorption processes (2)–(4). Bold curve—the experimental absorption coefficient from [28].

In accordance with the aims of this work, the calculations of the total absorption coefficients  $\kappa_{\text{tot}}(\lambda)$  have been performed for both cases (short and long pulses) in a wide region of values of shifts ( $\Delta_n$ ) and broadenings ( $\delta_n$ ) of atomic levels with  $n \geq 2$ . The calculations of  $\kappa_{\text{tot}}(\lambda)$  cover the wavelength region  $300 \text{ nm} \leq \lambda \leq 500 \text{ nm}$ . However, let us emphasize the fact that the values of the experimental absorption coefficient  $\kappa_{\text{exp}}(\lambda)$  characterize not only the bound-free (photo-ionization) processes (1) and the said additional absorption processes (2)–(4), but also the bound-bound (photo-excitation) processes, which are not considered in this work. Consequently, for the purpose of this work, the region  $\lambda \lesssim 450 \text{ nm}$  in the case of short pulse, and  $\lambda \lesssim 425 \text{ nm}$  in the case of long pulse (see tables 1 and 2), has the real significance, where the considered photo-ionization processes dominate in comparison with photo-excitation ones. The results of calculations are shown in figures 5–10 together with the corresponding experimental values  $\kappa_{\text{exp}}(\lambda)$  of the spectral absorption coefficient from [28].

Figures 5–8 illustrate the results of the calculations of  $\kappa_{\text{tot}}(\lambda)$  in the case when  $\Delta_n = \text{const}$ , while figures 9 and 10 present the calculations of  $\kappa_{\text{tot}}(\lambda)$  in the case when  $\Delta_n$  decreases (relative to  $\Delta_2$ ) with increasing  $n$ .

The bottom and the top curves of  $\kappa_{\text{tot}}(\lambda)$  in figures 5 and 6 illustrate strong influence of  $\Delta_n$  on the calculated total absorption coefficient:  $\Delta_n = \delta_n = 0.30$  eV and  $\Delta_n = \delta_n = 0.60$  eV for the short pulse;  $\Delta_n = \delta_n = 0.05$  eV and  $\Delta_n = \delta_n = 0.20$  eV for the long pulse. The groups of three curves, which lie between the corresponding bottom and top curves, demonstrate relatively small influence of  $\delta_n$  on the calculated values of  $\kappa_{\text{tot}}(\lambda)$ :  $\Delta_n = 0.45$  eV, and  $\delta_n = 0.40$  eV,  $\delta_n = 0.45$  eV and  $\delta_n = 0.50$  eV for the short pulse;  $\Delta_n = 0.125$  eV, and  $\delta_n = 0.120$  eV,  $\delta_n = 0.125$  eV and  $\delta_n = 0.130$  eV for the long pulse.

Also, the dashed curves in figures 5 and 6 demonstrate the behavior of the spectral absorption coefficient  $\kappa_{\text{add}}(\lambda)$ , defined by equations (26) and (20)–(24), in the case of short and long pulses, respectively. One can see that the total contribution of electron-ion, electron-

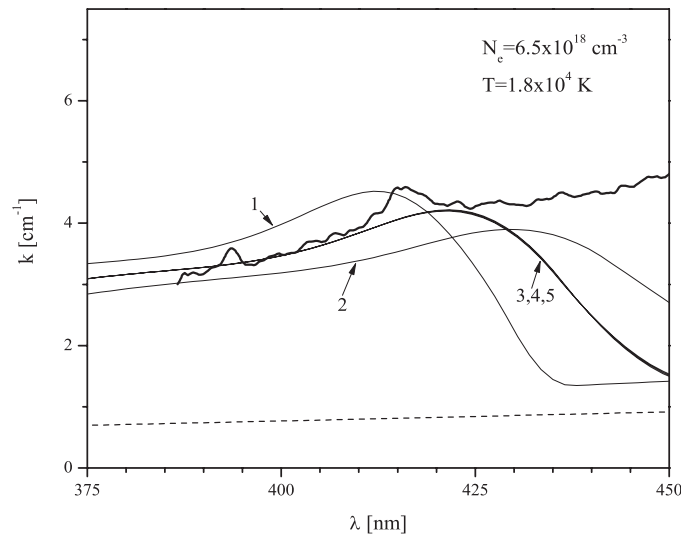


**Figure 6.** The influence of the shift and broadening to the calculated total absorption coefficient. Long pulse: 1—the absorption coefficient  $\kappa_{\text{tot}}(\lambda)$  calculated in the approximation of the constant shift with  $\Delta_n = \delta_n = 0.05$  eV; 2—the same, but with  $\Delta_n = \delta_n = 0.2$  eV; 3, 4 and 5—the same, but with  $\Delta_n = 0.125$  eV and  $\delta_n = 0.12, 0.125$  and  $0.13$  eV, respectively. Dashed curve—the absorption coefficient  $\kappa_{\text{add}}(\lambda)$  which characterizes the total contribution of absorption processes (2)–(4). Bold curve—the experimental absorption coefficient from [28].

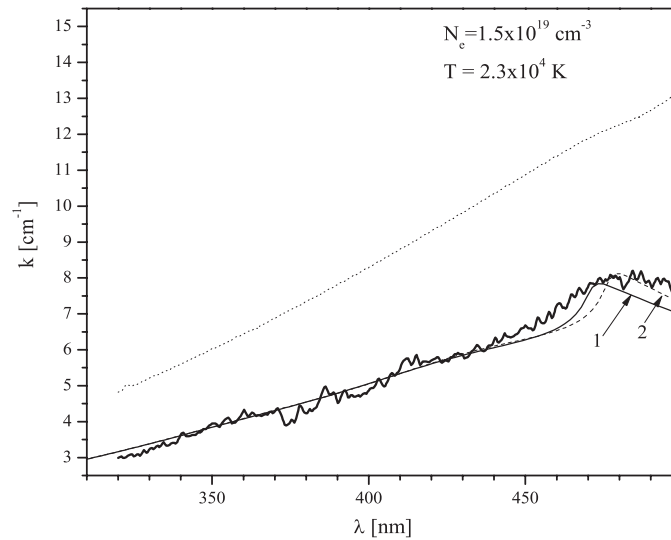


**Figure 7.** Short pulse: 1—the absorption coefficient  $\kappa_{\text{tot}}(\lambda)$  calculated in the approximation of the constant shift with the optimal values of  $\Delta_n$  and  $\delta_n$ , namely  $\Delta_n = 0.455$  eV and  $\delta_n = 0.525$  eV; 2—the absorption coefficient  $\kappa_{\text{tot}}(\lambda)$  calculated in the same approximation with  $\Delta_n = \delta_n = 0.455$  eV. Bold and dotted curve—the absorption coefficients obtained in [28] experimentally and by means of the perturbation theory.

atom and ion–atom absorption processes, described by equations (2)–(4) indeed cannot be neglected in the considered cases.

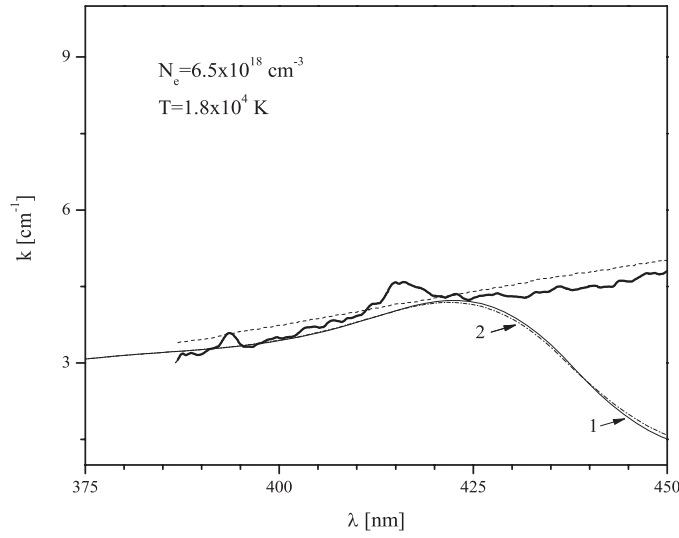


**Figure 8.** Long pulse: 1—the absorption coefficient  $\kappa_{\text{tot}}(\lambda)$  calculated in the approximation of the constant shift with the optimal values of  $\Delta_n$  and  $\delta_n$ , namely  $\Delta_n = 0.13$  eV and  $\delta_n = 0.11$  eV; 2—the absorption coefficient  $\kappa_{\text{tot}}(\lambda)$  calculated in the same approximation with  $\Delta_n = \delta_n = 0.13$  eV. Bold and dashed line—the absorption coefficients obtained in [28] experimentally and by means of the perturbation theory.

Figures 7 and 8 show the curves of  $\kappa_{\text{tot}}(\lambda)$  calculated with the values of  $\Delta_n$  and  $\delta_n$  which are treated as the optimal ones:  $\Delta_n = 0.455$  eV and  $\delta_n = 0.525$  eV for the short pulse, and  $\Delta_n = 0.13$  eV and  $\delta_n = 0.11$  eV for the long one. In order to estimate the possible error due to such a choice of shifts and broadenings, the results of calculations are shown in figures 9 and 10 in the case when  $\Delta_n$  decreases with the increase of  $n$ , proportionally to the ionization energies of the corresponding atomic levels. Let us note the fact that calculated curves presented in these figures correspond to the optimal values of  $\Delta_{n=2}$  and  $\delta_{n=2}$ . One can see that the calculated curves in figures 9 and 10 are very close to the calculated curves in figures 7 and 8, respectively. This fact is reflected in the values of  $\Delta_{n=2}$  and  $\delta_{n=2}$  which correspond to the curves in figures 9 and 10:  $\Delta_{n=2} = 0.49$  eV and  $\delta_{n=2} = 0.55$  eV for the short pulse, and  $\Delta_{n=2} = 0.14$  eV and  $\delta_{n=2} = 0.12$  eV for the long one.

Besides the curves  $\kappa_{\text{tot}}(\lambda)$  and  $\kappa_{\text{exp}}(\lambda)$ , the curves  $\kappa_{\text{p.th.}}(\lambda)$  are also presented in figures 7 and 8, which were obtained in [28] for the short and long pulse on the basis of the perturbation theory used in [20, 28]. For the sake of correct interpretation of the presented data, let us note the fact that the values of  $\kappa_{\text{p.th.}}(\lambda)$ , similar to  $\kappa_{\text{exp}}(\lambda)$ , characterize not only photo-ionization, but also the bound-bound (photo-excitation) processes, which are not considered in this work. One can see that in the case of strongly non-ideal plasmas (short pulse,  $N_e = 1.5 \times 10^{19} \text{ cm}^{-3}$ ) the difference between  $\kappa_{\text{exp}}(\lambda)$  and  $\kappa_{\text{p.th.}}(\lambda)$  is so large that it justifies any effort toward the development of an alternative method of calculation of the strongly non-ideal plasma absorption coefficient. However, in the case of long pulse ( $N_e = 0.65 \times 10^{19} \text{ cm}^{-3}$ ) the considered plasma is located by its parameters in the lower part of the region of strong non-ideality, where the perturbation theory should give much better results. This fact is reflected in a significant reduction of the difference between  $\kappa_{\text{exp}}(\lambda)$  and  $\kappa_{\text{p.th.}}(\lambda)$ .

Therefore, it is important to check whether relation (18) is valid also for  $N_e$  close to  $0.65 \times 10^{19} \text{ cm}^{-3}$ . Since in the case of constant shifts  $\Delta_n = 0.455$  and  $0.130$  eV for



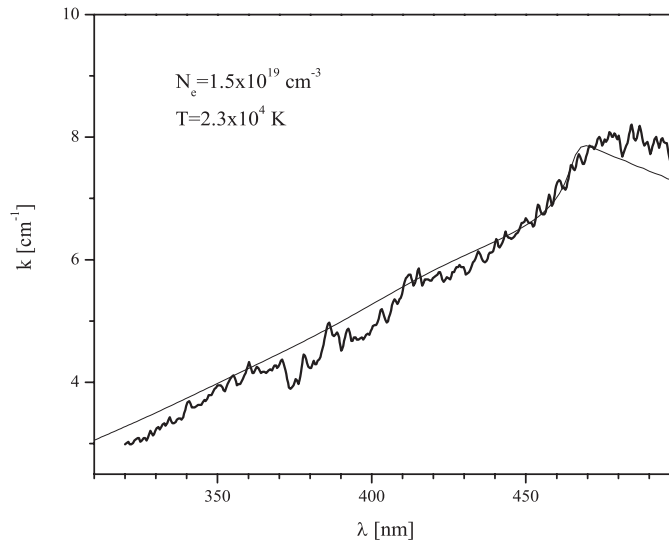


**Figure 9.** Short pulse: thin line—the absorption coefficient  $\kappa_{\text{tot}}(\lambda)$  calculated in the approximation of the variable shift with the optimal values of  $\Delta_{n=2}$  and  $\delta_{n=2}$ , namely  $\Delta_{n=2} = 0.49$  eV and  $\delta_{n=2} = 0.55$  eV. Bold line—the experimental absorption coefficient from [28].

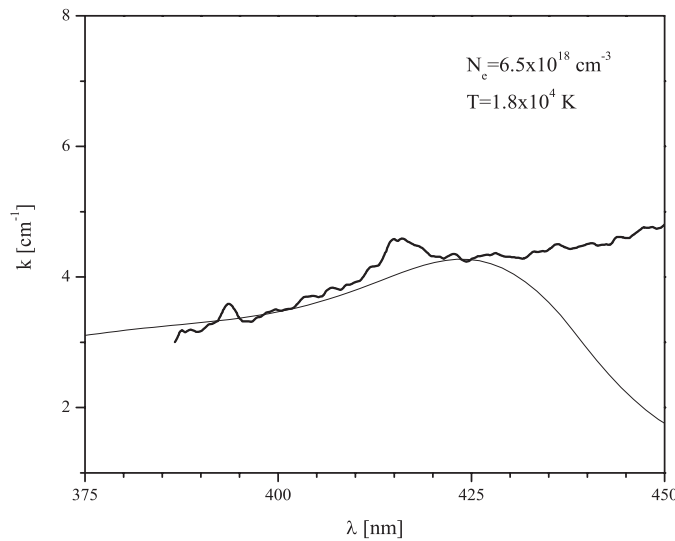


**Figure 10.** Long pulse: thin line—the absorption coefficient  $\kappa_{\text{tot}}(\lambda)$  calculated in the approximation of the variable shift with the optimal values of  $\Delta_{n=2}$  and  $\delta_{n=2}$ , namely  $\Delta_{n=2} = 0.14$  eV and  $\delta_{n=2} = 0.12$  eV. Bold line—the experimental absorption coefficient from [28].

short and long pulses, respectively, the validity of equation (18) means that  $0.455/0.130 = (1.5/0.65)^{3/2}$ , which is satisfied with an accuracy better than 1%. In the case of variable shift, we have that  $\Delta_{n=2} = 0.49$  and  $0.12$  eV for the short and long pulse, respectively, and the validity of equation (18) means now that  $0.49/0.14 = (1.5/0.65)^{3/2}$ , which is satisfied with the same accuracy.

This fact offers a possibility of determining  $\Delta_n$  or  $\Delta_{n=2}$  for any  $N_e$  and  $T$  from intervals  $0.65 \times 10^{19} \text{ cm}^{-3} < N_e < 1.5 \times 10^{19} \text{ cm}^{-3}$  and  $1.8 \times 10^4 \text{ K} \leq T \leq 2.3 \times 10^4 \text{ K}$ , and probably in some significantly wider regions, at least for  $5 \times 10^{18} \text{ cm}^{-3} \lesssim N_e \lesssim 5 \times 10^{19} \text{ cm}^{-3}$  and  $1.6 \times 10^4 \text{ K} \lesssim T \lesssim 2.5 \times 10^4 \text{ K}$ . Then, since it has been established that the influence of  $\delta_n$  is significantly weaker than the influence of  $\Delta_n$ , we can determine  $\delta_n$  for any  $N_e$  from those intervals, taking  $\delta_n = \Delta_n$ , as in the examples illustrated by the dashed curves in figures 7 and 8.

On the grounds of all that has been said, one can conclude that the presented method can already be used for calculations of the spectral absorption coefficients of dense hydrogen plasmas in the regions  $N_e \sim 10^{19} \text{ cm}^{-3}$  and  $T_e \approx 2 \times 10^4 \text{ K}$ , as long as electron–H<sup>+</sup> and electron–H(1s) inverse bremsstrahlung, negative ion H<sup>-</sup>(1s<sup>2</sup>) photo-detachment, H(1s)–H<sup>+</sup> absorption charge exchange and molecular ion H<sub>2</sub><sup>+</sup>(1Σ<sub>g</sub><sup>+</sup>) photo-dissociation can be described as in this paper. Let us note the fact that with some modifications related to the atom photo-ionization processes, which should enable the description of the influence of the atom core, the presented method can be applied to other kinds of laboratory dense hydrogen-like plasmas. Most of all, we mean alkali metals, helium and other rare-gas plasmas. Also, the obtained results can be of interest for some astrophysical plasmas, namely the plasma of the inner layers of solar atmosphere, as well as the plasmas of partially ionized layers of some other stellar atmospheres (for example some DA and DB white dwarfs).

Further development of the method described requires first of all an improvement of the procedure used, in order to replace the semi-empirical parameters with the ones determined within the procedure itself. Another step would be including into consideration atom bound-bound (photo-excitation) processes which have been omitted here, and extending the region of the method's applicability to the long wavelengths.

## Acknowledgments

The authors would like to express their gratitude to Professor V M Adamyan and Professor Lj M Ignjatović for their permanent attention, support and useful discussions. The authors are thankful to the University Pierre et Marie Curie of Paris, France, for financial support, as well as to the Ministry of Science of the Republic of Serbia for support within the project 176002 'Influence of collisional processes on astrophysical plasma line shapes'.

## References

- [1] Kobzev G, Jakubov I and Popovich M 1995 *Transport and Optical Properties of Non Ideal Plasmas* (New York: Plenum)
- [2] Adamyan V M, Djuric Z, Ermolaev A M, Mihajlov A A and Tkachenko I M 1994 *J. Phys. D: Appl. Phys.* **27** 111–8
- [3] Ichimaru S, Iyetomi H and Tanaka S 1987 *Phys. Rep.* **149** 91
- [4] Ebeling W, Kraeft W D and Kremp D 1976 *Theory of Bound States and Ionization Equilibrium in Plasmas and Solids* (Berlin: Akademie)
- [5] Kraeft W, Kremp D, Ebeling W and Ropke G 1986 *Quantum Statistics of Charged Particle System* (Berlin: Akademie)
- [6] Rinker G 1988 *Phys. Rev. A* **37** 1284  
Rinker G 1986 *Technical Report no LA-10608-MS* Los Alamos National Laboratory (unpublished)
- [7] Fortov V E and Jakubov I T 1989 *Physics of Nonideal Plasma* (New York: Hemisphere)
- [8] Adamyan V M, Djuric Z, Mihajlov A A, Sakan N M and Tkachenko I M 2004 *J. Phys. D: Appl. Phys.* **37** 1896–903
- [9] Srećković V A, Ignjatović L M, Mihajlov A A and Dimitrijević M S 2010 *Mon. Not. R. Astron. Soc.* **406** 590–6
- [10] Mihalas D 1978 *Stellar Atmospheres* 2nd edn (San Francisco: Freeman)

- [11] Mihajlov A A, Ignjatović L M, Sakan N M and Dimitrijević M S 2007 *Astron. Astrophys.* **469** 749–54
- [12] D’Ammando G, Pietanza L D, Colonna G, Longo S and Capitelli M 2010 *Spectrochim. Acta B* **65** 120–9
- [13] Omar B, Wierling A, Gunter S and Ropke G 2007 *Contrib. Plasma Phys.* **47** 315–23
- [14] Seaton M J, Yan Y, Mihalas D and Pradhan A K 1994 *Mon. Not. R. Astron. Soc.* **266** 805
- [15] Dimitrijević M S and Sahal-Brechot S 1996 *Phys. Scr.* **54** 50
- [16] Tkachenko I M and de Córdoba P F 1998 *Phys. Rev. E* **57** 2222–9
- [17] Reinholz H, Zaporoghets Y, Mintsev V, Fortov V, Morozov I and Röpke G 2003 *Phys. Rev. E* **68** 036403-1–10
- [18] Mintsev V B and Fortov V E 2006 *J. Phys. A: Math. Gen.* **39** 4319–27
- [19] Kalman G J, Rommel J M and Blagoev K 1998 *Strongly Coupled Coulomb Systems* (New York: Springer)
- [20] Gavrilova T V, Aver’yanov V P, Vitel Y, D’Yachkov L G and Kurilenkov Y K 2001 *Opt. Spectrosc.* **91** 667–74
- [21] D’Yachkov L, Khomkin A and Shumikhin A 2006 *Czech. J. Phys.* **56** B1035–9
- [22] Koester D, Spherhake U, Allard N F, Finley D S and Jordan S 1998 *Astron. Astrophys.* **336** 276
- [23] Kielkopf J F, Allard N F and Huber J 2004 *Astrophys. J.* **611** L129–32
- [24] Finley D S, Koester D and Basri G 1997 *Astrophys. J.* **488** 375
- [25] Mihajlov A A, Dimitrijević M S and Ignjatović L 1993 *Astron. Astrophys.* **276** 187–92
- [26] Mihajlov A A, Dimitrijević M S, Ignjatović L and Djurić Z 1994 *Astron. Astrophys. Suppl.* **103** 57–66
- [27] D’Yachkov I G, Kurilenkov Y K and Vitel Y 1998 *J. Quant. Spectrosc. Radiat. Transfer* **59** 53–64
- [28] Vitel Y, Gavrilova T V, D’Yachkov L G and Kurilenkov Y 2004 *J. Quant. Spectrosc. Radiat. Transfer* **83** 387–405
- [29] Zaghoul M R 2008 *J. Phys. D: Appl. Phys.* **41** 225206
- [30] Nuttall J and Cohen H L 1969 *Phys. Rev.* **188** 1542
- [31] Rescigno T N and McKoy V 1975 *Phys. Rev. A* **12** 522
- [32] Msezane A Z and Manson S T 1982 *Phys. Rev. Lett.* **48** 473
- [33] Fazio P M and Copeland G E 1984 *Phys. Rev. Lett.* **53** 163
- [34] Manson S T 1985 *Phys. Rev. A* **31** 3698
- [35] Fang T K and Ho Y K 1999 *Phys. Rev. A* **60** 2145
- [36] Sahoo S and Ho Y K 2009 *Res. Lett. Phys.* **2009** 1
- [37] Bethe H A and Salpeter E E 1957 *Quantum Mechanics Of One- And Two-Electron Atoms* (Berlin: Springer)
- [38] Murillo M S and Weisheit J C 1998 *Phys. Rep.* **302** 1
- [39] Zhao L B and Ho Y K 2004 *Phys. Plasmas* **11** 1695–700
- [40] Sahoo S and Ho Y K 2006 *Phys. Plasmas* **13** 063301–9
- [41] Shukla P K and Eliasson B 2008 *Phys. Lett. A* **372** 2897–9
- [42] Qi Y Y, Wang J G and Janev R K 2009 *Phys. Rev. A* **80** 063404
- [43] Sahoo S and Ho Y K 2010 *J. Quant. Spectrosc. Radiat. Transfer* **111** 52–62
- [44] Lin C Y and Ho Y K 2010 *Eur. Phys. J. D* **57** 21–6
- [45] Lin C Y and Ho Y K 2011 *Comput. Phys. Commun.* **182** 125–9
- [46] Mihajlov A A, Vitel Y and Ignjatovic L M 2009 *High Temp.* **47** 1–12
- [47] Mihajlov A A, Djordjevic D, Popovic M M, Meyer T, Luft M and Kraeft W 1989 *Contrib. Plasma Phys.* **29** 441
- [48] Suchy K 1964 *Beitr. Plasma Phys.* **4** 71
- [49] Kraeft W D, Luft M and Mihajlov A A 1983 *Physica A* **120** 263–78
- [50] Mihajlov A A, Djordjevic D, Vucic S, Kraeft W and Luft M 1986 *Contrib. Plasma Phys.* **26** 19–35
- [51] Mihajlov A A, Vitel Y and Ignjatovic L M 2008 *High Temp.* **46** 737–45
- [52] Debye P and Hückel E 1923 *Phys. Z.* **24** 185–206
- [53] Abramowitz M and Stegun I A 1965 *Handbook of Mathematical Functions* (New York: Dover)
- [54] Sobel’man I I 1979 *Atomic Spectra and Radiative Transitions* (Berlin: Springer)
- [55] Adamyan V M 2009 private communication
- [56] Ermolaev A M, Mihajlov A A, Ignjatovic L M and Dimitrijevic M S 1995 *J. Phys. D: Appl. Phys.* **28** 1045
- [57] Johnson L C 1972 *Astrophys. J.* **174** 227–36
- [58] Stille J L and Callaway J 1970 *Astrophys. J.* **160** 245
- [59] Wishart A W 1979 *Mon. Not. R. Astron. Soc.* **187** 59



## Review

Hydrogen Balmer lines for low electron number density plasma diagnostics<sup>☆</sup>N. Konjević<sup>a,\*</sup>, M. Ivković<sup>b</sup>, N. Sakan<sup>b</sup><sup>a</sup> Faculty of Physics, University of Belgrade, 11001 Belgrade, P.O. Box 368, Serbia<sup>b</sup> Institute of Physics, University of Belgrade, 11081 Belgrade, P.O. Box 68, Serbia

## ARTICLE INFO

## Article history:

Received 13 April 2012

Accepted 15 June 2012

Available online 28 June 2012

## Keywords:

Spectroscopic plasma diagnostics  
Spectral line shapes and intensities  
Stark broadening  
Hydrogen spectral lines  
Electron number density

## ABSTRACT

We present an analysis of the procedure for plasma electron number density,  $N_e$ , diagnostics based on the comparison of theoretical and experimental shape or width of hydrogen Balmer lines. Low  $N_e$  diagnostics, requiring an extension of available theoretical Stark broadening data tables was examined first. The difficulties encountered during experimental line profile analysis at low  $N_e$  are discussed and appropriate procedures suggested. The widely adopted deconvolution of experimental profile by fitting with a Voigt function is examined and it is shown that this deconvolution introduces large systematic error in Stark width determination. This uncertainty can be decreased but never completely avoided by fixing the Gaussian part of the Voigt function. Simple formulas of satisfactory accuracy for deconvolution at the half width of experimental profile were investigated and their application recommended. The contribution of Van der Waals broadening to the experimental profile is examined and the correction for its contribution discussed. Approximate and reliable formulas for the evaluation of  $N_e$  from the Stark width were critically evaluated. To estimate the applicability of different sets of theoretical data for  $N_e$  diagnostics, a comparison of theory versus experiments was carried out and best data tables were recommended. For low  $N_e$  diagnostics the application of higher members of Balmer series is advised whenever possible.

© 2012 Elsevier B.V. All rights reserved.

## Contents

|   |    |
|---|----|
| 1. Introduction . . . . .   | 16 |
| 2. Spectral line broadening . . . . .   | 17 |
| 3. Hydrogen Balmer line shapes below fine structure limit . . . . .           | 18 |
| 4. Hydrogen Balmer line shapes above fine structure limit . . . . .           | 18 |
| 4.1. Deconvolution of experimental profiles . . . . .                         | 19 |
| 4.1.1. Fitting with Voigt function . . . . .                                  | 19 |
| 4.1.2. Approximate formulas for deconvolution at the line halfwidth . . . . . | 20 |
| 4.1.3. Correction for Van der Waals broadening . . . . .                      | 21 |
| 4.2. Comparison theory versus experiment. . . . .                             | 23 |
| 4.3. Simple formulas for evaluation $N_e$ from the Stark width . . . . .      | 24 |
| 4.3.1. The $H_\beta$ line . . . . .   | 24 |
| 4.3.2. $H_\alpha$ and the $H_\gamma$ lines . . . . .                          | 24 |
| 4.4. Higher members of Balmer series . . . . .                                | 25 |
| 5. Summary and conclusions. . . . .   | 25 |
| Acknowledgment . . . . .  | 25 |
| References . . . . .  | 25 |

## 1. Introduction

Various  $N_e$  plasma diagnostic techniques were devised for the electron number density,  $N_e$ , one of the most important parameters for

<sup>☆</sup> This paper is dedicated to Gary M. Hieftje, on the occasion of his 70th birthday, in recognition of his boundless contributions to spectroscopy and analytical chemistry.

\* Corresponding author.

E-mail address: [konjevic@ipb.ac.rs](mailto:konjevic@ipb.ac.rs) (N. Konjević).

plasma characterization. Depending on  $N_e$  value and plasma geometry numerous modifications of microwave [1] and infrared heterodyne interferometry [2] were developed while optical interferometers [3,4] were successfully used for higher  $N_e$ . The application of visible and infrared interferometry is considerably increased after the discovery of coherent radiation sources. The lasers may be used not only as light sources, but also as detectors and amplifiers of laser radiation in the so called, laser interferometer arrangement [5], which has several

modifications, see e.g. [6]. Some important properties of interferometric  $N_e$  plasma diagnostic techniques are: no perturbation during the course of measurement and high sensitivity if appropriate wavelength used. The main drawback is that only an average  $N_e$  along interferometer beam path through plasma can be determined. In addition to interferometry, the lasers also enabled the development of Thomson scattering technique for simultaneous  $N_e$  and electron temperature,  $T_e$ , plasma diagnostics [7,8].

Parallel to the development of new techniques and improvements of the old ones, for the last fifty years the applications of Optical Emission Spectroscopy (OES) for plasma diagnostics were extensively studied. Several advantages of OES techniques attracted attention: lack of plasma perturbation during the course of measurement, high spatial resolution (as good as optical system set for plasma observation) and use of simple, robust and relatively cheap equipment usually available in laboratory. Last but not least, the OES techniques may be applied to study distant plasmas such as in astrophysics or for remote control of industrial plasma processing.

In this work the applications of the hydrogen line shape OES technique for  $N_e$  diagnostics is discussed. This technique is one of the first and most frequently used for  $N_e$  diagnostics [9]. Hydrogen lines are selected for plasma diagnostic applications because of their high line shape sensitivity (linear Stark effect) on microfield induced by charged particles – electrons and – ions. Moreover, Balmer lines are located in visible and near UV spectral region where sensitive photodetectors and other required spectroscopy equipment is widely available. As a consequence of all the advantages of Balmer lines and numerous requirements in astrophysics for plasma diagnostics, including applications such as opacity calculations (hydrogen is the most largely widespread element in the Universe), a large number of theoretical and experimental studies of these lines were carried out; see e.g. [10] and references therein. The results of this effort are evident. For example, the  $H_\beta$  line may be used for plasma diagnostic purposes in the  $N_e$  range  $(10^{22}–10^{23})\text{m}^{-3}$  with an accuracy of 5%–7% [11,12]. Here, we focus our attention on the application of hydrogen Balmer lines for low  $N_e$  diagnostics. To be more specific, the upper density limit of “low  $N_e$ ”, as defined here, is  $N_e$  for which Stark broadening dominates all other broadening mechanisms. This is plasma  $N_e$  where no deconvolution of experimental profile is required to determine  $N_e$  and depends primarily upon spectroscopic equipment used for line shape recording (instrumental broadening). It varies also from line to line within Balmer series. For example, for the  $H_\beta$  line, this limit is at  $N_e \approx 10^{21}\text{m}^{-3}$  while for the  $H_\alpha$ , it is close to  $10^{22}\text{m}^{-3}$  if lines are recorded with a medium spectral resolution instrument. For the sake of generalization, the  $N_e$  range is sometimes extended to higher electron densities.

The choice of Balmer line for diagnostics is determined by line intensity and by interference with neighboring lines in the presence of other gases. The line intensity is important for two reasons: if the line is too strong the self-absorption may be present, while weak line requires an acceptable signal to noise ratio. All in all, the  $H_\beta$  line is most frequently the best choice. The  $H_\beta$  line is also favored as the line with the most detailed sets of calculated data, which are experimentally tested in a number of studies, see e.g. [13]. Recently, the interest for the  $H_\alpha$  has considerably increased. This strong line appears when only traces of molecular hydrogen, water vapor or hydrocarbon compounds are present. In these cases, the intensity of the  $H_\beta$  is usually so low that it cannot be used for the line shape analysis.

For the correct application of line shape diagnostic techniques numerous precautions must be taken during experimental profile analysis. These are primarily related to the estimation of other broadening mechanisms, the deconvolution procedure, the self-absorption effect etc. Some of these interference effects and procedures to overcome difficulties were described and discussed already in our preceding publications [14–17] and will be mentioned here briefly for the sake

of completeness. It is useful to note that details of the various applications of hydrogen line shapes for plasma diagnostics can be found in the NIST bibliography on line shapes [13].

## 2. Spectral line broadening

The experimental line shape is the result of several plasma broadening mechanisms which are described in details in well known text books and articles, see e.g. [9,10,18]. These mechanisms are as follows:

- Natural broadening: usually negligible in most line shape plasma experiments. The line width of the Lorentz profile induced by natural broadening may be calculated if relevant transition probability data are available, see e.g. [14,16].
- Doppler broadening: unavoidable in the presence of thermal motion of emitters. If temperature of emitting particles is known and if emitters follow the Maxwellian velocity distribution, the line width is simple to evaluate, see e.g. [14,16]. The line shape in this case has a Gaussian form.
- Pressure broadening: includes three broadening mechanisms: resonance, Van der Waals (VdW) and Stark broadening. Although the evaluation of resonance and Van der Waals line widths is possible using sophisticated semiclassical and fully quantum mechanical calculations, see e.g. [19–21], the line widths are most often estimated using simple approximate formulas, see e.g. [9,14,16,22–24]. The procedure for evaluation of VdW line width is usually provided for an atomic emitter perturbed by inert gas. For the atomic emitter perturbed by molecules, see e.g. [23,24]. Both, resonance and VdW profiles have Lorentzian form. Apart from broadening, Van der Waals interaction shifts the spectral line in the red, approximately 1/3 of the FWHM, see [9]. Resonance broadening does not induce shift of spectral line. Since resonance broadening is usually negligible for the Balmer line in low electron density plasmas, we shall focus our further discussion on VdW broadening only. More details on VdW broadening contribution to Balmer lines width we refer reader to Section 4.1.3.

Stark broadening is the result of interaction between emitter and charged particles (electron and ions) in plasma; see e.g. [18]. For hydrogen lines, the disposition of energy levels and presence of Fine Structure Components (FSC) makes evaluation of line profiles laborious and time consuming. The resulting shape of Stark broadened hydrogen line has no simple Lorentz or Gauss form, which induce difficulties in its presentation and application. This is further complicated by the fact that the line shape varies with  $N_e$  and to the smaller extent with  $T_e$ . Hence, the results of hydrogen line shape calculations are usually presented in the form of tables; one table for single  $N_e$  followed by several tables for different  $T_e$ . For the evaluation of intermediate  $N_e$  and  $T_e$  profiles, one has to use an interpolation program usually supplied by the authors of data tables. In the case when one uses experimental line profile for  $N_e$  plasma diagnostics, apart from a numerical program for experimental data fitting, theoretical Stark broadening data tables with an interpolation subroutine are used to obtain best fit between theory and experiment. A simpler technique for  $N_e$  diagnostics consists of measuring line half width only and comparing it with theoretical calculations for the same  $T_e$ . Obviously, the half width technique is less accurate than the comparison of the whole line profile. Some important details of  $N_e$  diagnostics using both techniques will be discussed in the following sections.

- Instrumental broadening is an important quantity in particular at low  $N_e$  and low emitter's temperature when line profile is narrow i.e. when Stark broadening is small or comparable with other broadening mechanisms. In a large number of cases, the instrumental line shape of an imaging spectrometer is close to Gaussian but it has to be carefully determined and used in the deconvolution procedure. We recommend low-pressure discharge



as the light source for the measurement of the instrumental profile instead of a highly coherent directional light source such as the laser. However, if only the laser light source is available we recommend the removal of its directionality and spatial coherence, which can be done by transmitting the beam through lens tissue or matted glass.

- Self-absorption is the result of radiative transfer of line radiation through plasma. The central part of line profile (largest radiation intensity) is absorbed the most by the same species in the lower energy state of transition and the maximum of line profile decreases while relative line width increases if collisional deexcitation is present. If the test for self-absorption is not carried out, then we may deduce higher but erroneous  $N_e$  from the apparent increase in Stark width. The presence of self-absorption may be detected by the use of an external concave mirror which doubles the optical path of radiation through plasma, see e.g. [14]. In the case of homogenous plasma and if the line is not too much absorbed the correction of optically thick line profile to the optically thin may be performed, see e.g., [14,25]. Relative line intensities within multiplet may be used as a good indicator of the presence of self-absorption, see e.g. [17]. Unfortunately, this technique is not applicable to hydrogen lines along spectral series. Recently, a new technique for self-absorption detection was demonstrated in plasma induced by Electrolytic Oxidation (PEO). In PEO two plasma processes with different  $N_e$  and  $T_e$  occur almost simultaneously [26]. The line profiles of the  $H_{\alpha}$  and of the  $H_{\beta}$  in this case can be fitted only with two profiles of unequal widths. From the intensity ratio of two profiles within the  $H_{\alpha}$  and within the  $H_{\beta}$  it is possible to detect self-absorption of the stronger  $H_{\alpha}$  line, see Figs. 9, 10 and 13 in [26].

The use of line shapes for inhomogeneous plasma diagnostics is a very difficult task, in particular when a strong gradient of  $N_e$ ,  $T_e$  and consequently the density gradient of emitters, is present. The line profile is distorted by superposition of line radiation from cooler plasma layers onto the line profile from the central warmer part of the plasma. Then, instead of expected typical self-absorbed broadened profile we may get the resulting overall profile with smaller half width and/or distorted due to difference in line shifting in hot dense plasma and cold layer. In this case the distorted profiles cannot be used for plasma diagnostics without plasma modeling to fit experimental line shape.

Finally, in relation to self-absorption, its importance for line shape analysis and for OES plasma diagnostics in general is so large that it cannot be overemphasized.

### 3. Hydrogen Balmer line shapes below fine structure limit

As already pointed out the results of hydrogen line shape calculations are in most cases presented in the form of tables for different  $N_e$  and  $T_e$ . Stark profiles in these tables are usually given before and after convolution with Gaussian profile from Doppler broadening. Here, we discuss the results of several line shape calculations: Kepple and Griem – KG [27], Vidal Cooper and Smith – VCS [28], Stehle and Hutcheon (Model Microfield Method – MMM) [29], and Gigoso and Cardenoso (Computer Simulation – CS) [30]. Recently, Gigoso et al. [31] have performed CS Balmer line shape calculations for different hydrogen–ion–perturber combinations. It should be noted here that MMM calculation of Balmer line shapes [29] is performed for hydrogen plasma only, i.e. reduced emitter–perturber mass  $\mu = 0.5$ .

Most calculations, see [27,30,31], do not report data for  $N_e$  below certain limit. This  $N_e$  limit depends upon Fine Structure Splitting (FSS) of spectral line and varies from line to line along the spectral series [32,33]. Below this limit the separation between Fine Structure Components (FSC) becomes larger than Stark broadening width.

For example, the Fine Structure Limit (FSL) of the  $H_{\beta}$  is slightly below the lowest value in tables at  $N_e = 10^{20} \text{ m}^{-3}$ . To extend calculations below FSL we must treat each FSC separately and this includes convolution with Doppler and other broadening contributions. This is formidable task and such tables are not yet available. Since for plasma diagnostic purposes the theoretical data below  $N_e = 10^{20} \text{ m}^{-3}$  are needed, many authors linearly extrapolate Stark width,  $w_S(N_e)$ , data from the region above FSL, where  $w_S = N_e^{2/3}$  to the region below the limit, where  $w_S = N_e$ , for each FSC see Figs. 13 and 14 in [34]. The extrapolated data are then used with each FSC separately, see e.g. [23,24].

In the next step another erroneous assumption is usually made. The wavelength separation between FSC is assumed to be fixed and the Stark component (assumed Lorentzian) is convoluted with profiles of other broadening mechanisms (resonance, VdW, Doppler and instrumental). This is incorrect also, since in plasma microfield each FSC shifts differently [35,36]. To illustrate this, let us note that for  $N_e = 10^{16} \text{ m}^{-3}$  FSCs positions are shifted between  $-2.8$  and  $1.1$  MHz (depending upon component) with respect to the zero field according to theoretical calculations [35] or between  $-7.4$  and  $+5.8$  MHz in accordance with the experiment [36]. In addition to shift, it was also wrongly assumed that Stark width of each FSC is the same. On the contrary, the calculations [35] and experiment [36] at  $N_e = 10^{16} \text{ m}^{-3}$  report FSC Stark widths between  $3.7$  and  $8.8$  MHz or between  $12$  and  $14.2$  MHz, respectively. Finally, when all broadening contributions for each FSC are taken into account their profiles are summed up and the overall “Voigt like” profile obtained. In the last step, the “Voigt like” profile was deconvoluted and the half width of Lorentz fraction was used to deduce  $w_S$ , see e.g. [23,24]. Thus, it was assumed again that the resulting Stark profile has Lorentzian form which is another erroneous assumption, see Section 4.1. The described procedure for evaluation of theoretical  $w_S$  below FSL of the  $H_{\beta}$  line is burdened with so many dubious assumptions that any agreement between  $N_e$  determined this way and using another diagnostic technique is only accidental.

Here, one should note that the FSL depends primarily upon the upper quantum number of the spectral line and differs considerably along the Balmer series. The electron density at the FSL decreases for higher member of the series e.g.  $6 \times 10^{20}$  for the  $H_{\alpha}$ ,  $4 \times 10^{19} \text{ m}^{-3}$  for the  $H_{\beta}$ ,  $10^{19} \text{ m}^{-3}$  for the  $H_{\gamma}$  [33], etc. In addition to the difficulty caused by the appearance of FSC, in a number of cases Doppler and instrumental broadening introduce another limitation in determination of low electron densities. The influence of both effects was studied in [33]. In the conclusion of the discussion about the extension of Stark broadening data tables below FSL we state that the only correct approach would be an extension of the data tables. At this moment data from the tables may be extended safely by using  $w_S \sim N_e^{2/3}$  dependence to FSL of  $4 \times 10^{19} \text{ m}^{-3}$  for the  $H_{\beta}$  and increase FSL for the  $H_{\alpha}$  to  $6 \times 10^{20} \text{ m}^{-3}$  from tabulated value at  $10^{20} \text{ m}^{-3}$ . Experimental and theoretical studies in the vicinity of FSL are desirable.

### 4. Hydrogen Balmer line shapes above fine structure limit

For the electron densities above FSL in the region where Stark broadening tabulated data are available, large error in  $N_e$  diagnostics can be induced by the application of an inappropriate deconvolution procedure or by the use of inappropriate data tables. In the following sections we deal with both potential sources of error frequently met in reports of plasma characterization. To demonstrate difficulties encountered in the analysis of experimental profiles we used theoretical line shapes to avoid interference with the experimental data scatter, which blur the effects intended to demonstrate. In addition, the theoretical data are available in a wide range of plasma parameters, which helps to generalize conclusions.

#### 4.1. Deconvolution of experimental profiles

Whenever the contribution of other broadening mechanisms compared to Stark broadening is not negligible, the deconvolution procedure must be employed to determine Stark width –  $w_S$ , which is used to determine  $N_e$  from the comparison with theoretical widths at the same  $T_e$ . Another approach is to fit the whole experimental line shape with the theoretical Stark profile and determine  $N_e$  from the best fit. This approach will be discussed later.

##### 4.1.1. Fitting with Voigt function

As already pointed out, deconvolution is most frequently performed by the fitting experimental profile with the Voigt function and then, assuming that Stark width equals Lorentzian part of Voigt profile –  $w_L$ , the Stark width –  $w_S$  is extracted. The electron density  $N_e$  is determined from the comparison with theoretical Stark widths –  $w_S$  for the same  $T_e$ . Such a deconvolution procedure is employed in spite of the fact that the Stark profile has no Lorentz form neither below neither above FSL, see examples in Fig. 1. Otherwise there would be no need for Stark broadening tables and theoretical Stark widths would be presented as Lorentzian half widths.

**4.1.1.1. The  $H_\beta$  line.** To illustrate the inadequacy of the  $H_\beta$  line profile fitting with the Voigt function we convoluted the theoretical Stark profile tabulated for reduced mass  $\mu=1$  (e.g. hydrogen emitter in argon plasma);  $N_e=10^{20} \text{ m}^{-3}$ ;  $T_e=4168 \text{ K}$  [31] with Gaussian corresponding to Doppler temperature ( $T_g=T_e=4168 \text{ K}$ ). Then, the generated profile was fitted with the Voigt function using several commercial programs, all giving almost identical results. The typical fit is presented in Fig. 2a. The overall profile is in excellent agreement with the Voigt function, see the residue which is smaller than 1%. However, the results for the half widths obtained after deconvolution of the best fit Voigt profile in Fig. 2a are very different from starting broadening parameters. The half width of the Lorentz part of Voigt profile  $w_L$  is 2.74 times smaller than Stark width  $w_S$  used to generate overall profile. If one assumes  $w_L=w_S$  large error is introduced. On the other hand, the Gaussian part is enormously enlarged and the temperature of emitters determined from  $w_G$  exceeds  $T_e$  more than three times ( $T_g=3.21 * T_e$ ).

If the fitting procedure is performed with the Voigt function having a fixed Gaussian, which implies knowledge of emitters' temperature and instrumental profile width, the overall agreement of the best fit is worse, see residue in Fig. 2b, but the agreement with  $w_S$  used for the overall profile generation is better,  $w_L/w_S=0.76$ , which is still in large systematic disagreement with starting  $w_S$ .

In order to estimate the accuracy of Stark half width –  $w_S$  evaluated by fitting generated profiles with Voigt function in a broad range of plasma parameters we repeated fitting procedure, see Fig. 2, with all profiles tabulated in [31] for relative reduced mass  $\mu_R=1$ . Here,  $\mu_R$  corresponds to the reduced mass  $\mu=1$  where  $\mu_R=\mu * T_e/T_i$  while  $T_e$  and  $T_i$  are temperatures of electrons and heavy particles respectively and  $T_e=T_g$ .

In Fig. 3 the parameter –  $\rho$  is the ratio of distance between particles –  $\rho_0$  and Debye length –  $\rho_D$  ( $\rho = \rho_0 / \rho_D$ ):

$$\rho = (3/4\pi)^{1/3} * (q^2/\epsilon_0 k)^{1/2} * N_e^{1/6} * T_e^{1/2} = 0.00899 * N_e^{1/6} [m^{-3}] * T_e [K]^{1/2} \quad (1)$$

where  $q$  is electron charge,  $\epsilon_0$  is dielectric constant of vacuum and  $k$  – Boltzmann constant. To facilitate the analysis of the results in Fig. 3 and other results presented below, the values of the electron temperatures for different  $\rho$  and  $N_e$  are presented in Table 1.

The results in Fig. 3 show that fixing the Gaussian part of Voigt fitting function increases the accuracy of deconvolution with the

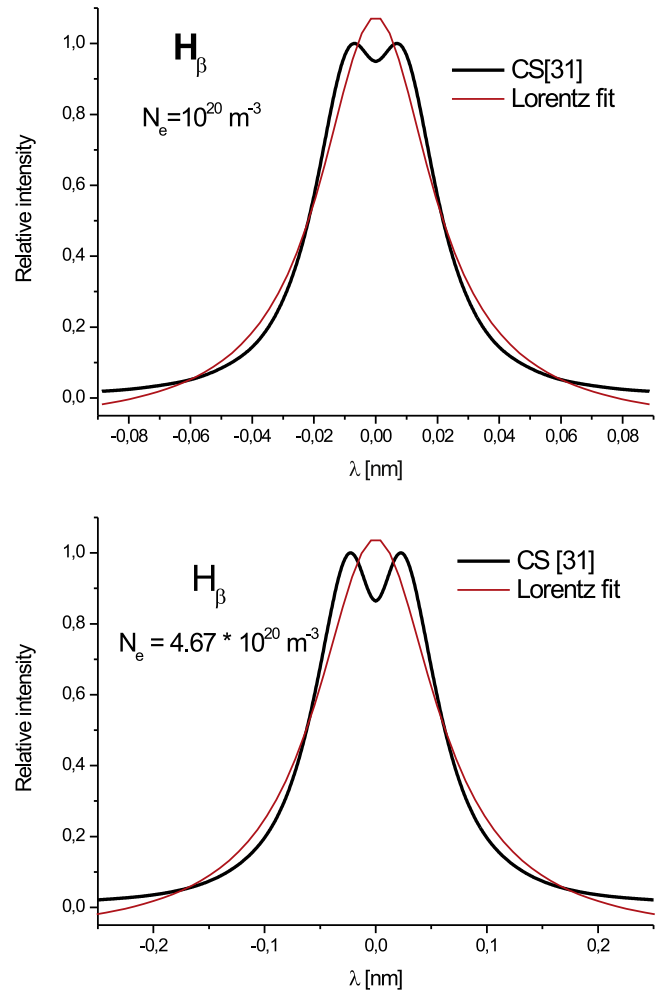


Fig. 1. The examples of Stark profiles for the  $H_\beta$  line at: a)  $N_e=10^{20} \text{ m}^{-3}$ ;  $T_e=4168 \text{ K}$  and b)  $N_e=4.67 * 10^{20} \text{ m}^{-3}$ ;  $T_e=5108 \text{ K}$ . For comparison with Stark profile best fit Lorentz function (thin line) is shown.

Voigt function for all studied plasma parameters, but a substantial error still remains.

Here and in other comments of the  $w_L/w_S$  ratio the term “accuracy” and “error” are used to describe deviation between half width  $w_L$  and starting Stark width  $w_S$ . Thus, the largest accuracy or zero error, is in the case of  $w_L/w_S=1$ .

The accuracy of deconvolution of generated Stark  $\otimes$  Gaussian profiles by fitting to the Voigt function depends on the deviation of the Stark profile from the Lorentz form and to a smaller extent upon the ratio of Stark and Gaussian half width  $w_G$ . The latter value can be calculated from

$$w_G^2 = w_{D1}^2 = w_D^2 + w_I^2 \quad (2)$$

where  $w_{D,1}$  is half width of the Gaussian resulting from convolution of Doppler,  $w_D$ , and instrumental,  $w_I$  profile. We assume here that instrumental profile has a Gaussian intensity distribution.

The degree of deviation of the Stark profile from the Lorentz shape can be illustrated using the ratio of line width at 1/10 and 1/2 of line intensity,  $w_{0.1}/w_{0.5}$ , which is 3.0 for Lorentz profile, see e.g. [37]. In the case of the  $H_\beta$  line the deviation from the Lorentz profile is largest, see Table 2. Thus, the accuracy of  $H_\beta$  line profile achieved by fitting with the Voigt function is worst in comparison with other two studied Balmer lines.

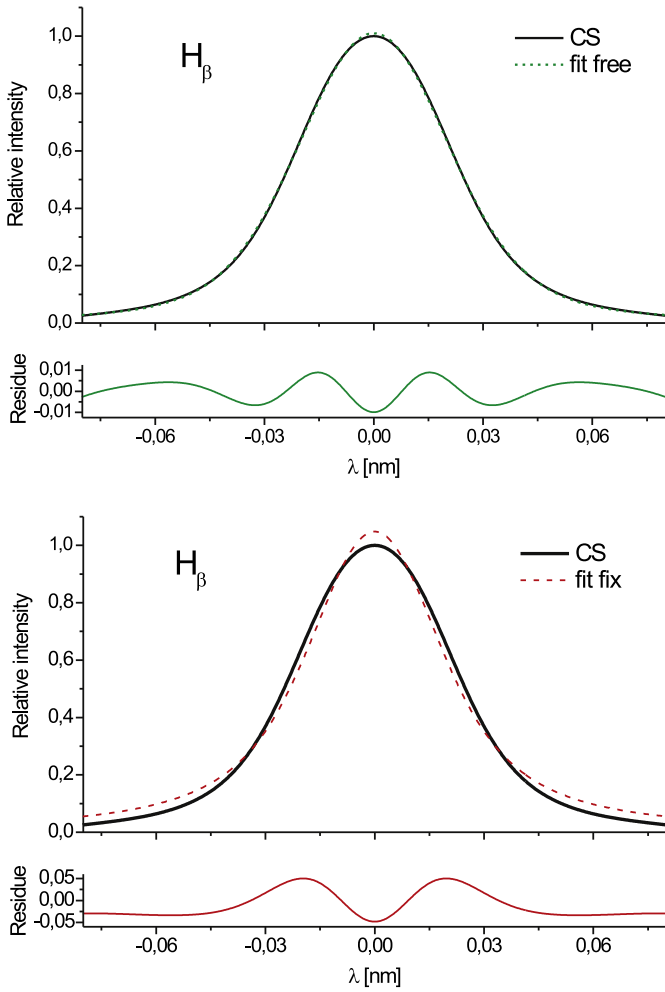


**Fig. 2.** The example of fitting the  $H_{\beta}$  profile at  $N_e = 10^{20} \text{ m}^{-3}$ ;  $T_e = T_g = 4168 \text{ K}$  (bold line) with Voigt function: a) without presumption about the Gaussian contribution (dotted line) and b) with fixed Gaussian contribution (dashed line). Lower curves correspond to residuals between generated and fitted functions.

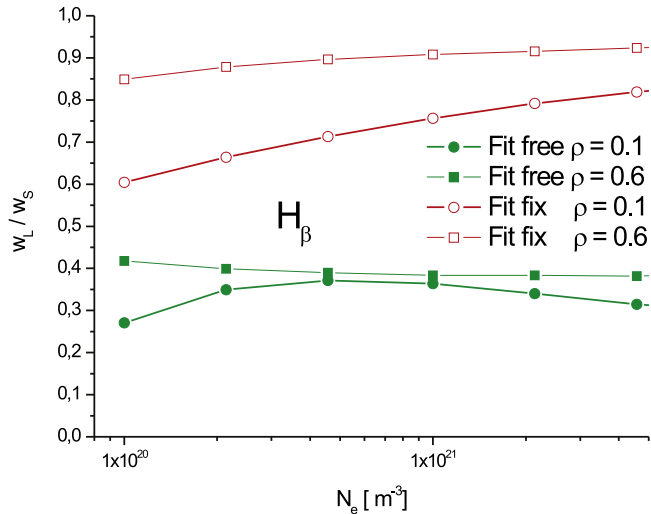


**Fig. 3.** The ratio of the halfwidths  $w_L/w_S$  versus electron number density  $N_e$  for the  $H_{\beta}$  line: two lower curves are border lines for the Voigt free parameter fit are for  $\rho$ , in the range (0.1–0.6) [31] while two upper curves are border lines for Voigt fitting with fixed Gaussian part of Voigt function.

4.1.1.2. *The  $H_{\alpha}$  and the  $H_{\gamma}$  lines.* The Stark profile of the  $H_{\alpha}$  is closer to the Lorentz function, see Fig. 4a. Thus, the overall line shape obtained after convolution of Stark profile with Gaussian is closer to Voigt as well, see Fig. 4b.

Under the same plasma conditions, however, the deconvolution error of the  $H_{\alpha}$  is larger than for the  $H_{\beta}$  line as a consequence of smaller Stark and larger Doppler width. This is especially evident at higher temperatures ( $\rho < 0.3$ ) and/or at lower  $N_e$  when Stark to Gaussian width ratio –  $w_S/w_G$  becomes small, see Table 2, causing lower accuracy in determination of the Lorentz fraction. Consequently, very small residuals are obtained even when fitting of the  $H_{\alpha}$  is performed with Gaussian. The influence of the contribution of Gaussian fraction to the accuracy of deconvolution for  $\rho = 0.3$  (most laboratory plasmas) is illustrated by Fig. 5.

From the point of view of the similarity with Lorentz function, see Table 2 and Fig. 6a, the fitting accuracy of the  $H_{\gamma}$  Stark profile with Voigt function is an intermediate case between first and second Balmer line. Fitting without fixing Gaussian parameter of the Voigt function looks good i.e. the residuals are small, see Fig. 6b, but the estimation of Stark half widths is poor. By fixing Gauss fraction when fitting with Voigt function, the  $w_L/w_S$  ratio becomes closer to one, see below Fig. 8c.

#### 4.1.2. Approximate formulas for deconvolution at the line halfwidth

In the foregoing section we have shown that the accuracy of  $w_S$  is improved by fitting the experimental profile with Voigt function having fixed Gaussian fraction –  $w_G$ . Here, we propose the use of the pre-determined Gauss fraction full width,  $w_G$ , with one of two following formulas for the Voigt function [38,39]:

$$w_V = w_L/2 + \left( (w_L/2)^2 + w_G^2 \right)^{1/2} \quad (3)$$

$$w_V = 0.5346 * w_L + \left( 0.2169 * w_L^2 + w_G^2 \right)^{1/2} \quad (4)$$

where  $w_V$  is the full half width (FWHM) of the Voigt profile.

We successfully used formulas (3) and (4) for deconvolution of Stark profile halfwidths, see below, with an accuracy exceeding the one for whole profile deconvolution technique, see Section 4.1.1.

4.1.2.1. *The  $H_{\beta}$  line.* First, a simple deconvolution formula was developed from the comparison of theoretical widths of VCS Stark profiles [28] before and after convolution with Gaussian (Doppler profile). The formula has the following form [40]:

$$w_S = \left( w_m^{1.4} - w_{D,I}^{1.4} \right)^{1/14} \quad (5)$$

where:  $w_m$  is measured halfwidth of experimental profile.

In addition to Eq. (5) we applied formulas (3) and (4) to deconvolute the  $H_{\beta}$  profiles for  $\rho$  between 0.1 and 0.6, see Fig. 7. The results in Fig. 7 show that the ratio  $w_L/w_S$  decreases for low  $N_e$  and low  $\rho$  values but the accuracy of the deduced  $w_S$  is always better with approximate formulas than by fitting the whole experimental profile with Voigt function.

To achieve the highest accuracy of  $N_e$  plasma diagnostics at lower  $N_e$  and higher  $T_e$ , the use of a program for line fitting of the  $H_{\beta}$  line [41] is recommended. However, in the gas mixtures when interference of hydrogen lines with neighboring lines occur the use of approximate deconvolution formulas (3)–(5) have an advantage.

4.1.2.2. *The  $H_{\alpha}$  and the  $H_{\gamma}$  lines.* The application of approximate formulas (3)–(5) with the  $H_{\alpha}$  line gives results with an accuracy exceeding the one estimated for the  $H_{\beta}$ . The value of  $w_L$  for medium temperatures –  $\rho = 0.3$  is only a few percent different from the  $w_S$  used to generate the Stark profile. This holds also for low electron densities of several



**Table 1**  
Electron temperatures  $T_e$  for different  $\rho$  and different electron number densities  $-N_e$ .

| log $N_e$ [ $m^{-3}$ ] | $T_e$ [K] |        |        |       |        |        |        |        |         |
|------------------------|-----------|--------|--------|-------|--------|--------|--------|--------|---------|
|                        | 20        | 20.333 | 20.667 | 21    | 21.333 | 22     | 23     | 24     | 25      |
| $\rho = 0.1$           | 37508     | 48444  | 26568  | 80809 | 104369 | 174098 | 375083 | 808092 | 1740981 |
| $\rho = 0.3$           | 4168      | 5383   | 6952   | 8979  | 11597  | 19344  | 41676  | 89788  | 193442  |
| $\rho = 0.6$           | 1042      | 1346   | 1738   | 2245  | 2899   | 4836   | 10419  | 22447  | 48361   |

times  $10^{20} m^{-3}$ , see Fig. 8a. It is interesting to note that the most accurate widths  $w_L$  are determined from Eq. (5), which is derived and originally applied to the  $H_\beta$  profiles only [40].

From the results of the analysis for the  $H_\alpha$  and  $H_\gamma$  line in Fig. 8 for  $\rho$  in the range 0.3–0.6 (plasmas with medium temperatures, see Table 1) follows that by using Eqs. (3)–(5) for profile deconvolution at the half width, the achieved accuracy is better than 10%.

#### 4.1.3. Correction for Van der Waals broadening

For low  $N_e$  plasmas operated at high pressures like e.g. microwave induced plasmas, atmospheric pressure arcs and jets, the Van der Waals broadening contribution may not be negligible in comparison with Stark broadening.

Up to now only the deconvolution of the Gauss (Doppler + instrumental broadening) from the Stark profile was considered. In the presence of VdW, after deconvolution of Gaussian components, the remaining part (Stark  $\otimes$  VdW) has to be deconvoluted also. The adopted procedure for this deconvolution, which is necessary to perform before evaluating  $w_S$ , is to subtract estimated VdW Lorentz width,  $w_{VdW}$ , from the Stark  $\otimes$  VdW part of the experimental profile. Here, we made an attempt to test this simple and, in its essence, incorrect deconvolution procedure. In addition to this, the overall VdW line shape of hydrogen lines has no Lorentz distribution at low perturber densities, see below.

First, it is necessary to estimate the shape and width of VdW contribution. As pointed out already in Section 3 the hydrogen lines consists of several FSC. The line shape of each FSC broadened by VdW is described by Lorentz function, see e.g. [23,42], whose FWHM can be calculated from the following formula, see e.g. [9,14]

$$w_{VdW}[cm] = 8.18 \times 10^{-12} * \lambda^2 * (\bar{\alpha} < R^2 >)^{2/5} * (T/\mu)^{3/10} * N \quad (6)$$

where  $<R^2>$  is the difference between the squares of the expectation values (in units of  $a_0$ ) of the coordinate vector of the radiating electron in the upper and lower state of the transition,  $\bar{\alpha}$  – the mean atomic polarizability of the neutral perturber and  $\mu$  is the atom-perturber reduced mass in a.m.u. Introducing

$$K_1 = \lambda^2 * <R^2>^{2/5} \quad K_p = \bar{\alpha}^{2/5} / \mu^{3/10} \quad (7)$$

and by substitution of  $N$  with pressure,  $p$ , the Eq. (6) may be written as

$$w_{VdW}[nm] = 5.925 * 10^{14} K_1 * K_p * p[mbar] * T[K]^{-0.7} \quad (8)$$

The coefficients in the above equation depend on line –  $K_1$  and perturber's parameters –  $K_p$ , see Table 3.

**Table 2**  
Parameters  $w_{0.1}/w_{0.5}$  and  $w_S/w_D$  for the first three hydrogen Balmer lines. The  $w_S$ ,  $w_D$  and  $w_S/w_D$  are given for  $N_e = 10^{20} m^{-3}$   $\rho = 0.3$   $T_e = T_g = 4$  168 K.

| Line       | $w_{0.1}/w_{0.5}$ |       | $w_S$  | $w_D$  | $w_S/w_D$ |
|------------|-------------------|-------|--------|--------|-----------|
|            | Min               | Max   |        |        |           |
| $H_\alpha$ | 2.686             | 3.65  | 0.013  | 0.03   | 0.433     |
| $H_\beta$  | 2.06              | 2.285 | 0.0437 | 0.0225 | 1.942     |
| $H_\gamma$ | 2.23              | 2.68  | 0.055  | 0.02   | 2.74      |

The examples of the  $H_\beta$  VdW line profiles in argon at 800 K for different gas pressures are presented in Fig. 9. The profiles were obtained by summing profiles of FSC having Lorentz widths as calculated from Eq. (8). Relative FSC line intensities and wavelengths are taken from [44].

With the exception of VdW profiles for low perturber pressures, see Fig. 9, the overall line shape can be approximated with Lorentz function whenever the  $w_{VdW}$  of FSC is greater than 0.05 nm (five times maximum separation between line components), see also [23]. For the  $H_\beta$  line in argon the range of  $p$  and  $T_g$  when VdW profile can be approximated with Lorentz function is presented in Fig. 10. For any other perturber or line, similar graph can be evaluated from Eq. (8) and Table 3. If FSC line width  $w_{VdW} < 0.05$  nm the deconvolution

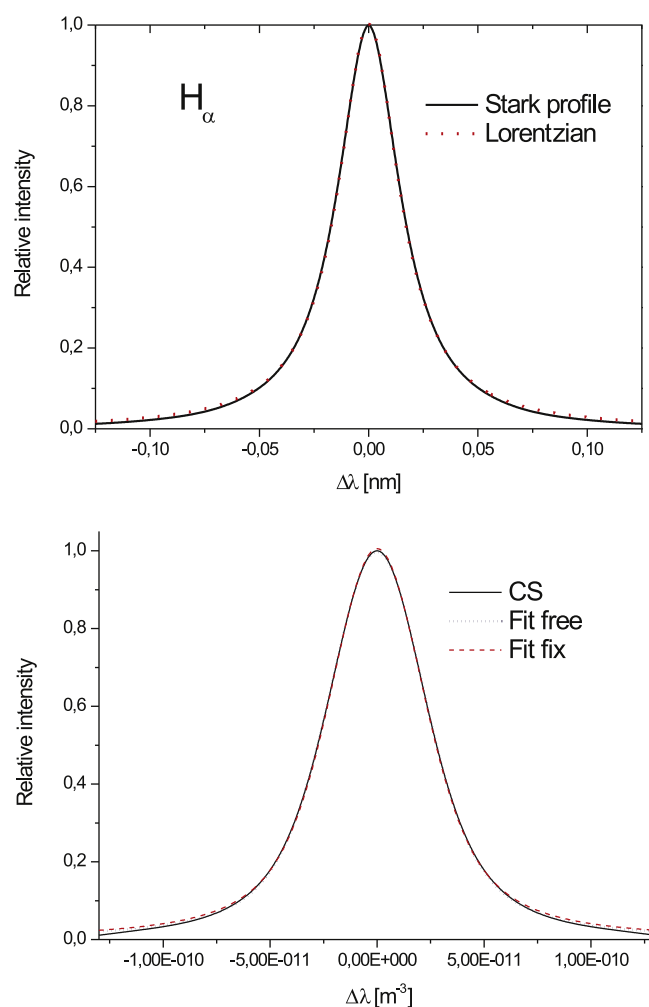


**Fig. 4.** The examples of the  $H_\alpha$  line profile fitting for  $N_e = 4.67 * 10^{20} m^{-3}$  and  $T_e = 5108$  K: a) Stark profile (thin line) with Lorentz function (dotted line) and b) Stark profile convoluted with Doppler for  $T_e = T_g$  (thick line) fitted with Voigt function: without presumption about the Gaussian contribution (dotted line) and with fixed Gaussian part (dashed line).

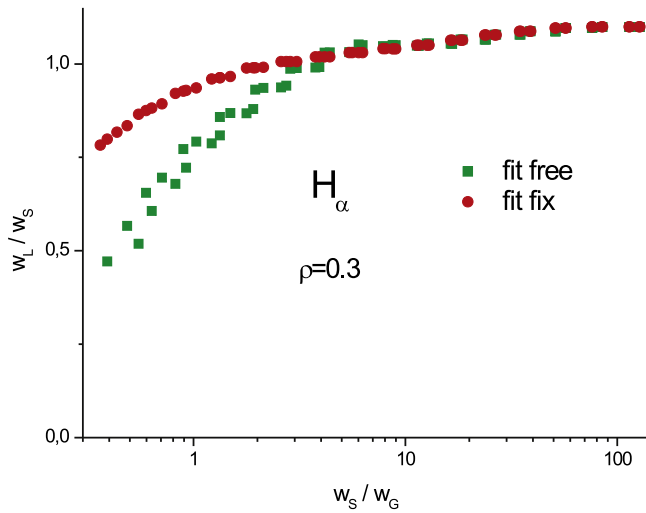


Fig. 5. The dependence of the ratios  $w_L/w_S$  on  $w_S/w_G$ .

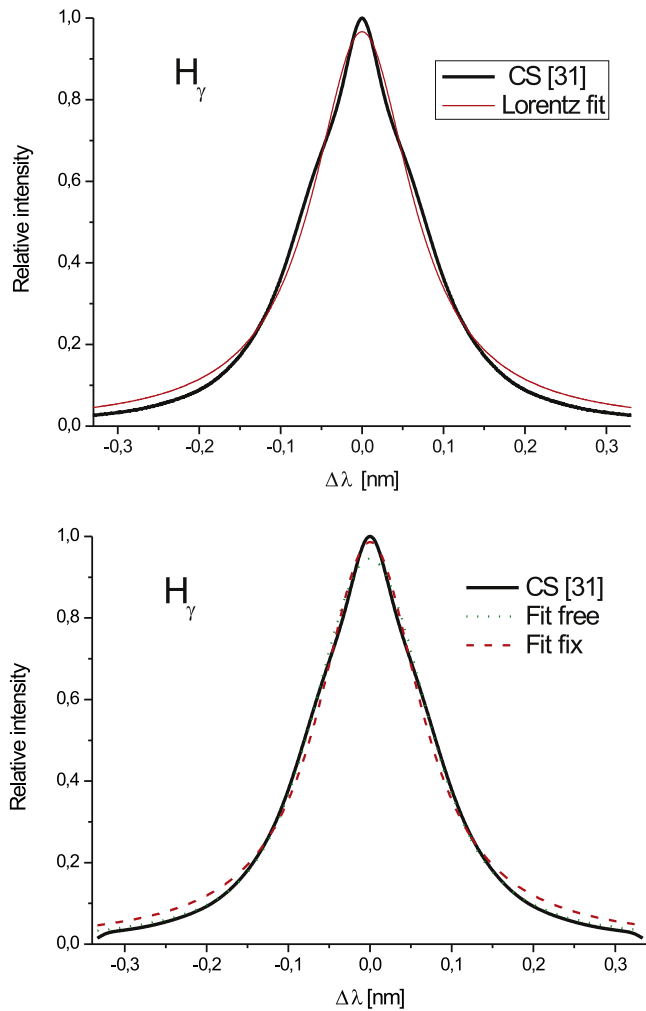


Fig. 6. The examples of the  $H_\gamma$  line profile for  $N_e = 4.67 \cdot 10^{20} \text{ m}^{-3}$  and  $T_e = 5 \text{ 108 K}$ : a) Stark profile (thick line) fitted with Lorentz function (thin line) and b) Stark profile convoluted with Doppler for  $T_e = T_g$  (thick line) and fitted with Voigt function: without presumption about the Gaussian contribution (dotted line) and with fixed Gaussian part (dashed line).

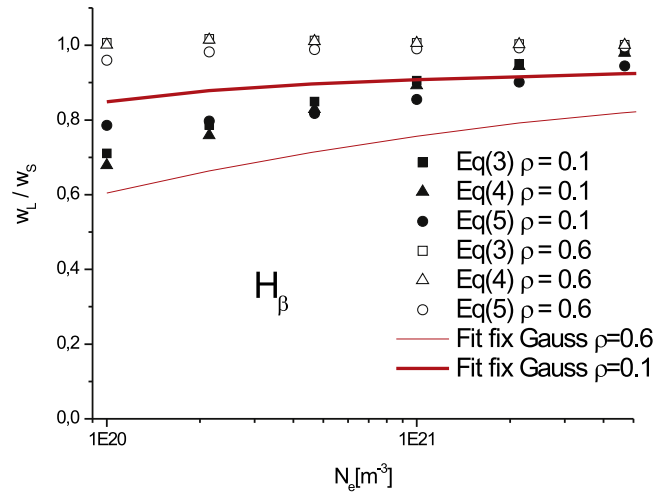


Fig. 7. The ratio  $w_L/w_S$  for the  $H_\beta$  line versus electron number density  $N_e$  for  $\rho = 0.1$  and  $0.6$  evaluated by fitting profile with Voigt function having fixed Gaussian and corresponding results from formulas (3)–(5).

of VdW contribution has to be performed using the line shape form evaluated from the sum of FSC.

After the evaluation of the VdW profile, an attempt is made to test the accuracy of the  $w_S$  determination by using deconvolution with simple subtraction ( $w_S \otimes w_{VdW}$ ) –  $w_{VdW}$ . For these tests VdW Lorentz profile is convoluted with Stark or Stark  $\otimes$  Doppler profiles.

**4.1.3.1. The  $H_\beta$  line.** In cases when VdW profile is approximated by Lorentz function, the error in determination of  $w_S$  by subtraction from convoluted Stark  $\otimes$  VdW profile becomes significant if  $w_{VdW}$  is comparable or larger than  $w_S$ . The error in the determination of  $w_S$  after the subtraction of  $w_{VdW}$  after deconvolution from Stark  $\otimes$  VdW  $\otimes$  Gauss using Eqs. (3)–(5) is approximately equal to the sum of errors caused by two deconvolution processes. Thus, the above analysis confirms that the deconvolution by subtraction of  $w_{VdW}$  is valid whenever VdW profile has Lorentz shape.

**4.1.3.2. The  $H_\alpha$  and the  $H_\gamma$  lines.** For the  $H_\alpha$  line the deconvolution error of VdW contribution is of the same magnitude as for the  $H_\beta$  line. For the same plasma conditions the largest source of error is usually lower Stark width in comparison to  $w_{VdW}$ . For the  $H_\gamma$  line the deconvolution by subtraction for the same plasma conditions is most accurate in comparison with other two studied Balmer lines. This is caused by higher  $w_S/w_{VdW}$  ratio than for the  $H_\alpha$  and for the  $H_\beta$  line. Smaller deviation of the  $H_\gamma$  from the Lorentz shape in comparison with the  $H_\beta$  line, see Table 2, is important also.

All conclusions in the above analysis are based on the assumption that each FSC has identical line shift. The VdW line shift,  $d_{VdW}$ , for all FSC is estimated to be equal to 1/3 of  $w_{VdW}$ :  $d_{VdW}$  is always red i.e. towards larger wavelengths, see e.g. [9]. It was shown [43] however, that  $d_{VdW}$  depends strongly upon the perturber. For example the ratio  $d_{VdW}/w_{VdW}$  for 2p–3d component of the  $H_\alpha$  line is equal to  $-0.046$ ,  $+0.027$  and  $+0.397$  for He, Ne and Ar perturbers respectively [43]. Since  $d_{VdW}$  for 2p–3d component of the  $H_\alpha$  is only available for three perturbers (to the authors' knowledge, data for the  $H_\beta$  are not available) we propose, as adopted already, to neglect the influence of variation from line to line of the  $d_{VdW}$  to  $N_e$  measurements.

Testing of the influence of  $d_{VdW}$  on deconvolution was performed only in cases when VdW profile is well approximated with Lorentz function. For these tests VdW Lorentz profile red shifted by  $w_{VdW}/3$  is convoluted with Stark  $\otimes$  Doppler profiles. For all tested cases the results remain the same or within 1% with results obtained without inclusion of VdW shift.

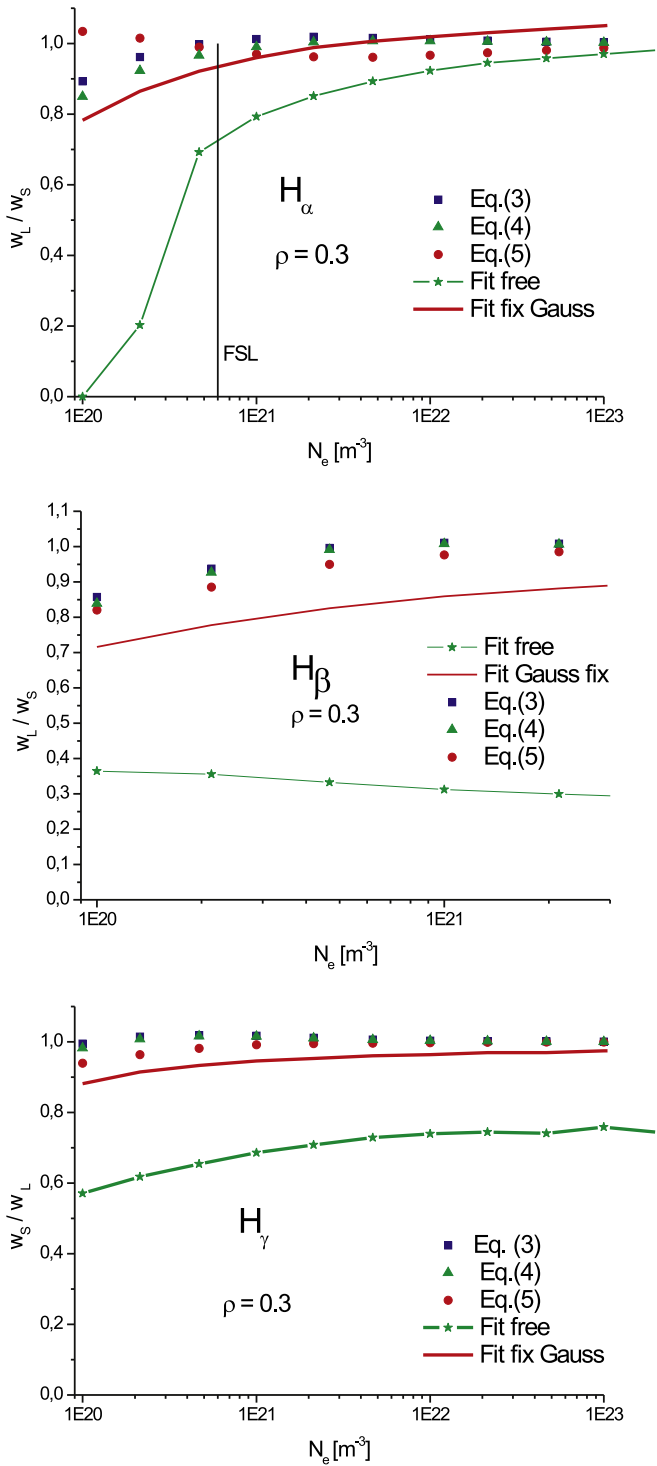


Fig. 8. The comparison of  $w_L/w_S$  evaluated for  $\rho = 0.3$  and  $w_L = 0.02$  nm from approximate formulas (3)–(5) for the: a)  $H_\alpha$ , b)  $H_\beta$ , and c)  $H_\gamma$  line. FSL – fine structure limit.

Table 3  
Line –  $K_i$  and perturber coefficients –  $K_p$ , see Eq. (7). Data for  $\alpha$  taken from [43].

| Perturber        | He         | Ne        | Ar    | Kr    | Xe    |       |
|------------------|------------|-----------|-------|-------|-------|-------|
| $K_p [10^{-10}]$ | 1.43       | 1.76      | 3.095 | 3.63  | 4.40  |       |
| Line             | $H_\alpha$ | $H_\beta$ |       |       |       |       |
| Transition       | 3d–2p      | 3p–2s     | 3s–2p | 4d–2p | 4p–2s | 4s–2p |
| $K_i [10^{-8}]$  | 2.695      | 3.077     | 3.402 | 2.757 | 2.945 | 3.069 |

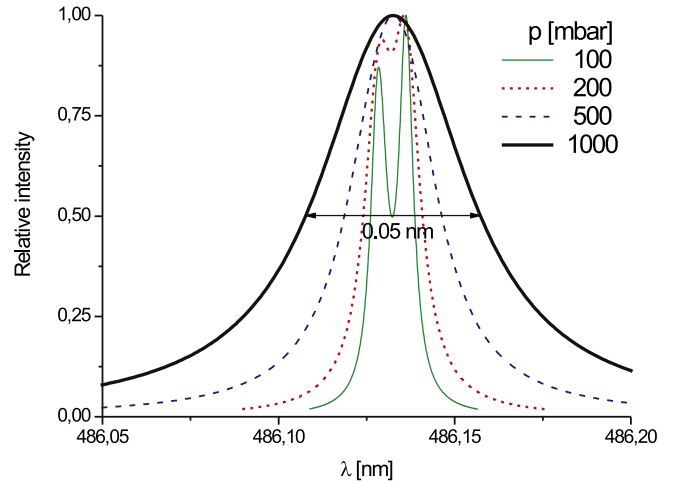


Fig. 9. The VdW profiles of the  $H_\beta$  line in argon at  $T_g = 800$  K at different pressures.

4.2. Comparison theory versus experiment

Numerous experiments were carried out to test theoretical calculations for hydrogen Balmer line shapes, see NIST bibliography [13]. For  $N_e < 10^{23} \text{ m}^{-3}$  and for the first three Balmer lines the experimental tests of theoretical calculations show the following:

The  $H_\beta$  line: mutual agreement of Stark widths from three sets of theoretical calculations, KG [27], VCS [28], MMM [29] and CS [30,31] is within 6–10% [11,31], see also Fig. 11. The overall agreement between theoretical calculations and experiment is in the range 10–15%, see e.g. [11,31,34].

The central part of the  $H_\beta$  line is not correctly described by KG [27] and VCS [28] calculations, which do not take into account ion dynamics effect. For the comparison of experimental the  $H_\beta$  line profiles with theory see e.g. [11,18].

Since the  $H_\beta$  line is frequently used for plasma diagnostics several numerical programs, which are developed for fitting experimental profiles and comparison with results of theoretical calculations; for an overview of different programs see e.g. [15]. Here, we recommend program for use with the  $H_\beta$  experimental profiles [41], with three sets of theoretical data (MMM, VCS and CS) for  $N_e$  diagnostics.

The  $H_\alpha$  and the  $H_\gamma$  lines. The comparison of theoretical results with experiments, see Figs. 12 and 13, shows best agreement between

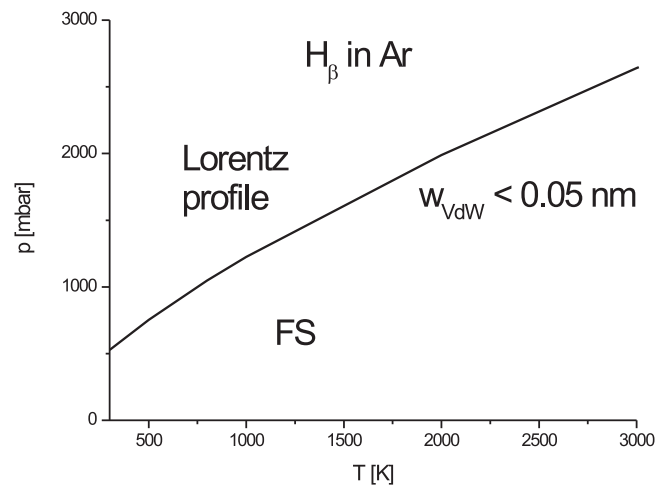
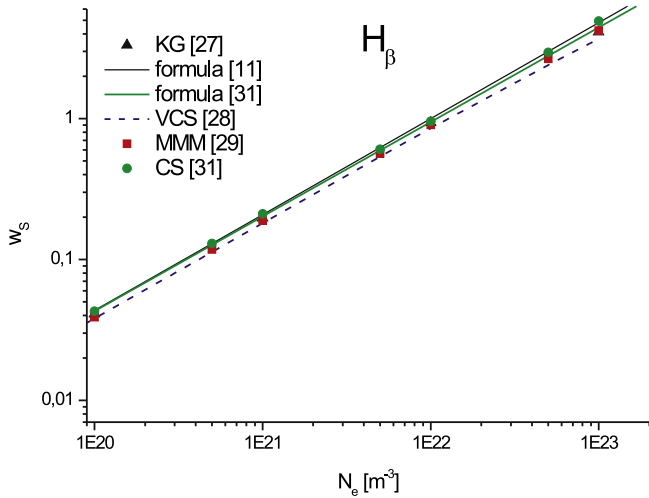


Fig. 10. The regions of VdW deconvolution for the  $H_\beta$  line profile with argon perturbers: above straight line VdW profile can be approximation with Lorentz function and the deconvolution with subtraction procedure may be applied.



**Fig. 11.** The comparison of  $w_s = f(N_e)$  for the  $H_\beta$  line deduced from different theories and approximate formulas.

experiment and CS [30,31] and MMM [29] calculations. For the  $H_\gamma$  mutual agreement between CS and MMM is better.

From the comparison of data in Figs. 12 and 13 follows that the results of MMM [29] and CS [30,31] calculations are recommended for low  $N_e$  plasma diagnostics. At  $N_e$  approaching  $10^{23} \text{ m}^{-3}$  mutual agreements of all theoretical calculations and the agreement with experiments improves considerably.

#### 4.3. Simple formulas for evaluation $N_e$ from the Stark width

If the approximate deconvolution formulas (3)–(5) are employed to determine Stark half width  $w_s$ , see Section 4.1.2, for  $N_e$  measurement, one can use simple approximate formulas that correlate  $w_s$  with  $N_e$ .

##### 4.3.1. The $H_\beta$ line

First approximate formula is deduced from the  $H_\beta$  experimental Stark widths for the  $N_e$  range  $(1.5 - 30) \times 10^{22} \text{ m}^{-3}$  in Ref. [11]:

$$N_e [\text{m}^{-3}] = 10^{22} * (w_s[\text{nm}]/0.94666)^{1.49} \quad (9)$$

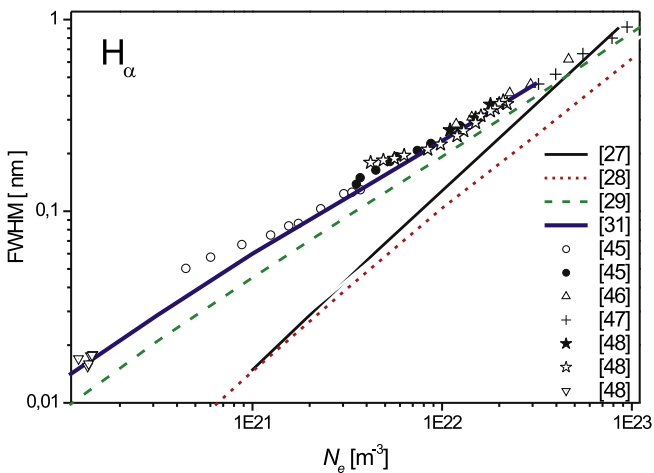


**Fig. 12.** Comparison of experimental and theoretical halfwidths –  $w_s$  for hydrogen Balmer alpha line. Theories: KG [27] – thin line, VCS [28] – dotted line, MMM [29] – dashed line, CS [31] – thick line. Experiment:  $\circ$  – Ehrich and Kelleher (70 Torr) [45],  $\bullet$  – Ehrich and Kelleher (1 atm) [45],  $\Delta$  – Ehrich and Kusch [46],  $+$  – Wiese et al. [47],  $\star$  – wall stabilized arc end-on [48],  $\star^*$  – wall stabilized arc side-on [48],  $\nabla$  – microwave induced plasma [48].

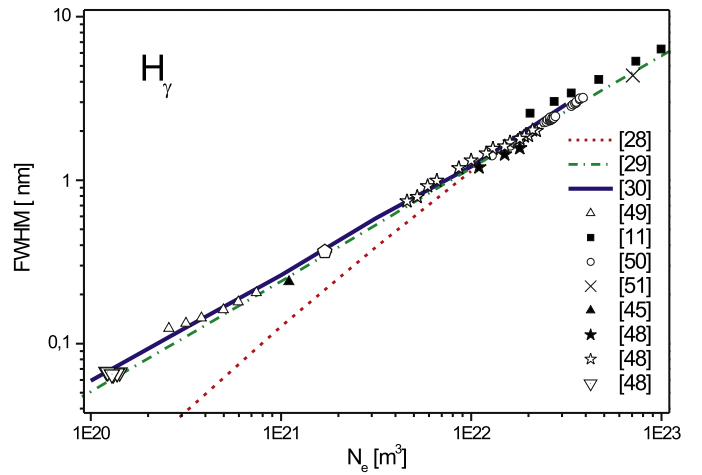


**Fig. 13.** Comparison of experimental and theoretical halfwidths –  $w_s$  of hydrogen Balmer gamma line. Theories: VCS [28] – dotted line, MMM [29] – dashed line, CS [31] – thick line. Experiment:  $\Delta$  – Bengston and Chester [49],  $\blacksquare$  – Wiese et al. [11],  $\circ$  – Hill and Gerrardo [50],  $\times$  – Wiese et al. [51],  $\blacktriangle$  – Ehrich and Kelleher [45],  $\star$  – wall stabilized arc end-on [48],  $\star^*$  – wall stabilized arc side-on [48],  $\nabla$  – microwave induced plasma [48].

where  $w_s$  is the full halfwidth (FWHM) of the Stark contribution to the experimental profile. The application of this formula was later extended to  $N_e \approx (0.2 - 1.3) \times 10^{22} \text{ m}^{-3}$  with minor modification [40] and frequently employed below  $10^{21} \text{ m}^{-3}$  where Eq. (6) is not experimentally tested. Recent calculations based on the CS [31] confirmed the applicability of Eq. (9) for diagnostics of plasma  $N_e$  as low as  $10^{20} \text{ m}^{-3}$ . We estimate the accuracy of Eq. (9) in the range 8–12%. This estimate does not include uncertainty in  $w_s$  measurement.

Another approximate formula

$$\log N_e = 22.578 + 1.478 * \log w_s - 0.144 * (\log w_s)^2 - 0.1265 * \log T_e \quad (10)$$

with an estimated accuracy of  $\pm 5\%$  was derived from the results of VCS calculations [52]. The applicability of Eq. (10) is in the  $N_e$   $(0.0316 - 3.16) \times 10^{22} \text{ m}^{-3}$  and  $T_e$  (5000–20000) K range [52]. The estimated accuracy does not include uncertainties in  $w_s$  and  $T_e$  measurement.

On the bases of CS calculations the authors [31] derived for the  $H_\beta$  line another formula similar to Eq. (9):

$$N_e [\text{m}^{-3}] = 10^{23} * (w_s[\text{nm}]/4.8)^{1.46808} \quad (11)$$

##### 4.3.2. $H_\alpha$ and the $H_\gamma$ lines

The approximate formulas [31] for the  $H_\alpha$  and the  $H_\gamma$  are reported only in the form that relates full width at half area,  $w_{SA}$  with  $N_e$ :

$$H_\alpha : N_e [\text{m}^{-3}] = 10^{23} * (w_{SA}[\text{nm}]/1.098)^{1.47135} \quad (12)$$

$$H_\gamma : N_e [\text{m}^{-3}] = 10^{23} * (w_{SA}[\text{nm}]/4.668)^{1.45826} \quad (13)$$

Here, one should note that the application of Eqs. (12) and (13) implies deconvolution of experimental profile and then determination of  $w_{SA}$  of the Stark profile only. This requires first the deconvolution of experimental profile and then reconstruction of theoretical Stark profile to determine  $w_{SA}$ . Thus, with an exception of the  $H_\alpha$ , formulas  $N_e = f(w_{SA})$  are not practical for  $N_e$  plasma diagnostics.

The profiles of the  $H_\alpha$  are close to Lorentzian, see Table 2 and Fig. 3, and it is justified to use  $w_{SA} = w_s = w_L$ . This simplifies the application of Eq. (12): one has to determine  $w_s$  by assuming  $w_s = w_L$  and to introduce this result in Eq. (12) instead of  $w_{SA}$ . Unfortunately

the same procedure cannot be applied to Eq. (13) for the  $H_\gamma$  line. Finally it should be pointed out that formulas (12) and (13) differ from the original ones [31] where HWHM are used instead of claimed FWHM [53].

#### 4.4. Higher members of Balmer series

The application of higher members of Balmer series for plasma diagnostic purposes have been discussed already [15]. Here, we draw attention to some advantages of this technique and to the recent work in this field. Namely, the use of higher member increases the sensitivity of  $N_e$  diagnostics and, what is very important, the line shape is almost independent on ion dynamics i.e. reduced mass emitter–perturber does not play an important role. To illustrate the increased sensitivity let us quote the result from low-pressure hydrogen microwave induced plasma where  $N_e \approx 10^{18} \text{ m}^{-3}$  is determined [54] from an experimental profile of the  $H_{16}$  line in conjunction with theoretical calculations of line shapes for higher members of Balmer series [55].

### 5. Summary and conclusions

For the characterization of plasmas used for numerous applications, the electron number density,  $N_e$ , is an important parameter, which has to be determined in a large density range starting from  $10^{18} \text{ m}^{-3}$  up to several times  $10^{23} \text{ m}^{-3}$ . In this work the attention is focused to relatively low  $N_e$  when other broadening mechanisms of hydrogen Balmer lines are comparable with Stark broadening. This is the case when deconvolution of experimental profile has to be performed to separate Stark contribution used for  $N_e$  diagnostics.

First part of this publication is devoted to the analysis of numerous attempts to extend Stark broadening data tables below those presented for lowest  $N_e$  and which are close to Fine Structure Limit (FSL). At this limit, which is different for each Balmer line, the line splits in several components. Each line becomes isolated from one another and therefore, Stark broadening has to be treated separately for each fine structure component. In other words, Stark broadening of each component is smaller than mutual wavelength separation of components. To the authors' knowledge data tables below FSL for Balmer lines are not available. In order to measure  $N_e$  below FSL several authors extrapolated Stark broadening data to lower densities below FSL which is wrong from several points of view, see Section 3. Unfortunately there is no correct way to extend Stark broadening data except performing theoretical calculations below FSL. The experimental testing of extended data is required also. Another possibility would be the measurement of line shapes below FSL in order to determine empirical formulas relating line shape parameters with  $N_e$ . This work requires careful measurements of atomic hydrogen temperature and determination of reduced mass emitter–perturber  $\mu$ , which is not always an easy task in non-equilibrium multi component plasma. In addition this experiment requires an independent technique for  $N_e$  plasma diagnostics. Presently however we can only recommend to use data tables above FSL, which is  $6 \times 10^{20}$  for the  $H_\alpha$ ,  $4 \times 10^{19} \text{ m}^{-3}$  for the  $H_\beta$ , and  $10^{19} \text{ m}^{-3}$  for the  $H_\gamma$  [33]. This means that data for the  $H_\alpha$  usually given in data tables from  $10^{20} \text{ m}^{-3}$  can be used only above  $6 \times 10^{20} \text{ m}^{-3}$  while data for the  $H_\beta$  can be extended to  $4 \times 10^{19} \text{ m}^{-3}$ . Here one should not forget Van der Waals, Doppler and instrumental broadening, which have to be taken into account since they can easily “cover” Stark broadening contribution.

For low  $N_e$  but above FSL, the authors who are not using numerical program for  $N_e$  diagnostics, for deconvolution of experimental profile usually apply fitting with Voigt function. In Section 4.1 it is shown how large error is introduced by this procedure. By fixing the Gaussian part of Voigt function the error is considerably decreased but remains still large and systematic. The deconvolution of experimental Stark profile at the half width may be improved by applying approximate

formulas (3)–(5). These simple and reasonably accurate formulas are recommended in particular cases when Balmer lines are interfering with neighboring lines in gas mixtures.

Here, it should not be forgotten that to obtain Stark width, the remaining part of an experimental profile after deconvolution from Doppler and instrumental contribution has to be corrected sometimes for Van der Waals broadening. In principle, to perform this correction is not easy because Stark or VdW profiles do not have the same line shape, see Section 4.1.3. To simplify deconvolution procedure, we recommend already adopted subtraction of estimated VdW width from the Stark  $\otimes$  VdW part of line profile. For more details about estimation of VdW contribution, see Section 4.1.3.

After deconvolution of experimental profile  $N_e$  can be evaluated either from the comparison of Stark width with those determined from theoretical data tables or by using approximate formulas (9)–(12). For the  $H_\beta$  formulas (9) and (10) are highly recommended while for the  $H_\alpha$  formula (11) is a good choice. Unfortunately Eq. (12) for the  $H_\gamma$  is not easy to apply.

Finally, we draw attention to Figs. 12 and 13 showing that Computer Simulation [31] and MMM [29] are recommended for low  $N_e$  plasma diagnostics from the  $H_\alpha$  and from the  $H_\gamma$  line Stark width. The use of higher members of Balmer series increases considerably the sensitivity of Stark broadening technique for  $N_e$  plasma diagnostics, see Section 4.4. Therefore, these lines are highly recommended for low  $N_e$  plasma diagnostics whenever line with good signal to noise ratio is detected.

### Acknowledgment

The communication with J. F. Kielkopf concerning the  $H_\alpha$  VdW shifts is very much appreciated. This work is supported by the Ministry of Education and Science of the Republic of Serbia under Project 171014.

### References

- [1] M.A. Heald, C.B. Wharton, Plasma Diagnostics with Microwaves, Wiley, New York, 1965..
- [2] B.N. Ganguly, W.R. Lempert, K. Akhtar, J.E. Scharer, F. Leibold, C.O. Laux, R.N. Zare, A.P. Yalin, Electron density measurements by millimeter interferometry and electron density measurements by infrared heterodyne interferometry, In: K.H. Becker, U. Kogelschatz, K.H. Schoenbach, R.J. Barker (Eds.), Non-equilibrium Air Plasmas at Atmospheric Pressure, Institute of Physics, Bristol, 2005, pp. 482–501.
- [3] R.A. Alpher, D.R. White, Optical interferometry, In: R.H. Huddleston, S.L. Leonard (Eds.), Plasma Diagnostic Techniques, Academic Press, New York, 1965.
- [4] F.C. Jahoda, J.A. Sawyer, Optical refractivity of plasma, In: H.H. Lovberg, H.R. Griem (Eds.), Methods of Experimental Physics, Plasma Physics, vol. 9, Academic Press, New York, 1971, pp. 1–47.
- [5] D.E.T.F. Ashby, D.F. Jephcott, Measurement of plasma density using gas laser as an infrared interferometer, Appl. Phys. Lett. 3 (1963) 13–16.
- [6] N. Konjević, W.L. Wiese, Experimental Stark widths and shifts for non-hydrogenic spectral lines of ionized atoms (a critical review and tabulation of selected data), J. Phys. Chem. Ref. Data 8 (1976) 259–308.
- [7] H.-J. Kunze, The laser as a tool for plasma diagnostics, In: W. Lochte-Holtgreven (Ed.), Plasma Diagnostics, North-Holland, Amsterdam, 1968, pp. 550–616.
- [8] J. Sheffield, Plasma Scattering of Electromagnetic Radiation, Academic Press, New York, 1975.
- [9] H.R. Griem, Plasma spectroscopy, McGraw-Hill, New York, 1964..
- [10] H.R. Griem, Principles of Plasma Spectroscopy, Cambridge University Press, 1997.
- [11] W.L. Wiese, D.E. Kelleher, D.R. Paquette, Detailed study of the Stark broadening of Balmer lines in a high density plasma, Phys. Rev. A6 (1972) 1132–1153.
- [12] V. Helbig, K.-P. Nick, Investigation of the Stark broadening of Balmer beta, J. Phys. B Atomic Mol. Opt. Phys. 14 (1981) 3573–3583.
- [13] <http://www.nist.gov/pml/data/asbib/index.cfm> or <http://physics.nist.gov/cgi-bin/ASBib1/LineBroadBib.cgi>.
- [14] N. Konjević, Plasma broadening and shifting of non-hydrogenic spectral lines: present status and applications, Phys. Rep. 316 (1999) 339–401.
- [15] M. Ivković, S. Jovičević, N. Konjević, Low electron density diagnostics: development of optical emission spectroscopic techniques and some applications to microwave induced plasmas, Spectrochim. Acta Part B 59 (2004) 591–605.
- [16] S. Djurović, N. Konjević, On the use of non-hydrogenic spectral lines for low electron density and high pressure plasma diagnostics, Plasma Sources Sci. Technol. 8 (2009) 035011 (8 pages).
- [17] N. Konjević, M. Ivković, S. Jovičević, Spectroscopic diagnostics of laser-induced plasmas, Spectrochim. Acta Part B 65 (2010) 593–602.



- [18] H.R. Griem, *Spectral Line Broadening by Plasmas*, Academic Press, New York, 1974.
- [19] N. Allard, J. Kielkopf, The effect of neutral nonresonant collisions on atomic spectral lines, *Rev. Mod. Phys.* 54 (1982) 1103–1182.
- [20] E.L. Lewis, Collisional relaxation of atomic excited states, line broadening and interatomic interaction, *Phys. Rep.* 58 (1980) 1–71.
- [21] G. Peach, *Collisional broadening of spectral lines*, in: *Atomic, molecular and optical physics handbook*, Editor: Gordon W.F. Drake AIP Woodbury, New York, 1996.
- [22] D.E. Kelleher, W.L. Wiese, Observation of ion motion in hydrogen Stark profiles, *Phys. Rev. Lett.* 31 (1973) 1431–1434.
- [23] C.O. Laux, T.G. Spence, C.H. Kruger, R.N. Zare, Optical diagnostics of atmospheric pressure air plasmas, *Plasma Sources Sci. Technol.* 12 (2003) 125–138.
- [24] B.N. Ganguly, W.R. Lempert, K. Akhtar, J.E. Scharer, F. Leibold, C.O. Laux, R.N. Zare, A.P. Yalin, Measurements of electron number density by optical emission spectroscopy, In: K.H. Becker, U. Kogelschatz, K.H. Schoenbach, R.J. Barker (Eds.), *Non-equilibrium Air Plasmas at Atmospheric Pressure*, Institute of Physics, Bristol, 2005, pp. 508–517.
- [25] H.-Y. Moon, K.K. Herrera, N. Omenetto, B.W. Smith, J.D. Winefordner, On the usefulness of a duplicating mirror to evaluate self-absorption effects in laser induced breakdown spectroscopy, *Spectrochim. Acta Part B* 64 (2009) 702–713.
- [26] S. Stojadinović, J. Jovović, M. Petković, R. Vasilčić, N. Konjević, Spectroscopic and real-time imaging investigation of tantalum plasma electrolytic oxidation (PEO), *Surf. Coat. Technol.* 205 (2011) 5406–5413.
- [27] P. Kepple, H.R. Griem, Improved Stark profile calculations for the hydrogen lines  $H_{\alpha}$ ,  $H_{\beta}$ ,  $H_{\gamma}$  and  $H_{\delta}$ , *Phys. Rev.* 173 (1968) 317–325.
- [28] C.R. Vidal, J. Cooper, E.W. Smith, Hydrogen Stark-broadening tables, *Astrophys. J.* 25 (1973) 37–136 (Suppl. No.).
- [29] C. Stehlé, R. Hutcheon, Extensive tabulations of Stark broadened hydrogen line profiles, *Astron. Astrophys. Suppl. Ser.* 140 (1999) 93–97.
- [30] M.A. Gigosos, V. Cardenoso, New plasma diagnosis tables of hydrogen Stark broadening including ion dynamics, *J. Phys. B Atomic Mol. Opt. Phys.* 29 (1996) 4795–4838.
- [31] M.A. Gigosos, M.A. Gonzalez, V. Cardenoso, Computer simulated Balmer-alpha, -beta and -gamma Stark line profiles for non-equilibrium plasmas diagnostics, *Spectrochim. Acta Part B* 58 (2003) 1489–1504.
- [32] R. Pastor, M.A. Gigosos, M.A. Gonzalez, Fine structure effects in the hydrogen Balmer- $\alpha$  line, In: *Spectral line shapes Volume 11*, 15th ICSLS, 10–14 July 2000, Berlin, AIP Conference Proceedings, 559, 2001, pp. 79–81.
- [33] W. Olchawa, R. Olchawa, B. Grabowski, Stark broadening of hydrogen spectral lines with fine structure effects, *Eur. Phys. J. D* 28 (2004) 119–124.
- [34] V. Helbig, Starkeffekt-verbreiterung von Balmerlinien bei mittleren elektronendichten, *Contrib. Plasma Phys.* 31 (1991) 183–197.
- [35] C. Stehle, N. Feautrier, Stark broadening of the hydrogen  $H_{\alpha}$  line at low densities: fine structure and spontaneous emission effects, *J. Phys. B Atomic Mol. Opt. Phys.* 18 (1985) 1297–1306.
- [36] E.W. Weber, R. Frankenberger, M. Schilling, Nonlinear plasma spectroscopy of the hydrogen Balmer- $\alpha$  line, *Appl. Phys. B* 32 (1983) 63–73.
- [37] J.T. Davies, J.M. Vaughan, A new tabulation of the Voigt profile, *Astrophys. J.* 137 (1963) 1302–1305.
- [38] N.M. Temme, Voigt function, In: W.J. Olver Frank, D.M. Lozier, R.F. Boisvert, et al., (Eds.), *NIST Handbook of Mathematical functions*, Cambridge University Press, ISBN: 978-0521192255, 2010.
- [39] J.J. Olivero, R.L. Longbothum, Empirical fits to the Voigt line width: a brief review, *J. Quant. Spectrosc. Radiat. Transf.* 17 (1977) 233–236.
- [40] D.E. Kelleher, Stark broadening of visible neutral helium lines in a plasma, *J. Quant. Spectrosc. Radiat. Transf.* 25 (1981) 191–220.
- [41] R. Zikić, M.A. Gigosos, M. Ivković, M.A. Gonzalez, N. Konjević, A program for the evaluation of electron number density from experimental hydrogen Balmer beta line profiles, *Spectrochim. Acta Part B* 57 (2002) 987–998.
- [42] J.F. Kielkopf, Impact broadening and shift of the  $H_{\alpha}$  line by helium, neon and argon, *J. Chem. Phys.* 62 (1975) 3784–3787.
- [43] C.W. Allen, In: *Astrophysical Quantities*, 3rd ed., Athlone Press, New York, 1973, p. 92.
- [44] W.L. Wiese, J.R. Fuhr, Accurate atomic transition probabilities for hydrogen, helium, and lithium, *J. Phys. Chem. Ref. Data* 38 (2009) 565–726 (Erratum: 38 (2009) 1129).
- [45] H. Ehrich, D.E. Kelleher, Experimental investigation of plasma-broadened hydrogen Balmer lines at low electron densities, *Phys. Rev. A* 21 (1980) 319–334.
- [46] H. Ehrich, H.J. Kusch, Experimentelle untersuchung zur Stark-verbreiterung der Balmer-linien  $H_{\alpha}$  und  $H_{\beta}$ , *Z. Naturforsch.* 28a (1973) 1794–1800.
- [47] W.L. Wiese, D.E. Kelleher, V. Helbig, Variation in Balmer-line Stark profiles with atom-ion reduced mass, *Phys. Rev. A* 11 (1975) 1854–1864.
- [48] N. Konjević, M. Ivković, S. Jovičević, Low-electron density plasma diagnostics by optical emission spectroscopy, In: V. Aubrecht, M. Bartlova (Eds.), *XVIIth Symposium on Physics of Switching Arc Phenomena*, Brno University of Technology, Brno Czech Republic, September 10–13, 2007, Volume II, Brno-Letohrad, 2007, pp. 27–36.
- [49] R.D. Bengtson, G.R. Chester, Stark broadening of Balmer lines in the density range  $(2-8) \times 10^{14} \text{ cm}^{-3}$ , *Phys. Rev. A* 13 (1976) 1762–1771.
- [50] R.A. Hill, J.B. Gerardo, Stark broadening of  $H_{\beta}$ ,  $H_{\gamma}$  and  $H_{\delta}$ : a comparison of theory and experiment, *Phys. Rev.* 162 (1967) 855–862.
- [51] W.L. Wiese, D.R. Paquette, J.E. Solariski, Profiles of Stark-broadened Balmer lines in hydrogen plasma, *Phys. Rev.* 129 (1963) 1225–1232.
- [52] A. Czernichowski, J. Chapelle, Use of the 447 nm He I line to determine electron concentrations, *J. Quant. Spectrosc. Radiat. Transf.* 33 (1985) 427–436.
- [53] M.A. Gonzalez, private, communication (2012).
- [54] N. Konjević, S. Jovičević, M. Ivković, Optical emission spectroscopy for simultaneous measurement of plasma electron density and temperature in a low-pressure microwave induced plasma, *Phys. Plasmas* 16 (2009) 103501 (6 pages).
- [55] M. Lemke, Extended VCS Stark broadening tables for hydrogen – Lyman to Brackett series, *Astron. Astrophys. Suppl. Ser.* 122 (1997) 285–292.

# Comparison of single extraction procedures and the application of an index for the assessment of heavy metal bioavailability in river sediments

Sanja Sakan<sup>1</sup> · Aleksandar Popović<sup>2</sup> · Sandra Škrivanj<sup>2</sup> · Nenad Sakan<sup>3</sup> · Dragana Đorđević<sup>1</sup>

Received: 10 November 2015 / Accepted: 29 July 2016 / Published online: 10 August 2016  
© Springer-Verlag Berlin Heidelberg 2016

**Abstract** Metals in sediments are present in different chemical forms which affect their ability to transfer. The objective of this body of work was to compare different extraction methods for the bioavailability evaluation of some elements, such as Ba, Cd, Co, Cr, Cu, Fe, K, Mg, Mn, Ni, Pb, V and Zn from Serbian river sediments. A bioavailability risk assessment index (BRAI) was used for the quantification of heavy metal bioavailability in the sediments. Actual and potential element availability was assessed by single extractions with mild ( $\text{CaCl}_2$  and  $\text{CH}_3\text{COONH}_4$ ) and acidic ( $\text{CH}_3\text{COOH}$ ) extractants and complexing agents (EDTA). Aqua regia extraction was used for the determination of the pseudo-total element content in river sediments. In different single extraction tests, higher extraction of Cd, Cu, Zn and Pb was observed than for the other elements. The results of the single extraction tests revealed that there is a considerable chance of metal leaching from the sediments assessed in this study. When the BRAI was applied, the results showed a high risk of heavy metal bioavailability in Serbian river sediments.

**Keywords** BRAI · Heavy metal · Bioavailability · Single extraction · Sediment · River

## Introduction

Sediments make up an integral part of the aquatic environment and are the main carriers of all types of pollutants. From an ecotoxicological view point, one of the most important groups of pollutants is heavy metals (Kastratović et al. 2013). The presence of metals in sediments can be attributed to natural weathering processes that affect soils and rocks and potentially additional anthropogenic inputs. It is believed that most of the metal content, as much as 90 %, in aquatic systems is bound to sediments (Calmano et al. 1993; Jamshidi-Zanjani et al. 2015).

Elements in sediments are associated with a number of physico-chemical processes that act as a reservoir or sink for environmental elements (exchangeable or specifically adsorbed carbonate, secondary Fe and Mn oxides, organic matter, sulphides, silicates etc.). These phases can strongly affect the behaviour of the element within the sediment in terms of its biological availability, potential toxicity, chemical interactions and mobility within the profile (Anju and Banerjee 2011).

Numerous studies have been conducted to assess and establish the extent of metal contamination in rivers (Villaescusa-Celaya et al. 2000; Vicente-Martorell et al. 2009; Mohiuddin et al. 2010; Massolo et al. 2012; Jiao et al. 2015; Guan et al. 2016). Most of the previous studies have been limited to the determination of the total content of metals in sediments, which is a poor contamination-risk indicator and reflects only the maximum amount of contamination, when metal properties basically depend on their binding state, sediment properties such as pH, total organic carbon (TOC), redox conditions and their chemical speciation (Ma et al. 2016). Using only the total metal content in potential risk

Responsible editor: Philippe Garrigues

**Electronic supplementary material** The online version of this article (doi:10.1007/s11356-016-7341-6) contains supplementary material, which is available to authorized users.

✉ Sanja Sakan  
ssakan@chem.bg.ac.rs

<sup>1</sup> ICTM, Chemistry Center, University of Belgrade, Njegoševa 12, P. O. Box 815, Belgrade 11000, Serbia

<sup>2</sup> Faculty of Chemistry, University of Belgrade, Studentski trg 12-16, P. O. Box 51, Belgrade 11000, Serbia

<sup>3</sup> Institute of Physics, University of Belgrade, Pregrevica 118, P.O. Box 68, Belgrade 11081, Serbia

assessments may overestimate environmental pollution and the risks due to heavy metals, as only a portion of the total metal content is bioavailable (Madrid et al. 2008; Li et al. 2009; Jamshidi-Zanjani et al. 2015; Ren et al. 2015). The exchangeable fraction corresponds to the metal form that is most available and can be released by merely changing the ionic strength of the medium (Anju and Banerjee 2011). The use of single extractions for sediment evaluation allows a more nuanced assessment of heavy metal forms and their mobility within the sediment. Various one-step extraction methods are frequently used for bioavailability evaluation because of their simplicity and ease of operation.

Although there are numerous methods used for partial extractions, they generally fall into the following groups: (1) water soluble metals fractions released using water as the extraction agent; (2) exchangeable trace metals (electrostatically weakly bound), extraction with:  $\text{CaCl}_2$ ,  $\text{CH}_3\text{COONH}_4$ ,  $\text{NH}_4\text{NO}_3$ ,  $\text{Ca}(\text{NO}_3)_2$ ,  $\text{NaNO}_3$ ,  $\text{AlCl}_3$ ,  $\text{BaCl}_2$ ,  $\text{MgCl}_2$  and  $\text{Mg}(\text{NO}_3)_2$ , which function through leaching cations that are adsorbed onto solid materials due to permanent structural charges: phyllosilicates, phyllo-manganates and sometimes organic matter (Leleyter et al. 2012); (3) elements that are sensitive to acidification processes (e.g. bound to carbonates), extraction with  $\text{CH}_3\text{COOH}$ ,  $\text{HCl}$  and  $\text{CH}_3\text{COONa}$ , which simulate the effect of an acid input (e.g. through acid rain or an accidental spill), as low pH conditions favour the dissociation of the existing complexes (Leleyter et al. 2012) and (4) elements that are sensitive to complexation processes (e.g. non-silicate bound phases), extraction using complexing or reducing extraction agents, such as EDTA, DTPA and  $\text{CH}_3\text{COONH}_4\text{-CH}_3\text{COOH/EDTA}$  (Sahuquillo et al. 2003; Rao et al. 2010; Qasim et al. 2015).

The comparison of aqua regia, as the standard method for pseudo-total heavy metal assessment in sediment, with several widely used single extraction procedures for evaluating the heavy metal availability is presented in this research. Since the aqua regia is a standard method, exploring its relationship with the metal availability yielded with the milder chemical reagents procedures is of great importance for the metal assessment in river sediments. Four single extraction agents ( $\text{CaCl}_2$ ,  $\text{CH}_3\text{COONH}_4$ , EDTA and  $\text{CH}_3\text{COOH}$ ) were applied to examine the bioavailability of Ba, Cd, Co, Cr, Cu, Fe, K, Mg, Mn, Ni, Pb, V and Zn in river sediments from Serbia. An index (BRAI) based on EDTA extraction and described by Jamshidi-Zanjani et al. (2015) was used for the formal categorisation and quantification of the heavy metal bioavailability. Since the issue of quantifying the bioavailability of potentially harmful metals has not been intensively explored or applied in previous studies, the importance of the application of this index as a quantitative measure of metal bioavailability in sediments is of great importance in future eco-chemical investigations. The innovative of this approach lies in the comparison of several methods and yielding a relationship between the results. There is a need to estimate and quantify the bioavailability of potentially harmful

metals on measurements based on samples that are no more available. Also, there is an importance for providing rapid indications based on the new samples, and it could be achieved by the help of yielded connections. Because of usefulness of studied methods on different heavy metals groups, the presented relationship has importance in anthropogenic influence estimation.

## Materials and methods

### Study area

Serbia has an extensive inland waterway network comprised of three international rivers and a channel network of almost 2000 km of inland waterways. The rivers in Serbia belong to the watersheds of the Black, Adriatic and Aegean seas. On more than 90 % of the Serbian territory, there are rivers that join with the Danube before emptying into the Black Sea. Approximately 588 km of the Danube River passes through Serbia and it is considered to be one of the most important components of the region's transport infrastructure. The Danube also represents the main inland transport corridor linking Eastern and Western Europe. It crosses Germany, Austria, Slovakia, Hungary, Croatia, Serbia, Romania, Bulgaria, Moldova and Ukraine and connects the North Sea with the Black Sea via the Rhine-Main-Danube Canal (RIS 2007).

The eco-chemical status of Serbian rivers is a constant topic of interest, both at local and international level. Teodorović (2009) reported that several hot spots of severe freshwater pollution and sediment contamination have been identified in Serbia, which can be attributed to outdated environmental legislation, negligible amounts of properly treated waste waters and accidental spills. Heavy metals appear to be the most significant problem.

### Sampling sites and sampling

Sediment river samples were collected from 32 sites in Serbia during 2008; sampling site numbers are denoted within the parentheses: the Tisa (7), the Danube (5), the Sava (4), the Ibar (2), the Great Morava (2), the West Morava (1), the South Morava (1), the Nišava (2), the Tamiš (1), the Vrbas (1), the Topčiderska river (1), the Porečka river (1), the

**Fig. 1** Map of the study area and sampling sites (site number is rendered in *italics*). Explanation: Tisa (Martonoš, 1); Tisa (Titel, 2); Tisa (Titel, 3); Tisa (Martonoš, 4); Tisa (Martonoš, 5); Tisa (Martonoš, 6); Tisa (Martonoš, 7); Danube (Bezdan, 8); Danube (Bezdan, 9); Danube (Bezdan, 10); Danube (Bezdan, 11); Danube (Gruja, 12); Sava (Ostružnica, 13); Sava (S. Mitrovica, 14); Sava (Šabac, 15); Sava (Jamena, 16); Ibar (Raška, 17); Ibar (Kraljevo, 18); Great Morava (Ljubičevski most, 19); Great Morava (Bagrdan, 20); West Morava (Masakare, 21); South Morava (Mojsinje, 22); South Morava (Vladičin Han, 23); Nišava (Niš, 24); Nišava (Dimitrovgrad, 25); Tamiš (Jaša Tomić, 26); Canal DTD (Vrbas, 27); Topčiderska r. (Rakovica-Belgrade, 28); Porečka r. (Mosna, 29); Kolubara (Draževac, 30); Pek (Kusiće, 31) and Toplica (Doljevac, 32)





Kolubara (1), the Pek (1) and the Toplica (1). Locations of the sampling sites are shown in Fig. 1 and Table 1. The sampling of sediments in this research was conducted using a Van Veen grab sampler, designed to collect an accurate representative sediment sample. The sediment samples were stored at 4 °C to prevent changes in the chemical composition. The micro- and macro-elemental contents were determined in the granulometric fraction, i.e. <63 µm of the bottom sediment sample (grab sample), after air drying for 8 days. Analysis of the metal concentration in the fine sediment fraction (less than 63 µm) is recommended as these particles are the most important sources of bioavailable metals in sediments (Villaescusa-Celaya et al. 2000).

The moisture content of each sample was determined by drying a separate 1 g sample in an oven (105 ± 2 °C) until a constant weight was reached. From this, a correction to dry

mass was obtained, which was then applied to all reported metal content results.

### Extraction of heavy metals

To evaluate the mobile fractions, representative aliquots of each sample were leached by four different chemical reagents: 0.01 M CaCl<sub>2</sub>, 0.05 M EDTA, 1 M CH<sub>3</sub>COONH<sub>4</sub> and 0.11 M CH<sub>3</sub>COOH.

### Extraction with 0.01 M CaCl<sub>2</sub>

A 20-mL aliquot of a 0.01 M CaCl<sub>2</sub> solution was added to 2.0 g of sediment in a 50-mL centrifuge tube and the suspension was shaken on a shaker for 3 h in a room at 20 ± 2 °C

**Table 1** Locations of sampling sites

| Number | Sampling site     | River             | Latitude (x° y' z") | Longitude (x° y' z") |
|--------|-------------------|-------------------|---------------------|----------------------|
| 1      | Martonoš          | Tisa              | 46 06 52            | 20 05 13             |
| 2      | Titel             | Tisa              | 45 11 52            | 20 19 07             |
| 3      | Titel             | Tisa              | 45 11 52            | 20 19 07             |
| 4      | Martonoš          | Tisa              | 46 06 52            | 20 05 13             |
| 5      | Martonoš          | Tisa              | 46 06 52            | 20 05 13             |
| 6      | Martonoš          | Tisa              | 46 06 52            | 20 05 13             |
| 7      | Martonoš          | Tisa              | 46 06 52            | 20 05 13             |
| 8      | Bezdan            | Danube            | 44 52 56            | 25 26 29             |
| 9      | Bezdan            | Danube            | 44 52 56            | 25 26 29             |
| 10     | Bezdan            | Danube            | 44 52 56            | 25 26 29             |
| 11     | Bezdan            | Danube            | 44 52 56            | 25 26 29             |
| 12     | Gruja             | Danube            | 44 15 45            | 22 41 10             |
| 13     | Ostružnica        | Sava              | 44 43 54            | 20 19 02             |
| 14     | Sremska Mitrovica | Sava              | 44 58 00            | 19 36 24             |
| 15     | Šabac             | Sava              | 44 46 18            | 19 42 12             |
| 16     | Jamena            | Sava              | 44 52 41            | 19 05 21             |
| 17     | Raška             | Ibar              | 43 17 01            | 20 37 43             |
| 18     | Kraljevo          | Ibar              | 43 43 06            | 20 41 39             |
| 19     | Ljubičevski most  | Great Morava      | 44 35 12            | 21 08 18             |
| 20     | Bagrdan           | Great Morava      | 44 04 06            | 21 12 12             |
| 21     | Maskare           | West Morava       | 43 40 19            | 21 24 07             |
| 22     | Mojsinje          | South Morava      | 43 37 50            | 21 29 27             |
| 23     | Vladičin Han      | South Morava      | 42 43 30            | 22 04 06             |
| 24     | Niš               | Nišava            | 43 19 36            | 21 54 30             |
| 25     | Dimitrovgrad      | Nišava            | 43 00 27            | 22 49 01             |
| 26     | Jaša Tomić        | Tamiš             | 45 25 55            | 20 51 50             |
| 27     | Vrbas             | DTD (Vrbas)       | 45 35 15            | 19 37 34             |
| 28     | Rakovica-Belgrade | Topčiderska river | 44 45 05            | 20 27 09             |
| 29     | Mosna             | Porečka river     | 44 25 22            | 22 10 43             |
| 30     | Draževac          | Kolubara          | 44 35 36            | 20 13 18             |
| 31     | Kusiće            | Pek               | 44 29 00            | 21 39 24             |
| 32     | Doljevac          | Toplica           | 43 12 12            | 21 50 12             |

(Quevauviller 1998). The extract was separated immediately from the solid phase by centrifugation at 3000 rpm for 20 min. Then, the supernatant was decanted and diluted to 50 mL with 1 M HNO<sub>3</sub> and stored in a polyethylene bottle at 4 °C until needed for analysis.

**Extraction with 0.05 M EDTA**

A 20-mL aliquot of a 0.05-M EDTA solution was added to 2.0 g of sediment in a 50-mL centrifuge tube and the suspension was shaken on a shaker for 1 h in a room at 20 ± 2 °C (Quevauviller 1998). The extract was separated immediately from the solid phase by centrifugation at 3000 rpm for 20 min. Then, the supernatant was decanted and diluted to 50 mL with 1 M HNO<sub>3</sub> and stored in a polyethylene bottle at 4 °C until needed for analysis.

**Extraction with 1 M CH<sub>3</sub>COONH<sub>4</sub>**

A 40-mL aliquot of a 1-M CH<sub>3</sub>COONH<sub>4</sub> solution was added to 1 g of sediment in a 50-mL centrifuge tube and the suspension was shaken on a shaker for 2 h in a room at 20 ± 2 °C (Sakan et al. 2009; Petrović et al. 2010). The extract was separated from the solid phase by centrifugation at 3000 rpm for 20 min. Then, the supernatant was decanted and diluted to 50 mL with 1 M HNO<sub>3</sub> and stored in a polyethylene bottle at 4 °C until needed for analysis.

**Extraction with 0.11 M CH<sub>3</sub>COOH**

A 40-mL aliquot of a 0.11-M acetic acid solution was added to 1 g of sediment in a 50-mL centrifuge tube and the suspension was shaken on a shaker for 16 h in a room at 20 ± 2 °C (Sutherland 2010; Relić et al. 2013; Sakan et al. 2015). The extract was separated from the solid phase by centrifugation at

3000 rpm for 20 min. Then, the supernatant was decanted and diluted to 50 mL with 1 M HNO<sub>3</sub> and stored in a polyethylene bottle at 4 °C until needed for analysis.

**Digestion with aqua regia**

Approximately 500 mg of sample sediment and 12 mL of aqua regia (9 mL HCl and 3 mL HNO<sub>3</sub>) were added to a microwave vessel (DIN 38414 S7 1983, SW-846 EPA Method 3051a 2007). Microwave digestion was performed in a pressurised microwave oven (Ethos 1, Advanced Microwave Digestion System, Milestone, Italy) equipped with a rotor holding ten microwave vessels (PTFE). During digestion, the temperature of the microwave oven was raised to 165 °C over 10 min (holding time 0 s), then to 175 °C over 3 min, after which it was maintained at 175 °C for 10 min (max power 1200 W) (Rönkkömäki et al. 2008). One control vessel per rack contained a temperature and pressure probe. The vessels were removed from the oven after the temperature had dropped to less than 50 °C and the pressure to less than 69 kPa. At the end of the digestion cycle, the vessels were allowed to cool to room temperature before continuing the sample preparation, to align with security protocols and to avoid the leakage of volatile substances. After cooling, the sample digests were filtered with Whatman No. 42 filter paper, to remove solids which remained after the microwave digestion process. The digests were then transferred into a flask, diluted to 100 mL with 1 M HNO<sub>3</sub> and stored in a polyethylene bottle at 4 °C until needed for analysis (Sakan et al. 2011).

**Certificate reference materials**

Quality assurance and quality control were assessed by duplicate sample analysis, method blanks and standard reference materials. The accuracy of the applied analytical procedures

**Table 2** Comparison of analysed and certified values of BCR-701, BCR-143 and BCR-146

|                     | Cd                   | Cr   | Cu   | Ni   | Pb   | Zn   | Mn   | Co   |
|---------------------|----------------------|------|------|------|------|------|------|------|
|                     | CH <sub>3</sub> COOH |      |      |      |      |      |      |      |
| Analysed            | 7.52                 | 1.82 | 48.9 | 13.5 | 3.45 | 189  | nd*  | nd   |
| Certified (BCR-701) | 7.34                 | 2.26 | 49.3 | 15.4 | 3.18 | 205  | nd   | nd   |
| Recovery (%)        | 102                  | 80.5 | 99.2 | 87.7 | 108  | 90.9 | nd   | nd   |
|                     | Aqua regia           |      |      |      |      |      |      |      |
| Analysed            | 70.5                 | 469  | 111  | 272  | 156  | 960  | 822  | 12.0 |
| Certified (BCR-143) | 72.0                 | 426  | 128  | 296  | 174  | 1063 | 858  | 11.8 |
| Recovery (%)        | 97.9                 | 110  | 86.4 | 92.0 | 89.7 | 90.4 | 95.8 | 102  |
|                     | Aqua regia           |      |      |      |      |      |      |      |
| Analysed            | 16.4                 | 148  | 680  | 54.0 | 494  | 2622 | 270  | 7.6  |
| Certified (BCR-146) | 18.4                 | 174  | 831  | 65   | 583  | 3040 | 298  | 6.5  |
| Recovery (%)        | 89.2                 | 85.0 | 81.8 | 83.1 | 84.7 | 86.2 | 84.7 | 117  |

\* nd



was verified by analysis of the certified reference materials: BCR-701 for extraction with  $\text{CH}_3\text{COOH}$  and BCR-143 and BCR-146 for aqua regia digestion. The obtained results are shown in Table 2.

### Determination of element content

The element content in the extracts was determined using an inductively coupled plasma optical emission spectrometer iCAP-6500Duo (ThermoScientific, UK). The detector was a RACID86 Charge injector device (CID). This instrument operates sequentially with both radial and axial torch configurations. The analytical performance of the iCAP 6000 Series is demonstrated by its improved detection limits, enhanced linearity, superior long-term stability and high-resolution images (Sakan et al. 2011).

External standard solutions were prepared from 1000  $\text{mg L}^{-1}$  stock metal solutions. To minimise interference, a multi-element standard stock solution was prepared in which the ratios of the metals in the multiple element calibration standard were analogous to their ratios in the samples. The multi-element standards and blanks were prepared in the same matrix as the extracting reagents to minimise matrix effects and for background correction. The instrumental calibration was checked after the analysis of every 10 to 12 samples.

### Bioavailability risk assessment index

Bioavailability is defined as the extent to which living receptors are exposed to contaminants in soil or sediment (Feng et al. 2005). In this study, an index (bioavailability risk assessment index, BRAI) proposed by Jamshidi-Zanjani et al. (2015) was used to quantify metal bioavailability in sediments, which is based on the results of single extraction methods to ensure a more reliable assessment of the potential risks. It should be noted that this index was developed based on single extraction methods with EDTA as the extractant, with a view to assessing the risk of metal bioavailability.

The proposed formula to calculate BRAI is:

$$\text{BRAI} = \sum \text{Bdi} (i = 1 \text{ to } n) / \sum \text{TEi} (i = 1 \text{ to } n),$$

where Bdi denotes the bioavailable degree of each metal in the sediment sample, which is calculated by:

$$\text{Bdi} = \text{SEi} \times \text{TEi} \text{ and } \text{SEi} = (\text{Bi}/\text{TCi}) \times 100,$$

where n is the number of metals, TE is the toxic effect of the metal derived from the effect range median (ERM) values proposed by Long et al. (1995), SE or source effect represents the release potential of the bioavailable fraction of each of the metals, Bi is the amount of the extracted metal using single extraction methods ( $\text{mg/kg}$ ) and TCi is the total concentration of metal in the sediment samples ( $\text{mg/kg}$ ). A detailed description is given elsewhere (Jamshidi-Zanjani et al. 2015).

Based on the TE and SE values, the proposed categories for BRAI are presented in Table 3.

**Table 3** The categories of BRAI and its criteria

| BRAI value               | BRAI category                     |
|--------------------------|-----------------------------------|
| $\text{BRAI} \leq 1$     | Low risk of bioavailability       |
| $1 < \text{BRAI} \leq 3$ | Medium risk of bioavailability    |
| $3 < \text{BRAI} \leq 5$ | High risk of bioavailability      |
| $\text{BRAI} > 5$        | Very high risk of bioavailability |

### Statistical analysis

Mean, minimum, maximum and standard deviation were determined for all data. Correlation analysis was performed using Pearson's coefficient between the element content values. All statistical analyses were carried out using SPSS 21 for Windows.

## Results and discussion

### The accuracy check

Comparative results of analysed and certified values of BCR-701, BCR-143 and BCR-146 are shown in Table 2. Good concordance between the determined and the certified values were obtained, confirming the accuracy of the results reported in this manuscript. The precision is expressed as relative standard deviation (RSD). The RSD values of the mean values obtained from duplicate measurements were less than 8 % for all the measured elements and methods. No reference material was available for the extractions with  $\text{CaCl}_2$ , EDTA and  $\text{CH}_3\text{COONH}_4$ ; therefore, a difference of less than 8 % among replicates was considered acceptable. The accuracy and precision values calculated in this work confirm the high performance of the adopted procedures.

### Single-extraction analyses and total metal content in sediments

The total element content and the results obtained for the element content after the execution of four single extraction methods are presented in Table 4 and Figs. 2–6. The percentages of the extracted elements in the mobile fraction compared to the total content obtained with aqua regia digestion were also calculated. Table 4 and Supplementary Figs. 1–4 detail the results obtained for all the elements for the four extraction techniques used.

It is possible to observe similar trends when the average value of extractable element content (shown in  $\text{mg kg}^{-1}$ ) and the mean percent of extracted elements are compared (Table 4). A difference can be observed for the maximum percentage of individual extracted elements, for example, for Fe and Ni using EDTA. These results can be explained by the

**Table 4** Element content in studied sediments (mg kg<sup>-1</sup>) and percent of extracted elements (%)

|  | Ba   | Cd   | Co   | Cr   | Cu   | Fe     | K      | Mg     | Mn    | Ni    | Pb   | V    | Zn   |
|--|------|------|------|------|------|--------|--------|--------|-------|-------|------|------|------|
| CaCl <sub>2</sub>                        |      |      |      |      |      |        |        |        |       |       |      |      |      |
| <sup>a</sup> Mean (mg kg <sup>-1</sup> ) | 2.07 | 0.01 | 0.01 | <DL  | 0.39 | 1.83   | 69.3   | 292    | 17.8  | 0.11  | 0.03 | 0.02 | 0.18 |
| Max                                      | 3.50 | 0.06 | 0.10 | <DL  | 2.40 | 7.14   | 117    | 896    | 77.3  | 0.42  | 0.08 | 0.14 | 1.70 |
| Min                                      | 1.10 | <DL  | <DL  | <DL  | 0.08 | 0.04   | 35.0   | 143    | 2.17  | 0.03  | <DL  | 0.00 | 0.00 |
| <sup>b</sup> Average (%)                 | 0.82 | 0.73 | 0.08 | 0    | 0.63 | 0.00   | 0.72   | 2.17   | 1.49  | 0.16  | 0.07 | 0.02 | 0.04 |
| Max                                      | 1.73 | 1.89 | 0.45 | 0    | 1.11 | 0.01   | 1.46   | 8.27   | 7.87  | 0.53  | 0.3  | 0.13 | 0.23 |
| Min                                      | 0.42 | 0.1  | 0.02 | 0    | 0.21 | 0      | 0.34   | 0.64   | 0.3   | 0.03  | 0    | 0    | 0    |
| EDTA                                     |      |      |      |      |      |        |        |        |       |       |      |      |      |
| <sup>a</sup> Mean (mg kg <sup>-1</sup> ) | 12.6 | 0.94 | 0.62 | 0.07 | 26.2 | 762    | 218    | 487    | 276   | 2.46  | 33.1 | 1.76 | 56.7 |
| Max                                      | 47.2 | 2.94 | 1.92 | 0.25 | 280  | 3141   | 373    | 1361   | 890   | 18.0  | 172  | 11.0 | 231  |
| Min                                      | 0.77 | 0.10 | 0.04 | 0.00 | 4.30 | 192    | 25.0   | 84     | 76.0  | 0.00  | 2.30 | 0.00 | 8.92 |
| <sup>b</sup> Average (%)                 | 4.77 | 36.3 | 3.29 | 0.14 | 32.1 | 1.84   | 2.27   | 3.55   | 23.42 | 2.65  | 43.8 | 1.90 | 14.4 |
| Max                                      | 14.5 | 58.6 | 8.8  | 0.57 | 46.8 | 7.1    | 3.99   | 7.63   | 45.6  | 23.4  | 61.0 | 11.6 | 61.2 |
| Min                                      | 0.28 | 3.9  | 0.21 | 0    | 5.43 | 0.43   | 0.2    | 0.73   | 8     | 0     | 4.59 | 0    | 4.05 |
| CH <sub>3</sub> COOH                     |      |      |      |      |      |        |        |        |       |       |      |      |      |
| <sup>a</sup> Mean (mg kg <sup>-1</sup> ) | 26.8 | 1.18 | 1.75 | 0.15 | 10.5 | 360    | 177    | 1877   | 609   | 4.60  | 2.91 | 0.11 | 89.2 |
| Max                                      | 47.3 | 5.62 | 5.17 | 0.46 | 166  | 2108   | 329    | 7278   | 1651  | 26.1  | 34.6 | 1.64 | 544  |
| Min                                      | 13.2 | 0.04 | 0.35 | <DL  | 0.18 | 5.40   | 83.0   | 483    | 129   | <DL   | <DL  | <DL  | 5.80 |
| <sup>b</sup> Average (%)                 | 10.5 | 41.3 | 8.73 | 0.29 | 8.66 | 0.84   | 1.84   | 12.7   | 51.4  | 4.63  | 2.71 | 0.12 | 19.1 |
| Max                                      | 16.1 | 66.9 | 22.2 | 1.05 | 57.1 | 4.27   | 3.76   | 31.2   | 77.3  | 13.8  | 10.7 | 1.73 | 45.1 |
| Min                                      | 5.08 | 9.12 | 2.47 | 0    | 0.83 | 0.01   | 0.8    | 4.39   | 21.45 | 0     | 0    | 0    | 5.44 |
| CH <sub>3</sub> COONH <sub>4</sub>       |      |      |      |      |      |        |        |        |       |       |      |      |      |
| <sup>a</sup> Mean (mg kg <sup>-1</sup> ) | 60.1 | 0.74 | 0.15 | 0.02 | 4.98 | 2.48   | 242    | 719    | 173   | 1.24  | 0.77 | 0.23 | 16.8 |
| Max                                      | 97.0 | 1.80 | 0.87 | 0.08 | 82.0 | 14.8   | 446    | 2403   | 581   | 5.84  | 10.5 | 2.88 | 122  |
| Min                                      | 32.8 | 0.05 | 0.03 | <DL  | 0.38 | 0.94   | 156    | 384    | 50.5  | 0.28  | <DL  | <DL  | 1.10 |
| <sup>b</sup> Average (%)                 | 23.1 | 28.8 | 0.81 | 0.04 | 4.80 | 0.00   | 2.50   | 5.22   | 14.8  | 1.59  | 0.71 | 0.25 | 3.45 |
| Max                                      | 32.4 | 60.6 | 3.99 | 0.15 | 12.1 | 0.03   | 4.83   | 13.5   | 32.6  | 8.2   | 4.89 | 2.7  | 10.2 |
| Min                                      | 12.7 | 6.69 | 0.19 | 0    | 0.73 | 0      | 1.41   | 1.56   | 4.72  | 0.37  | 0    | 0    | 0.33 |
| Aqua regia                               |      |      |      |      |      |        |        |        |       |       |      |      |      |
| <sup>a</sup> Mean (mg kg <sup>-1</sup> ) | 260  | 3.00 | 19.0 | 55.0 | 72.0 | 40,490 | 9986   | 14,335 | 1134  | 88.0  | 71.0 | 87.0 | 350  |
| Max                                      | 426  | 9.01 | 27.0 | 120  | 676  | 50,230 | 12,887 | 24,983 | 3185  | 284   | 323  | 110  | 1207 |
| Min                                      | 135  | 0.30 | 5.30 | 26.7 | 21.8 | 20,299 | 5089   | 6915   | 507   | 32.04 | 16.6 | 40.3 | 67.6 |

<sup>a</sup> Mean content of extracted element, shown in mg kg<sup>-1</sup>

<sup>b</sup> (Metal content (mobile) / metal content (aqua regia)) × 100

<DL below detection limit

high heterogeneity of the sediments studied with significant differences in the geochemical composition of the substrates. Also, the observed differences may be due to presence of different anthropogenic contributions to the sediment composition. The individual maximum content of the extracted elements varied from 1.05 % (for Cr) to 77.30 % (for Mn), which highlights the large differences between the bioavailabilities of the elements studied.

Compared to the other extraction reagents, the least elemental content was extracted using CaCl<sub>2</sub>. Less than 9 % of the total content (Table 4) was extracted with CaCl<sub>2</sub>. These results are consistent with previously published results

(Bakircioglu et al. 2011) and can be explained by the fact that unbuffered salt solutions such as CaCl<sub>2</sub> extract only the water-soluble fraction (Jamshidi-Zanjani et al. 2015).

The highest amount of elemental content was extracted using CH<sub>3</sub>COOH as the extracting reagent. In terms of the relative amounts of elements extracted using the four approaches, the highest amount of Ba and K was extracted using CH<sub>3</sub>COONH<sub>4</sub>; Cu, Fe, Pb and V with EDTA and Cd, Co, Cr, Mg, Mn and Ni with CH<sub>3</sub>COOH (Table 3).

As previously outlined, the highest amount of Ba and K was extracted using CH<sub>3</sub>COONH<sub>4</sub> as the extracting agent. The neutral 1-M ammonium acetate extraction method is the

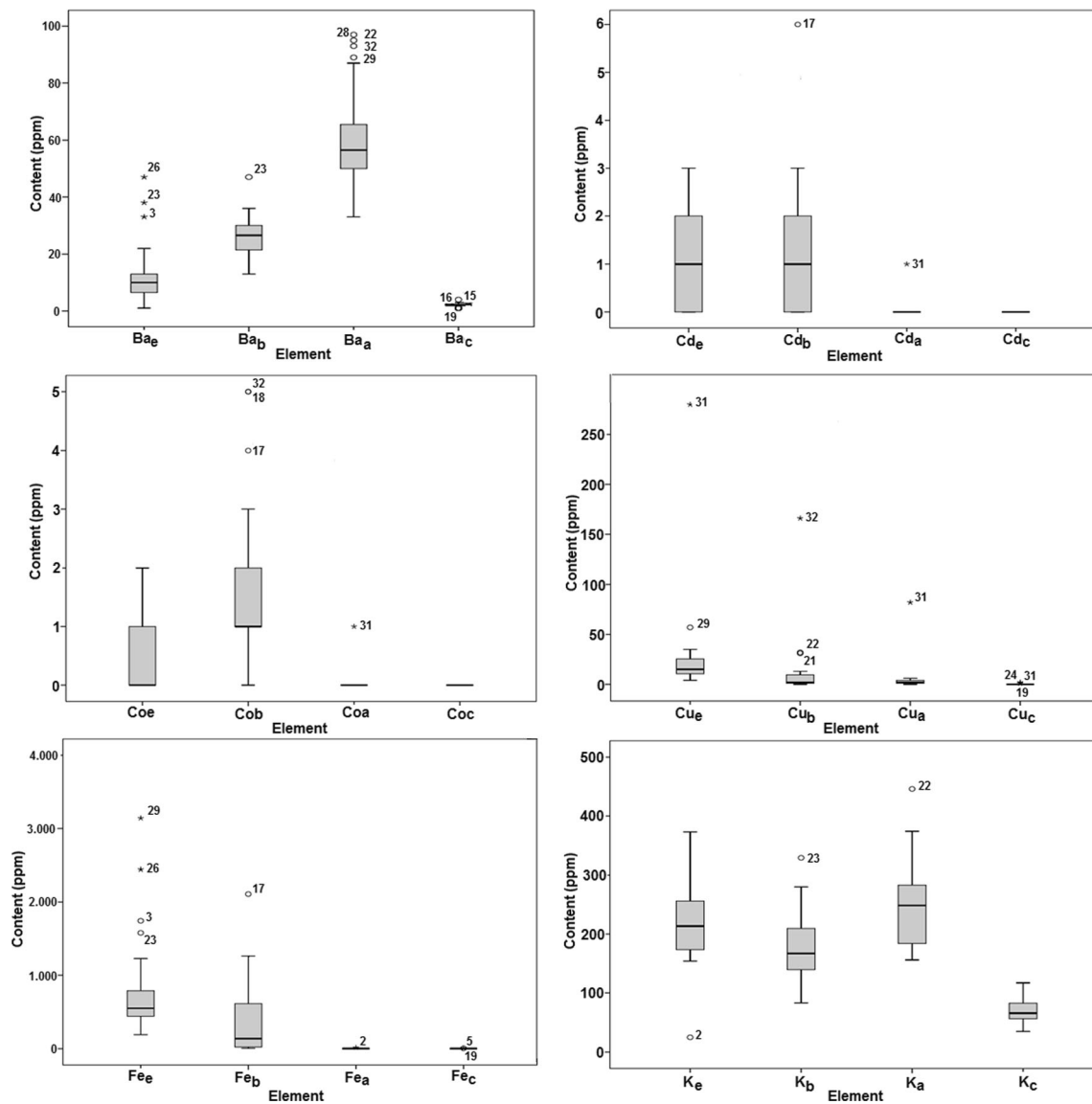


**Fig. 2** Box plot showing the variation of Ba, Cd, Co, Cu, Fe and K content in mobile fractions in the studied sediments (explanation: *e*—EDTA; *b*—CH<sub>3</sub>COOH; *a*—CH<sub>3</sub>COONH<sub>4</sub>; *c*—CaCl<sub>2</sub>). Open circle represents outlying points, while asterisk represents extreme points

most widely used procedure to extract water-soluble and rapidly exchangeable fractions. This method extracts the water-soluble and rapidly exchangeable fractions of the alkali and alkaline earth cations by displacement with NH<sub>4</sub><sup>+</sup> from exchangeable sites. Since NH<sub>4</sub><sup>+</sup> forms inner-sphere surface complexes with 2:1 layer-type clay minerals, the use of this method to measure soil cation exchange capacity has significant potential for inaccuracy (Carter 1993). Compared to CaCl<sub>2</sub>, CH<sub>3</sub>COONH<sub>4</sub> showed better extraction ability for all the elements studied (Fig. 5a, b). The average proportion of extracted Ba and Cd were 23.1 and 28.8 % of their total content, respectively. For other elements, the extracted amount was less than 15 % of their total content. The results obtained are consistent with others previously reported (Meers et al. 2005; Jamshidi-Zanjani et al. 2015). The fact that higher extraction was shown

for toxic elements such as Cd, Zn and Cu using CH<sub>3</sub>COONH<sub>4</sub> instead of CaCl<sub>2</sub> highlights the high potential risk of their release into the environment. Furthermore, considerable fractions of these elements could be available for biota metabolism. Ba and K were extracted in higher amounts with CH<sub>3</sub>COONH<sub>4</sub> than with EDTA and CH<sub>3</sub>COOH, which is consistent with previously published results, which propose that this method may be used to assess the amount of available K, Na, Li, Ba, Mg and Ca (Carter 1993).

According to the results detailed in Table 4, the mean proportions of Cu, Fe, Pb and V and the maximum values of Ni and Zn, from samples taken from particular regions, are extracted in higher content with EDTA than with the other extracting reagents. This indicates that these elements are more easily remobilised by complexation than by acidification

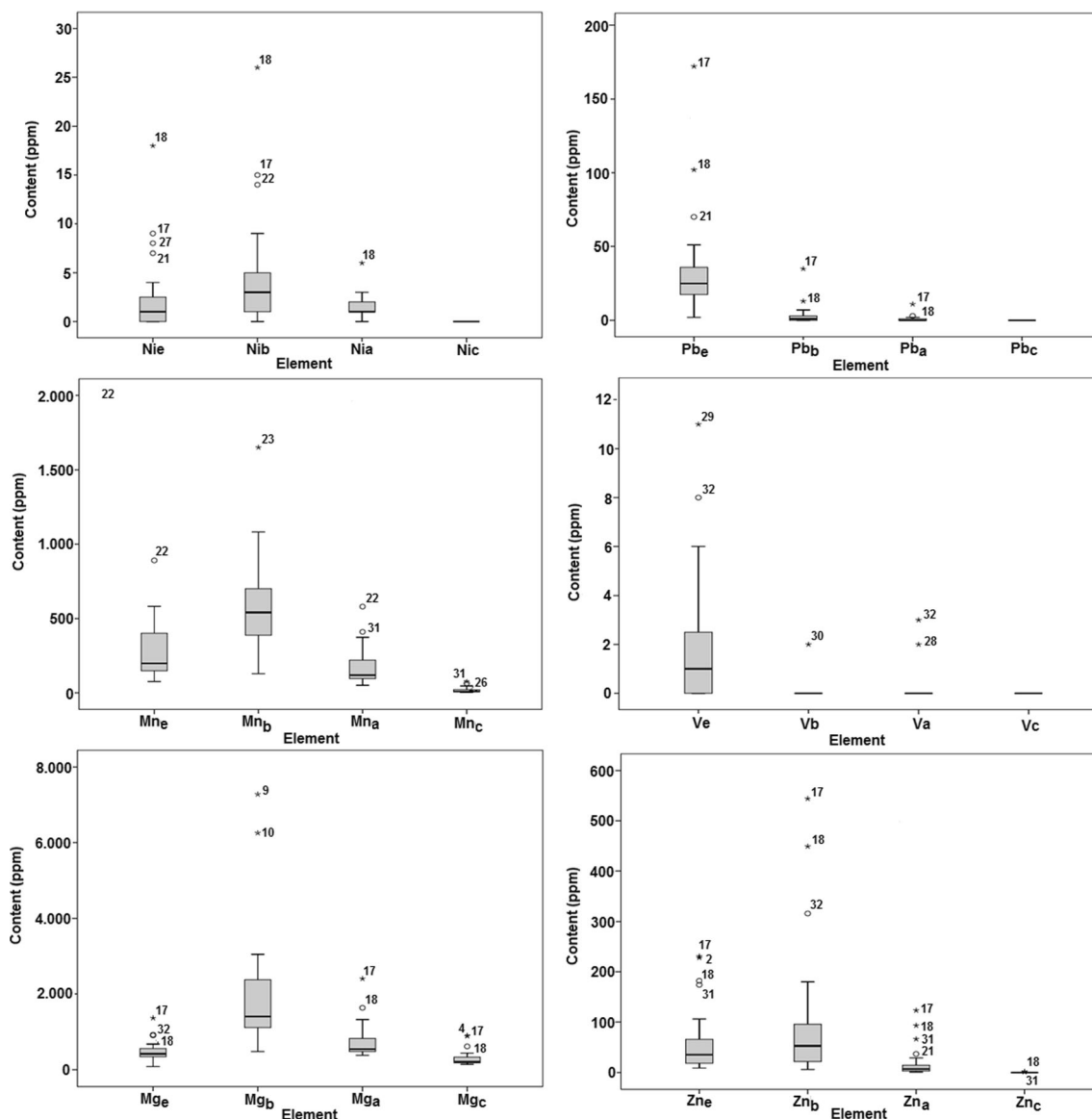
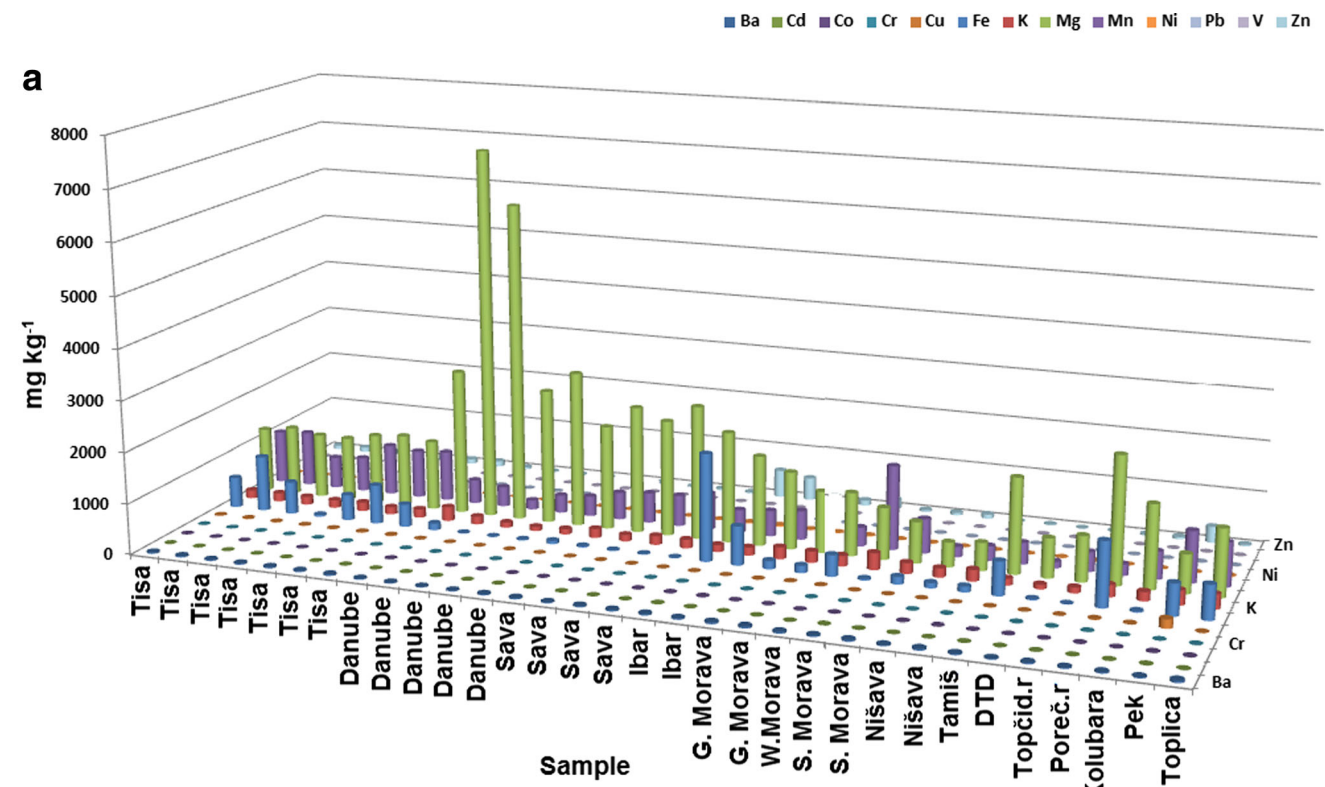


**Fig. 3** Box plot showing the variation of Ni, Pb, Mn, V, Mg, and Zn content in mobile fractions in the studied sediments (explanation: *e*—EDTA; *b*—CH<sub>3</sub>COOH; *a*—CH<sub>3</sub>COONH<sub>4</sub>; *c*—CaCl<sub>2</sub>). *Open circle* represents outlying points, while *asterisk* represents extreme points

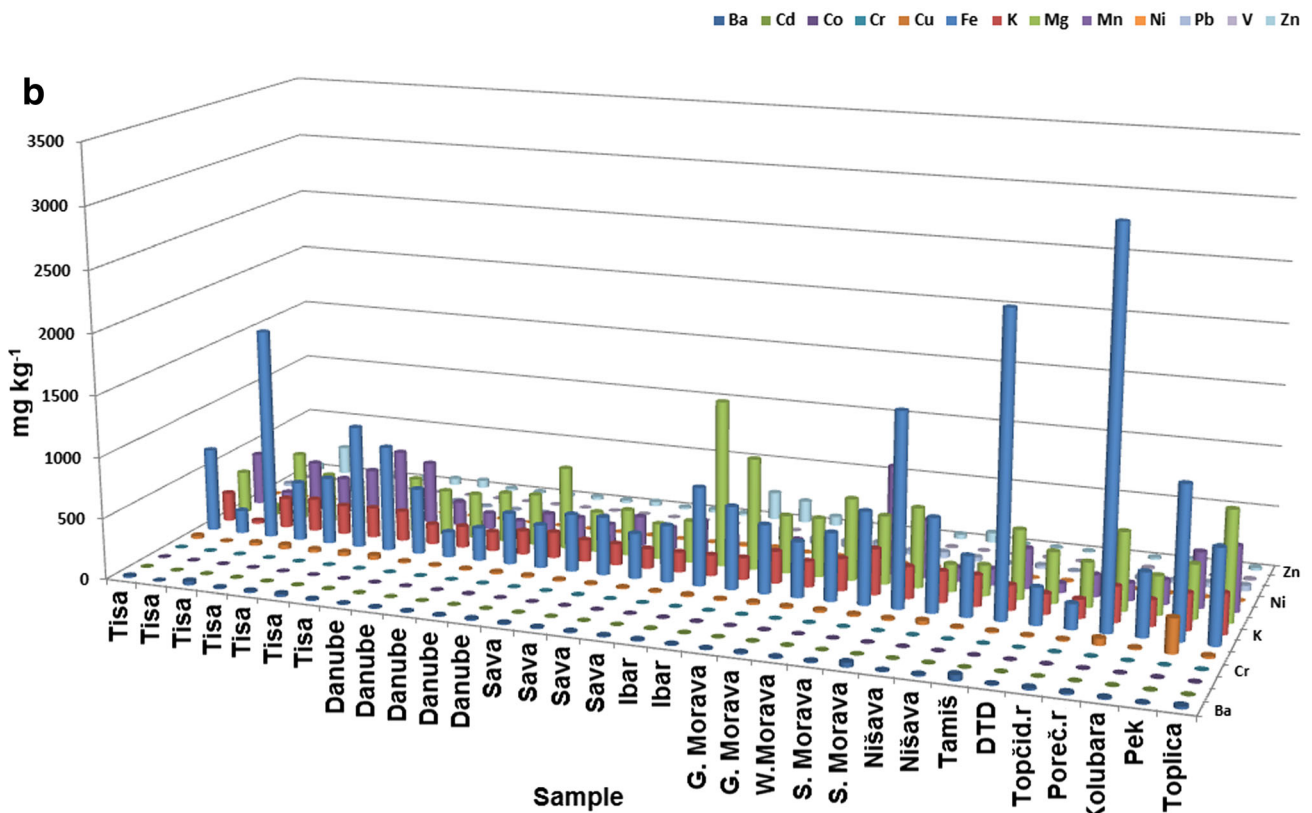
processes. EDTA is a widely used complexing agent due to its high extraction capacity (Sahuquillo et al. 2003). EDTA is assumed to extract metals on exchange sites of both inorganic and organic complexes. Additionally, EDTA is recognised to concurrently complex with soil and sediments components, such as Fe and Al oxides, aluminosilicates and carbonates (Chao, 1984; Sahuquillo et al. 2003; Gismera et al. 2004), resulting in their dissolution and competitive phenomena among metals (Tsang et al. 2007). In general, EDTA is considered as an extractor of water soluble, partially exchangeable, and partially organic-bound elements (Zhang et al. 2010; Jamshidi-Zanjani et al. 2015).

It can be assumed that Cu, Zn and Pb are mostly associated to a mineralogical fraction that is not attacked at all by other extracting reagents, but is solubilised by EDTA, which also is

in agreement with work reported by Leleyter et al. (2012). This scenario implies that these metals are not associated to any carbonate phase, or exchangeable fraction, but may be present as highly complexed forms, adsorbed on minerals. Additionally, the proposed complexes would have to be less stable than the complexes they can form with EDTA. Sahuquillo et al. (2003) explained the reasons for the higher extractability observed for Cu and Pb when using a complexing agent for extraction: firstly, Cu and Pb have high complexation constants with EDTA (log K = 17.8 and 18.3, respectively). Secondly, these two metals are highly associated with Fe oxides and hydroxides and can be remobilised due to the complexation of Fe with EDTA (log K = 25.1). Di Palma and Mecozzi (2007) point out that in the remediation of copper contaminated soil and sediments, the effectiveness



CH<sub>3</sub>COOH



EDTA

Fig. 4 Content of element after extraction with CH<sub>3</sub>COOH (a) and with EDTA (b)



of EDTA has been widely demonstrated as a chelating agent in washing treatments.

Leleyter et al. (2012) describe that for the estimation of metal mobility, EDTA is adapted for Pb. Pb bound in the organic fraction is an important non-residual fraction due to  $\text{Pb}^{2+}$  having high stability constants with humic acids. Very little lead bound to the exchangeable and carbonate fraction was noted which is in agreement with the research carried out by Anju and Banerjee (2011). Some data have shown that in uncontaminated soils 20–60 % of the total Pb content can be extracted with EDTA, which is in line with the results reported here (Table 4). Results generally confirm EDTA effectiveness in removing metals weakly bound to carbonate, oxide and hydroxide fractions.

Dominant extraction of Zn, Cd, Co, Cr, Mg, Mn and Ni was observed when  $\text{CH}_3\text{COOH}$  was used as the extraction reagent (Table 4, Figs. 2 and 3), which means that these metals are more sensitive to acidification than to complexation processes (Sahuquillo et al. 2003). Similar percentages of extracted Cr, Cu, Pb, Ni, Zn and Cd with  $\text{CH}_3\text{COOH}$  were also shown for the Sava river (Milačič et al. 2010). Leleyter et al. (2012) concluded that EDTA leaching appears to be the best method to estimate Pb mobility, whereas sequential extraction appears more appropriate to estimate Zn mobility. Successful extraction of Cd with  $\text{CH}_3\text{COOH}$  has also been reported by other researchers (Kartal et al. 2006; Di Palma and Mecozzi 2007; Massolo et al. 2012). The Cd was mainly associated with the fraction dissolved in acetic acid (Fig. 4a), which is thought to remove predominantly water-soluble, exchangeable, and carbonate-bound metals from the sediment. The very low solubility of cadmium carbonate and the low adsorption constant of the complex formed with the organic matter causes Cd to become more concentrated in the carbonates and the exchangeable fractions. Mn was considered to be the most mobile element since it was present in the highest relative percentage (a mean content of 51.4 %) when extracted with  $\text{CH}_3\text{COOH}$  (Fig. 4a). This is probably because of the known close association of Mn with carbonates, as endorsed by other researchers (Massolo et al. 2012).

The box and whisker plots shown in Figs. 2 and 3 summarise the basic statistics for the concentrations of heavy metals investigated in the studied sediments. It is obvious that the extractable amounts of elements by various single extractants displayed wide differences in their variance. Some elements have anomalies of higher extractable amounts in some of the river sediments: Cd (Ibar, Pek); Co (Toplica, Ibar, Pek); Cu (Pek, Toplica, Porečka river, South and West Morava, Nišava); Ni (Ibar, South and West Morava, DTD canal); Pb (Ibar, West Morava) and Zn (Ibar, Toplica, Tisa, Pek, West Morava). These elements at quoted localities mainly originate from anthropogenic sources. Anthropogenic metals entering the aquatic environment are participated in geochemical fractions that are environmentally reactive and as result their

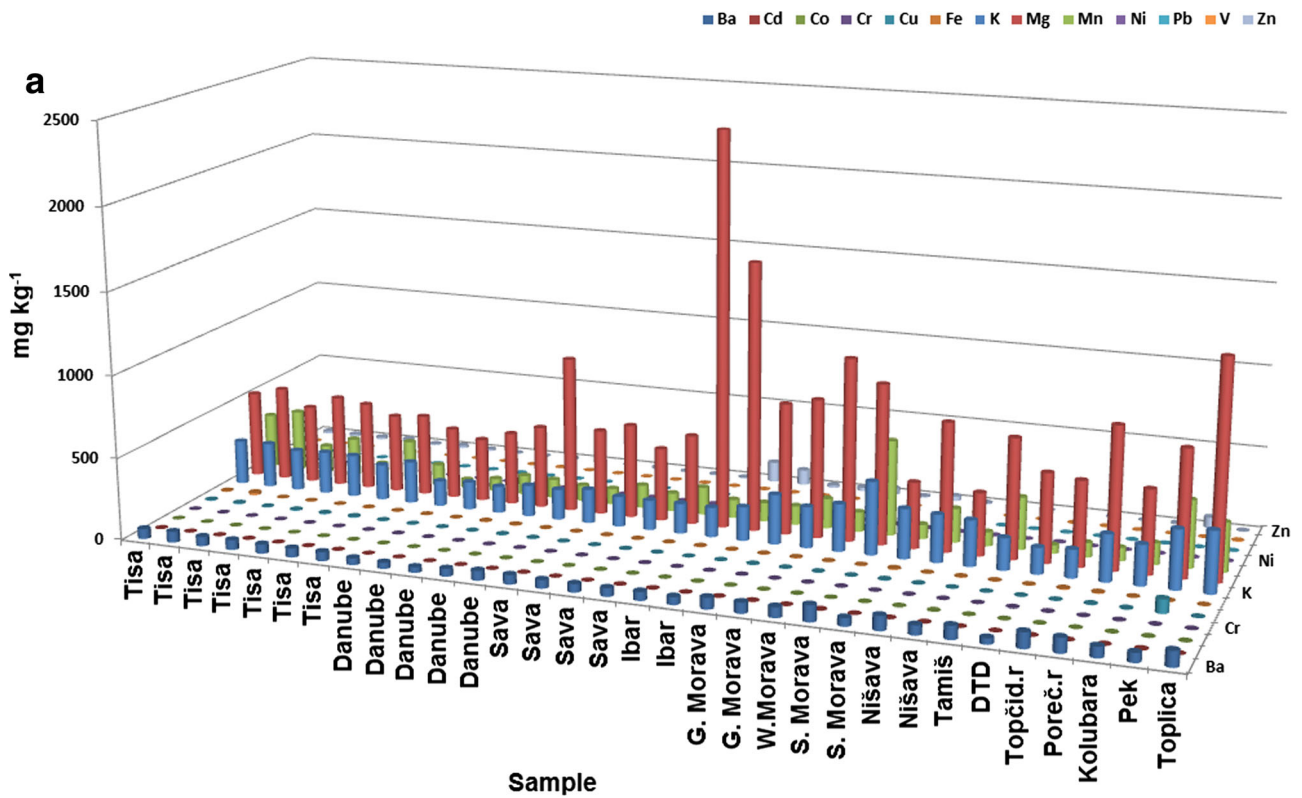
bioavailability is higher. Anomalies of higher extractable amounts of Ba, Fe, K, Mn, V and Mg are consequence of significant differences in the geochemical composition of the sediments.

### Bioavailability risk assessment index

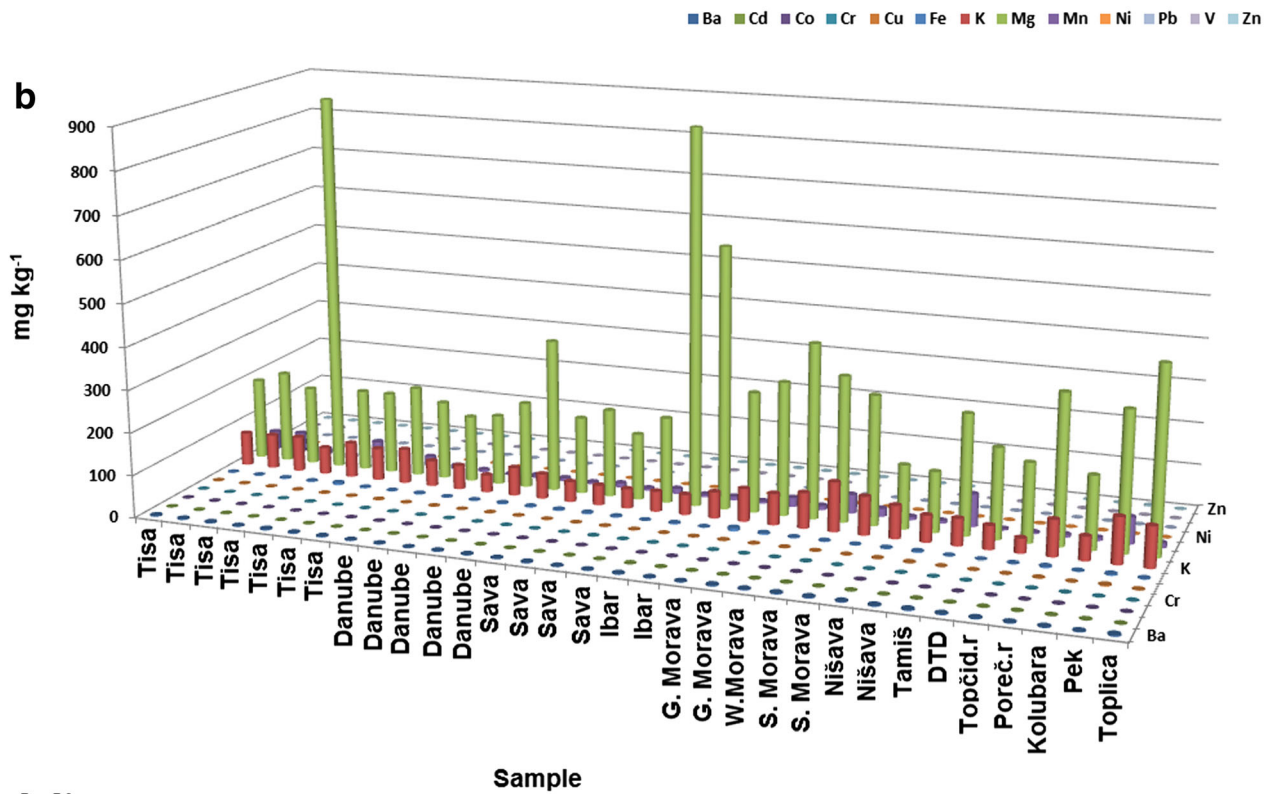
The results of the calculated bioavailability risk assessment index (BRAI) with EDTA as the extractant are presented in Fig. 7. In general, for all the sediments studied, the BRAI values were higher than one, which means medium to high risk levels of the researched elements. The BRAI values from the Tisa; the Danube (Bezdan and Gruja, two of five samples); the Sava (Ostružnica); the Ibar (Raška); the Great, West and South Morava; the Nišava; the Tamiš; the Kolubara; the Pek and the Toplica were all higher than three. The highest values of BRAI (higher than four) were from the Tisa and the Pek. The mean of the calculated BRAI for the sediments studied were 3.13 (high risk of bioavailability). Therefore, it can be concluded that the sediments in this study have considerable potential to leach metals. Comparing the BRAI values reported here with other published results, the mean BRAI value in this research was higher than urban soil in Sevilla (Madrid et al. 2008), but lower than mining areas in India (Anju and Banerjee 2011), agricultural soils from Italy (Poggio et al. 2009) and residential sites in Italy (Poggio et al. 2009). The results obtained for the studied river sediments are consistent with results reported for the Sava (Milačič et al. 2010), where it was shown that the environmental status of the Sava river is generally comparable to other moderately polluted rivers in Europe.

### Correlation between single extractions and pseudo-total element content

Supplementary Table 1 presents an overview of the significant correlation between the element content obtained with different single extraction procedures and the pseudo-total content of elements obtained with aqua regia. A significant linear correlation was found between the following: EDTA—extractable and total concentrations of Cd, Co, Cu, Ni, V and Zn;  $\text{CH}_3\text{COOH}$ —extractable and total concentrations of Cd, Co, Mg, Ni, Pb and Zn;  $\text{CH}_3\text{COONH}_4$ —extractable and total concentrations of Ba, Cd, Cu, Mn, Ni, Pb and Zn and  $\text{CaCl}_2$ —extractable and total concentrations of Cu and Zn. These correlations indicate that studied elements originate from anthropogenic source rather than geochemical background. Positive correlation of mobile Mn content with total Mn content indicate that Mn oxides were the main substrate for some of the elements (Relić et al. 2005). Correlation between the mobile fractions of Mg and pseudo-total content of Mg indicating that carbonates are significant substrates of elements in studied sediments, considering that metal mobilisation with acetic



$\text{CH}_3\text{COONH}_4$



$\text{CaCl}_2$

Fig. 5 Content of element after extraction with  $\text{CH}_3\text{COONH}_4$  (a) and with  $\text{CaCl}_2$  (b)

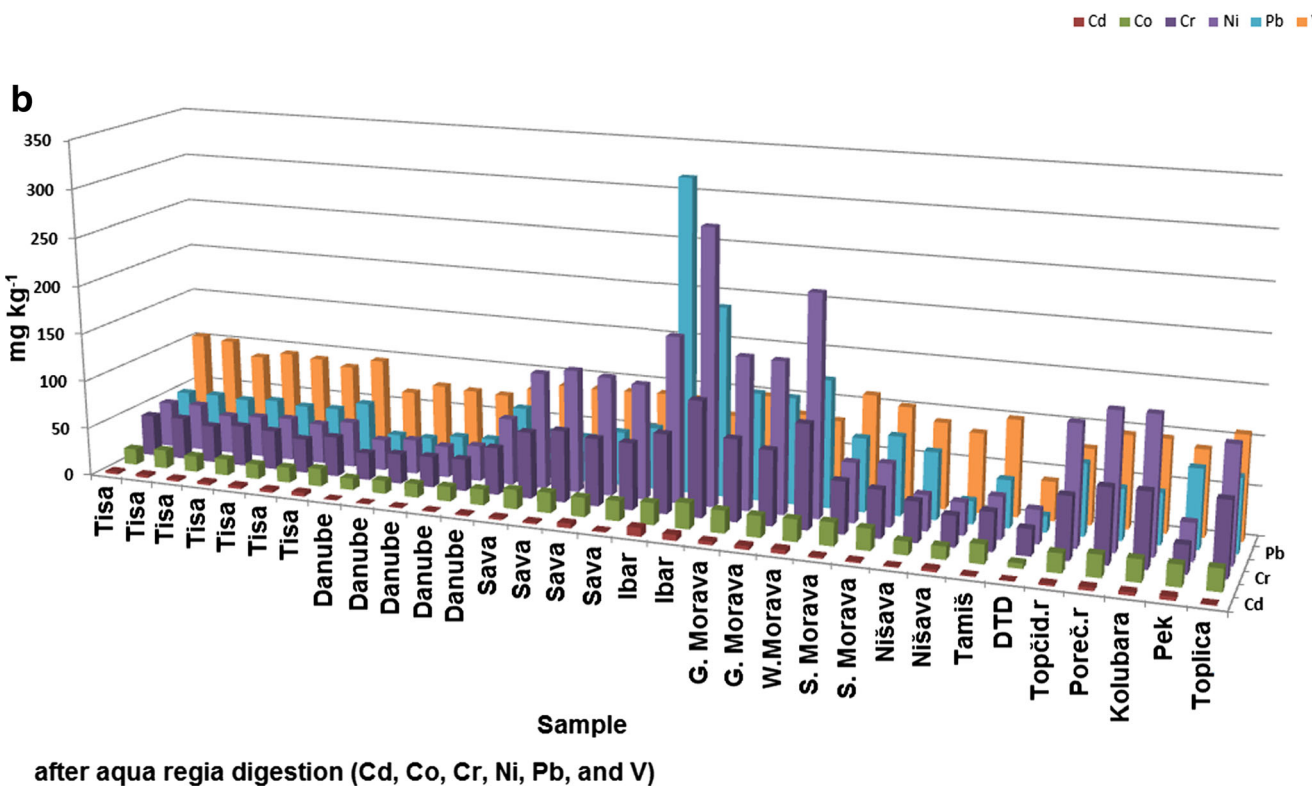
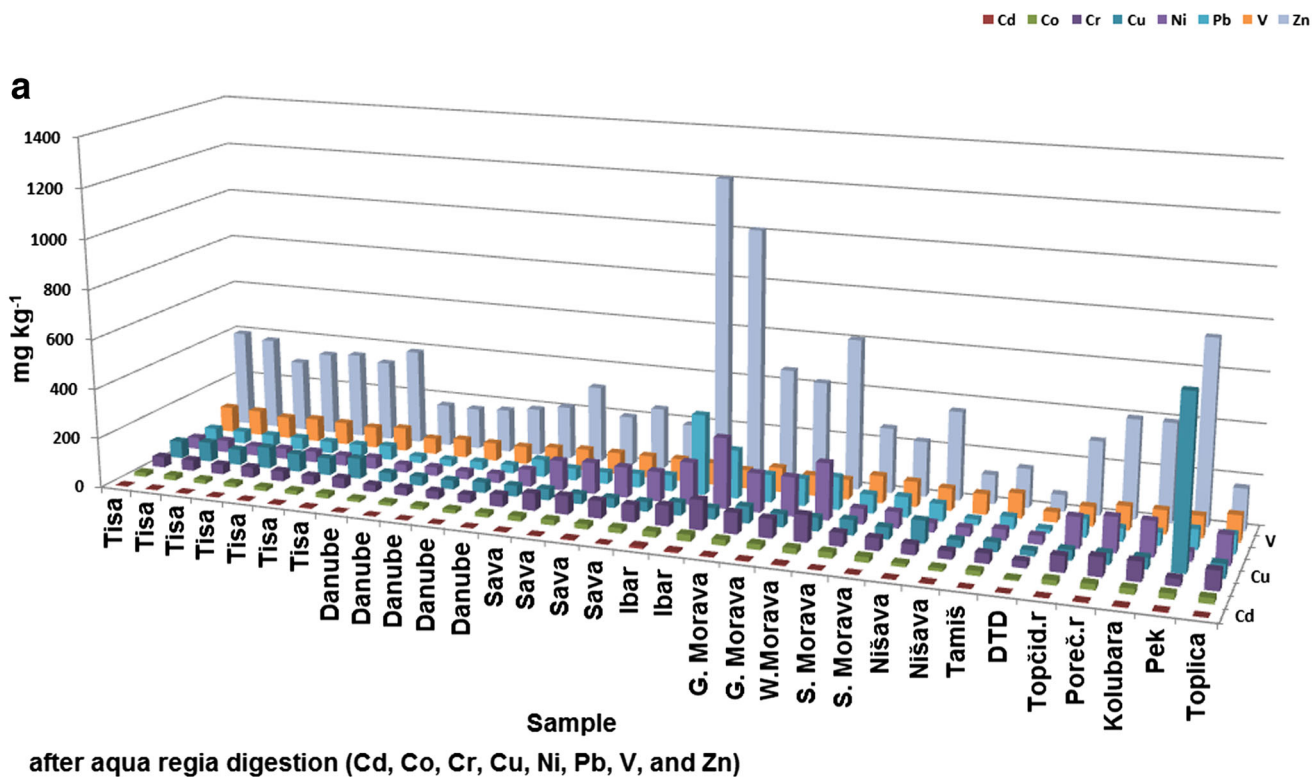
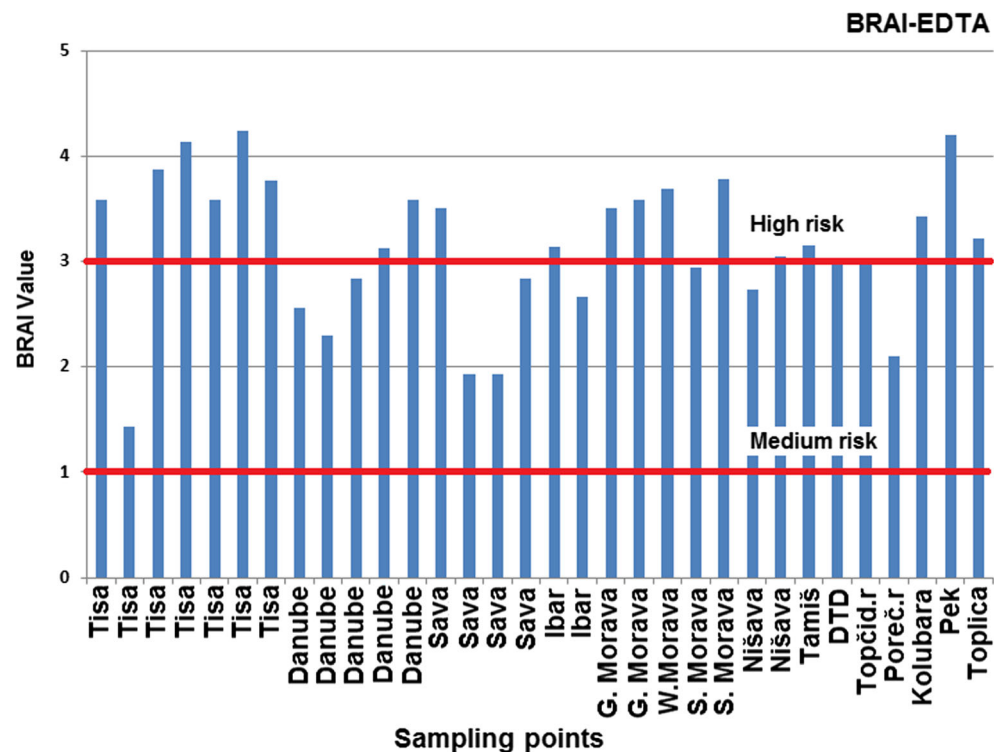


Fig. 6 Content of element after aqua regia digestion. (a) Cd, Co, Cr, Cu, Ni, Pb, V and Zn and (b) Cd, Co, Cr, Ni, Pb and V (without Cu and Zn)

acid is basically attributed to carbonate dissolution. No correlation was found between the mobile fraction and the total

content for Cr, Fe and K. This can be explained by the fact that aqua regia extracts the inert fraction of the sediment

**Fig. 7** BRAI values in the surface sediment based on EDTA extraction



components that is not related to the available chemical forms (Kelepertzis et al. 2015). Cr was found to be the least mobile element and was generally not released in significant amounts. Also, Fe and K are elements that are predominantly bound with oxides and silicates in sediments, and are generally immobile. These elements are retained within the crystal lattice of minerals and in well-crystallised oxides, and could be used as an indicator of natural sources input (Favas et al. 2015).

It is possible to conclude that single extractions offer the possibility to perform fast screening analysis of the mobilisable pool of elements in soils and sediments. No correlation between all the single extractions and the total extraction confirmed that total concentration is a poor indicator of bioavailability.

## Conclusions

Various single extraction procedures were used to evaluate Ba, Cd, Co, Cr, Cu, Fe, K, Mg, Mn, Ni, Pb, V and Zn extractability in Serbian river sediments. The results of the single extraction methods reveal that the studied sediments hold considerable potential to leach metals. Among the protocols used for the determination of heavy metal pool, the highest amount of elemental content was extracted using acetic acid as the extracting reagent. The highest amount of Ba and K was extracted using ammonium acetate; Cu, Fe, Pb and V with EDTA, and Cd, Co, Cr, Mg, Mn and Ni with acetic acid. Compared to calcium chloride, ammonium acetate showed

better extraction ability for all the elements studied. The fact that higher extraction was shown for toxic elements such as Cd, Zn and Cu using ammonium acetate instead of calcium chloride highlights the high potential risk of their release into the environment. Cd, Cu, Zn and Pb were among the metals that show the highest potential bioavailability in the Serbian river sediments tested. No correlation between all the single extractions and the total extraction confirmed that total concentration is a poor indicator of bioavailability. Results of this study imply that the potential risk arising from elevated contents of toxic elements in the river sediments does not solely rely on the total content, but on the determination of bioavailable fractions. In general, single extractions offer the possibility to perform fast screening analysis of the mobilisable pool of elements in soils and sediments.

BRAI was used to quantify metal bioavailability in sediments. This index is very important in environmental research due to its ability to quantify metal bioavailability in sediments from which more reliable potential risks can be assessed. For all the sediments studied, the BRAI values were higher than one, which means medium to high risk levels of the researched elements. These results may be of great importance to researchers since the quantification of the bioavailability of heavy metals in Serbian river systems using the BRAI has never been previously reported. Also, the results provide baseline information for overall management of the river's environment.

Based on the results obtained, we recommend the use of single extraction procedures and the BRAI in future studies.



Furthermore, our recommendation would be to perform extraction with glycine for the prediction of the effects of heavy metal contamination on human health and to calculate an index to quantify human bioaccessibility.

**Acknowledgments** This study was supported by the Ministry of Education, Science and Technological Development of Serbia, Grant Nos. 172001 and 43007. In addition, we would like to thank the Republic Hydrometeorological Service of Serbia for the sediment samples. The authors are grateful to anonymous reviewers whose comments greatly improved the paper.

## References

- Anju M, Banerjee DK (2011) Associations of cadmium, zinc, and lead in soils from a lead and zinc mining area as studied by single and sequential extractions. *Environ Monitor Assess* 176:67–85
- Bakircioglu D, Kurtlus YB, Ibar H (2011) Comparison of extraction procedures for assessing soil metal bioavailability of wheat grains. *Clean-Soil Air Water* 39:728–734
- Calmano W, Hong J, Förstner U (1993) Binding and mobilization of heavy metals in contaminated sediments affected by pH and redox potential. *Water Sci Technol* 28:223–235
- Carter MR (1993) *Soil sampling and methods of analysis*. Lewis Publishers, Canadian Society of soil Science
- Chao TT (1984) Use of partial dissolution techniques in geochemical exploration. *J Geochem Explor* 20:101–135
- DIN 38414 S7 (1983), Deutsche Einheitsverfahren zur Wasser-, Abwasser- und Schlammuntersuchung, Schlamm und Sedimente (Gruppe S), Aufschluß mit Königswasser zur nachfolgenden Bestimmung des säurelöslichen Anteils von Metallen (S7) (Sludge and sediments-decomposition with aqua regia for the measurement of the acid soluble metal load), Beuth Berlin
- Favas PJC, Sarkar SK, Rakshit D (2015) Geochemical fractionation of trace elements in stream sediments contaminated by mining activity. *Clean-Soil Air Water* 43:446–455
- Feng MH, Shan XQ, Zhang S, Wen B (2005) A comparison of the rhizosphere-based method with DTPA, EDTA,  $\text{CaCl}_2$ , and  $\text{NaNO}_3$  extraction methods for prediction of bioavailability of metals in soil to barley. *Environ Pollut* 137:231–240
- Gismera MJ, Lacal J, da SP, Garcia R, Sevilla MT, Procopio JR (2004) Study of metal fractionation in river sediments. A comparison between kinetic and sequential extraction procedures. *Environ Pollut* 127:175–182
- Guan Q, Wang L, Pan B, Guan W, Sun X, Cai A (2016) Distribution features and controls of heavy metals in surface sediments from the riverbed of the Ningxia-inner Mongolian reaches, Yellow River, China. *Chemosphere* 144:29–42
- Jamshidi-Zanjani A, Saeedi M, Li LY (2015) A risk assessment index for bioavailability of metals in sediments: Anzali international wetland case study. *Environ Earth Sci* 73:2115–2126
- Jiao W, Ouyang W, Hao F, Lin C (2015) Anthropogenic impact on diffuse trace metal accumulation in river sediments from agricultural reclamation areas with geochemical and isotopic approaches. *Sci Total Environ* 536:609–615
- Kartal Ş, Aydin Z, Tokahoğlu Ş (2006) Fractionation of metals in street sediment samples by using the BCR sequential extraction procedure and multivariate statistical elucidation of the data. *J Hazard Mater* 132:80–89
- Kastratović VR, Đurović DD, Krivokapić SD, Mugoša BP (2013) Mobility and bioavailability of metals in sediments of Skadar lake—Montenegro. *E3S Web of Conferences* 1, 33006.doi: 10.1051/e3conf/20130133006
- Kelepertzis E, Paraskevopolou V, Argyraki A, Fligos G, Chalkiadaki O (2015) Evaluation of single extraction procedures for the assessment of heavy metal extractability in citrus agricultural soil of a typical Mediterranean environment (Argolida, Greece). *J Soils Sediments* 15:2265–2375
- Leleyter L, Rousseau C, Biree L, Baraud F (2012) Comparison of EDTA, HCl and sequential extraction procedures, for selected metals (Cu, Mn, Pb, Zn), in soils, riverine and marine sediments. *J Geochem Explor* 116–117:51–59
- Li LY, Hall K, Yi Y, Mattu G, McCallum D, Chen M (2009) Mobility and bioavailability of trace metals in the water-sediment system of the highly urbanized brunette watershed. *Water Air Soil Pollut* 197: 249–266
- Long ER, MacDonald DD, Smith SL, Calder FD (1995) Incidence of adverse biological effects within ranges of chemical concentrations in marine and estuarine sediments. *Environ Manag* 19:81–97
- Ma X, Zuo H, Tian M, Zhang L, Meng J, Zhou X, Min N, Chang X, Liu Y (2016) Assessment of heavy metals contamination in sediments from three adjacent regions of the Yellow River using metal chemical fractions and multivariate analysis techniques. *Chemosphere* 144:264–272
- Madrid F, Diaz-Barrientos E, Madrid L (2008) Availability and bioaccessibility of metals in the clay fraction of urban soils of Sevilla. *Environ Pollut* 156:605–610
- Massolo S, Bignasca A, Sarkar SK, Chatterjee M, Bhattacharya BD, Alam A (2012) Geochemical fractionation of trace elements in sediments of Hugli River (Ganges) and Sundarban wetland (West Bengal, India). *Environ Monit Assess* 184:7561–7577
- Meers E, Lamsal S, Vervake P, Hopgood M, Lust N, Tack FMG (2005) Availability of heavy metals for uptake by *Salix viminalis* on a moderately contaminated dredged sediment disposal site. *Environ Pollut* 137:351–364
- Milačić R, Ščančar J, Murko S, Kocman D, Horvat M (2010) A complex investigation of the extent of pollution in sediments of the Sava river. Part 1: selected elements. *Environ Monit Assess* 163:263–275
- Mohiuddin KM, Zakir HM, Otomo K, Sharmin S, Shikazono N (2010) Geochemical distribution of trace metal pollutants in water and sediments of downstream of an urban river. *Int J Environ Sci Technol* 7: 17–28
- Di Palma L, Mecozzi R (2007) Heavy metals mobilization from harbour sediments using EDTA and citric acid as chelating agents. *J Hazard Mater* 147:768–775
- Petrović D, Todorović M, Manojlović D, Krsmanović V (2010) A simulation experiment as a method for the investigation of the mobility of heavy metals from inundated land. *J Serb Chem Soc* 75:1005–1018
- Poggio L, Vrščaj B, Schulin R, Hepperle E, Ajmone Marsan F (2009) Metals pollution and human bioaccessibility of topsoils in Grugliasco (Italy). *Environ Pollut* 157:680–689
- Qasim B, Motelica-Heino M, Joussein E, Soubrand M, Gauthier A (2015) Potentially toxic element phytoavailability assessment in technosols from former smelting and mining areas. *Environ Sci Pollut Res* 22:5961–5974
- Quevauviller P (1998) Operationally defined extraction procedures for soil and sediment analysis I. Standardization. *TRAC-Trend Anal Chem* 17(5):289–298
- Rao CRM, Sahuquillo A, Lopez-Sanchez JF (2010) Comparison of single and sequential extraction procedures for the study of rare earth elements remobilization in different types of soils. *Anal Chim Acta* 662:128–146
- Relić D, Đorđević D, Popović A, Blagojević T (2005) Speciations of trace metals in the Danube alluvial sediments within an oil refinery. *Environ Int* 31:661–669
- Relić D, Đorđević D, Sakan S, Anđelković I, Pantelić A, Stanković R, Popović A (2013) Conventional, microwave, and ultrasound

- sequential extractions for the fractionation of metals in sediments within the petrochemical industry, Serbia. *Environ Monit Assess* 185:7627–7645
- Sahuquillo A, Rigol A, Rauret G (2003) Overview of the use of leaching/extraction tests for risk assessment of trace metals in contaminated soils and sediments. *TRAC-Trend Anal Chem* 22:152–159
- Sakan S, Đorđević D, Manojlović D, Polić P (2009) Assessment of heavy metal pollutants accumulation in the Tisza river sediments. *J Environ Manag* 90:3382–3390 doi:10.1007/s12665-014-3562-5
- Sakan S, Đorđević D, Dević G, Relić D, Anđelković I, Đuričić J (2011) A study of trace element contamination in river sediments in Serbia using microwave-assisted aqua regia digestion and multivariate statistical analysis. *Microchem J* 99:492–502
- Sakan S, Popović A, Anđelković I, Đorđević D (2015) Aquatic sediments pollution estimate using the metal fractionation, secondary phase enrichment factor calculation, and used statistical methods. *Environ Geochem Health*. doi:10.1007/s10653-015-9766-0
- Sutherland RA (2010) BCR-701: a review of 10-years of sequential extraction analyses. *Anal Chim Acta* 680:10–20
- SW-846 EPA Method 3051a (2007) Microwave assisted acid digestion of sediments, sludges, soils, and oils, 1. Revision
- Ren J, Williams PN, Luo J, Ma H, Wang X (2015) Sediment metal bioavailability in Lake Taihu, China: evaluation of sequential extraction, DGT, and PBET techniques. *Environ Sci Pollut Res* 22:12919–12928
- RIS-Danube River Information System (2007) Standard Summary Project Fiche—IPA centralized programmes ([http://ec.europa.eu/enlargement/pdf/serbia/ipa/river\\_information\\_system\\_en.pdf](http://ec.europa.eu/enlargement/pdf/serbia/ipa/river_information_system_en.pdf))
- Rönkkömäki H, Pöykio R, Nurmesniemi H, Popov K, Merisalu E, Tuomi T, Välimäki I (2008) Particle size distribution and dissolution properties of metals in cyclone fly ash. *Int J Environ Sci Tech* 5:485–494
- Teodorović I (2009) Ecotoxicological research and related legislation in Serbia. *Environ Sci Pollut Res* 16(Suppl 1):S123–S129
- Tsang DCW, Lo IMC, Chan KL (2007) Modeling the transport of metals with rate-limited EDTA-promoted extraction and dissolution during EDTA-flushing of copper-contaminated soils. *Environ Sci Technol* 41:3660–3666
- Vicente-Martorell JJ, Galindo-Riaño MD, García-Vargas M, Granado-Castro MD (2009) Bioavailability of heavy metals monitoring water, sediments and fish species from a polluted estuary. *J Hazard Mat* 162:823–836
- Villaescusa-Celaya JA, Gutiérrez-Galindo EA, Flores-Muñoz G (2000) Heavy metals in the fine fraction of coastal sediments from Baja California (Mexico) and California (USA). *Environ Pollut* 108:453–462
- Zhang MK, Liu ZY, wang H (2010) Use of single extraction methods to predict bioavailability of heavy metals in polluted soils to rice. *Commun Soil Sci Plan* 41:820–831

# Free–free absorption coefficients and Gaunt factors for dense hydrogen-like stellar plasma

V. A. Srećković,<sup>1,2★</sup> N. Sakan,<sup>1★</sup> D. Šulić,<sup>3</sup> D. Jevremović,<sup>4</sup> Lj. M. Ignjatović<sup>1,2</sup>  
and M. S. Dimitrijević<sup>2,4,5★</sup>

<sup>1</sup>University of Belgrade, Institute of Physics, PO Box 57, 11001 Belgrade, Serbia

<sup>2</sup>Isaac Newton Institute of Chile, Yugoslavia Branch, Volgina 7, 11060 Belgrade, Serbia

<sup>3</sup>University Union – Nikola Tesla, 11000, Belgrade, Serbia

<sup>4</sup>Astronomical Observatory, Volgina 7, 11160 Belgrade 74, Serbia

<sup>5</sup>LERMA, Observatoire de Paris, PSL Research University, CNRS, Sorbonne Universités, UPMC (Univ. Pierre, and Marie Curie) Paris 06, 5 Place Jules Janssen, 92190 Meudon, France

Accepted 2017 December 12. Received 2017 November 28; in original form 2017 October 25

## ABSTRACT

In this work, we present a study dedicated to determination of the inverse bremsstrahlung absorption coefficients and the corresponding Gaunt factor of dense hydrogen-like stellar-atmosphere plasmas where electron density and temperature change in a wide range. A method suitable for this wide range is suggested and applied to the inner layers of the solar atmosphere, as well as the plasmas of partially ionized layers of some other stellar atmospheres (for example, some DA and DB white dwarfs) where the electron densities vary from  $10^{14} \text{ cm}^{-3}$  to  $10^{20} \text{ cm}^{-3}$  and temperatures from 6000 K to 300 000 K in the wavelength region of  $10 \text{ nm} \leq \lambda \leq 3000 \text{ nm}$ . The results of the calculations are illustrated by the corresponding figures and tables.

**Key words:** atomic processes – Sun: atmosphere – stars: atmospheres – white dwarfs.

## 1 INTRODUCTION

Although, of all the plasma internal absorption processes, we have so far considered only ion–atom radiative ones, we are aware of the need to consider other possible absorption processes too. Namely, some of them must be treated as concurrent to the ones that we have studied, and others warrant our attention for more diverse reasons. One such kind of process is that of electron–ion bremsstrahlung, which, by its very nature, suggests its importance, as its efficiency increases proportionally to the square of the free-electron density. Anyone interested in these processes must be fascinated by the amount of works about them. Indeed, so much has been done in this field that any new work should contain a very important result. However, we believe that for some time now we have had results of significant importance; we mean the possibility of determining the spectral characteristics of inverse bremsstrahlung (absorption coefficients and Gaunt factors) in the same way in a wide range of electron densities and temperatures. We note that some preliminary results have been presented at the X Serbian Conference on Spectral Line Shapes in Astrophysics (Mihajlov, Srećković & Sakan 2015), in order to inform other researchers of the potential possibilities existing in the field of inverse bremsstrahlung processes.

The aims of this work require determination of the corresponding spectral absorption coefficients for the inverse bremsstrahlung process and the corresponding Gaunt factors for a broad class of weakly non-ideal plasmas, as well as for plasmas of higher non-ideality. It is shown that this process can be successfully described in the frame of the cut-off Coulomb potential model within the range of the physical parameters that cover the area important for modelling astrophysical plasma (white dwarfs, solar atmospheres, etc). The physical sense and the properties of a group screening parameter for two-component systems that are used in this paper are discussed in detail in our previous papers (Mihajlov, Vitel & Ignjatović 2009a,b). This method for describing the electrostatic screening in two-component systems is applicable to systems of higher non-ideality degree. On the basis of data from the above-mentioned papers are determined new characteristic lengths that complete a new system of screening lengths in plasma. This topic itself, the discussion and search for more consistent models of screening and more realistic potentials in plasmas is still continuing and is very current (see Mihajlov et al. 2009b; Demura 2010, and references therein).

For the sake of further considerations, we will introduce some designations that are used below:  $E$  and  $E'$ : respectively, the energies of the initial and final states of the electron–ion system (absorber);  $\varepsilon_{\text{ph}}$ : the energy of the absorbed photon and  $\hbar k$ : its impulse;  $\hbar q$ : the impulse of the electron in its initial state; and  $m$ ,  $e$ : respectively, the mass of the electron and the modulus of its charge.

\* E-mail: vlada@ipb.ac.rs (VAS); nsakan@ipb.ac.rs (NS); mdimitrijevic@aob.rs (MSD)

## 2 NECESSARY THEORETICAL REMARKS

### 2.1 The potential and electrostatic screening model

In Mihajlov et al. (2015) the significance of the model potential used in this paper was emphasized. One of the model Coulomb screening potentials, known as the cut-off potential, had already been introduced in Suchy (1964), and had been investigated in connection with the transport plasma properties in Mihajlov et al. (1986). This potential is given by

$$U(r) = \begin{cases} -\frac{e^2}{r} + \frac{e^2}{r_{\text{cut}}} & 0 < r \leq r_{\text{cut}} \\ 0 & r_{\text{cut}} < r, \end{cases} \quad (1)$$

where  $r$  is the distance from the coordinate origin and  $r_{\text{cut}}$  is a parameter defined and determined further on in the text.

This is the model, illustrated by Fig. 1, used in this work. Let us note that in Mihajlov et al. (2011) the universality of the screening model did not arise at all. However, in the case of the electron–ion inverse bremsstrahlung process, which is possible in plasmas with enormous differences in electron densities and temperature, the situation is the other way round. Namely, in this case we have to start from the inner plasma electrostatic screening model of any considered system and to solve the problem of its applicability. For that purpose we will first consider the models used in the papers that exist in the literature (Hazak et al. 2002; Armstrong et al. 2014; van Hoof et al. 2014).

One can see that the electron–ion scattering is treated in those models as scattering of the electron upon the adequate Debye potential. This fact is a serious handicap of the mentioned models, as was discussed in our previous papers.

This is caused by the fact that the Debye potential is defined as a potential of the observed ion and the entirety of its surrounding as a function of the distance from the ion, and can be used only for determination of its average potential energy in the observed plasma. Because of this, in Mihajlov et al. (2011) the model of the inner plasma screening was applied for the first time. Fig. 1 implies that in this screening model the potential energy of the free electron  $U_{\text{scr.}}(r)$  is of a strictly Coulomb nature:  $U_{\text{scr.}}(r) = -e^2/r$  in the region  $r < r_{\text{cut}}$ , where  $r_{\text{cut}}$  is the corresponding cut-off radius, and  $U_{\text{scr.}}(r) = \text{const} = U_{\text{cut}}$  in the region  $r > r_{\text{cut}}$ , where  $U_{\text{cut}}$  is equal to the average energy of the free electron in the considered system. In further consideration of this, we take  $U_{\text{cut}} = -e^2/r_{\text{cut}}$  as the zero of the energy and describe such plasma just by means of the model cut-off potential given by equation (1), which is especially suitable for describing electron–ion scattering within plasma. Certainly, we assume that the above-described electrostatic screening model could be applicable in such a wide range of electron densities and temperatures that this allows one to consider it as an almost universal model. For that very reason the cut-off potential equation (1) could also be considered as almost universal.

### 2.2 Transformation of the dipole moments

It is only after an explanation of the universality of the potential equation 1 that the procedures gain importance for the determination of inverse bremsstrahlung processes as characteristic spectral absorption coefficients, Gaunt factors, and the possibility of improvement of these procedures.

As the first improvement, for the inverse bremsstrahlung cross-section  $\sigma_{\text{i.b.}}^{(\text{ex})}$ , the standard expressions from Sobelman (1979) will be used here, since the potential equation (1) has a finite radius.

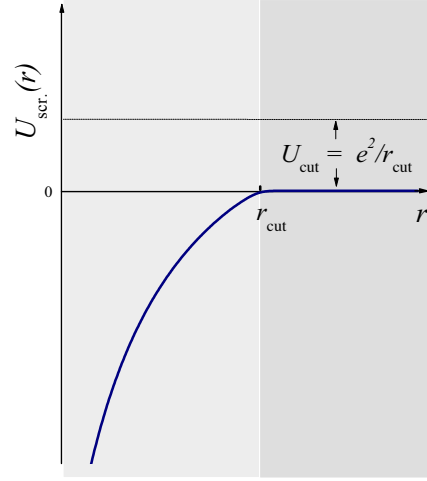


**Figure 1.** Behaviour of the potential  $U_{\text{scr.}}(r)$ , where  $r_{\text{cut}}$  is the cut-off parameter presented in equations (6) and (7).

Consequently,

$$\sigma_{\text{i.b.}}^{(\text{ex})}(E; E') = \frac{8\pi^4 \hbar e^2 k}{3 q^2} \sum_{l'=l\pm 1}^{l_{\text{max}}} l_{\text{max}} |\hat{D}_{E,l;E'l'}|^2, \quad (2)$$

$$\hat{D}_{E,l;E'l'} = \int_0^\infty P_{E'l'}(r) \cdot r \cdot P_{E,l}(r) dr,$$

where  $l_{\text{max}}$  is defined in section 2.4, the radial functions  $P_{E,l}(r)$  and  $P_{E'l'}(r)$  are the solutions of the radial Schrödinger equation

$$\frac{d^2 P_{E,l}(r)}{dr^2} + \left[ \frac{2m}{\hbar^2} (E - U(r)) - \frac{l(l+1)}{r^2} \right] P_{E,l}(r) = 0, \quad (3)$$

and  $U(r)$  is the cut-off Coulomb potential given by equation (1). The radial functions  $P_{E,l}(r)$  of all states that are possible in the potential  $U(r)$  are described and discussed by Mihajlov et al. (1986). As the next step, using the transformation characteristics of the matrix element of the solutions  $P_{E,l}(r)$  we will replace the dipole matrix element  $\hat{D}_{E,l;E'l'}$  in equation 2 by the matrix element of the gradient of the potential energy  $U(r)$ . This procedure is described by the expressions

$$|\hat{D}(r)_{E,l;E'l'}|^2 = \frac{\hbar^4}{m^2 (E - E')^4} |\nabla U_{E,l;E'l'}|^2, \quad (4)$$

$$\nabla_r U_{E,l;E'l'} = \int_0^{r_{\text{cut}}} P_{E,l}(r) \cdot \nabla_r U(r) \cdot P_{E'l'}(r) dr, \quad (5)$$

where  $U(r)$  is given by equation (1).

It is known that the transition from the dipole matrix element  $\hat{D}_{E,l;E'l'}$  to the dipole matrix element  $\nabla_r U_{E,l;E'l'}$  in principle does not mean much. However, in the case of  $U(r)$ , which is given by equation (1), it means a transition from determination of the quantity  $\hat{D}_{E,l;E'l'}$ , which cannot be factually calculated, to determination of a quantity that can be calculated routinely. Namely, in the case of this potential the integral of two functions of the Coulomb continuum from 0 to  $\infty$  gets replaced by the integral of the same two functions, but from 0 to  $r_{\text{cut}}$ .

### 2.3 Determination of the cut-off radius

In order to complete the described model we have to determine the cut-off parameter  $r_{\text{cut}}$  and the energy parameter  $U_{\text{cut}}$  as functions of the electron density  $N_e$  and the temperature  $T$ . Here we will



**Table 1.** Values of the Gaunt factor for  $N_e = 1 \times 10^{17} \text{ cm}^{-3}$  as a function of wavelength  $\lambda$  and temperature  $T$ . The tables are available in their entirety for  $10^{14} \text{ cm}^{-3}$  to  $10^{20} \text{ cm}^{-3}$  and temperatures from 6000 K to 300 000 K in the wavelength region of  $10 \text{ nm} \leq \lambda \leq 3000 \text{ nm}$  in machine-readable form in the online journal as additional data. A portion is shown here for guidance regarding their form and content.

| $\lambda [\text{nm}]/T [\text{K}]$ | 10 000    | 20 000    | 40 000    | 50 000    | 100 000   | 150 000   | 200 000   | 250 000   | 300 000   |
|------------------------------------|-----------|-----------|-----------|-----------|-----------|-----------|-----------|-----------|-----------|
| 10                                 | 1.084E+00 | 1.101E+00 | 1.121E+00 | 1.133E+00 | 1.207E+00 | 1.244E+00 | 1.291E+00 | 1.341E+00 | 1.415E+00 |
| 100                                | 1.088E+00 | 1.104E+00 | 1.166E+00 | 1.217E+00 | 1.588E+00 | 1.813E+00 | 2.053E+00 | 2.303E+00 | 2.562E+00 |
| 200                                | 1.093E+00 | 1.151E+00 | 1.402E+00 | 1.565E+00 | 2.522E+00 | 3.053E+00 | 3.609E+00 | 4.185E+00 | 4.778E+00 |
| 500                                | 1.167E+00 | 1.512E+00 | 2.425E+00 | 2.932E+00 | 5.769E+00 | 7.322E+00 | 8.940E+00 | 1.061E+01 | 1.233E+01 |
| 1000                               | 1.469E+00 | 2.340E+00 | 4.401E+00 | 5.533E+00 | 1.182E+01 | 1.524E+01 | 1.877E+01 | 2.240E+01 | 2.611E+01 |
| 1500                               | 1.845E+00 | 3.251E+00 | 6.532E+00 | 8.330E+00 | 1.825E+01 | 2.359E+01 | 2.908E+01 | 3.469E+01 | 4.039E+01 |
| 2000                               | 2.251E+00 | 4.207E+00 | 8.762E+00 | 1.125E+01 | 2.486E+01 | 3.213E+01 | 3.957E+01 | 4.715E+01 | 5.484E+01 |
| 2500                               | 2.675E+00 | 5.197E+00 | 1.106E+01 | 1.424E+01 | 3.157E+01 | 4.075E+01 | 5.014E+01 | 5.968E+01 | 6.934E+01 |
| 3000                               | 3.110E+00 | 6.216E+00 | 1.339E+01 | 1.729E+01 | 3.833E+01 | 4.942E+01 | 6.074E+01 | 7.223E+01 | 8.385E+01 |

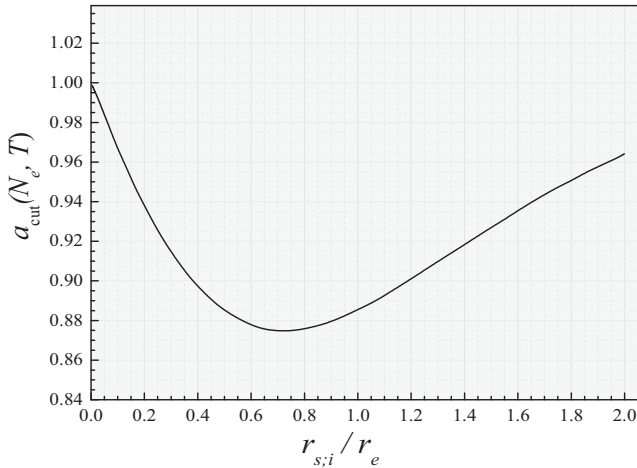


**Figure 2.** Behaviour of the parameters  $a_{\text{cut}} = r_{\text{cut}}/r_e$  as a function of the ratio  $r_{s,i}/r_e$ , where  $r_e$  is given by equation (6) and  $r_{s,i}$  is the ion Wigner–Seitz radius for the considered electron–ion plasma. The presented curve is obtained on the basis of data presented in Mihajlov et al. (2009a).

use the fact that these parameters can be determined by means of Fig. 2, which is obtained using the data from Mihajlov et al. (2009a). Namely, the curve presented in Fig. 2 shows the behaviour of the parameter  $a_{\text{cut}} = r_{\text{cut}}/r_e$  as a function of the ratio  $r_{s,i}/r_e$ , where  $r_e$  and the ion Wigner–Seitz radius  $r_{s,i}$  are given by the relations

$$r_{s,i} = \left[ \frac{3}{4\pi N_i} \right]^{1/3}, \quad r_e = \left[ \frac{kT}{4\pi N_e e^2} \right]^{1/2}, \quad (6)$$

where  $N_i$  is the ion density. After that the cut-off radius  $r_{\text{cut}}$  is determined here as a function of  $N_e, T$  by means of the relation

$$r_{\text{cut}} = a_{\text{cut}} \cdot r_e, \quad (7)$$

where the parameter  $a_{\text{cut}}$  can be directly determined from Fig. 2. The procedure for the determination of  $a_{\text{cut}}$  is to calculate the ratio  $r_{s,i}/r_e$  (by equation 6) for the required values of plasma parameters (electron density and temperature) and to directly obtain (download) the  $y$  values on the curve in Fig. 2 for the known  $x$  value.

## 2.4 The numerical procedure

The numerical procedure consists of two important elements. The *first element* refers to the way of determining  $P_{E,l}(r)$  in the area  $r > r_{\text{cut}}$ . As known, the necessary solution of equation 3 is given by superposition of the spherical Bessel functions, i.e.  $C_1 j_n(z) + C_2 y_n(z)$ , where  $j_n(z)$  and  $y_n(z)$  are spherical Bessel

functions of the first and second kinds and they are of the  $n$ th order. However, here is used the fact that these functions are expressed over the Coulomb functions  $F_l(0, \frac{\sqrt{2mE}}{\hbar} r)$  and  $G_l(0, \frac{\sqrt{2mE}}{\hbar} r)$  by means of the relations (see e.g. Gough 2009)  $j_L(\rho) = \rho^{-1} F_L(0, \rho)$  and  $y_L(\rho) = -\rho^{-1} G_L(0, \rho)$ , where  $G_L(0, \rho)$  is the Coulomb function that is irregular at the coordinate origin. In accordance with that, the necessary radial function  $P_{E,l}(r)$  in the case  $r > r_{\text{cut}}$  is used here in the form

$$P_{E,l}(r) = C_N^c \left\{ C_F F_l \left( 0, \frac{\sqrt{2mE}}{\hbar} r \right) + C_G G_l \left( 0, \frac{\sqrt{2mE}}{\hbar} r \right) \right\}, \quad (8)$$

where  $C_N^c$  is the normalization constant and  $C_F$  and  $C_G$  are the constants that provide the behaviour of the solution according to the convergent value for infinite radii. In such a way, we have fully standardized the expressions for the necessary (continual) radial solutions of equation (3).

The *second element* of the numerical procedure refers to the method of summing in equation 2 for the inverse bremsstrahlung cross-section  $\sigma_{i,b}^{(ex)}(E; E')$ . After a detailed investigation, the following method of summation is chosen: the sum goes over  $l'$  from 0 to  $l_{\text{max}}$  with no need for initial checking of the convergence, and for  $l' > l_{\text{max}}$  the sum is checked for convergence, e.g. when  $l'$  is greater than  $l_{\text{max}}$  the Cauchy criteria for the convergence test is applied since it is expected that the sum monotonically converges towards the limit value. The behaviour of the sum after reaching the limiting value  $l_{\text{max}}$  was examined and convergence is proved in the limiting series of  $r_{\text{cut}}$ , when the cut-off radius converges towards infinity  $r_{\text{cut}} \rightarrow \infty$ . To determine the start of the checking boundary we use  $l_{\text{max}} = [l^*] + 1$  where  $l^*$  is determined from the relation  $\frac{\hbar^2 l(l+1)}{2mr_{\text{cut}}^2} = E$ . From here, keeping in mind that  $l(l+1) = (l+1/2)^2 - 1/4$ , we get the boundary value  $l^*$  in the form  $l^* = 0.5 \cdot (\sqrt{1 + 8 \cdot \frac{2mE}{\hbar^2} r_{\text{cut}}^2} - 1)$ . It has been shown that summing over  $l$  in the region  $l > l_{\text{max}}$  ends very quickly, so that the total number of summands is not much greater than  $l_{\text{max}}$ . Such behaviour of the sum is proof of a well defined  $l_{\text{max}}$  boundary. After these improvements we could use the possibilities provided by the universality of the electrostatic screening model that we used and finally perform extensive calculations of the inverse bremsstrahlung characteristics that could be the basis for creation of the corresponding data base.

## 3 THE CALCULATED QUANTITIES

We consider here plasmas with electron densities from  $10^{14} \text{ cm}^{-3}$  to  $1 \cdot 10^{20} \text{ cm}^{-3}$  and temperatures from 6000 K to 300 000 K. In

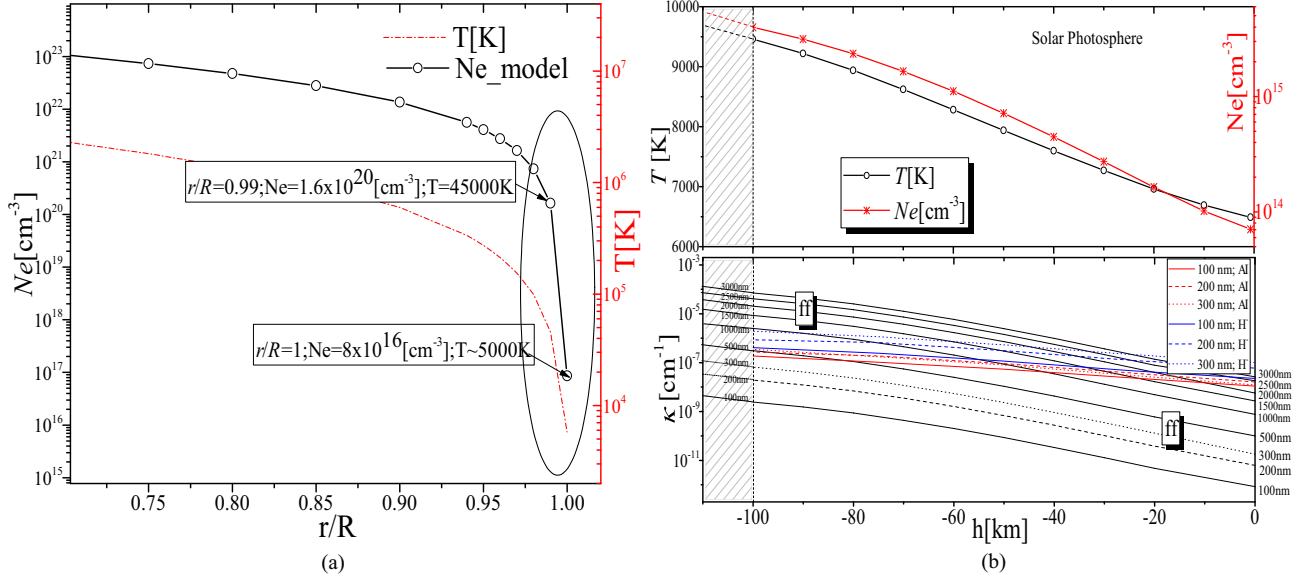


**Figure 3.** (a) Electron density and temperature in the interior of the Sun as a function of radius for the Standard Solar Models (Bahcall, Serenelli & Basu 2006). (b) Upper panel: behaviour of the temperature  $T$  and  $N_e$  as a function of height  $h$  within the considered part of the solar atmosphere model of Fontenla, Balasubramaniam & Harder (2007). Lower panel: plots of the absorption coefficients (equation (9)) of the absorption processes considered for the case of a solar atmosphere model from Fontenla et al. (2007). Black lines denote free–free (ff) absorption processes, i.e. inverse bremsstrahlung absorption coefficients, blue electron–atom and red ion–atom absorption coefficients (Ignjatović et al. 2014; Srećković et al. 2014). The extrapolated values are in the left shaded region in front of the dashed line.

accordance with Mihajlov et al. (1993) and Adamyan et al. (1994), for such conditions we find that, for the electron component, treated as an appropriate electron gas on a positively charged background, the value of the chemical potential is practically equal to the classical one, so that the distribution function for electrons is Maxwellian  $f_T(v) = 4\pi(m/2\pi kT)^{3/2}v^2e^{-mv^2/2kT}$ , for a given temperature  $T$ . Consequently,

$$\kappa_{i,b}^{(ex)}(\varepsilon_\lambda; N_e, T) = N_e^2 \cdot \int_0^\infty \sigma_{i,b}^{(ex)}(E; E')v \cdot f_T(v)dv \cdot \left(1 - \exp\left[-\frac{\hbar\omega}{kT}\right]\right), \quad (9)$$

where the expression in parentheses takes into account the effect of stimulated emission. Additionally, we take the quasi-classical Kramer's  $k_{i,b}^{q.c.}(\lambda, T; N_e)$  (see e.g. Sobelman 1979) as

$$k_{i,b}^{q.c.}(\lambda, T; N_e) = N_e^2 \cdot \frac{16\pi^{5/2}\sqrt{2}e^6}{3\sqrt{3}cm^{3/2}\varepsilon_{ph}^3} \frac{\hbar^2}{(kT)^{1/2}} \left(1 - \exp\left[-\frac{\hbar\omega}{kT}\right]\right), \quad (10)$$

where  $\varepsilon_{ph} = 2\pi\hbar c/\lambda$ , and the averaged Gaunt factor  $G_{i,b}(\lambda, T)$  is

$$k_{i,b}^{(ex)}(\lambda, T; N_e) = k_{i,b}^{q.c.}(\lambda, T; N_e) \cdot G_{i,b}(\lambda, T), \quad (11)$$

where  $k_{i,b}^{(ex)}(\lambda, T; N_e)$  and  $k_{i,b}^{q.c.}(\lambda, T; N_e)$  are given by equations (9) and (10).

## 4 RESULTS AND DISCUSSION

The contribution of inverse bremsstrahlung to the total absorption in stellar atmospheres is not so important, but its contribution increases with density, and for very dense plasmas it becomes dominant. For example, Grinenko & Gericke (2009) stated that inverse bremsstrahlung is the dominant absorption mechanism for lasers

with parameters typical for inertial confinement fusion. Plasma in inertial confinement fusion experiments has properties that are similar to the conditions in stellar interiors. Consequently, it is of interest to investigate the role of inverse bremsstrahlung in subphotospheric and deeper layers, and to examine its influence on radiative transfer through such layers.

In addition to other factors that determine the importance of inverse bremsstrahlung, we should bear in mind the existence of a physical area where inverse bremsstrahlung is dominant compared to other processes. The examples that demonstrate this can be found in the literature (Rozsnyai 2001; Grinenko & Gericke 2009). Moreover, we expect a major contribution to the inverse bremsstrahlung process in a dense highly ionized plasma (see e.g. Fig. 3(a), the marked region of  $r$ ) in the process of transfer of radiation. Here we mean the high electron density and temperature that occur in the interior of the Sun, which are in Fig. 3(a) presented as a function of radius (Standard Solar Models, Bahcall et al. 2006).

In the lower panel in Fig. 3(b), the plot of each absorption coefficient of the considered absorption processes for the case of a solar atmosphere model from Fontenla et al. (2007) is shown as a function of height for various values of wavelengths. Here  $h$  is the height of the considered layer with respect to the chosen referent one. The corresponding plasma parameters are presented in the upper panel of Fig. 3(b). The electron–atom processes that are sometimes treated as the  $H^-$  continuum. With AI, i.e.  $\kappa_{ai}$ , atom–ion symmetric and non-symmetric processes (Ignjatović et al. 2014; Srećković et al. 2014) are represented. From this figure one can see that the inverse bremsstrahlung absorption coefficients are comparable with the concurrent ones, especially in the region of higher electron density and temperature  $h \leq -70$  km (left-hand part of Fig. 3(b)). Consequently, we can conclude that the influence of the inverse bremsstrahlung process increases with temperature and density.

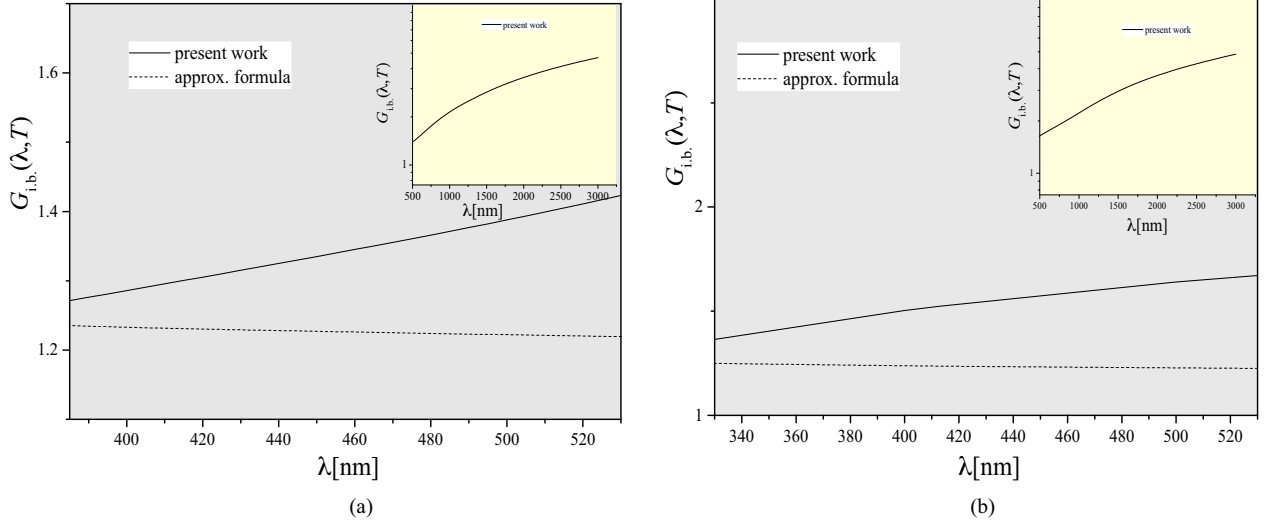


**Figure 4.** (a) Dynamics of the Gaunt factor data from this work (equation (11)) and data obtained by the approximation formula (D'yachkov 1990) for the electron density  $N_e = 6.5 \cdot 10^{18} \text{ cm}^{-3}$  and temperature  $T = 18000 \text{ K}$  (from Vitel et al. 2004; Mihajlov et al. 2011). (b) Behaviour of the mean Gaunt factor data from this work and data obtained by the approximation formula (D'yachkov 1990) for the electron density  $N_e = 1.5 \cdot 10^{19} \text{ cm}^{-3}$  and  $T = 23000 \text{ K}$  (from Vitel et al. 2004; Mihajlov et al. 2011).

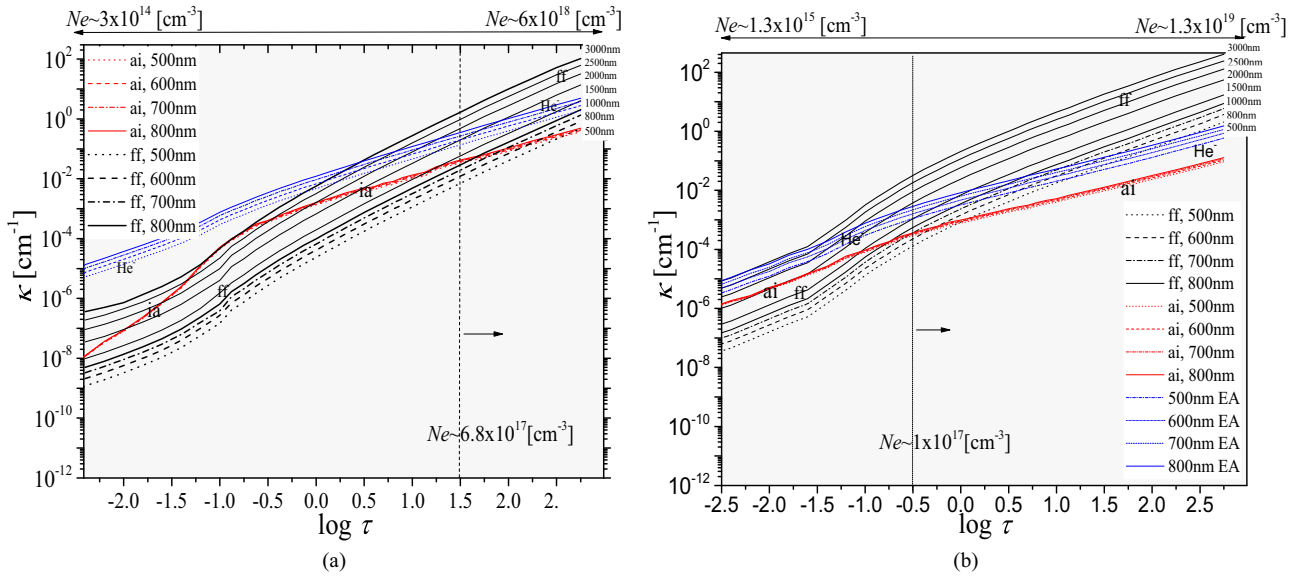


**Figure 5.** (a) Plots of the absorption coefficients (equation (9)) of the considered absorption processes for the case of a DB white dwarf with  $T_{\text{eff}} = 12000 \text{ K}$  and  $\log g = 8$  as functions of  $\log \tau$ , where  $\tau$  is the Rosseland optical depth. (b) Plots of the absorption coefficients (equation (9)) of the considered absorption processes for the case of a DB white dwarf with  $T_{\text{eff}} = 16000 \text{ K}$  and  $\log g = 8$  as functions of  $\log \tau$ , where  $\tau$  is the Rosseland optical depth. Black lines denote ff absorption processes, i.e. inverse bremsstrahlung absorption coefficients, blue concurrent electron–atom (EA) processes (He<sup>−</sup> continuum) and red concurrent ion–atom absorption coefficients (ai).

The behaviour of the Gaunt factor in the area of higher parameters of non-ideality is shown in Figs 4(a) and (b). In these figures are presented the dynamics of the Gaunt factor for the electron density  $N_e = 6.5 \cdot 10^{18} \text{ cm}^{-3}$  and temperature  $T = 18000 \text{ K}$  as well as for  $N_e = 1.5 \cdot 10^{19} \text{ cm}^{-3}$  and  $T = 23000 \text{ K}$  (parameters obtained in the experiment by Vitel et al. 2004; Mihajlov et al. 2011). The data from this work are marked by solid lines and data obtained by the use of the approximation formula (D'yachkov 1990) by the dashed line. The insets show the data from this work but in a wider wavelength region. One can notice that there is an evident difference between the data presented here and data obtained by the use of the approximation formula (D'yachkov

1990). These differences are affected by the principal differences in the way of describing the electron–ion scattering in the rest of the plasma (see Mihajlov et al. 2009a). It is understood that some of these results may be useful for further laboratory plasma investigations.

Good conditions for studying the impact of the increase of electron density and temperature on the inverse bremsstrahlung contribution is provided by plasmas of white dwarf atmospheres. This is illustrated in Figs 5(a) and (b), where the plots of the considered absorption processes, including the inverse bremsstrahlung processes, are shown for the case of a DB white dwarf with  $\log g = 8$ ,  $T_{\text{eff}} = 12000 \text{ K}$  and  $T_{\text{eff}} = 16000 \text{ K}$  from the atmosphere model

of Koester (2015, private communication). The electron–atom processes ( $\text{He}^-$  continuum), are represented in these figures by blue lines marked by EA ( $\kappa_{\text{EA}}$ ). ai, i.e.  $\kappa_{\text{ai}}$ , represents atom–ion symmetric and non-symmetric processes. From these figures one can see that the inverse bremsstrahlung absorption coefficients are comparable with concurrent ones, especially in the region of higher electron density (the parts of Figs 5(a) and (b) marked with arrows). Finally, within the considered DB white dwarf atmospheres, the investigated radiative processes strongly influence the atmosphere’s opacity, especially for the cases of white dwarf atmospheres with larger effective temperature, i.e. higher electron densities and temperatures.

Concerning the accuracy, a number of factors may affect it. First, we discuss the screening parameters. It is likely that such a change in the screening length will affect the accuracy. Since the method that is used here is applicable to systems of higher non-ideality degree, its use is limited to certain areas of plasma temperatures and densities. For plasmas with low non-ideality (i.e. low density and high temperature) or plasmas with extreme non-ideality with the coupling parameter  $\Gamma$  much greater than 1 (high density and very low temperature), this approach is not capable of providing high accuracy (here  $\Gamma = e^2/(akT)$  and  $a = (3/4\pi N_e)^{1/3}$ ). Finally, we are also able to notice that the data are highly sensitive to changes in temperature.

To summarize, the presented exact quantum-mechanical method is used to obtain the spectral coefficients for the inverse bremsstrahlung process and the corresponding Gaunt factors for a broad class of moderately non-ideal plasmas, as well as for plasmas of higher non-ideality. The range of the physical parameters covers the area important for plasma modelling from an astrophysical standpoint (white dwarfs, central stars of planetary nebulae, etc). For this purpose, calculation of the Gaunt factors in a wide region of wavelengths for series of electron densities and plasma temperatures was done. The results of the calculations are illustrated by the corresponding tables in the online version of this article (table for every  $N_e$  and  $T$  taken).

Further directions in the development of the method would be determination of absorption coefficients and Gaunt factors for two-component systems (ions with an arbitrary charge  $Z$  and electron component) as well as for three-component systems.

## ACKNOWLEDGEMENTS

We acknowledge the contribution of the late Dr A. A. Mihajlov, who participated in the discussions and preparation of this paper. This work is partially supported by the Ministry of Education, Science and Technological Development of the Republic of Serbia under grants III 44002 and 176002.

## REFERENCES

- Adamyán V. M., Djuric Z., Ermolaev A. M., Mihajlov A. A., Tkachenko I. M., 1994, *J. Phys. D*, 27, 927  
 Armstrong G. S. J., Colgan J., Kilcrease D. P., Magee N. H., 2014, *High Energy Density Phys.*, 10, 61

- Bahcall J. N., Serenelli A. M., Basu S., 2006, *ApJS*, 165, 400  
 D’yachkov L. G., 1990, *J. Phys. B*, 23, L429  
 Demura A. V., 2010, *Int. J. Spectrosc.*, 2010, 671073  
 Fontenla J. M., Balasubramanian K. S., Harder J., 2007, *ApJ*, 667, 1243  
 Gough C., 2009, *GNU Scientific Library Reference Manual—Third Edition*. Network Theory Ltd., available online at: <http://www.gnu.org/software/gsl/>  
 Grinenko A., Gericke D. O., 2009, Dense plasma heating by inverse Bremsstrahlung, in: *Central Laser Facility, Annual Report 2008/2009*, Science and Technology Facilities Council, Rutherford Appleton Laboratory, Harwell Science and Innovation Campus, Didcot, Oxfordshire, p. 110  
 Hazak G., Metzler N., Klapisch M., Gardner J., 2002, *Phys. Plasmas* 9, 345  
 Ignjatović L. M., Mihajlov A. A., Srećković V. A., Dimitrijević M. S., 2014, *MNRAS*, 441, 1504  
 Mihajlov A. A., Djordjević D., Vučić S., Kraeft W. D., Luft M., 1986, *Contr. Plasma Phys.*, 26, 19  
 Mihajlov A. A., Ermolaev A. M., Djuric Z., Ignjatović L., 1993, *J. Phys. D*, 26, 1041  
 Mihajlov A. A., Vitel Y., Ignjatović L. M., 2009a, *High Temperature*, 47, 1  
 Mihajlov A. A., Vitel Y., Ignjatović L. M., 2009b, *High Temperature*, 47, 147  
 Mihajlov A. A., Sakan N. M., Srećković V. A., Vitel Y., 2011, *J. Phys. A*, 44, 095502  
 Mihajlov A. A., Srećković V. A., Sakan N. M., 2015, *JA&A*, 36, 635  
 Rozsnyai B. F., 2001, *J. Quant. Spectrosc. Radiative Transfer*, 71, 655  
 Sobelman I. I., 1979, *Atomic Spectra and Radiative Transitions*. Springer, Berlin  
 Srećković V. A., Mihajlov A. A., Ignjatović L. M., Dimitrijević M. S., 2014, *Advances Space Res.*, 54, 1264  
 Suchy K., 1964, *Beitr. Plasmaphys.* 4, 71  
 van Hoof P. A. M., Williams R. J. R., Volk K., Chatzikos M., Ferland G. J., Lykins M., Porter R. L., Wang Y., 2014, *MNRAS*, 444, 420  
 Vitel Y., Gavrilova T. V., D’yachkov L. G., Kurilenkov Y., 2004, *J. Quant. Spectrosc. Radiative Transfer*, 83, 387

## SUPPORTING INFORMATION

Supplementary data are available at [MNRAS](https://doi.org/10.1093/mnras/rtz168) online.

Additional Supporting Information (tables) may be found in the online version of this article. The tables are available in their entirety for  $10^{14} \text{ cm}^{-3}$  to  $10^{20} \text{ cm}^{-3}$  and temperatures from 6000 K to 300 000 K in the wavelength region of  $10 \text{ nm} \leq \lambda \leq 3000 \text{ nm}$  in machine-readable form in the online journal as additional data.

**Table 1.** This table gives values of the Gaunt factor for  $N_e = 1 \times 10^{17} [\text{cm}^{-3}]$  for temperatures  $10\,000 \text{ K} \leq T \leq 300\,000 \text{ K}$  in the wavelength region  $10 \text{ nm} \leq \lambda \leq 3000 \text{ nm}$ .

Please note: Oxford University Press is not responsible for the content or functionality of any supporting materials supplied by the authors. Any queries (other than missing material) should be directed to the corresponding author for the article.

This paper has been typeset from a  $\text{\TeX}/\text{\LaTeX}$  file prepared by the author.



# The electron-impact broadening of the Nb III for 5p–5d transitions

Zoran Simić<sup>1★</sup> and Nenad M. Sakan<sup>2</sup>

<sup>1</sup>*Astronomical Observatory, Volgina 7, 11060 Belgrade, Serbia*

<sup>2</sup>*Institute of Physics, University of Belgrade, PO Box 57, 11001 Belgrade, Serbia*

Accepted 2019 November 27. Received 2019 November 14; in original form 2019 October 24

## ABSTRACT

In this work, we present the data of Stark widths of rare-earth element Nb III, calculated for 21 spectral lines by using the modified semi-empirical method. Obtained results have been used to study the influence of Stark broadening on spectral lines in hot stars atmospheres such as A-type star and DA and DB white dwarfs.

**Key words:** atomic data – atomic processes – line: formation.

## 1 INTRODUCTION

Abundances analyses show presence of different rare-earth elements (REE) in stellar spectra of hot star atmospheres. The primary astrophysical source of the REE is the rapid neutron-capture process also known as r-process (Mumpower et al. 2016). This mechanism is responsible for the majority of the Solar system REE abundances. Stark broadening data of REE spectral lines are important for abundance determination and also for laboratory and technological plasma.

In the spectrum of Canopus, single ionized niobium is noted by Reynolds, Hearnshaw & Cottrell (1988). Also, Gopka et al. (1991) analyse the abundances of REE elements: strontium, yttrium, zirconium, niobium, molybdenum, ruthenium, rhodium, barium, lanthanum, cerium, praseodymium, neodymium, samarium, europium, and gadolinium in the atmospheres of K giants by the model atmosphere method using synthetic spectra method. From a spectroscopic analysis of the rapidly oscillating chemically peculiar star  $\gamma$  Equ with model of  $T_{\text{eff}} = 7700$  K,  $\log g = 4.20$ , Ryabchikova et al. (1997) derived that Nb and Mo are the most overabundant elements in this star relative to the Sun. An example of a very sharp-lined chemically peculiar star,  $\gamma$  Equ, is of spectral class near F0V. This star is a member of the rapidly oscillating CP2 (roAp) stars. It was discovered oscillations with a period of 12.44 min and an amplitude that was variable between 0.5 and 1.5 mmag from night to night.

Identification and quantitative analysis of REE abundance show the spectral lines of the first ions, often the spectral lines of the second and third ions, of REE are dominant in stellar atmospheres due to low ionization potentials (Popović, Dimitrijević & Ryabchikova 1999).

We started to investigate ionized niobium spectral lines in Simić, Dimitrijević & Popović (2014), and we obtained electron-impact (Stark) full width at half-maximum (FWHM) intensity of 15 Nb III spectral lines from  $4d^2$  ( $^3F$ ) $5s$ – $4d^2$  ( $^3F$ ) $5p$  transitions.

This result shows importance of Stark broadening effect for plasma conditions in atmospheres of A-type stars and DB white dwarfs.

The crucial work on niobium in ionized states II and III is presented in Nilsson et al. (2010). The accurate transition probabilities for astrophysically interesting spectral lines of Nb II and Nb III were derived in order to determine the niobium abundance in the Sun and in metal-poor stars rich in neutron-capture elements. The quality of the presented data lines in laboratory measurements of 17 radiative lifetimes in Nb II. By combining these lifetimes with branching fractions for lines depopulating the levels, Nilsson et al. (2010) derived the transition probabilities of 107 Nb II lines from  $4d^25p$  configuration in the wavelength range 2240–4700 Å, and have presented the theoretical transition probabilities of 76 Nb III transitions with wavelengths in the range 1430–3140 Å.

Complex spectra of REE produce difficulties in calculations for the same approach (Popović & Dimitrijević 1998). Often there are no available data on the energy levels and the reliable transition probabilities for the REE that direct to use the approximate methods suitable for Stark broadening calculations. As we mentioned in Simić et al. (2014), there are many cases where we can use estimate of Stark broadening parameters on the basis of regularities and systematic trends to complete the atomic data needed for calculation (Dimitrijević & Popović 1989).

The spectrum of doubly charged Nb ion is given by Gayazov, Ryabtsev & Churilov (1998), with 908 identified lines in recorded region. The LS coupling is a quite good approximation for niobium in the studied configurations. The analysis of the third niobium spectrum was based on the theoretical level energies and transition probabilities calculated using the COWAN code. The mixing of the terms in the third niobium spectrum configuration is denoted as a mixing configuration term (Gayazov et al. 1998). Details will be given in Section 3 of this paper.

In this work, we presented new electron-impact (Stark) FWHM intensity for 21 Nb III spectral lines and completed a list of obtained results in Simić et al. (2014) within modified semi-empirical approach (MSE; Dimitrijević & Konjević 1980) including the case of complex spectra (Popović & Dimitrijević 1997). This considered

\* E-mail: zsimic@aob.rs

transitions will be used to investigate the importance of Stark broadening for plasma conditions in hot stellar atmospheres such as A-type star and DA and DB white dwarfs.

No available experimental data that can be used to compare with our electron-impact full widths.

## 2 THE MODIFIED SEMI-EMPIRICAL METHOD

The electron-impact (Stark) full width (FWHM) of an isolated ion line is given for an ionized emitter within the MSE approach (Dimitrijević & Konjević 1980) as

$$w_{\text{MSE}} = N \frac{4\pi}{3c} \frac{\hbar^2}{m^2} \left( \frac{2m}{\pi k T} \right)^{1/2} \frac{\lambda^2}{\sqrt{3}} \cdot \left\{ \sum_{\ell_i \pm 1} \sum_{L_i J_i} \mathfrak{R}_{\ell_i, \ell_i \pm 1}^2 \tilde{g}(x_{\ell_i, \ell_i \pm 1}) \right. \\ + \sum_{\ell_f \pm 1} \sum_{L_f J_f} \mathfrak{R}_{\ell_f, \ell_f \pm 1}^2 \tilde{g}(x_{\ell_f, \ell_f \pm 1}) \\ + \left( \sum_{i'} \mathfrak{R}_{i i'}^2 \right)_{\Delta n \neq 0} g(x_{n_i, n_i + 1}) \\ \left. + \left( \sum_{f'} \mathfrak{R}_{f f'}^2 \right)_{\Delta n \neq 0} g(x_{n_f, n_f + 1}) \right\}, \quad (1)$$

where  $i$  represent the initial level, and  $f$  the final one,  $\mathfrak{R}_{\ell_k, \ell_{k'}}^2$ ,  $k = i, f$  is the square of the matrix element, and

$$\left( \sum_{k'} \mathfrak{R}_{k k'}^2 \right)_{\Delta n \neq 0} = \left( \frac{3n_k^*}{2Z} \right)^2 \frac{1}{9} (n_k^{*2} + 3\ell_k^2 + 3\ell_k + 11)$$

(in Coulomb approximation). The electron density is denoted with  $N$ , while  $T$  is the electron temperature, equation (1). With  $g(x)$  (Griem 1968) and  $\tilde{g}(x)$  (Dimitrijević & Konjević 1980) are denoted Gaunt factors for width, for  $\Delta n \neq 0$  and  $\Delta n = 0$ , respectively. Also, this function depends on

$$x_{l_k, l_{k'}} = \frac{E}{\Delta E_{l_k, l_{k'}}}, \quad k = i, f,$$

here  $E = \frac{3}{2} k T$  is the electron kinetic energy and  $\Delta E_{l_k, l_{k'}} = |E_{l_k} - E_{l_{k'}}|$  is the energy difference between levels  $l_k$  and  $l_k \pm 1$  ( $k = i, f$ ),

$$x_{n_k, n_{k+1}} \approx \frac{E}{\Delta E_{n_k, n_{k+1}}},$$

where for  $\Delta n \neq 0$  the energy difference between energy levels with  $n_k$  and  $n_k + 1$ ,  $\Delta E_{n_k, n_{k+1}}$ , is estimated as  $\Delta E_{n_k, n_{k+1}} \approx 2Z^2 E_H / n_k^{*3}$ .  $n_k^* = [E_H Z^2 / (E_{\text{ion}} - E_k)]^{1/2}$  is the effective principal quantum number,  $Z$  is the residual ionic charge, for example  $Z = 1$  for neutral atoms, and  $E_{\text{ion}}$  is the appropriate spectral series limit.

We used Gayazov et al. (1998) for atomic energy levels needed for our calculation of Nb III Stark linewidths.

## 3 COMPLEX SPECTRA OF IONIZED NIOBIUM

In Morton (2000), we found report on energy levels for neutral niobium and single, double, and triple charged niobium. Especially for Nb III origin of the data for levels are from Iglesias (1955). This third spectrum of niobium photographed in the region from 540 to 3200 Å and it was measured 700 lines. It established 58 new levels originating from the  $4d^2 3s$ ,  $4d^2 5s$ ,  $4d^2 5d$ ,  $4d^2 6s$ , and  $4d^2 5p$  configurations and to classify a total of 319 lines. The source was condensed spark in He between Nb electrodes, and for lines of

longer wavelengths it was used plates and light source a condensed spark in air.

A detailed study of Iglesias (1955) of the spectrum of doubly ionized Nb was motivated Gayazov et al. (1998) to perform new research of Nb III spectrum. All levels below  $80\,000 \text{ cm}^{-1}$ , found by Iglesias (1955), were confirmed including the ones. Their values have been slightly modified due to better accuracy of observations (Gayazov et al. 1998). Accuracy of the energy levels is estimated as  $0.1 \text{ cm}^{-1}$  or better.

In the third niobium spectrum configuration we can find mixing configuration, term with different configurations (Gayazov et al. 1998). For example,  $63686.35 \text{ cm}^{-1}$  observed energy is represented with term with configuration mixing: 83 per cent  $4d^2 5p (^3F) ^4G_{5/2}$  and 11 per cent  $4d^2 5p (^3F) ^2F_{5/2}$ . In distinction from next example observed energy  $78793.62 \text{ cm}^{-1}$  with 61 per cent  $4d^2 5p (^1G) ^2G_{7/2}$  and 16 per cent  $4d^2 5p (^3F) ^2D_{7/2}$ . In the case when we can neglect the contribution of other configurations, as the first example here, we can apply MSE approach. Otherwise, we need a calculate the square of the matrix element as

$$\mathfrak{R}_{j, j'}^2 = P_1 \mathfrak{R}_{\alpha, \alpha'}^2 + P_2 \mathfrak{R}_{\beta, \beta'}^2,$$

where  $P_1$  is the part of the leading configuration and  $P_2$  of the second one of any term represented as a mixture ( $P_1 + P_2 = 1$ ),  $\alpha, \alpha'$  denote the energy level corresponding to the leading configuration, and its perturbing levels, and  $\beta, \beta'$  is the same for the second configuration (see details in Dimitrijević & Popović 1993).

## 4 RESULTS AND DISCUSSION

In our previous study of doubly charged niobium ion (Simić et al. 2014), we considered 5s–5p transitions, and noted that it is possible to apply MSE approach (Dimitrijević & Konjević 1980) in the case of complex spectra where contributions of leading term of initial and final energy level are at least 80 per cent. This criterion allows us to take new 21 lines of Nb III for calculations of Stark widths for 5p–5d transitions. In Table 1, we represent the Stark full widths for Nb III for 5p–5d transitions. All calculations taken in account an electron density of  $10^{23} \text{ m}^{-3}$  and temperatures from 10 000 up to 300 000 K. The temperature dependence of Stark widths for 5p–5d transitions, can be seen in Fig. 1, shows the usual trend where widths decrease with temperature. At the high temperatures Stark width becomes very close with respect to each other.

In the Nilsson et al. (2010), the probabilities of 76 Nb III transitions with wavelengths in the range 1430–3140 Å are presented. In accordance with Iglesias (1955) the terms listed in tables from Nilsson et al. (2010) have short designation. For our range of interest there are data only on a–z transitions, where ‘a’ represents parent term  $4d^3$  for lower level and ‘z’ designates parent term  $4d^2 (^3F) 5p$  for upper level accordingly. In our investigation, with the spectral range of 1680–2060 Å, all of the lines measured in Nilsson et al. (2010) are not applicable for our calculated values of 5p–5d transitions. The possibility of comparison of our calculations with the presented results would lead us to include the calculations for some of the lines presented in Nilsson et al. (2010), in our further research.

The electron-impact broadening effect in hot stars for Nb III spectral lines can be considered in two models: A-type and white dwarfs. In the case of white dwarfs we will take both DA and DB types. For that matter we chosen 1771.5 Å spectral lines of Nb III for transitions, it could be seen in Table 1 as  $5p (^3F) ^4G_{9/2}$ – $5d (^3F) ^4F_{7/2}^o$  transition with a relative intensity of 277 (Gayazov et al. 1998).

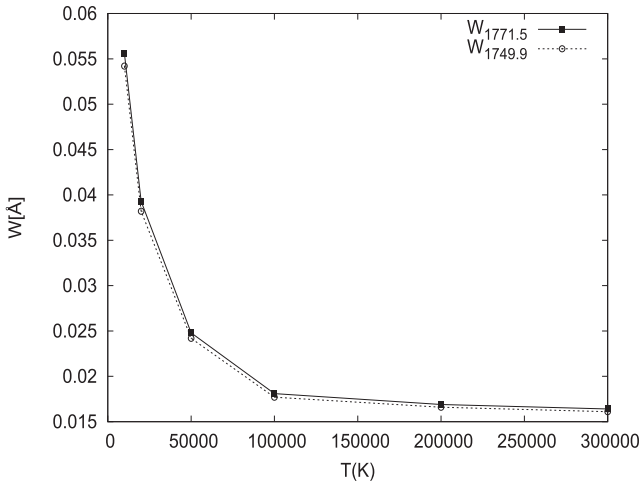
We compared thermal Doppler and Stark widths for Nb III spectral line  $5p (^3F) ^4G_{9/2}$ – $5d (^3F) ^4F_{7/2}^o$  ( $\lambda = 1771.5 \text{ Å}$ ) in A-type stars, a

**Table 1.** Nb III electron-impact broadening parameters (full width at half-maximum) for  $4d^2\ (^3F) 5s-4d^2\ (^3F) 5p$  transitions obtained by the modified semi-empirical method (Dimitrijević & Konjević 1980) for a perturber density of  $10^{23}\ \text{m}^{-3}$  and temperatures from 10 000 up to 300 000 K.

| Transition                                | $T$ (K) | Width (Å) | Transition                                  | $T$ (K) | Width (Å) |
|---|---------|-----------|---|---------|-----------|
|   | 10 000  | 0.0599    |   | 10 000  | 0.0626    |
| Nb III                                    | 20 000  | 0.0423    | Nb III                                      | 20 000  | 0.0442    |
| 1838.0 Å                                  | 50 000  | 0.0267    | 1869.8 Å                                    | 50 000  | 0.0280    |
| $5p\ (^3F) 4G_{5/2}-5d\ (^3F) 4F_{3/2}^o$ | 100 000 | 0.0193    | $5p\ (^3F) 4G_{7/2}-5d\ (^3F) 4F_{5/2}^o$   | 100 000 | 0.0202    |
|   | 200 000 | 0.0175    |   | 200 000 | 0.0184    |
|   | 300 000 | 0.0174    |   | 300 000 | 0.0182    |
|   | 10 000  | 0.0592    |   | 10 000  | 0.0525    |
| Nb III                                    | 20 000  | 0.0418    | Nb III                                      | 20 000  | 0.0371    |
| 1824.8 Å                                  | 50 000  | 0.0264    | 1727.2 Å                                    | 50 000  | 0.0234    |
| $5p\ (^3F) 4G_{5/2}-5d\ (^3F) 4F_{5/2}^o$ | 100 000 | 0.0191    | $5p\ (^3F) 4G_{7/2}-5d\ (^3F) 4F_{7/2}^o$   | 100 000 | 0.0171    |
|   | 200 000 | 0.0174    |   | 200 000 | 0.0160    |
|   | 300 000 | 0.0173    |   | 300 000 | 0.0158    |
|   | 10 000  | 0.0498    |   | 10 000  | 0.0512    |
| Nb III                                    | 20 000  | 0.0352    | Nb III                                      | 20 000  | 0.0362    |
| 1688.7 Å                                  | 50 000  | 0.0222    | 1706.6 Å                                    | 50 000  | 0.0229    |
| $5p\ (^3F) 4G_{5/2}-5d\ (^3F) 4F_{7/2}^o$ | 100 000 | 0.0163    | $5p\ (^3F) 4G_{7/2}-5d\ (^3F) 4F_{9/2}^o$   | 100 000 | 0.0167    |
|   | 200 000 | 0.0153    |   | 200 000 | 0.0157    |
|   | 300 000 | 0.0142    |   | 300 000 | 0.0153    |
|   | 10 000  | 0.0556    |   | 10 000  | 0.0577    |
| Nb III                                    | 20 000  | 0.0393    | Nb III                                      | 20 000  | 0.0408    |
| 1771.5 Å                                  | 50 000  | 0.0248    | 1800.4 Å                                    | 50 000  | 0.0258    |
| $5p\ (^3F) 4G_{9/2}-5d\ (^3F) 4F_{7/2}^o$ | 100 000 | 0.0181    | $5p\ (^3F) 4G_{11/2}-5d\ (^3F) 4F_{9/2}^o$  | 100 000 | 0.0189    |
|   | 200 000 | 0.0169    |   | 200 000 | 0.0176    |
|   | 300 000 | 0.0164    |   | 300 000 | 0.0172    |
|   | 10 000  | 0.0542    |   | 10 000  | 0.0670    |
| Nb III                                    | 20 000  | 0.0382    | Nb III                                      | 20 000  | 0.0474    |
| 1749.9 Å                                  | 50 000  | 0.0242    | 1926.8 Å                                    | 50 000  | 0.0299    |
| $5p\ (^3F) 4G_{9/2}-5d\ (^3F) 4F_{9/2}^o$ | 100 000 | 0.0177    | $5p\ (^3F) 4G_{11/2}-5d\ (^3F) 4H_{13/2}^o$ | 100 000 | 0.0216    |
|   | 200 000 | 0.0166    |   | 200 000 | 0.0198    |
|   | 300 000 | 0.0161    |   | 300 000 | 0.0195    |
|   | 10 000  | 0.0700    |   | 10 000  | 0.0701    |
| Nb III                                    | 20 000  | 0.0495    | Nb III                                      | 20 000  | 0.0495    |
| 1963.1 Å                                  | 50 000  | 0.0313    | 1963.0 Å                                    | 50 000  | 0.0313    |
| $5p\ (^3F) 4F_{7/2}-5d\ (^3F) 4D_{5/2}^o$ | 100 000 | 0.0225    | $5p\ (^3F) 4F_{9/2}-5d\ (^3F) 4D_{7/2}^o$   | 100 000 | 0.0226    |
|   | 200 000 | 0.0205    |   | 200 000 | 0.0207    |
|   | 300 000 | 0.0203    |   | 300 000 | 0.0204    |
|   | 10 000  | 0.0674    |   | 10 000  | 0.0605    |
| Nb III                                    | 20 000  | 0.0477    | Nb III                                      | 20 000  | 0.0428    |
| 1928.3 Å                                  | 50 000  | 0.0301    | 1847.8 Å                                    | 50 000  | 0.0270    |
| $5p\ (^3F) 4F_{7/2}-5d\ (^3F) 4D_{7/2}^o$ | 100 000 | 0.0218    | $5p\ (^3F) 4F_{9/2}-5d\ (^3F) 4F_{7/2}^o$   | 100 000 | 0.0197    |
|   | 200 000 | 0.0199    |   | 200 000 | 0.0184    |
|   | 300 000 | 0.0196    |   | 300 000 | 0.0178    |
|   | 10 000  | 0.0702    |   | 10 000  | 0.0589    |
| Nb III                                    | 20 000  | 0.0496    | Nb III                                      | 20 000  | 0.0417    |
| 1975.5 Å                                  | 50 000  | 0.0314    | 1824.3 Å                                    | 50 000  | 0.0263    |
| $5p\ (^3F) 4F_{7/2}-5d\ (^3F) 4F_{5/2}^o$ | 100 000 | 0.0226    | $5p\ (^3F) 4F_{9/2}-5d\ (^3F) 4F_{9/2}^o$   | 100 000 | 0.0192    |
|   | 200 000 | 0.0205    |   | 200 000 | 0.0180    |
|   | 300 000 | 0.0203    |   | 300 000 | 0.0174    |
|   | 10 000  | 0.0583    |   | 10 000  | 0.0703    |
| Nb III                                    | 20 000  | 0.0412    | Nb III                                      | 20 000  | 0.0497    |
| 1817.0 Å                                  | 50 000  | 0.0261    | 2061.4 Å                                    | 50 000  | 0.0314    |
| $5p\ (^3F) 4F_{7/2}-5d\ (^3F) 4F_{7/2}^o$ | 100 000 | 0.0190    | $5p\ (^3F) 4D_{1/2}-5d\ (^3F) 4D_{1/2}^o$   | 100 000 | 0.0225    |
|   | 200 000 | 0.0177    |   | 200 000 | 0.0206    |
|   | 300 000 | 0.0172    |   | 300 000 | 0.0204    |

**Table 1** – *continued*

| Transition   | $T$ (K) | Width ( $\text{\AA}$ ) | Transition   | $T$ (K) | Width ( $\text{\AA}$ ) |
|--|---------|------------------------|--|---------|------------------------|
| Nb III<br>1794.2 $\text{\AA}$<br>$5p\ (^3F)\ ^4F_{7/2} - 5d\ (^3F)\ ^4F_{9/2}^o$ | 10 000  | 0.0568                 | Nb III<br>2041.1 $\text{\AA}$<br>$5p\ (^3F)\ ^4D_{1/2} - 5d\ (^3F)\ ^4D_{3/2}^o$ | 10 000  | 0.0691                 |
|  | 20 000  | 0.0402                 |  | 20 000  | 0.0488                 |
|  | 50 000  | 0.0254                 |  | 50 000  | 0.0309                 |
|  | 100 000 | 0.0186                 |  | 100 000 | 0.0222                 |
|  | 200 000 | 0.0174                 |  | 200 000 | 0.0203                 |
|  | 300 000 | 0.0168                 |  | 300 000 | 0.0201                 |
| Nb III<br>2044.6 $\text{\AA}$<br>$5p\ (^3F)\ ^4D_{1/2} - 5d\ (^3F)\ ^4F_{3/2}^o$ | 10 000  | 0.0761                 |  |         |                        |
|  | 20 000  | 0.0538                 |  |         |                        |
|  | 50 000  | 0.0340                 |  |         |                        |
|  | 100 000 | 0.0244                 |  |         |                        |
|  | 200 000 | 0.0221                 |  |         |                        |
|  | 300 000 | 0.0220                 |  |         |                        |

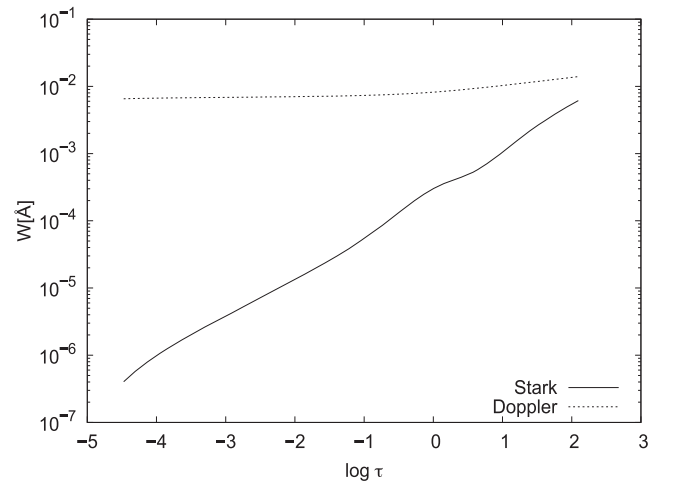
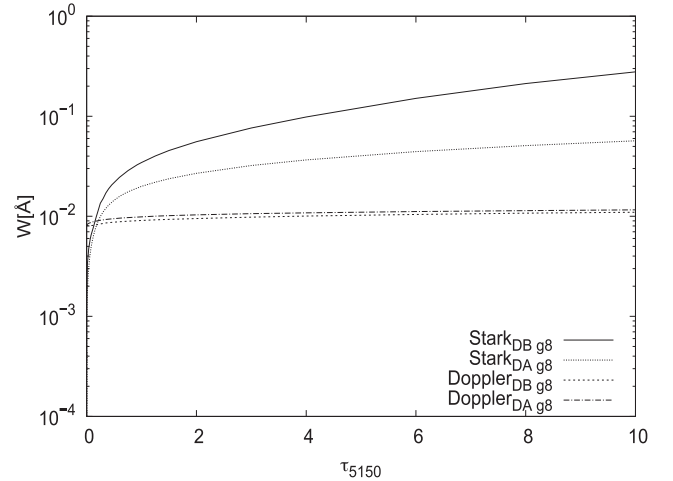

**Figure 1.** Stark widths as a function of temperatures for doubly ionized niobium spectral lines 1771.5 and 1749.9  $\text{\AA}$ .

model atmosphere with  $T_{\text{eff}} = 10\,000$  K and  $\log g = 4.5$  (Kurucz 1979), in Fig. 2. In considered case the Stark width is smaller than Doppler one, although in such case Stark broadening must be considered since its influence on line wings is still dominant. Stark broadening increases in line wings with the increase of niobium abundance as expected.

For the model of white dwarfs DA and DB types, we considered the same Nb III spectral line  $5p\ (^3F)\ ^4G_{9/2} - 5d\ (^3F)\ ^4F_{7/2}^o$  ( $\lambda = 1771.5$   $\text{\AA}$ ). In Fig. 3, the comparison of Stark and Doppler width as a function of optical depth is shown for both models, with  $T_{\text{eff}} = 15\,000$  K and  $\log g = 8$  (Wickramasinghe 1972). Here, thermal Doppler broadening has much less importance in comparison with the Stark broadening mechanism than in A-type stellar atmospheres. The optical depth points at the standard wavelength  $\lambda_s = 5150$   $\text{\AA}$  ( $\tau_{5150}$ ) are used in Wickramasinghe (1972) and here, in distinction from (Kurucz 1979) where the Rosseland optical depth scale ( $\tau_{\text{Ross}}$ ) has been used for the A-type star model.

Stark broadening is more significant than the thermal Doppler broadening even in the surface atmosphere layers of DA and DB white dwarfs, see Fig. 2. Also, electron-impact broadening is larger in DB type of white dwarfs.

Generally, from our results it follows that in atmosphere of A-type stars and white dwarfs exists layers where Stark broadening


**Figure 2.** Thermal Doppler and Stark widths for Nb III spectral lines  $5p\ (^3F)\ ^4G_{9/2} - 5d\ (^3F)\ ^4F_{7/2}^o$  ( $\lambda = 1771.5$   $\text{\AA}$ ) for an A-type star atmosphere model with  $T_{\text{eff}} = 10\,000$  K and  $\log g = 4.5$ , as a function of the Rosseland optical depth.

**Figure 3.** Thermal Doppler and Stark widths for Nb III spectral lines  $5p\ (^3F)\ ^4G_{9/2} - 5d\ (^3F)\ ^4F_{7/2}^o$  ( $\lambda = 1771.5$   $\text{\AA}$ ) for DA and DB white dwarf atmosphere model with  $T_{\text{eff}} = 15\,000$  K and  $\log g = 8$ , as a function of optical depth  $\tau_{5150}$ .



effect should be taken into account for modelling and investigating stellar plasmas.

## ACKNOWLEDGEMENTS

This work is a part of the Project 176002 ‘Influence of collisional processes on astrophysical plasma line shapes’ supported by the Ministry of Education, Science and Technological Development of Serbia.

## REFERENCES

- Dimitrijević M. S., Konjević N., 1980, *J. Quant. Spectrosc. Radiat. Transf.*, 24, 451
- Dimitrijević M. S., Popović M. M., 1989, *A&A*, 217, 201
- Dimitrijević M. S., Popović L. Č., 1993, *A&AS*, 101, 583
- Gayazov R. R., Ryabtsev A. N., Churilov S. S., 1998, *Phys. Scr.*, 57, 45
- Gopka V. F., Komarov N. S., Mishenina T. V., Yuschenko A. V., 1991, *Pis'ma Astron. Zh.*, 17, 368
- Griem H. R., 1968, *Phys. Rev.*, 165, 258
- Iglesias R. L., 1955, *J. Opt. Soc. Am.*, 45, 10
- Kurucz R. L., 1979, *ApJS*, 40, 1
- Morton D. C., 2000, *ApJS*, 130, 403
- Mumpower M. R., McLaughlin G. C., Surman R., Steiner A. W., 2016, *ApJ*, 833, 6
- Nilsson H. et al., 2010, *A&A*, 511, A16
- Popović L. Č., Dimitrijević M. S., 1997, in Vujičić B., Djurović S., Purić J., eds, *The Physics of Ionized Gas*. Institute of Physics, Novi Sad, Serbia, p. 477
- Popović L. Č., Dimitrijević M. S., 1998, in North P., Schnel A., Žižňovský J., eds, *Proc. of the 26th Meeting and Workshop of the European Working Group on CP Stars*. Astron. Inst. Slovak Acad. Sci., Tatranska Lomnica, p. 353
- Popović L. Č., Dimitrijević M. S., Ryabchikova T., 1999, *A&A*, 350, 719
- Reynolds S. E., Hearnshaw J. B., Cottrell P. L., 1988, *MNRAS*, 235, 1423
- Ryabchikova T. A., Adelman S. J., Weiss W. W., Kuschnig R., 1997, *A&A*, 322, 234
- Simić Z., Dimitrijević M. S., Popović L. Č., 2014, *Adv. Space Res.*, 54, 1231
- Wickramasinghe D. T., 1972, *Mem. R. Astron. Soc.*, 76, 129

This paper has been typeset from a  $\text{\TeX}/\text{\LaTeX}$  file prepared by the author.

# Risk assessment of trace element contamination in river sediments in Serbia using pollution indices and statistical methods: a pilot study

Sanja Sakan · Gordana Dević · Dubravka Relić ·  
Ivan Anđelković · Nenad Sakan · Dragana Đorđević

Received: 14 March 2014 / Accepted: 15 November 2014 / Published online: 28 November 2014  
© Springer-Verlag Berlin Heidelberg 2014

**Abstract** To effectively manage potential environmental and human health impacts of contaminated river sediments, it is important that information about the source (anthropogenic vs geogenic), variability and environmental risks associated with the contamination are well understood. The present study was carried out to assess the source and severity of contamination and to undertake a risk assessment for selected elements (As, Cd, Co, Cr, Cu, Fe, Mn, Ni, Pb, V and Zn) in river sediments in Serbia. The estimate of the anthropogenic component of contamination was derived by determining the total element content and the background values for elements in sediments, and the severity of pollution was assessed by calculating a number of pollution indices including the contamination factor, the enrichment factor, the index of geoaccumulation, the ecological risk factor, the potential ecological risk index, the pollution load index, the combined pollution index, the modified degree of

contamination and the toxic unit factor. This analysis indicates that river sediments in Serbia are primarily polluted with Zn, Cu and Cd. The most contaminated river systems are the Ibar, Pek, West Morava and Great Morava rivers. Mining activities were found to have a significant influence on sediment. Multivariate analyses suggested anthropogenic origins for Pb, Zn, Cd, As, Ni and Cu, whilst Fe, V, Mn, Co and Cr appear to have a mixed origin (both lithogenic and anthropogenic sources). A geochemical approach, with a calculation of pollution indices and statistical methods, is recognised as useful for the risk management of trace elements in sediments around the world.

**Keywords** Trace elements · River sediments · Enrichment factor · Modified degree of contamination · Multivariate analysis

---

**Electronic supplementary material** The online version of this article (doi:10.1007/s12665-014-3886-1) contains supplementary material, which is available to authorized users.

---

S. Sakan (✉) · G. Dević · D. Đorđević  
ICTM, Chemistry Centre, University of Belgrade, Njegoševa 12,  
P. O. Box 815, 11000 Belgrade, Serbia  
e-mail: ssakan@chem.bg.ac.rs

D. Relić  
Faculty of Chemistry, Applied Chemistry,  
University of Belgrade, P. O. Box 51, 11000 Belgrade, Serbia

I. Anđelković  
Innovation Centre of the Faculty of Chemistry,  
11158 Belgrade, Serbia

N. Sakan  
Institute of Physics, University of Belgrade, Pregrevice 118,  
P.O. Box 68, 11081 Belgrade, Serbia

## Introduction

Heavy metals are widely distributed in nature, in places such as water, soil, sediments, air and various forms of organisms (Zhang et al. 2009). Metals are non-biodegradable and accumulative in nature. Contamination of the aquatic environment by heavy metals occurs as the result of various human activities (Behra et al. 2002). Elevated emissions and their deposition over time can lead to anomalous enrichment, causing metal contamination of the surface environment (Wong et al. 2006). Metal contamination in these sediments could directly affect the river water quality, resulting in potential consequences to the sensitive lowest levels of the food chain and ultimately to human health (Kabir et al. 2011).

The sediments consist of inorganic and organic particles with complex physical, chemical and biological

characteristics. They can scavenge some elements, thus acting as an adsorptive sink with metal concentrations in sediments often being many times greater than in the water column (Kalantzi et al. 2013). These metals may present both natural and anthropogenic origin. Main natural sources of heavy metals are weathering of soils and rocks and atmospheric deposition. Discharge of agricultural, municipal and industrial wastewaters into water bodies is dominant contribution from anthropogenic sources (Lin et al. 2011). To identify pollution problems, the anthropogenic contributions should be distinguished from the natural sources. Geochemical approaches, such as the enrichment factor (EF) and geochemical index methods, have been successfully used to estimate the impact of the human activities on sediments (Chabukdhara and Nema 2012) and many scientists have studied metal contamination in sediments using these approaches (Gao et al. 2013; Hui-na et al. 2012; Hu et al. 2011; Kabir et al. 2011; Harikumar et al. 2009; Abraham and Parker 2008). Calculating pollution indices of heavy metal is a powerful tool for ecological geochemistry assessment. These indexes evaluate the degree to which the sediment-associated chemical status might adversely affect aquatic organisms and are designed to assist sediment assessors and managers responsible for the interpretation of sediment quality (Caeiro et al. 2005).

Multivariate chemometric techniques, such as principal component analysis (PCA) and cluster analysis (CA), are often used as additional methods of monitoring heavy metals (Wang et al. 2014; Jamshidi-Zanjani and Saeedi et al. 2013; Chabukdhara and Nema 2012; Iqbal et al. 2013; Relić et al. 2010, 2011; Varol 2011; Li and Zhang 2010; Yang et al. 2009). These statistical techniques appeared to be very useful in solving many environmental compartments and the identification of existing pollution pattern.

In this study, the evaluation of the metal pollution level and possible sources compared to background pollution was performed for river sediments in Serbia. The main objectives were (1) to determine the total content of As, Cd, Co, Cr, Cu, Fe, Mn, Ni, Pb, V and Zn; (2) to carry out calculations of the contamination factor (CF), EF, index of geoaccumulation (I<sub>geo</sub>), ecological risk factor (Er), potential ecological risk index (RI), pollution load index (PLI), combined pollution index (CPI), modified degree of contamination (mC<sub>d</sub>) and toxic units to estimate the anthropogenic input of the elements and to assess the pollution status of the area; and (3) to identify the main sources of toxic elements. The authors consider that the combination of a wide range of indices as well as the use of multivariate statistical methods is a novel approach for assessing the distribution of metals in sediments which can be extended to other similar contaminated aquatic systems.

## Materials and methods

### Study area

European rivers are affected by a wide variety of pollution problems. European catchments are under pressure from ever-increasing water stresses and land-use change, especially those with a high conservation value in the Mediterranean area. In Western European rivers, very high levels of cadmium, mercury, lead and zinc have been recorded. Record levels of contaminations are observed in river basins that receive considerable discharges from industrial and mining activities and from large cities (Tockner et al. 2009). This is the case for many mining sites in the Western Balkans, where copper, lead, zinc and other elements are frequently found (Stuhlberger 2014). In Serbia, the primary extracted minerals include copper, coal, lead–zinc with associated gold, silver, bismuth and cadmium, red bauxite and modest quantities of oil and gas.

The largest and most important rivers that flow through Serbia are the Danube, Sava, Great Morava, West Morava, South Morava, Tisa, Ibar, Drina, Timok, Nišava, Tamiš and Begej Rivers. The Danube is the largest river in the country, flowing for 588 km inside Serbia, whilst forming the border with Romania, and is the second largest river in Europe. The basin drains parts of 19 countries. Some major tributaries of the Danube are still heavily polluted. Water quality in the Middle and Lower Danube remained relatively high (class II) between 1950 and the 1970s, but deteriorated afterwards due to rapid industrial development, poor pollution control and inputs from heavily polluted tributaries (Tockner et al. 2009).

The 945-km-long Sava River is the largest tributary of the Danube by volume (average discharge: 1,572 m<sup>3</sup>/s) and the second largest, after the Tisza, by catchment area (95,793 km<sup>2</sup>). In Serbia, it remains a typical lowland river. Until the 1990s, the Sava was affected by heavy pollution from the metallurgical, chemical, leather, textile, food, cellulose and paper industries, as well as from agricultural activities. The Sava is the main recipient of wastewater from many cities and is impacted by the polluted water of the tributaries (Tockner et al. 2009).

The River Tisza (966 km; 157,220 km<sup>2</sup>) is the largest Danube tributary in its length and catchment area. A small part of the Tisza watershed area lies within Serbian territory and covers only 6 % or 8,994 km<sup>2</sup>. This area belongs to the Autonomous Province of Vojvodina. It is predominantly lowland and part of the Pannonian basin, which is the largest of the sediment-filled, postorogenic basins of the Alpine region (Adriano et al. 2003). Ecological accidents that took place in 2000 in the superior watershed and their effects on the rivers upstream with resulting transboundary influences proved the necessity of a regional approach to

environmental protection and the active involvement of riverside countries in establishing common strategies and programs for preventing and reducing the risk of accidental pollution (Adriano et al. 2003).

The 308-km-long West Morava drains south-western Serbia (catchment area: 15,567 km<sup>2</sup>). The largest tributary is the Ibar.

Description of the sampling site and sampling

As riverine pollution can cross national borders, it is important that levels of pollutants in water and sediment are assessed in all the countries through which the river flows. Due to this factor, sediment samples in this study were collected from all of the main rivers in Serbia. A total of 35 samples of river sediment from 15 rivers in Serbia were collected during the year 2008 (Table 1). For the larger rivers, sampling was conducted at several locations (Fig. 1; Table 1). The sediment samples were stored at 4 °C to prevent changes in the chemical composition of the sediments. The contents of the micro- and macro-elements were determined in the granulometric fraction <63 μm of the bottom sediment samples (“grab”—the samples) after air drying for 8 days (Sakan et al. 2011). Detailed information about natural variability and sediment and soil properties in studied region is shown in paper Sakan et al. (2014).

Analytical procedures and element analysis

The total content of elements in the sediments was determined by digestion with very strong acids: HNO<sub>3</sub> + HCl + HF. A 0.5-g sediment sample was placed in a

Teflon vessel and then 9 ml HCl (37 %), 3 ml HNO<sub>3</sub> (70 %) and 3 ml HF (48 %) were added to the vessel. One Teflon vessel only contains the acid mixture for a blank. A microwave digestion system brings the sample to 165 °C in 10 min (holding time 0 s), then 175 °C in 3 min, where it was kept for 10 min (max power was 1200 W) (Rönkkömäki et al. 2008). Microwave digestion was performed in a pressurised microwave oven (Ethos 1, Advanced Microwave Digestion System, Milestone, Italy) equipped with a rotor holding 10 microwave vessels (PTFE).

After cooling the digestion system, 10 ml H<sub>3</sub>BO<sub>3</sub> (5 g/100 ml water) is added. Again, the microwave digestion system brings the sample to 175 °C in 10 min at 1420 W and holds the temperature at 170 °C for 3 min. The digestate is then diluted to a final volume of 100 ml (Nam et al. 2001).

In this research, the following elements were determined in each sample: As, Cd, Co, Cr, Cu, Fe, Mn, Ni, Pb, V and Zn. The results are expressed in mg kg<sup>-1</sup> dry sediment. The analytical determination of the studied elements was realised with an atomic emission spectrometer with an inductively coupled plasma iCAP-6500 Duo (Thermo Scientific, UK). The detector was a RACID86 charge injector device (CID). Analytical grade chemicals were used throughout the study without any further purification. The metal standards were prepared from a stock solution of 1,000 mg L<sup>-1</sup> by successive dilutions. The concentrations obtained for all the elements in the blanks were close to the detection limit of the method, indicating that contamination was not a problem in the digestion.

Assessment of sediment contamination

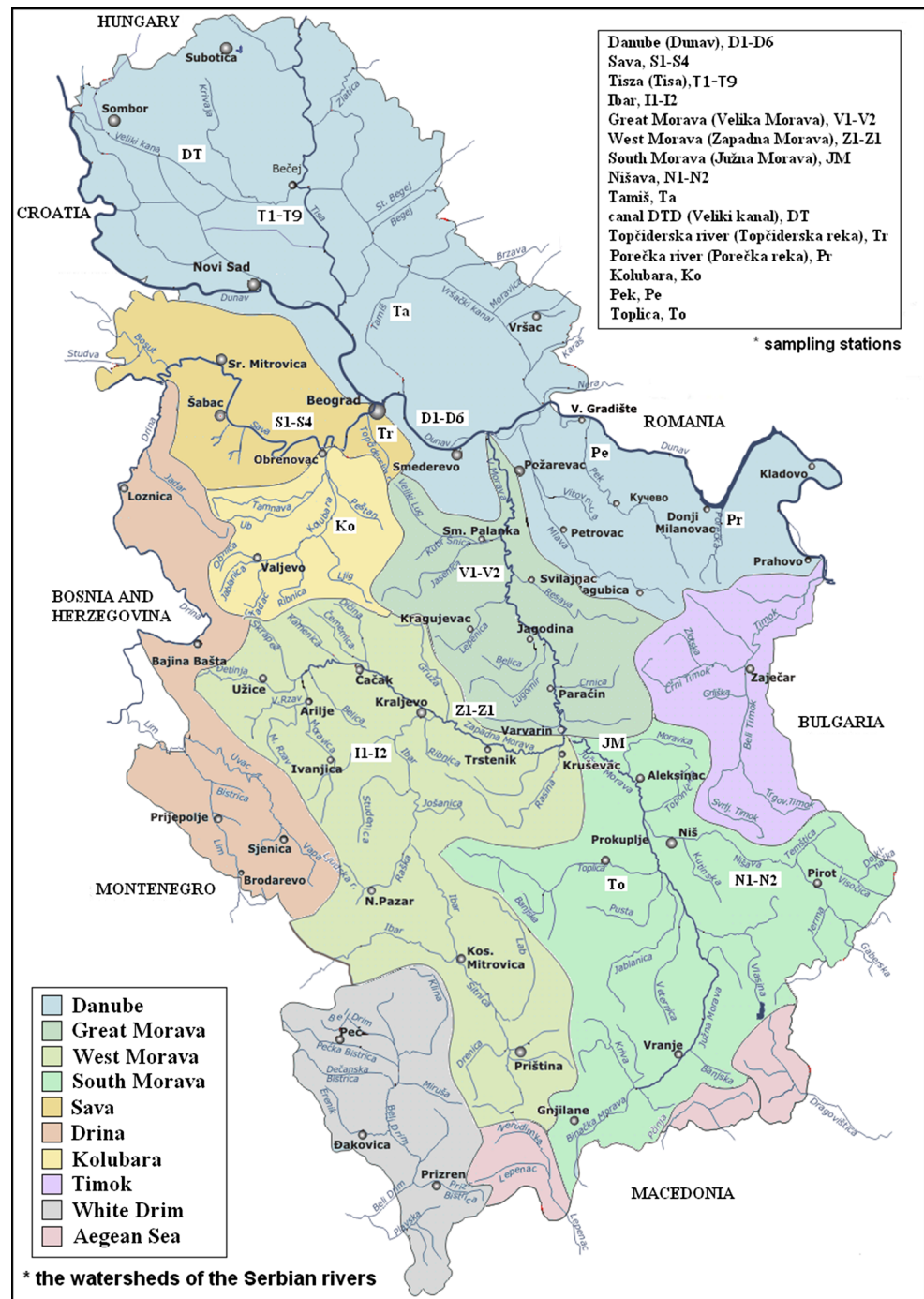
The degree of metal enrichment in sediments was carried out using following formulas:

CF was calculated as the ratio between the metal content in the sediment at a given station and the normal concentration levels (background concentration), reflecting the degree of metal enrichment in the sediment:  $CF = C_s/C_b$ . CF was classified into four groups in Hakanson (1980) and Pekey et al. (2004). EF was calculated as:  $EF = (M/Y)_{sample}/(M/Y)_{background}$ , where *M* is the concentration of the potentially enriched element and *Y* is the concentration of the proxy element. I<sub>geo</sub> was calculated as  $I_{geo} = \log_2 [C_{metal}/1.5 C_{metal (control)}]$ , where *C<sub>metal</sub>* is the concentration of the heavy metal in sample and *C<sub>metal (control)</sub>* is the concentration of the metal in the unpolluted sample or control. The factor 1.5 is attributed to lithogenic variations in the sediment (Mendiola et al. 2008). Ecological risk factor (*Er<sup>i</sup>*):  $Er^i = Tr^i C^i f$ , where *Tr<sup>i</sup>* is the toxic–response factor for a given substance [for Hg, Cd, As, Cr and Zn, they are 40, 30, 10, 2 and 1, respectively; and 5 for Pb, Cu and Ni (Yang et al. 2009)], and *C<sup>i</sup>f* is the contamination

**Table 1** Sampling locations

| River             | Watershed    | Sampling sites |
|-------------------|--------------|----------------|
| Danube            | Black Sea    | D1–D6          |
| Sava              | Danube       | S1–S4          |
| Tisa              | Danube       | T1–T9          |
| Ibar              | West Morava  | I1, I2         |
| Great Morava      | Danube       | V1, V2         |
| West Morava       | Great Morava | Z1, Z2         |
| South Morava      | Great Morava | JM             |
| Nišava            | South Morava | N1, N2         |
| Tamiš             | Danube       | Ta             |
| DTD canal         | Danube       | DT             |
| Topčiderska River | Sava         | Tr             |
| Porečka River     | Danube       | Pr             |
| Kolubara          | Sava         | Ko             |
| Pek               | Danube       | Pe             |
| Toplica           | South Morava | To             |

**Fig. 1** Location map of the study area



factor (Hakanson, 1980). Ecological risk index (RI):  $RI = \sum (T_i \times C_i/C_0)$ , where  $n$  is the number of heavy metals,  $T_i$  is the toxic-response factor for a given substance,  $C_i$  represents the metal content in the sediment and  $C_0$  is the regional background value of heavy metals (Hakanson, 1980; Yang et al. 2009). PLI: the PLI for a single site is the  $n$ th root of the number ( $n$ ) of multiple CF multiplied together (Tomlinson et al. 1980; Mohiuddin et al. 2012):  $PLI = (CF_1 \times CF_2 \times CF_3 \times \dots \times CF_n)^{1/n}$ .

CPI: there are two steps in this assessment process. The first step is to determine the contamination coefficient of each heavy metal which is obtained by:  $C_f^i = C^i/C_n^i$ . In the second step: the CPI is obtained by  $CPI = \sum C_f^i/m$ , where  $C_f^i$  is the contamination coefficient of heavy metal,  $C^i$  is the concentration of each heavy metal in the sediment,  $C_n^i$  is the background values, and  $m$  is number of heavy metals and CPI.  $mC_d$ : this factor is similar to CPI according to the method of calculation:  $mC_d = \sum C_f^i (i = 1, i = n)/n$ , where



$n$  = the number of analysed elements,  $i$  = the  $i$ th element (or pollutant) and  $C_f$  = contamination factor, but differs in the gradation degree of contamination (Abraham and Parker 2008). TU is defined as the ratio of the determined content to the probable effect level (PEL) (Gao et al. 2013; Harikumar et al. 2009; Pedersen et al. 1998). The PEL is defined as the lower limit of the range of chemical concentrations that is usually or always associated with adverse biological effects (Gao et al. 2013). Sediments with measured chemical concentrations equal to or greater than the PEL are considered to represent significant and immediate hazards to exposed organisms. The PEL represents the lower limit of the range of chemical concentrations that is usually or always associated with adverse biological effects (CCME 1995). It was derived using a weight of evidence approach in which matching biological and chemical data from numerous modelling, laboratory, and field studies performed on freshwater sediments were compiled and analysed, i.e. the geometric mean of the 50th percentile of the effect data set and the 85th percentile of the no effect data set (Smith et al. 1996; CCME 1995). In this manuscript, for TU calculation used PEL values are published in Smith et al. (1996) and MacDonald et al. (2000).

#### Statistical analysis

Multivariate analysis was performed using PCA and CA. The statistical analyses were conducted using SPSS 11.0 using the log-transform normalised data set. The element used for sediment normalisation is aluminium. This element was chosen because Al is a conservative element and a major constituent of clay minerals, and has been successfully used in previous investigations (Rubio et al. 2000).

## Results and discussion

#### Performance of the analytical procedure

The accuracy and precision of the obtained results were checked by analysing sediment reference material (BCR standards, 143 and 146R). The percentage recovery of each element was obtained as: [(measured concentration in  $\text{mg kg}^{-1}$ )/mean certified value for CRM in  $\text{mg kg}^{-1}$ ]  $\times$  100]. The results indicate a good agreement between the certified and analytical values (Table 2). The recovery of elements being practically complete for most of them and the values were in the acceptable range (recovery 80–120 %) (Chang et al. 2009).

The precision is expressed as relative standard deviations. The relative standard deviations of the means of

duplicate measurement were less than 4 % (0.03–3.80 %) for all the measured elements.

#### Descriptive statistics of elements contents in sediments

The total contents and basic statistics (minimum and maximum, as well as the means and standard deviations) for the total contents of all the measured elements in the investigated river sediments are shown in Table 3. The distribution of heavy metals in studied sediments showed large spatial variations amongst the different rivers suggesting large natural variability of metal concentrations in sediments and different origins of these elements. The order of the total element content was  $\text{Zn} > \text{Cu} > \text{Pb} > \text{Ni} > \text{Cr} > \text{V} > \text{Co} > \text{Cd} > \text{As}$  (not taking into account Fe and Mn). The contents of all elements were higher than the background values for the investigated elements (Table 4). Also, the contents of Cd, Cr, Cu, Ni, Pb and Zn were above the PEL, which indicates that the investigated river systems are polluted with toxic elements and that the content of these elements in sediments poses a potential risk to aquatic life. Because of that, additional calculations were performed the severity of contamination by these elements in sediments.

#### Calculating the grade of contamination and risk category

Contamination of the investigated river sediments with the studied trace elements was assessed using: CF, EF, Igeo, Er, RI, PLI, CPI, mCd and TU. Tables 5 and 6 show the predicted severity of contamination determined by these indices and ecological risk based on the calculated factors.

Table 4 shows the background values for the elements in sediments given by other authors (Rubio et al. 2000; Sakan et al. 2009) and calculated for the investigated river sediment, as well as values for the element content in continental crust (Wedepohl 1995) and the PEL values (Smith et al. 1996; MacDonald et al. 2000). The element contents in the DTD canal (station in Vrbas) were chosen as the background values for elements in this research because there are no significant anthropogenic sources of toxic elements at this locality and the sediment samples are similar to the other investigated river sediments in geochemical characteristics and composition. Many researchers recommend that it is better to use the regional background values (Rubio et al. 2000) than the element content in continental crust or the average values of the element contents in world soils, etc. In this research, the same background values (quoted in Table 4) are used for calculating all the pollution indices. For the background value of As, the content in the continental crust is used since the content of As extracted from the DTD canal (station in Vrbas) was below the detection limit.

**Table 2** The result of accuracy and precision of applied method

| Element | Certified 146R<br>(mg kg <sup>-1</sup> ) | Measured<br>(mg kg <sup>-1</sup> ) | Accuracy<br>(%) | Certified 143R<br>(mg kg <sup>-1</sup> ) | Measured<br>(mg kg <sup>-1</sup> ) | Accuracy<br>(%) |
|---------|--|------------------------------------|-----------------|--|------------------------------------|-----------------|
| Cd      | 18.8                                     | 18.3                               | 97.3            | 71.8                                     | 70.5                               | 98.2            |
| Co      | 7.39                                     | 7.62                               | 103             | 12.3                                     | 12.0                               | 101.6           |
| Cu      | 838                                      | 678                                | 80.9            | 130.6                                    | 111.4                              | 85.3            |
| Pb      | 609                                      | 532                                | 87.4            | 179.7                                    | 212.9                              | 118.5           |
| Mn      | 323                                      | 347                                | 107.5           | 904                                      | 834                                | 92.2            |
| Ni      | 70                                       | 60                                 | 85.4            | 299                                      | 248                                | 82.9            |
| Zn      | 3,060                                    | 2,749                              | 89.8            | 1,055                                    | 1,116                              | 106             |
| Cr      | 196                                      | 167                                | 85.2            |  |                                    |                 |

### Contamination factor (CF)

Values of the CF (CF, Table 6) were classified into four groups using the classification scheme given by Pekey et al. (2004) and Hakanson (1980). The results of the CF groupings are presented in Table 7 and Supplementary Table 1. The highest CF value, for Cu (very high contamination), was found at site 33 (the river Pek). CF values >6, which indicate “very high contamination”, were observed for Zn, Cu, Ni, Cd and As. For other elements, the CF values indicated: no metal enrichment to considerable contamination (Cr), no metal enrichment to very high contamination (As, Ni), moderate contamination to very high contamination (Cd, Cu, Zn); moderate contamination to considerable contamination (Fe, Mn, Co, Pb), and moderate contamination for V. From the CF values, contamination with the investigated elements can be observed, especially with Zn, Cu, Ni and Cd.

### Enrichment factor (EF)

The EF values were interpreted as suggested by Acevedo-Figueroa et al. (2006) (Table 5) and were calculated separately for all the sampling sites (Table 5, Supplementary Table 1). River sediments in Serbia showed a wide range of trace element enrichment. In general, the order of the average EF values was Cu > Zn > Cd > Co > Pb > Ni > Mn > Cr > As. According to the categories (Table 5), these findings indicate that Cu, Zn and Cd enrichment was high. From the pollution point of view, the EF of Cu in the river Pek (35.03) was the highest amongst the elements in the investigated sediments, suggesting significant contamination at this locality.

### Index of geoaccumulation (Igeo)

Müller (1979) proposed seven grades or classes based on the increasing numerical value of the Igeo index (Table 5). The greatest number of samples and elements belong to Class 1 (Fig. 2; Table 7, Supplementary Table 3), i.e.

unpolluted to moderately polluted sediment (with As, Cd, Co, Cr, Cu, Fe, Mn, Ni, Pb and V), Class 2 (Cd, Cu, Zn, and Pb in some samples), Class 3 (Cu in the river Pek and the West Morava 1, and Zn in the Ibar 1 and Ibar 2 and Pek) and the largest Igeo value -3.92 had the sediment from the Pek for Cu (Class 4, heavy pollution). These findings indicate that the primary contaminants in the rivers are Cu and Zn, like Cd. These results are consistent with EF values.

### Ecological risk factor (Er)

The ecological risk assessment results are summarised in Table 7 and the Supplementary Table 4. The potential Er indices of Cr, Ni, Pb, Zn and As were lower than 40 (except for arsenic at two locations in the river Ibar), which indicates a slight potential ecological risk of these elements in the main Serbian river. Amongst the studied elements, Cd and Cu present a higher ecological risk than any other elements because of their higher toxicity coefficient.

### Ecological risk index (RI)

The RI was calculated as the sum of all the calculated risk factors (Table 8 and Supplementary Table 4). The potential RI values were generally lower than 300, which suggest that sediment samples from the river catchments exhibited low and moderate ecological risk for the investigated elements. However, three (two sediment samples from the Ibar and one from the Pek Rivers) of the 34 samples of sediments had large RI values (300–600), which indicates a high ecological risk of these elements.

The contribution percent of the individual element to the overall potential ecological risk revealed that the most toxic element, Cd, is the main contributor to the total potentially ecological risk. Because Cd pollution, in general, was the result of a long history of accumulation, there is a strong potential risk to the ecosystem and the health of the residents in this region (Gao et al. 2013).

**Table 3** Total contents and descriptive statistics of elements in different river sediments, this study (mg kg<sup>-1</sup>)

|        | As   | Cd   | Co    | Cr   | Cu   | Fe    | Mn   | Ni   | Pb   | V    | Zn   | Al    |
|--------|------|------|-------|------|------|-------|------|------|------|------|------|-------|
| T1     | 3.26 | 5.05 | 10.0  | 59.8 | 47.8 | 33105 | 1276 | 39.2 | 95.7 | 87.2 | 330  | 54345 |
| T2     | 0.46 | 4.23 | 20.5  | 103  | 64.5 | 49098 | 1234 | 46.2 | 118  | 131  | 335  | 63956 |
| T3     | 1.39 | 4.97 | 21.2  | 95.8 | 74.1 | 46711 | 1324 | 45.0 | 124  | 122  | 391  | 72870 |
| T4     | 0.79 | 4.41 | 19.1  | 90.2 | 63.8 | 42246 | 1399 | 39.2 | 124  | 109  | 338  | 75717 |
| T5     | 0.41 | 6.37 | 22.6  | 106  | 88.3 | 46480 | 1722 | 47.7 | 112  | 122  | 360  | 39331 |
| T6     | 0.91 | 6.89 | 21.3  | 99.8 | 90.5 | 50118 | 2108 | 42.4 | 142  | 131  | 420  | 67904 |
| T7     | 0.51 | 6.23 | 19.8  | 92.8 | 74.0 | 43445 | 1870 | 42.8 | 90.3 | 115  | 346  | 26311 |
| T8     | 0.83 | 6.09 | 19.3  | 89.5 | 71.1 | 43281 | 1683 | 41.5 | 119  | 114  | 337  | 71782 |
| T9     | 1.49 | 7.00 | 21.5  | 96.3 | 87.1 | 46932 | 1816 | 46.3 | 140  | 123  | 411  | 83795 |
| D1     | 0.53 | 2.25 | 16.2  | 73.4 | 28.0 | 40134 | 1387 | 33.2 | 90.0 | 95.5 | 168  | 44340 |
| D2     | 3.70 | 2.12 | 16.3  | 75.0 | 23.8 | 39637 | 1036 | 36.0 | 114  | 106  | 157  | 89119 |
| D3     | 0.52 | 2.49 | 16.8  | 79.9 | 31.4 | 40922 | 979  | 35.8 | 104  | 107  | 208  | 54910 |
| D4     | 0.41 | 2.35 | 15.4  | 76.1 | 28.9 | 37534 | 896  | 35.0 | 132  | 95.5 | 220  | 62215 |
| D5     | 0.29 | 2.78 | 19.0  | 78.4 | 40.7 | 40389 | 1352 | 37.9 | 80.3 | 97.7 | 221  | 23482 |
| D6     | 0.75 | 5.31 | 21.5  | 123  | 41.9 | 44697 | 1185 | 70.8 | 136  | 113  | 228  | 54034 |
| S1     | 0.48 | 3.46 | 21.7  | 112  | 32.0 | 36506 | 1025 | 93.6 | 89.0 | 87.5 | 270  | 44354 |
| S2     | 0.58 | 3.02 | 28.5  | 154  | 36.4 | 46480 | 1759 | 126  | 115  | 108  | 213  | 57957 |
| S3     | 0.50 | 3.74 | 26.4  | 140  | 36.4 | 43872 | 1660 | 119  | 113  | 104  | 272  | 57781 |
| S4     | 0.65 | 4.69 | 27.3  | 145  | 31.3 | 45780 | 1819 | 119  | 110  | 113  | 213  | 54741 |
| I1     | 8.89 | 10.5 | 13.6  | 102  | 29.0 | 36863 | 904  | 142  | 318  | 72.1 | 947  | 36516 |
| I2     | 6.56 | 8.32 | 36.2  | 230  | 39.4 | 47630 | 1352 | 274  | 263  | 101  | 1095 | 59195 |
| V1     | 0.80 | 7.91 | 32.3  | 170  | 65.6 | 55319 | 1734 | 42.6 | 182  | 129  | 499  | 29759 |
| V2     | 1.60 | 6.82 | 27.7  | 152  | 53.0 | 46593 | 1226 | 156  | 182  | 110  | 449  | 61204 |
| Z1     | 2.15 | 3.60 | 12.2  | 85.6 | 155  | 33860 | 808  | 84.2 | 77.2 | 94.5 | 250  | 47320 |
| Z2     | 2.06 | 7.50 | 31.8  | 222  | 52.6 | 46461 | 1032 | 236  | 213  | 110  | 660  | 57360 |
| JM     | 1.11 | 3.88 | 23.4  | 106  | 47.9 | 50105 | 3688 | 55.1 | 150  | 124  | 238  | 74056 |
| N1     | 0.48 | 2.65 | 16.3  | 86.3 | 85.0 | 38745 | 731  | 35.9 | 138  | 111  | 411  | 59353 |
| N2     | 0.34 | 5.53 | 16.2  | 70.7 | 22.1 | 34881 | 770  | 34.6 | 84.1 | 101  | 114  | 42827 |
| Ta     | 1.17 | 3.12 | 26.5  | 112  | 51.9 | 62800 | 1413 | 50.4 | 137  | 149  | 191  | 95849 |
| DT     | 1.10 | 1.28 | 8.2   | 62.1 | 11.5 | 24556 | 648  | 34.7 | 57.8 | 60.4 | 66.7 | 36323 |
| Tr     | 0.78 | 3.91 | 27.9  | 161  | 40.9 | 50739 | 1226 | 133  | 144  | 128  | 338  | 52416 |
| Pr     | 0.98 | 3.13 | 23.8  | 118  | 137  | 51266 | 868  | 59.0 | 119  | 138  | 155  | 72811 |
| Ko     | 1.13 | 5.45 | 28.7  | 146  | 39.4 | 47245 | 1352 | 132  | 126  | 114  | 417  | 61971 |
| Pe     | 1.47 | 6.26 | 30.5  | 88.7 | 870  | 50977 | 1997 | 41.6 | 157  | 127  | 922  | 78474 |
| To     | 0.64 | 5.23 | 29.5  | 148  | 55.6 | 50808 | 1685 | 115  | 135  | 137  | 167  | 34488 |
| Min    | 0.29 | 1.28 | 8.22  | 59.8 | 11.5 | 24556 | 648  | 33.2 | 57.8 | 60.4 | 66.6 | 23482 |
| Max    | 8.89 | 10.5 | 36.2  | 230  | 870  | 62800 | 3688 | 274  | 318  | 149  | 1095 | 95848 |
| Mean   | 1.42 | 4.82 | 21.97 | 113  | 78.5 | 44177 | 1399 | 77.8 | 132  | 111  | 353  | 57110 |
| SD     | 1.44 | 2.08 | 6.63  | 41.0 | 141  | 7200  | 556  | 58.5 | 51.0 | 18.4 | 232  | 17544 |
| Median | 0.80 | 4.69 | 21.5  | 102  | 47.9 | 45780 | 1352 | 46.3 | 124  | 111  | 330  | 57781 |

*Pollution load index (PLI)*

Supplementary Table 1 presents the PLI values of the studied elements. When the PLI > 1, it means that pollution exists; otherwise, if the PLI < 1, there is no metal

pollution (Varol 2011). The PLI values varied from 1.4 to 4.27 for the investigated sediments, suggesting that pollution exists. The highest PLI values were observed in the following sediments: Ibar, Pek, West Morava and Great Morava and these river systems are significantly polluted.



**Table 4** Comparison between background values for elements given by other authors and calculated for the investigated river sediment ( $\text{mg kg}^{-1}$ )

| Element | Barreiro <sup>a</sup> | Continental crust <sup>b</sup> | Ría de Vigo <sup>c</sup> | Tisa River (Serbia) <sup>d</sup> | River sediment <sup>e</sup> | PEL   |
|---------|-----------------------|--------------------------------|--------------------------|----------------------------------|-----------------------------|-------|
| Cd      | nd <sup>f</sup>       | 0.1                            | nd                       | nd                               | 1.28                        | 3.53  |
| Co      | 16                    | 24                             | 11.66                    | nd                               | 8.22                        | nd    |
| Cr      | 43                    | 126                            | 34.04                    | 11.37                            | 62.13                       | 90.0  |
| Cu      | 25                    | 25                             | 29.41                    | 41.97                            | 11.50                       | 197.0 |
| Fe      | 2.69                  | 43,200                         | 3.51                     | nd                               | 24,555.8                    | nd    |
| Mn      | 225                   | 716                            | 244.33                   | nd                               | 647.8                       | nd    |
| Pb      | 25                    | 14.8                           | 51.29                    | 19.3                             | 57.79                       | 91.3  |
| Ni      | 30                    | 56                             | 30.32                    | 42.27                            | 34.69                       | 36    |
| Zn      | 100                   | 65                             | 105.35                   | 127.3                            | 66.65                       | 315   |
| V       | nd                    | 98                             | nd                       | nd                               | 60.43                       | nd    |
| Al      | nd                    | 79,600                         | nd                       | nd                               | 36,323.4                    | nd    |
| As      | nd                    | 1.7                            | nd                       | nd                               | nd                          | 17    |

PEL—Probable effect level-above which harmful effects are likely to be observed (Smith et al. 1996; MacDonald et al. 2000)

<sup>a</sup> Background values of trace elements for Ría de Vigo (Barreiro) (Rubio et al. 2000)

<sup>b</sup> Element content in Continental crust (Wedepohl 1995)

<sup>c</sup> Background values for Ría de Vigo (Rubio et al. 2000)

<sup>d</sup> Background values for the Tisa river (Sakan et al. 2009)

<sup>e</sup> Background values in the studied sediments

<sup>f</sup> No data

**Table 5** Grades of enrichment factor, index of geoaccumulation, and modified degree of contamination

| Enrichment factor (EF) |                    | Index of geoaccumulation ( $I_{\text{geo}}$ ) |  | Modified degree of contamination ( $mC_d$ ) |                    |
|------------------------|--------------------|---|--|---|--------------------|
| Value                  | Pollution category | Value   | Pollution category                           | Value                                       | Pollution category |
| $EF < 1$               | No enrichment      | $I_{\text{geo}} < 0$                          | uncontaminated/unpolluted ( <i>class 0</i> ) | $mC_d < 1.5$                                | Nil/very low       |
| $1 \leq EF \leq 3$     | Minor              | $0 \leq I_{\text{geo}} < 1$                   | unpolluted/moderately ( <i>class 1</i> )     | $1.5 \leq mC_d < 2$                         | Low                |
| $3 \leq EF \leq 5$     | Moderate           | $1 \leq I_{\text{geo}} < 2$                   | moderately ( <i>class 2</i> )                | $2 \leq mC_d < 4$                           | Moderate           |
| $5 \leq EF \leq 10$    | Moderately severe  | $2 \leq I_{\text{geo}} < 3$                   | moderately/<br>heavily ( <i>class 3</i> )    | $4 \leq mC_d < 8$                           | High               |
| $10 \leq EF \leq 25$   | Severe             | $3 \leq I_{\text{geo}} < 4$                   | heavily ( <i>class 4</i> )                   | $8 \leq mC_d < 16$                          | Very high          |
| $25 \leq EF \leq 50$   | Very severe        | $4 \leq I_{\text{geo}} < 5$                   | heavily/extremely<br>( <i>class 5</i> )      | $16 \leq mC_d < 32$                         | Extremely high     |
| $EF > 50$              | Extremely severe   | $I_{\text{geo}} \geq 5$                       | extremely ( <i>class 6</i> )                 | $mC_d \geq 32$                              | Ultra high         |

### Combined pollution index (CPI)

The CPI values are shown in Supplementary Table 4. When the  $CPI < 1$ , the sediment is unpolluted; when the  $CPI \geq 1$ , the sediment is contaminated by heavy metals (Hui-na et al. 2012; Jian-Min et al. 2007). The CPI values range from 1.65 to 10.19, which indicates that the investigated sediments are contaminated with the studied trace elements. A more detailed discussion will be presented through a discussion of the  $mC_d$ , considering that these two factors are calculated in the same manner.

### Modified degree of contamination ( $mC_d$ )

The  $mC_d$  is based on integrating and averaging all the available analytical data for a set of sediment samples. Based on the values of the  $mC_d$  factors (Supplementary Table 4), it is possible to distinguish differing levels of metal contamination (Table 5). The  $mC_d$  values for the investigated sediments generally lie in the range 1.65–10.19. Using the classification system proposed for this parameter, the overall range of  $mC_d$  values indicates a low to very high degree of contamination. The  $mC_d$  data

**Table 6** Grades of ecological risk factor, contamination factor, and ecological risk index

| Ecological risk factor (Er) |               | Contamination factor (CF) |                            | Ecological risk index (RI) |               |
|-----------------------------|---------------|---------------------------|----------------------------|----------------------------|---------------|
| Value                       | Risk category | Value                     | Pollution category         | Value                      | Risk category |
| Er < 40                     | Low           | CF < 1                    | No metal enrichment        | RI < 150                   | Low risk      |
| 40 ≤ Er < 80                | Moderate      | 1 ≤ CF ≤ 3                | Moderately contamination   | 150 ≤ RI < 300             | Moderate      |
| 80 ≤ Er < 160               | Considerable  | 3 ≤ CF ≤ 6                | Considerable contamination | 300 ≤ RI < 600             | Considerable  |
| 160 ≤ Er < 320              | High          | CF > 6                    | Very high contamination    | RI ≥ 600                   | Very high     |
| Er ≥ 320                    | Very high     | – <sup>a</sup>            | –                          | –                          | –             |

<sup>a</sup> No data

**Table 7** CF, EF, Igeo, Er and TU values of elements in sediment samples

|      | As    | Cd    | Co   | Cr    | Cu    | Fe   | Mn   | Ni    | Pb    | V    | Zn    |
|------|-------|-------|------|-------|-------|------|------|-------|-------|------|-------|
| CF   |       |       |      |       |       |      |      |       |       |      |       |
| Min  | 0.26  | 1.66  | 1.22 | 0.96  | 1.92  | 1.35 | 1.13 | 0.96  | 1.34  | 1.19 | 1.71  |
| Max  | 8.08  | 8.23  | 4.40 | 3.71  | 75.67 | 2.56 | 5.69 | 7.89  | 5.51  | 2.47 | 16.43 |
| Mean | 1.30  | 3.84  | 2.72 | 1.84  | 7.00  | 1.82 | 2.19 | 2.28  | 2.33  | 1.86 | 5.42  |
| SD   | 1.63  | 1.57  | 0.76 | 0.65  | 12.4  | 0.26 | 0.85 | 1.70  | 0.86  | 0.27 | 3.45  |
| EF   |       |       |      |       |       |      |      |       |       |      |       |
| Min  | 0.22  | 0.68  | 0.81 | 0.49  | 0.84  | 0.66 | 0.65 | 0.42  | 0.80  | 0.72 | 0.96  |
| Max  | 8.04  | 8.18  | 4.79 | 3.35  | 35.03 | 2.75 | 3.99 | 4.84  | 5.48  | 2.63 | 14.13 |
| Mean | 0.90  | 2.77  | 1.90 | 1.29  | 4.37  | 1.27 | 1.53 | 1.58  | 1.62  | 1.29 | 3.78  |
| SD   | 1.42  | 1.78  | 0.90 | 0.65  | 5.84  | 0.50 | 0.81 | 1.20  | 0.93  | 0.50 | 2.82  |
| Igeo |       |       |      |       |       |      |      |       |       |      |       |
| Min  | <0    | 0.10  | <0   | <0    | 0.25  | <0   | <0   | <0    | <0    | <0   | 0.13  |
| Max  | 1.68  | 1.70  | 1.08 | 0.20  | 3.92  | 0.53 | 1.33 | 1.66  | 1.30  | 0.50 | 2.39  |
| Mean | 0.84  | 0.86  | 0.60 | 0.18  | 1.15  | 0.22 | 0.42 | 0.80  | 0.43  | 0.24 | 1.14  |
| SD   | 0.60  | 0.42  | 0.25 | 0.03  | 0.68  | 0.12 | 0.28 | 0.45  | 0.29  | 0.12 | 0.53  |
| Er   |       |       |      |       |       |      |      |       |       |      |       |
| Min  | 2.60  | 49.80 | –    | 1.92  | 9.60  | –    | –    | 4.80  | 6.70  | –    | 1.71  |
| Max  | 80.80 | 247   | –    | 7.42  | 378   | –    | –    | 39.45 | 27.55 | –    | 16.43 |
| Mean | 12.99 | 115   | –    | 3.68  | 34.99 | –    | –    | 11.39 | 11.64 | –    | 5.42  |
| SD   | 16.35 | 47.19 | –    | 1.31  | 62.01 | –    | –    | 8.49  | 4.33  | –    | 3.45  |
| TU   |       |       |      |       |       |      |      |       |       |      |       |
| Min  | 0.02  | 0.60  | –    | 0.66  | 0.11  | –    | –    | 0.92  | 0.85  | –    | 0.36  |
| Max  | 0.52  | 2.98  | –    | 2.56  | 4.42  | –    | –    | 7.60  | 3.49  | –    | 3.48  |
| Mean | 0.085 | 1.394 | –    | 1.272 | 0.408 | –    | –    | 2.196 | 1.473 | –    | 1.145 |
| SD   | 0.106 | 0.569 | –    | 0.452 | 0.725 | –    | –    | 1.636 | 0.548 | –    | 0.731 |

indicate a significant anthropogenic impact in sediment from the Pek, Ibar and West Morava Rivers. The mC<sub>d</sub> values in the Danube sediments indicate a low degree of contamination, whilst in other mC<sub>d</sub> sediment values indicate a moderate degree of contamination.

*Ecological toxicity (TU)*

Figure 3 shows the TU value for each metal and the sum of the TU values of all the trace elements in the

investigated sediments. The PEL values used for calculating the TU in this paper are shown in Table 4. The average trace element TU at the investigated localities followed the order: Ni > Pb > Cd > Cr > Zn > Cu > As. Based on the mean value of ΣTU, it can be concluded that potential toxicity existed for the quoted elements. All the values were higher than 4. From the toxic unit values, stations I1 and I2 (Ibar), Z2 (West Morava), V2 (Great Morava 2) and Pe (Pek) are more polluted compared to the others (ΣTU > 10).

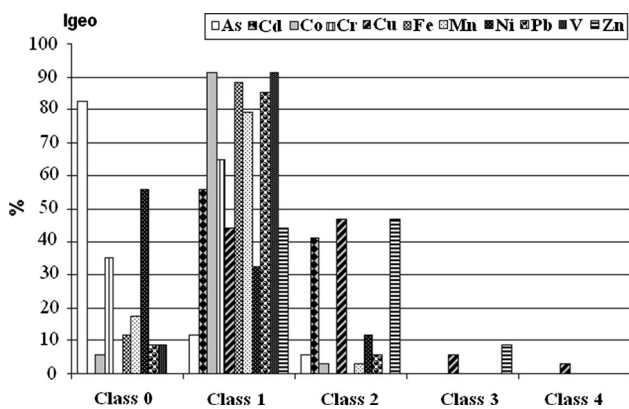


**Fig. 2** Index of geoaccumulation (*Igeo*) of analysed elements in the sediments

**Table 8** The average values of RI, PLI, CPI, mCd and TU in sediment samples

|      | RI    | PLI  | CPI   | mCd   | TU    |
|------|-------|------|-------|-------|-------|
| Min  | 87.29 | 1.40 | 1.65  | 1.65  | 4.07  |
| Max  | 575   | 4.27 | 10.19 | 10.19 | 19.46 |
| Mean | 195   | 2.37 | 2.96  | 2.96  | 7.974 |
| SD   | 97.03 | 0.64 | 1.50  | 1.50  | 3.486 |

Trace elements and sample site grouping using principal component analysis (PCA) and hierarchical cluster analysis (HCA)

**PCA**

A PCA with Varimax normalised rotation was performed in this research. The scores and loadings of the principal components are presented in Table 9 and Fig. 4. PC1, explaining 60.86 % of the total variance, has strong positive loadings for Fe, Mn, Co, Cr, V, Pb, Cd, and Ni. PC2, explaining 15.67 % of the total variance, has strong

loadings for As, Pb, Zn, Cd and Ni. PC3, explaining 10.58 % of the total variance, has a strong positive loading on Cu.

Figure 5 displays isolated three groups of samples: 20 (I1), 21 (I2), 23 (V2) and 25 (Z2)—first group, 33 (Pe)—second group, and the other sediment samples constitute the third group. With regard to PCA (Q mode), sampling site 33 (Pek river) has the most polluted river sediments at the investigated localities. The contribution of Cu to the overall pollution is the most significant compared to other elements in this sediment. In the group with samples 20, 21, 23 and 25, the sediment with significant pollution is compared to other moderately polluted studied sediments.

**HCA**

Hierarchical cluster analysis (HCA) was performed on the dataset on both variables (R mode) and samples (Q mode), to identify clusters of elements and sites. The hierarchical methods are used because they are not limited to pre-determined numbers of clusters and can display the similarity of samples across a wide range of scales.

The results of the CA (R mode) are shown in a dendrogram (Fig. 6) where all the elements were grouped into four significant clusters: cluster 1 includes Fe, V, Co, Cr and Mn; cluster 2 contains Pb, Zn, Cd, and Ni, cluster 3 contains Cu, and cluster 4 contains As.

The results of the spatial cluster analysis (Q mode) are shown in a dendrogram (Fig. 7), where all 34 river sediment sampling sites were grouped into four significant clusters: Cluster 1 (T2–T9, V1, D1, D3–D6, Ta, JM, N1, and N2, CPI mean is 2.50, TU mean is 6.26), Cluster 2 (V2, Ko, Z2, S1–S4, Tr, To, Z1, Pr, T1, and D2, CPI mean is

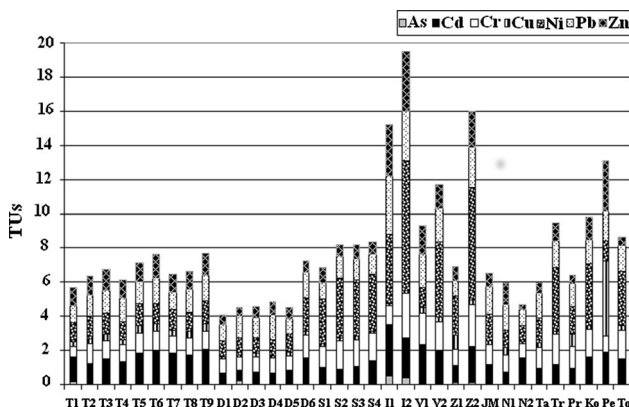


**Fig. 3** The TU of each element and the sum of TUs of elements in the investigated sediments

**Table 9** Loadings of experimental variables on significant principal components for the river sediments in Serbia

|                       | PC1    | PC2    | PC3    |
|-----------------------|--------|--------|--------|
| As                    |        | 0.906  |        |
| Fe                    | 0.933  |        |        |
| Mn                    | 0.778  |        |        |
| Co                    | 0.933  |        |        |
| Cr                    | 0.862  |        |        |
| Pb                    | 0.590  | 0.720  |        |
| Zn                    |        | 0.774  |        |
| Cd                    | 0.596  | 0.624  |        |
| Ni                    | 0.579  | 0.630  |        |
| Cu                    |        |        | 0.893  |
| V                     | 0.911  |        |        |
| Eigenvalue            | 6.694  | 1.724  | 1.164  |
| % Total variance      | 60.855 | 15.669 | 10.578 |
| Cumulative % variance | 60.855 | 76.525 | 87.103 |

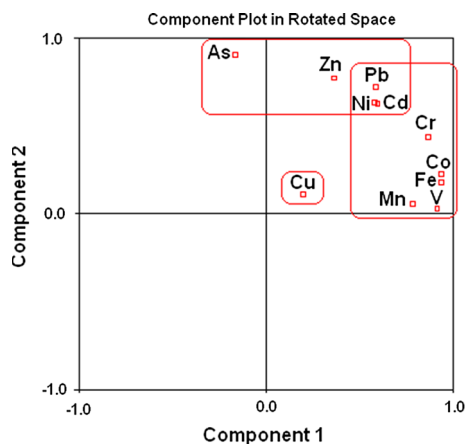


Fig. 4 PCA of selected elements (R mode)

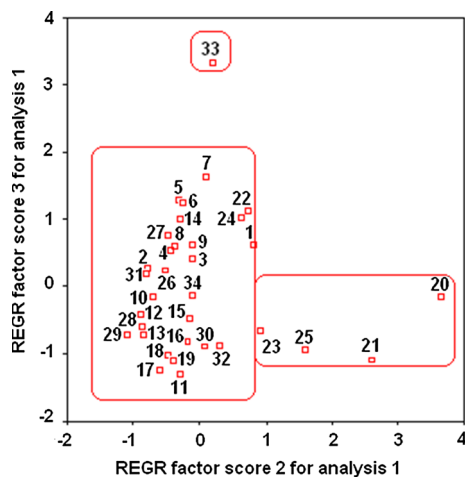


Fig. 5 PCA of selected elements (Q mode). Explanation: 1–9 (Tisa), 10–15 (Danube), 16–19 (Sava), 20, 21 (Ibar), 22, 23 (Great Morava), 24, 25 (West Morava), 26 (Južna Morava), 27, 28 (Nišava), 29 (Tamiš), 30 (Topčiderska River), 31 (Porečka River), 32 (Kolubara), 33 (Pek), 34 (Toplica)

2.75, TU mean is 8.52), Cluster 3 (I1 and I2, CPI is 4.94 and TU mean is 17.35) and Cluster 4 (Pe, CPI is 10.18 and TU mean is 13.06). The sampling sites in Clusters 1, 2 and 3 represented sediments from relatively to moderate polluted regions. Cluster 4 site (river Pek) was located in high-pollution region.

The HCA results were similar to those obtained with PCA. Elements with similar origins are (1) Fe, V, Mn, Co and Cr; (2) Pb, Zn, Cd, As and Ni; and (3) Cu. It is observed that the sources of Cu are different from the other elements.

Fe, V, Mn, Co and Cr have a combined source and these elements are derived from both lithogenic and anthropogenic sources. Iron is abundant in the Earth’s crust, though the pollution indices suggest the existence of anthropogenic sources of this element at some localities. Also, enrichment is observed for Mn in some of sediments. Cr is

Dendrogram using Average Linkage (Between Groups)

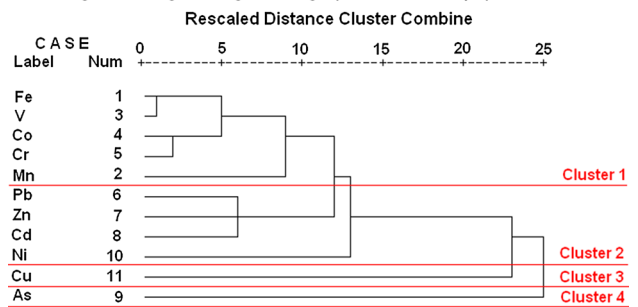


Fig. 6 Dendrogram showing clustering of the analysed elements

Dendrogram using Average Linkage (Between Groups)

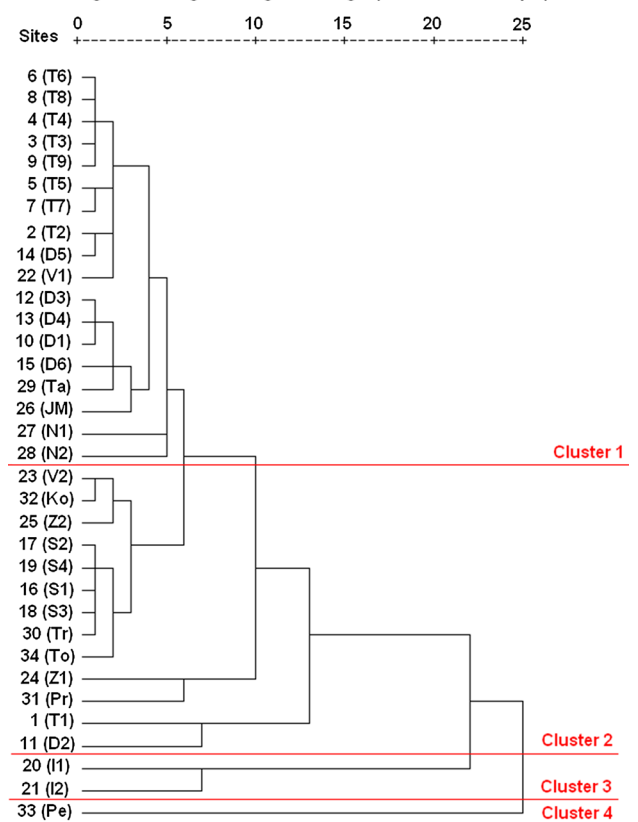


Fig. 7 Dendrogram showing clustering of sampling sites (HCA, Q mode)

generally a marker of the paint and metal industries, V is greatly impacted by anthropogenic activities such as mining and agricultural processes, and Co is mainly from anthropogenic signatures, i.e., paint, fertiliser or agrochemical industries (Li and Zhang, 2010). The low content of V, Co and Cr in the investigated sediments and the values of the calculated pollution indices, which indicate insignificant pollution, confirmed the mixed sources of Fe, V, Mn, Co and Cr at the studied locality.

Pb, Zn, Cd, As and Ni are likely to be mainly derived from anthropogenic sources. The significant anthropogenic

source of these elements is mining and smelting complexes in Serbia. These results are in accordance with Bird et al. (2010) that throughout the River Danube drainage basin, the mining and processing of metal ores lead to point-source releases of contaminant metals (Cd, Cu, Pb, Zn) and As to the local surface drainage network. The Trepca mining complex is the dominant source of lead and zinc. In addition to mining, anthropogenic sources of these elements may be direct discharges from local point sources, such as industrial and urban discharges carrying metal and metalloid contaminants. Contaminants mainly come from metallurgy and coal burning. Fertiliser and pesticides containing As can also lead to an increase in As. Ni is also mainly derived from anthropogenic activities, especially industrial sources (Gao et al. 2013).

Cu is derived from anthropogenic sources, most significantly from metallic wastewater discharges. The significant anthropogenic source of Cu is the open-pit mine in Majdanpek. Another source of Cu may be discharges from industries, as well as agricultural activities.

The obtained results indicate that the most polluted sediments at the studied localities are sediments from the Ibar and the Pek Rivers. Additionally, calculated indices suggest that the Great Morava and West Morava are also significantly polluted river systems. Pollution of these rivers is mainly caused by permanent and accidental pollution from industrial plants and mines that are located in the basins of these rivers.

One of the main sources of industrial pollution of the River Ibar is likely to be the Trepca mining complex. This huge industrial mining site had been in operation and engaged in large-scale exploitation since 1925. Since then, and until the year 2000, lead and zinc have been mined and smelted and the tailings still threaten the environment and keep polluting the Ibar (Pedersen and Klitgaard 2004). Results of Rexhepi et al. (2010) are shown that high zinc, lead and copper content in the sediment of Ibar River suggests that the lead and zinc smelter in Mitrovica still discharges strongly polluted effluents into this stream and that the high metal content could also reflect the accumulation of fine, strongly polluted particles in the river bed for a fairly long time.

The significant pollution with Cu of sediments from the Pek River is probably due to discharge from the Cu mining complex in Majdanpek. Bird et al. (2010) have shown that metal mining in Serbia is focused on the Bor and Majdanpek Cu deposits. The copper ore treatment process produced large amounts of ore waste and flotation tailing heaps, located in the vicinity of the towns of Bor and Majdanpek. In addition to permanent pollution, accidental pollution significantly affects the pollution of the Pek. The most serious incidents listed are the breaches of tailing dams at Majdanpek and Veliki Majdan causing direct,

serious contamination of the river Pek by heavy metals (Stuhlberger 2014).

In general, the results obtained using multivariate statistical analysis are consistent with that obtained using the calculation of pollution indices. Sediments in rivers in the same statistical grouping appear to indicate the same source of pollution and a similar degree of contamination. The applied methods can classify sediments in the whole investigated region according to the degree of pollution and to identify the main sources of toxic elements. The combined application of PCA and pollution indices can effectively identify the comprehensive and single pollution levels of elements in sediments, thus important to the extent determination of heavy metals pollution around the world.

## Conclusion

The impact of trace element pollution on the quality of the river sediments in Serbia was evaluated using CF, EF, Igeo, Er, RI, PLI, CPI,  $mC_d$ , and TU. The source identification carried out using multivariate analyses (PCA and CA) shows that (1) Fe, V, Mn, Co and Cr are derived from lithogenic and anthropogenic sources, (2) Pb, Zn, Cd, As and Ni are mainly derived from anthropogenic sources, and (3) Cu is derived from anthropogenic sources, most significantly from metallic wastewater discharges.

Contamination was observed in the studied elements, most of all with Zn, Cu and Cd. Cd and Cu present a higher ecological risk than any other element because of their higher toxicity coefficient. The potential Er varied amongst the studied elements in the sediments as well as in the different areas. The values of the PLI and  $mC_d$  suggest that the degree of contamination ranges from low to very high. The highest values of the pollution indices suggest a significant contribution of elements from anthropogenic sources in the river sediments from the Ibar, Pek, West Morava and Great Morava. Significant pollution indexes are also observed in the Tisa and Sava rivers. Pollution of these rivers is mainly caused by permanent and accidental pollution from industrial plants and mines that are located in the basins of these rivers. Significant influences are evident from mining complexes (mainly in Trepca and Majdanpek) on river contamination with toxic trace elements.

The above results confirmed the existence of pollution with trace elements in the studied river sediments. The calculated pollution indices and the appliance of statistical methods are recognised as useful for improving ecological risk assessment and the management of trace elements in sediments. A future fractionation sediment study is recommended to determine the proportion of the total metal pool that might be bioavailable.

**Acknowledgments** This study was supported by the Ministry of Education, Science and Technological Development of Serbia, Grant Nos. 172001 and 43007. In addition, we would like to thank the Republic Hydrometeorological Service of Serbia for the sediment samples.

**References**

Abraham GMS, Parker PJ (2008) Assessment of heavy metal enrichment factors and the degree of contamination in marine sediment from Tamaki Estuary, Auckland, New Zealand. *Environ Monit Assess* 136:227–238

Acevedo-Figueroa D, Jiménez BD, Rodríguez-Sierra CJ (2006) Trace metals in sediments of two estuarine lagoons from Puerto Rico. *Environ Pollut* 141:336–342

Adriano DC, Németh T, Györi Z (2003) Natural attenuation of metals along the Tisza River–Floodplain–Wetlands Continuum, University of Debrecen, Centre of Agricultural Sciences, Hungary

Behra R, Landwehrjohann R, Vogel K, Wagner B, Sigg L (2002) Copper and zinc content of periphyton from two rivers as a function of dissolved metal concentration. *Aquat Sci* 64:300–306

Bird GH, Brewer PA, Macklin MG (2010) Management of the Danube drainage basin: implications of contaminant-metal dispersal for the implementation of the EU Water Framework Directive. *Intl J River Basin Manag* 8:63–78

Caeiro S, Costa MH, Ramos TB, Fernandes F, Silveira N, Coimbra A, Medeiros G, Painho M (2005) Assessing heavy metal contamination in Sado Estuary Sediment: an index analysis approach. *Ecol Indic* 5:151–169

CCME (1995) Protocol for the derivation of Canadian sediment quality guidelines for the protection of aquatic life. Canadian Council of Ministers for the Environment, Report CCME EPC-98E

Chabukdhara M, Nema AK (2012) Assessment of heavy metal contamination in Hindon River sediments: a chemometric and geochemical approach. *Chemosphere* 87:945–953

Chang CY, Wang CF, Mui DT, Chiang HL (2009) Application of methods (sequential extraction procedures and high-pressure digestion method) to fly ash particles to determine the element constituents: a case study for BCR 176. *J Hazard Mater* 163:578–587

Gao H, Bai J, Xiao R, Liu P, Jiang W, Wang J (2013) Levels, sources and risk assessment of trace elements in wetland soils of a typical shallow freshwater lake, China. *Stoch Env Res Risk A* 27:275–284

Hakanson L (1980) Ecological risk index for aquatic pollution control, a sedimentological approach. *Water Res* 14:975–1001

Harikumar PS, Nasir UP, Mujeebu Rahman MP (2009) Distribution of heavy metals in the core sediments of a tropical wetland system. *Int J Environ Sci Tech* 6:225–232

Hu X, Wang C, Zou L (2011) Characteristic of heavy metals and Pb isotopic signatures in sediments cores collected from typical urban shallow lakes in Nanjing, China. *J Environ Manag* 92:742–748

Hui-na Z, Xing-zhong Y, Guang-ming Z, Min J, Jie L, Chang Z, Juan Y, Hua-jun H, Zhi-feng L, Hong-wei J (2012) Ecological risk assessment of heavy metals in sediments of Xiawan Port based on modified potential ecological risk index. *T Nonferr Met Soc* 22:1470–1477

Iqbal J, Tirmizi SA, Shah MH (2013) Statistical apportionment and risk assessment of selected metals in sediments from Rawal lake (Pakistan). *Environ Monit Assess* 185:729–743

Jamshidi-Zanjani A, Saeedi M (2013) Metal pollution assessment and multivariate analysis in sediment of Anzali international wetland. *Environ Earth Sci* 70:1791–1808

Jian-Min Z, Zhi D, Mei-Fang C, Cong-Qiang L (2007) Soil heavy metal pollution around the Dabaoshan mine, Guangdong province, China. *Pedosphere* 17:588–594

Kabir I, Lee H, Kim G, Jun T (2011) Correlation assessment and monitoring of the potential pollutants in the surface sediments of Pyeongchang River. *Int J Sedim Res* 26:152–162

Kalantzi I, Shimmied TM, Pergantis SA, Papageorgiou N, Black KD, Karakassis I (2013) Heavy metals, trace elements and sediment geochemistry at four Mediterranean fish farms. *Sci Total Environ* 444:128–137

Li S, Zhang Q (2010) Spatial characterization of dissolved trace elements and heavy metals in the upper han river (China) using multivariate statistical techniques. *J Hazard Mater* 176:579–588

Lin CE, Chen CT, Kao CM, Hong A, Wu CY (2011) Development of the sediment and water quality management strategies for the salt-water river. *Taiwan Mar Pollut Bull* 63(5–12):528–534

MacDonald DD, Ingersoll CG, Berger TA (2000) Development and evaluation of consensus-based sediment quality guidelines for freshwater ecosystems. *Arch Environ Contam Toxicol* 39:20–31

Mendiola L, Dominguez MCD, Sandoval MRG (2008) Environmental assessment of and active tailings pile in the State of Mexico (Central Mexico). *Res J Environ Sci* 2:197–208

Mohiuddin KM, Otomo K, Ogawa Y, Shikazono N (2012) Seasonal and spatial distribution of trace elements in the water and sediments of the Tsurumi river in Japan. *Environ Monit Assess* 184:265–279

Müller G (1979) Schwermetalle in den Sedimenten des Rheins-Veränderungen seit 1971. *Umschau* 79:778–783

Nam SH, Kim MJ, Park YI, Lee SJ (2001) A study on various pretreatment and preparation for the determination of inorganic elements in sediment. *Anal Sci* 17:a263–a265

Pedersen F, Bjørnstad E, Andersen HV, Kjøl HJ, Poll C (1998) Characterization of sediments from Copenhagen harbour by use of biotests. *Water Sci Technol* 37:233–240

Pedersen EK, Klitgaard R (2004) Environmental management in Kosovo, Heavy metal emission from Trepca. TekSam (Institut for Miljo, YTeknologi og Samfund)

Pekey H, Karakaş D, Ayberk S, Tolun L, Bakoğlu M (2004) Ecological risk assessment using trace elements from surface sediments of Izmit Bay (Northeastern Marmara Sea) Turkey. *Mar Pollut Bull* 48:946–953

Relić D, Đorđević D, Popović A, Jadranić M, Polić P (2010) Fractionation and potential mobility of trace metals in Danube alluvial aquifer within an industrialized zone. *Environ Monit Assess* 171:229–248

Relić D, Đorđević D, Popović A (2011) Assessment of the pseudo total metal content in alluvial sediments from Danube River, Serbia. *Environ Earth Sci* 63:1303–1317

Rexhepi F, Rugova A, Arbneshi T (2010) Assessment of heavy metal pollution in Ibër river sediment, Kosova. Balowis, Ohrid, Republic of Macedonia

Rönkkömäki H, Pöykiö R, Nurmesniemi H, Popov K, Merisalu E, Tuomi T, Välimäki I (2008) Particle size distribution and dissolution properties of metals in cyclone fly ash. *Int J Environ Sci Te* 5:485–494

Rubio B, Nombela MA, Vilas F (2000) Geochemistry of major and trace elements in sediments of the Ria de Vigo (NW Spain): an assessment of metal pollution. *Mar Pollut Bull* 40:968–980

Sakan SM, Đorđević DS, Manojlović DD, Polić PS (2009) Assessment of heavy metal pollutants accumulation in the Tisza river sediments. *J Environ Manag* 90:3382–3390

Sakan SM, Đorđević DS, Dević G, Relić D, Anđelković I, Đuričić J (2011) A study of trace element contamination in river sediments

- in Serbia using microwave-assisted aqua regia digestion and multivariate statistical analysis. *Microchem J* 99:492–502
- Sakan S, Dević G, Relić D, Anđelković I, Sakan N, Đorđević D (2014) Evaluation of sediment contamination with heavy metals: the importance of determining appropriate background content and suitable element for normalization. *Environ Geochem Health*. doi:10.1007/s10653-014-9633-4
- Smith SL, MacDonald DD, Keenleyside KA, Ingersoll CG, Field LJ (1996) A preliminary evaluation of sediment quality assessment values for freshwater ecosystems. *J Gt Lakes Res* 22:624–638
- Stuhlberger C (2014) Mining and environment in the western balkans, C. Stuhlberger, produced by zoi environment network ([http://www.unep.org/pdf/MiningBalkans\\_screen.pdf](http://www.unep.org/pdf/MiningBalkans_screen.pdf))
- Tockner K, Robinson C, Uehlinger U (2009) Rivers of Europe (in press)
- Tomlinson DC, Wilson JG, Harris CR, Jeffrey DW (1980) Problems in the assessment of heavy-metal levels in estuaries and the formation of a pollution index. *Helgol Mar Res* 33:566–575
- Varol M (2011) Assessment of heavy metal contamination in sediments of the Tigris river (Turkey) using pollution indices and multivariate statistical techniques. *J Hazard Mater* 195:355–364
- Wang L, Wang Y, Wenzao Z, Xu C, An Z (2014) Multivariate statistical techniques for evaluating and identifying the environmental significance of heavy metal contamination in sediments of the Yangtze River, China. *Environ Earth Sci* 71:1183–1193
- Wedepohl KH (1995) The composition of the continental crust. *Geochim Cosmochim Acta* 59:1217–1232
- Wong CSC, Li X, Thornton I (2006) Urban environmental geochemistry of trace metals. *Environ Pollut* 142:1–16
- Yang Z, Wang Y, Shen Z, Niu J, Tang Z (2009) Distribution and speciation of heavy metals in sediments from the mainstream, tributaries, and lakes of the Yangtze river catchment of Wuhan, China. *J Hazard Mater* 166:1186–1194
- Zhang M, Cui L, Sheng L, Wang Y (2009) Distribution and enrichment of heavy metals among sediments, water body and plants in Hengshuihu Wetland of Northern China. *Ecol Eng* 35:563–569



# CLEAN

## Soil Air Water

Renewables

Sustainability

Environmental Monitoring





Sanja M. Sakan<sup>1</sup>  
Gordana J. Dević<sup>1</sup>  
Dubravka J. Relić<sup>2</sup>  
Ivan B. Andelković<sup>3</sup>  
Nenad M. Sakan<sup>4</sup>  
Dragana S. Dorđević<sup>1</sup>

## Research Paper

# Environmental Assessment of Heavy Metal Pollution in Freshwater Sediment, Serbia

<sup>1</sup>ICTM, Center for Chemistry,  
University of Belgrade, Belgrade,  
Serbia

<sup>2</sup>Faculty of Chemistry, Applied  
Chemistry, University of Belgrade,  
Belgrade, Serbia

<sup>3</sup>Innovation Center of the Faculty of  
Chemistry, Belgrade, Serbia

<sup>4</sup>Institute of Physics, University of  
Belgrade, Belgrade, Serbia

The purpose of this study was to evaluate sediment heavy metals (Cd, Cu, Co, Mn, Cr, Ni, Pb and Zn) related to pollution in freshwater sediments in Serbia. The heavy metal enrichment determination in studied sediments was conducted by using total metal content with strong acidic digestion (HCl + HNO<sub>3</sub> + HF), a calculated enrichment factor (EF), and application of correlation analysis and the box plot method. For identification of appropriate elemental normalisers for enrichment factor calculations, Fe, Al, Ti and Si were used. The significant variation in heavy metal distribution among samples collected in this large region, encompassing all Serbian watersheds, suggests the selective contamination of sediments by heavy metals. Values for EF indicate nil to moderate enrichment for most studied elements, except for Cd, Cu, and Zn at some sampling points, where the enrichment was, in some cases, even severe. The high content of heavy metals and EFs in Serbia is related to the human activities around the sampling sites. The results indicate that all elements used for normalisation in this paper can also be used to estimate the anthropogenic influence, with an exception of Co, which should be considered as an element for normalisation in future studies.

**Keywords:** Anthropogenic input; Enrichment factor; Normalisers; Statistical analysis

*Received:* April 8, 2014; *revised:* July 24, 2014; *accepted:* August 16, 2014

**DOI:** 10.1002/clen.201400275

## 1 Introduction

The investigation of heavy metal pollution in water and sediments of lakes and rivers has gained an increased attention of many environmental researchers over the past few decades [1]. Potentially hazardous trace elements, often in literature referred to as “heavy metals”, are deemed serious pollutants due to their toxicity, persistence and non-degradability in the environment [2]. Pollution with these contaminants poses a worldwide environmental threat [3].

Heavy metals are natural constituents of sediments. They are derived from rocks and soils by erosion, transport and deposition. They can also be derived from anthropogenic sources, in which case they are incorporated into sediments as artificial pollutants from industrial or urban releases and wastes [4]. Then, sediments act as environmental archives that indicate the timeline of an aquatic environmental contamination [5]. While heavy metals may be transferred from water to sediments through settling of particles, their remobilization may occur via aquatic biota [6] as well as with changes in environmental conditions.

The evaluation of the pollution status of river bed sediments is a complex task with a series of difficulties in its application (climate/seasonal change, depth size, etc.). The bed sediments are highly influenced by geology, so, they present a strong local influence

which impedes a standardization of what should be defined as “non-contaminated sediments”. In the assessment of heavy metal sediment pollution, one major problem is the choice of data analysis methods [7]. Different methods and pollution criteria are applied in pollution assessment: fractionation and determination of heavy metals speciation [8–11], statistical analysis [3, 11–15], geochemical normalisation and pollution indices [3, 5–7, 12, 13, 16–18]. Geochemical normalisation with conservative elements has been effectively used for assessing the enrichment of metal pollutants and distinguishing their natural and anthropogenic sources. Different research sources recommend the use of Fe, Li, Al and Si. Since it is difficult to identify the proportion of natural and anthropogenic sources of heavy metals, in enrichment assessment it is important to determine suitable elements for normalisation.

Over the last decades in Europe, the rapid economic development and land exploitation changes have resulted in a large impact on the environment, especially on rivers. Therefore, European countries have a wide range of pollution problems. Several hot spots with severe freshwater pollution and sediment contamination (mostly heavy metals, polyaromatic hydrocarbons and polychlorinated biphenyls) have been isolated in Serbia, as the consequence of outdated environmental legislation, negligible quantity of properly treated wastewater and accidental spills [19]. Data and publications on element pollution in Serbia are still limited [20]. Despite several studies carried out to evaluate the quality of sediments in some locations in Serbia [19, 20], only few studies are pertinent to the freshwater sediments of the entire Serbia region. Therefore, in this paper were determined and quantified contents of Cd, Cu, Co, Mn, Cr, Ni, Pb and Zn in river sediments of the country. The main objectives of the study are: (i) to present the total concentrations of

**Correspondence:** Dr S. M. Sakan, ICTM, Center for Chemistry, University of Belgrade, Njegoševa 12, Belgrade 11000, Serbia.  
E-mail: ssakan@chem.bg.ac.rs

**Abbreviations:** EF, enrichment factor; MAQ, maximum allowed quantity

studied elements; (ii) to select the appropriate normaliser for estimating the heavy metal enrichment; and (iii) to identify the anthropogenic and natural sources of trace metals by statistical analyses and enrichment factor (EF) calculation.

## 2 Materials and Methods

### 2.1 Sampling

This study considers heavy metal concentrations in bottom sediment samples collected from major rivers in Serbia. The set of 35 samples of 15 river sediments in Serbia was taken during 2008: the Danube (Black Sea watershed), the Sava (Danube watershed), the Tisa (Danube watershed), the Ibar (West Morava watershed), the Great Morava (Danube watershed), the West Morava (Great Morava watershed), the South Morava (Great Morava watershed), the Nišava (South Morava watershed), the Tamiš (Danube watershed), the DTD canal (Danube watershed), the Topčiderska River (Sava watershed), the Porečka River (Danube watershed), the Kolubara (Sava watershed), the Pek (Danube watershed) and the Toplica (South Morava watershed). For the larger rivers, sampling was conducted at several locations (Fig. 1). The sediment samples were collected by using a grab sampler from the specified sampling stations. The sampling of sediments in this research was conducted using a Van Veen grab sampler, designed to collect an accurate representative sample of the sediment. Sediments in surface water are frequently heterogeneous due to small-scale changes in hydrological regime and geomorphologic changes in the catchment area. Equal volumes of sediment from nearby locations (five subsamples) were mixed for each site in order to make a composite sample to expand the area of each site represented by the sample. Immediately after sampling, the sediment was transported to the laboratory in a portable cooler. Samples were stored at 4°C in order to prevent changes in the chemical composition of the sediments. Contents of the micro and macro-elements were determined in the granulometric fraction <63 µm of the bottom sediment samples ("grab", the sample), after air drying for eight days [21].

### 2.2 Sediment analysis

Sediment samples were digested in a microwave digestion system (Ethos 1, Advanced Microwave Digestion System, Milestone, Italy) with a HNO<sub>3</sub>/HCl/HF mixture for element analyses [22]. The analytical determination of the studied elements was realised with atomic emission spectrometry with inductively coupled plasma iCAP-6500 Duo (Thermo Scientific, UK). For analysis calibrations, solution preparation, analytical-grade quality reagents and stock solutions were employed. External standard solutions were prepared from 1000 mg L<sup>-1</sup> stock metal solutions. For minimized interferences, a multi-element standard stock solution was prepared with the ratios of the metals in this multiple element calibration standard being analogous to their ratios in samples. These multi-element standards and blanks were prepared in the same matrix as the extracting reagents to minimize matrix effects and for background correction. The instrumental calibration was checked every 10–12 samples. The quality of the analytical data was ensured by careful standardization, procedural blank measurements, and duplicate samples. The operational conditions for inductively coupled plasma were adjusted in accordance with the manufacturer's guidelines to obtain optimal determination. The detection limit was determined as three times the

standard deviation of the blank measurements. The obtained values were: 0.03 mg kg<sup>-1</sup> Cd, 0.1 mg kg<sup>-1</sup> Cu, 0.03 mg kg<sup>-1</sup> Co, 0.03 mg kg<sup>-1</sup> Mn, 0.1 mg kg<sup>-1</sup> Cr, 0.1 mg kg<sup>-1</sup> Ni, 0.5 mg kg<sup>-1</sup> Pb, 0.05 mg kg<sup>-1</sup> Zn, 0.5 mg kg<sup>-1</sup> Al and 0.3 mg kg<sup>-1</sup> Fe. The accuracy and precision of the obtained results were verified by analysing sediment reference material (BCR standards, 143R and 146 R). The recovery was practically complete for most elements and the values in the acceptable range (recovery: 80–120%). Accuracy with BCR 146 R were: 97.3% Cd, 103% Co, 80.9% Cu, 87.4% Pb, 108% Mn, 85.4% Ni, 89.8% Zn and 85.2% Cr. Accuracy of methods, calculated with BCR 143 R were: 98.2% Cd, 102% Co, for 85.3% Cu, for 118% Pb, for 92.2% Mn, for 82.9% Ni, and 106% Zn. The calculated accuracy and precision confirmed the good performance of the adopted procedures.

The data reported in this paper are calculated as dry weight.

### 2.3 EF

For the purpose of quantifying the degree of metal enrichment, the EF is used in this paper. EF is used as an index to evaluate anthropogenic influences of harmful elements in sediments; it is generally defined as:

$$EF = (M/Y)_{\text{sample}} / (M/Y)_{\text{background}} \quad (1)$$

where *M* is the concentration of the potentially enriched element and *Y* is the concentration of the proxy element. Normalisation of the data is an attempt to compensate for the natural variability of trace metals in sediments, so that any anthropogenic metal contributions may be detected and quantified. This evaluating technique is carried out by normalizing the metal concentration based on geological characteristics of sediments. Widely used elements for normalization are Al and Fe. Aluminium is a major metallic element found in the earth crust; its concentration is somewhat high in sediments and is not affected by man-made factors. Si and Ti contents also reflect the sediment texture, and these elements may be used as conservative tracers to differentiate natural from anthropogenic components. Al, Fe, Si, and Ti can be used as normalisers in areas where substantial anthropogenic contributions of these elements are absent. In this manuscript, normalisation elements in calculating the EFs were Fe, Al, Ti and Si, followed by results comparison. The enrichment was assessed from the EF values as follows: EF <1 = nil; <3 = minor; 3–5 = moderate; 5–10 = moderately severe and >10 = severe [5].

In the interpretation of sediment pollution and determination of EF, the choice of background concentration values plays an important role. While many previous studies used the average values of shale or crustal abundance as a reference baseline, the best alternative proposed is to compare concentrations of the contaminated sediment with mineralogically and texturally comparable, uncontaminated sediments [18]. As shown in [15], reference values for the element content in sediments are not always available and comparison with average crustal values may not be appropriate in the case of a very heterogeneous studied area such as this. In such cases the preferable method for assessing enrichment is to use local uncontaminated sediments as background values [5]. In this paper, the background values of elements were determined for studied areas utilising the process of EF coefficients calculation, and these values are shown in Section 3.

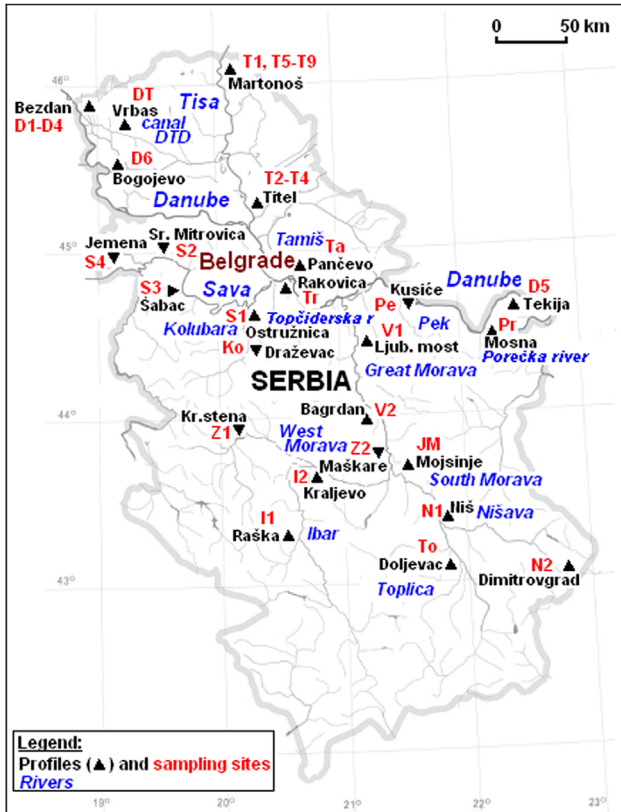


**Figure 1.** Map of sampling locations. Explanation for Danube: Bezdán (D1-D4), Tekija (D5) and Bogojevo (D6); for Sava: Ostružnica (S1), Sremska Mitrovica (S2), Sabac (S3) and Jemena (S4); for Tisa: Martonoš (T1, T5-T9) and Titel (T2-T4); for Great Morava: Ljubicevski most (V1) and Bagrdan (V2); for West Morava: Kratovska stena (Z1) and Maskare (Z2); for Ibar Raška (I1) and Kraljevo (I2); for Nišava: Niš (N1) and Dimitrograd (N2); for DTD canal: Vrbas (DT); for Tamiš: Pančevo (Ta); for Topčiderska River: Rakovica (Tr); for Kolubara: Draževac (Ko); for South Morava: Mojsinje (JM); for Toplica: Doljevac (To); for Pek: Kusiće (Pe) and for Porečka River (Pr).

For a better clarification of the changes in EF values of metals in sediments, the box plot method was applied in this research. This method is employed to maximize insight into a data set, uncover underlying structures and detect outliers and anomalies [23].

### 2.4 Statistical analysis

In order to determine the interrelationships between various normalisers and other elements, to determine the correlation between any two contents of measured heavy metals, and also the EFs for the elements, calculated with different normalisers, the Pearson correlation analysis was conducted using the SPSS statistical package (vers. 11.5). The Pearson correlation shows the linear relationship between two sets of data. This widely-used coefficient measures the strength of a linear association between variables. Bivariate correlations provide information about both the strength of the relationship (from uncorrelated, when the correlation is zero, to perfectly correlated, when the correlation is +1 or -1), and the direction of the relationship (positive or negative).

The statistical treatment and interpretation of data is explained more in detail in the literature [21, 24]. In the presented

manuscript we have followed the mentioned procedure with an addition of the critical value for Pearson's correlation coefficient and alpha level ( $\alpha$ ). In this paper, the Pearson correlation coefficient ( $r$ ) represents a significant linear correlation for values  $r \geq 0.334$  ( $\alpha = 0.05$  and degree of freedom (df) = 33). The interpretation of correlation strength is used as quoted and reported in [5]:  $r < 0.3$  = poor;  $r: 0.3-0.6$  = moderate;  $r: 0.6-0.9$  = strong; and  $r > 0.9$ : excellent.

## 3. Results and Discussion

### 3.1 Element content

The total contents of studied elements are presented as logarithm values in Fig. 2, due to the wide range of heavy metal content. Contents were in the range of:  $1.28-10.5 \text{ mg kg}^{-1}$  Cd,  $11.5-870 \text{ mg kg}^{-1}$  Cu,  $8.22-36.2 \text{ mg kg}^{-1}$  Co,  $648-3688 \text{ mg kg}^{-1}$  Mn,  $59.8-230 \text{ mg kg}^{-1}$  Cr,  $33.2-274 \text{ mg kg}^{-1}$  Ni,  $57.8-318 \text{ mg kg}^{-1}$  Pb,  $66.6-1095 \text{ mg kg}^{-1}$  Zn,  $24 \text{ mg kg}^{-1}$  Fe,  $556-62 \text{ mg kg}^{-1}$  Fe,  $23 \text{ mg kg}^{-1}$  Fe,  $482-95 \text{ mg kg}^{-1}$  Fe.

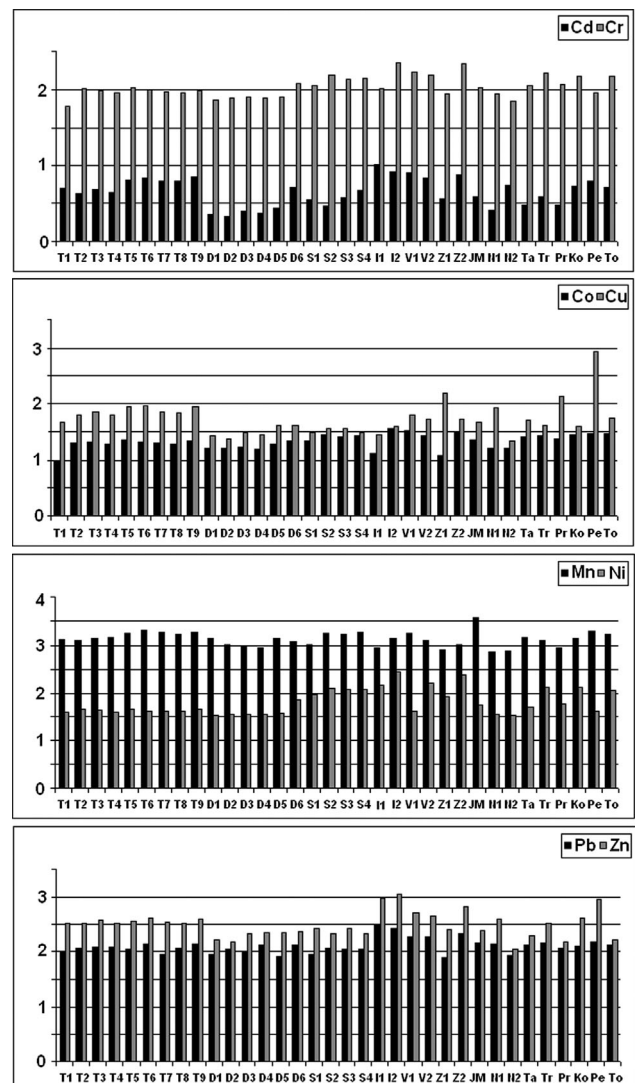


**Figure 2.** Total contents of elements ( $\text{mg kg}^{-1}$ ) in studied river sediments (logarithm value).

mg kg<sup>-1</sup> Al, 3687–7517 mg kg<sup>-1</sup> Ti, and 89 865–231 439 mg kg<sup>-1</sup> Si, with a mean content of: 4.82 mg kg<sup>-1</sup> Cd, 78.5 mg kg<sup>-1</sup> Cu, 22.0 mg kg<sup>-1</sup> Co, 1399 mg kg<sup>-1</sup> Mn, 113 mg kg<sup>-1</sup> Cr, 77.8 mg kg<sup>-1</sup> Ni, 132 mg kg<sup>-1</sup> Pb, 353 mg kg<sup>-1</sup> Zn, 44 177 mg kg<sup>-1</sup> Fe, 57 110 mg kg<sup>-1</sup> Al, 5278 mg kg<sup>-1</sup> Ti, and 197 390 mg kg<sup>-1</sup> Si. The obtained results were compared with element concentrations in the continental crust [25]: 0.1 mg kg<sup>-1</sup> Cd, 25 mg kg<sup>-1</sup> Cu, 24 mg kg<sup>-1</sup> Co, 716 mg kg<sup>-1</sup> Mn, 126 mg kg<sup>-1</sup> Cr, 56 mg kg<sup>-1</sup> Ni, 14.8 mg kg<sup>-1</sup> Pb, 65 mg kg<sup>-1</sup> Zn, 43 200 mg kg<sup>-1</sup> Fe, 79 600 mg kg<sup>-1</sup> Al, 4010 mg kg<sup>-1</sup> Ti, and 288 000 mg kg<sup>-1</sup> Si. The mean content of measured elements in the sediments was higher than the element concentrations in the continental crust for Cd, Cu, Mn, Ni, Pb, and Zn, which may indicate an influence of anthropogenic activities on metal content in the studied region, but also may indicate influence by geogenic (natural) factors. The obtained values for Co, Cr and Fe are similar with crustal values, indicating the dominant geochemical origin of these elements in the system. Lower contents of Si and Al in the sediments compared to the continental crust indicate that the silicate lattice was not completely destroyed, while the increased content of Ti in river sediments in Serbia may suggest a significant presence of Ti minerals in the soil.

The results have also shown large variations in the content of Al, Fe, and Si in these sediments. A possible explanation for the variability of Al, Fe and Si contents should be linked to a large sampling area, showing inherent spatial heterogeneity. A wider spread of the concentration of Al, as well as Fe, could reflect a higher degree of variation in the sediment chemical composition, in the context of different sub-basins areas for main rivers and their effluents.

An assessment of metal pollution levels was made by comparing mean values for the obtained results from the studied river sediments and soil standards for Serbia [26]. The maximum allowed quantity (MAQ) for soil in Serbia is: 300 mg kg<sup>-1</sup> Zn, 2 mg kg<sup>-1</sup> Cd, 100 mg kg<sup>-1</sup> Pb, 50 mg kg<sup>-1</sup> Ni, 100 mg kg<sup>-1</sup> Cu and 100 mg kg<sup>-1</sup> Cr. The concentration levels of Zn, Cd, Pb, Ni and Cr in river sediments are unsafe, when compared with the Serbian MAQ. The mean content of Cu is below the MAQ for the Serbian soil standard, but for some areas the Cu content exceeded this criterion.

The distribution of heavy metals in drainage sediments showed large spatial variations among the different rivers (Fig. 2), suggesting different origins of these elements, as well as

the existence of their anthropogenic sources. These findings are in accordance with results reported in the literature [23]. Dević et al. showed that pollution of groundwater in Serbia is derived from both scattered point sources (industrial and urban effluent) and diffuse sources—agricultural activity [23]. Increased contents of the studied elements were observed in some river systems: Mn in the South Morava, Zn and Cu in the Pek, Zn in the Ibar and West Morava, Cd in the Tisa, Ibar, Great Morava and so on. These results highlight the need to quantify elemental pollution.

### 3.2 Statistical analysis

Table 1 shows the correlation matrix of heavy metals and normalisers in the studied river sediments. Investigation of the relationship between metals and different normalisers (Fe, Al, Ti, and Si), examination of the relationships between the measured heavy metals, and assessment of their possible sources, is performed through correlation analysis. The positive correlation between heavy metal content is observed from the correlation matrix (Table 1). It can be seen that the majority of interrelationships between metals are in the moderate and strong range. The highest values of correlation coefficients are between Cr and Ni ( $r=0.869$ ), Cr and Co ( $r=0.858$ ) and Zn and Pb ( $r=0.824$ ). The positive correlations between Cd, Co, Cr, Pb and Zn show that these elements mostly originate from an identical source. These correlations also may indicate their common sink in stream sediments. Cu was positively correlated only with Zn ( $r=0.421$ ), with this correlation being moderate, indicating that Cu originates from various sources in respect to other elements, mainly from mines in river basins. There was also a possibility that different substrates are dominated in Cu-binding in relation to the other elements.

Positive correlations between normalisers and studied elements exist among certain elements; here, Si is positively correlated with Cd, Ti with Co and Mn, and Fe with Co, Cr, and Mn. In sediments, Si mainly represents aluminosilicates. In addition, Si may represent quartz, which has no affinity for metal binding [24]. In the literature [27] it is shown that differences of trace element concentrations between fine-grained and sand-grained fractions became less significant when the site is more contaminated. This fact suggests that excessive metals from non-natural sources may be accumulated in the sand-sized fraction. Since quartz is the main

**Table 1.** Correlation matrix of heavy metals and normalisers in studied river sediments ( $n=35$ )

|    | Cd            | Co            | Cr           | Cu            | Mn            | Ni           | Pb           | Zn     | Fe            | Al     | Ti           | Si |
|----|---------------|---------------|--------------|---------------|---------------|--------------|--------------|--------|---------------|--------|--------------|----|
| Cd | 1             |               |              |               |               |              |              |        |               |        |              |    |
| Co | <b>0.387*</b> | 1             |              |               |               |              |              |        |               |        |              |    |
| Cr | <b>0.451</b>  | <b>0.858</b>  | 1            |               |               |              |              |        |               |        |              |    |
| Cu | 0.144         | 0.215         | -0.110       | 1             |               |              |              |        |               |        |              |    |
| Mn | 0.194         | <b>0.387*</b> | 0.120        | 0.191         | 1             |              |              |        |               |        |              |    |
| Ni | <b>0.452</b>  | <b>0.609</b>  | <b>0.869</b> | -0.137        | -0.064        | 1            |              |        |               |        |              |    |
| Pb | <b>0.743</b>  | <b>0.427*</b> | <b>0.571</b> | 0.065         | 0.063         | <b>0.627</b> | 1            |        |               |        |              |    |
| Zn | <b>0.759</b>  | <b>0.415*</b> | <b>0.459</b> | <b>0.421*</b> | 0.070         | <b>0.552</b> | <b>0.824</b> | 1      |               |        |              |    |
| Fe | 0.273         | <b>0.779</b>  | <b>0.513</b> | 0.210         | <b>0.496</b>  | 0.172        | 0.318        | 0.201  | 1             |        |              |    |
| Al | -0.125        | 0.145         | -0.041       | 0.238         | 0.184         | -0.081       | 0.084        | 0.042  | <b>0.391*</b> | 1      |              |    |
| Ti | 0.173         | 0.367*        | 0.140        | 0.268         | <b>0.372*</b> | -0.163       | 0.029        | -0.028 | <b>0.707</b>  | 0.342* | 1            |    |
| Si | 0.461         | 0.255         | 0.221        | 0.121         | 0.257         | 0.069        | 0.170        | 0.208  | <b>0.372*</b> | -0.004 | <b>0.712</b> | 1  |

\*Correlation is significant at the 0.05 level.

Bold numbers indicate that the correlation is significant at the 0.01 level.

**Table 2.** Minimum, maximum and median values of EF ( $n = 35$ )

| Parameter | EF <sub>Fe-Cd</sub> | EF <sub>Fe-Co</sub> | EF <sub>Fe-Cr</sub> | EF <sub>Fe-Cu</sub> | EF <sub>Fe-Mn</sub> | EF <sub>Fe-Ni</sub> | EF <sub>Fe-Pb</sub> | EF <sub>Fe-Zn</sub> |
|-----------|---------------------|---------------------|---------------------|---------------------|---------------------|---------------------|---------------------|---------------------|
| Minimum   | 0.95                | 0.90                | 0.69                | 1.28                | 0.64                | 0.55                | 0.85                | 1.11                |
| Maximum   | 5.48                | 2.27                | 1.91                | 36.45               | 2.79                | 4.07                | 3.67                | 9.47                |
| Median    | 2.02                | 1.39                | 1.00                | 2.24                | 1.08                | 0.71                | 1.15                | 2.72                |
|           | EF <sub>Al-Cd</sub> | EF <sub>Al-Co</sub> | EF <sub>Al-Cr</sub> | EF <sub>Al-Cu</sub> | EF <sub>Al-Mn</sub> | EF <sub>Al-Ni</sub> | EF <sub>Al-Pb</sub> | EF <sub>Al-Zn</sub> |
| Minimum   | 0.68                | 0.81                | 0.49                | 0.84                | 0.65                | 0.42                | 0.80                | 0.96                |
| Maximum   | 8.18                | 4.79                | 3.35                | 35.03               | 3.99                | 4.84                | 5.48                | 14.13               |
| Median    | 2.32                | 1.90                | 1.01                | 2.70                | 1.29                | 1.06                | 1.27                | 2.87                |
|           | EF <sub>Ti-Cd</sub> | EF <sub>Ti-Co</sub> | EF <sub>Ti-Cr</sub> | EF <sub>Ti-Cu</sub> | EF <sub>Ti-Mn</sub> | EF <sub>Ti-Ni</sub> | EF <sub>Ti-Pb</sub> | EF <sub>Ti-Zn</sub> |
| Minimum   | 1.60                | 1.27                | 1.03                | 2.02                | 1.00                | 0.91                | 1.27                | 1.79                |
| Maximum   | 9.37                | 4.58                | 3.97                | 62.06               | 4.80                | 8.42                | 6.14                | 18.16               |
| Median    | 3.29                | 2.28                | 1.44                | 4.03                | 2.03                | 1.23                | 1.88                | 4.41                |
|           | EF <sub>Si-Cd</sub> | EF <sub>Si-Co</sub> | EF <sub>Si-Cr</sub> | EF <sub>Si-Cu</sub> | EF <sub>Si-Mn</sub> | EF <sub>Si-Ni</sub> | EF <sub>Si-Pb</sub> | EF <sub>Si-Zn</sub> |
| Minimum   | 1.95                | 1.27                | 1.01                | 2.04                | 1.23                | 1.02                | 1.39                | 1.85                |
| Maximum   | 8.32                | 4.57                | 3.88                | 73.43               | 5.91                | 8.14                | 5.56                | 16.79               |
| Median    | 3.72                | 2.72                | 1.66                | 4.39                | 2.03                | 1.36                | 2.12                | 4.66                |

component of sand-grained fractions, it can be concluded that there are significant anthropogenic sources of Cd present.

Ti has a positive relationship with Co and Mn. It is a common lithophile element that forms several minerals (limonite, magnetite, rutile, anatase, brookite, sphene, pyroxene, amphibole, mica and garnet), and may also substitute for Mg<sup>2+</sup> or Fe<sup>2+</sup> in silicate minerals, leading to the enrichment of Ti content in amphibole and mica ([http://weppi.gtk.fi/publ/foregsatlas/text/Ti\\_TiO2.pdf](http://weppi.gtk.fi/publ/foregsatlas/text/Ti_TiO2.pdf)). The results of

the mineralogical composition of the most important studied soils in Serbia showed the presence of mica, garnets and pyroxene [28]. Based on this fact, it is possible that the presence of minerals enriched with Ti is due to various processes of soil erosion and weathering in river systems. A positive correlation between Ti and Fe, Al, Mn and Si can be explained by the fact that in sedimentary rocks, the concentration of TiO<sub>2</sub> is determined by the abundance of detrital oxides and silicates.

**Table 3.** Correlation matrices of EFs with different normalisers

|                  | EF               |                  |                  |                  | EF               |                  |                  |                  |
|------------------|------------------|------------------|------------------|------------------|------------------|------------------|------------------|------------------|
|                  | Cd <sub>Al</sub> | Cd <sub>Fe</sub> | Cd <sub>Ti</sub> | Cd <sub>Si</sub> | Co <sub>Al</sub> | Co <sub>Fe</sub> | Co <sub>Ti</sub> | Co <sub>Si</sub> |
| Cd <sub>Al</sub> | 1                |                  |                  |                  | Co <sub>Al</sub> | 1                |                  |                  |
| Cd <sub>Fe</sub> | <b>0.775</b>     | 1                |                  |                  | Co <sub>Fe</sub> | <b>0.556</b>     | 1                |                  |
| Cd <sub>Ti</sub> | <b>0.776</b>     | <b>0.965</b>     | 1                |                  | Co <sub>Ti</sub> | <b>0.526</b>     | <b>0.946</b>     | 1                |
| Cd <sub>Si</sub> | <b>0.777</b>     | <b>0.928</b>     | <b>0.967</b>     | 1                | Co <sub>Si</sub> | <b>0.432</b>     | <b>0.804</b>     | <b>0.878</b>     |
| Cr               |                  |                  |                  |                  | Cu               |                  |                  |                  |
|                  | Cr <sub>Al</sub> | Cr <sub>Fe</sub> | Cr <sub>Ti</sub> | Cr <sub>Si</sub> | Cu <sub>Al</sub> | Cu <sub>Fe</sub> | Cu <sub>Ti</sub> | Cu <sub>Si</sub> |
| Cr <sub>Al</sub> | 1                |                  |                  |                  | Cu <sub>Al</sub> | 1                |                  |                  |
| Cr <sub>Fe</sub> | <b>0.669</b>     | 1                |                  |                  | Cu <sub>Fe</sub> | <b>0.971</b>     | 1                |                  |
| Cr <sub>Ti</sub> | <b>0.650</b>     | <b>0.969</b>     | 1                |                  | Cu <sub>Ti</sub> | <b>0.969</b>     | <b>0.998</b>     | 1                |
| Cr <sub>Si</sub> | <b>0.606</b>     | <b>0.883</b>     | <b>0.936</b>     | 1                | Cu <sub>Si</sub> | <b>0.965</b>     | <b>0.995</b>     | <b>0.999</b>     |
| Mn               |                  |                  |                  |                  | Ni               |                  |                  |                  |
|                  | Mn <sub>Al</sub> | Mn <sub>Fe</sub> | Mn <sub>Ti</sub> | Mn <sub>Si</sub> | Ni <sub>Al</sub> | Ni <sub>Fe</sub> | Ni <sub>Ti</sub> | Ni <sub>Si</sub> |
| Mn <sub>Al</sub> | 1                |                  |                  |                  | Ni <sub>Al</sub> | 1                |                  |                  |
| Mn <sub>Fe</sub> | <b>0.589</b>     | 1                |                  |                  | Ni <sub>Fe</sub> | <b>0.933</b>     | 1                |                  |
| Mn <sub>Ti</sub> | <b>0.593</b>     | <b>0.951</b>     | 1                |                  | Ni <sub>Ti</sub> | <b>0.920</b>     | <b>0.991</b>     | 1                |
| Mn <sub>Si</sub> | <b>0.498</b>     | <b>0.880</b>     | <b>0.937</b>     | 1                | Ni <sub>Si</sub> | <b>0.907</b>     | <b>0.980</b>     | <b>0.991</b>     |
| Pb               |                  |                  |                  |                  | Zn               |                  |                  |                  |
|                  | Pb <sub>Al</sub> | Pb <sub>Fe</sub> | Pb <sub>Ti</sub> | Pb <sub>Si</sub> | Zn <sub>Al</sub> | Zn <sub>Fe</sub> | Zn <sub>Ti</sub> | Zn <sub>Si</sub> |
| Pb <sub>Al</sub> | 1                |                  |                  |                  | Zn <sub>Al</sub> | 1                |                  |                  |
| Pb <sub>Fe</sub> | <b>0.774</b>     | 1                |                  |                  | Zn <sub>Fe</sub> | <b>0.862</b>     | 1                |                  |
| Pb <sub>Ti</sub> | <b>0.758</b>     | <b>0.969</b>     | 1                |                  | Zn <sub>Ti</sub> | <b>0.857</b>     | <b>0.984</b>     | 1                |
| Pb <sub>Si</sub> | <b>0.641</b>     | <b>0.861</b>     | <b>0.926</b>     | 1                | Zn <sub>Si</sub> | <b>0.824</b>     | <b>0.965</b>     | <b>0.981</b>     |

\*Correlation is significant at the 0.05 level.

Bold indicates that the correlation is significant at the 0.01 level.



The correlation between Fe and Mn implies the presence of Fe/Mn oxides [5]. A positive correlation of Fe with Co, Cr, and Mn can be observed. It can be concluded that in the studied sediments, Fe–Mn oxides are the main carriers of Co and Cr. The significance of Fe–Mn oxides in binding affinities of Co and Cr is shown in the literature [8, 9]. Wang et al. could also show that heavy metals were associated with Fe-oxides, since iron oxides have a relatively higher adsorption capacity than clay minerals and Al-oxides [12].

In general, the absence of strong relations between normalisers and heavy metals may be impacted by numerous factors, as shown in the literature [5]. A lack of the relationship between Al and other normalisers with most of the studied heavy metals indicates contamination from different sources and this nonlinear relationship indicates anthropogenic sources rather than natural ones, which is also shown in [7].

### 3.3 Determination of EF and selection of appropriate normalisers

In this paper, EF was calculated for each of the studied heavy metals. The calculation of this factor was based on the background value determined for the studied area. The element content in the DTD canal (station in Vrba) was chosen as background values for elements in this research, due to the lack of significant anthropogenic sources of toxic elements at this area, and similarity of the sediment samples to other investigated river sediments in their geochemical characteristics and composition. Background values of elements in this research are: 1.28 mg kg<sup>-1</sup> Cd, 11.5 mg kg<sup>-1</sup> Cu,

8.22 mg kg<sup>-1</sup> Co, 648 mg kg<sup>-1</sup> Mn, 62.1 mg kg<sup>-1</sup> Cr, 34.7 mg kg<sup>-1</sup> Ni, 57.8 mg kg<sup>-1</sup> Pb, 66.6 mg kg<sup>-1</sup> Zn, 24 556 mg kg<sup>-1</sup> Fe, 36 323 mg kg<sup>-1</sup> Al, 4958 mg kg<sup>-1</sup> Ti and 198 667 mg kg<sup>-1</sup> Si.

The EF values are calculated with different elements for normalisation: Fe, Al, Ti and Si and were interpreted as suggested by Swarnalatha [5]. The minimum, median and maximum EFs were calculated for all analysed elements and the results are given in Table 2. For comparison purposes the median EF values of elements are considered. Significant differences were observed in EF values calculated with different elements used for the normalisation. The EF values are more than 40% higher when Ti and Si are used as normalisers in respect to EF values obtained with Al and Fe. The studied heavy metals in sediments show decreasing EF values for different normalisers in the following sequence: Si > Ti > Al > Fe. The obtained values for EF indicate “nil” to “moderate” enrichment for all studied elements, except for Cd, Cu, and Zn on some sampling points, for which the enrichment was even up to “severe”. There is a positive correlation between all EF values calculated with different elements for normalisation (Table 3).

Correlation analysis was performed also between heavy metals and their EFs (Table 4). A significantly high correlation was observed for all studied elements (Cd, Co, Cr, Cu, Mn, Ni, Pb, and Zn) and their EFs were calculated with different elements for normalisation (Al, Ti, Si and Fe). These positive correlations point to anthropogenic contributions of heavy metal distributions in the studied sediments. In addition, these correlations confirmed the use of Al, Ti, Si and Fe for normalisation and for describing the enrichment status in this research.

**Table 4.** Correlation matrix of heavy metals and EFs

|                      | Cd    | Co    | Cr    | Cu    | Mn    | Ni    | Pb    | Zn    |
|----------------------|-------|-------|-------|-------|-------|-------|-------|-------|
| EF <sub>Al</sub> -Cd | 0.783 |       |       |       |       |       |       |       |
| EF <sub>Fe</sub> -Cd | 0.933 |       |       |       |       |       |       |       |
| EF <sub>Ti</sub> -Cd | 0.940 |       |       |       |       |       |       |       |
| EF <sub>Si</sub> -Cd | 0.954 |       |       |       |       |       |       |       |
| EF <sub>Al</sub> -Co |       | 0.564 |       |       |       |       |       |       |
| EF <sub>Fe</sub> -Co |       | 0.904 |       |       |       |       |       |       |
| EF <sub>Ti</sub> -Co |       | 0.847 |       |       |       |       |       |       |
| EF <sub>Si</sub> -Co |       | 0.811 |       |       |       |       |       |       |
| EF <sub>Al</sub> -Cr |       |       | 0.968 |       |       |       |       |       |
| EF <sub>Fe</sub> -Cr |       |       | 0.934 |       |       |       |       |       |
| EF <sub>Ti</sub> -Cr |       |       | 0.923 |       |       |       |       |       |
| EF <sub>Si</sub> -Cr |       |       | 0.898 |       |       |       |       |       |
| EF <sub>Al</sub> -Cu |       |       |       | 0.967 |       |       |       |       |
| EF <sub>Fe</sub> -Cu |       |       |       | 0.995 |       |       |       |       |
| EF <sub>Ti</sub> -Cu |       |       |       | 0.998 |       |       |       |       |
| EF <sub>Si</sub> -Cu |       |       |       | 0.999 |       |       |       |       |
| EF <sub>Al</sub> -Mn |       |       |       |       | 0.581 |       |       |       |
| EF <sub>Fe</sub> -Mn |       |       |       |       | 0.944 |       |       |       |
| EF <sub>Ti</sub> -Mn |       |       |       |       | 0.921 |       |       |       |
| EF <sub>Si</sub> -Mn |       |       |       |       | 0.895 |       |       |       |
| EF <sub>Al</sub> -Ni |       |       |       |       |       | 0.922 |       |       |
| EF <sub>Fe</sub> -Ni |       |       |       |       |       | 0.983 |       |       |
| EF <sub>Ti</sub> -Ni |       |       |       |       |       | 0.988 |       |       |
| EF <sub>Si</sub> -Ni |       |       |       |       |       | 0.987 |       |       |
| EF <sub>Al</sub> -Pb |       |       |       |       |       |       | 0.757 |       |
| EF <sub>Fe</sub> -Pb |       |       |       |       |       |       | 0.926 |       |
| EF <sub>Ti</sub> -Pb |       |       |       |       |       |       | 0.933 |       |
| EF <sub>Si</sub> -Pb |       |       |       |       |       |       | 0.874 |       |
| EF <sub>Al</sub> -Zn |       |       |       |       |       |       |       | 0.833 |
| EF <sub>Fe</sub> -Zn |       |       |       |       |       |       |       | 0.968 |
| EF <sub>Ti</sub> -Zn |       |       |       |       |       |       |       | 0.972 |
| EF <sub>Si</sub> -Zn |       |       |       |       |       |       |       | 0.982 |

\*Correlation is significant at the 0.01 level.

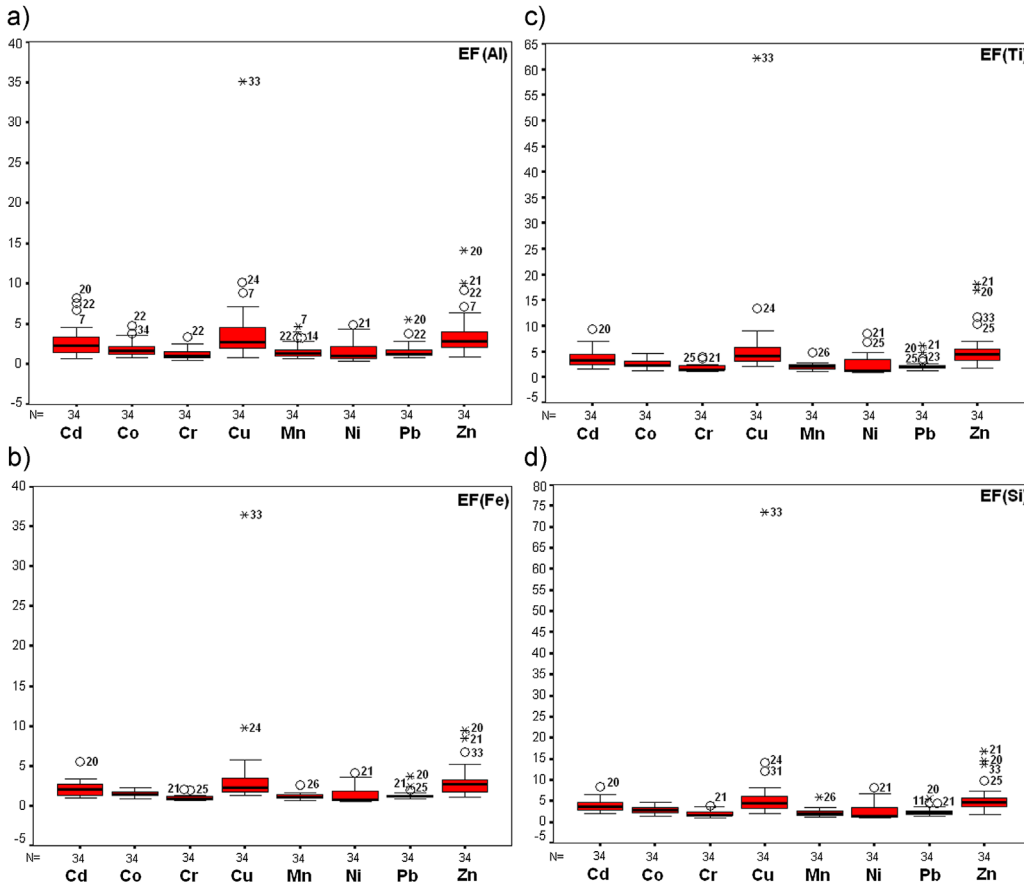


**Figure 3.** Box plots showing the variation of EF in the studied sediments with: (a) Al, (b) Fe, (c) Ti and (d) Si as normaliser. Solid line within the box indicates a median value. Horizontal lines in the boxes represent 25, 50 (median) and 75% of values; error bars indicate 5 and 105% of these values. Open circle represents outlying points, while (\*) represents extreme points.

Figure 3 shows a variation of EF in the studied sediments using the Box plot. For Cd, Cu and Zn, the median value is slightly elevated and has a wide distribution of coefficients, whilst others had a compact distribution, suggesting a slight increase in Cd, Cu and Zn contamination. Outlier and extreme values of EF were observed in: Tisa (Cd, Cu, Mn and Zn), Ibar (Cd, Cr, Ni, Pb and Zn), Great Morava (Cd, Co, Mn, Pb, Zn, and Cr), West Morava (Cr, Cu, Ni, Pb, and Zn), Toplica (Co), Pek (Cu, Pb, and Zn), Danube (Mn) and South Morava (Mn), suggesting that these are the most critical sites in terms of metal contamination. The pollution of these rivers is mainly caused by permanent and accidental pollution from industrial plants and mines that are located in the basins of these rivers: Trepca mining complex – Pb and Zn (Ibar), mining complex in Majdanpek – Cu (Pek) and other basins, agricultural products, mainly due to the use of manganese-containing products, such as fertilizers and fungicides.

#### 4. Concluding remarks

The process of distinguishing anthropogenic pollutants from natural contents of sediments using EFs is valuable in quantifying the level of pollution. Heavy metal contamination of sediments is established as being present in the examined rivers of Serbia. The studied sediments are contaminated to various degrees by heavy metals. The selection of background values, as well as the identification of appropriate normalisers has been very important

in the calculation of EF. All elements used for normalisation (Al, Ti, Si, and Fe) were successfully used to estimate the anthropogenic influence in this research. The positive correlation of the studied elements with Co and its content, which is similar to the average concentration of this element in the continental crust, suggests the possibility of using Co as normalisation element in further research.

#### Acknowledgments

This study was supported by the Ministry of Education, Science and Technological Development of Serbia, Grant Nos. 172001 and 43007. In addition, we would like to thank the Republic Hydrometeorological Service of Serbia for the sediment samples. The authors are grateful to anonymous reviewers whose comments greatly improved the paper.

*The authors have declared no conflict of interest.*

#### References

- [1] M. S. Rahman, N. Saha, A. H. Molla, Potential ecological risk assessment of heavy metal contamination in sediment and water body around Dhaka export processing zone, Bangladesh, *Environ. Earth Sci.* **2014**, *71*, 2293–2308.



- [2] H. Pekey, The distribution and sources of heavy metals in Izmit Bay surface sediments affected by a polluted stream, *Mar. Pollut. Bull.* **2006**, *52*, 1197–1208.
- [3] L. Zhang, H. Shao, Heavy metal pollution in sediments from aquatic ecosystems in China, *Clean – Soil Air Water* **2013**, *41* (9), 878–882.
- [4] M. A. Benamar, I. Toumert, S. Tobbeche, A. Tchantchane, A. Chalabi, Assessment of the state of pollution by heavy metals in the surficial sediments of Algiers Bay, *Appl. Radiat. Isot.* **1999**, *50*, 975–980.
- [5] K. Swarnalatha, J. Letha, S. Ayoob, A. M. Sheela, Identification of silicon (Si) as an appropriate normalizer for estimating the heavy metals enrichment of an urban lake system, *J. Environ. Manage.* **2013**, *129*, 54–61.
- [6] O. I. Davutluoglu, G. Seckin, C. B. Ersu, T. Yilmaz, B. Sari, Assessment of metal pollution in water and surface sediments of the Seyhan river, Turkey, using different indexes, *Clean – Soil Air Water* **2011**, *39*, 185–194.
- [7] J. H. Rule, Assessment of trace element geochemistry of Hampton roads harbor and Lower Chesapeake bay area sediments, *Environ. Geol. Water Sci.* **1986**, *8*, 209–219.
- [8] S. Carroll, P. A. O'Day, B. Esser, S. Randall, Speciation and fate of trace metals in estuarine sediments under reduced and oxidized conditions, Seaplane Lagoon, Alameda Naval Air Station (USA), *Geochem. Trans.* **2002**, *3*, 81–101.
- [9] R. J. Krupdam, P. Smita, S. R. Wate, Geochemical fractionation of heavy metals in sediments of the Tapi estuary, *Geochem. J.* **2006**, *40*, 513–522.
- [10] S. Sakan, I. Gržetić, D. Đorđević, Distribution and fractionation of heavy metals in the Tisa (Tisza) River sediments, *Environ. Sci. Pollut. Res.* **2007**, 229–236.
- [11] B. Gupta, R. Kumar, M. Rani, Speciation of heavy metals in water and sediments of an urban lake system, *J. Environ. Sci. Health, Part A* **2013**, *48*, 1231–1242.
- [12] X.-C. Wang, H. Feng, H.-Q. Ma, Assessment of metal contamination in surface sediments of Jiaozhou Bay, Qingdao, China, *Clean – Soil Air Water* **2007**, *35*, 62–70.
- [13] M. A. Hortellani, J. E. S. Sarkis, L. C. B. Menezes, R. Bazante-Yamaguishi, A. S. A. Pereira, P. F. G. Garcia, L. S. Maruyama, et al. Assessment of metal concentration in the Billings reservoir sediments, São Paulo state, Southeastern Brazil, *J. Brazil Chem. Soc.* **2013**, *24*, 58–67.
- [14] A. Jamshidi-Zanjani, M. Saeedi, Metal pollution assessment and multivariate analysis in sediment of Anzali international wetland, *Environ. Earth Sci.* **2013**, *70*, 1791–1808.
- [15] S. Comero, S. Vaccaro, S. Locoro, L. De Capitani, B. M. Gawlik, Characterization of the Danube River sediments using PMF multivariate approach, *Chemosphere* **2014**, *95*, 329–335.
- [16] H. Gao, J. Bai, R. Xiao, P. Liu, J. Wang, Levels, sources and risk assessment of trace elements in wetland soils a typical shallow freshwater lake, China, *Stochastic Environ. Res. Risk Assess.* **2013**, *27*, 275–284.
- [17] D. Krčmar, M. Prica, B. Dalmacija, M. Watson, J. Trčković, L. Rajić, Z. Tamaš, Correlation of different pollution criteria in the assessment of metal sediment pollution, *J. Environ. Sci. Health, Part A* **2013**, *48*, 380–393.
- [18] M. Fujita, Y. Ide, D. Sato, P. S. Kench, Y. Kuwahara, H. Yokoki, H. Kayanne, Heavy metal contamination of coastal lagoon sediments: Fongafale Islet, Funafuti Atoll, Tuvalu, *Chemosphere* **2014**, *95*, 628–634.
- [19] I. Teodorović, Ecotoxicological research and related legislation in Serbia, *Environ. Sci. Pollut. Res.* **2009**, *16*, S123–S129.
- [20] S. Subotić, Z. Višnjić Jeftić, S. Spasić, A. Hegediš, J. Krpo-Četković, M. Lehardt, Distribution and accumulation of elements (As, Cu, Fe, Hg, Mn, and Zn) in tissues of fish species from different trophic levels in the Danube River at the confluence with the Sava River (Serbia), *Environ. Sci. Pollut. Res.* **2013**, *20*, 5309–5317.
- [21] S. Sakan, D. Đorđević, G. Dević, D. Relić, I. Anđelković, J. Đuričić, A study of trace element contamination in river sediments in Serbia using microwave-assisted aqua regia digestion multivariate statistical analysis, *Microchem. J.* **2011**, *99*, 492–502.
- [22] H. Rönkkömäki, R. Pöykiö, H. Nurmesniemi, K. Popov, E. Merisalu, T. Tuomi, I. Välimäki, Particle size distribution and dissolution properties of metals in cyclone fly ash, *Int. J. Environ. Sci. Technol.* **2008**, *5*, 485–494.
- [23] G. Dević, D. Đorđević, S. Sakan, Natural and anthropogenic factors affecting the groundwater quality in Serbia, *Sci. Total Environ.* **2014**, 468–469, 933–942.
- [24] S. Sakan, D. Đorđević, D. Manojlović, P. Predrag, Assessment of heavy metal pollutants accumulation in the Tisza river sediments, *J. Environ. Manage.* **2009**, *90*, 3382–3390.
- [25] K. H. Wedepohl, The composition of the continental crust, *Geochim. Cosmochim. Acta* **1995**, *59*, 1217–1232.
- [26] Official Gazette of the Republic of Serbia, *Serbia* **1990**, *11*, 239.
- [27] N. F. Y. Tam, Y. S. Wong, Y. S. Spatial variation of heavy metals in surface of Hong Kong mangrove swamps, *Environ. Pollut.* **2000**, *110*, 195–205.
- [28] N. M. Kostić, M. D. Jakovljević, V. B. Hadžić, J. Protić, Mineralogy and agrochemistry of magnesium in soils of Vojvodina, Šumadija and Northern Pomoravlje, *Matica Srpska Proc. Nat. Sci.* **2001**, *100*, 115–126.

# Evaluation of sediment contamination with heavy metals: the importance of determining appropriate background content and suitable element for normalization

Sanja Sakan · Gordana Dević · Dubravka Relić ·  
Ivan Anđelković · Nenad Sakan ·  
Dragana Đorđević

Received: 9 September 2013 / Accepted: 5 July 2014 / Published online: 18 July 2014  
© Springer Science+Business Media Dordrecht 2014

**Abstract** In the present study, concentrations of heavy metals (Cd, Cu, Co, Mn, Cr, Ni, Pb, and Zn) were determined at 35 river sediments in Serbia. The anthropogenic heavy metals input and quantification of the metal enrichment degree in sediments were estimated by calculating geo-accumulation indices ( $I_{geo}$ ) and enrichment factors (EF). These pollution indices have been calculated using different background values (continental crust and local background values) and different element used for normalization (Al and Fe), followed by result comparison. The EF values calculated with continental crust as background (minor to extremely severe enrichment) were higher than when regional background values were used (minor to moderate enrichment). Significant influence of background values on the  $I_{geo}$  values is observed.

Values of geo-accumulation index ( $<2$ ) revealed that studied river sediments are remaining unpolluted to moderately polluted with Co, Mn, Cr, and Ni. Significant pollution in the sediments was observed for Cd, Cu, Pb, and Zn elements. The results of this study confirm the relevance of precise and accurate determining of local background concentrations while assessing sediment pollution. The values of EFs for studied elements were more influenced by the choice of background values than selection of element used for normalization. Our recommendation would be to use the local and regional background content in quantification of metal contamination in sediments, since these values differ and are site and region dependent.

**Keywords** Heavy metals · Background values · Sediments · Geo-accumulation indices · Enrichment factors

S. Sakan (✉) · G. Dević · D. Đorđević  
ICTM, Chemistry Centre, University of Belgrade,  
Njegoševa 12, P. O. Box 815, 11000 Belgrade, Serbia  
e-mail: ssakan@chem.bg.ac.rs

D. Relić  
Faculty of Chemistry, Applied Chemistry, University of  
Belgrade, P. O. Box 51, 11000 Belgrade, Serbia

I. Anđelković  
Innovation Centre of the Faculty of Chemistry,  
11158 Belgrade, Serbia

N. Sakan  
Institute of Physics, University of Belgrade, Pregrevica  
118, P. O. Box 68, 11081 Belgrade, Serbia

## Introduction

It is well established that human activities have great impact on the geochemical cycles of metals, resulting in widespread environmental contamination (Nriagu and Pacyna 1988). Large uncontrolled metal inputs from industrial sources have contributed to increased river pollution. Depending on hydrodynamics and environmental conditions, metals tend to accumulate

in sediments at the bottom of the water column, and if toxic levels are reached, metals can affect benthic organisms and food chain, raising the possibility of a threat to human health in local population (Louriño-Cabala et al. 2011).

Metal pollutants have received considerable attention due to their persistence, biogeochemical recycling, and environmental risk (Silva et al. 2012; Gao et al. 2013). However, high metal concentrations in sediment do not automatically imply that contamination has occurred, but may simply reflect the natural mineralogical composition of the parent geological material and the grain size and organic matter content of the host sediment (Silva et al. 2012).

Several studies have been conducted to assess distribution and contamination of heavy metals and to determine quantity of pollution load in different sediments. In assessing the metal contamination, geo-accumulation index ( $I_{geo}$ ) and the enrichment factor (EF), respectively, are often used (Rubio et al. 2000; Abraham and Parker 2008; Deveza-Rey et al. 2009; Botsou et al. 2011; Louriño-Cabala et al. 2011; Hu et al. 2011; Asa et al. 2013; Cukrov et al. 2013; and Swarnalatha et al. 2013). The metal pollution load index, ecological and geo-accumulated risk (Kabir et al. 2011), trace metal to iron ratios (Bartoli et al. 2012), heavy metal fractionation and KSPEF calculation (Yang et al. 2012), ecological toxicity (sum of the toxic units), and potential ecological risk index method (Gao et al. 2013) are also very popular in evaluating the heavy metal contamination status. Impact of heavy metal pollution, as well as numerous calculation methods for determination of background values and different normalizing element assessment has been used. Rubio et al. (2000) showed that both,  $I_{geo}$  and EF, were associated with on “background” data. Numerous elements were used as normalizers: aluminum–(Al), iron–(Fe), cobalt–(Co), manganese–(Mn), titanium–(Ti), and silicon–(Si).  $I_{geo}$  and EF have been calculated with Al as grain-size proxy and three different background values (which of two were regional and third global average shale values) in Rubio et al. (2000). Abraham and Parker (2008) calculated  $I_{geo}$ , EF, and modified levels of contamination (mCd) in sediments, using Fe as normalizer and average metal concentrations, determined in the lower part of the core and continental shale abundance as background values. Botsou et al. (2011) used Al and average shale and local background values to

distinguish natural and anthropogenic sources in sediments and calculation of EF. EFs have been calculated on the basis of box-plot method. Derived backgrounds were compared with EF values obtained by using average crustal and shale values, and local surface pristine values in Deveza-Rey et al. (2009). In this research, Al was used as a normalizing element. Louriño-Cabala et al. (2011) used international and national reference contents as the geochemical background for the selected metals while calculating the  $I_{geo}$ . Hu et al. (2011) calculated  $I_{geo}$  and EF. EF was calculated with Al and average shale concentrations of metals. For  $I_{geo}$ , an average shale concentration of metals was used as reference material. Asa et al. (2013) used different risk indices for determining anthropogenic pollution. In EF calculation, Fe is selected as the element for normalization and the EFs for all metals were determined with respect to Indian river average and world river average. For  $I_{geo}$  calculation was used the world surface rock average as the geochemical background. Cukrov et al. (2013) calculated EF with Al and unpolluted marine sediment from the nearby area as background sample. Swarnalatha et al. (2013) used the EF and contamination factor to estimate anthropogenic input. In this study, average shale values are used as background values for calculation of EF. Fe, Al, Co, Mn, Ti, and Si were tested as possible normalizers. The obtained results from cited researches showed that different conclusions depend on using different risk assessment methods, background values, and normalization elements. In this paper, EF factor and index of geo-accumulation were estimated using Al and Fe as normalizers and two different background values, as well as determined interrelations of obtained factors. The relations of the two index methods, with indices calculated for different background values and normalization elements, as well as determination of: (a) metals/Al ratio for metals in river sediments, (b) ratio between the EF (using Al and background values) and EF (using Fe and background values), (c) ratio between the EF (using Al and continental crust) and EF (using Fe and continental crust), and (d) ratio between calculated EF values with different background values and different element for normalization, were explored to discover their differences in the environmental risk assessment of heavy metals. Since the EF and  $I_{geo}$  are very popular in evaluating the environmental risk, we hope to provide useful and

novel information about these indices and that a new approach with the determined quantitative relations between these parameters can be very important in the application in prospective research.

In the present study, through the evaluation of enrichment of heavy metals (Cd, Cu, Co, Mn, Cr, Ni, Pb, and Zn) in river sediments of Serbia, we have illustrated the importance of selecting suitable elements for normalization and appropriate background values in realistic contamination quantification. The chemical analyses also include Al and Fe, which are considered indicative of the sediment grain size. In addition, there was shown the application of test with the determination of the *M/Al* ration as a rapid method for detecting the existence of potential anthropogenic sources.

## Materials and methods

### Study area

Surface river sediments were collected from 35 points in Serbia. All rivers in Serbia belong to the drainage basins of three seas: the Black Sea, the Adriatic, or the Aegean Sea. The largest in area is the Black Sea drainage basins, which covers an area of 81,261 km<sup>2</sup> or 92 % of the territory of Serbia. The entire basin is drained by only one river, the Danube, which flows into the Black Sea. All major rivers, such as Tisa, Sava, and the Great Morava belong to it.

### Sampling locations

Sediment samples (Fig. 1) were taken from 15 rivers during the year 2008. Sampling locations are given in Fig. 1: for the Danube: Bezdan (D1–D4), Tekija (D5), and Bogojevo (D6); for Sava: Ostružnica (S1), Sremska Mitrovica (S2), Šabac (S3), and Jemena (S4); for Tisa: Martonoš (T1, T5–T9) and Titel (T2–T4); for Great Morava: Ljubičevski most (V1) and Bagrdan (V2); for West Morava: Kratovska stena (Z1) and Maskare (Z2); for Ibar: Raška (I1) and Kraljevo (I2); for Nišava: Niš (N1) and Dimitrovgrad (N2); for DTD canal: Vrbas (DT); for Tamiš: Pančevo (Ta); for Topčiderska River: Rakovica (Tr); for Kolubara: Draževac (Ko); for South Morava: Mojsinje (JM); for Toplica: Doljevac (To); for Pek: Kusiće (Pe); and for Porečka River: Mosna (Pr). Localities: Bezdan (for

the Danube), Martonoš (for Tisa), and Jemena (for Sava) are outskirts points of sediment collection. The granulometric fraction (< 63 μm) of the bottom sediment samples (“grab”–the sample) were used to determinate the element contents after air-drying for 8 days (Sakan et al. 2011). The sampling was conducted using Van Veen grab sampler.

### Sediment and soil properties in Serbia

In the paper presented by Kostić et al. (2001), was given the mineralogical composition of the most relevant Serbian soil types, collected from Vojvodina, Šumadija, and Northern Pomoravlje. Said composition of the observed soils is complex with results showing predominance of quartz, mica, associated with altered feldspars (plagioclase and orthoclase), carbonate (calcite and dolomite), and minor to trace amounts of chlorite, clay minerals, hornblende, and rare goethite and talc, indicating the mineralogy and variety of parent rocks, e.g., loess, schist, flisch sediments, and sandstones. Magnetite, limonite, and other accompanying minerals (garnets, epidote, apatite, and pyroxene) are found in heavy mineral fractions. Variation in quartz content might result from weathering processes; district cambisols and luvisols contain higher quartz content in comparison with less affected soils, such as fluvisols, rankes, and regosols, on the same and similar parent rocks (Kostić et al. 2001).

The Danube catchment passes through wide area of nine countries. The mineralogy of the Danube River is very complex due to heterogeneity of rock types present along its course (Comero et al. 2014). The rock types outlining the river basin are differentiated vastly, both in terms of lithological composition and age. Drainage basins of most affluent have the same predominant lithology of the Danube course, probably with a greater contribution from sedimentary lithologies (Comero et al. 2014). The results of mineralogical analyses using the Danube alluvial sediments from Pančevo (Sakan et al. 2012) show the presence of quartz, calcite, illite, kaolinite, and quartz–feldspar transformed as abundant minerals, with quartz and calcite being predominant. The Tisa River sediments consisted mostly of quartz, illite, kaolinite, feldspar transformed, and calcite (Sakan et al. 2012).

Analysis of Corine Land Cover Database for the 2006 shows the presence of 28 out of 44 Class CLC

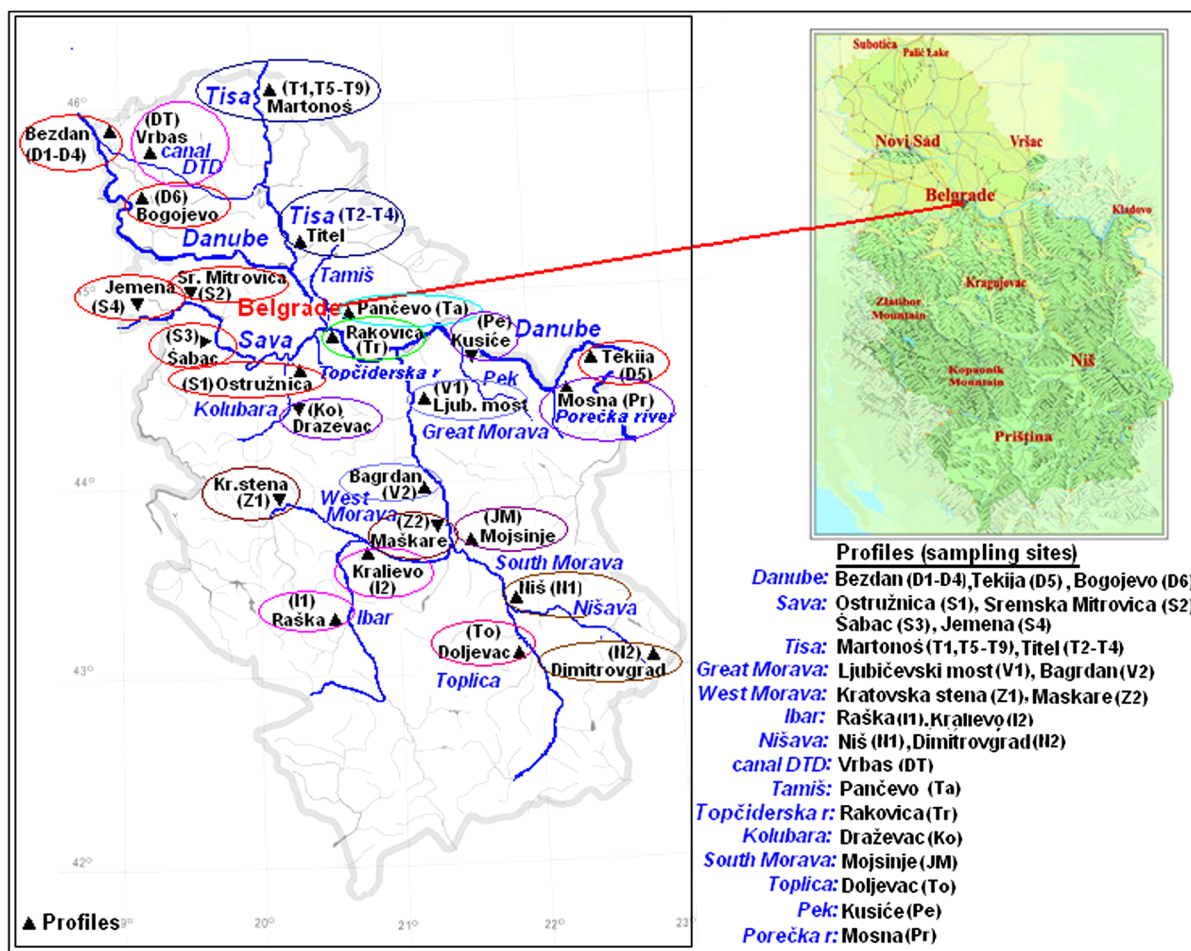


**Fig. 1** Map of Serbia and sampling locations. Explanation: D1–D6 (the Danube), S1–S4 (the Sava), T1–T9 (the Tisa), V1–V2 (the Great Morava), Z1–Z2 (the West Morava), I1–I2 (the

Ibar), N1–N2 (the Nišava), DT (the DTD canal), Ta (the Tamiš), Tr (the Topčiderska River), Ko (the Kolubara), JM (the South Morava), To (the Toplica), Pe (the Pek), Pr (the Porečka River)

nomenclature in Serbia (excluding Kosovo and Metohija). Majority share is of agricultural areas with 58 % of the total territory of the country. About 26 % is under the complex plots that are processed, while 13 % of predominantly agricultural land is mostly under natural vegetation. Forests and seminatural areas encompass nearly 40 % of the country. The land classified as an artificial surface covers nearly 3 % of the territory, and the remaining approximately 1.6 % is classified as wetlands and water basins (SEPA 2009).

#### Analysis of element content

Analysis of metals was carried out using the atomic emission spectrometer with an inductively coupled

plasma iCAP-6500 Duo (Thermo Scientific, United Kingdom), after triacid total digestion (HCl, HNO<sub>3</sub>, and HF). A 0.5-g sediment sample was placed in a Teflon vessel. Then 9 mL HCl (37 %), 3 mL HNO<sub>3</sub> (70 %), and 3 mL HF (48 %) were added to the vessel. One Teflon vessel only contains the acid mixture for a blank. A microwave digestion system brings the sample to 165 °C in 10 min (holding time 0 s), then 175 °C in 3 min, where held for 10 min (max power was 1200 W) (Rönkkömäki et al. 2008). Microwave digestion was performed in a pressurized microwave oven (Ethos 1, Advanced Microwave Digestion System, Milestone, Italy) equipped with a rotor holding 10 microwave vessels (PTFE).

After cooling the digestion system, 10 mL H<sub>3</sub>BO<sub>3</sub> (5 g/100 mL water) is added. Again, the microwave



digestion system brings the sample to 175 °C in 10 min at 1420 W and holds the temperature at 170 °C for 3 min. The digestate is then diluted to a final volume of 100 mL (Nam et al. 2001). The solutions were stored in polyethylene flasks for later determination of metals using ICP OES.

All reagents used in the analytical procedure were of analytical grade. Deionized water was used throughout the study. Analytical blanks were run in the same way as the samples, and concentrations determined using standard solutions prepared in the same acid matrix. The metal standards were prepared from a stock solution of 1,000 mg L<sup>-1</sup> by successive dilutions. The instrumental calibration was checked every 10–12 samples; if deviated by more than 2.5 %, the machine was recalibrated before analysis continued.

For each digestion were obtained reagent blanks. They were prepared in the same way as the samples without the sediments and CRMs. Blank samples, reflecting blank values for the sampling bottles, reagents, digestion vessels, filtration, and any contamination during the whole procedure were prepared and digested in parallel with the batch of samples, using the same procedure, the same quantities of all reagents, but omitting the test portion. The concentrations obtained for all metals in the blanks were close to the detection limit of the method, indicating a zero contamination effect in digestion method.

The accuracy and precision of our results were checked by analyzing sediment reference materials (BCR standards, 143R, and 146R). Accuracy was determined by comparing the measured concentration with the certified value and then expressed in percentage. The percentage recovery of each element was determined as: [measured concentration in mg kg<sup>-1</sup>/mean certified value for BCR 143 in mg kg<sup>-1</sup>] and [measured concentration in mg kg<sup>-1</sup>/mean certified value for BCR 146 in mg kg<sup>-1</sup>]. Accuracy was assessed as percentage-relative standard deviation (RSD), with RSD < 20 % being deemed acceptable (Chen and Ma 1998; Chand and Prasad 2013). Calculation results for the accuracy and precision of applied method are given in Table 1. Obtained results indicate a good concordance of the certified and analytical values for BCR 143 and BCR 146 reference materials; the accuracy ranged from 80.9 to 118 %, and precision was <10 % (from 0.03 to 3.80 %).

Results are expressed in mg kg<sup>-1</sup> of dry sediment. The detection limit was determined as three times the standard deviation of the blank measurements. The obtained values were (in mg kg<sup>-1</sup>): Cd–0.03, Cu–0.1, Co–0.03, Mn–0.03, Cr–0.1, Ni–0.1, Pb–0.5, Zn–0.05, Al–0.5, and Fe–0.3.

#### Metal pair ratio (M/Al) for elements in sediments

Results from several studies have indicated that the relative proportions of metals and aluminum in crustal material are fairly constant (Schropp and Windom 1988). Aluminum, a major component of clay minerals, is usually associated with fine-grained aluminosilicate minerals. The relative constancy of natural crustal materials composition was used as the basis for different studies of metal data interpretation. Duce et al. (1976) compared metal/aluminum ratios in atmospheric dust samples to those in average crustal material in order to estimate the relative atmospheric enrichment of metals due to anthropogenic sources.

The metal pair ratios depend on numerous processes in the geochemical cycle including weathering, transport, and deposition. Many studies were carried out to assess the extent of contamination in freshwater coastal sediments using a reference element normalization approach and employing various reference elements (Al and Fe) (Carvalho et al. 2002). Assessment of heavy metal contamination in sediments is based on geochemical elemental concentrations ratios in paper Jain et al. (2005). Sun et al. (2008) show that Al normalization is a reasonable approach for correcting dilution and assessing the enrichment of trace elements. In this research, Al-normalized elemental ratios were input as variance. The principal component analyses were performed in determining processes controlling the geochemical composition of the South China Sea sediments during the last climatic cycle.

Bartoli et al. (2012) have shown that using a comparison of metal concentration ratios in the sediments is a quick and practical method for tracing heavy metal enrichment. In natural river systems, elements and metals coexist in relative proportions. The ratios of trace metals to conservative elements may reveal geochemical imbalances due to elevated trace metal concentrations normally attributed to anthropogenic activities (Bartoli et al. 2012).

**Table 1** Total contents of heavy metals in certified reference materials (146R and 143R)

| Element | Certified 146R<br>(mg kg <sup>-1</sup> ) | Found<br>(mg kg <sup>-1</sup> ) | Accuracy<br>(%) | Certified 143R<br>(mg kg <sup>-1</sup> ) | Found<br>(mg kg <sup>-1</sup> ) | Accuracy<br>(%) |
|---------|--|---------------------------------|-----------------|--|---------------------------------|-----------------|
| Cd      | 18.8                                     | 18.3                            | 97.3            | 71.8                                     | 70.5                            | 98.2            |
| Co      | 7.39                                     | 7.62                            | 103             | 12.3                                     | 12.0                            | 102             |
| Cu      | 838                                      | 678                             | 80.9            | 130.6                                    | 111.4                           | 85.3            |
| Pb      | 609                                      | 532                             | 87.4            | 179.7                                    | 212.9                           | 118             |
| Mn      | 323                                      | 347                             | 108             | 904                                      | 834                             | 92.2            |
| Ni      | 70                                       | 60                              | 85.4            | 299                                      | 248                             | 82.9            |
| Zn      | 3060                                     | 2749                            | 89.8            | 1055                                     | 1116                            | 106             |
| Cr      | 196                                      | 167                             | 85.2            |  |                                 |                 |

### Enrichment factors (EF)

The enrichment factor (EF) can be used for assessing whether the presence of an element in sediment samples coincident with anthropogenic activities. EF represents the actual contamination level in the sediment, and it is a good tool for tracing heavy metal enrichment (Lin et al. 2011). The EF calculations compare each value with a given background level, either from the local site, using older deposits formed under similar conditions, but without anthropogenic impact, or from a regional or global average composition (Choi et al. 2012). The EF is defined as:

$$EF = (M/Y)_{\text{sample}} / (M/Y)_{\text{background}}$$

where  $M$  is the concentration of the potentially enriched element and  $Y$  is the concentration of the proxy element. To calculate the EF of the metals, the normalizer and the background levels of the metals should be determined.

### Geo-accumulation index ( $I_{\text{geo}}$ )

The geo-accumulation index, first described by Müller (1979), was used here as a second criterion to identify contaminated sediments.  $I_{\text{geo}}$  of an element in sediment can be calculated with the formula:

$$I_{\text{geo}} = \log_2 [C_{\text{metal}} / 1.5 C_{\text{metal}(\text{control})}]$$

where  $C_{\text{metal}}$  is the concentration of the heavy metal in the enriched sediment and  $C_{\text{metal}(\text{control})}$  is the concentration of the metal in the unpolluted sediment or control. The factor 1.5 is introduced to minimize the effect of the possible variations in the background or control values, which may be attributed to lithogenic variations in the sediment (Mediolla et al. 2008).  $I_{\text{geo}}$  is

a quantitative measure of the metal pollution in aquatic sediments and can be used as a reference to estimate the extent of metal pollution, in a similar way as enrichment factor. The index is based on a qualitative pollution intensity scale, whereby sediments can be classified as: uncontaminated/unpolluted (class 0, for  $I_{\text{geo}} < 0$ ); unpolluted to moderately polluted (class 1, for  $0 \leq I_{\text{geo}} < 1$ ); moderately polluted (class 2, for  $1 \leq I_{\text{geo}} < 2$ ); moderately to highly polluted (class 3, for  $2 \leq I_{\text{geo}} < 3$ ); highly polluted (class 4, for  $3 \leq I_{\text{geo}} < 4$ ); highly to extremely polluted (class 5, for  $4 \leq I_{\text{geo}} < 5$ ); and extremely polluted (class 6, for  $I_{\text{geo}} \geq 5$ ).

## Results and discussion

### Metal content

The metal contents of the sediment samples are presented in Table 2, as well as soil standards for Serbia (Official Gazette of Serbia, 1990). The ranges of metals in sediment were 23,482–89,119 mg kg<sup>-1</sup> for Al; 24,556–62,800 mg kg<sup>-1</sup> for Fe; 1.28–10.5 mg kg<sup>-1</sup> for Cd; 8.20–36.2 mg kg<sup>-1</sup> for Co; 59.8–230 mg kg<sup>-1</sup> for Cr; 11.5–870 mg kg<sup>-1</sup> for Cu; 648–3,688 mg kg<sup>-1</sup> for Mn; 33.2–274 mg kg<sup>-1</sup> for Ni; 57.8–318 mg kg<sup>-1</sup> for Pb; and 66.7–1,095 mg kg<sup>-1</sup> for Zn. The significant higher values of all analyzed elements were observed in the sediment samples from Tisa, Toplica, Pek, Porečka River, West Morava, and Ibar. In the studied region, said river systems are the most critical sites of metal contamination. Their pollution is mainly caused by permanent and accidental pollution from industrial plants and mines located in the basins: Trepca mining complex–Pb and Zn (Ibar), mining complex in



**Table 2** Content of studied elements in sediments, expressed in (mg kg<sup>-1</sup>)

| Sample | Al     | Fe     | Cd   | Co   | Cr    | Cu   | Mn    | Ni   | Pb   | Zn    |
|--------|--------|--------|------|------|-------|------|-------|------|------|-------|
| T1     | 54,345 | 33,105 | 5.05 | 10.0 | 59.8  | 47.8 | 1,276 | 39.2 | 95.7 | 330   |
| T2     | 63,956 | 49,098 | 4.23 | 20.5 | 103.3 | 64.5 | 1,234 | 46.2 | 118  | 335   |
| T3     | 72,870 | 46,711 | 4.97 | 21.2 | 95.8  | 74.1 | 1,324 | 45.0 | 124  | 391   |
| T4     | 75,717 | 42,246 | 4.41 | 19.1 | 90.2  | 63.8 | 1,399 | 39.2 | 124  | 338   |
| T5     | 39,331 | 46,480 | 6.37 | 22.6 | 106   | 88.3 | 1,722 | 47.7 | 112  | 360   |
| T6     | 67,904 | 50,118 | 6.89 | 21.3 | 99.8  | 90.5 | 2,108 | 42.4 | 142  | 420   |
| T7     | 26,311 | 43,445 | 6.23 | 19.8 | 92.8  | 74.0 | 1,870 | 42.8 | 90.3 | 346   |
| T8     | 71,782 | 43,281 | 6.09 | 19.3 | 89.5  | 71.1 | 1,683 | 41.5 | 119  | 337   |
| T9     | 83,795 | 46,932 | 7.00 | 21.5 | 96.3  | 87.1 | 1,816 | 46.3 | 140  | 411   |
| D1     | 44,340 | 40,134 | 2.25 | 16.2 | 73.4  | 28.0 | 1,387 | 33.2 | 90.0 | 168   |
| D2     | 89,119 | 39,637 | 2.12 | 16.3 | 75.0  | 23.8 | 1,036 | 36.0 | 114  | 157   |
| D3     | 54,910 | 40,922 | 2.49 | 16.8 | 79.9  | 31.4 | 979   | 35.8 | 104  | 208   |
| D4     | 62,215 | 37,534 | 2.35 | 15.4 | 76.1  | 28.9 | 896   | 35.0 | 132  | 220   |
| D5     | 23,482 | 40,389 | 2.78 | 19.0 | 78.4  | 40.7 | 1,352 | 37.9 | 80.3 | 221   |
| D6     | 54,034 | 44,697 | 5.31 | 21.5 | 123   | 41.9 | 1,185 | 70.8 | 136  | 228   |
| S1     | 44,354 | 36,506 | 3.46 | 21.7 | 112   | 32.0 | 1,025 | 93.6 | 89.0 | 270   |
| S2     | 57,957 | 46,480 | 3.02 | 28.5 | 154   | 36.4 | 1,759 | 126  | 115  | 213   |
| S3     | 57,781 | 43,872 | 3.74 | 26.4 | 140   | 36.4 | 1,660 | 119  | 113  | 272   |
| S4     | 54,741 | 45,780 | 4.69 | 27.3 | 145   | 31.3 | 1,819 | 119  | 110  | 213   |
| I1     | 36,516 | 36,863 | 10.5 | 13.6 | 102   | 29.0 | 904   | 142  | 318  | 947   |
| I2     | 59,195 | 47,630 | 8.32 | 36.2 | 230   | 39.4 | 1,352 | 274  | 263  | 1,095 |
| V1     | 29,759 | 55,319 | 7.91 | 32.3 | 170   | 65.6 | 1,734 | 42.6 | 182  | 499   |
| V2     | 61,204 | 46,593 | 6.82 | 27.7 | 152   | 53.0 | 1,226 | 156  | 182  | 449   |
| Z1     | 47,320 | 33,860 | 3.60 | 12.2 | 85.6  | 155  | 808   | 84.2 | 77.2 | 250   |
| Z2     | 57,360 | 46,461 | 7.50 | 31.8 | 222   | 52.6 | 1,032 | 236  | 213  | 660   |
| JM     | 74,056 | 50,105 | 3.88 | 23.4 | 106   | 47.9 | 3,688 | 55.1 | 150  | 238   |
| N1     | 59,353 | 38,745 | 2.65 | 16.3 | 86.3  | 85.0 | 731   | 35.9 | 138  | 411   |
| N2     | 42,827 | 34,881 | 5.53 | 16.2 | 70.7  | 22.1 | 770   | 34.6 | 84.1 | 114   |
| Ta     | 95,849 | 62,800 | 3.12 | 26.5 | 112   | 51.9 | 1,413 | 50.4 | 137  | 191   |
| DT     | 36,323 | 24,556 | 1.28 | 8.2  | 62.1  | 11.5 | 648   | 34.7 | 57.8 | 66.7  |
| Tr     | 52,416 | 50,739 | 3.91 | 27.9 | 161   | 40.9 | 1,226 | 133  | 144  | 338   |
| Pr     | 72,811 | 51,266 | 3.13 | 23.8 | 118   | 137  | 868   | 59.0 | 119  | 155   |
| Ko     | 61,971 | 47,245 | 5.45 | 28.7 | 146   | 39.4 | 1,352 | 132  | 126  | 417   |
| Pe     | 78,474 | 50,977 | 6.26 | 30.5 | 88.7  | 870  | 1,997 | 41.6 | 157  | 922   |
| To     | 34,488 | 50,808 | 5.23 | 29.5 | 148   | 55.6 | 1,685 | 115  | 135  | 167   |
| MAQ    |        |        | 2    |      | 100   | 100  |       | 50   | 100  | 300   |

MAQ maximum allowed quantity (Official Gazette of Serbia 1990)

Majdanpek–Cu (Pek) and other basins, agricultural products, mainly due to the use of manganese-containing products, such as fertilizer and fungicide. The landfill Trepča has the greatest impact on the lead and zinc pollution of the Ibar, since in this area is located vast number of production and manufacturing plants of the mining–metallurgical system Trepča–nine lead and zinc mines, three flotations, two of metallurgy, the chemical

industry, and a battery factory (Barać et al. 2009). The highest content of heavy metals was found at sediments from river Pek. The spring of the Pek River is near to Majdanpek, and since there is a Cu mine in Majdanpek, it is fair to assume that Cu presence is associated with this mine. Tisa River was in the past contaminated by industrial accidents, resulting in cyanide and heavy metals spill (Sakan et al. 2009). For Tisa, Great Morava,

and Sava affluent, literature confirmed impact of mining industry and industrial facilities discharge on sediment contamination (Comero et al. 2014). In Serbia, the primary extracted minerals include copper, coal, lead–zinc with associated gold, silver, bismuth and cadmium, red bauxite, and modest quantities of oil and gas. River Toplica is mostly affected by the wood-processing and processing fruits and vegetables plants, ranging from Kursumljia and Prokuplje, but this region is also exposed to the impact of waters from illegal dumps formed in river beds or on their banks (Samardžić 2013). The Porečka River pollution is caused by waste waters from a copper mine in Majdanpek tailings reservoirs (Marinos et al. 1997).

The concentration levels of Cd, Cr, Ni, Pb, and Zn are unsafe when compared with Serbian MAQ (Maximum Allowed Quantity) of soils for the majority of the sediment samples and for Cu in sediment samples from the Pek and Porečka River. The maximum contents for most elements are higher than the background values (Table 2) in the studied sediments. These results suggested existence of some anthropogenic inputs of studied elements in addition to the natural inputs. The significant anthropogenic source of these elements is mining and smelting complexes in Serbia.

For tracing and determination of the heavy metal enrichment, three indices were calculated in this paper: ratios of trace metals to conservative elements, enrichment factor, and *I*<sub>geo</sub>.

#### Metal pair ratio (M/Al) for studied element in sediments

Table 4 presents trace metal to aluminum ratio for studied elements in river sediments. From the results, it can be concluded that sediments at sites I1, I2 (Ibar), and V1 (Great Morava) are the most polluted with heavy metals, followed by the sediments from T5 and T7 (Tisa), D5 (the Danube), Z1 and Z2 (West Morava), Pr (Porečka River), and To (Toplica), having enrichment of almost all the metals.

From elements, the highest M/Al ratios were for Mn, Zn, Cu, and Pb, indicating that these elements represent significant pollution substances of the studied locality. Since that value of M/Al for some of studied elements point to the existence of pollution, it should quantify the degree of pollution.

#### Enrichment factors (EF)

In order to determine the extent of contamination of the sediments, EF values are calculated for all heavy metals. Metal content was normalized with content of iron and aluminum followed by result comparison. In general, Al or Fe was used as a suitable element for normalization in researches (Radakovich et al. 2008), due to their relative abundance in the Earth's crust and thus decreased the tendency to be heavily influenced by human activities (Jain et al. 2005). The EF values were interpreted as suggested by (Acevedo-Figueroa et al. 2006), where:  $EF < 1$  indicates no enrichment;  $< 3$  is minor; 3–5 is moderate; 5–10 is moderately severe; 10–25 is severe; 25–50 is very severe; and  $> 50$  is extremely severe. For the purposes of comparison, the degree of enrichment by heavy metals for studied sediments is also assessed with different background concentrations: reference values for the average continental crust and local background values. The background concentrations of elements in investigated sediments, values for the element content in continental crust, as well as background values for the elements in sediments given by other authors are shown in Table 3.

The element contents in sediments from the DTD canal (station in Vrbas) were chosen as the local background values for elements in this research because there are no significant anthropogenic sources of toxic elements at this locality, and the sediment samples are similar to the other investigated river sediments in geochemical characteristics and composition. Concentration result for the DTD canal (station in Vrbas) is shown in Table 3, as the background values of observed sediments. As suggested by some authors, the establishment of local background levels is necessary to compare contents of the target heavy metals and similarity of mineralogy and texture in contaminated sediments with uncontaminated sediments (Ho et al. 2012).

Figures 2 and 3 show calculated sediment EF for studied elements. The summary statistics for the EFs of metals are shown in Table 5. The results show that EF values are highly dependent on the normalizer selected for analysis and selected background values. The higher values were obtained when EF was calculated using continental crust as background, than when used regional background values. The highest discrepancy of EF values was obtained for Cd

**Table 3** Background concentrations of elements in sediments, expressed in (mg kg<sup>-1</sup>)

|    | Crust <sup>a</sup> | River sediment <sup>b</sup> | Stream sediment <sup>c</sup> | Range in soils <sup>c</sup> | River sediments <sup>f</sup> | River sediments <sup>g</sup> | River sediments <sup>h</sup> | Lake sediments <sup>i</sup> |
|----|--------------------|-----------------------------|------------------------------|-----------------------------|------------------------------|------------------------------|------------------------------|-----------------------------|
| Al | 79,600             | 36,323                      | nd <sup>d</sup>              | nd                          | nd                           | nd                           | 44,000                       | nd                          |
| Fe | 43,200             | 24,556                      | nd                           | nd                          | 2,400 ± 500                  | nd                           | 27,700                       | nd                          |
| Cd | 0.1                | 1.28                        | nd                           | 0.06–1.1                    | nd                           | 0.66 ± 0.69                  | 0.075                        | 0.42                        |
| Co | 24                 | 8.22                        | 3.13                         | 21.6–21.5                   | 6.1 ± 1.5                    | 14.2 ± 10.0                  | nd                           | nd                          |
| Cr | 126                | 62.1                        | 40.06                        | 7–221                       | 63 ± 14                      | nd                           | 145                          | 94.90                       |
| Cu | 25                 | 11.5                        | 9.19                         | 6–80                        | 12 ± 3                       | 49.3 ± 39.3                  | 11.9                         | 90.10                       |
| Mn | 716                | 648                         | 140.87                       | 80–1,300                    | nd                           | nd                           | 559                          | nd                          |
| Ni | 56                 | 34.7                        | 15.73                        | 4–55                        | 26 ± 10                      | 32.4 ± 18.2                  | 191                          | nd                          |
| Pb | 14.8               | 57.8                        | 18.82                        | 10–84                       | 27 ± 7                       | 7.3 ± 9.6                    | 10.8                         | 38.10                       |
| Zn | 65                 | 66.6                        | 65.90                        | 17–125                      | 55 ± 11                      | 91.6 ± 41.5                  | 64.5                         | 156.0                       |

<sup>a</sup> Element content in Continental crust (Wedepohl 1995)

<sup>b</sup> Background values in the studied sediments (element content in the DTD canal, this study)

<sup>c</sup> Background values in stream sediments (mean values) around the Aluminum Smelting Company, Nigeria (Ekwere and Elueze 2012)

<sup>d</sup> No data

<sup>e</sup> Range of means in soils (worldwide, background concentration, McBride 1994)

<sup>f</sup> Range of metal concentrations for the background values in sediments from Ferrol Ria, Spain (Cobelo-García and Prego 2003)

<sup>g</sup> Sediments from Pasvik River, Russia, average background values with standard deviation (Dauvalter and Rognerrud 2001)

<sup>h</sup> Sediments from Asopos River, Central Greece, total metal contents of the reference stations (Botsou et al. 2011)

<sup>i</sup> Lake sediments from Dianchi Lake, China, mean values (Ren-Ying et al. 2007)

(Table 4), which was related to significantly different values of crust and background concentrations (Table 2) for the given elements. EF values are also dependent on element used for normalization (Al or Fe), but they are more influenced by selection of background values. Results indicate that heavy metals were enriched in most sediment from different areas (EF > 1). However, significant differences can be observed in the grade of pollution in studied localities, since the range of EF values is from <1 to >50 for studied elements.

The average EF values calculated using local sediment background values as background and (1) Al as a normalizer are: Cu (moderate enrichment) > Zn (moderate enrichment) > Cd (minor enrichment) > Co (minor enrichment) > Pb (minor enrichment) > Ni (minor enrichment) > Mn (minor enrichment) > Cr (minor enrichment), and (2) Fe as a normalizer are: Cu (moderate enrichment) > Zn (moderate enrichment) > Cd (minor enrichment) > Co (minor enrichment) > Pb (minor enrichment) > Ni (minor enrichment) > Mn (minor enrichment) > Cr (minor enrichment). It is possible to conclude that the order of the calculated EF of

elements is the same when used Al and Fe as elements for normalization. Results indicate that enrichment with studied elements is minor to moderate.

In Table 4, are shown values of ratio between EF calculated with Al, and EF calculated with Fe as normalization elements: EF (Al and background values)/EF (Fe and background values). It is possible to conclude that the ratio for EFs in the majority of sediments is approximately 1. Values 2 for this ratio were observed in sediment samples with observed contamination of heavy metals (higher values of EF for some elements, such as: Tisa, T5, and T7; Danube, D5; Great Morava, V1, and Toplica, To).

The average EF values calculated using continental crust values as background and: (1) Al as a normalizer are: Cd (extremely severe enrichment) > Pb (severe enrichment) > Zn (moderately severe enrichment) > Cu (moderate enrichment) > Mn (moderate enrichment) > Ni (minor enrichment) > Co (minor enrichment) > Cr (minor enrichment), and (2) Fe as a normalizer are: Cd (very severe enrichment) > Pb (moderately severe enrichment) > Zn (moderately severe enrichment) > Cu (moderate enrichment) > Mn (minor enrichment) > Ni (minor

**Table 4** Metals/Al ratio for different metals in river sediments and relationship between the enrichment factors

| Sample | Cd <sup>a</sup><br>( $\times 10^{-3}$ ) | Co<br>( $\times 10^{-3}$ ) | Cr<br>( $\times 10^{-3}$ ) | Cu<br>( $\times 10^{-3}$ ) | Mn<br>( $\times 10^{-3}$ ) | Ni<br>( $\times 10^{-3}$ ) | Pb<br>( $\times 10^{-3}$ ) | Zn<br>( $\times 10^{-3}$ ) | EFb <sup>b</sup> | EFc <sup>c</sup> |
|--------|---|----------------------------|----------------------------|----------------------------|----------------------------|----------------------------|----------------------------|----------------------------|------------------|------------------|
| T1     | 0.09                                    | 0.18                       | 1.10                       | 0.88                       | 23.5                       | 0.72                       | 1.76                       | 6.08                       | 0.90             | 1.12             |
| T2     | 0.07                                    | 0.32                       | 1.61                       | 1.01                       | 19.3                       | 0.72                       | 1.85                       | 5.24                       | 1.14             | 1.41             |
| T3     | 0.07                                    | 0.29                       | 1.32                       | 1.02                       | 18.2                       | 0.62                       | 1.70                       | 5.37                       | 0.95             | 1.18             |
| T4     | 0.06                                    | 0.25                       | 1.19                       | 0.84                       | 18.5                       | 0.52                       | 1.64                       | 4.46                       | 0.83             | 1.03             |
| T5     | 0.16                                    | 0.58                       | 2.68                       | 2.25                       | 43.8                       | 1.21                       | 2.86                       | 9.14                       | 1.75             | 2.17             |
| T6     | 0.10                                    | 0.31                       | 1.47                       | 1.33                       | 31.0                       | 0.62                       | 2.09                       | 6.18                       | 1.09             | 1.36             |
| T7     | 0.24                                    | 0.75                       | 3.53                       | 2.81                       | 71.1                       | 1.63                       | 3.43                       | 13.2                       | 2.44             | 3.04             |
| T8     | 0.09                                    | 0.27                       | 1.25                       | 0.99                       | 23.4                       | 0.58                       | 1.66                       | 4.69                       | 0.89             | 1.11             |
| T9     | 0.08                                    | 0.26                       | 1.15                       | 1.04                       | 21.7                       | 0.55                       | 1.67                       | 4.91                       | 0.83             | 1.03             |
| D1     | 0.05                                    | 0.37                       | 1.66                       | 0.63                       | 31.3                       | 0.75                       | 2.03                       | 3.80                       | 1.34             | 1.66             |
| D2     | 0.02                                    | 0.18                       | 0.84                       | 0.27                       | 11.6                       | 0.40                       | 1.28                       | 1.76                       | 0.66             | 0.82             |
| D3     | 0.05                                    | 0.31                       | 1.46                       | 0.57                       | 17.8                       | 0.65                       | 1.89                       | 3.79                       | 1.10             | 1.37             |
| D4     | 0.04                                    | 0.25                       | 1.22                       | 0.47                       | 14.4                       | 0.56                       | 2.11                       | 3.54                       | 0.89             | 1.11             |
| D5     | 0.12                                    | 0.81                       | 3.34                       | 1.73                       | 57.6                       | 1.61                       | 3.42                       | 9.40                       | 2.55             | 3.16             |
| D6     | 0.10                                    | 0.40                       | 2.28                       | 0.78                       | 21.9                       | 1.31                       | 2.51                       | 4.23                       | 1.22             | 1.52             |
| S1     | 0.08                                    | 0.49                       | 2.52                       | 0.72                       | 23.1                       | 2.11                       | 2.01                       | 6.10                       | 1.22             | 1.51             |
| S2     | 0.05                                    | 0.49                       | 2.65                       | 0.63                       | 30.3                       | 2.17                       | 1.99                       | 3.68                       | 1.19             | 1.47             |
| S3     | 0.07                                    | 0.46                       | 2.43                       | 0.63                       | 28.7                       | 2.05                       | 1.95                       | 4.70                       | 1.12             | 1.40             |
| S4     | 0.09                                    | 0.50                       | 2.65                       | 0.57                       | 33.2                       | 2.17                       | 2.00                       | 3.88                       | 1.24             | 1.54             |
| I1     | 0.29                                    | 0.37                       | 2.81                       | 0.79                       | 24.7                       | 3.90                       | 8.72                       | 25.9                       | 1.49             | 1.86             |
| I2     | 0.14                                    | 0.61                       | 3.89                       | 0.67                       | 22.8                       | 4.62                       | 4.44                       | 18.5                       | 1.19             | 1.48             |
| V1     | 0.27                                    | 1.08                       | 5.72                       | 2.20                       | 58.3                       | 1.43                       | 6.12                       | 16.8                       | 2.75             | 3.42             |
| V2     | 0.11                                    | 0.45                       | 2.49                       | 0.87                       | 20.0                       | 2.55                       | 2.97                       | 7.33                       | 1.13             | 1.40             |
| Z1     | 0.08                                    | 0.26                       | 1.81                       | 3.28                       | 17.1                       | 1.78                       | 1.63                       | 5.28                       | 1.06             | 1.32             |
| Z2     | 0.13                                    | 0.56                       | 3.87                       | 0.92                       | 18.0                       | 4.12                       | 3.72                       | 11.5                       | 1.20             | 1.49             |
| JM     | 0.05                                    | 0.32                       | 1.43                       | 0.65                       | 49.8                       | 0.74                       | 2.03                       | 3.21                       | 1.00             | 1.24             |
| N1     | 0.05                                    | 0.27                       | 1.45                       | 1.43                       | 12.3                       | 0.60                       | 2.32                       | 6.92                       | 0.97             | 1.20             |
| N2     | 0.13                                    | 0.38                       | 1.65                       | 0.52                       | 18.0                       | 0.81                       | 1.97                       | 2.66                       | 1.20             | 1.50             |
| Ta     | 0.03                                    | 0.28                       | 1.17                       | 0.54                       | 14.7                       | 0.53                       | 1.43                       | 1.99                       | 0.97             | 1.20             |
| Tr     | 0.04                                    | 0.23                       | 1.71                       | 0.32                       | 17.8                       | 0.96                       | 1.59                       | 1.84                       | 1.43             | 1.78             |
| Pr     | 0.08                                    | 0.53                       | 3.07                       | 0.78                       | 23.4                       | 2.53                       | 2.76                       | 6.44                       | 1.04             | 1.29             |
| Ko     | 0.04                                    | 0.33                       | 1.62                       | 1.88                       | 11.9                       | 0.81                       | 1.64                       | 2.13                       | 1.13             | 1.40             |
| Pe     | 0.09                                    | 0.46                       | 2.36                       | 0.64                       | 21.8                       | 2.13                       | 2.03                       | 6.73                       | 0.96             | 1.19             |
| To     | 0.08                                    | 0.39                       | 1.13                       | 11.1                       | 25.5                       | 0.53                       | 2.00                       | 11.7                       | 2.18             | 2.71             |

<sup>a</sup> Metals/Al ratio for different metals

<sup>b</sup> Relationship between the enrichment factors calculated with local background values (content in DTD canal) and different normalization elements:  $EFb = EF(\text{with Al and background values})/EF(\text{with Fe and background values})$

<sup>c</sup> Relationship between the enrichment factors calculated with continental crust and different normalization elements:  $EFc = EF(\text{with Al and continental crust})/EF(\text{with Fe and continental crust})$

enrichment) > Co (no enrichment) > Cr (enrichment). Results indicated that enrichment with studied elements ranged from minor to extremely severe. Results of EFs with values of continental crust and

local background values for studied sediments were different, especially for Cd and Pb.

Ratio  $EF(\text{Al and continental crust})/EF(\text{Fe and continental crust})$  has been calculated, and results were

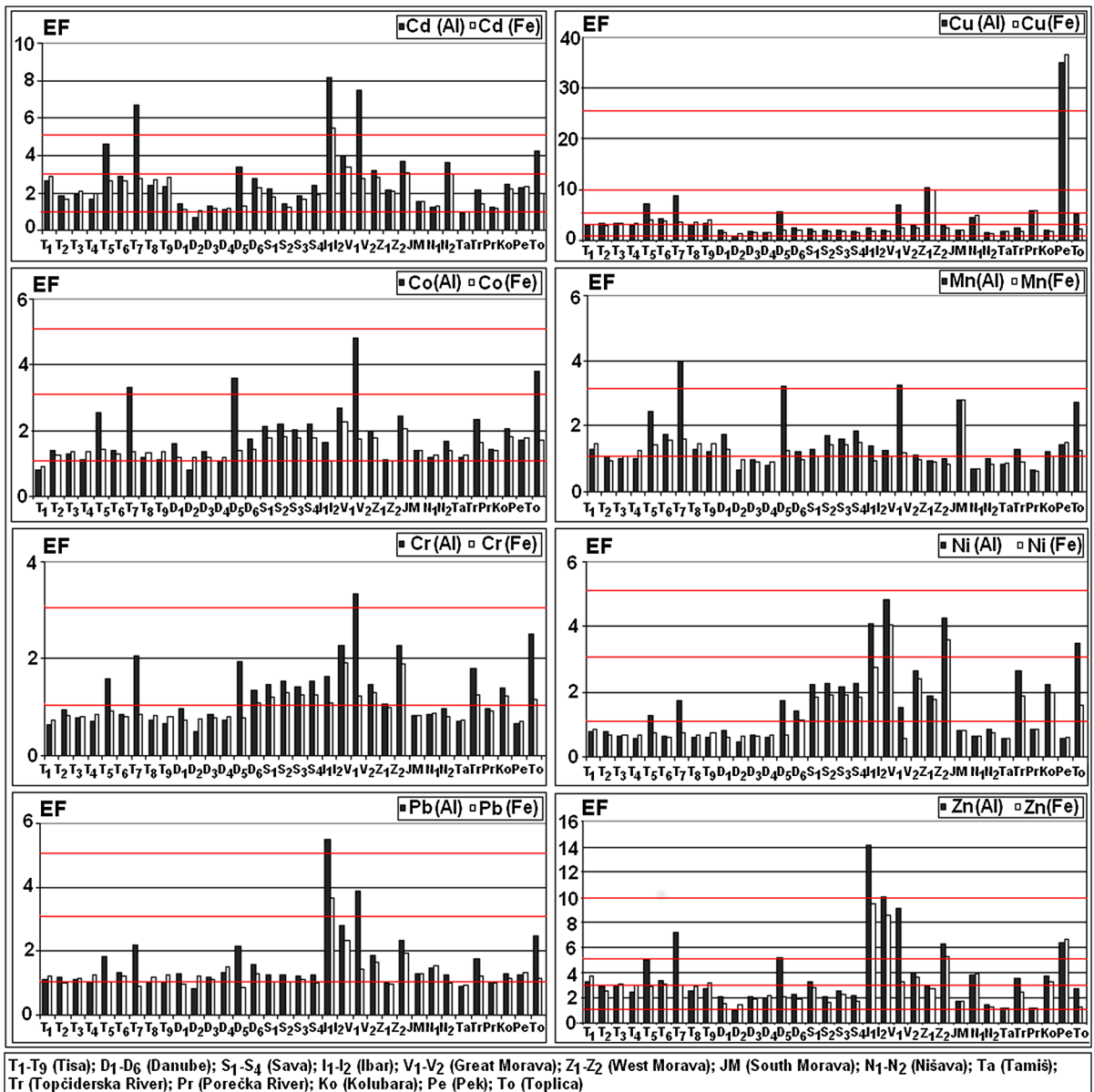


**Fig. 2** EF values (with calculated background values) depending on the element that was used for normalization (Al and Fe)

shown in Table 4. It can be concluded that for most of sediments, values of the ratio of EFs are mainly 1, except in the sediments with higher EF values. In these sediments, EF values were 2 (T5–Tisa) and 3 (T7–Tisa, D5–Danube, V1–Great Morava, and To–Toplica).

In Table 6, it was shown that the ratios between calculated EF values with different background values and elements are used for normalization. A significant difference was observed between EF for Cd (28.1 and

22.6) and Pb (8.4 and 6.9), which was related to different values of crust and background concentrations (Table 6), as these values were significantly different for the given elements (Table 3). Also, the Fe and Al contents in the calculated background and crust were different, which also affected EF values. Results shown that EF values with continental crust as background were higher than EF values calculated with regional background values for most elements.

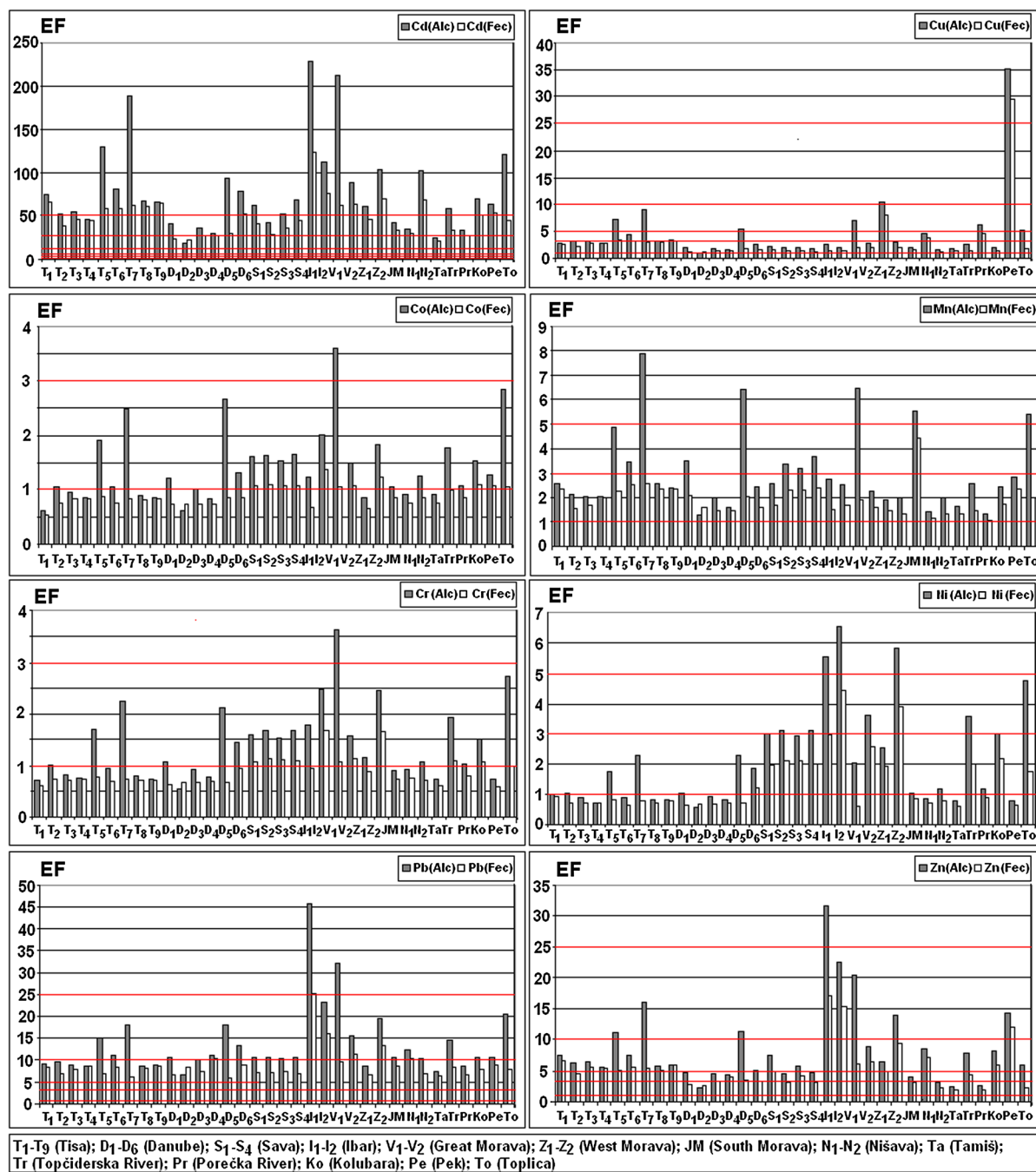


**Fig. 3** EF values (with crust content as background values) depending on the element that was used for normalization (Al and Fe)

It is possible to conclude that the choice of element for geochemical normalization and background values is very important. For a specific site and region, it is significant to have good assessment

of said values. Also, obtained results indicate that the value of EF is more influenced by the choice of background values than with selection of element used for normalization.

**Table 5** Enrichment factors for studied heavy metals

|                              | Parameter | Cd    | Co   | Cr   | Cu    | Mn   | Ni   | Pb   | Zn    |
|------------------------------|-----------|-------|------|------|-------|------|------|------|-------|
| EF<br>(BV <sub>c</sub> , Al) | Average   | 2.77  | 1.90 | 1.29 | 4.37  | 1.53 | 1.58 | 1.62 | 3.78  |
|                              | S.D.      | 1.78  | 0.90 | 0.65 | 5.84  | 0.81 | 1.20 | 0.93 | 2.82  |
|                              | Minimum   | 0.68  | 0.81 | 0.49 | 0.84  | 0.65 | 0.42 | 0.80 | 0.96  |
|                              | Maximum   | 8.18  | 4.79 | 3.35 | 35.03 | 3.99 | 4.84 | 5.48 | 14.13 |
| EF<br>(BV <sub>c</sub> , Fe) | Average   | 2.13  | 1.48 | 1.00 | 3.73  | 1.20 | 1.25 | 1.29 | 3.00  |
|                              | S.D.      | 0.92  | 0.30 | 0.30 | 6.01  | 0.39 | 0.90 | 0.51 | 1.91  |
|                              | Minimum   | 0.95  | 0.90 | 0.69 | 1.28  | 0.64 | 0.55 | 0.85 | 1.11  |
|                              | Maximum   | 5.48  | 2.27 | 1.91 | 36.4  | 2.79 | 4.07 | 3.67 | 9.47  |
| EF<br>(Cr, Al)               | Average   | 77.7  | 1.42 | 1.40 | 4.40  | 3.04 | 2.15 | 13.6 | 8.47  |
|                              | S.D.      | 50.1  | 0.67 | 0.71 | 5.89  | 1.62 | 1.62 | 7.77 | 6.32  |
|                              | Minimum   | 18.9  | 0.60 | 0.53 | 0.85  | 1.29 | 0.57 | 6.72 | 2.15  |
|                              | Maximum   | 229   | 3.59 | 3.62 | 35.3  | 7.91 | 6.56 | 45.9 | 31.6  |
| EF<br>(Cr, Fe)               | Average   | 48.1  | 0.89 | 0.87 | 3.02  | 1.90 | 1.37 | 8.84 | 5.41  |
|                              | S.D.      | 20.7  | 0.18 | 0.26 | 4.86  | 0.62 | 0.98 | 3.56 | 3.44  |
|                              | Minimum   | 21.5  | 0.54 | 0.60 | 1.04  | 1.02 | 0.59 | 5.80 | 2.01  |
|                              | Maximum   | 123.7 | 1.37 | 1.66 | 29.5  | 4.44 | 4.43 | 25.2 | 17.1  |

BV<sub>c</sub> background values in the studied sediments (element content in DTD canal), Cr element content in Continental crust

**Table 6** Ratio between calculated EF values with different background values and element for normalization

|                | EF(Cd)               | EF(Co)  | EF(Cr)  | EF(Cu)  | EF(Mn)  | EF(Ni)  | EF(Pb)  | EF(Zn)  |
|----------------|----------------------|---------|---------|---------|---------|---------|---------|---------|
| L <sup>a</sup> | Fec/Feb <sup>b</sup> | Fec/Feb | Fec/Feb | Fec/Feb | Fec/Feb | Fec/Feb | Fec/Feb | Fec/Feb |
|                | 22.6                 | 0.6     | 0.9     | 0.8     | 1.6     | 1.1     | 6.9     | 1.8     |
| L              | Alc/Alb <sup>c</sup> | Alc/Alb | Alc/Alb | Alc/Alb | Alc/Alb | Alc/Alb | Alc/Alb | Alc/Alb |
|                | 28.1                 | 0.8     | 1.1     | 1.0     | 2.0     | 1.4     | 8.4     | 2.2     |

<sup>a</sup> Studied locality

<sup>b</sup> EF calculated with Fe as element for normalization and different background content (c-Continental crust and b-content in DTD canal)

<sup>c</sup> EF calculated with Al as element for normalization and different background content (c-Continental crust and b-content in DTD canal)

Geo-accumulation index ( $I_{geo}$ )

The geo-accumulation index of heavy metals in sediments and grading of pollution levels are shown in Fig. 4. When calculating  $I_{geo}$ , two different values were taken as background contents: Continental crust and local background values (determined for studied sediments) and results were compared.

Based on the results of the geo-accumulation index, it can be observed

1. If local background is used for calculation  $I_{geo}$ : Cd (class 1 to 2), Cu (class 1 to 4), Co (class 1 to 2), Mn

(class 0 to 2), Cr (class 0 to 1), Ni (class 0 to 2), Pb (class 1 to 2), and Zn (class 1 to 3).

2. If continental crust is used for calculation  $I_{geo}$ : Cd (class 1 to 5), Cu (class 0 to 1), Co (class 0), Mn (class 0 to 2), Cr (class 0 to 1), Ni (class 0 to 2), Pb (class 1 to 3), and Zn (class 1 to 3).

Differences in the values of  $I_{geo}$  can be observed depending on the choice of background values used for calculation. The highest value for  $I_{geo}$  was observed for Cu and Zn, if  $I_{geo}$  was calculated using the local background values while the continental crust as the background for Cd and Zn. The smallest difference in  $I_{geo}$  values is obtained for Zn, which is a consequence of the similar values for background value and continental



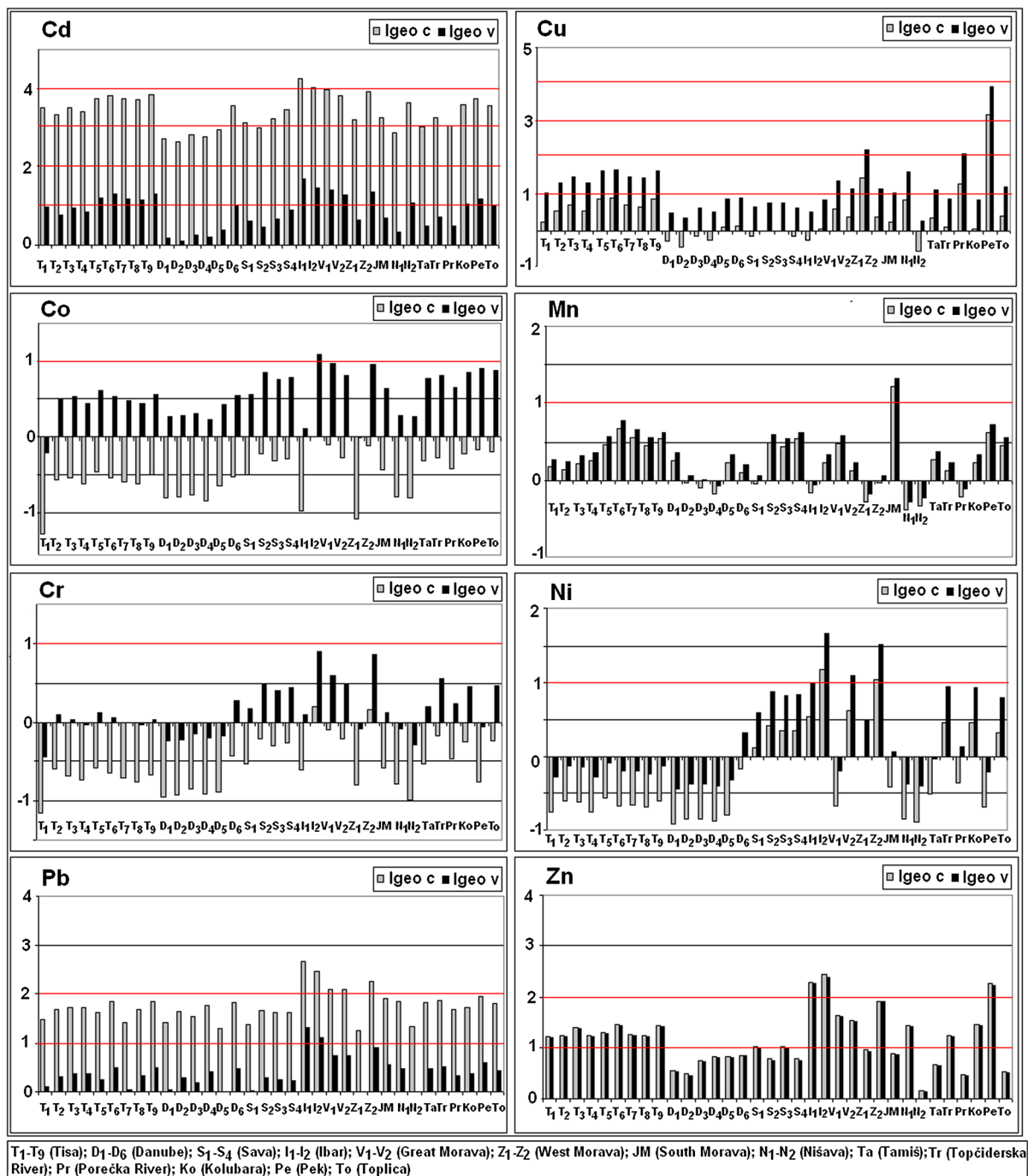


**Fig. 4**  $I_{geo}$  values depending on the choice of background values (crust,  $I_{geo\ c}$ , and calculated background for studied sediments,  $I_{geo\ v}$ )

crust content for Zn. Greater differences in values of  $I_{geo}$  are observed among elements that are significant pollutants. There was very little difference in values of  $I_{geo}$  between the Mn, Cr, and Ni.

Present results of geo-accumulation index (Fig. 4) revealed that studied river sediments were remaining unpolluted to moderately polluted with Co, Mn, Cr, and Ni ( $I_{geo} < 2$ ). Significant pollution in the

sediments was observed for the elements Cd, Cu, Pb, and Zn. Enrichment with these heavy metals at studied locations indicated the existence of significant anthropogenic sources of these elements. From the studied river systems, the highest value for  $I_{geo}$  is determined in the following river systems: (1) with Cd: Tisa, Ibar, the Great Morava, West Morava, Kolubara, Pek, and Toplica; (2) with Cu: Tisa, the Great Morava, West Morava, Porecka River, and Pek; (3) with Pb: Ibar, West Morava, and (4) with Zn: Ibar, Pek, Kolubara, and West and the Great Morava. Contamination in these river basins was mainly consequence of industrial and mining activities (Bor and Majdanpek Cu deposits and the Trepča deposits, Baia Mare and Baia Borsa mine in Romania) and city inputs.

Due to differences in the obtained  $I_{geo}$  values calculated with different background contents for studied elements, it was important to perform precise and accurate determination of background values in assessment of pollution status and calculation of contamination indices. Our recommendation would be to use the local and regional background content in calculation contamination factors and pollution indices.

## Conclusion

The obtained results show that  $I_{geo}$  and EF were useful in assessing metal pollution from both natural and anthropogenic processes. The calculation of EF and  $I_{geo}$  indicated that the studied river sediments were greatly contaminated by anthropogenic activities. Results isolate Cd, Cu, Pb, and Zn as potential threat to water environment safety.

Due to complexity of the local lithology, it is recommended that environmental monitoring and assessment include selection of an appropriate background content to gain understanding of the geochemistry and potential source of pollution in that environment. This study also emphasizes the need for the systematic selection of the most appropriate normalizer for observed systems.

The results obtained in this study can be used as useful reference for future researches, because they exhibited metal pollution as problem for observed river systems in Serbia. Further analysis is necessary to assess the pollution status of the cited localities, since there is significant discharge of heavy metal

from the urban industrial and mining activities into the rivers.

**Acknowledgments** This study was supported by the Ministry of Education, Science and Technological Development of Serbia, Grant Nos. 172001 and 43007. In addition, we would like to thank the Republic Hydrometeorological Service of Serbia for the sediment samples. The authors are grateful to anonymous reviewers whose comments greatly improved the paper.

## References

- Abraham, G. M. S., & Parker, R. J. (2008). Assessment of heavy metal enrichment factors and the degree of contamination in marine sediments from Tamaki Estuary, Auckland, New Zealand. *Environmental Monitoring and Assessment*, *136*, 227–238.
- Acevedo-Figueroa, D., Jiménez, B. D., & Rodríguez-Sierra, C. J. (2006). Trace metals in sediments of two estuarine lagoons from Puerto Rico. *Environmental Pollution*, *141*, 336–342.
- Asa, S. C., Rath, P., Panda, U. C., Parhi, P. K., & Bramha, S. (2013). Application of sequential leaching, risk indices and multivariate statistics to evaluate heavy metal contamination of estuarine sediments: Dhamara Estuary, east Coast of India. *Environmental Monitoring and Assessment*. doi:10.1007/s10661-013-3060-3.
- Barać, M., Vitas, N., & Janićijević, S. (2009). Heavy metals and Trepče landfills in the middle flow of the river Ibar. *Ecologica*, *16*, 401–408. (in Serbian).
- Bartoli, G., Papa, S., Sagnella, E., & Fioretto, A. (2012). Heavy metal content in sediments along the Calore River: Relationships with physical-chemical characteristics. *Journal of Environmental Management*, *95*, S9–S14.
- Botsou, F., Karageorgis, A. P., Dassenakis, E. M., & Scoullou, M. (2011). Assessment of heavy metal contamination and mineral magnetic characterization of the Asopos River sediments (Central Greece). *Marine Pollution Bulletin*, *62*, 547–563.
- Carvalho, A., Schropp, S. J., Sloane, G., Biernacki, T. P., & Seal, T. L. (2002). *Development of an interpretive tool for assessment of metal enrichment in Florida freshwater sediment*. Florida: Florida Department of Environmental Protection Tallahassee.
- Chand, M., & Prasad, S. (2013). ICP-OES assessment of heavy metal contamination in tropical marine sediments: A comparative study of two digestion techniques. *Microchemical Journal*, *111*, 53–61.
- Chen, M., & Ma, L. Q. (1998). Comparison of four USEPA digestion methods for trace metal analysis using certified and Florida soils. *Journal of Environmental Quality*, *27*, 1294–1300.
- Choi, K. Y., Kim, S. H., Hong, G. H., & Chon, H. T. (2012). Distributions of heavy metals in the sediments of South Korean harbors. *Environmental Geochemistry and Health*, *34*, 71–82.

- Cobelo-García, A., & Prego, R. (2003). Heavy metal sedimentary record in Galician Ria (NW Spain): background values and recent contamination. *Marine Pollution Bulletin*, *46*, 1253–1262.
- Comero, S., Vaccaro, S., Locoro, G., Capitani, L. D., & Gawlik, B. M. (2014). Characterization of the Danube River sediments using the PMF multivariate approach. *Chemosphere*, *95*, 329–335.
- Corazza, M. Z., Abrão, T., Lepri, F. G., Gimenez, S. M. N., Oliviera, E., & Santos, M. J. (2012). Monte Carlo method applied to modeling copper transport in river sediments. *Stochastic Environmental Research and Risk Assessment*, *26*, 1063–1079.
- Cukrov, N., Frančišković-Bilinski, S., & Bogner, D. (2013). Metal contamination recorded in the sediment of the semi-closed Bakar Bay (Croatia). *Environmental Geochemistry and Health*. doi:10.1007/s10653-013-9558-3.
- Dauvalter, V., & Rognerrud, S. (2001). Heavy metal pollution in sediments of the Pasvik River drainage. *Chemosphere*, *42*, 9–18.
- Deveza-Rey, R., Díaz-Fierros, F., & Barral, M. T. (2009). Normalization strategies for river bed sediments: A graphical approach. *Microchemical Journal*, *91*, 253–265.
- Duce, R. A., Hoffman, G. L., Ray, B. J., Fletcher, I. S., Wallace, G. T., Tiotrowicz, S. R., et al. (1976). Trace metals in the marine atmosphere: sources and fluxes. In H. L. Windom & R. A. Duce (Eds.), *Marine pollutant transfer*. Lexington, Massachusetts: Lexington Books.
- Ekwere, A. S., & Elueze, A. A. (2012). Trace element assessment of stream sediments around the aluminium smelting company in Ikot-Abasi, South-Eastern Nigeria. *Research Journal of Applied Sciences, Engineering and Technology*, *4*, 256–261.
- Gao, H., Bai, J., Xiao, R., Liu, P., Jiang, W., & Wang, J. (2013). Levels, sources and risk assessment of trace elements in wetland soils of a typical shallow freshwater lake, China. *Stochastic Environmental Research and Risk Assessment*, *27*, 275–284.
- Ho, H. H., Swennen, R., Cappuyns, V., Vassilieva, E., & Tran, T. V. (2012). Necessity of normalization to aluminum to assess the contamination by heavy metals and arsenic in sediments near Haiphong Harbor, Vietnam. *Journal of Asian Earth Sciences*, *56*, 229–239.
- Hu, X., Wang, C., & Zou, L. (2011). Characteristics of heavy metals and Pb isotopic signatures in sediments cores collected from typical urban shallow lakes in Nanjing, China. *Journal of Environmental Management*, *92*, 742–748.
- Jain, C. K., Singhal, D. C., & Sharma, M. K. (2005). Metal pollution assessment of sediment and water in the river Hindon, India. *Environmental Monitoring and Assessment*, *105*, 193–207.
- Kabir, M. I., Lee, H., Kim, G., & Jun, T. (2011). Correlation assessment and monitoring of the potential pollutants in the surface sediments of Pyeongchang River, Korea. *International Journal of Sediment Research*, *26*, 152–162.
- Kostić, N. M., Jakovljević, M. D., Hadžić, V. B., & Protić, J. (2001). Mineralogy and agrochemistry of magnesium in soils of Vojvodina, Šumadija and Northern Pomoravlje. *Proceedings for Natural Sciences*, *100*, 115–126. Matica Srpska.
- Lin, C. E., Chen, C. T., Kao, C. M., Hong, A., & Wu, C. Y. (2011). Development of the sediment and water quality management strategies for the Salt-water River Taiwan. *Marine Pollution Bulletin*, *63*, 528–534.
- Louriño-Cabala, B., Levsen, L., Charriau, A., Billon, G., Oudane, B., & Boughriet, A. (2011). Potential risks of metal toxicity in contaminated sediments of Deûle river in Northern France. *Journal of Hazardous Materials*, *186*, 2129–2137.
- Marinos, P. G., Koukis, G. C., Tsiambaos, G. C., & Stournaras, G. C. (1997). *Engineering Geology and the Environment, Tom 3*. Rotterdam: Balkema.
- McBride, M. B. (1994). *Environmental Chemistry of Soils*. New York: Oxford University Press. 406 pp.
- Mediolla, L. L., Domingues, M. C. D., & Sandoval, M. R. G. (2008). Environmental Assessment of and Active Tailings Pile in the State of Mexico (Central Mexico). *Research Journal of Environmental and Earth Sciences*, *2*, 197–208.
- Müller, G. (1979). Schwermetalle in den Sedimenten des Rheins-Veränderungen seit 1971. *Umschau*, *79*, 778–783.
- Nam, S. H., Kim, M. J., Park, Y. I., & Lee, S. J. (2001). A study on various pretreatment and preparation for the determination of inorganic elements in sediment. *Analytical Sciences*, *17*, a263–a265.
- Nriagu, J. O., & Pacyna, J. M. (1988). Quantitative assessment of worldwide contamination of air, water and soils by trace metals. *Nature*, *333*, 134–139.
- Official Gazette, Republic of Serbia (1990). No. 11, p 239.
- Radakovich, O., Roussiez, V., Ollivier, P., Ludwig, W., Grenz, C., & Probst, J.-L. (2008). Input of particulate heavy metals from rivers and associated sedimentary deposits on the Gulf of Lion continental shelf. *Estuarine Coastal and Shelf Science*, *77*, 285–295.
- Ren-Ying, L., Hao, Y., Zhi-Gao, Z., Jun-Jie, L., Xiao-Hua, S., & Feng, J. (2007). Fractionation of heavy metals in sediments from Dianchi Lake, China. *Pedosphere*, *17*, 265–272.
- Rönkkömäki, H., Pöykiö, R., Nurmesniemi, H., Popov, K., Merisalu, E., Tuomi, T., et al. (2008). Particle size distribution and dissolution properties of metals in cyclone fly ash. *International Journal of Environmental Science and Technology*, *5*, 485–494.
- Rubio, B., Nombela, M. A., & Vilas, F. (2000). Geochemistry of major and trace elements in sediments of the Ria de Vigo (NW Spain): An assessment of metal pollution. *Marine Pollution Bulletin*, *40*, 968–980.
- Sakan, S., Đorđević, D., Manojlović, D., & Predrag, P. (2009). Assessment of heavy metal pollutants accumulation in the Tisa river sediments. *Journal of Environmental Management*, *90*, 3382–3390.
- Sakan, S., Đorđević, D., Dević, G., Relić, D., Anđelković, I., & Đuričić, J. (2011). A study of trace element contamination in river sediments in Serbia using microwave-assisted aqua regia digestion and multivariate statistical analysis. *Microchemical Journal*, *99*, 492–502.
- Sakan, S., Đorđević, D., Lazić, M., & Tadić, M. (2012). Assessment of arsenic and mercury contamination in the Tisa River sediments and industrial canal sediments (Danube alluvial formation), Serbia. *Journal of Environmental Science and Health, Part A*, *47*, 109–116.

- Samardžić, M. (2013). Temporal and spatial dispersal of pollutants in the basin of Great Morava. Ph.D thesis, University of Novi Sad, Faculty of Agriculture, Serbia.
- Schropp, S. J., & Windom, H. L. (1988). *A guide to the interpretation of metal concentrations in estuarine sediments coastal zone management section*. Florida: Florida Department of Environmental Regulation.
- SEPA (2009). Report on the status of land in Serbia, Republic of Serbia, Ministry of Energy, Development and the Environment Agency for Environmental Protection, Belgrade, (in Serbian). [www.sepa.gov.rs/download/Stanje\\_zemljista.pdf](http://www.sepa.gov.rs/download/Stanje_zemljista.pdf).
- Silva, A., Lima, G. R. S., Alves, J. C., Santos, S. H., Garcia, A. B. G., Alves, J. P. H., et al. (2012). Evaluation of trace metal levels in surface sediments of the Sergipe River hydrographic basin, Northeast Brazil. *Journal of the Brazilian Chemical Society*, 23, 1669–1679.
- Sun, Y., Wu, F., Clemens, S. C., & Oppo, D. W. (2008). Processes controlling the geochemical composition of the South China Sea sediments during the last climatic cycle. *Chemical Geology*, 257, 240–246.
- Swarnalatha, K., Letha, J., Ayoob, S., & Sheela, A. M. (2013). Identification of silicon (Si) as an appropriate normaliser for estimating the heavy metals enrichment. *Journal of Environmental Management*, 129, 54–61.
- Wedepohl, K. H. (1995). The composition of the continental crust. *Geochimica et Cosmochimica Acta*, 59, 1217–1232.
- Yang, Y., Chen, F., Zhang, L., Liu, J., Wu, S., & Kang, M. (2012). Comprehensive assessment of heavy metal contamination in sediment of the Pearl River Estuary and adjacent shelf. *Marine Pollution Bulletin*, 64, 1947–1955.



## Study of potential harmful elements (arsenic, mercury and selenium) in surface sediments from Serbian rivers and artificial lakes



Sanja Sakan<sup>a,\*</sup>, Nenad Sakan<sup>b</sup>, Ivan Anđelković<sup>c</sup>, Snežana Trifunović<sup>d</sup>, Dragana Đorđević<sup>a</sup>

<sup>a</sup> ICTM, Chemistry Center, University of Belgrade, Njegoševa 12, P. O. Box 815, Belgrade 11000, Serbia

<sup>b</sup> Institute of Physics, University of Belgrade, Pregrevica 118, P.O. Box 68, 11081 Belgrade, Serbia

<sup>c</sup> Innovation Center of the Faculty of Chemistry, University of Belgrade, Studentski Trg 12-16, Belgrade, Serbia

<sup>d</sup> Faculty of Chemistry, University of Belgrade, Studentski Trg 12-16, 11000 Belgrade, Serbia

### ARTICLE INFO

#### Keywords:

Arsenic  
Mercury  
Selenium  
Sediment  
River  
Se:Hg ratio  
S:Se ratio

### ABSTRACT

This investigation examines surface sediment samples from rivers and artificial lakes (Serbia) to quantify levels of potentially harmful elements (As, Hg, and Se) and several ancillary elements (Al, Fe, Mn, Ca, Mg, C, H, N, and S). These data provide the first global analysis of Hg, As and Se levels in a well-studied system. Combination of different methods was applied for estimation of the environmental status of sediments and to determine the potential risk of ecological damage: digestion with aqua regia and determination of element content, determination of elements mobile forms by ammonium-acetate extraction, calculation of contamination indexes - index of geoaccumulation and enrichment factor, comparison with sediment quality guidelines and other literature data, and use of statistical methods. Results indicate that the sediments are slightly enriched with As and Hg, but not with Se. Fact that values for Se contents was less than the international threshold levels, suggesting the very probable absence of risk of contamination over the catchment with this element. The average pollution levels in Serbian river and artificial lakes expressed in terms of geoaccumulation indexes of As and Hg indicate that the environment is uncontaminated to moderately contaminated. All values of EF for Hg were below 2, indicating deficiency to minimal enrichment with Hg on studied localities. The EF values of As indicate deficiency to moderate enrichment (EF ranged from 0.11 to 3.54). According to the comparison to quality standard, the As in sediments of the studied area have potential risk. High content of arsenic in river and lake sediments indicate that arsenic pollution problem that lasts longer period of time.

### 1. Introduction

In a natural environment, As, Hg, and Se are considered potential harmful elements (PHEs) when their concentrations exceed certain levels. They can also be categorized as atmophile elements, because their mass transport through the atmosphere is often greater than via streams (Li et al., 2016). In recent years, much attention has been focused on the geochemical behaviour of these elements (Rezende et al., 2011; Zhang, 2014; Jagtap and Maher, 2015; Jiang et al., 2015; T. Chen et al., 2016, H. Chen et al., 2016; Tepanosyan et al., 2016).

Arsenic is a toxic, ubiquitous element with metalloid properties, is almost often present in environmental samples. It is found in nature in metal ore deposits, mainly as arsenides of Cu, Ni and Fe. Arsenic compounds are used mainly in agriculture and forestry as pesticides and herbicides; and in smaller amounts, as additive in the glass and ceramic industries as feed additives (Patel et al., 2005). Although it is classified as a metalloid, it is also referred to as a metal, and in the context of

toxicology as a heavy metal. Sediments are important sinks of inorganic arsenic in natural systems. However, inorganic arsenic is not permanently fixed, since pH, temperature or redox potential changes and presence of organic matter or ionic exchange processes can mobilise arsenic compounds from the sediment (Raposo et al., 2004).

Selenium in the environment is a significant research area as environmental selenium provides a source for biological uptake. Selenium is generally widely distributed and is cycled through environmental compartments via both natural and anthropogenic processes. Approximately, 40% of total Se emissions result from anthropogenic activities (Savery et al., 2013). Interest in selenium concentrations in the environment stem from the dual role of selenium as an essential nutrient at low concentrations and as toxic substance at higher levels of concentrations (Hagarová et al., 2005). Selenium usually occurs in association with various sulphide minerals/metallic ores in which it replaces sulphur atoms and only forms minerals with elements having a comparatively high atomic number, e.g., Pb, Hg, Bi, Ag, Cu etc.

\* Corresponding author at: ICTM, Chemistry Center, University of Belgrade, Njegoševa 12, Belgrade 11000, Serbia.  
E-mail address: [ssakan@chem.bg.ac.rs](mailto:ssakan@chem.bg.ac.rs) (S. Sakan).



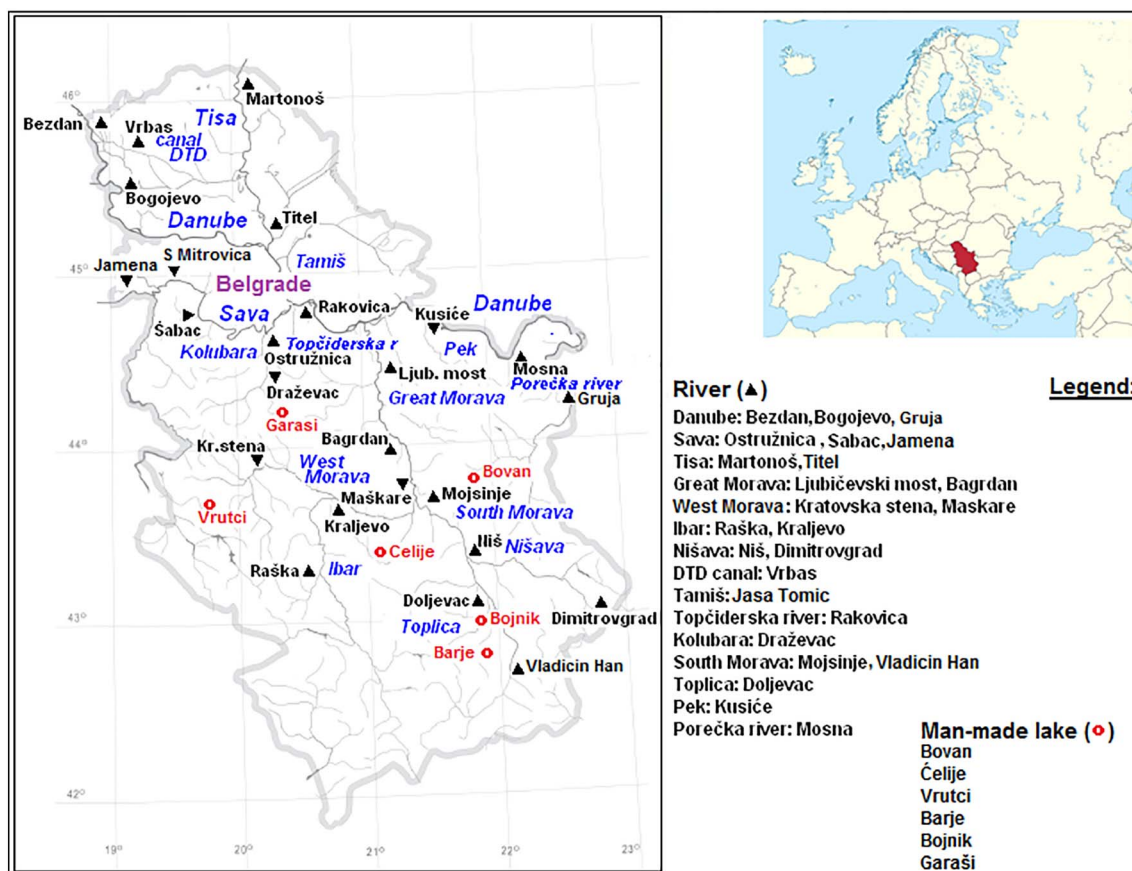


Fig. 1. Location map of sampling sites.

Particularly, selenium has strong affinity for copper and accumulation of copper in ores is usually accompanied by concentration of selenium (Tarin, 2006). In surface waters, Se is found mostly as selenate and selenite, which are both highly bioavailable species allowing for bioaccumulation and biomagnification posing a threat to aquatic wildlife (Savery et al., 2013).

Mercury is one of the most hazardous environmental pollutants with a large number of physical and chemical forms. Mercury is released into the environment from three major sources: natural deposits in soils, anthropogenic release, and wet and dry atmospheric deposition from both of these sources (Jagtap and Maher, 2015). Although all forms of mercury are poisonous, alkylmercury compounds are of special concern because of their easy penetration through biological membranes, efficient bio-accumulation, high volatility and long-term elimination from tissues. In the aquatic environments, mercury accumulates in sediments, where the methylation and demethylation processes preferably seem to occur (Berzas Nevado et al., 2010). The major discovery in recent years that Se can inhibit the toxicity and enrichment of MeHg in aquatic organisms has provided a potential approach to solving problems of Hg contamination in water (Zhang, 2014). A large number of scientific studies have confirmed that interactions between selenium and mercury are a very important topic of study for the systematic understanding of the environmental behaviour, fate and toxicological effects of Hg (or Se). Research (Yang et al., 2008) indicates that adding Se to lake sediments can significantly reduce the formation of MeHg in these sediments.

Mercury in contaminated sediments could be extracted by various chemical reagents in order to determine the different mercury species and partitions, providing useful information of toxicology, bioavailability and biochemical reactivity. Unfortunately, at present, neither specific extractants nor standard protocols exist for the isolation of particular mercury species (Issaro et al., 2009). Hagarová et al. (2005)

report that the application of extraction methods to selective removal of selenium is complicated by the fact that selenium may exist in more than one oxidation state (selenate (VI), selenite (IV), elemental selenium (0) and selenide (II)), each of which has a unique behaviour. Selenium determination with microwave digestion with aqua regia is recommended in paper Prachei et al. (2010). The determination of Hg total content in sediments with aqua regia is proposed by the U.S. Environmental Protection Agency (1986). In paper Rezende et al. (2011) is recommended the aqua regia digestion procedure for As and Hg determination in sediments, and obtained results are with high precision and accuracy.

In the presented manuscript, the arsenic, mercury and selenium levels in the Serbian River and artificial lake sediments were determined using microwave digestion with aqua regia and extraction with ammonium–acetate. The main objective of this study was to determine the distribution of studied elements in sediments and to estimate the degree of contamination and potential risk of ecological damages, on the basis of: calculation of pollution indexes (Igeo and EF), comparison with the corresponding sediment quality guidelines, comparison of the obtained results with those found in the literature, and prediction of mobility of studied potential harmful elements. There were also calculated Se:Hg and S:Se ratios, and were determined content of several ancillary parameters: Al, Fe, Mn, Ca, Mg, C, H, N, and S. In order to establish relationships among elements and determine the common source (and/or carrier substances), a correlation and cluster analysis was performed. To our knowledge, this is the first systematic investigations of arsenic, mercury and selenium content in river and artificial lake systems from Serbian localities.

## 2. Materials and methods

### 2.1. Study area and sampling sites

Serbia has many rivers and lakes. Serbia's rivers belong to the drainage basins of the Black, the Adriatic, and the Aegean seas, where the largest and the most important in the area is the Black Sea drainage basin covering an area of 81,261 km<sup>2</sup> or 92% of the territory of Serbia. The number of natural lakes in the total area is relatively small; however, when the increasing number of artificial reservoirs is included, the hydrographic networks become richer and more complex (Dević et al., 2014). Most lakes of Serbia are artificial, created by damming numerous rivers of Serbia for the purpose of obtaining hydroelectric power or as water reservoirs.

A total of 48 surface sediment samples were collected from Serbian rivers (36) and artificial lakes (12) during 2008. Sampling site numbers are denoted with the brackets: the Tisa (9), the Danube (6), the Sava (4), the Ibar (2), the Great Morava (2), the West Morava (2), the South Morava (2), the Nišava (2), the Tamiš (1), the Vrbas (1), the Topčiderska River (1), the Porečka river (1), the Kolubara (1), the Pek (1) and the Toplica (1) - rivers and the Barje (3), the Čelije (3), the Vrutci (1), the Garaši (1), the Bojnik (2) and the Bovan (2) - lakes. Locations of the sampling sites are shown in Fig. 1 and Table 1. The sampling of sediments in this research was conducted using a Van Veen grab sampler, designed to collect an accurate representative sediment sample. The sediment samples were stored at 4 °C to prevent changes in the chemical composition. The micro and macroelemental levels were determined in the granulometric fraction, i.e., < 63 μm of the bottom sediment sample (grab sample). Analysis of the metal concentration in the fine sediment fraction (< 63 μm) is recommended as these particles are the most important sources of bioavailable metals in sediments (Villaescusa-Celaya et al., 2000), as well as for comparability of data to other river basins (Milačić et al., 2010).

The moisture content of each sample was determined by drying a separate 1 g sample in an oven (105 ± 2 °C) until a constant weight was reached. From this, a correction to dry mass was obtained, which was then applied to all reported metal content results.

### 2.2. Chemical analysis

#### 2.2.1. Digestion with aqua regia

Total As, Hg, Se, Al, Fe, and Mn levels were determined using microwave digestion with aqua regia. Approximately 500 mg of sample sediment and 12 mL of aqua regia (9 mL HCl and 3 mL HNO<sub>3</sub>) were added to a microwave vessel (DIN 38414 S7 1983, SW-846 EPA Method 3051a 2007). Microwave digestion was performed in a pressurised microwave oven (Ethos 1, Advanced Microwave Digestion System, Milestone, Italy) equipped with a rotor holding 10 microwave vessels (PTFE). During digestion, the temperature of the microwave oven was raised to 165 °C over 10 min (holding time 0 s), then to 175 °C over 3 min, after which it was maintained at 175 °C for 10 min (max power 1200 W) (Rönkkömäki et al., 2008). One control vessel per rack contained a temperature and pressure probe. The vessels were removed from the oven after the temperature had dropped to < 50 °C and the pressure to < 69 kPa. At the end of the digestion cycle the vessels were allowed to cool to room temperature before continuing the sample preparation, to align with security protocols and to avoid the leakage of volatile substances. After cooling, the sample digests were filtered with Whatman No. 42 filter paper, to remove solids which remained after the microwave digestion process. The digests were then transferred into a flask, diluted to 100 mL with 1 M HNO<sub>3</sub> and stored in a polyethylene bottle at 4 °C until needed for analysis (Sakan et al., 2011).

#### 2.2.2. Extraction with 1 M CH<sub>3</sub>COONH<sub>4</sub>

A 40-mL aliquot of a 1 M CH<sub>3</sub>COONH<sub>4</sub> solution was added to 1 g of sediment in a 50-mL centrifuge tube. The suspension was shaken on a

**Table 1**

Content of studied elements [mg kg<sup>-1</sup>], dry weight basis and Se:Hg and S:Se ratios.

| Number          | Sampling location               | R/L <sup>a</sup> | Hg                | As    | Se    | Se:Hg | S:Se   |
|-----------------|---------------------------------|------------------|-------------------|-------|-------|-------|--------|
| 1               | Tisa (Martonoš)                 | R                | < dl <sup>b</sup> | 20.1  | 0.542 |       | 6827   |
| 2               | West Morava (Kratovska stena)   | R                | < dl              | 23.5  | 0.605 |       | 8099   |
| 3               | Ibar (Raška)                    | R                | 0.086             | 103   | 0.357 | 4.15  | 13,165 |
| 4               | Tamiš (Jaša Tomić)              | R                | < dl              | 9.77  | 0.341 |       | 8504   |
| 5               | Tisa (Titel)                    | R                | < dl              | 13.6  | 0.399 |       | 6266   |
| 6               | Vrbas DTD (Vrbas)               | R                | < dl              | 7.58  | 0.152 |       | 13,158 |
| 7               | Danube (Bezdan)                 | R                | < dl              | 13.8  | 0.352 |       | 5682   |
| 8               | Danube (Bezdan)                 | R                | < dl              | 13.1  | 0.365 |       | 5753   |
| 9               | Danube (Bezdan)                 | R                | 0.259             | 12.5  | 0.382 | 1.47  | 5131   |
| 10              | Topčiderska river (Rakovica)    | R                | 0.242             | 17.6  | 0.266 | 1.10  | 7143   |
| 11              | Danube (Bogojevo)               | R                | 0.123             | 8.44  | 0.291 | 2.37  | 6873   |
| 12              | Porečka river (Mosna)           | R                | < dl              | 16.6  | 1.004 |       | 3586   |
| 13              | Barje                           | L                | < dl              | 9.69  | 0.128 |       | 14,922 |
| 14              | South Morava (Mojsinje)         | R                | 0.075             | 16.8  | 0.486 | 6.48  | 5967   |
| 15              | Čelije                          | L                | < dl              | 9.46  | 0.128 |       | 15,391 |
| 16              | Čelije                          | L                | 0.009             | 9.70  | 0.056 | 6.22  | 35,000 |
| 17              | Barje                           | L                | 0.002             | 37.2  | 0.117 | 58.50 | 16,667 |
| 18              | Nišava (Niš)                    | R                | 0.492             | 11.2  | 0.650 | 1.32  | 5538   |
| 19              | Danube (Bezdan)                 | R                | 0.500             | 16.6  | 0.388 | 0.78  | 5052   |
| 20              | Barje                           | L                | < dl              | 44.7  | 0.127 |       | 15,354 |
| 21              | Tisa (Titel)                    | R                | 0.203             | 20.4  | 0.290 | 1.43  | 6897   |
| 22              | Tisa (Titel)                    | R                | 0.056             | 14.4  | 0.176 | 3.14  | 11,080 |
| 23              | Kolubara (Draževac)             | R                | 0.345             | 19.5  | 0.206 | 0.60  | 9466   |
| 24              | Ibar (Kraljevo)                 | R                | 0.357             | 66.0  | 0.216 | 0.61  | 12,130 |
| 25              | Vrutci                          | L                | 0.135             | 5.96  | 0.084 | 0.62  | 22,619 |
| 26              | Sava (Ostružnica)               | R                | 0.331             | 17.6  | 0.272 | 0.82  | 7132   |
| 27              | Čelije                          | L                | 0.147             | 8.95  | 0.090 | 0.61  | 21,889 |
| 28              | Pek (Kusiće)                    | R                | 0.130             | 23.4  | 0.983 | 7.56  | 6419   |
| 29              | Sava (Sremska Mitrovica)        | R                | 0.341             | 14.8  | 0.323 | 0.95  | 6037   |
| 30              | Sava (Šabac)                    | R                | 0.368             | 17.5  | 0.342 | 0.93  | 5702   |
| 31              | Great Morava (Ljubičevski most) | R                | 0.500             | 30.7  | 0.451 | 0.90  | 4279   |
| 32              | Tisa (Martonoš)                 | R                | 0.206             | 15.1  | 0.347 | 1.68  | 5620   |
| 33              | Tisa (Martonoš)                 | R                | 0.254             | 19.6  | 0.433 | 1.70  | 4411   |
| 34              | South Morava (Vladičin Han)     | R                | 0.271             | 19.6  | 0.301 | 1.11  | 6379   |
| 35              | Toplica (Doljevac)              | R                | 0.352             | 25.2  | 0.491 | 1.39  | 3951   |
| 36              | Bojnik                          | L                | 0.321             | 4.95  | 0.230 | 0.72  | 8435   |
| 37              | Tisa (Martonoš)                 | R                | 0.360             | 17.4  | 0.400 | 1.11  | 4875   |
| 38              | Garaši                          | L                | 0.337             | 6.2   | 0.159 | 0.47  | 12,327 |
| 39              | West Morava (Maskare)           | R                | 0.717             | 31.3  | 0.363 | 0.51  | 7218   |
| 40              | Bojnik                          | L                | 0.178             | 5.81  | 0.263 | 1.48  | 7338   |
| 41              | Nišava (Dimitrovgrad)           | R                | < dl              | 4.10  | 0.446 |       | 4731   |
| 42              | Bovan                           | L                | 0.021             | 9.41  | 0.274 | 13.05 | 7080   |
| 43              | Bovan                           | L                | < dl              | 9.29  | 0.301 |       | 6412   |
| 44              | Tisa (Martonoš)                 | R                | 0.051             | 15.8  | 0.316 | 6.20  | 6203   |
| 45              | Great Morava (Baگردan)          | R                | 0.441             | 24.3  | 0.373 | 0.85  | 5308   |
| 46              | Tisa (Martonoš)                 | R                | 0.08              | 18.2  | 0.365 | 4.56  | 5342   |
| 47              | Sava (Jamena)                   | R                | 0.217             | 16.3  | 0.390 | 1.80  | 5000   |
| 48              | Danube (Gruja)                  | R                | 0.269             | 17.1  | 0.276 | 1.03  | 7609   |
| Median          |                                 |                  | 0.141             | 16.4  | 0.332 |       |        |
| GM <sup>c</sup> |                                 |                  | 0.134             | 15.3  | 0.292 |       |        |
| HM <sup>d</sup> |                                 |                  | 0.081             | 12.8  | 0.242 |       |        |
| Avg             |                                 |                  | 0.183             | 19.0  | 0.340 | 3.95  | 8874   |
| Max             |                                 |                  | 0.717             | 103   | 1.004 | 58.5  | 35,000 |
| Min             |                                 |                  | < dl              | 4.10  | 0.056 | 0.47  | 3586   |
| SDEV            |                                 |                  | 0.180             | 16.48 | 0.191 |       |        |

<sup>a</sup> River/lake.

<sup>b</sup> Below detection limit (< 0.0001 mg kg<sup>-1</sup>).

<sup>c</sup> Geometric mean.

<sup>d</sup> Harmonic mean.

shaker for 2 h in a room at 20 ± 2 °C (Todorović et al., 2001; Sakan et al., 2009; Petrović et al., 2010; Sakan et al., 2012). The extract was separated from the solid phase by centrifugation at 3000 rpm for 20 min. Then, the supernatant was decanted and diluted to 50 mL with 1 M HNO<sub>3</sub> and stored in a polyethylene bottle at 4 °C until needed for



analysis.

### 2.2.3. Determination of element content

In this research, the following elements were determined in each sample: As, Hg, Se, Al, Fe, and Mn. The analytical determination of the studied elements was realised with an atomic emission spectrometer with an inductively coupled plasma iCAP-6500 Duo (Thermo Scientific, United Kingdom). The detector was a RACID86 Charge injector device (CID). For As, Hg, and Se determination, ICP OES coupled with hydride generation technique was used. Hydride technique was used to minimize interferences from sample matrices.

Analytical grade chemicals were used throughout the study without any further purification. The metal standards were prepared from a stock solution of 1000 mg L<sup>-1</sup> by successive dilutions. The concentrations obtained for all the elements in the blanks were close to the detection limit of the method, indicating that contamination was not a problem in the digestion.

The wavelengths used in this analysis were: As - 189.0 nm, Hg - 194.2 nm, Se - 196.0 nm, Mn - 257.6 nm, Fe - 261.1 nm, Ca - 184.2 nm, Mg - 279.5 nm, and Al - 237.3 nm. The detection limit was determined as three times the standard deviation of the blank measurements. The obtained values were (in mg kg<sup>-1</sup>) were: As - 0.0001, Hg - 0.0001, Se - 0.0001, Mn - 0.03, Al - 0.5 and Fe - 0.3.

The obtained results are expressed in mg kg<sup>-1</sup> dry sediment.

### 2.2.4. Elemental analysis

The determination of C, H, N, and S content in the investigated sediments was performed by elemental analysis, using the Vario EL III C, H, N, S/O elemental analyser (Elementar). Determined C content represented total carbon content, i.e. sum of inorganic and organic carbon.

## 2.3. Contamination indexes

The *index of geoaccumulation* ( $I_{geo}$ ), originally introduced by Muller (1979), was employed here to separate the anthropogenic influences on the sediment from the natural influences (Li et al., 2016). The index is defined by the following equation:

$$I_{geo} = \log_2(C_n/1.5 B_n),$$

where  $C_n$  is the measured sediment concentration of the element of interest (n) and  $B_n$  is the geochemical background concentration of element (n). The  $I_{geo}$  classifies the sampling locations into seven classes as follows:  $I_{geo} \leq 0$  - practically uncontaminated;  $0 < I_{geo} < 1$  - uncontaminated to moderately contaminated;  $1 < I_{geo} < 2$  - moderately contaminated;  $2 < I_{geo} < 3$  - moderately to heavily contaminated;  $3 < I_{geo} < 4$  - heavily contaminated;  $4 < I_{geo} < 5$  - heavily contaminated; and  $5 \leq I_{geo}$  - extremely contaminated.

The *enrichment factor* (EF) was calculated according to the following equation:

$$EF = (C_{n(\text{sample})}/C_{\text{ref}(\text{sample})})/(B_{n(\text{background})}/B_{\text{ref}(\text{background})}),$$

where  $C_{n(\text{sample})}$  is the content of the examined element in the examined environment;  $C_{\text{ref}(\text{sample})}$  is the content of the reference element in the examined environment;  $B_{n(\text{background})}$  is the content of the examined element in the reference environment, and  $B_{\text{ref}(\text{background})}$  is the content of the reference element in the reference environment (Bernalte et al., 2015). Five contamination categories are recognized on the basis of the enrichment factor:  $EF < 2$  (deficiency to minimal enrichment),  $EF = 2-5$  (moderate enrichment),  $EF = 5-20$  (significant enrichment),  $EF = 20-40$  (very high enrichment), and  $EF > 40$  (extremely high enrichment).

## 2.4. Statistics and data processing

In order to establish relationships among elements and determine

the common source (and/or carrier substances), a correlation matrix was calculated for the elements in the sediments. Hierarchical Cluster Analysis also was performed to classify the sediments according to the values of the studied variables into clusters and generate dendrogram. Data were analyzed using SPSS 21.0.

## 3. Results and discussion

### 3.1. The accuracy check

The accuracy of the analytical procedures applied was checked by analysis of the certified reference material (BCR-143R, 'Sewage sludge amended soil'). The materials were handled according to the supplier's specifications. The percentage recovery for Hg and Mn was obtained as: [(measured concentration in mg kg<sup>-1</sup>) / (mean certified value for CRM in mg kg<sup>-1</sup>) × 100]. The determined concentration for Hg was 1.03 mg kg<sup>-1</sup>, which is 93.6% of the certified values. The determined concentration for Mn was 822 mg kg<sup>-1</sup>, which is 95.8% of the certified values. Good agreement between determined and the certified values confirming the accuracy of the obtained result.

The precision is expressed as relative standard deviations. The relative standard deviations of the means of duplicate measurement were < 10% for all the measured elements.

### 3.2. Mercury, arsenic and selenium content in sediment

The total As, Se and Hg contents in studied sediments are summarized in Table 1, while the contents of determined ancillary parameters (Al, Fe, Mn, Ca, Mg, C, H, N, and S) are summarized in Supplementary Table 1. Comparison of the obtained results in this research with those found in the literature for the elements in soil and sediments from India, China, Spain, Armenia, France, Ghana, Scotland, Danube and Sava river is shown in Table 2.

In general, contents of elements vary along studied localities (Table 1). The total content of As in sediment were in the range 4.10–103 mg kg<sup>-1</sup>. The average content of As in the sediment (19.0 ± 16.5 mg kg<sup>-1</sup>) was comparable to that of the sediment from Yangtze river (Tang et al., 2014), Sava river (Milačić et al., 2010), Danube river (Woitke et al., 2003), and was significantly lower compared with the values reported by Patel et al. (2005) for sediment from central India. Average concentration of As found in this study was also lower than values reported in Dhivert et al. (2015). However, the average concentration of As was found to be slightly higher in this study compared with the values reported by Xu et al. (2016) - for soil from China (Beijing), Roig et al. (2011) - for river sediments (Spain), Tepanosyan et al. (2016) - for topsoil (Armenia), and Frémion et al. (2016) - for Loire river sediments (France). Comparison of As content in Tisa river sediments in this study with those published for Tisa sediment in Sakan et al. (2012) indicate that values in this study was higher than values in Sakan et al. (2012). Possible reason for this maybe fact that in this research was determined total content of As (by aqua regia), since in Sakan et al. (2012) present results for total extractable amount of As represented as the sum of As released in all five fractions of sequential extraction. As extractant in residual fraction in Sakan et al. (2012) is used 6 M HCl, not aqua regia.

Total Hg content ranged from below detection limit to 0.72 mg kg<sup>-1</sup>. Hg pristine concentrations vary between 0.08 and 0.4 mg kg<sup>-1</sup> (Issaro et al., 2009), indicating mercury emissions from anthropogenic sources in the studied area. Results of comparisons of the obtained results with other published results for mercury (Table 2) indicate that mercury contents in Serbian river and lakes are higher than the levels measured in topsoil in Armenia Tepanosyan et al. (2016) and river sediment from Spain (Roig et al., 2011), but roughly similar to measured values in soil from China (Xu et al., 2016), river sediments from Ghana (Oppong et al., 2010), Sava river (Milačić et al., 2010) and Tisa river (Sakan et al., 2012). The sediments mercury contents

**Table 2**

The average contents and ranges of As, Hg, and Se, compared with data published for other sediments and soils and sediment quality guidelines (in mg kg<sup>-1</sup>, only if it is not otherwise stated).

|   | As                             | Hg  | Se                             | Literature                          |
|---|--------------------------------|---|--------------------------------|-------------------------------------|
| Sediment (Kupa river, Croatia)            | ND-12.96 (5.036 ± 2.829)       | 13.4–206 (86.8 ± 48.2) <sup>b</sup>           | 0.12–1.26(0.61 ± 0.26)         | Frančičković-Bilinski (2007)        |
| Sediment (rivers <sup>c</sup> , Slovenia) | 10.87–30.46 (17.33 ± 6.94)     | 121–1087 (425 ± 312) <sup>b</sup>             | 0.34–2.72(1.26 ± 0.57)         | Frančičković-Bilinski et al. (2006) |
| Sediment (Sava river <sup>d</sup> )       | 1.89–46.01(14.13 ± 7.94)       | 16.8–6918(1163–1415) <sup>b</sup>             | ND-3.94(1.25 ± 0.81)           | Frančičković-Bilinski (2008)        |
| Sediment (central India)                  | 19–489 (105 <sup>a</sup> )     |   |                                | Patel et al. (2005)                 |
| Soil (northwest China)                    | 6.28–12.96 (9.88)              | 0.52–5.05 (1.39)                              |                                | T. Chen et al. (2016)               |
| Background                                | 11.70                          | 0.13  |                                | T. Chen et al. (2016)               |
| Scottish topsoils                         |                                |   | 0.19–1.46                      | Shand et al. (2010)                 |
| Finnish sediment (silt)                   |                                |   | (90 <sup>b</sup> )             | Koljonen (1974)                     |
| Finnish sediment (clay)                   |                                |   | (320 <sup>b</sup> )            | Koljonen (1974)                     |
| Soil (northeast-southwest China)          |                                |   | 0.08–0.215                     | Lv et al. (2014)                    |
| Soil (China, Fujiang River B)             |                                |   | (0.200)                        | Yu et al. (2014)                    |
| Soil (China, Beijing)                     | 4.05–18.3 (8.38)               | 0.01–0.67 (0.07)                              |                                | Xu et al. (2016)                    |
| Sediments (river, NE Spain)               | 1.09–13.17                     | ND-0.22                                       |                                | Roig et al. (2011)                  |
| Topsoil (Yerevan, Armenia)                | 0.050–4.900 (0.050)            | 0.010–0.270 (0.115)                           |                                | Tepanosyan et al. (2016)            |
| Sediments (Rhue river, France)            | 9.4                            |   |                                | Frémion et al. (2016)               |
| Sediment (Upper Loire River, France)      | 44.7                           |   |                                | Dhivert et al. (2015)               |
| Sediment (Yangtze River, China)           | 17.0                           |   |                                | Tang et al. (2014)                  |
| Sediment (River Pra Basin, Ghana)         |                                | 0.390–0.707                                   |                                | Oppong et al. (2010)                |
| Sediment (Sava river, spring - outfall)   | 7–25                           | 0.2–0.6                                       |                                | Milačić et al. (2010)               |
| Sediment (Danube river)                   | 9.0–68.9 (17.6 ± 1.9)          | < 0.10–2.37 (0.22 ± 0.05)                     |                                | Woitke et al. (2003)                |
| Sediment (Danube-tributaries)             | 8.1–388 (20.1 ± 15.9)          | < 0.10–2.56 (0.22 ± 0.21)                     |                                | Woitke et al. (2003)                |
| Sediment-background values                | 10                             | 0.2   |                                | Woitke et al. (2003)                |
| Sediment (this study)                     | <b>4.10–103 (19.0 ± 16.48)</b> | <b>&lt; dl<sup>e</sup>–0.72 (0.18 ± 0.18)</b> | <b>0.06–1.00 (0.34 ± 0.19)</b> |                                     |
| MAC (Serbia)                              | 25                             | 2   |                                | Republic of Serbia (1994)           |
| Benchmarks                                | 9.8                            | 0.18  | 2                              | US EPA, 2007                        |
| PEC                                       | 25                             | 1.1   |                                | MacDonald and Ingersoll (2002)      |

ND: not detected.

<sup>a</sup> Mean.

<sup>b</sup> µg kg<sup>-1</sup>.

<sup>c</sup> Savinja, Voglajna, and Hudinja.

<sup>d</sup> Slovenia and Croatia.

<sup>e</sup> dl - 0.0001 mg kg<sup>-1</sup>.

measured in this study area, however, lower than those found in soil from sewage irrigation area of northwest China (T. Chen et al., 2016, H. Chen et al., 2016). The average contents of Hg found in this study is similar to measured values of Hg in Danube river and Danube tributaries (Woitke et al., 2003), but on some location along the entire course and some tributaries, maximum values were higher than studied values.

Total Se content in this study ranged from 0.056 to 1.000 mg kg<sup>-1</sup> (Table 1). The river and lakes sediments selenium contents are higher than the levels measured in soils from China (Lv et al., 2014), but similar to measured values in Scottish topsoil (Shand et al., 2010), Finnish sediment (Koljonen, 1974), and soils from China (Yu et al., 2014).

To estimate the environmental status of sediments and to determine the potential risk of ecological damage, the Hg, As and Se contents in the sediment were compared with the corresponding sediment quality guidelines (SQGs, Table 2): US EPA benchmarks (US EPA, 2007; De Castro-Catalá et al., 2016), PEC - probable effect concentrations (MacDonald and Ingersoll, 2002) and Serbia national legislation (Republic of Serbia, 1994). Screening ecological benchmarks are used to identify chemical concentrations in environmental media that are at or below thresholds for effects to ecological receptors. No benchmarks were exceeded for Se, but for As and Hg on some sites measured values exceeded the benchmarks (Fig. 2, Table 2). Lemly (2002) also described the sedimentary toxic effect threshold for Se in sediment as 2 µg/g, which is in accordance with US EPA benchmarks. The fact that Se levels were less than the international threshold levels suggests the very probable absence of risk of contamination with this element over the catchment.

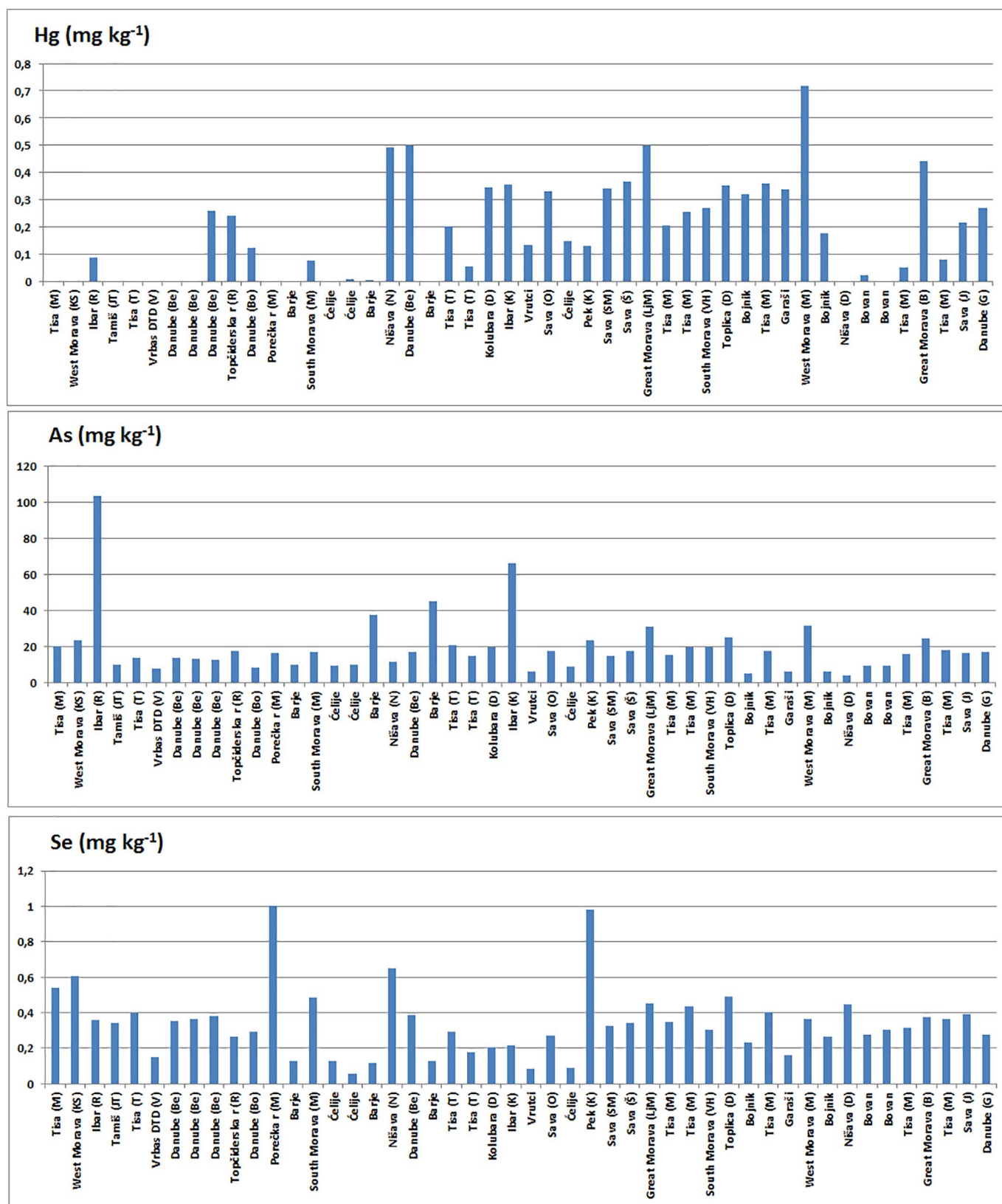
The collation of contents of As and Hg with maximum acceptable concentrations (MAC) approved by Serbian legislation (Table 2) showed that only arsenic exceeded MAC on some localities: Great Morava, West Morava, Ibar and Toplica (rivers) and Barje (artificial

lake). Data from Table 2 further indicate that most of sediments exceeded PEC values for As, but did not exceeded for Hg. PEC (probable effect concentrations) are SQGs that were established as concentrations of individual chemicals above which adverse effects in sediments are expected to frequently occur. Thus, it is possible to conclude that on studied localities Hg was found to be present in slightly elevated concentration. The highest Hg content was found at site West Morava. Elevated Hg content in this river was also shown in paper Milošковиć et al. (2016).

High content of arsenic on some localities are mainly caused by pollution with exogenous substances. Stafilov et al. (2010) report very heavy pollution with As of the area around the Ibar and Sitnica valleys. Dević et al. (2016) reported high levels of As in river water in Serbia. The authors explain that, with the use of arsenic-containing herbicides, high concentrations of naturally occurring arsenic in some quaternary sedimentary aquifers, and as a consequence of mining activities. These results suggest that a large proportion of the Serbian population is chronically exposed to As. High content of arsenic in river and lake sediments indicate that arsenic pollution problem that lasts longer period of time.

The box-plot (Supplementary Fig. 1) shows that Se and As have some outliers and extreme values. Since that Se content not exceeded MAC values, it can be supposed that geology is the primary control on the selenium concentration in sediments. This is partially because of different background Se content in different regions.

In the sediment samples which are analyzed in this paper shown that elevated concentrations of elements, mainly those that exceed the MAC, in most cases were detected in samples of river sediments. It is possible to assume that this is due to the fact that the artificial lake reservoirs are usually built in rural areas, where the less anthropogenic pollution. Unlike lakes, rivers often flow through the towns, but these bodies of water more or less burdened with micronutrients, toxic

Fig. 2. Hg, As, and Se content (mg kg<sup>-1</sup>) in sediments from rivers and lakes.

substances, organic or inorganic, waste materials, depending on the type and industrial process which, particularly in Serbia, without needed and compulsory technology treatment directly discharged into them.

### 3.3. Se:Hg ratio

It was proposed as early as 1972 that the Hg-to-Se molar ratio should be used as a reference standard for Hg pollution (Ganter et al., 1972). However, this proposal has attracted little attention because the

specific underlying mechanism has only gradually become clear in recent years (Zhang, 2014). In Burger et al. (2012) was written that Ralston (2008) suggest that selenium:mercury molar ratios above 1 are protective for adverse mercury effects. The Se:Hg ratio are calculated for studied sediments and results are shown in Table 1. The ratio Se:Hg > 1 was observed in sediments with lower mercury and higher selenium content, suggest a protective effect of Hg toxicity. For sediments with higher Hg content, Se:Hg was < 1, which indicates that the higher content of selenium is required in order to neutralize the negative impact mercury effects. In general, when the concentration of Se is significantly higher than that of Hg, Se plays a dominant role in Hg assimilation processes.

### 3.4. S:Se ratio

Malisa (2001) reported that S/Se ratios are distinct in different rock types and can thus be used to elucidate the origin of rocks, ores, and sediments. The obtain values for S:Se ratios in studied sediments in present research (3586–35,000, Table 1) are in accordance for values in clayey and organic-rich sediments (1000–10,000) for most of the studied samples, but in some areas, obtained Se/S ratio was higher. This ratio in sediments depends on the abundance of selenium during sedimentation, since there is a usually about the same amount of sulphur present, which can be bound to sediments (Malisa, 2001). High value for S/Se ratios at some locations in this research may be a consequence of geochemical composition of sediment.

### 3.5. Analysis of the easily soluble element fraction of sediments

In order to estimate the extent of pollution of selected elements in sediments, extraction in  $\text{CH}_3\text{COONH}_4$ , was performed. The neutral 1 M ammonium acetate extraction method is the most widely used procedure to extract water-soluble and rapidly exchangeable fractions. The percentages of the extracted elements in the soluble fraction compared to the total content obtained with aqua regia digestion were calculated and results shown in Supplementary Fig. 2 only for As, since the extracted amounts of Se and Hg in this fraction was below detection limits. Other studies also shown that a significant proportion of insoluble and non-bioavailable elemental Se naturally present in sediment (Wiramanaden et al., 2010). Sakan et al. (2012) reported that in investigated river and alluvial sediment mercury is quite stable and present low chemical availability, which is comparable with data found in this study.

Data from Supplementary Fig. 2 showed that the percentages of the easily soluble metal fraction of arsenic were in general below 10%, indicating its low mobility into the aquatic environment. Obtained results are comparable to results for Sava River (Milačić et al., 2010) and Tisa river and Danube alluvial sediments (Sakan et al., 2012).

### 3.6. Determination of background values

The selection of appropriate background values is very important in assessment of the sediment contamination level, based on ecological risk-assessment criteria, such as  $I_{\text{geo}}$  and EF (Li et al., 2016; Sakan et al., 2015). Unfortunately, no earlier background data for the three selected element were available for the study area. The As and Hg data reported in Woitke et al. (2003) were chosen as the background values for the current study due to the following reasons: (i) contaminated and mineralogically and texturally comparable river sediments, (ii) similarity with other published background values (Table 2) and (iii) similarity with US EPA benchmarks (Table 2).

### 3.7. The index of geoaccumulation

The calculated values for  $I_{\text{geo}}$  are shown in Fig. 3.  $I_{\text{geo}}$  for As ranging from < 0 to 1.93, indicating practically uncontaminated to moderately

contaminated sediments; for Hg,  $I_{\text{geo}}$  was from < 0 to 0.87, indicating practically uncontaminated to moderately contaminated sediment. The percentage of sediments that had  $I_{\text{geo}} < 0$  were 45.8% for As and 75.0% for Hg. The percentage of samples that had  $0 < I_{\text{geo}} < 1$  were 47.9% for As and 25% for Hg. Only three sediments (Ibar (2) and Barje lake (1)) had  $I_{\text{geo}} > 1$  for As (6.2%), indicating moderately contaminated areas. The average pollution levels in Serbian river and artificial lakes expressed in terms of geoaccumulation indexes of As and Hg indicate that the environment is uncontaminated to moderately contaminated. Therefore, although there was a significant proportion of samples for which As and Hg exceeded the benchmarks, they had the least number of samples that exceeded the  $I_{\text{geo}}$  values when background values were taken into consideration.

### 3.8. Enrichment factor

The calculated EFs are shown in Fig. 4. EF values range for As was from 0.113 to 3.537 (mean 0.586). All values of EF for Hg were below 2, indicating deficiency to minimal enrichment with Hg on studied localities. The EF values of As indicate deficiency to minimal enrichment to moderate enrichment (EF ranged from 0.11 to 3.54). The calculated values of EF indicate that 95.8% sites for As had values for EF < 2 (deficiency to minimal enrichment). Two stations in the studied area had values > 2 for As (moderate enrichment), for Ibar river (stations 1280 and 1281). Obtained results are consistent with the results of  $I_{\text{geo}}$ .

### 3.9. Correlation analysis

The correlation coefficients between each pair of variable elements in the sediments were calculated using the Pearson correlation matrix approach and values are shown in Supplementary Table 2. The results obtained show that there are both positive and negative correlations between the elements with regard to their source. Results of correlation analysis indicate that Hg does not show a significant correlation with any of the elements. The lack of significant linear correlation between Hg and the other studied elements suggests that its sources were quite different from those of the others. As is positive correlated with: Fe, Mg and S, and Se are positive correlated with C and S. Correlation between Se and S is highly significant. Positive correlation among As and Fe is also shown in paper T. Chen et al. (2016) and H. Chen et al. (2016), which may indicate that As is present as insoluble Fe-arsenate complexes. Also, arsenate (As(V)) is expected to be very sparingly soluble in most environments, because of a very efficient inner-sphere complexation adsorption mechanism on Fe and Al oxides (Gustafsson and Tin, 1994). Frémion et al. (2016) found that a correlation between As and major elements could reflect the fact that after their release in aquatic medium, they sorb through time onto Al- and Fe-oxides present in high concentration in sediments matrix. As and S may form very insoluble compounds, such as arsenopyrite (Gustafsson and Tin, 1994). Positive correlation of As with Mg may be due to Mg has the capacity to precipitate with arsenate (Fendorf et al., 2010). The positive correlation between Se and S reflect the association of Se with various sulphide minerals. Because of the similar ionic radii of sulphide ion and selenide ion, selenium readily substitutes for sulphur ion sulphide minerals. Correlation of Se with total carbon content indicates that selenium in sediments accumulated via organic matter also, which is in accordance with the results of Wiramanaden et al. (2010). Čuvarđić (2003) shows that in sedimentary rocks, Se is bond to organic fractions. Wiramanaden et al. (2010) suggest that microbial activity may be very important in the biogeochemical cycling of Se in fresh-water ecosystems.

Fe is negatively correlated with Ca and C, and positively with K, Mn, and H. Obtained correlations may be consequence of different origin of elements; Ca and C represented carbonates, and Fe is mainly present in form oxide. Fe oxides are building associations with Mn oxides and clay minerals in soils and sediments. The positive correlations of total C with Ca, Mg, and N confirmed dual nature of carbon content, since that total



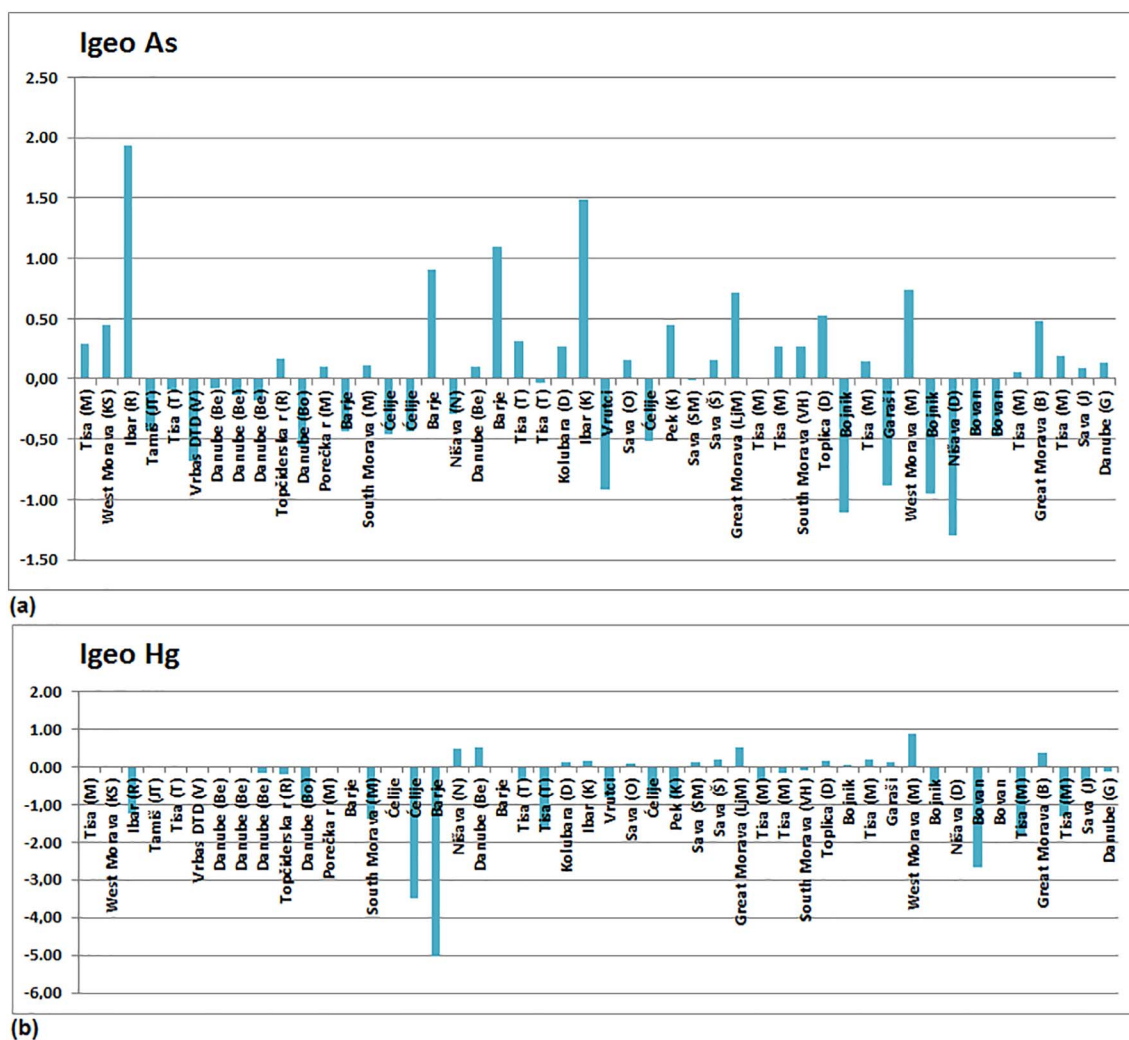


Fig. 3. Arsenic (a) and mercury (b) index of geoaccumulation of studied sediments.

carbon includes inorganic and organic sample constituents. Inorganic carbon forms are present in soils and sediments typically as carbonates (represented with Ca and Mg in this research) and total N content represent organic matter. Nitrogen in soil and sediment is mainly derived by decomposition of the plants and animals or plankton and plays an important role as a source of nutrients (Avramidis et al., 2015).

### 3.10. Cluster analysis (CA)

The results obtained by CA (R mode) are presented by dendrogram, where the distance axis represents the degree of association between groups of variables, i.e. lower the value on the axis, the more significant the association. According to the dendrogram (Supplementary Fig. 3), two main clusters can be observed. Cluster one consists of H, N, Se, S, Fe, K, Mn, and As. Cluster two consists of Ca, C, Mg and Hg. The first cluster, based on the degree of dependence on elements, can be divided into three subclusters H and N (1), Se and S (2) and Fe, K, Mn, and As (3). H and N were significantly correlated with each other indicating adsorption of organic matter to clay minerals; Se and S represented sulphides and Fe, K, and Mn present Fe and Mn oxides and associations of these oxides and clay minerals in sediments. As(V) is very strongly sorbed by Fe/Mn oxides (Li et al., 2016), which explain the presence of arsenic in this subcluster.

The second cluster can be divided into two subclusters: Ca, C, and Mg (1) and Hg (2). As expected, Hg was isolated from the other elements, which is indicative of lack of association with the others in the

sediments. Ca, C, and Mg represented carbonates and form separate sub-cluster.

Results obtained by applying this multivariate method are consistent with those obtained by content distribution in sediments and inter-element relationships of studied elements.

## 4. Conclusion

Sediment pollution with As, Hg, and Se is a widespread concern due to the global distribution of these elements and the associated potential for toxicity, bioaccumulation and biomagnification. In the Serbian river and artificial lake sediments studied, mercury was found to be present in slightly elevated concentration. High content of arsenic on some localities, mainly caused by pollution with exogenous substances indicate that arsenic pollution problem that lasts longer period of time. Elevated concentrations of elements, mainly arsenic, in most cases were detected in samples of river sediments, since artificial lake reservoirs are usually built in rural areas, where the less anthropogenic pollution rivers often flow through the towns. Concentration of total selenium content in sediments is too low to be of toxicological significance in the aquatic environment.

The average pollution levels in studied sediments, expressed in terms of geoaccumulation indexes of As and Hg indicate that the environment is uncontaminated to moderately contaminated. All values of EF for Hg were below 2, indicating deficiency to minimal enrichment with Hg on studied localities. The calculated values of EF for As indicate

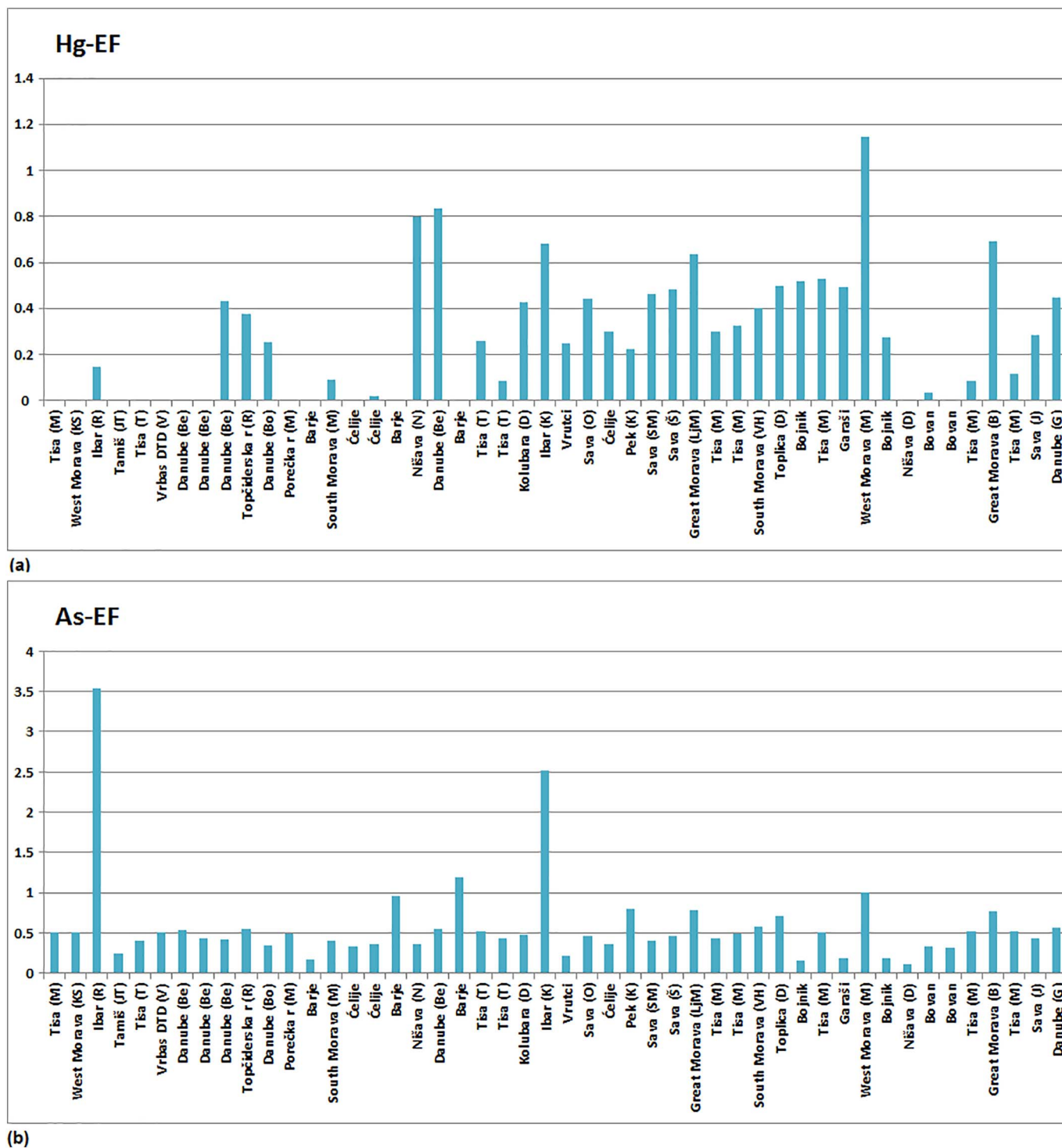


Fig. 4. Enrichment factors values of Hg (a) and As (b) at each sampling site.

that 95.8% sites for As had values for EF < 2, indicating deficiency to minimal enrichment. Two stations in the studied area had values > 2 for As, indicating moderate enrichment. These sediments were taken from Ibar river, and obtained values may be explained by increased load of As due to anthropogenic pressures in these region. The percentages of the easily soluble metal fraction of arsenic were in general below 10%, indicating its low mobility into the aquatic environment.

Due to the potential risk of arsenic and mercury pollution in sediment, with potential impacts on the entire ecosystem, pollution prevention and remediation measurements seem essential, especially in areas where we found increased levels of this element.

**Acknowledgements**

This study was supported by the Ministry of Education, Science and Technological Development of Serbia, Grant Nos. 172001 and 43007. In addition, we would like to thank the Republic Hydrometeorological Service of Serbia for the sediment samples.

**Appendix A. Supplementary data**

Supplementary data to this article can be found online at <http://dx.doi.org/10.1016/j.gexplo.2017.06.006>.

## References

- Avramidis, P., Nikolaou, K., Bekiari, V., 2015. Total organic carbon and total nitrogen in sediments and soils: a comparison of the wet oxidation-titration method with the combustion-infrared method. *Agric. Agric. Sci. Procedia* 4, 425–430.
- Bernalte, E., Salmanighabeshi, S., Rueda-Holgado, F., Palomo-Marín, M.R., Marín-Sánchez, C., Cereceda-Balic, F., Pimilla-Gil, E., 2015. Mercury pollution assessment in soils affected by industrial emissions using miniaturized ultrasonic probe extraction and ICP-MS. *Int. J. Environ. Sci. Technol.* 12, 817–826.
- Berzas Nevado, J.J., Rodríguez Martín-Doimeadios, R.C., Guzmán Bernardo, F.J., Jiménez Moreno, M., Herculano, A.M., do Nascimento, J.L.M., Crespo-López, M.E., 2010. Mercury in the Tapajós River basin, Brazilian Amazon: a review. *Environ. Int.* 36, 593–608.
- Burger, J., Gochfeld, M., Jeinter, C., Donio, M., Pittfield, T., 2012. Interspecific and intraspecific variation in selenium:mercury molar ratios in saltwater fish from the Aleutians: potential protection on mercury toxicity by selenium. *Sci. Total Environ.* 431, 46–56.
- Chen, T., Chang, Q., Liu, J., Clevers, J.G.P.W., Kooistra, L., 2016. Identification of soil heavy metal sources and improvement in spatial mapping based on soil spectral information: a case study in northwest China. *Sci. Total Environ.* 565, 155–164.
- Chen, H., Chen, R., Teng, Y., Wu, J., 2016. Contamination characteristics, ecological risk and source identification of trace metals in sediments of the Le'an River (China). *Ecotoxicol. Environ. Saf.* 125, 85–92.
- Čuvarčić, M.S., 2003. Selenium in soil. In: *Proceedings for Natural Sciences*. vol. 104. Matica Srpska, Novi Sad, pp. 23–37.
- De Castro-Catalá, N., Kuzmanović, M., Roig, N., Sierra, J., Ginebreda, A., Barceló, D., Pérez, S., Petrović, M., Picó, Y., Schuhmacher, M., Muñoz, I., 2016. Ecotoxicity of sediments in rivers: invertebrate community, toxicity bioassays and the toxic unit approach as complementary assessment tools. *Sci. Total Environ.* 540, 297–306.
- Dević, G., Đorđević, D., Sakan, S., 2014. Freshwater environmental quality parameters of man-made lakes of Serbia. *Environ. Monit. Assess.* 186, 5221–5234.
- Dević, G., Sakan, S., Đorđević, D., 2016. Assessment of the environmental significance of nutrients and heavy metal pollution in the river network of Serbia. *Environ. Sci. Pollut. Res.* 23 (1), 282–297.
- Dhivert, E., Grosbois, C., Coynel, A., Lefèvre, I., Desmet, M., 2015. Influences of major flood sediment inputs on sedimentary and geochemical signals archived in a reservoir core (Upper Loire Basin, France). *Catena* 126, 75–85.
- Fendorf, S., Nico, P.S., Kocar, B.D., Masue, Y., Tufano, K.J., 2010. Arsenic chemistry in soils and sediments. *Dev. Soil Sci.* 34, 357–378.
- Frančičković-Bilinski, S., 2007. An assessment of multielemental composition in stream sediments of Kupa River drainage basin, Croatia for evaluating sediment quality guidelines. *Fresen. Environ. Bull.* 16 (5), 561–575.
- Frančičković-Bilinski, S., 2008. Detection of geochemical anomalies in stream sediments of the upper Sava River drainage basin (Slovenia, Croatia). *Fresen. Environ. Bull.* 17 (2), 188–196.
- Frančičković-Bilinski, S., Bilinski, H., Tibljaš, D., Hanžel, D., 2006. Sediments from Savinja, Voglajna and Hudinja rivers (Slovenia), reflecting anomalies in an old metallurgic area. *Fresen. Environ. Bull.* 15 (3), 220–228.
- Frémion, F., Bordas, F., Mourier, B., Lenain, J., Kestens, T., Courtin-Nomade, A., 2016. Influence of dams on sediment continuity: a study case of a natural metallic contamination. *Sci. Total Environ.* 547, 282–294.
- Ganther, H.E., Goudie, C., Wagner, P., Sunde, M.L., Kopecky, M.J., Oh, S.H., Hoekstra, W.G., 1972. Selenium relation to decreased toxicity of methylmercury added to diets containing tuna. *Science* 175, 1122–1124.
- Gustafsson, J.P., Tin, N.T., 1994. Arsenic and selenium in some Vietnamese acid sulphate soils. *Sci. Total Environ.* 151, 153–158.
- Hagarová, I., Zemberyová, M., Bajčan, D., 2005. Sequential and single step extraction procedures used for fractionation of selenium in soil samples. *Chem. Pap.* 59, 93–98.
- Issaro, N., Abi-Ghanem, C., Bermond, A., 2009. Fractionation studies of mercury in soils and sediments: a review of the chemical reagents used for mercury extraction. *Anal. Chim. Acta* 631, 1–12.
- Jagtap, R., Maher, W., 2015. Measurement of mercury species in sediments and soils by HPLC-ICPMS. *Microchem. J.* 121, 65–98.
- Jiang, Y., Zeng, X., Fan, X., Chao, S., Zhu, M., Cao, H., 2015. Levels of arsenic pollution in daily foodstuffs and soils and its associated human health risk in town in Jiangsu Province. *Ecotoxicol. Environ. Saf.* 122, 198–204.
- Koljonen, T., 1974. Selenium in certain Finnish sediments. *Bull. Geol. Soc. Finl.* 46, 15–21.
- Lemly, A.D., 2002. *Selenium Assessment in Aquatic Ecosystems: A Guide for Hazard Evaluation and Water Quality Criteria*. Springer, New York, NY.
- Li, L., Ciu, J., Liu, J., Gao, J., Bai, Y., Shi, X., 2016. Extensive study of potential harmful elements (Ag, As, Hg, Sb, and Se) in surface sediments of the Bohai Sea, China: sources and environmental risks. *Environ. Pollut.* <http://dx.doi.org/10.1016/j.envpol.2016.05.034>.
- Lv, Y., Yu, T., Yang, Z., Zhao, W., Zhang, M., Wang, Q., 2014. Constraint on selenium bioavailability caused by its geochemical behavior in typical Kaschin-Beck disease areas in Aba, Sichuan Province of China. *Sci. Total Environ.* 493, 737–749.
- MacDonald, D.D., Ingersoll, C.G., 2002. *A Guidance Manual to Support the Assessment of Contaminated Sediments in Freshwater Ecosystems*. (<http://www.epa.gov/great-lakes/sediment/Vol3.pdf>).
- Malisa, E.P., 2001. The behaviour of selenium in geological processes. *Environ. Geochem. Health* 23, 137–158.
- Milačić, R., Ščančar, J., Murko, S., Kocman, D., Horvat, M., 2010. A complex investigation of the extent of pollution in sediments of the Sava River. Part I: selected elements. *Environ. Monit. Assess.* 163, 263–275.
- Milošković, A., Dojčinović, B., Kovačević, S., Radojković, N., Radenković, M., Milošević, D., Simić, V., 2016. Spatial monitoring of heavy metals in the inland waters of Serbia: a multispecies approach based on commercial fish. *Environ. Sci. Pollut. Res.* <http://dx.doi.org/10.1007/s11356-016-6207-2>.
- Muller, G., 1979. Schwermetalle in den sedimenten des Rheins-Veränderungen seit, 1971. *Umschau* 79 (24), 778–783.
- Oppong, S.O., Voegborlo, R.B., Agorku, S.E., Adimado, A.A., 2010. Total mercury in fish, sediments and soil from the River Pra Basin, Southwestern Ghana. *Bull. Environ. Contam. Toxicol.* 85, 324–329.
- Patel, K.S., Shrivastava, K., Brandt, R., Jakubowski, N., Corns, W., Hoffmann, P., 2005. Arsenic contamination in water, soil, sediment and rice of central India. *Environ. Geochem. Health* 27, 131–145.
- Petrović, D., Todorović, M., Manojlović, D., Krsmanović, V., 2010. A simulation experiment as a method for the investigation of the mobility of heavy metals from inundated land. *J. Serb. Chem. Soc.* 75, 1005–1018.
- Prachei, B.M., Snow, D.D., Pegg, M., 2010. Distribution of selenium, mercury, and methylmercury in surficial Missouri River sediments. *Bull. Environ. Contam. Toxicol.* 84, 331–335.
- Ralston, N.V.C., 2008. Selenium health benefit values as seafood safety criteria. *EcoHealth* 5, 442–455.
- Raposo, J., Olazabal, M.A., Madariaga, J.M., 2004. Validation of chemical speciation model of inorganic arsenic in river waters with mobilisation processes. *Chem. Speciat. Bioavailab.* 16, 9–15.
- Republic of Serbia, 1994. *Official Gazette of Republic Serbia*, 23/1994. (Rule book of allowed concentrations of dangerous and hazardous materials in soil and in water for irrigation and methods for analysis) pp. 23.
- Rezende, P., Moura, P.A.S., Durão Jr., W.A., Nascentes, C.C., Windmöller, C.C., Costa, L.M., 2011. Arsenic and mercury mobility in Brazilian sediments from the São Francisco River basin. *J. Braz. Chem. Soc.* 22, 910–918.
- Roig, N., Nadal, M., Sierra, J., Ginebreda, A., Schuhmacher, M., Domingo, J., 2011. Novel approach for assessing heavy metal pollution and ecotoxicological status of rivers by means of passive sampling methods. *Environ. Int.* 37, 671–677.
- Rönkkömäki, H., Pöykö, R., Nurmesniemi, H., Popov, K., Merisalu, E., Tuomi, T., Välimäki, I., 2008. Particle size distribution and dissolution properties of metals in cyclone fly ash. *Int. J. Environ. Sci. Technol.* 5, 485–494.
- Sakan, S., Đorđević, D., Manojlović, D., Polić, P., 2009. Assessment of heavy metal pollutants accumulation in the Tisza River sediments. *J. Environ. Manag.* 90, 3382–3390.
- Sakan, S., Đorđević, D., Dević, G., Relić, D., Anđelković, I., Đuričić, J., 2011. A study of trace element contamination in river sediments in Serbia using microwave-assisted aqua regia digestion and multivariate statistical analysis. *Microchem. J.* 99, 492–502.
- Sakan, S., Đorđević, D., Lazić, M., Tadić, M., 2012. Assessment of arsenic and mercury contamination in the Tisa River sediments and industrial canal sediments (Danube alluvial formation), Serbia. *J. Environ. Sci. Health A* 47, 109–116.
- Sakan, S., Dević, G., Relić, D., Anđelković, I., Sakan, N., Đorđević, D., 2015. Environmental assessment of heavy metal pollution in freshwater sediment, Serbia. *Clean: Soil, Air, Water* 43, 838–845.
- Savery, L.C., Evers, D.C., Wise, S.S., Falank, C., Wise, J., Gianios Jr., C., Kerr, I., Payne, R., Thompson, W.D., Perkins, C., Zheng, T., Zhu, C., Benedict, L., Wise Sr., J.P., 2013. Global mercury and selenium concentrations in skin from free-ranging sperm whales (*Physeter macrocephalus*). *Sci. Total Environ.* 450–451, 59–71.
- Shand, C.A., Balsam, M., Hillier, S.J., Hudson, G., Newman, G., Arthur, J.R., Nicol, F., 2010. Aquaregia extractable selenium concentrations of some Scottish topsoils measured by ICP-MS and the relationship with mineral and organic soil components. *J. Soil. Food Agric.* 90, 972–980.
- Stafilov, T., Aliu, M., Sajn, R., 2010. Arsenic in surface soils affected by mining and metallurgical processing in K Mitrovica region, Kosovo. *Int. J. Environ. Res. Public Health* 7, 4050–4061.
- Tang, Q., Bao, Y., He, X., Zhou, H., Cao, Z., Gao, P., Zhong, R., Hu, Y., Zhang, X., 2014. Sedimentation and associated trace metal enrichment in the riparian zone of the Three Gorges Reservoir, China. *Sci. Total Environ.* 479–480, 258–266.
- Tarin, P., 2006. *Distribution, Speciation and Geochemistry of Selenium in Contaminated Marine Sediments—Port Kembla Harbour, NSW, Australia*. PhD thesis School of Earth Environmental Sciences, University of Willongong (<http://ro.uow.edu.au/thesis/714>).
- Teapanosyan, G., Sahakyan, L., Belyaeva, O., Saghatelian, A., 2016. Origin identification and potential ecological risk assessment of potentially toxic inorganic elements in the topsoil of the city of Yerevan, Armenia. *J. Geochem. Explor.* 167, 1–11.
- Todorović, Z., Polić, P., Đorđević, D., Antonijević, S., 2001. Lead distribution in water and its association with sediment constituents of the “Barje” lake (Leskovac, Yugoslavia). *J. Serb. Chem. Soc.* 66, 697–708.
- U.S. Environmental Protection Agency, 1986. *Test Methods for Evaluating Solid Wastes, SW 846*, third ed. vol. 1. U.S. Environmental Protection Agency, Washington, DC, pp. 7471 Sec. A, Method.
- US EPA, 2007. *Freshwater Sediment Screening Benchmarks*. US Environmental Protection Agency.
- Villaescusa-Celaya, J.A., Gutiérrez-Galindo, E.A., Flores-Muñoz, G., 2000. Heavy metals in the fine fraction of coastal sediments from Baja California (Mexico) and California (USA). *Environ. Pollut.* 108, 453–462.
- Wiramanaden, C.I.E., Forster, E.K., Liber, K., 2010. Selenium distribution in a lake system receiving effluent from a metal mining and milling operation in Northern Saskatchewan, Canada. *Environ. Toxicol. Chem.* 29, 606–616.
- Woitke, P., Wellnitz, J., Helm, D., Kube, P., Lepom, P., Lithertay, P., 2003. Analysis and assessment of heavy metal pollution in suspended solids and sediments of the river Danube. *Chemosphere* 51, 633–642.
- Xu, L., Cao, S., Wang, J., Lu, A., 2016. Which factors determine metal accumulation in



- agricultural soils in the severely human-coupled ecosystem? *Int. J. Environ. Res. Public Health* 13, 510. <http://dx.doi.org/10.3390/ijerph13050510>.
- Yang, D.Y., Chen, Y.W., Gunn, J.M., Belzile, N., 2008. Selenium and mercury in organisms: interactions and mechanisms. *Environ. Rev.* 16, 71–92.
- Yu, T., Yang, Z., Lv, Y., Hou, Q., Xia, X., Feng, H., Zhang, M., Lixin, J., Kan, Z., 2014. The origin and geochemical cycle of soil selenium in a Se-rich area of China. *J. Geochem. Explor.* 139, 97–108.
- Zhang, H., 2014. Impacts of Selenium on the Biogeochemical Cycles of Mercury in Terrestrial Ecosystems in Mercury Mining Areas. Springer Theses Springer-Verlag, Berlin Heidelberg. [http://dx.doi.org/10.1007/978-3-642-54919-9\\_2](http://dx.doi.org/10.1007/978-3-642-54919-9_2).

Article

# Geochemical Fractionation and Assessment of Probabilistic Ecological Risk of Potential Toxic Elements in Sediments Using Monte Carlo Simulations

Sanja Sakan <sup>1,\*</sup> , Nenad Sakan <sup>2</sup> , Aleksandar Popović <sup>3</sup>, Sandra Škrivanj <sup>3</sup> and Dragana Đorđević <sup>1,\*</sup>

<sup>1</sup> Centre of Excellence in Environmental Chemistry and Engineering–ICTM, University of Belgrade, Njegoševa 12, 11158 Belgrade, Serbia

<sup>2</sup> Institute of Physics, University of Belgrade, Pregrevica 118, 11080 Zemun, Serbia; nsakan@ipb.ac.rs

<sup>3</sup> Faculty of Chemistry, University of Belgrade, Studentski trg 12-16, 11000 Belgrade, Serbia; apopovic@chem.bg.ac.rs (A.P.); sandra\_skrivanj@chem.bg.ac.rs (S.Š.)

\* Correspondence: ssakan@chem.bg.ac.rs (S.S.); dragadj@chem.bg.ac.rs (D.Đ.); Tel.: +381-11-3336-801 (S.S.)

Received: 15 April 2019; Accepted: 21 May 2019; Published: 6 June 2019



**Abstract:** The need for further research into potentially toxic elements in Serbian rivers led to an investigation of distributions, sources, and ecological risks in a sample base of sediments from 15 rivers. The analyses were carried out through both experimental and theoretical methods. Geochemical fractionation of Cd, Co, Cr, Cu, Fe, Mn, Ni, Pb, As, V, and Zn in sediments was studied using a sequential extraction procedure. Both a Håkanson risk index (RI) and a Monte Carlo simulation (MCS) were used in order to estimate ecological risk, applying the probability distribution of RI values instead of single-point calculations. In order to both further the development of the used method and include additional processes, software for the simulations was developed instead of using proprietary solutions. Metal fractionation showed high percentage recoveries of Cd, Cr, Co, Cu, Fe, Ni, and V in residual fractions. The high content of Pb, Mn, and Zn in mobile fractions might cause serious environmental concerns. In some localities, Cu and Cd could be problematic elements, since their mobility was high. An environmental assessment based on the described criteria provided risk levels varying from low to median (mainly contributed by Cd and Cu).

**Keywords:** geochemical fractionation; probabilistic ecological risk; Monte Carlo simulation; toxic elements; sediments; hierarchical clustering

## 1. Introduction

As an essential part of the overall ecological system, water is a subject and special responsibility in terms of improving the quality and sustainability of the quantity and needs of future generations. Due to intensive technological and industrial development, a large amount of harmful and toxic substances is polluting rivers and river sediments and is causing environmental damage. Among these substances, pollution by toxic and potentially toxic elements (PTEs) is a major problem due to their ubiquity coinciding with their toxicity and persistence [1]. River sediment quality is estimated by the presence of the sought toxic elements in fluvial sediments and fine suspended particles, since the solubility of the investigated PTEs in water is low under normal conditions [2].

When PTEs are found in an aquatic environment, they can be accumulated in sediment. River sediment is characteristic of the great complexity and diversity of its composition. The binding capacity for these elements depends primarily on the composition of the original rock and climatic

conditions. Reactivity or PTE mobility, and therefore potential toxicity, depends on the substrate to which it is related and the strength of the bound. The biological activity and chemical reactions in a water column can mobilize some of the toxic elements from sediment, and they can be carried out down the stream [3]. From the point of view of the environment, it is important to determine under what conditions PTEs can be released from sediment.

PTEs can be bounded in various matrices in different ways: occluded in amorphous materials; adsorbed on clay surfaces or iron/manganese oxyhydroxides; presenting in lattice of secondary minerals like carbonates, sulfates or oxides; complexed with organic matter (OM) or lattice of primary minerals such as silicates [4]. The strength of the element's binding determines its bioavailability as well as the risk associated with its presence in the investigated system. The strength values can, therefore, give a clear indication of sediment reactivity, which in turn allows an assessment of the risk connected with the presence of metals in the environment [5]. In an unaffected ecosystem, PTEs are almost immobile, as they are bound to silicates and minerals, but under the influence of human activities, these elements may be found in other labile forms, such as oxides, carbonates, hydroxides, and sulfides [1].

Extensive studies of different extraction methods for environmental samples have been carried out [6–10]. Since metals are bound into different chemical forms associated with a matrix, an analysis requires the application of sequential extraction methods [11]. Sequential extraction (SE) is an important and widely applied tool for gathering information on the potential mobility (hence, potential bioavailability and toxicity) of potentially toxic metals in the environment [12].

Different evaluation methods are used to determine the degree of contamination for sediments using numerous pollution indices [3,7,9,13–16]. Most current ecological risk assessment of sediments, including RI method, assume and combine a series of average, conservative and worst case values to derive a conservative point estimate of risk [17]. An evaluation of complex situations involving random behavior can be carried out with the help of Monte Carlo methods, which can help reduce uncertainty in estimating future outcomes in areas such as risk assessment or actuarial analyses [18]. This technique provides a quantitative way to obtain probability distributions for risks within the validity of the assessment model and provides more information for decision-making [17].

Serbia is very rich in water resources, not only due to the Sava, Danube, and Tisa rivers, but also due to mountain springs. Water pollution is a significant problem in Serbia and comes mainly from outdated technology, a lack of pollution abatement installations, inadequate storage and disposal of byproducts, untreated industrial and municipal wastewater, drainage water from agriculture, etc. Considering the large pollution of many river flows in Serbia, research related to their quality in Serbia are very important. First of all, new approaches and methods should be developed for applications with which it would be possible to monitor the quality of water.

A thorough investigation of the mobility of PTEs in river sediments was carried out within this manuscript by applying experimental and theoretical methods. This investigation was conducted to (i) quantify and assess the spatial variations of the studied elements, Cd, Co, Cr, Cu, Fe, Mn, Ni, Pb, V, and Zn, in river sediments collected from 15 rivers in Serbia; (ii) evaluate the potential mobility of elements in various fractions of sediments using a modified Tessier's sequential extraction method; (iii) determine the contamination factor to assess the degree of toxic element risk to the environment in relation to retention time; (iv) perform an ecological risk assessment of potentially toxic elements using a Monte Carlo simulation (MCS); and (v) determine the interrelations and similarities of the extracted element contents in each extraction step using cluster analysis.

To our knowledge, this is the first report evaluating the probabilistic ecological risk of potentially toxic elements in Serbian river basins by performing a Monte Carlo simulation. The information presented as a result of the carried-out study could be directly used in planning appropriate strategies for the environmental management of these drainage basins.

## 2. Materials and Methods

### 2.1. Studied Area

The territory of Serbia is characterized by a varied lithographic composition. Several geotectonic compositions can be singled out within this territory: the Pannonian Basin, Inner Dinarides, Vardar Zone, Serbo-Macedonian Massif, Carpatho-Balkanides, and Dacian Basin. Masses of karstified limestone are the main water-bearing media in morphologically broken-up regions (the Dinarides and Carpatho-Balkanides). Water-bearing media in the Vardar zone consist almost exclusively of rocks with fracture porosity, and water-bearing media of young depressions (the Pannonian and Dacian basins, as well as depressions within the Serbo-Macedonian Massif) are represented by alluvial formations and Neogene lacustrine sediments, i.e., water-bearing media with intergranular porosity [19].

The river network in the region of Serbia is relatively dense. The greatest part of Serbian territory belongs to the Danube drainage basin. The most important tributaries of the Danube in Serbia are the Tisa, Sava, and Great Morava rivers [20].

### 2.2. Sampling Sites

Thirty-two samples of river sediment from 15 rivers in Serbia were collected for this research (Table 1, Figure 1): the Danube, the Sava, the Tisa, the Ibar, the Great Morava, the West Morava, the South Morava, the Nišava, the Tamiš, the Danube–Tisa–Danube Canal (DTD, Vrbas), the Topčiderska River, the Porečka River, the Kolubara, the Pek, and the Toplica. For the larger rivers, sampling was conducted at several locations (Figure 1). The sediment samples were stored at 4 °C. The contents of the micro- and macroelements were determined from the granulometric fraction <63 µm of the bottom sediment [21].

**Table 1.** Sediment samples: Number, river, and sampling site.

| Sample | River and Sampling Site         |
|--------|---------------------------------|
| 1      | Tisa (Martonoš)                 |
| 2      | Tisa (Martonoš)                 |
| 3      | Tisa (Martonoš)                 |
| 4      | Tisa (Martonoš)                 |
| 5      | Tisa (Martonoš)                 |
| 6      | Tisa (Titel)                    |
| 7      | Tisa (Titel)                    |
| 8      | Danube (Gruja)                  |
| 9      | Danube (Bezdan)                 |
| 10     | Danube (Bezdan)                 |
| 11     | Danube (Bezdan)                 |
| 12     | Danube (Bezdan)                 |
| 13     | Sava (Sremska Mitrovica)        |
| 14     | Sava (Šabac)                    |
| 15     | Sava (Ostružnica)               |
| 16     | Sava (Jamena)                   |
| 17     | DTD canal (Begej, Vrbas)        |
| 18     | Tamiš (Jaša Tomić)              |
| 19     | Pek (Kusiće)                    |
| 20     | Kolubara (Draževac)             |
| 21     | Porečka river (Mosna)           |
| 22     | Ibar (Raška)                    |
| 23     | Ibar (Kraljevo)                 |
| 24     | Topčiderskariver (Rakovica)     |
| 25     | South Morava (Mojsinje)         |
| 26     | Great Morava (Ljubičevski most) |
| 27     | Great Morava (Bagrdan)          |
| 28     | West Morava (Maskare)           |
| 29     | Nišava (Niš)                    |
| 30     | Nišava (Dimitrovgrad)           |
| 31     | South Morava (Vladičin Han)     |
| 32     | Toplica (Doljevac)              |



**Figure 1.** Locations of sampling sites.

### 2.3. Chemical and Data Analysis

Geochemical fractionation was conducted through a modification of Tessier's sequential extraction, which included five phases: F1 ("ion-exchangeable"), which was adsorbed and water-soluble metal forms and much less metal bound to carbonate ( $1\text{ M CH}_3\text{COO}(\text{NH}_4)$ ); F2, which was metal bound to carbonate and easily reducible species ( $0.01\text{ M HCl}$  and  $0.1\text{ M NH}_2\text{OH}\cdot\text{HCl}$ ); F3, which was metal bound to moderately reducible phases or the Fe oxide fraction ( $0.2\text{ M H}_2\text{C}_2\text{O}_4$  and  $0.2\text{ M }(\text{NH}_4)_2\text{C}_2\text{O}_4$ ); F4, which was organic matter and sulfides ( $30\%\text{ H}_2\text{O}_2$  adjusted to pH 2 with  $\text{HNO}_3$ , followed by extraction with  $3.2\text{ M CH}_3\text{COO}(\text{NH}_4)$ ); and F5, which was a "residual" fraction (aqua regia). A description of the procedure for fractions 1–4 is shown in Reference [5], and the fifth fraction is in Reference [12]. Samples were microwave-digested to determine the total contents of the studied elements [14,21]. The concentrations of elements from the extracts were determined by ICP/OES (inductively coupled plasma atomic emission spectrometry; iCAP-6500 Duo, Thermo Scientific, Cambridge, UK).

Quality control, accuracy, and the precision of the measurement and concentration values were performed using a certified reference material, BCR-143R. The measured values were in excellent agreement with the certified values of the BCR 143 reference materials (the accuracy ranged from 81.5% to 114%). Precision was expressed as the relative standard deviation. The relative standard deviations of the means of duplicate measurements were less than 10%.

Descriptive statistics and a hierarchical cluster analysis (HCA) were carried out using SPSS version 21 for Windows.

Determination of the toxic element contamination factor is an important aspect that indicates the degree of toxic element risks to the environment in relation to its retention time [3]. These factors are defined as the sum of element contents in the mobile phases (nonresidual phases) of the sample divided by the residual phase content ( $C_f = \Sigma$  (step 1 + 2 + 3 + 4)/residual, step 5). The lower the  $C_f$  value is, the higher the relative metal retention is [13].

#### 2.4. Ecological Risk Analysis

Håkanson's method could be used to evaluate the potential ecological risk of metal contaminants in sediments [22]. A potential ecological risk index (RI) shows the potential ecological risk caused by various pollutants in the environment [23,24]. According to Håkanson's method, the RI of metal contaminants in sediments can be calculated using the following equation:

$$RI = \sum_{i=1}^m E_r^i, \quad (1)$$

where  $E_r^i = T_r^i \cdot C_f^j$  and  $C_f^j = C^i/C_n^i$ .

RI are calculated as the sum of all risk factors for heavy metals in sediments,  $E_r^i$  is the potential ecological risk for a single factor,  $T_r^i$  is the toxic response factor for a given metal,  $C_f^j$  is the contamination factor,  $C^i$  is the measure concentration of metals in sediment, and  $C_n^i$  is the reference value for metals.

#### 2.5. Monte Carlo Simulation

A Monte Carlo analysis based on mathematical statistics and probability theory was used to assess model uncertainty through random sampling of a probability distribution for each variable [25]. In this manuscript, instead of Håkanson's RI, the probabilistic distribution of the RI was calculated using a Monte Carlo simulation to randomly sample values from the distribution of exposure concentrations [24].

The Monte Carlo method has been proven as a modeling procedure for stochastic processes, and its application originates from the nuclear age era [26], when it was usually applied to particle transport problems. As such, it is also an applicable, if not unavoidable, tool for risk assessment. As could be seen from Qu et al. [17] and Wu et al. [27], the Monte Carlo method is very applicable in heavy metal pollution risk assessment. Based on their work, we developed our software, which is written in Qt [28], and a random number generator produces a normal distribution with long-term repeatability. The program used was tested on several models, and as a final test the results from Qu et al. [17] and Wu et al. [27] were reproduced in their entirety based on input data. It is expected that the use of our specific software could lead us to more easily extend its capabilities based on the current need in research.

### 3. Results and Discussion

#### 3.1. Distribution by Fraction of Studied Elements

A sequential extraction procedure was applied to fractionate the studied elements within sediments. The percentage element distribution by fraction was calculated as the average content of the extracted element in each fraction with respect to the total extracted element content (Table 2). The residual fractions of the sediment were the dominant ones for Cd, Cr, Co, Cu, Fe, Ni, As, and V, as shown in Figure 2 and Table 2. This fact indicated that crystal forms of iron oxides as well as aluminosilicates were a significant substrate of the studied elements.



**Table 2.** Distribution of metals in the fractions of the sequential extraction.

| Element | Distribution by Fraction |
|---------|--------------------------|
| Cd      | F5 > F2 > F1 > F4 > F3   |
| Cr      | F5 > F4 > F3 > F2 > F1   |
| Co      | F5 > F2 > F3 > F4 > F1   |
| Cu      | F5 ≈ F3 > F4 ≈ F2 > F1   |
| Fe      | F5 > F3 > F4 > F2 > F1   |
| Mn      | F2 > F1 > F5 > F4 > F3   |
| Ni      | F5 > F4 ≈ F2 ≈ F3 > F1   |
| Pb      | F2 > F4 > F3 ≈ F5 ≈ F1   |
| Zn      | F2 > F5 > F4 > F3 > F1   |
| V       | F5 > F3 > F2 > F4 > F1   |
| As      | F5 > F3 > F2 > F4 > F1   |

F1: ion-exchangeable; F2: metal bound to carbonate and easily reducible species; F3: the Fe oxide fraction; F4: organic matter and sulfides; F5: the "residual" fraction.

Those residual fractions were relatively stable and did not show significant transformations in various conditions: Namely, the metals still remained in sediment. Residual fractions of both geogenic and anthropogenic origin represented the more stable metal forms, and their influence on the ecological system was much less than the others under normal conditions. The dominant fractions for the extraction of Co, As, and V were F5, F2, and F3. This distribution indicated the fact that Fe oxide of different degrees of crystallinity was the most significant for the binding of Co, As, and V. The change in oxidation state of Fe and Mn could lead to the release of the elements that were retained in this form, and this accidental situation could lead to a long-term source of contamination. The Mn, Pb, and Zn are extracted significantly in mobile, the second fractions. This distribution indicated that carbonates and oxide fractions, principally mobile fractions, were the most significant for the binding of these elements. As shown in Tessier et al. [29], metals bound in carbonate and exchangeable, Fe-Mn oxide, and organic fractions are the most likely to mobilize from the sediments if oxygen or the geochemical conditions change in the surface water and hence are more available for the food chain. The fractions bound to Mn oxides and organic materials were reviewed as the most important components in sediments for metal binding, and they represented a potentially mobile component under changing conditions.

An organic fraction may be associated with various forms of organic material, such as living organisms, detritus, or coatings on mineral particles, through complexation or a bioaccumulation process. This kind of metal can exist in sediment for longer periods, and can also be released with OM decomposition. An exchangeable fraction, referring to metals directly adsorbing on sediments, was not significant for elements in the studied sediments. However, in some localities, it was possible to observe a substantial proportion of Cd and Cu extracted in the mobile, first, and second fractions (Figure 2). Since exchangeable and carbonate bound fractions (weakly bound forms) are partially introduced through anthropogenic intrusions [10], it can be assumed that in some localities there existed local anthropogenic sources of Cd and Cu.

In the current investigation, Pb, Mn, and Zn were noted to be highly mobile, and their high concentration in the mobile fractions might cause serious environmental concerns. In addition, in some localities, Cu and Cd could be problematic elements, since their mobility was high.



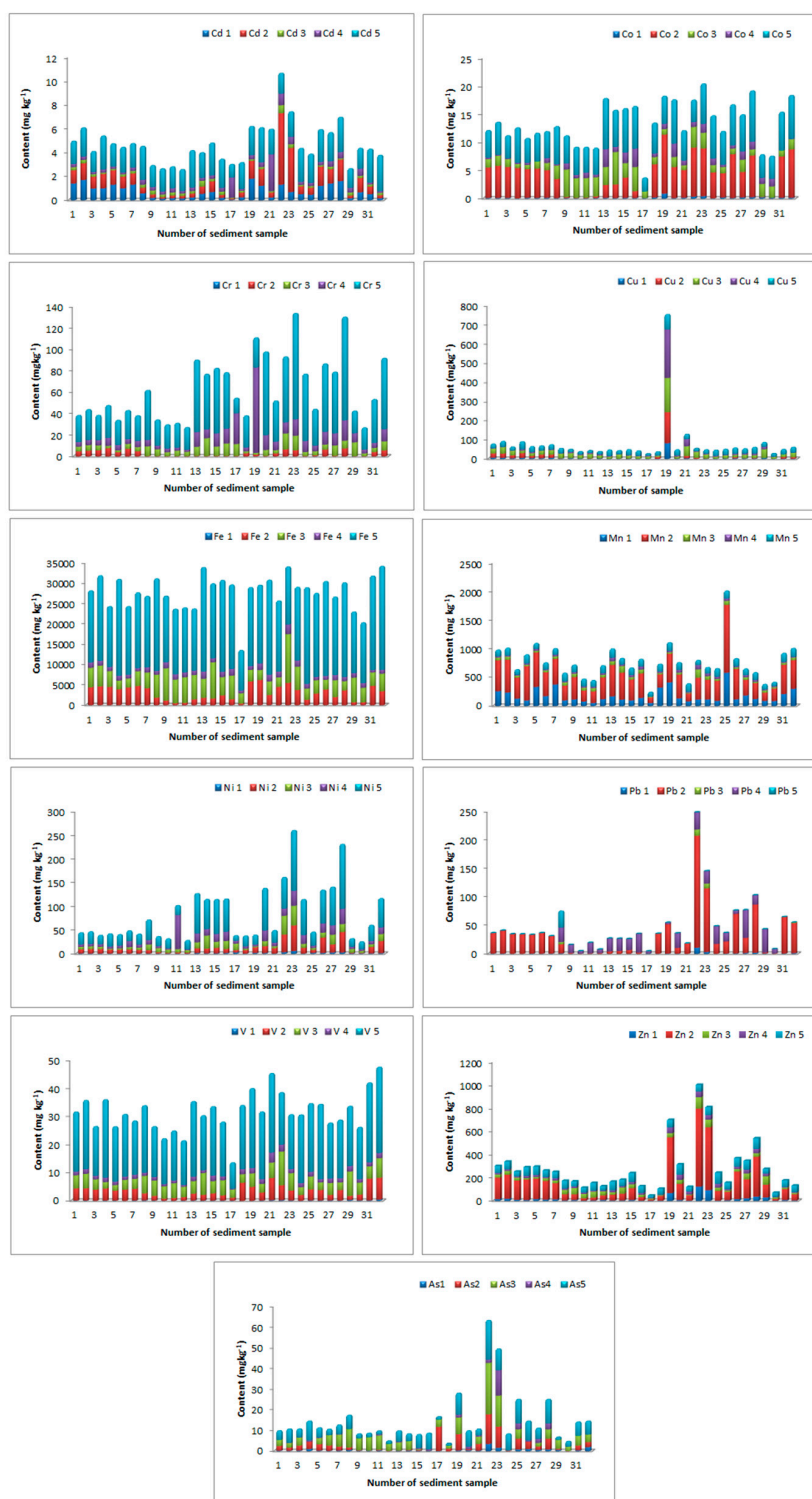


**Figure 2.** Distribution of Cd, Cr, Cu, Fe, Mn, Ni, Pb, V, Zn, and As by fraction and sampling site. \*E1: “ion-exchangeable”; E2: metal bound to carbonate and easily reducible species; E3: the Fe oxide fraction; E4: organic matter and sulfides; E5: the “residual” fraction.

### 3.2. Distribution of Elements by Sampling Site

The total content of elements after digestion with aqua regia, the guideline values of Serbia, background values, and earth crust values of elements in the studied sediments are presented in Table 3.

The distribution of elements by sampling site is given in Figure 2. A comparison of the quantitative distribution of the contents of the various elements in the sediments is shown in a boxplot (Figure 3).

**Table 3.** Comparison of the total element contents in surface river sediments to the guideline values of Serbia, earth crust values, and background values ( $\text{mg kg}^{-1}$ ).

|                                | Cd   | Co   | Cr   | Cu   | Fe     | Mn   | Ni   | Pb   | V    | Zn   | As   |
|--------------------------------|------|------|------|------|--------|------|------|------|------|------|------|
| Min                            | 1.28 | 8.22 | 59.8 | 11.5 | 24,556 | 648  | 33.2 | 57.8 | 60.4 | 66.6 | 3.67 |
| Max                            | 10.5 | 36.2 | 230  | 870  | 62,800 | 3688 | 274  | 318  | 149  | 1095 | 63.2 |
| Mean                           | 4.82 | 22.0 | 113  | 78.5 | 44,177 | 1399 | 77.8 | 132  | 111  | 353  | 14.7 |
| Guideline v. <sup>1</sup>      | 3    | /    | 100  | 100  | /      | /    | 50   | 100  | /    | 300  | 25   |
| Earth crust <sup>2</sup>       | 0.13 | 18   | 83   | 47   | 46,500 | 1000 | 58   | 16   | 90   | 83   | 1.7  |
| Background v. <sup>3</sup>     | 1.28 | 8.22 | 62.1 | 11.5 | 24,556 | 648  | 33.2 | 57.8 | 60.4 | 66.6 | 3.67 |
| Toxic response f. <sup>4</sup> | 30   | /    | 2    | 5    | /      | /    | 5    | 5    | /    | 1    | 10   |

<sup>1</sup> The guideline values of Serbia [30]; <sup>2</sup> earth crust values [31]; <sup>3</sup> background values of the studied sediments; <sup>4</sup> toxic response factors. Here, v.: Values; f.: Factors.

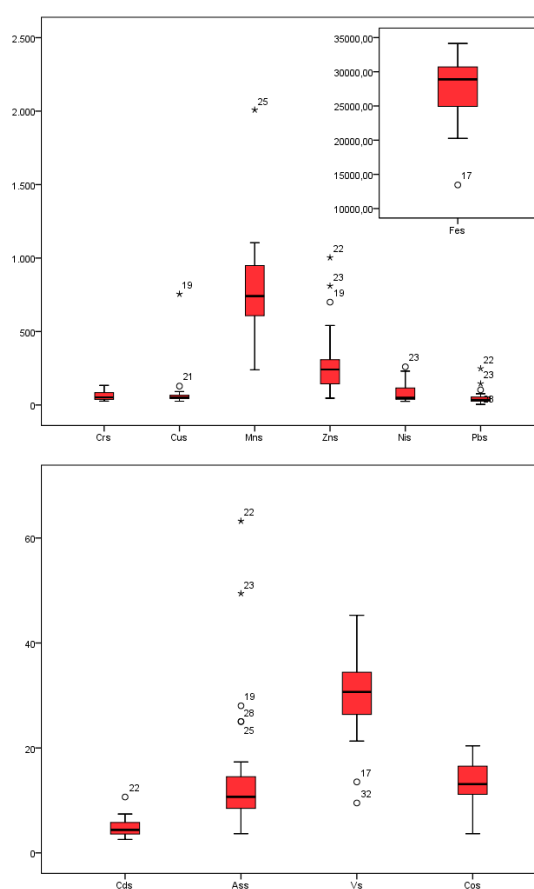


**Figure 3.** Box plot diagrams of Cd, Cr, Cu, Fe, Mn, Ni, Pb, V, As, and Zn.

Outlier and extreme values of the element contents suggested that the most critical sites in terms of metal contamination were observed in West Morava (Pb), Ibar (Cd, Zn, Pb, and Ni), the Porečka River (Cu), Ibar (Cu, Zn), and South Morava (Mn). The maximum content of Cd, Cr, Cu, Ni, Pb, and Zn exceeded the standard values given by Serbian guidelines. Permanent and accidental pollution from industrial plants and mines that are located in the basins of these rivers, alongside agricultural use of manganese-containing products such as fertilizers and fungicides, were the main cause of pollution in these rivers [32]. Given the existence and position of a Cu mine in Majdanpek close to the source of the Pek River, it is justifiable to assume that the origin of the Cu was associated with this mine [21].

As the greatest tributary of the West Morava, the Ibar River is affected with lead and zinc pollution, since in this area are a vast number of production and manufacturing plants of the mining-metallurgical

system, Trepča-nine lead and zinc mines, three flotations, two of metallurgy, the chemical industry, and a battery factory [33].

### 3.3. Cluster Analysis (CA)

A cluster analysis (R-mode, Pearson method) was carried out by using the contents of the elements extracted in the different fractions. The results of the cluster analysis by fraction of sequential extraction are shown in Figure 4.

Fraction F1: The results for the F1 fraction distinguished the elements into three groups, which were formed by mixing different mineralogical species. Group 1 was characterized by elements Pb1, As1, Zn1, and Ni1, mainly due to the presence of secondary carbonate minerals that were partially destroyed in this fraction. Group 2 was constituted by Cu1, Co1, and Cd1, which did not show a clear association and could form a mixing group where different mineral species such as hydrated oxides of iron and manganese, humic acids, or sulfates could present their substrates. Group 3 was constituted by Cr1, Mn1, V1, and Fe1, which could be attributed to the important role proposed for Fe and Mn oxyhydroxides in the retention of elements in this fraction.

Fraction F2: Fraction F2 could be differentiated into three groups with a high association level. Group 1 was characterized by elements such as Cd2, Zn2, Pb2, Ni2, and As2 due to the presence of carbonate minerals, and these had a high-potential capacity to collect and retain metallic elements on the surface [2]. Group 2 was constituted by Fe2, Co2, V2, and Cr2, which may indicate Co, V, and Cr were associated with hydrated oxides of iron and that Group 3 was associated with Cu3 and Mn3, which may indicate an association of Cu with hydrated oxides of manganese.

Fraction F3: An analysis of the F3 fraction did not show as clear a differentiation as the other fractions. Cd3, Fe3, Mn3, V3, Zn3, Co3, Cr3, Ni3, Pb3, and As3 made one group and isolated only Cu3. This distribution was the result of the dissolution of the partially crystalline and amorphous iron oxide forms at this stage, as they are important substrates of those elements. A possible cause for the separation of Cu3 as a special group was probably the different origin of this element with respect to the other elements.

Fraction F4: Fraction F4 could be differentiated into two groups with a high association level. Group 1 was characterized by elements Cr4, Cu4, Cd4, and V4, mainly due to associations of these elements with organic matter. Group 2 was constituted by Fe4, Mn4, Co4, Zn4, Pb4, Ni4, and As4, since these elements are associated with sulfides. As and S may form very insoluble compounds, such as arsenopyrite [34].

Fraction F5: An analysis of the residual fraction showed a differentiation of the elements into three groups. The first group consisted of Cd5, Fe5, Co5, Mn5, V5, and Cu5, where major parts of the elements were related to the presence of crystalline Fe oxides. The second group was composed of Cr5, Ni5, and Zn5, which are mainly related to the presence of silicates; and the third group was isolated Pb5 and As5, which are recognized as having an affinity with sulfides or secondary sulfates (arsenic–lead sulfide minerals). As shown in Noguchi and Nakagawa [34], the following lead–arsenic sulfide minerals are known: Jordanite  $4\text{PbS}\cdot\text{As}_2\text{S}_3$ , gratonite  $9\text{PbS}\cdot\text{As}_2\text{S}_3$ , guitermanite  $10\text{PbS}\cdot 3\text{As}_2\text{S}_3$ , dufrenoyite  $2\text{PbS}\cdot\text{As}_2\text{S}_3$ , rathite  $13\text{PbS}\cdot 9\text{As}_2\text{S}_3$ , baumhauerite  $4\text{PbS}\cdot 3\text{As}_2\text{S}_3$ , liveingite  $5\text{PbS}\cdot 4\text{As}_2\text{S}_3$ , and sartorite  $\text{PbS}\cdot\text{As}_2\text{S}_3$ .

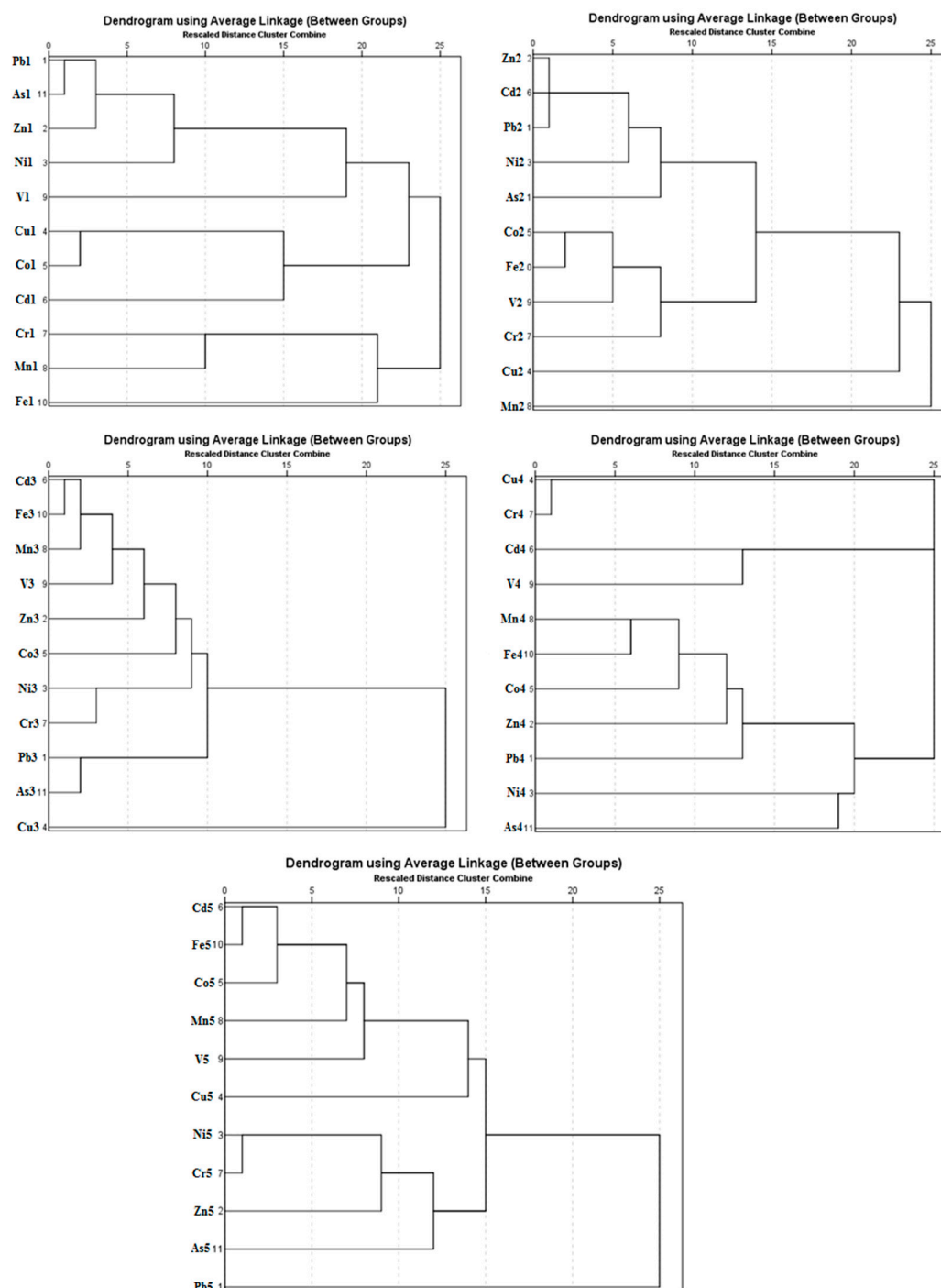


**Figure 4.** Presentation of the cluster analysis (CA) for the different steps recovered in the sequential extraction procedure (SEP). The number shown next to the element represents a fraction of the sequential extraction.

### 3.4. Contamination Factors

The individual contamination factor (Cf) of elements was used to estimate the relative retention time of heavy metals retained in the sediment. Higher Cf values demonstrated a lower retention time and a higher risk to the environment. In this research, contamination factors were calculated for Cu, Cr, Pb, Cd, Ni, Co, Fe, Mn, Zn, As, and V in the sediments at all stations.

The obtained results (Figure 5) showed that relative metal retention was not the same for all of the elements. The calculated factors showed the highest Cfs for Pb, Zn, Mn, Cu, and Cd and showed

their ability to be released from Serbian river sediments; whereas As, Co, Cr, Fe, Ni, and V showed the lowest mobility and hence the ability to be released. The combined risk of Cd, Zn, Cu, and Pb, the great contributors to highly mobile fractions, was a consequence of their large concentrations, toxicity, and mobility, and as such this presents an increased possible risk of these metals to the environment. The highest contamination factors were obtained for Mn, Zn, and Pb in the sediment samples obtained from Pek and Ibar sediments (locations 19 and 22). It can be concluded that Fe and V had a high relative metal retention with respect to the other elements.

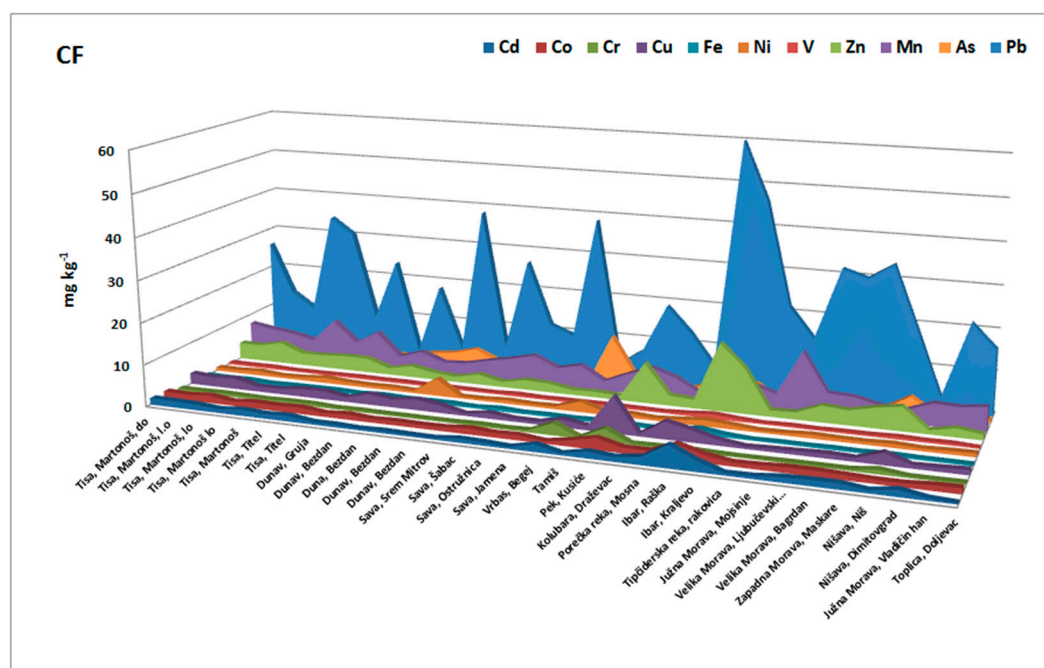


**Figure 5.** Contamination factor for each element in the investigated sediments.

### 3.5. Ecological Risk Assessment of Potentially Toxic Elements Using the Monte Carlo Simulation

A distribution curve of  $E_r^i$  and HRI (Total ecological risk comprehensive index) values is shown in Figure 6. The probability that ecological risk appeared at different risk levels with reference to a risk level classification standard was analyzed, as shown in Table 4.

The risks of Zn, Pb, and Cr were all low. The risks for Ni and As were also low (Ni 99.07% and 99.99% for As). The Monte Carlo simulations indicated that Cu and Cd posed a relatively high ecological risk in the studied areas, from a low to median risk. These results suggest that Cd and Cu are the most important risk factors in Serbian river basins (especially Cd), given that the probability of a median risk level was 31.70%. The obtained results were in line with the results of the sequential extractions, calculated contamination factors, and box plot method results. The results of the Monte Carlo simulations indicate that mobility, in addition to the high content of an element, is very important in risk assessment.

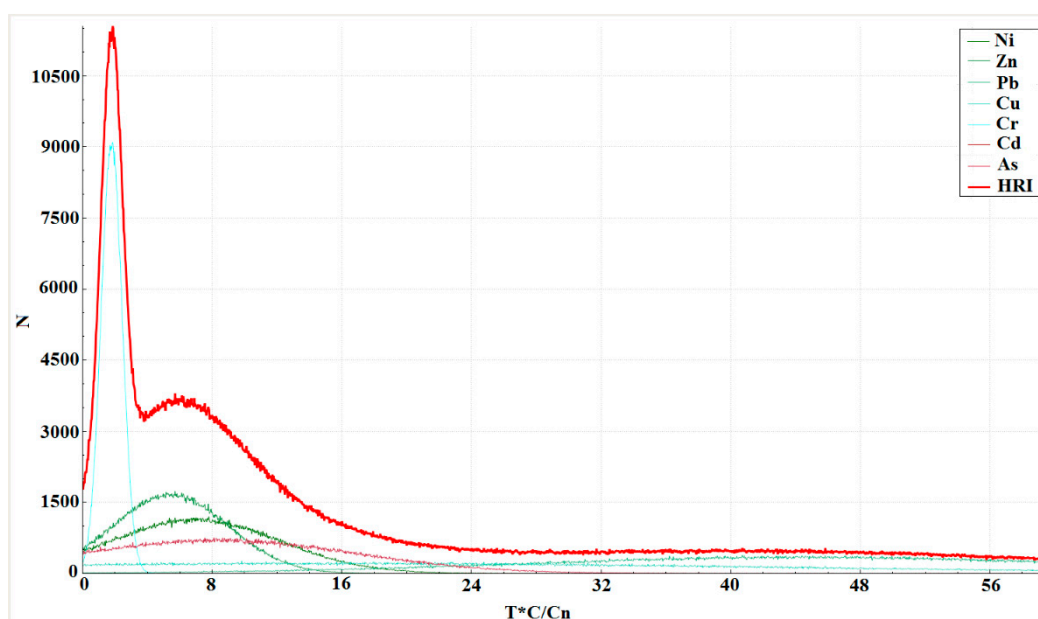


**Figure 6.** Distribution curve and exceedance probability curves of the risk index (RI) and total ecological risk comprehensive index HRI based on a Monte Carlo simulation run 100,000 times. Local backgrounds are the reference values for the calculation of  $E_r$ .

**Table 4.** Ecological risk analysis results of each heavy metal pollutant.

| Value of $E_r^i$       | Risk Level     | Probability (%) |     |     |       |     |       |       |
|------------------------|----------------|-----------------|-----|-----|-------|-----|-------|-------|
|                        |                | Ni              | Zn  | Pb  | Cu    | Cr  | Cd    | As    |
| $E_r^i < 40$           | Low            | 99.97           | 100 | 100 | 45.33 | 100 | 16.24 | 99.99 |
| $40 \leq E_r^i < 80$   | Lower          | 0.03            | 0   | 0   | 42.29 | 0   | 52.06 | 0.01  |
| $80 \leq E_r^i < 160$  | Median         | 0               | 0   | 0   | 12.37 | 0   | 31.70 | 0     |
| $160 \leq E_r^i < 320$ | High           | 0               | 0   | 0   | 0     | 0   | 0     | 0     |
| $E_r^i \geq 320$       | Extremely high | 0               | 0   | 0   | 0     | 0   | 0     | 0     |

As shown in Table 5, the probability of the HRI values being at a low risk level was 100%, i.e., the total ecological risk level of heavy metal pollutants in the sediments of rivers in Serbia.

**Table 5.** Total ecological risk analysis results of the rivers.

| HRI Value            | Risk Level | Probability (%) |
|----------------------|------------|-----------------|
| $HRI < 150$          | Low        | 100             |
| $150 \leq HRI < 300$ | Lower      | 0               |
| $300 \leq HRI < 600$ | Median     | 0               |
| $HRI \geq 600$       | High       | 0               |

#### 4. Conclusions

Content, spatial distribution, and distribution by fraction, as well as an ecological risk assessment of elements (Cd, Co, Cr, Cu, Fe, Mn, Ni, Pb, V, As, and Zn), were studied in surface sediments from 15 rivers in Serbia. The study demonstrated that the sediments contained significant contents of elements. The maximum content of Cd, Cr, Cu, Ni, Pb, and Zn exceeded the standard values given by Serbian guidelines. Outlier and extreme values of element contents were observed in West Morava (Pb), Ibar (Cd, Zn, Pb, and Ni), the Porečka River (Cu), Pek (Cu, Zn), and South Morava (Mn), suggesting that these were the most critical sites in terms of metal contamination.

Among the studied elements, Cd, Cr, Co, Cu, Fe, Ni, As, and V showed dominant levels in residual fractions of the sediments. Mn, Pb, and Zn were extracted significantly in mobile and second



fractions. This distribution indicated that carbonates and oxide fractions, principally mobile fractions, were the most significant for the binding of these elements. The combined effects of a high content of Cd, Zn, Cu, and Pb and their high mobility potential present an increased possible risk of these metals to the environment.

Since a high percentage of Cr, Co, Cu, V, and As was extracted in the third extraction stage, it is necessary to emphasize the importance of extraction with an oxalate reagent, considering that poorly crystallized Fe oxide represented a significant substrate of the examined elements. Although this step is not included in many sequential extraction procedures (nor in the sequential extraction procedure proposed by the Community Bureau of Reference (BCR) standard procedure), the results obtained in this study suggest the need for the addition of oxalate reagents in SE procedures, especially when it comes to river sediment as substrate. The developed MCS software gave an opportunity for its further improvement in order to describe complex mathematical models of stochastic systems. The goal for the development of our software is to have the ability to follow both the experimental basis and the theoretical modeling developments of risk pollution assessments. In its current state, it is a good tool for risk pollution assessments, and work on improving its modeling is in progress.

**Author Contributions:** Conceptualization, S.S.; software, N.S.; methodology, S.S., N.S., A.P., D.Đ.; investigations, S.S., N.S., A.P., D.Đ.; formal analysis, S.Š.; writing—original draft preparation, S.S., N.S., D.Đ.; writing—review and editing, S.S., N.S., A.P., D.Đ.

**Funding:** This study was supported by the Ministry of Education, Science, and Technological Development of Serbia, Grant No. 172001.

**Acknowledgments:** We would like to thank the Republic Hydrometeorological Service of Serbia for the sediment samples.

**Conflicts of Interest:** The funders had no role in the design of the study; in the collection, analyses, or interpretation of data; in the writing of the manuscript; or in the decision to publish the results.

## References

1. Pérez-Sirvent, C.; García-Lorenzo, M.L.; Hernández-Pérez, C.; Martínez-Sánchez, M.J. Assessment of potentially toxic element contamination in soils from Portman Bay (SE, Spain). *J. Soils Sediments* **2018**, *18*, 2248–2258. [[CrossRef](#)]
2. García-Ordiales, E.; Covelli, S.; Esbrí, J.M.; Loredó, J.; Higuera, P.L. Sequential extraction procedure as a tool to investigate PTHE geochemistry and potential geoavailability of dam sediments (Almadén mining district, Spain). *Catena* **2016**, *147*, 394–403. [[CrossRef](#)]
3. Nemati, K.; Bakar, N.K.A.; Abas, M.R.B.A.; Sobhanzadeh, E.; Low, K.H. Comparison of unmodified and modified BCR sequential extraction schemes for the fractionation of heavy metals in shrimp aquaculture sludge from Selangor, Malaysia. *Environ. Monit. Assess.* **2011**, *176*, 313–320. [[CrossRef](#)] [[PubMed](#)]
4. Peng, J.; Song, Y.; Yuan, P.; Cui, X.; Qiu, G. The remediation of heavy metals contaminated sediment. *J. Hazard. Mater.* **2009**, *161*, 633–640. [[CrossRef](#)] [[PubMed](#)]
5. Sakan, S.; Sakan, N.; Đorđević, D. Trace element study in Tisa River and Danube alluvial sediment in Serbia. *Int. J. Sediment Res.* **2013**, *28*, 234–245. [[CrossRef](#)]
6. Davutoglu, O.I.; Seckin, G.; Ersu, C.B.; Yilmaz, T.; Sari, B. Heavy metal content and distribution in surface sediments of the Seyhan River, Turkey. *J. Environ. Manag.* **2011**, *92*, 2250–2259. [[CrossRef](#)]
7. Liu, G.; Yu, Y.; Hou, J.; Xue, W.; Liu, X.; Liu, Y.; Wang, W.; Alsaedi, A.; Hayat, T.; Liu, Z. An ecological assessment of heavy metal pollution of the agricultural ecosystem near lead-acid battery factory. *Ecol. Indic.* **2014**, *47*, 210–218. [[CrossRef](#)]
8. Chaudhary, S.; Banerjee, D.K.; Kumar, N.; Yadav, S. Assessment of bioavailable metals in the sediments of Yamuna flood plain using two different single extraction procedures. *Sustain. Environ. Res.* **2016**, *26*, 28–32. [[CrossRef](#)]
9. Poznanovic-Spahić, M.; Sakan, S.; Cvetković, Ž.; Tančić, P.; Trifković, J.; Nikić, Z.; Manojlović, D. Assessment of contamination, environmental risk, and origin of heavy metals in soils surrounding industrial facilities in Vojvodina, Serbia. *Environ. Monit. Assess.* **2018**, *190*, 4.
10. Saleem, M.; Iqbal, J.; Akhter, G.; Shah, M.H. Fractionation, bioavailability, contamination and environmental risk of heavy metals in the sediments from a freshwater reservoir, Pakistan. *J. Geochem. Explor.* **2018**, *184*, 199–208. [[CrossRef](#)]



11. Pérez-Cid, B.; Lavilla, I.; Bendicho, C. Application of microwave extraction for partitioning of heavy metals in sewage sludge. *Anal. Chim. Acta* **1999**, *378*, 201–210. [[CrossRef](#)]
12. Relić, D.; Đorđević, D.; Sakan, S.; Anđelković, I.; Pantelić, A.; Stanković, R.; Popović, A. Conventional, microwave, and ultrasound sequential extractions for the fractionation of metals in sediments within the Petrochemical Industry, Serbia. *Environ. Monit. Assess.* **2013**, *185*, 7627–7645. [[CrossRef](#)] [[PubMed](#)]
13. Jamali, M.K.; Kazi, T.G.; Afridi, H.I.; Arain, M.B.; Jalbani, N.; Memon, A.R. Speciation study of heavy metals in untreated domestic wastewater sludge by time saving BCR sequential extraction method. *J. Environ. Sci. Health A* **2007**, *42*, 649–659. [[CrossRef](#)] [[PubMed](#)]
14. Sakan, S.; Dević, G.; Relić, D.; Anđelković, I.; Sakan, N.; Đorđević, D. Risk assessment of trace element contamination in river sediments in Serbia using pollution indices and statistical methods: A pilot study. *Environ. Earth Sci.* **2015**, *73*, 6625–6638. [[CrossRef](#)]
15. Jahan, S.; Strezov, V. Comparison of pollution indices for the assessment of heavy metals in the sediments of seaports of NSW, Australia. *Mar. Pollut. Bull.* **2018**, *128*, 295–306. [[CrossRef](#)]
16. Marković, M.; Zuliani, T.; Belanović Simić, S.; Mataruga, Z.; Kostić, O.; Jarić, S.; Vidmar, J.; Milačić, R.; Ščančar, J.; Mitrović, M.; et al. Potentially toxic elements in the riparian soils of the Sava River. *J. Soils Sediments* **2018**, *18*, 3404–3414. [[CrossRef](#)]
17. Qu, C.; Li, B.; Wu, H.; Wang, S.; Li, F. Probabilistic ecological risk assessment of heavy metals in sediments from China's major aquatic bodies. *Stoch. Environ. Res. Risk Assess.* **2016**, *30*, 271–282. [[CrossRef](#)]
18. Reible, D.D. *Processes, Assessment and Remediation of Contaminated Sediments*; Springer Science + Business Media: New York, NY, USA, 2014; p. 446. ISBN 978-1-4614-6726-7.
19. Komatina, M. *Developments in Earth & Environmental Sciences 2. Medical Geology—Effects of Geological Environments on Human Health*; Elsevier: Amsterdam, The Netherlands, 2004.
20. Petković, S.; Dragović, N.; Marković, S. Erosion and sedimentation problems in Serbia. *Hydrol. Sci. J.* **2009**, *44*, 63–77. [[CrossRef](#)]
21. Sakan, S.; Đorđević, D.; Dević, G.; Relić, D.; Anđelković, I.; Đuričić, J. A study of trace element contamination in river sediments in Serbia using microwave-assisted aqua regia digestion and multivariate statistical analysis. *Microchem. J.* **2011**, *99*, 492–502. [[CrossRef](#)]
22. Håkanson, L. An ecological risk index for aquatic pollution control. A sedimentological approach. *Water Res.* **1980**, *14*, 975–1001. [[CrossRef](#)]
23. Yi, Y.; Yang, Z.; Zhang, S. Ecological risk assessment of heavy metals in sediment and human health risk assessment of heavy metals in fishes in the middle and lower reaches of the Yangtze River basin. *Environ. Pollut.* **2011**, *159*, 2575–2585. [[CrossRef](#)] [[PubMed](#)]
24. Zhao, L.; Mi, D.; Chen, Y.; Wang, L.; Sun, Y. Ecological risk assessment and sources of heavy metals in sediment from Daling River basin. *Environ. Sci. Pollut. Res.* **2015**, *22*, 5975–5984. [[CrossRef](#)] [[PubMed](#)]
25. Qu, L.; Hunag, H.; Xia, F.; Liu, Y.; Dahlgren, R.A.; Yhang, M.; Mei, K. Risk analysis of heavy metal concentration in surface waters across the rural-urban interface of the Wen-Rui Tang River, China. *Environ. Pollut.* **2018**, *237*, 639–649. [[CrossRef](#)] [[PubMed](#)]
26. Kahn, H.; Harris, T.E. Estimation of particle transmission by random sampling. *Natl. Bur. Stand. Appl. Math. Ser.* **1951**, *12*, 27–30.
27. Wu, H.; Li, B.; Qu, C.; Wang, S.; Wan, W.; Zhou, J. A Method for Determining Ecological Risks of Heavy Metal Pollution in River and Lake Sediments. U.S. Patent 20160110835A1, 21 April 2016.
28. Tessier, A.; Campbell, P.G.C.; Bisson, M. Sequential extraction procedure for the speciation of particulate trace metals. *Anal. Chem.* **1979**, *51*, 844–851. [[CrossRef](#)]
29. Official Gazette of the Republic Serbia 23/1994.
30. Vinogradov, A.P. Average Contents of Chemical Elements in the Major Types of Terrestrial Igneous Rocks. *Geokhimiya* **1962**, *7*, 555–571.
31. Mousavi, S.R.; Shahsavari, M.; Rezaei, M. A general overview on manganese (Mn) importance for crops production. *Aust. J. Basic Appl. Sci.* **2011**, *5*, 1799–1803.
32. Milošković, A.; Dojčinović, B.; Kovačević, S.; Radojković, N.; Radenković, M.; Milošević, D.; Simić, V. Spatial monitoring of heavy metals in the inland waters of Serbia: A multispecies approach based on commercial fish. *Environ. Sci. Pollut. Res.* **2016**, *23*, 9918–9933. [[CrossRef](#)]

33. Gustafsson, J.P.; Tin, N.T. Arsenic and selenium in some Vietnamese acid sulphate soils. *Sci. Total Environ.* **1994**, *151*, 1122–1124. [[CrossRef](#)]
34. Noguchi, K.; Nakagawa, R. Arsenic and arsenic-lead sulfides sediments from Tamagawa hot springs, Akita Prefecture. *Proc. Jpn. Acad.* **1969**, *45*, 1969. [[CrossRef](#)]



© 2019 by the authors. Licensee MDPI, Basel, Switzerland. This article is an open access article distributed under the terms and conditions of the Creative Commons Attribution (CC BY) license (<http://creativecommons.org/licenses/by/4.0/>).

## Article

# Evaluation of Element Mobility in River Sediment Using Different Single Extraction Procedures and Assessment of Probabilistic Ecological Risk

Sanja Sakan <sup>1,\*</sup>, Stanislav Frančišković-Bilinski <sup>2,\*</sup>, Dragana Đorđević <sup>1</sup>, Aleksandar Popović <sup>3</sup>,  
Nenad Sakan <sup>4</sup>, Sandra Škrivanj <sup>3</sup> and Halka Bilinski <sup>2</sup>

- <sup>1</sup> Centre of Excellence in Environmental Chemistry and Engineering–ICTM, University of Belgrade, Njegoševa 12, 11158 Belgrade, Serbia; dragadj@chem.bg.ac.rs
- <sup>2</sup> Ruđer Bošković Institute, Division for Marine and Environmental Research, 10000 Zagreb, Croatia; bilinski@irb.hr
- <sup>3</sup> Faculty of Chemistry, University of Belgrade, Studentski trg 12–16, 11000 Belgrade, Serbia; apopovic@chem.bg.ac.rs (A.P.); sandra\_skrivanj@chem.bg.ac.rs (S.Š.)
- <sup>4</sup> Institute of Physics, University of Belgrade, Pregrevica 118, 11080 Zemun, Serbia; nsakan@ipb.ac.rs
- \* Correspondence: ssakan@chem.bg.ac.rs (S.S.); francis@irb.hr (S.F.-B.)

**Abstract:** In this manuscript, samples of Kupa River sediments were examined using three different extraction agents. The aim of this study was to evaluate the applicability of single extraction procedures to investigate the bioavailability and mobility of major and trace elements (Al, As, Ba, Cd, Co, Cr, Cu, Fe, K, Li, Mg, Mn, Na, Ni, P, Pb, S, Si, Sr, Ti, V, and Zn) from river sediment. Two forms of studied elements were evaluated: mobile, the most toxic element form (extraction with 1 M CH<sub>3</sub>COONH<sub>4</sub> and 0.01 M CaCl<sub>2</sub>) and potentially mobilized form (2 M HNO<sub>3</sub> extraction). The estimation of the ecological risk, with the application of the probability distribution of RI (potential ecological risk index) values, is yielded with the help of the Monte Carlo simulation (MCS). Ammonium acetate is proved to be a better extraction agent than calcium chloride. A positive correlation between the content of all extracted elements with nitric acid and the total element content indicates that 2 M HNO<sub>3</sub> efficiently extracts all studied elements. Results showed anthropogenic sources of cadmium and copper and high barium mobility. The MCS suggests that risk of Cr, Cu, Ni, Pb, and Zn was low; As and Cd posed a lower and median ecological risk in the studied areas.

**Keywords:** Kupa River (Croatia); ecological risk; element mobility; probabilistic ecological risk; Monte Carlo simulation



**Citation:** Sakan, S.; Frančišković-Bilinski, S.; Đorđević, D.; Popović, A.; Sakan, N.; Škrivanj, S.; Bilinski, H. Evaluation of Element Mobility in River Sediment Using Different Single Extraction Procedures and Assessment of Probabilistic Ecological Risk. *Water* **2021**, *13*, 1411. <https://doi.org/10.3390/w13101411>

Academic Editor: Laura Bulgariu

Received: 18 March 2021

Accepted: 12 May 2021

Published: 18 May 2021

**Publisher's Note:** MDPI stays neutral with regard to jurisdictional claims in published maps and institutional affiliations.



**Copyright:** © 2021 by the authors. Licensee MDPI, Basel, Switzerland. This article is an open access article distributed under the terms and conditions of the Creative Commons Attribution (CC BY) license (<https://creativecommons.org/licenses/by/4.0/>).

## 1. Introduction

Sediments play an important role in the transport of nutrients, metals, and other contaminants through river systems to the world's oceans and seas [1]. River sediments are reservoirs of materials derived from both anthropogenic and natural weathering processes and have been used as an important tool to assess the health status of aquatic ecosystems and are an integral component for the functioning of ecological integrity [2].

Petrographic, mineralogical, and geochemical composition of watercourse sediment samples, if sampled in an uninhabited area, reflects lithology upstream of the sampling site, if the anthropogenic impact is small or absent. However, if a large lithological diversity is present, it causes difficulties in interpreting the origin of the source material, as a result of the large mixing of eroded material and its downstream transport. Some authors, such as [3], also point out the problem of the opposite effect in cases of long and narrow valleys without tributaries, when samples of watercourse sediments taken along the valley are only replicas of the same material from the same source, without new geochemical information. According to the same authors, active watercourse sediments are recent deposits, originating from a limited number of currently active material sources.

The contamination of sediments is widespread and is a potential threat to the environment in the short and long term [4]. It is widely recognized that the availability of contaminants should be considered in environmental risk and life cycle assessments and regulation [5]. In recent years, increasing attention was drawn to the environmental fate of potentially toxic elements (PTEs). PTEs refer to chemical elements including both metals and non-metals that may potentially cause harmful effects on the organisms in the environment if present in high concentrations [6]. Toxic elements include those elements that act exclusively toxic, such as: cadmium, lead, mercury, arsenic, thallium, uranium, etc. [7]. Some elements in low concentrations are essential minerals for normal growth, development, and functioning of the organism, while at high concentrations they cause a toxic effect.

Mobility and availability depend on the reactivity and on the binding behavior of toxic elements with the components of the matrix, and cannot be assessed only from the values of the total concentrations [8]. In order to assess their distribution between residual and non-residual fractions and their environmental availability i.e., their ability to be available to living organisms in case of changes in environmental parameters, many authors use chemical extractions [9]. Extraction is one of the most common methods for isolating chemical elements and compounds. Different extraction agents are recommended for isolation of major and trace elements from soils and sediments, and they have purpose to simulate natural processes, such as acidification or oxidation. Single and sequential extractions are current and useful tools for estimating the availability of metals in soils and sediments [9]. Although the sequential extraction procedure proposed by the European Standard, Measurements and Testing (SM&T) program, formerly the Community Bureau of Reference (BCR) sequential extraction method is standardized, it is not enough to solve all problems and doubts about metals' availability just by applying this method. In the manuscript [9] is described why it is important to apply different extraction methods (single and sequential), as well as why a comparison between different chemical procedures is necessary to assess the metals' availability in sediments better. Single extractions may be used for estimating the potentially most mobile element fraction [8]. These extractions offer possibilities to perform a fast screening of the mobilizable pool of elements in sediments. Obtained element concentrations represent bioavailable fraction which is strongly correlated with their leaching potential from soil and sediments [10]. The biggest advantage of these extractions is that the results are obtained quickly, and that they are simple, practical, and cost-effective. Additionally, they also offer possibilities to perform a fast screening of the mobilizable pool of elements in soils and sediments [10]. In manuscript [11],  $\text{CaCl}_2$  is recommended as suitable single extractions for obtaining the concentrations of Cu and S which could originate from the same source. As a general conclusion, in [12] is shown that the 0.01 M  $\text{CaCl}_2$  extraction procedure seems to be a suitable method for the determination of Cd, Cu, Pb, and Zn mobility in soils, since this procedure presents an appropriate extraction capacity for this type of studies and also uses the lowest salt concentration. Dilute strong acids are often used to estimate the mobile fractions of soils and sediments [9].

Ecological risk assessment is performed to evaluate the likelihood that adverse ecological effects may occur or are occurring as a result of exposure to one or more stressors [13]. The potential ecological risk of PTEs can be determined using several methods [14]. In recent years, a new method called probabilistic risk assessment is described for ecological risk assessment [13]. The EPA (Environmental Protection Agency) and the National Academy of Sciences recognized Monte Carlo methods of quantifying variability and uncertainty in risk assessments [15]. The Monte Carlo simulation is used in a variety of physical and chemistry problems. As such, it is also widely used as a computational method for generating probability distributions of variables that depend on other variables or parameters represented as probability distributions [15].

Research in this manuscript was performed on sediment samples from the Kupa River, Croatia and its tributaries, which is a unique river system, serving as an ideal "natural laboratory" for studying different chemical processes in rivers. Since an extreme barium

anomaly in sediments in the Kupica and Kupa rivers was discovered during work on the Ph.D. thesis of Frančišković-Bilinski and was published in 2006 [16], it is very important to examine the mobility of barium and other trace elements in more detail. Several studies investigated the contamination of the Kupa River [16–19], but in the current manuscript, it is the first time the use of different types of extractions as a tool to assess the potential element availability in river sediments was evaluated. A single extraction method was carried out to determine mobility and bioavailability of elements from sediments and, for this reason, different single extraction procedures were evaluated. The extraction was performed using three extraction agents: calcium chloride (0.01 M  $\text{CaCl}_2$ ), ammonium acetate (1 M  $\text{CH}_3\text{COONH}_4$ ), and nitric acid (2 M  $\text{HNO}_3$ ). Obtained results were compared with total element content, after BCR sequential extraction. In addition, for the first time, evaluation of probabilistic ecological risk of PTEs in these river sediments was computed using a Monte Carlo simulation.

## 2. Materials and Methods

### 2.1. Study Area

The Kupa River basin occupies the west-central part of Croatia and is shared by two neighboring countries (Slovenia, Bosnia and Herzegovina). Details about the Kupa River can be found in [18], who investigated and described for the first time its geomorphology, tectonic setting, lithological framework, granulometric properties, and pollution status of this transboundary river basin. The Kupa itself is a tributary to the Sava River and meets the latter at Sisak after traversing a distance of 294 km. The Sava River belongs to the Danube River watershed and enters the Danube River at Belgrade (Serbia). The Kupa River drainage basin is situated at the very south of the Danube drainage basin.

The map of Croatia, with a rectangle indicating the position of the Kupa drainage basin, the course of the Kupa River, and its catchment area showing sediment sampling locations are presented in Figure 1. The total area of 10,605 km<sup>2</sup> of the Kupa River drainage basin is divisible into several sub-basins as per its countrywide distributions: 79.32% belongs to Croatia, 18.32% to Slovenia, and 2.36% to Bosnia and Herzegovina. The river basin is one of the most significant water resources in Croatia. Although shared by other adjoining countries, about 85% of the river water, being chiefly derived from carbonate karst springs, river springs, precipitation, and run off, discharges on the Croatian side. The karst aquifers of the Dinarides are highly vulnerable because of the rapid water exchange with the groundwater through numerous shallow holes. The availability of about 3.5 m<sup>3</sup>/s of very good quality spring water has given a strategic importance to the area based on the fact that the whole Adriatic coast and numerous settlements in the continental area have come into existence [20].

### 2.2. Sampling and Sample Preparation

Positions of sampling locations are presented in Figure 1 and in Table 1. Two locations (IŠ and 51) are on the Kupica River; one location (52) is on the Kupa River upstream Kupica inflow, while all other locations are in Kupa River downstream from the Kupica River inflow. Sample DN-2 is taken from the upper flow of Dobra River between villages Gornja and Donja Dobra. This location is located very close to the Brod na Kupi and Čedan locations on the Kupica and Kupa rivers (5–7 km air distance), but it does not have any direct connections with those locations. Therefore, despite its relative vicinity to sampling locations IŠ, 51, 52, ČD, and 50 and similar geological composition of surrounding areas, on sampling point DN-2, there is no influence of waste from the abundant barite mine in Homer.

Locations where fine-grained sediment accumulates along the river bank were chosen. On each sampling site, at least three grab samples of active fine-grained surface sediment (0–5 cm deep) were collected from different places in an area of 5 m<sup>2</sup>. From this material, a composite sample was taken weighing up to 1.5 kg. This procedure decreased the possible bias caused by local variability.



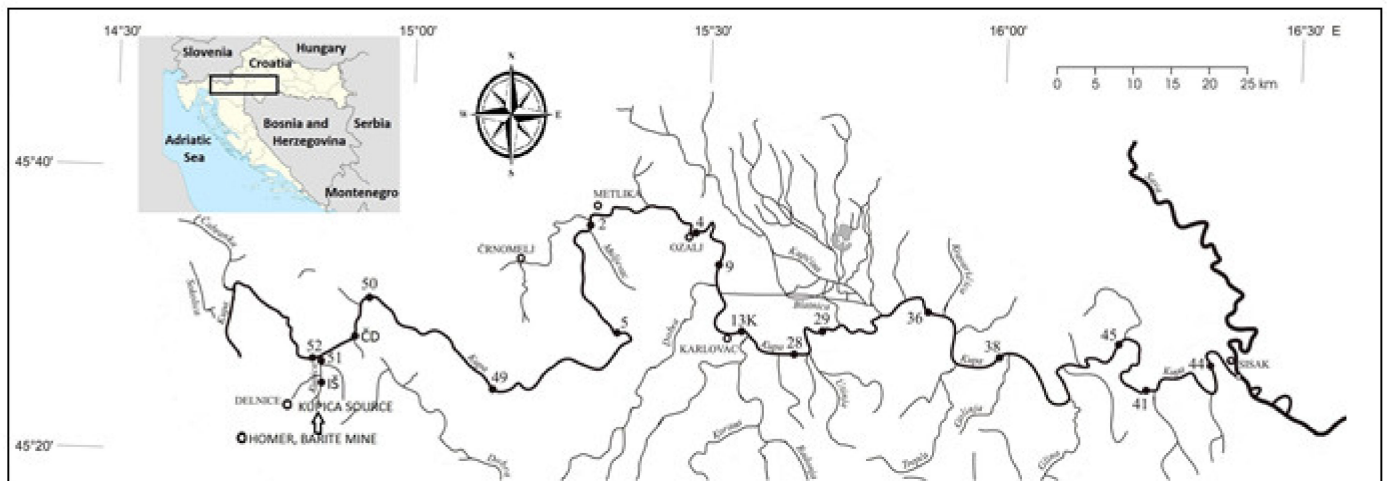


Figure 1. Sampling locations.

Table 1. Sampling locations.

| Number | Label | Fraction ( $\mu\text{m}$ ) | Clarification of the Locality   |
|--------|-------|----------------------------|---|
| 1      | DN-2  | <63                        | Dobra River, upper course, only about 5 km downstream from the source, between the villages of Gornja and Donja Dobra   |
| 2      | IŠ    | <63                        | the river Kupica, approximately 1.5 km upstream from its confluence with the Kupa   |
| 3      | K-4   | <63                        | Kupa River in Ozalj, right bank, just below the dam of the Ozalj hydroelectric power plant  |
| 4      | K-2   | <63                        | Kupa River in Jurovo, right bank, about 250 m upstream from the mouth of the river Lahinja  |
| 5      | 38    | <63                        | Kupa River in the settlement Sunčani brijeg, about 500 m downstream, left bank  |
| 6      | ČD    | <63                        | Kupa River, right bank, the village of Čedan, located approximately 5 km downstream from Brod na Kupu   |
| 7      | 44    | <63                        | Kupa River, Sisak, right bank, about 2 km before the confluence of the Odra and Kupa  |
| 8      | 51    | <63                        | Kupica River in Brod na Kupu, just before the confluence with the Kupa River  |
| 9      | IŠ    | 63–2000                    | Kupica River, approximately 1.5 km upstream from its confluence with the Kupa River   |
| 10     | 44    | 63–2000                    | Kupa River, Sisak, Zibel beach, right bank, about 2 km before the confluence of the Odra and Kupa   |
| 11     | 45    | 63–2000                    | Kupa River, Letovanić, left bank  |
| 12     | K-2   | 63–2000                    | Kupa River in Jurovo, right bank, about 250 m upstream from Lahinja River inflow  |
| 13     | 51    | 63–2000                    | Kupica River in Brod na Kupu, just before the confluence with the Kupa River  |
| 14     | K-5   | 63–2000                    | Kupa River, Jakovci Netretički, in the part where Kupa passes from its upper to middle course, was sampled from the right bank near the waterfall below the village |
| 15     | K-9   | 63–2000                    | Kupa River, between the villages of Levkušje and Zorkovac, right bank, about 3.5 km upstream from the Dobra River inflow  |
| 16     | 38    | 63–2000                    | Kupa River in the settlement Sunčani breg, about 500 m downstream, left bank  |
| 17     | 52    | 63–2000                    | Kupa River in Brod na Kupu, right bank, sample taken about 100 m upstream from the mouth of the Kupica River  |
| 18     | ČD    | 63–2000                    | Kupa River, right bank, the village of Čedan, located approximately 5 km downstream from Brod na Kupu   |
| 19     | 28    | 63–2000                    | Kupa River, Donja Rečica, left bank, on the location right across from Brođani  |
| 20     | 41    | 63–2000                    | Kupa River, Petrinja, town beach, 800 m downstream from the bridge on the main road from Petrinja to Zagreb, right bank   |
| 21     | 49    | 63–2000                    | Kupa River, the upper course of the Kupa in Gorski Kotar, about 1 km upstream from the village of Severin na Kupu   |
| 22     | 29    | 63–2000                    | Kupa River, Zamršlje, about 7 km downstream from point 28   |
| 23     | 36    | 63–2000                    | Kupa River, Lijevo Sredičko, left bank, lower course, 12 km upstream from Pokupsko  |
| 24     | K-4   | 63–2000                    | Kupa River in Ozalj, right bank, just below the dam of the Ozalj hydroelectric power plant  |
| 25     | DN-2  | 63–2000                    | Dobra River, upper course, only about 5 km downstream from the source, between the villages of Gornja and Donja Dobra   |

After sampling, the sediments were dried in air at room temperature and then sieved through 2000  $\mu\text{m}$  and 63  $\mu\text{m}$  sieves (Fritsch, Weimar, Germany) to obtain two sediment fractions: fine fraction containing clay and silt ( $<63 \mu\text{m}$ ) and coarser fraction containing sand (63–2000  $\mu\text{m}$ ). Obtained sediment fractions were used for further analysis.

### 2.3. Sample Extractions and Measurement Using ICP-OES

Sediment samples were crushed and homogenized and after measuring certain sample masses, extracted with three extraction agents: 0.01 M  $\text{CaCl}_2$ , 1 M  $\text{CH}_3\text{COONH}_4$ , and 2 M  $\text{HNO}_3$ .

**Calcium chloride extractable** About 2 g of the sediment sample was weighed into a 50 mL centrifuge tube, and 20 mL 0.01 M  $\text{CaCl}_2$  was added. The solution thus prepared was shaken for 3 h on a rotary shaker (Heidolph) [21–23].

**Ammonium acetate extractable** About 1 g of the soil sample was weighed into a 50 mL centrifuge tube, and 40 mL of 1 M  $\text{CH}_3\text{COONH}_4$  was added into each sediment sample. The solution thus prepared was shaken for 2 h on a rotary shaker (Heidolph) [23].

**Extraction with  $\text{HNO}_3$**  About 2 g of sediment sample was weighed into a centrifuge tube. A 20 mL of 2 M  $\text{HNO}_3$  was added into each sediment sample. The solution thus prepared was shaken for 1 h on a rotary shaker (Heidolph) at room temperature [24,25].

After the extraction process, all samples were centrifuged at 3000 rpm for 10 min. The supernatant was filtered, and the filtrate was filled up to 50 mL with 1 M  $\text{HNO}_3$  and stored in a polyethylene bottle at 4 °C until needed for analysis.

The total amounts of elements in this manuscript are defined as the sum of extracted elements in the four binding fractions (BCR extractions). A detailed description of this method is shown in [19].

### 2.4. Measurement Using ICP-OES

The content of elements in the extracts was determined using ICP-OES (inductively coupled plasma optical emission spectrometer) devices (iCAP-6500Duo, ThermoScientific, Paisley, UK). The detector was a RACID86 Charge injector device (CID). This instrument operates sequentially with both radial and axial torch configurations. The analytical performance of the iCAP 6000 Series is demonstrated by its improved detection limits, enhanced linearity, superior long-term stability, and high-resolution images [20].

### 2.5. Pollution Risk Assessment and Monte Carlo Simulation

As it could be seen from Qu et al. [26] and Wu et al. [27], the Monte Carlo method is very applicable in PTEs' pollution risk assessment. Based on their work, we developed our software, which is written in Qt, and a proven pseudo random number generator produces a normal distribution with long-term repeatability. The program used was tested on several models, and as a final test, a reproduction of the results from Qu et al. [26] and Wu et al. [27] was conducted in its entirety, based on the input data, and calculated with the help of our software. The first time our software was applied occurred in Sakan et al. 2020 [19].

In the presented research, instead of Håkanson's RI, the probabilistic distribution of RI was calculated using the Monte Carlo simulation. The potential ecological risk index (RI) in sediments can be calculated using the following equation [28,29]:  $RI = \sum E_r^i$ , where  $E_r^i = T_r^i C^i f$ ,  $T_r^i$  is the toxic-response factor for a given substance (for Hg, Cd, As, Cr, and Zn, they are 40, 30, 10, 2, and 1, respectively; and five for Pb, Cu, and Ni) [29,30], and  $C^i f$  is the contamination factor [28].  $E_r^i$  is the potential ecological risk for single factor, and RI is calculated as the sum of all risk factors for heavy metals in sediments.

### 2.6. Determination of Magnetic Susceptibility

Magnetic susceptibility was measured using SM30, a small magnetic susceptibility meter, which can assess the high sensitivity measure sediments and rocks with an extremely low level of magnetic susceptibility and, in addition, can distinctly measure diamagnetic materials such as limestone, quartz, and also water. Sensitivity of SM30 is  $1 \times 10^{-7}$  SI units,



what is about ten times better than the sensitivity of most of the competitive instruments. The operating frequency is 8 kHz, measurement time less than 5 s, and operating temperature  $-20\text{ }^{\circ}\text{C}$  to  $50\text{ }^{\circ}\text{C}$ . The SM30 has an 8 kHz LC (inductor-capacitor) oscillator with a large-size pick-up coil as a sensor. The oscillation frequency is measured when the coil is put to the surface of the measured sample and when the coil is removed tens of cm away. Each sample was measured three times, and the mean value was taken as final result of measurement to assure as precise data as possible.

### 3. Results and Discussion

#### 3.1. Quality Control and Assurance

To check the quality of the element analyses, the certified reference material BCR 483 (Sewage Sludge Amended Soil) was analyzed for extraction with  $\text{CaCl}_2$ . In Table 2 is shown results of comparisons of the obtained calcium chloride extractable content and indicative values for BCR 483. The recoveries for Cd, Cr, Cu, Ni, Pb, and Zn were between 97.6 and 117.1%.

**Table 2.** Comparison of calcium chloride extractable element content-obtained and indicative values of BCR-483 certified reference material.

|            | Cd              | Cr              | Cu            | Ni            | Pb               | Zn            |
|------------|-----------------|-----------------|---------------|---------------|------------------|---------------|
| Obtained   | $0.48 \pm 0.03$ | $0.41 \pm 0.06$ | $1.4 \pm 0.1$ | $1.6 \pm 0.1$ | BDL <sup>1</sup> | $8.1 \pm 0.5$ |
| Indicative | $0.45 \pm 0.05$ | $0.35 \pm 0.09$ | $1.2 \pm 0.4$ | $1.4 \pm 0.2$ | <0.06            | $8.3 \pm 0.7$ |
| Recovery   | 106.7%          | 117.1%          | 116.7%        | 114.3%        | /                | 97.6%         |

<sup>1</sup> Below detection limit by ICP OES.

#### 3.2. Discussion about Extracted Elements Contents by Different Extraction Agents

The extraction was performed using three extraction agents: calcium chloride (0.01 M  $\text{CaCl}_2$ ), ammonium acetate (1 M  $\text{CH}_3\text{COONH}_4$ ), and nitric acid (2 M  $\text{HNO}_3$ ).  $\text{CaCl}_2$  and  $\text{CH}_3\text{COONH}_4$  are classified in groups of unbuffered salts, called “soft” or “mild” extractants. Obtained results are presented in Tables 3 and 4 and Figures 2 and 3. The relationship between the contents of the elements extracted by different extraction agents is also considered, and the relationship between the extracted contents is shown as a percentage (Supplementary Material, Tables S1–S3). Ratios were calculated only in samples in which element content is greater than the detection limits. From the calculated concentration ratios, it can be concluded which extraction agent is more efficient for the extraction of a certain element, depending on whether the obtained value is less than or greater than one, or calculated as a percentage less than or greater than 100.

Nitric acid extraction in comparison with  $\text{CaCl}_2$  extraction gave better results during the extraction of the following elements: Al, As, Ba, Cd, Co, Cr, Cu, Fe, K, Mg, Mn, Na, Ni, P, S, Si, Sr, Ti, V, and Zn, where the observed relationship is noticeable for the elements: Al, Ba, Cu, K, Mg, Mn, Na, S, and Si. This result may indicate that Al, Ba, Cu, K, Mg, Mn, Na, S, and Si do not have high mobility in the examined sediments. During the extraction of beryllium, lithium, and lead, values below the detection limit in all samples were obtained, so these ratios could not be calculated. It is possible to conclude that nitric acid is a more efficient extraction agent in relation to calcium chloride. These results are expected given that the extract after extraction with  $\text{HNO}_3$  contains elements bounded to sulphide and phosphates (released forms) and represents maximum contents of potentially available fraction. The low content of elements extracted using  $\text{CaCl}_2$  indicates that studied elements in the examined river sediments do not have high mobility, since this solution simulates the natural soil solution, and element contents approximately correspond to their water soluble and exchangeable contents [30].

**Table 3.** Statistical analysis of elements' contents (Al, As, Ba, Be, Ca, Cd, Co, Cr, Cu, Fe, K, and Li).

| [mg kg <sup>-1</sup> ] | CaC <sup>1</sup>  | Fraction: <63 µm |        |        | BCR   | Fraction: 63–2000 µm |        |        |
|------------------------|-------------------|------------------|--------|--------|-------|----------------------|--------|--------|
|                        |                   | AA               | NA     | CaC    |       | AA                   | NA     | BCR    |
|                        |                   | <b>Al</b>        |        |        |       | <b>Al</b>            |        |        |
| <b>Mean</b>            | 0.092             | 1.60             | 914    | 9836   | 0.140 | 0.80                 | 255    | 3791   |
| <b>Max</b>             | 0.144             | 6.55             | 1200   | 11,865 | 0.772 | 3.95                 | 418    | 7659   |
| <b>Min</b>             | 0.023             | 0.35             | 522    | 6252   | 0.005 | 0.21                 | 119    | 1206   |
|                        |                   | <b>As</b>        |        |        |       | <b>As</b>            |        |        |
| <b>Mean</b>            | <BDL <sup>2</sup> | <BDL             | 0.969  | 6.40   | <BDL  | <BDL                 | 0.335  | 3.93   |
| <b>Max</b>             | <BDL              | <BDL             | 1.740  | 10.70  | 0.004 | <BDL                 | 0.734  | 9.60   |
| <b>Min</b>             | <BDL              | <BDL             | 0.568  | 2.64   | <BDL  | <BDL                 | 0.171  | 1.92   |
|                        |                   | <b>Ba</b>        |        |        |       | <b>Ba</b>            |        |        |
| <b>Mean</b>            | 0.733             | 91.59            | 74.13  | 447.1  | 0.390 | 22.39                | 16.90  | 46.7   |
| <b>Max</b>             | 1.430             | 143.00           | 137.43 | 1347.0 | 0.833 | 47.30                | 39.15  | 210.0  |
| <b>Min</b>             | 0.270             | 37.40            | 31.41  | 63.9   | 0.125 | 7.89                 | 4.44   | 9.8    |
|                        |                   | <b>Be</b>        |        |        |       | <b>Be</b>            |        |        |
| <b>Mean</b>            | <BDL              | <BDL             | 0.315  | 0.89   | <BDL  | <BDL                 | 0.107  | 0.37   |
| <b>Max</b>             | <BDL              | 0.002            | 0.433  | 1.11   | <BDL  | 0.004                | 0.202  | 0.82   |
| <b>Min</b>             | <BDL              | <BDL             | 0.189  | 0.56   | <BDL  | <BDL                 | 0.053  | 0.13   |
|                        |                   | <b>Ca</b>        |        |        |       | <b>Ca</b>            |        |        |
| <b>Mean</b>            | /                 | 10,457           | 38,110 | 39,469 | /     | 7498                 | 33,834 | 37,257 |
| <b>Max</b>             | /                 | 13,628           | 76,460 | 78,479 | /     | 12,313               | 64,672 | 86,503 |
| <b>Min</b>             | /                 | 3686             | 11,498 | 12,026 | /     | 1074                 | 7019   | 8604   |
|                        |                   | <b>Cd</b>        |        |        |       | <b>Cd</b>            |        |        |
| <b>Mean</b>            | <BDL              | 0.063            | 0.213  | 0.43   | <BDL  | 0.017                | 0.073  | 0.19   |
| <b>Max</b>             | 0.001             | 0.118            | 0.310  | 0.59   | 0.001 | 0.048                | 0.163  | 0.35   |
| <b>Min</b>             | <BDL              | 0.042            | 0.139  | 0.26   | <BDL  | <BDL                 | 0.041  | 0.10   |
|                        |                   | <b>Co</b>        |        |        |       | <b>Co</b>            |        |        |
| <b>Mean</b>            | 0.001             | 0.018            | 3.75   | 9.47   | 0.002 | 0.006                | 1.36   | 4.33   |
| <b>Max</b>             | 0.003             | 0.033            | 5.00   | 12.70  | 0.017 | 0.016                | 2.98   | 8.21   |
| <b>Min</b>             | <BDL              | 0.011            | 2.08   | 5.52   | <BDL  | <BDL                 | 0.72   | 2.28   |
|                        |                   | <b>Cr</b>        |        |        |       | <b>Cr</b>            |        |        |
| <b>Mean</b>            | <BDL              | <BDL             | 4.58   | 25.70  | <BDL  | <BDL                 | 1.84   | 10.32  |
| <b>Max</b>             | 0.001             | <BDL             | 27.00  | 65.50  | 0.002 | <BDL                 | 14.61  | 29.30  |
| <b>Min</b>             | <BDL              | <BDL             | 0.71   | 12.40  | <BDL  | <BDL                 | 0.01   | 4.12   |
|                        |                   | <b>Cu</b>        |        |        |       | <b>Cu</b>            |        |        |
| <b>Mean</b>            | 0.011             | 0.466            | 17.1   | 18.5   | 0.005 | 0.360                | 12.6   | 8.1    |
| <b>Max</b>             | 0.015             | 0.552            | 28.3   | 26.2   | 0.011 | 1.420                | 22.9   | 14.9   |
| <b>Min</b>             | 0.006             | 0.347            | 10.1   | 10.2   | <BDL  | 0.188                | 3.6    | 2.9    |
|                        |                   | <b>Fe</b>        |        |        |       | <b>Fe</b>            |        |        |
| <b>Mean</b>            | 0.190             | 2.16             | 2903   | 27,903 | 0.275 | 1.13                 | 1267   | 15,019 |
| <b>Max</b>             | 0.307             | 5.99             | 4208   | 39,145 | 1.090 | 3.41                 | 2082   | 34,941 |
| <b>Min</b>             | 0.067             | <BDL             | 2091   | 20,314 | 0.040 | <BDL                 | 681    | 4092   |
|                        |                   | <b>K</b>         |        |        |       | <b>K</b>             |        |        |
| <b>Mean</b>            | 2.25              | 78.8             | 122.2  | 723.5  | 0.76  | 21.3                 | 44.8   | 269.0  |
| <b>Max</b>             | 2.61              | 105.0            | 152.3  | 930.0  | 1.87  | 55.7                 | 70.3   | 510.0  |
| <b>Min</b>             | 1.66              | 65.2             | 88.1   | 482.0  | 0.27  | 9.6                  | 14.8   | 77.9   |
|                        |                   | <b>Li</b>        |        |        |       | <b>Li</b>            |        |        |
| <b>Mean</b>            | <BDL              | 0.070            | 5.70   | 25.01  | <BDL  | 0.027                | 4.91   | 14.27  |
| <b>Max</b>             | <BDL              | 0.094            | 10.42  | 29.40  | <BDL  | 0.039                | 8.50   | 25.50  |
| <b>Min</b>             | <BDL              | 0.041            | 2.47   | 18.00  | <BDL  | 0.017                | 1.37   | 3.93   |

<sup>1</sup> CaC—calcium chloride; AA—ammonium acetate; NA—nitric acid; BCR—total element content; <sup>2</sup> BDL—below detection limit.

**Table 4.** Statistical analysis of elements' contents (Mg, Mn, Na, Ni, P, Pb, S, Si, Sr, Ti, V, and Zn).

| [mg kg <sup>-1</sup> ] | CaC <sup>1</sup> | Fraction: <63 µm |        |        | Fraction: 63–2000 µm |        |        |        |
|------------------------|------------------|------------------|--------|--------|----------------------|--------|--------|--------|
|                        |                  | AA               | NA     | BCR    | CaC                  | AA     | NA     | BCR    |
|                        |                  | <b>Mg</b>        |        |        | <b>Mg</b>            |        |        |        |
| <b>Mean</b>            | 37.0             | 503              | 6468   | 9072   | 20.2                 | 178    | 10,233 | 10,578 |
| <b>Max</b>             | 73.8             | 891              | 10,152 | 11,502 | 56.5                 | 355    | 23,943 | 27,520 |
| <b>Min</b>             | 17.6             | 339              | 3240   | 4949   | 4.7                  | 74     | 1123   | 1455   |
|                        |                  | <b>Mn</b>        |        |        | <b>Mn</b>            |        |        |        |
| <b>Mean</b>            | 0.68             | 24.6             | 231    | 457    | 0.85                 | 11.1   | 101    | 286    |
| <b>Max</b>             | 1.23             | 54.2             | 423    | 881    | 2.72                 | 22.0   | 321    | 946    |
| <b>Min</b>             | 0.08             | 10.9             | 69     | 164    | 0.12                 | 3.0    | 30     | 83     |
|                        |                  | <b>Na</b>        |        |        | <b>Na</b>            |        |        |        |
| <b>Mean</b>            | 2.87             | 48.8             | 45.4   | 105.5  | 0.66                 | 16.7   | 20.6   | 48.5   |
| <b>Max</b>             | 5.64             | 87.7             | 73.5   | 159.0  | 1.16                 | 26.0   | 34.4   | 69.6   |
| <b>Min</b>             | 1.48             | 29.8             | 31.1   | 64.0   | 0.43                 | 10.9   | 8.9    | 18.6   |
|                        |                  | <b>Ni</b>        |        |        | <b>Ni</b>            |        |        |        |
| <b>Mean</b>            | 0.004            | 0.222            | 4.30   | 23.29  | 0.007                | 0.082  | 1.32   | 9.47   |
| <b>Max</b>             | 0.010            | 0.330            | 6.00   | 31.50  | 0.035                | 0.125  | 2.33   | 18.00  |
| <b>Min</b>             | 0.002            | 0.141            | 1.93   | 13.40  | 0.000                | 0.042  | 0.59   | 4.11   |
|                        |                  | <b>P</b>         |        |        | <b>P</b>             |        |        |        |
| <b>Mean</b>            | 0.081            | 6.64             | 216.2  | 5817   | 0.031                | 2.12   | 88.8   | 2877   |
| <b>Max</b>             | 0.137            | 13.00            | 260.8  | 6999   | 0.147                | 9.86   | 154.5  | 4635   |
| <b>Min</b>             | 0.015            | 0.00             | 180.0  | 4414   | <BDL <sup>2</sup>    | 0.00   | 45.4   | 1058   |
|                        |                  | <b>Pb</b>        |        |        | <b>Pb</b>            |        |        |        |
| <b>Mean</b>            | <BDL             | <BDL             | 11.45  | 22.78  | <BDL                 | <BDL   | 3.26   | 8.21   |
| <b>Max</b>             | <BDL             | <BDL             | 15.65  | 31.80  | <BDL                 | <BDL   | 5.42   | 20.80  |
| <b>Min</b>             | <BDL             | <BDL             | 5.47   | 10.60  | <BDL                 | <BDL   | 1.57   | 2.89   |
|                        |                  | <b>S</b>         |        |        | <b>S</b>             |        |        |        |
| <b>Mean</b>            | 8.08             | 100.51           | 95.9   | 364    | 3.02                 | 34.82  | 28.0   | 123    |
| <b>Max</b>             | 18.40            | 230.00           | 187.8  | 600    | 15.60                | 163.00 | 112.5  | 656    |
| <b>Min</b>             | 3.26             | 41.70            | 32.8   | 158    | 0.36                 | 6.21   | 5.2    | 35     |
|                        |                  | <b>Si</b>        |        |        | <b>Si</b>            |        |        |        |
| <b>Mean</b>            | 6.24             | 101.1            | 730    | 1585   | 2.11                 | 17.7   | 245    | 739    |
| <b>Max</b>             | 7.93             | 165.0            | 874    | 2115   | 4.32                 | 57.9   | 458    | 1531   |
| <b>Min</b>             | 4.43             | 54.3             | 566    | 1111   | 1.00                 | 5.6    | 128    | 393    |
|                        |                  | <b>Sr</b>        |        |        | <b>Sr</b>            |        |        |        |
| <b>Mean</b>            | 0.104            | 9.27             | 16.40  | 24.59  | 0.008                | 5.12   | 10.94  | 14.16  |
| <b>Max</b>             | 0.253            | 14.40            | 27.15  | 37.20  | 0.073                | 10.20  | 18.49  | 31.80  |
| <b>Min</b>             | 0.011            | 4.87             | 6.59   | 10.10  | <BDL                 | 1.29   | 2.81   | 4.35   |
|                        |                  | <b>Ti</b>        |        |        | <b>Ti</b>            |        |        |        |
| <b>Mean</b>            | <BDL             | <BDL             | 5.06   | 76.06  | 0.004                | 0.013  | 2.89   | 53.85  |
| <b>Max</b>             | 0.001            | 0.003            | 7.87   | 104.00 | 0.053                | 0.229  | 8.36   | 100.00 |
| <b>Min</b>             | <BDL             | <BDL             | 3.42   | 49.30  | <BDL                 | <BDL   | 0.82   | 27.40  |
|                        |                  | <b>V</b>         |        |        | <b>V</b>             |        |        |        |
| <b>Mean</b>            | 0.001            | 0.041            | 2.13   | 19.21  | <BDL                 | 0.024  | 0.83   | 8.84   |
| <b>Max</b>             | 0.003            | 0.104            | 3.13   | 25.00  | 0.002                | 0.073  | 1.51   | 14.60  |
| <b>Min</b>             | <BDL             | 0.018            | 1.20   | 11.90  | <BDL                 | 0.003  | 0.48   | 4.91   |
|                        |                  | <b>Zn</b>        |        |        | <b>Zn</b>            |        |        |        |
| <b>Mean</b>            | 0.002            | 0.557            | 19.08  | 60.96  | 0.007                | 0.358  | 6.68   | 26.65  |
| <b>Max</b>             | 0.008            | 0.904            | 28.07  | 85.35  | 0.091                | 1.000  | 12.86  | 56.26  |
| <b>Min</b>             | <BDL             | 0.238            | 13.02  | 37.49  | <BDL                 | 0.054  | 3.26   | 8.52   |

<sup>1</sup> CaC—calcium chloride; AA—ammonium acetate; NA—nitric acid; BCR—total element content; <sup>2</sup> BDL—below detection limit.

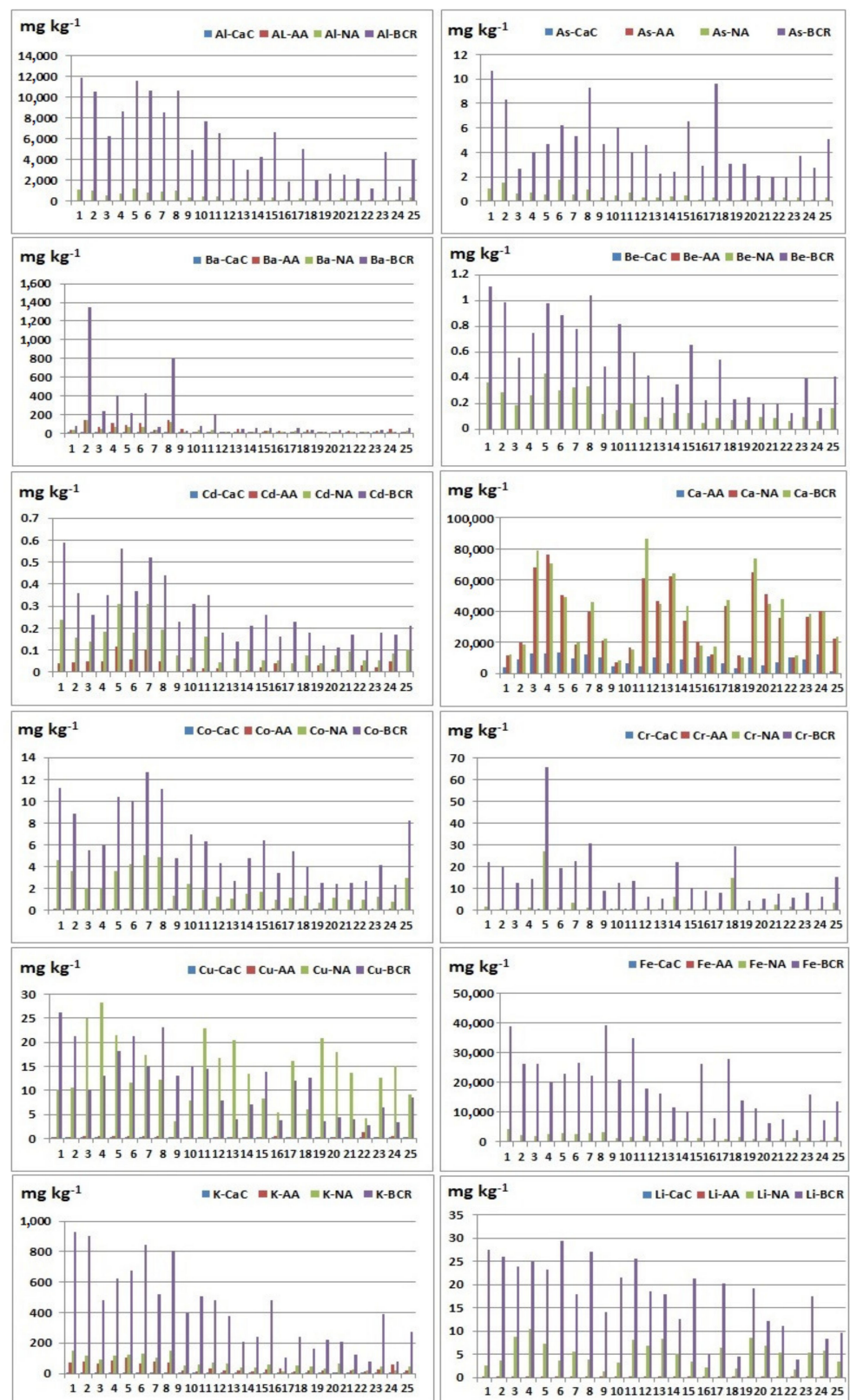


**Figure 2.** Extracted element contents (Al, As, Ba, Be, Cd, Ca, Co, Cr, Cu, Fe, K, and Li) using different reagents: CaC—calcium chloride; AA—ammonium acetate; NA—nitric acid; BCR—total element content (extracted element using BCR extraction procedure).

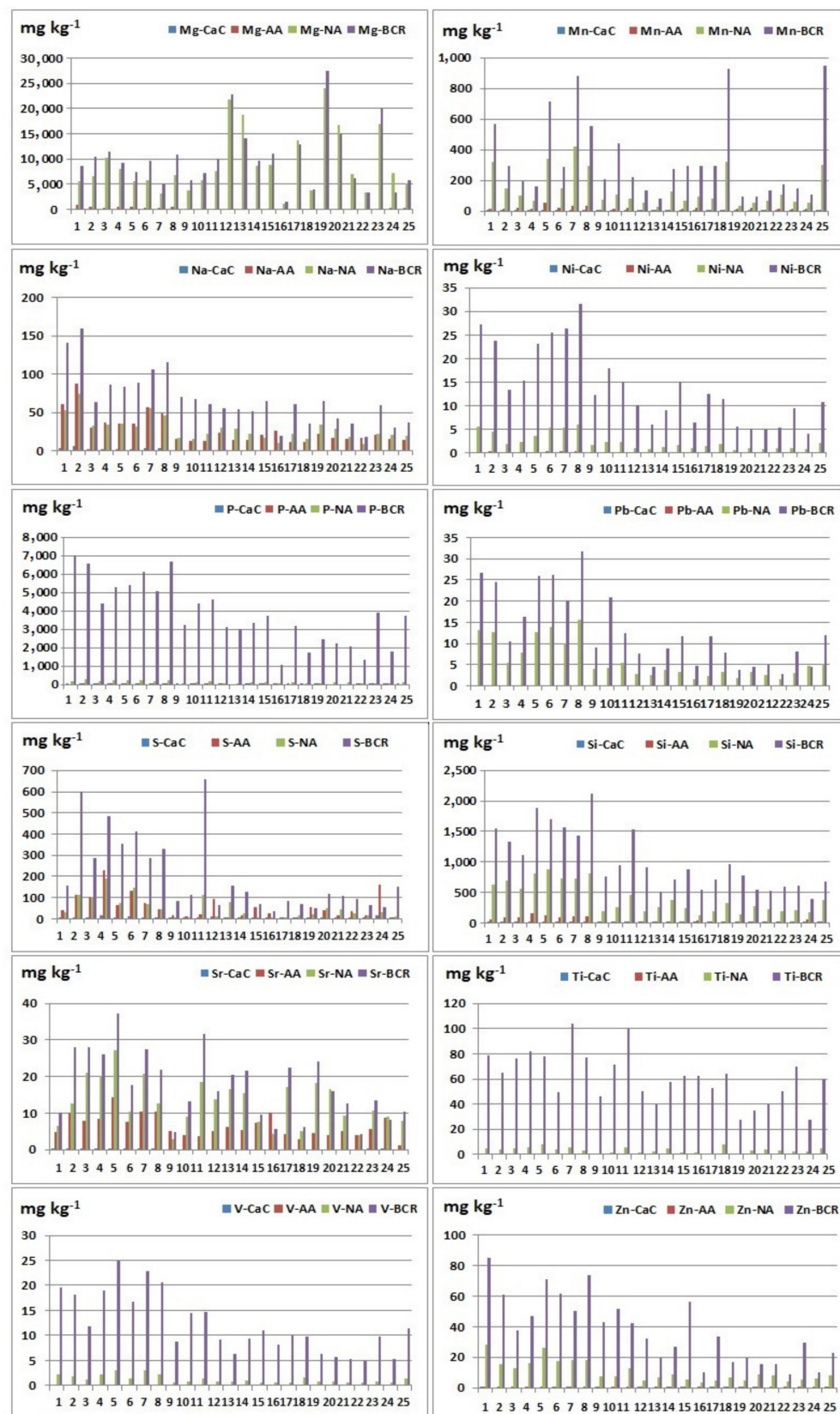


Figure 3. Extracted element contents (Mg, Mn, Na, Ni, P, Pb, S, Si, Sr, Ti, V, and Zn) using different reagents: *CaC*—calcium chloride; *AA*—ammonium acetate; *NA*—nitric acid; *BCR*—total element content (extracted element using BCR extraction procedure).



Nitric acid extraction in comparison with  $\text{CH}_3\text{COONH}_4$  gave better results when extracting the following elements: Al, Be, Ca, Cd, Co, Cu, Fe, K, Li, Mg, Mn, Ni, P, S, Sb, Si, Sr, Ti, V, and Zn, where the observed ratio is noticeable for the elements: Al, Co, Cu, Fe, Li, Mg, Mn, P, Ni, Si, V, and Zn (Table S2). During the extraction of arsenic, chromium, and lead, values below the detection limit in all samples were obtained, so these ratios could not be calculated. When determining barium, the observed ratio was calculated in 25 samples, in which in 20 samples, a better result was obtained during extraction with ammonium acetate. When determining sodium, the observed ratio was calculated in 25 samples, in which in 12 samples, a better result was obtained during extraction with ammonium acetate. When determining sulphur, the observed ratio was calculated in 25 samples, in which in 13 samples, a better result was obtained during extraction with ammonium acetate. These results can be explained by the high heterogeneity of the studied sediments with significant differences in the geochemical composition of the substrates. In most samples, better results were obtained after nitric acid extraction, but it should be noted that a significant amount of barium and sodium was extracted using ammonium acetate. This result is consistent with [23] and [31] that extraction with ammonium acetate may be used to assess the amount of available K, Na, Li, Ba, Mg, and Ca.

Extraction with ammonium acetate in comparison with  $\text{CaCl}_2$  gave better results when extracting the following elements: Al, Ba, Cd, Co, Cu, Fe, K, Mg, Mn, Na, Ni, P, S, Si, Sr, Ti, V, and Zn, where the largest differences were observed in the following elements: Ba, Al, K, Mg, Mn, Na, and Si (Tables 3 and 4). During the extraction of arsenic, beryllium, chromium, lithium, and lead, values below the detection limit in all samples were obtained, so these ratios could not be calculated for these elements. Since that better results were obtained during extraction with ammonium acetate, the conclusion is that ammonium acetate is a more efficient extraction agent than calcium chloride.

### *3.3. Discussion of Concentration Ratios of Studied Elements Using Different Extraction Agents with Results of Amounts of Elements Extracted by the BCR Sequential Extraction Procedure (Total Element Content)*

Concentration ratios of studied elements are presented separately for each extraction agent (calcium chloride, ammonium acetate, and nitric acid) in Supplementary Materials, Tables S4–S6. Total element contents represent the sum of elements extracted during the BCR extraction [19].

Ratios between concentrations obtained by calcium chloride, which is the mildest of used extraction agents, and concentrations obtained by total extraction showed that values for the majority of elements are extremely low. Only a few elements, which will be mentioned, show slightly higher values. Barium has values  $>1$  on several locations only in the coarser fraction, with the highest value reaching a bit above 6%. This finding has significant implications, as it could be a sign of increased bioavailability of Ba in Kupa River sediments. Concentrations of Ba are extremely high in the upper and middle flow of the river due to the Ba-anomaly originating from uncaredful disposal of waste from a barite mine in the Homer mine, Lokve, Gorski Kotar. An especially high Ba-concentration is in the Kupica River spring, to which it penetrated through vulnerable karstic underground, and this spring is used as the main water supply for the Delnice town, which is the central settlement of the whole Gorski Kotar area. Taking in account that Ba is being dissolved with an extraction agent as weak as calcium chloride is, it may imply that its concentration might get elevated, and what could cause problems with tap-water quality. It is known that some forms of Ba are toxic, so it could lead to health problems of local inhabitants. Unfortunately, Ba is not measured in the routine monitoring of water quality in Croatia. Therefore, it would be important to initiate some additional research on this topic in the affected area, as up to now only one preliminary study dealing with Ba's influence on health was performed [17]. In that study, authors applied geochemical and medical methods to investigate the possible impact of disposal of waste from the barite mine on human health in Lokve. The necessity of such measurements in future studies has been highlighted. Their preliminary study of diseases diagnosed in Lokve shows that about 18% of the total

inhabitants have serious medical problems. Diseases of the circulatory system, as well as endocrine, nutritional, and metabolic diseases, neoplasms, and respiratory diseases predominate. They called for further multidisciplinary research on the health effects of barium and trace elements, as well as for bioremediation of contaminated gardens and for watershed management of vulnerable karstic aquifers. From other studied elements, only sulphur has several elevated percentages, with the highest value of about 12.5% in the coarser fraction. This probably could be explained with the fact that the barite ( $\text{BaSO}_4$ ) mineral from the abundant mine is being dissolved, so together with Ba itself, S is also being released from this compound. All other elements show very small percentages.

Ratios between concentrations obtained by ammonium acetate, which is a slightly stronger agent, and concentrations obtained by total extraction, showed that ratios for the majority of elements are higher than when using calcium chloride. Similarly, as with the previous extraction agent, the highest values are observed for Ba and S, confirming everything mentioned in the previous paragraph. From other elements, excluding natural lithogenic elements such as Ca, Si, etc. originating from nearby carbonate rocks, the following elements have rather high percentages: Cd, Cu, K, Mn, and Na. This indicates their potential bioavailability.

Ratios between concentrations obtained by nitric acid, which is the strongest of all three used agents within the current research, and total element content showed the highest values among all three of them. This observation can be explained as follows: During the extraction with  $\text{HNO}_3$ , maximum contents of potentially available fraction were released. Fractions obtained during extraction with  $\text{CaCl}_2$  and ammonium acetate, so-called mobile forms, contain mainly elements in their ion-changing form.

Table 5 shows a statistical analysis of the data about the relationship between content of elements extracted with 2 M  $\text{HNO}_3$  and total extracted element contents (with BCR extraction). When it comes to the finer fraction ( $<63 \mu\text{m}$ ), it is possible to notice that Ca and Cu were extracted in a high percentage using 2 M  $\text{HNO}_3$ , which indicates that this extraction agent is very efficient for extraction of these two elements from the fine sediment fraction. These results indicate that calcium is predominantly present as carbonate at the examined localities. When it comes to copper, it is possible to conclude that this element is not significantly bound to silicates, but is probably bounded to manganese and iron oxides, which are very efficiently destroyed by the use of 2 M  $\text{HNO}_3$ . When the maximum values of the extracted elements are observed, it is possible to notice that a high content of magnesium and strontium was extracted at certain localities, which is probably a consequence of the significant carbonate content. Additionally, a high percentage of extracted zinc using 2 M  $\text{HNO}_3$  (up to 85.30%) was observed at some localities, which indicates high mobility and possible local contamination with this element. Chromium should also be pointed out, since it is a lithophilic and very immobile element in nature, which is confirmed by the results for the average percentage of extracted chromium using 2 M  $\text{HNO}_3$  (about 11% in both fractions). An increased percentage of the extracted element was observed at some localities (up to 41.22% in the fraction  $<63 \mu\text{m}$ , or 49.85% in the fraction  $63\text{--}2000 \mu\text{m}$ ), which may indicate increased mobility of this element in some localities.

When the fraction  $63\text{--}2000 \mu\text{m}$  is observed, 2 M  $\text{HNO}_3$  proved to be an extremely efficient means for extraction of Ca and Cu, but also Mg and Sr, while in some localities lead was also extracted up to 100%. Considering that the average value of extracted lead in this fraction is 46.10%, the high efficiency of extraction at certain localities can be explained by the existence of anthropogenic sources of lead, as a result of which lead is present in more mobile fractions.

At some sites, it was observed that a higher content of Cu was obtained by extraction with 2 M  $\text{HNO}_3$  than by destruction using BCR extraction. Given that the measurements were not made in the same time period, as well as that the ICP OES technique is a sensitive technique, and sediment is a complex matrix, it should be noted that this is a problem of a technical nature and can be seen only in a small number of samples. A similar situation was observed with magnesium.



**Table 5.** Ratio: content of elements extracted with 2 M HNO<sub>3</sub>/total extracted element contents (BCR extraction) \* 100 (%).

|    | <63 µm |        |       | 63–2000 µm |        |       |
|----|--------|--------|-------|------------|--------|-------|
|    | Mean   | Max    | Min   | Mean       | Max    | Min   |
| Zn | 60.95  | 85.30  | 37.50 | 26.65      | 56.30  | 8.52  |
| Al | 9.25   | 11.00  | 7.95  | 7.58       | 13.90  | 4.66  |
| As | 16.36  | 27.84  | 9.91  | 9.89       | 18.30  | 3.02  |
| Ba | 26.13  | 49.15  | 10.20 | 42.71      | 58.87  | 18.64 |
| Be | 35.63  | 44.21  | 29.66 | 32.29      | 52.87  | 17.42 |
| Ca | 96.84  | 108.76 | 86.80 | 93.41      | 114.40 | 70.37 |
| Cd | 49.44  | 59.33  | 40.39 | 39.29      | 67.70  | 17.62 |
| Co | 39.24  | 43.56  | 34.17 | 32.23      | 46.47  | 21.49 |
| Cu | 111.50 | 244.79 | 38.60 | 142.28     | 278.00 | 28.00 |
| Fe | 10.67  | 13.50  | 7.92  | 10.74      | 30.49  | 3.83  |
| K  | 17.26  | 20.11  | 12.75 | 18.77      | 32.54  | 10.99 |
| Li | 23.77  | 41.84  | 9.00  | 37.60      | 68.23  | 9.79  |
| Mg | 70.79  | 88.26  | 59.82 | 100.37     | 219.08 | 66.61 |
| Mn | 50.12  | 56.79  | 41.89 | 39.63      | 62.43  | 22.70 |
| Na | 43.25  | 52.84  | 35.21 | 45.15      | 71.42  | 23.13 |
| Ni | 17.99  | 20.63  | 14.41 | 14.51      | 21.47  | 10.11 |
| Pb | 50.28  | 53.15  | 47.25 | 46.10      | 108.19 | 20.19 |
| S  | 25.91  | 38.96  | 14.26 | 24.88      | 55.30  | 6.09  |
| Si | 46.74  | 52.29  | 38.31 | 34.73      | 57.13  | 17.86 |
| Sr | 65.79  | 76.73  | 44.91 | 79.09      | 109.38 | 58.15 |
| Ti | 6.74   | 10.16  | 4.45  | 5.46       | 13.13  | 1.62  |
| V  | 10.93  | 13.72  | 8.58  | 9.80       | 15.57  | 4.83  |
| P  | 3.76   | 4.32   | 2.68  | 3.26       | 4.81   | 2.08  |
| Cr | 11.22  | 41.22  | 3.60  | 11.87      | 49.85  | 0.07  |

Many elements have similar concentrations when extracted with nitric acid as well as when BCR extraction was performed on them. This means that this type of extraction, which is much easier than total sequential extraction, could be enough to get reasonable results for total content of some elements (Ca, Cu, Mg, and Sr) in sediments. Additionally, it should be noted that this acid can be used for rapid screening of sediment and soil contamination, given that high extraction efficiency was shown for Zn, Pb, and Cd in some localities. In Ref. [30], it is shown that the distribution of Zn is controlled by a similar mechanism as Pb.

In Table 6 is shown results of comparisons of extracted elements' content in this research with similar investigations.

**Table 6.** Comparison of extracted elements content in this research with similar investigations [mg kg<sup>-1</sup>].

|                  | Pb                     | Ni    | Cu                    | Cr               | Cd                  | Zn       |
|------------------|------------------------|-------|-----------------------|------------------|---------------------|----------|
| <sup>1</sup> CaC | <BDL                   | 0.004 | 0.011                 | <BDL             | <BDL                | 0.002    |
| AA               | <BDL                   | 0.222 | 0.466                 | <BDL             | 0.063               | 0.557    |
| NA               | 11.45                  | 4.30  | 17.1                  | 4.58             | 0.213               | 19.08    |
| BCR              | 22.78                  | 23.29 | 18.5                  | 25.70            | 0.43                | 60.96    |
| <sup>2</sup> CaC | 6.83                   | 0.13  | 0.15                  | 4.4 <sup>3</sup> | 0.7 <sup>3</sup>    | <BDL     |
| <sup>2</sup> PTC | 29                     | 17    | 106                   | 11.0             | 4.0                 | 8.2      |
| <sup>4</sup> CaC | <BDL-5974 <sup>3</sup> | nd    | 101–5589 <sup>3</sup> | nd               | 27–932 <sup>3</sup> | 0.22–217 |

<sup>1</sup> This study (fraction of studied sediment: <63 µm); CaC—calcium chloride; AA—ammonium acetate; NA—nitric acid; BCR—total element content; <sup>2</sup> PTC—pseudo total content (aqua regia) [11]. <sup>3</sup> µg kg<sup>-1</sup>; <sup>4</sup> Pueyo [12]; nd—not detected; BDL—below detection limit.

In general, contents of Pb, Ni, Cu, Cr, Cd, and Zn extracted by CaCl<sub>2</sub> from studied river sediments were lower than data for elements extracted from soil samples [11]. Total

content of Cu and Cd was higher in soils [11] than in studied sediments in this manuscript. Obtained higher values for Cu and Cd in soils are due to treatment of soils by fertilizer and pesticides. Total content of extracted Zn from river sediments was higher than in soil [11] because of possible different sources of zinc pollution in the river basin. The total content of the other examined elements (Pb, Ni, and Cr) in sediments (this study) and soils [11] is fairly uniform. Higher content of  $\text{CaCl}_2$  in extractable Pb, Cu, Cd, and Zn content in [12] can be explained by the fact that the investigated soil was largely contaminated (Table 6). The low extractability observed for Pb while using  $\text{CaCl}_2$  as reagent was observed in our research, but also in [11] and [12]. An explanation for this is that lead concentrations in contaminated soil extracts are controlled by precipitation processes (such as carbonates, hydroxides, sulphates, and phosphates), limiting the use of un-buffered salt solutions for the estimation of lead availability in soils [12]. The higher content of elements extracted using ammonium acetate in the yield of other extraction agents (in our case, it is calcium chloride, Table 6) is a consequence of the fact that 1 M ammonium acetate (pH 7) is perhaps the most preferred reagent for exchangeable metals because of its relatively high concentration and the metal complexing power of the acetate ion, both of which prevent re-adsorption or precipitation of released metal ions [32]. This reagent released bigger amounts of heavy metals than did ammonium nitrate [33].

### 3.4. Correlation Analysis

The Pearson correlation coefficients ( $r$ ) measure the strength and direction of linear relationships between two or more random variables. In the present study,  $r$  is used to describe the interrelationships between the analyzed elements, and the results of correlation analysis are shown in Table 7.

**Table 7.** Correlation analysis of extracted element contents.

|                    | E_AA  | E_NA   | E_BCR  |
|--------------------|---|--|--|
| <sup>1</sup> E_CaC | Ba **, K **, Mg **, Na **, P **, S **, Si **, Sr ** | Ba **, K **, Na **, P *, S **, Si **, Sr *                                   | Ba **, Cu *, K **, Mn *, Na **, Si **, Sr **   |
| E_AA               |   | Al *, Ba **, Cd **, Co *, Fe *, K **, Mn **, Na **, Ni **, S **, Si **, Sr * | Al *, Ba **, Cd **, K **, Li **, Na **, Ni **, S **, Si **, Sr *, Ti *, V *  |
| E_NA               |   |  | Al **, As **, Ba **, Be **, Ca **, Cd **, Co **, Cr **, Fe **, K **, Mg **, Mn **, Na **, Ni **, P **, Pb **, S **, Si **, Sr **, Ti **, V **, Zn ** |

<sup>1</sup> E—element; CaC—calcium chloride; AA—ammonium acetate; NA—nitric acid; BCR—total element content; \* Correlation is significant at the 0.05 level; \*\* Correlation is significant at the 0.01 level.

It can be observed that there is a positive correlation between the content of all extracted elements with nitric acid (NA) and the total element content (BCR content). This indicates that the use of 2 M  $\text{HNO}_3$  efficiently extracts all studied elements. The results of the correlation analysis indicate that there is a positive correlation between the total extracted element content and the elements extracted using AA—ammonium acetate (Al, Ba, Cd, K, Li, Na, Ni, S, Si, Sr, Ti, and V) and CaC—calcium chloride (Ba, Cu, K, Mn, Na, Si, and Sr). In the case of more mobile fractions, the content of elements extracted with calcium chloride is positively correlated with the content of Ba, K, Mg, Na, P, S, Si, and Sr, extracted with ammonium acetate. A positive correlation was observed between the content of elements extracted with nitric acid and calcium chloride (Ba, K, Na, P, S, Si, and Sr) and those extracted with ammonium acetate (Al, Ba, Cd, Co, Fe, K, Mn, Na, Ni, S, Si, and Sr). The observed correlations show that ammonium acetate is a more efficient means of extracting the most mobile fraction of elements. Correlations of the mobile contents

of the elements with the total content indicate the existence of anthropogenic sources of cadmium and copper at the examined localities.  $\text{CaCl}_2$  is recommended in [11] and [12] as a suitable reagent for extraction in the mobile form of Cu. In Ref. [30], it is shown that mobilization of Cu is mainly controlled by soil reaction.

A positive correlation between  $\text{CaCl}_2$ -extractable and total content of Cu in this manuscript indicated that in parts of the Kupa basin, there are vineyards that have been treated by fungicide copper (II)-sulphate. Additionally, positive correlations of mobile barium fractions using CaC and AA indicate the high mobility of this element. The positive correlation between the content of mobile contents of macroelements and the total content of elements indicates that the application of weaker extraction agents leads to complete or partial decomposition of carbonates, sulfates, phosphates, and even manganese oxides, and to the release of toxic elements related to them. We recommend extraction with ammonium acetate to assess mobile fraction elements that are equivalent to the “actually available” metal fraction, while nitric acid can be used to assess mobilizable fraction, i.e., the potentially available forms of trace elements in soils and sediments.

### 3.5. Ecological Risk Assessment of Potentially Toxic Elements Using Monte Carlo Simulation

A distribution curve on  $E_r^i$  and HRI (Total ecological risk comprehensive index) values is shown in Figure 4. The probability that ecological risk appeared at different risk levels with reference to a risk level classification standard was analyzed, as shown in Table 8. The Monte Carlo simulation suggests that risk of Cr, Cu, Ni, Pb, and Zn was low, and As and Cd posed a lower ecological risk in the studied areas. Cd is the most important factor in the Kupa River basin.

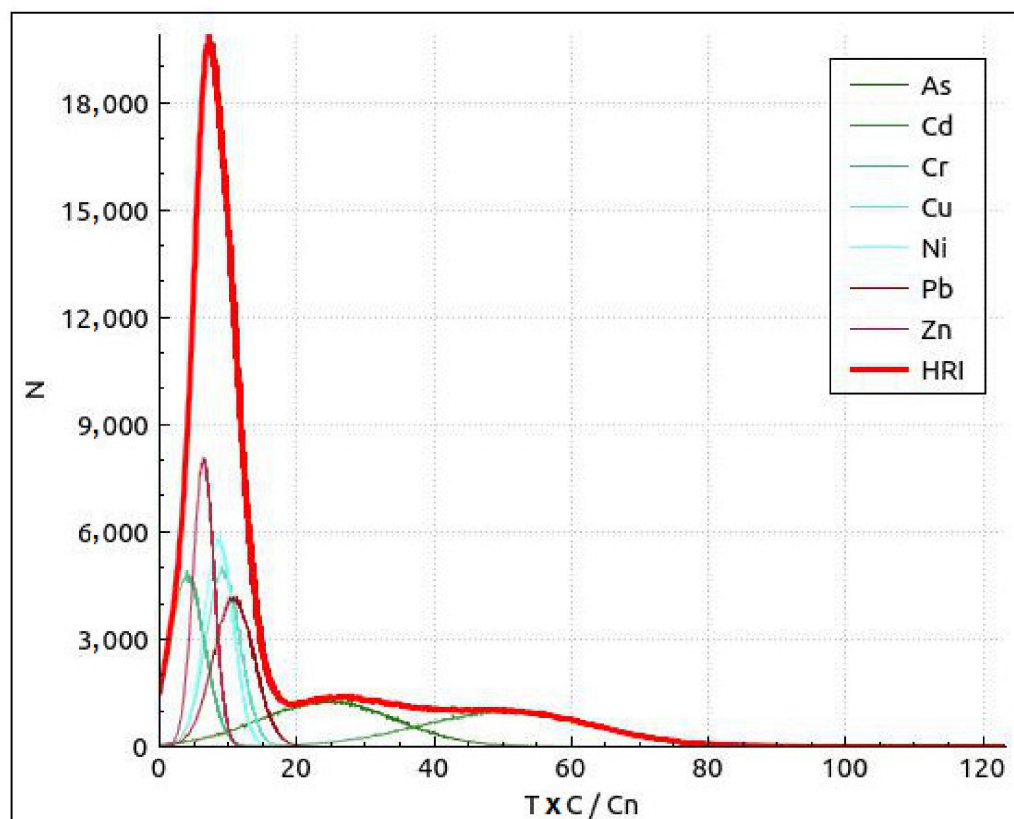


**Figure 4.** Distribution curve and exceedance probability curves of the risk index (RI) and total ecological risk comprehensive index HRI based on a Monte Carlo simulation run 100,000 times. Local backgrounds are the reference values for the calculation of  $E_r^i$ .

**Table 8.** Ecological risk analysis results of each PTEs.

| Value of $Er^i$       | Risk Level     | Probability (%) |       |     |     |     |     |     |
|-----------------------|----------------|-----------------|-------|-----|-----|-----|-----|-----|
|                       |                | As              | Cd    | Cr  | Cu  | Ni  | Pb  | Zn  |
| $Er^i < 40$           | Low            | 94.07           | 19.98 | 100 | 100 | 100 | 100 | 100 |
| $40 \leq Er^i < 80$   | Lower          | 5.93            | 78.93 | 0   | 0   | 0   | 0   | 0   |
| $80 \leq Er^i < 160$  | Median         | 0               | 1.09  | 0   | 0   | 0   | 0   | 0   |
| $160 \leq Er^i < 320$ | High           | 0               | 0     | 0   | 0   | 0   | 0   | 0   |
| $Er^i \geq 320$       | Extremely high | 0               | 0     | 0   | 0   | 0   | 0   | 0   |

As shown in Table 9, the probability of the HRI values being at a low risk level was 100%, i.e., the total ecological risk level of PTEs pollutants in the sediments of the Kupa river.

**Table 9.** Total ecological risk analysis results of the studied rivers.

| HRI Value             | Risk Level | Probability (%) |
|-----------------------|------------|-----------------|
| $HRI < 150$           | Low        | 100             |
| $150 \leq HRI < 300$  | Lower      | 0               |
| $300 \leq Er^i < 600$ | Median     | 0               |
| $Er^i \geq 600$       | High       | 0               |

### 3.6. Magnetic Susceptibility (MS) Measurements vs. Element Concentrations in Different Dissolution

Correlations between MS and elements contents obtained using three extraction agents were performed, and only one significant correlation is detected. For dissolution with 2 M  $HNO_3$ , the only significant correlation was found for Mg (0.50). From all three used agents in this paper,  $HNO_3$  is the strongest one, dissolving a significant part of the sediment, including both elements of anthropogenic and natural origin. Mg in Kupa River sediments is an element of natural origin, deriving from carbonate rocks, mostly dolomites.

## 4. Conclusions

Based on presented results for the Kupa river, it is possible to conclude that differences in amounts of a single element extracted from sediment by different procedures varied from location to location and from element to element, which is the result of high heterogeneity of the studied river sediments in the geochemical composition. These results indicated the significance of the application of different extractions reagents on the assessment of mobility of trace elements. Nitric acid is a more efficient extraction agent in relation to calcium chloride and ammonium-acetate, and ammonium acetate is a more efficient extraction agent than calcium chloride. The results of the single extraction methods indicate increased bioavailability of Ba, Cd, Cu, K, Mn, and Na and low bioavailability for chromium, since it is a lithophilic and very immobile element in nature. Numerous elements were extracted in similar contents when sediments were extracted with nitric acid as well as when performing BCR extraction (total element content). Extraction with 2 M  $HNO_3$ , which is much easier than sequential extraction and total element content determination, could be enough to get reasonable results for the determination of total content of Ca, Cu, Mg, and Sr in sediments. High extraction efficiency was shown also for Zn, Pb, and Cd in some localities. Additionally, it should be noted that 2 M  $HNO_3$  can be used for rapid screening of sediment and soil contamination. We recommend extraction with ammonium acetate to assess mobile fraction elements that are equivalent to the “actually available” metal fraction, while nitric acid can be used to assess mobilizable fraction, i.e., the potentially available forms of trace elements in soils and sediments.  $CaCl_2$  extraction is recommended for the determination of Cu mobile forms in sediments.

Based on a Monte Carlo simulation, it was found that the lower risk probabilities of Cd were 78.93% and 1.09% for median risk, which indicate that Cd was the most important

toxic element in the Kupa River. The probability of ecological risk for all factors indicated that the potential ecological risk of toxic elements in the Kupa River is low at present. However, despite the low risk at present, there are indications that contents of some toxic metals are increasing at some locations, especially in the Kupa River lower flow, which could increase the ecological risk in the future. Therefore, we suggest the need for future systematic monitoring of the Kupa River and its drainage basin with respect to toxic element and ecological risk estimations.

**Supplementary Materials:** The following are available online: <https://www.mdpi.com/article/10.3390/w13101411/s1>, Table S1: Relationship between the contents of elements extracted with  $\text{CaCl}_2$  and  $\text{HNO}_3$  (%); Table S2: Relationship between the contents of elements extracted with  $\text{CH}_3\text{COONH}_4$  and  $\text{HNO}_3$ ; Table S3: Relationship between the contents of elements extracted with  $\text{CaCl}_2$  and  $\text{CH}_3\text{COONH}_4$ ; Table S4: Relationship between the contents of elements extracted with  $\text{CaCl}_2$  and total element content—BCR extraction (%); Table S5: Relationship between the contents of elements extracted with  $\text{CH}_3\text{COONH}_4$  and total element content—BCR extraction (%); Table S6: Relationship between the contents of elements extracted with  $\text{HNO}_3$  and total element content—BCR extraction (%).

**Author Contributions:** Conceptualization, S.S. and S.F.-B.; methodology, S.S., S.F.-B., D.Đ. and H.B.; software, N.S.; sampling, S.F.-B. and H.B.; investigations, S.S. and S.F.-B.; formal analysis, S.S., S.F.-B. and S.Š.; writing—original draft preparation, S.S. and S.F.-B.; writing—review and editing, S.S., S.F.-B., D.Đ., A.P., N.S., S.Š. and H.B. All authors have read and agreed to the published version of the manuscript.

**Funding:** This manuscript was supported by the Centre of Excellence in Environmental Chemistry and Engineering—ICTM, Faculty of Chemistry, and Institute of Physics, Belgrade, University of Belgrade, through the grants by the Ministry of Education, Science and Technological Development of Republic of Serbia. The authors would like to thank the Ministry of Education, Science and Technological Development of Republic of Serbia (Grant No: 451-03-9/2021-14/200026) for financial support. Field trips in the Kupa River basin were funded by Ministry of Science and Education of Republic of Croatia (Grant No: 0411FI18), which is also thanked for financial support.

**Acknowledgments:** We would like to thank the Krešimir Maldini from Hrvatske vode (Croatian water authorities) who helped us with the drying and sieving of sediment samples collected in 2018.

**Conflicts of Interest:** The authors declare no conflict of interest.

## References

1. Davutluoglu, O.I.; Seckin, G.; Ersu, C.B.; Yilmaz, T.; Sari, B. Heavy metal content and distribution in surface sediments of the Seyhan River, Turkey. *J. Environ. Manag.* **2011**, *92*, 2250–2259. [[CrossRef](#)]
2. Zahra, A.; Hashmi, M.Z.; Malik, R.N.; Ahmed, Z. Enrichment and geo-accumulation of heavy metals and risk assessment of sediments of the Kurang Nallah—Feeding tributary of the Rawal Lake Reservoir, Pakistan. *Sci. Total Environ.* **2014**, *470–471*, 925–933. [[CrossRef](#)] [[PubMed](#)]
3. Ottesen, R.T.; Bogen, J.; Bølviken, B.; Volden, T. Overbank sediment: A representative sampling medium for regional geochemical mapping. *J. Geochem. Explor.* **1989**, *32*, 257–277. [[CrossRef](#)]
4. Cappuyns, V. A critical evaluation of single extractions from the SMT program to determine trace element mobility in sediments. *Appl. Environ. Soil Sci.* **2012**, *672914*. [[CrossRef](#)]
5. Groenenberg, J.E.; Römkens, P.F.A.M.; Zomeren, A.V.; Rodrigues, S.M.; Comans, R.N.J. Evaluation of the single dilute (0.43 M) nitric acid extraction to determine geochemically reactive elements in Soil. *Environ. Sci. Technol.* **2017**, *51*, 2246–2253. [[CrossRef](#)]
6. Antoniadis, V.; Shaheen, S.M.; Levizou, E.; Shahid, M.; Niazi, N.K.; Vithanage, M.; Ok, Y.S.; Bolan, N.; Rinklebe, J. A critical prospective analysis of the potential toxicity of trace element regulation limits in soils worldwide: Are they protective concerning health risk assessment?—A review. *Environ. Internat.* **2019**, *127*, 819–847. [[CrossRef](#)]
7. Kastori, R.R.; Petrović, M.; Petrović, N.M.; Štrbac, D. Effect of heavy metals on water relations in plants. *Zb. Matice Srp. Prir. Nauke* **1995**, *88*, 5–17.
8. Abollino, O.; Malandrino, M.; Giacomino, A.; Mentasti, E. The role of chemometrics in single and sequential extraction assays: A review Part I. Extraction procedures, uni- and bivariate techniques and multivariate variable reduction techniques for pattern recognition. *Anal. Chim. Acta.* **2011**, *688*, 104–121. [[CrossRef](#)]
9. Cuvier, A.; Leleyter, L.; Probst, A.; Probst, J.-L.; Prunier, J.; Poucelot, L.; Le Roux, G.; Lemoine, M.; Reinert, M.; Baraud, F. Why comparison between different chemical extraction procedures is necessary to better assess the metals availability in sediments? *J. Geochem. Explor.* **2021**, *225*, 106762. [[CrossRef](#)]



10. Pantović Spajić, K.; Sakan, S.; Đorđević, D.; Šošarić, T.; Lopičić, Z.; Janičijević, A.; Stojanović, K. Comparison of extraction agents for metal determination in sediments from artificial lakes and rivers in Serbia. *Acta Period. Technol.* **2019**, *50*, 189–196. [[CrossRef](#)]
11. Milićević, T.; Relić, D.; Škrivanj, S.; Tešić, Ž.; Popović, A. Assessment of major and trace element bioavailability in vineyard soil applying different single extraction procedures and pseudo-total digestion. *Chemosphere* **2017**, *171*, 284–293. [[CrossRef](#)] [[PubMed](#)]
12. Pueyo, M.; López-Sánchez, J.F.; Rauret, G. Assessment of  $\text{CaCl}_2$ ,  $\text{NaNO}_3$  and  $\text{NH}_4\text{NO}_3$  extraction procedures for the study of Cd, Cu, Pb and Zn extractability in contaminated soils. *Anal. Chim. Acta* **2004**, *504*, 217–226. [[CrossRef](#)]
13. Zhao, L.; Mi, D.; Wang, L.; Sun, Y. Ecological risk assessment and sources of heavy metals in sediment from Daling River basin. *Environ. Sci. Pollut. Res.* **2015**, *22*, 5975–5984. [[CrossRef](#)] [[PubMed](#)]
14. Yuan, H.; Song, S.; An, S.; Liu, E. Ecological risk assessment of potentially toxic elements (PTEs) in the soil-plant system after reclamation of dredged sediment. *Environ. Sci. Poll. Res.* **2018**, *25*, 29181–29191. [[CrossRef](#)] [[PubMed](#)]
15. Poulter, S.R. Monte Carlo Simulation in Environmental Risk Assessment—Science, Policy and Legal Issues. *RISK* **1998**, *9*, 7.
16. Frančičković-Bilinski, S. Barium anomaly in Kupa River drainage basin. *J. Geochem. Explor.* **2006**, *88*, 106–109. [[CrossRef](#)]
17. Frančičković-Bilinski, S.; Bilinski, H.; Grbac, R.; Žunić, J.; Nečemer, M.; Hanžel, D. Multidisciplinary work on barium contamination of the karstic upper Kupa River drainage basin (Croatia and Slovenia); calling for watershed management. *Environ. Geochem. Health* **2007**, *29*, 69–79. [[CrossRef](#)] [[PubMed](#)]
18. Frančičković-Bilinski, S.; Bhattacharya, A.K.; Bilinski, H.; Bhattacharya, B.D.; Mitra, A.; Sarkar, S.K. Fluvial geomorphology of the Kupa River drainage basin, Croatia: A perspective of its application in river management and pollution studies. *Zeitschrift für Geomorphologie* **2012**, *56*, 93–119. [[CrossRef](#)]
19. Sakan, S.; Frančičković-Bilinski, S.; Đorđević, D.; Popović, A.; Škrivanj, S.; Bilinski, H. Geochemical fractionation and risk assessment of potentially toxic elements in sediments from Kupa River, Croatia. *Water* **2020**, *12*, 2024. [[CrossRef](#)]
20. Biondić, B.; Biondić, R.; Kapelj, S. Protection of the Karst aquifers in the river Kupa catchment area and sustainable development. *RMZ Mater. Geov. Geoenv.* **2003**, *50*, 33–36.
21. Cappuyns, V.; Swennen, R.; Verhulst, A. Assessment of Heavy Metal Mobility in Dredged Sediments: Porewater Analysis, Single and Sequential Extractions. *Soil Sedim. Cont.* **2006**, *15*, 1–18. [[CrossRef](#)]
22. Sihlahla, M.; Mouri, H.; Nomngongo, P.N. Assessment of bioavailability and mobility of major and trace elements in agricultural soils collected in Port St Johns, Eastern Cape, South Africa using single extraction procedures and pseudo-total digestion. *J. Environ. Health Sci. Eng.* **2020**, *18*, 1615–1628. [[CrossRef](#)]
23. Sakan, S.; Popović, A.; Škrivanj, S.; Sakan, N.; Đorđević, D. Comparison of single extraction procedures and the application of an index for the assessment of heavy metal bioavailability in river sediments. *Environ. Sci. Pollut. Res.* **2016**, *23*, 21485–21500. [[CrossRef](#)]
24. Šestinová, O.; Hančulák, J.; Brehuv, J.; Fedorová, E. The mobility of heavy metals in sediments using the sequential extraction method. In Proceedings of the Conference Materials, 4th European Conference Bioremediation, Chania Crete, Greece, 3–6 September 2008.
25. Šmejkalová, M.; Mikanová, O.; Borůvka, L. Effects of heavy metal concentrations on biological activity of soil micro-organisms. *Plant Soil Environ.* **2003**, *49*, 321–326. [[CrossRef](#)]
26. Qu, C.; Li, B.; Wu, H.; Wang, S.; Li, F. Probabilistic ecological risk assessment of heavy metals in sediments from China's major aquatic bodies. *Stoch. Environ. Res. Risk Assess.* **2016**, *30*, 271–282. [[CrossRef](#)]
27. Wu, H.; Li, B.; Qu, C.; Wang, S.; Wan, W.; Zhou, J. A Method for Determining Ecological Risks of Heavy Metal Pollution in River and Lake Sediments. U.S. Patent 20160110835A1, 21 April 2016.
28. Håkanson, L. An ecological risk index for aquatic pollution control. A sedimentological approach. *Water Res.* **1980**, *14*, 975–1001. [[CrossRef](#)]
29. Yang, Z.; Wang, Y.; Shen, Z.; Niu, J.; Tang, Z. Distribution and speciation of heavy metals in sediments from the mainstream, tributaries, and lakes of the Yangtze river catchment of Wuhan, China. *J. Hazard. Mater.* **2009**, *166*, 1186–1194. [[CrossRef](#)] [[PubMed](#)]
30. Pavlů, L.; Drábek, O.; Borůvka, L.; Nikodem, A.; Němeček, K. Degradation of forest soils in the vicinity of an industrial zone. *Soil Water Res.* **2015**, *10*, 65–73. [[CrossRef](#)]
31. Carter, M.R. *Soil Sampling and Methods of Analysis*; Lewis Publishers: Boca Raton, FL, USA; Canadian Society of Soil Science: Pinawa, MB, Canada, 1993.
32. Podlesáková, E.; Nemeček, J.; Vácha, R. Mobility and Bioavailability of Trace Elements in Soils. In *Trace Elements in Soil: Bioavailability, Flux, and Transfer*; Iskandar, I.K., Kirkham, M.B., Eds.; Lewis Publishers: Boca Raton, FL, USA, 2001.
33. Sabienė, N.; Brazauskienė, D.M.; Rimmer, D. Determination of heavy metal mobile forms by different extraction methods. *Ekologija* **2004**, *1*, 36–41.

## Modeling of the Continuous Absorption of Electromagnetic Radiation in Dense Hydrogen Plasma

A. A. Mihajlov<sup>1,2</sup> and N. M. Sakan<sup>1</sup> and V. A. Srećković<sup>1,2</sup> and Y. Vitel<sup>3</sup>

<sup>1</sup> *Institute of Physics, Belgrade University,  
Pregrevica 118, Zemun, 11080 Belgrade, Serbia*

<sup>2</sup> *Isaac Newton Institute of Chile, Yugoslavia Branch,  
Volgina 7, 11060 Belgrade Serbia*

<sup>3</sup> *UPMC Univ Paris 6, Laboratoire des Plasmas Denses,  
3 rue Galilee, 94200 Ivry sur Seine, France*

Received: 2011 June 10; accepted: 2011 December 15

**Abstract.** In this work is examined a new modeling way of describing the continuous absorption of electromagnetic (EM) radiation in a dense partially ionized hydrogen plasmas with electron densities about  $5 \cdot 10^{18} \text{ cm}^{-3}$  -  $1.5 \cdot 10^{19} \text{ cm}^{-3}$  and temperatures about  $1.6 \cdot 10^4 \text{ K}$  -  $2.5 \cdot 10^4 \text{ K}$  in the wavelength region  $300 \text{ nm} < \lambda < 500 \text{ nm}$ . The obtained results can be applied to the plasmas of the partially ionized layers of different stellar atmospheres.

**Key words:** ISM: extinction – stars: continuous absorption

### 1. INTRODUCTION

In this paper testing is started of a new model way of describing some of atomic photo-ionization processes in dense strongly ionized plasmas, which is based on the approximation of cut-off Coulomb potential. By now this approximation has been used only in order to describe transport properties of dense plasmas (see for example Mihajlov et al. (1989)), but it was clear that it could be applied to the mentioned absorption processes in non-ideal plasmas too. Because of exceptional simplicity of the hydrogen atom, for the first application of the mentioned approximation the following photo-ionization processes are chosen here:

$$\epsilon_\lambda + H^*(n, l) \rightarrow H^+ + e_E, \quad (1)$$

where  $\epsilon_\lambda$  is the energy of the photon with wavelength  $\lambda$ ,  $n$  and  $l$  - principal and orbital quantum numbers of hydrogen atom excited states,  $e_E$  - the free electron in one of the states with energy  $E = \hbar^2 k^2 / 2m$ , and  $m$  and  $\hbar$  - the electron mass and Planck's constant. It is clear that describing the processes of the type of Eq. (1) in strongly non-ideal plasmas is one of the most complicated problems. Namely, while in weakly and moderately non-ideal plasma the interaction of an excited atom with its neighborhood can be neglected, as for example in Solar photosphere (Mihalas (1978); Mihajlov et al. (2007)), or described within the framework of a



perturbation theory, this is not possible in strongly non-ideal plasmas. This is due to the fact that in such plasmas the energy of the mentioned interaction reaches the order of the corresponding ionization potential.

Here a new model method having a semi-empirical character of determination of the spectral absorption coefficients, characterizing the bound-free (photo-ionization) processes (II) in strongly non-ideal hydrogen plasmas, is presented. As landmarks we take hydrogen plasmas with electron densities  $N_e \sim 1 \cdot 10^{19} \text{cm}^{-3}$  and temperatures  $T \approx 2 \cdot 10^4 \text{K}$ , which were experimentally studied in Vitel et al. (2004). The presented method is tested within the optical range of photon wavelengths  $350 \text{nm} \leq \lambda_{h\nu} \leq 500 \text{nm}$ .

## 2. THEORY

The absorption processes (II) in non-ideal plasma are considered here as a result of radiative transition in the whole system "electron-ion pair (atom) + the neighborhood", namely:  $\epsilon_\lambda + (H^+ + e)_{n,l} + S_{rest} \rightarrow (H^+ + e)_E + S'_{rest}$ , where  $S_{rest}$  and  $S'_{rest}$  denote the rest of the considered plasma. However, as it is well known, many-body processes can sometimes be simplified by their transformation to the corresponding single-particle processes in an adequately chosen model potential. Here, in accordance with the previous paper (Mihajlov et al. 1989) the screening cut-off Coulomb potential is taken as an adequate model potential, which can be presented in the form

$$U_c(r) = \begin{cases} -e^2/r + e^2/r_c, & 0 < r \leq r_c, \\ 0, & r_c < r < \infty, \end{cases} \quad (2)$$

which is illustrated by Fig. 1. Here  $e$  is the modulus of the electron charge,  $r$  - distance from the ion, and cut-off radius  $r_c$  - the characteristic screening length of the considered problem. Namely, within this model it is assumed that quantity  $U_{p;c} = -e^2/r_c$  is the mean potential energy of an electron in the considered hydrogen plasma. It is important that the cut-off radius  $r_c$  can be determined as a given function of  $N_e$  and  $T$ , using two characteristic lengths:  $r_i = [k_B T / (4\pi N_i e^2)]^{1/2}$  and  $r_{s;i} = [3 / (4\pi N_i)]^{1/3}$ , where  $N_i$  and  $r_{s;i}$  are the  $H^+$  density and the corresponding Wigner-Seitz's radius and  $k_B$  - Boltzman's constant. Namely, taking that  $N_i = N_e$  and

$$r_c = a_{c;i} \cdot r_i, \quad (3)$$

we can directly determine the factor  $a_{c;i}$  as a function of ratio  $r_{s;i}/r_i$ , on the basis of the data about the mean potential energy of the electron in the single ionized plasma from Mihajlov et al. (2009). The behavior of  $a_{c;i}$  in a wide region of values of  $r_{s;i}/r_i$  is presented in Fig. 2.

In diluted hydrogen plasma (see for example Mihalas 1978) the spectral absorption coefficients, characterizing the photo-ionization processes (II) can be described within the approximation of the non-perturbed energy levels in the potential  $U_c(r)$ , namely:  $\kappa_{ph}^{(0)}(\lambda; N_e, T) = \sum_{n,l} N_{n,l} \cdot \sigma_{ph}(\lambda; n, l, E_{n,l})$ , where  $N_{n,l}$  is the density of the atoms in the realized excited states with given  $n$  and  $l$ , and  $\sigma_{ph}(\lambda; n, l, E_{n,l})$  - the corresponding photo-ionization cross section for  $n \geq 2$ . According to the above mentioned, it cannot model the absorption coefficients of the dense non-ideal plasmas described in Vitel et al. (2004).

It can be shown, using the results from Adamyan (2009), that  $\kappa_{ph}(\lambda; N_e, T)$  can be obtained within the approximation based on adequately chosen shifts  $\Delta_{n,l}$  and broadenings  $\delta_{n,l}$  of the energy levels with given  $n$  and  $l$ . It is assumed that energies  $\epsilon$  of the perturbed atomic states are dominantly grouped around energy  $\epsilon_{n,l}^{(max)} = E(n, l) + \Delta_{n,l}$ , inside the interval  $(\epsilon_{n,l}^{(max)} - \delta_{n,l}/2, \epsilon_{n,l}^{(max)} + \delta_{n,l}/2)$ , similarly to the known cases (Gaus, Lorentz, uniform etc.).

Let us note that it is possible to describe the quantity  $\Delta_n$  as a function of  $N_e$ . Namely, for well-known physical reasons all shifts  $\Delta_{n,l}$ , and consequently  $\Delta_n$ , have to change proportionally with the density of the perturbers, the relative atom-perturber velocity and the characteristic perturbation energy. Consequently, we will have that:  $\Delta_n \sim N_e \cdot v_{ea}(T) \cdot e^2/l(N_e, T)$ , where  $v_{ea}(T)$  and  $l(N_e, T)$  are the characteristic electron-atom velocity and distance. On the basis of the results of Mihajlov et al. (2009) in the considered cases ( $N_e \sim 1 \cdot 10^{19} \text{cm}^{-3}$ ,  $T \sim 2 \cdot 10^4 \text{K}$ ) any relevant characteristic length has to be close to the radius  $r_i$ . From here, since  $v_{ea}(T) \sim (k_B T)^{1/2}$  and  $r_i \sim (k_B T/N_e)^{1/2}$ , the relation follows

$$\Delta_n \approx Const. \cdot N_e^{3/2}, \quad (4)$$

which is in accordance with Adamyan (2009) and can be useful in further considerations.

Here, we will describe the perturbed atomic states in the first order of the perturbation theory and, in accordance with what was said above, we will have it that

$$\kappa_{ph}(\lambda; N_e, T) = \sum_{n,l} N_{n,l} \cdot \frac{1}{\delta_n} \int_{\epsilon_{n,l}^{(max)} - \delta_n/2}^{\epsilon_{n,l}^{(max)} + \delta_n/2} \frac{\epsilon_\lambda}{\epsilon_\lambda + \epsilon} \cdot \sigma_{ph}(\lambda^{(\epsilon)}; n, l, E_{n,l}) d\epsilon, \quad (5)$$

where  $n \geq 2$ ,  $\epsilon_{n,l}^{(max)} = E_{n,l} + \Delta_n$ , and  $\sigma_{ph}(\lambda^{(\epsilon)}; n, l, E_{n,l})$  is the corresponding photo-ionization cross section for  $\lambda^{(\epsilon)} = \lambda \cdot \epsilon_\lambda / (\epsilon_\lambda + \epsilon)$ , i.e. for the wavelength of the photon with energy  $(\epsilon_\lambda + \epsilon)$ .

### 3. RESULTS AND DISCUSSION

In this paper the approximation of cut-off Coulomb potential (2) is applied to the modeling of spectral absorption coefficients of the hydrogen plasma, obtained in Vitel et al. (2004) in two experiments: a short and a long pulse, respectively. In the first case (short pulse) plasma with  $N_e = 1.5 \cdot 10^{19} \text{cm}^{-3}$  and  $T = 2.3 \cdot 10^4 \text{K}$  was studied, while in the second case (long pulse) - one with  $N_e = 6.5 \cdot 10^{18} \text{cm}^{-3}$  and  $T = 1.8 \cdot 10^4 \text{K}$ . It has been found that:  $r_c = 44.964$  a.u. for a short pulse, and  $r_c = 55.052$  a.u. for the long one.

In order to compare the obtained theoretical results with the experimental data from Vitel et al. (2004), we had to take into account other relevant absorption processes, namely:  $(e + H^+)$ -inverse "bremsstrahlung", as well as  $H^-$  and  $H_2^+$  absorption continuums, which cannot be neglected in the considered hydrogen plasmas. Therefore, when comparing our theoretical results with the experimental data from Vitel et al. (2004) we use the total spectral absorption coefficient  $\kappa_{tot}(\lambda)$  given by:  $\kappa_{tot}(\lambda) = \kappa_{ph}(\lambda) + \kappa_{add}(\lambda)$ , where the member  $\kappa_{ph}(\lambda) \equiv \kappa_{ph}(\lambda; N_e, T)$  is

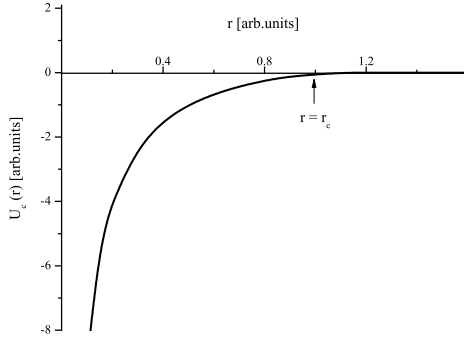


Figure 1: Cut-off potential  $U_c(r)$ , where  $r_c$  is cut-off parameter.

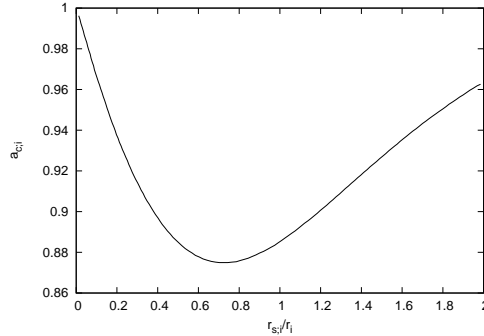


Figure 2: The parameter  $a_{c;i} \equiv r_c/r_i$  as the function of the ratio  $r_{s;i}/r_i$ .

given by Eq. (5), while the member  $\kappa_{add}(\lambda)$  is the sum of the absorption coefficients of all additional processes. Let us note that electron-ion process is described by the absorption coefficient from Sobel'man (1979), while the electron-atom and ion-atom processes - by the ones determined as in previous paper (Mihajlov et al. 2007) dedicated to the same absorption processes in the solar photosphere.

In accordance with the aims of this work the calculations of the total absorption coefficient, are performed for both cases (short and long pulse) in wide regions of values of shifts ( $\Delta_n$ ) and broadening ( $\delta_n$ ) of atomic levels with  $n \geq 2$ . The calculations of  $\kappa_{tot}(\lambda)$  cover wavelength region  $350\text{nm} \leq \lambda \leq 500\text{nm}$ . The results of calculations are shown in Figs. 3 and 4 together with the corresponding experimental values  $\kappa_{exp}(\lambda)$  of the spectral absorption coefficient from Vitel et al. (2004). This figures show the results of the calculations of  $\kappa_{tot}(\lambda)$  in the case  $\Delta_n = const.$ , with the values of  $\Delta_n$  and  $\delta_n$  which are treated as optimal ones:  $\Delta_n = 0.455\text{eV}$  and  $\delta_n = 0.625\text{eV}$  for the short pulse, and  $\Delta_n = 0.13\text{eV}$  and  $\delta_n = 0.11\text{eV}$  for the long pulse.

Here it is important to check whether relation Eq. (4) is valid also for  $N_e$  close to  $0.65 \cdot 10^{19}\text{cm}^{-3}$ . Since in the case of constant shifts  $\Delta_n = 0.455\text{eV}$  and  $0.130\text{eV}$  for short and long pulses respectively, validity of Eq. (4) means that  $0.455/0.130 = (1.5/0.65)^{3/2}$ , which is satisfied with an accuracy better than 1%. In the case of variable shift we have it that  $\Delta_{n=2} = 0.49\text{eV}$  and  $0.12\text{eV}$  for the short and long pulses respectively, and validity of Eq. (4) means now that  $0.49/0.14 = (1.5/0.65)^{3/2}$ , which is satisfied with the same accuracy. The fact that Eq. (4) is satisfied for  $N_e = 1.5 \cdot 10^{19}\text{cm}^{-3}$  and  $0.65 \cdot 10^{19}\text{cm}^{-3}$  offers a possibility to determine  $\Delta_n$  or  $\Delta_{n=2}$  not only for these densities but also for any  $N_e$  from interval  $0.65 \cdot 10^{19}\text{cm}^{-3} < N_e < 1.5 \cdot 10^{19}\text{cm}^{-3}$  and probably in a significantly wider region. Also, using the fact that the influence of  $\delta_n$  over the absorption coefficients is significantly weaker than the influence of  $\Delta_n$ , we can determine the values of  $\delta_n$  for any  $N_e$  using the values of ratio  $\delta_n/\Delta_n$  from the considered examples.

On the grounds of all that was said one can conclude that the presented method can already be used for calculations of the spectral absorption coefficients of dense hydrogen plasmas with  $N_e \sim 10^{19} \text{cm}^{-3}$  and  $T_e \approx 2 \cdot 10^4 \text{K}$ . Let us note that, with some minor modifications, the presented method can be applied to any kind of dense single-ionized plasma (laboratorial alkali-metal plasmas, helium plasmas in some DB white dwarfs etc.

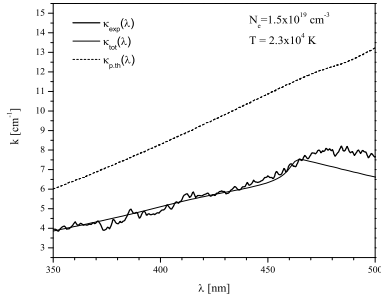


Figure 3: The absorption coefficient  $\kappa_{tot}(\lambda)$  calculated in the case of the short pulse with  $\Delta_n = 0.455 \text{eV}$  and  $\delta_n = 0.625 \text{eV}$ . Dashed line - the theoretical curve from Vitel et al. (2004).

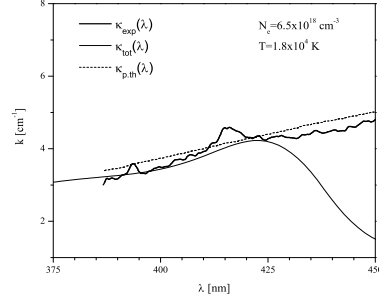


Figure 4: The absorption coefficient  $\kappa_{tot}(\lambda)$  calculated in the case of the Long pulse with  $\Delta_n = 0.13 \text{eV}$  and  $\delta_n = 0.11 \text{eV}$ . Dashed line - the theoretical curve from Vitel et al. (2004).

ACKNOWLEDGMENTS. The authors are thankful to the University P. et M. Curie of Paris (France) for financial support, as well as to the Ministry of Science of the Republic of Serbia for support within the Projects 176002, III44002 and 171014.

## REFERENCES

- Adamyan V. M. 2009, *private communication*
- Mihajlov A. A., Djordjevic D., Popovic M. M. et al. 1989, *Contrib. Plasma Phys.*, 29, 441
- Mihajlov A. A., Ignjatović L. M., Sakan N. M. et al. 2007, *A&A*, 437, 1023
- Mihajlov A. A., Vitel Y., Ignjatovic L. M. 2009, *High Temperature*, 47, 5
- Mihalas D. 1978, in *Stellar Atmospheres*, San Francisco
- Sobel'man I. I. 1979, in *Atomic Spectra and Radiative Transitions*, Springer Verlag, Berlin
- Vitel Y., Gavrilova T. V., D'yachkov L. G. et al. 2004, *JQSRT*, 83, 387

## Trace element study in Tisa River and Danube alluvial sediment in Serbia

Sanja M. SAKAN<sup>1</sup>, Nenad M. SAKAN<sup>2</sup>, and Dragana S. ĐORĐEVIĆ<sup>3</sup>

### Abstract

The contaminated sediment serves as a long-term source of toxic elements, since that mobility and transport in the environment of these elements are strongly influenced to associated solid phase. In this study, the modified Tessier sequential extraction procedure was applied for the fractionation of Cd, As, Hg, Cu, Zn, Cr, Pb, Ni and V in the sediments (Tisa River and canal sediments - Danube alluvial formation), to obtain an overall classification of trace element pollution in these areas through its spatial distribution. Investigations of this region are important due to the widespread occurrence of metal mining activities throughout the Tisa and Danube drainage basins and possibilities of contamination with toxic elements at studies localities. Five steps of the sequential extraction procedure partitioned elements into CH<sub>3</sub>COONH<sub>4</sub> extractable (F1), NH<sub>2</sub>OH•HC carbonate extractable and easily reducible (F2), H<sub>2</sub>C<sub>2</sub>O<sub>4</sub>/(NH<sub>4</sub>)<sub>2</sub>C<sub>2</sub>O<sub>4</sub> moderately reducible (F3), H<sub>2</sub>O<sub>2</sub>-HNO<sub>3</sub> organic extractable (F4), and HCl acid soluble residue (F5). Analyses of the extracts were performed by flame atomic absorption spectrometry. To indicate the degree of risk of toxic elements, risk assessment code and contamination factor have been used. The results of partitioning study indicate that more easily mobilized forms (metals in adsorbed/exchangeable/carbonate forms or bound to amorphous Fe and Mn oxyhydroxides and Fe and Mn oxides) were predominant for copper, zinc, cadmium and lead, which can be used as indicators for input from anthropogenic source. In contrast, the largest amount of chromium and nickel were associated with the inert fraction, which reduced their solubility and rendered them immobile under natural conditions and indicative of natural origins. Most of remaining portion of metals was bound to ferromanganese oxides fraction. It is concluded that sequential extraction results proved useful to distinguish between anthropogenic and geochemical sources of elements in the sediments.

**Key Words:** Sequential extraction, Modified Tessier procedure, Metals, Metalloids, Risk assessment code

### 1 Introduction

Numerous human activities, including municipal, industrial, commercial and agricultural operations, release a variety of toxic and potentially toxic pollutants into the environment. Within the urban environment, where these activities are especially intense, emissions of both metal and organic pollutants are often vastly accelerated, inevitably rendering the urban environment particularly susceptible to environmental degradation and contamination (Wong et al., 2006).

Contaminants originating from urban, industrial and agricultural activities, atmospheric deposition and from natural geological sources may accumulate in sediments up to several times the background concentrations and may serve as potential storage from both the inorganic and organic contaminants (Sultan and Shazili, 2010). In recent years, the rapid development of industry and agriculture has resulted in increased pollution of heavy metals which are a significant environmental hazard for invertebrates, fish, and humans (Yi et al., 2008).

The toxicity and fate of toxic elements in sediments is dependent on their chemical form and therefore the quantification of the different forms of elements is more meaningful than an estimation of their total concentrations. Metals are bound to different sediment fractions, with the strength of the binding determining their bioavailability and the risk associated with their presence in the investigated system. The strength values can, therefore, give a clear indication of sediment reactivity, which in turn allows an assessment of the risk connected with the presence of metals in the environment (Jain, 2004). In the absence of anthropogenic influences, trace elements in sediments are mainly associated with silicates and primary minerals and, therefore, have limited mobility. Chemical elements introduced from human activity show greater mobility, and are associated with other sediment phases, such as carbonates, oxides,

<sup>1</sup> Dr., ICTM, Department of Chemistry, University of Belgrade, Njegoševa 12, P. O. Box 815, 11001 Belgrade, SERBIA. Tel.No. +381 11 3336 801, Fax No. +381 11 2636 061. Corresponding author, E-mail: [ssakan@chem.bg.ac.rs](mailto:ssakan@chem.bg.ac.rs)

<sup>2</sup> Dr., Institute of Physics, University of Belgrade, 11081 Belgrade, P.O. Box 68, SERBIA, E-mail: [nsakan@ipb.ac.rs](mailto:nsakan@ipb.ac.rs)

<sup>3</sup> Dr., ICTM, Department of Chemistry, University of Belgrade, Njegoševa 12, P.O. Box 815, 11001Belgrade, SERBIA. E-mail: [dragadj@chem.bg.ac.rs](mailto:dragadj@chem.bg.ac.rs)

Note: The original manuscript of this paper was received in Apr. 2011. The revised version was received in Mar. 2013. Discussion open until June 2014.

hydroxides and sulfides (de Andrade Passos et al., 2010).

During recent years, the pollution of soils and sediments by metals has attracted a lot of attention of the scientific community (Bourenane et al., 2010; Acosta et al., 2011; Lin et al., 2011; Planojević et al., 2011; Relić et al., 2011; Varol, 2011; Shikazano et al., 2012; Varol and Şen., 2012).

An approach that has been widely applied is the fractionation of elements (or species) of interest into operationally defined forms under the sequential action of different extractants. Most of these are based on the scheme introduced by Tessier (Relić et al., 2005; Sakan et al., 2007) and the BCR protocol (Baig et al., 2009; Rodríguez et al., 2009; Devesa-Rey et al., 2010; Vasile and Vlădescu, 2010). The selective extractants used in sequential extraction procedures are aimed at the simulation of conditions whereby trace elements associated with certain components of the solids can be released. These operationally defined forms can help in an estimation of the amounts of metals and metalloids in different fractions that could be mobilized due to changes in chemical the properties of the responsible matrix. The method of sequential extraction is based on the successive application of extraction solvents with increasing strength for each subsequent phase of the extraction. Sorbed heavy metals could be displaced from the geochemical phases through the use of these extracting agents.

In some studies (Perin et al., 1985; Jain, 2004; de Andrade Passos et al., 2010; Varejão et al., 2010), risk assessment codes (RAC) were used to assess environmental risks and estimate possible damage to organisms caused by contaminated sediments. The RAC classification defines risk levels as zero, low, medium, high and very high (Jain, 2004). This criterion (RAC) indicates that sediment which releases less than 1 % of the total metal in exchangeable and carbonate fractions shall be considered safe for the environment. On the contrary, sediment releasing more than 50 % of the total metals in the same fractions must be considered highly dangerous as the pollutants can easily enter the food chain (Perin et al., 1985).

The present paper presents the distributions by fractions of the trace elements Cd, As, Hg, Cu, Zn, Cr, Pb, Ni and V in the Tisa River sediment and alluvial sediments from the Danube, which were taken in the industrial zone of Pančevo. Interpretation of results was based on the reduction of element bioavailability or mobility at each successive extraction step. The risk assessment code was determined for each element. Investigations of this region are significant due to the widespread occurrence of metal mining activities throughout the Tisa (Nguyen et al., 2009) and Danube drainage basins (Bird et al., 2010). In accordance with results (Bird et al., 2010), the Danube drainage basin provides a clear example of the challenges to catchment and water resource management posed by point and diffuse-source release of contaminant metals associated with mining and metallurgy, as well as with other industrial and municipal sources.

## 2 Research area and methods

### 2.1 Research area

Representative sediments of the study area were taken at two locations. One part of the samples was sediment of the Tisa River and its tributaries, and the second part were alluvial sediments from the Danube, which were taken in the industrial zone of Pančevo. The drainage basin system of the River Danube covers an area exceeding 800,000 km<sup>2</sup> and incorporates 14 countries. This drainage basin contains a number of major centres of base precious metal mining with ore deposits associated with volcanic rocks of varying ages and lithologies (Bird et al., 2010). Through the River Danube drainage basin, the mining and processing of metal ores lead to point-source release of contaminant metals (Cd, Cu, Pb, Zn) and As to the local surface drainage network (Bird et al., 2010). The investigated alluvial sediments were taken from the canal located in the industrial zone south-east of the City of Pančevo (44°52'15" north, 20°38'25" east), about 15 km east of Belgrade (Fig. 1). Pančevo is an industrial town, located in South Vojvodina, at the confluence of the Tamiš and the Danube Rivers. It is a centre of commercial and industrial activities. The most important economic industries in Pančevo are crude oil processing, HIP Petrochemical Complex, fertilizers (Nitrogen Plant), the textile and fashion industry and agriculture. Industrial complex is located at the southern end of the city of Pančevo, the so-called "South zone industrial complex" (SZIC), 20 km to the northeast of Belgrade (Planojević et al., 2011). The SZIC complex includes a petrochemical factory (HIP Petrohemija), an oil Refinery (NIS Rafinerija, Pančevo) and chemical fertilizers factory (HIP Azotara). Potential source of pollutants for alluvial sediments is related to automobile exhaust.

The Tisa (Tisza) River is the longest tributary (977 km) of the Danube River, also having the largest drainage basin (157,200 km<sup>2</sup>), which is shared by five countries: Ukraine, Romania, Slovakia, Hungary and Serbia (Laszlo et al., 2000). The upper Tisa River, flowing through Hungary, has been subjected to severe metal pollution due to mining activities and major industrial complexes in Romania, near the border of Romania with Hungary. Heavy floods, which occur regularly due to snow-melting and intensive precipitation, are a great potential risk for the enhancement of pollution by metals *via* the leaching of mine tailings, which are stocked near to river banks, as well as the spreading of the contamination from the river bed and further downstream (Nguyen et al., 2009). The largest recent accidental pollution of the Tisa River occurred in 2000, first during the night between 30th and 31st of January, at the site of Baia Mare in Romania, caused by the breaking of the dam of the flotation spoil banks of the gold mine, which caused the spilling of water and silt with a high concentration of cyanides and heavy metals. The second accidental pollution of the River Tisa occurred on March 10th, at Baia Borsa. The dam of the waste reservoir Novat-Baia Borsa broke, causing the leakage of

20,000 tons of wastewater and industrial silt into the River Viso, a tributary of the Tisa River. The silt contained high concentrations of zinc, iron and lead. Anthropogenic impact over territory is also caused by permanent pollution (industrial activities, municipal sewage discharges, agriculture). The Tisa is an international river and from its confluence with the Danube, the pollution is transmitted towards the Black Sea.

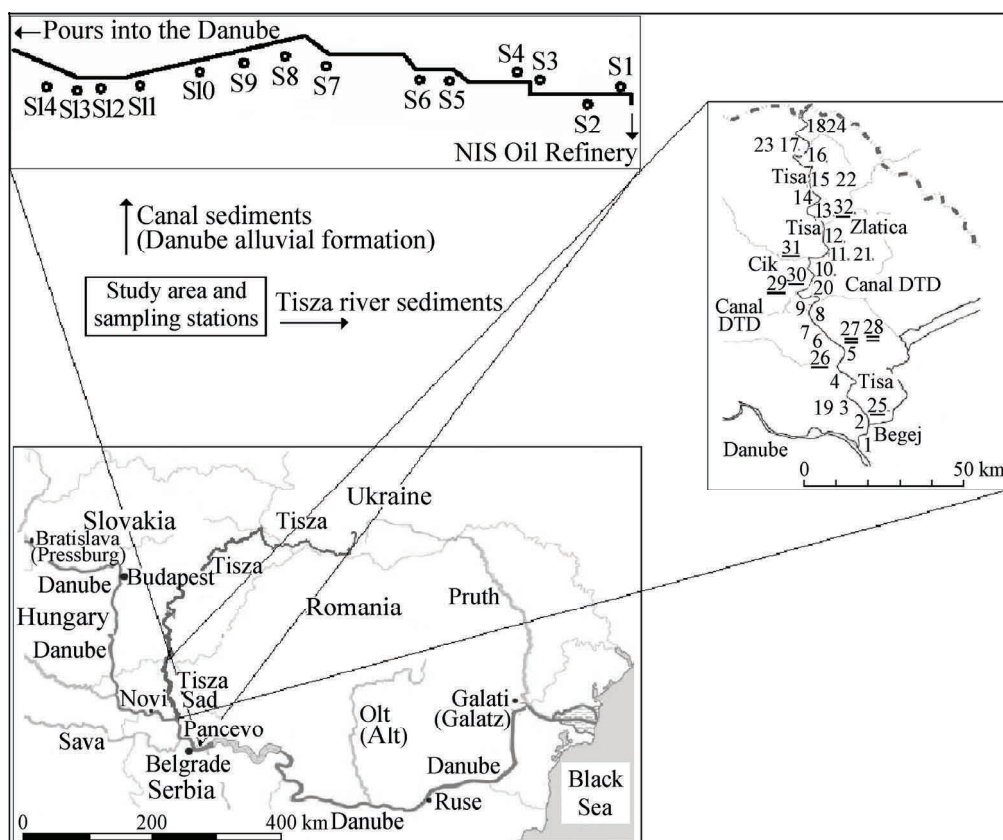


**Fig. 1** Sampling stations and investigated area. Sampling sites along the Tisa river are shown as numbers in respect to the distance from the Tisa mouth, as follows: (a) surface sediments - 1 (0 km), 2 (10 km), 3 (21 km), 4 (30 km), 5 (40 km), 6 (50 km), 7 (60 km), 8 (64 km), 9 (70 km), 10 (80 km), 11 (90 km), 12 (100 km), 13 (110 km), 14 (120 km), 15 (130 km), 16 (140 km), 17 (150 km), and 18 (158 km); (b) buried sediments - 19 (21 km), 20 (70 km), 21 (90 km), 22 (130 km), 23 (150 km), and 24 (158 km), and (c) Tisa tributaries and pools, surface sediments: 25 (Begej), 26 (Jegricka), 27 (Čikos pool), 28 (Okanj pool), 29 (Canal BB), 30 (Mrtva Tisa), 31 (Čik), and 32 (Zlatica). On the figure, samples of tributaries are underlined and the pools are underlined twice. Sampling sites for canal sediments (Danube alluvial formation) are marked as S1 to S14 (14 drill-holes).

## 2.2 Sampling and sample preservation

The samples of alluvial sediments were taken in August and September of 2001 along the canal which begins at the Oil Refinery Pančevo and passes through different industrial complexes. A pipeline for wastewater and atmospheric water, which begins at the Pančevo Oil Refinery, is placed in this canal and water from the pipeline flows into a wastewater canal that flows into the Danube River. The samples were taken from 14 drill-holes (marked as S1–S14) at different depths, up to 5 m. The drill-hole (DH) denoted S1 is nearest to the Refinery and S14 is nearest to the entrance of the canal into the Danube River (Fig. 1).

For the present investigations, the Serbian part of the Tisa watershed was selected. Sediment samples were collected in the period of July, 2<sup>nd</sup> – 17<sup>th</sup>, 2001, from 32 locations of the Tisa River system in Serbia. The locations of the 24 sampling sites of the River Tisa [18 surface sediments (0–5 cm) and 6 buried sediments (6–30 cm)] and 8 sampling sites of tributaries and pools [surface sediments (0–5 cm)] are presented in Fig. 1. The samples of surface sediments were collected using a plastic scoop, and the samples of buried sediments were collected by a corer made of PVC tubes of 10 cm in diameter and 60 cm in length. After sampling, the sediment samples were packed in pouches and frozen in order to prevent changes in chemical composition of the sediment.

Since that the same method was applied to the different types of sediment that had a similar geochemical background, but different sources of contamination, it was expected that the results would highlight the importance of the application of sequential extraction to assess risks connected with the presence of metals in different environments.



### 2.3 Determination of the metal contents

The sequential extraction procedure applied in the present investigation to determine metal fractionation in the sediments (modified Tessier procedure) is described elsewhere (Polić and Pfendt 1992; Relić et al., 2005; Sakan et al., 2007).

The extractants and operationally defined chemical fractions applied in this research were as follows:

(F1) The first step (exchangeable fraction): 10 g sediment sample was extracted with 1 M  $\text{CH}_3\text{COO}(\text{NH}_4)$ ;

(F2) The second step (represents metals bound to carbonates and easily reducible phases): extractant 0.6 M HCl and 0.1 M  $\text{NH}_2\text{OH}\cdot\text{HCl}$ .

(F3) The third step (metals bound to moderately reducible phases): a mixture of 0.2 M  $\text{H}_2\text{C}_2\text{O}_4/(\text{NH}_4)_2\text{C}_2\text{O}_4$  was used as the extractant;

(F4) The fourth step (metals bound to organic matter and sulphides): extractant 30 %  $\text{H}_2\text{O}_2$  adjusted to pH 2.0 with  $\text{HNO}_3$ ;

(F5) The fifth step (residual fraction): extractant 6 M HCl.

The main purposes of each extraction phase are described as follows: the first fraction (F1) of the extraction is defined as the 'Exchangeable fraction', in which the most mobile portion of metals (adsorbed and ion-exchange bound) are expected to be dissolved; in the second fraction (F2), the dissolution of carbonates occurs and the heavy metals, which are precipitated or co-precipitated, are released. Besides the carbonates, the dissolution of manganese oxides and the amorphous oxides of iron takes place in the second phase; metals are specifically adsorbed or co-precipitated. This phase is called the 'easily reducible phase' or the 'Carbonate and Mn-oxide fraction'; in the third fraction (F3), the stronger reduction dissolvent is applied and the dissolution of amorphous and partially crystalline oxides of iron occurs. This phase is called the 'stronger reducible phase' or 'Fe-oxides fraction'; the degradation of the organic substances and sulfides occurs in the fourth fraction (F4). In the organic fraction, the metals are complexed and adsorbed, and become available through oxidation. This phase is called the 'oxidation phase' or 'Organic fraction and sulfides'. Metals bound in carbonate and exchangeable, Fe-Mn oxide, and organic fractions are most likely to mobilize from sediments if oxygen or the geochemical conditions change in surface water, and hence are more available for food chain.

In the final, the fifth fraction (F5), the degradation of crystalline iron oxides occurs and the metals bound to them are released. This phase is called the 'Residual fraction'. The heavy metals are strongly bound in the crystal lattices of minerals, and have low mobility.

All the chemicals used in this paper were of analytical reagent grade. All glassware and plastic material employed had previously been treated for 1 week with 2 M nitric acid, rinsed with distilled water and then with ultra pure water.

For each sequential extraction series, 10.00 g of defrosted sediment was taken without drying in order to avoid chemical transformation due to chelating, oxidation processes, etc. Control samples were processed for each extraction step. The solid/liquid ratios was kept as close to 1:45 as possible during the extraction of the first, second, and third fractions.

Flame atomic absorption spectrometry (FAAS) was used to determine the levels of the trace elements (SpectraAA55 Varian spectrophotometer, equipped with a hydride vapour system). The wavelengths used in these analyses were: 232.0 nm for Ni, 213.9 nm for Zn, 324.7 nm for Cu, 217.0 nm for Pb, 357.9 nm for Cr, 228.8 nm for Cd, and 318.5 nm for V. The hydride system was applied in this investigation for the determination of the content of As (193.7 nm) and Hg (253.7 nm). External standard solutions were prepared from 1000 mg  $\text{L}^{-1}$  stock metal solutions. For minimized interferences, a multi-element standard stock solution was prepared in which the ratios of the metals in the multiple element calibration standards were analogous to their ratios in the samples. These multi-element standards and blanks were prepared in the same matrix as employed for the extraction to minimize matrix effects and for background correction (Relić et al., 2005). In order to simulate the composition of the investigated samples, the multi-element standards also contained elements which were not determined. Possible interference effects were minimized in this manner. The calibration was checked every 10–12 samples. As a quality control, duplicate analyses were performed on all samples and the precision was controlled. The relative standard deviations of the means of duplicate measurement were less than 10 %. The values of limit of detection (*DL*) for each determined element, expressed in  $\mu\text{g ml}^{-1}$ , were: Cr (0.03), Zn (0.005), Pb (0.05), Cd (0.01), Ni (0.05), Cu (0.02), V (0.5), As (0.002), and Hg (0.001). All concentrations values below the detection limit were replaced by half of the *DL*, as suggested by Reimann and Filmozer (1999) and Relić et al., (2005). The moisture content of each sample was determined by drying a separate 1 g sample in an oven ( $105 \pm 2$  °C) to constant weight. From this, a correction to dry mass was obtained, which was applied to all reported element concentrations.

### 2.4 Environmental implications/ Risk assessment code

The Risk Assessment Code (RAC, Table 1) was determined based on the percentage of the metal content in the first fraction (% F1), where binding is weak and the metals pose a greater risk to the environment (de Andrade Passos et al., 2010). Since in the first fraction. ammonium acetate was used as the extractant, the application of which leads to a noticeable dissolving of carbonates (Schoer and Eggersgluess, 1982), and in the second phase of extraction (F2), metals

bound to carbonates and easily reducible phases are released, it is possible to conclude that the application of ammonium acetate in the first fraction did not completely dissolve the carbonates, but only part.

**Table 1** Risk assessment code

| Risk           | Metal in carbonate and exchangeable fractions (%) |
|----------------|---|
| No risk        | < 1   |
| Low risk       | 1-10  |
| Medium risk    | 11-30   |
| High risk      | 31-50   |
| Very high risk | 75  |

### 3 Results and discussion

All the sediment samples collected were estimated, to confirm the fraction contents of investigated elements by the five-step sequential extraction procedure. The distributions by fractions of different elements are given in Table 2, Table 3, and Fig. 2. The Tables show the average content of extracted elements by fraction of the sequential extraction. The results are presented in the form of the arithmetic mean  $\pm$  standard deviation for each extraction fraction for the Tisa sediment (Table 2) and alluvial sediment from Pančevo (Table 3). Based on the average contents by fraction of the extracted elements, the percentage of the extracted element in each fraction was calculated and the results are shown in Fig. 2. The discussion of the results of the distribution of the elements by fraction is presented separately for each element.

**Table 2** Distribution by fractions in the Tisa sediment ( $\text{mg kg}^{-1}$ )

|    | F1 fraction     | F2 fraction       | F3 fraction     | F4 fraction     | F5 fraction       |
|----|-----------------|-------------------|-----------------|-----------------|-------------------|
| Cu | $3.34 \pm 2.54$ | $21.7 \pm 15.4$   | $33.1 \pm 10.4$ | $1.96 \pm 1.69$ | $14.8 \pm 5.3$    |
| Cr | $0.44 \pm 0.42$ | $2.08 \pm 0.95$   | $4.74 \pm 1.41$ | $1.42 \pm 0.82$ | $7.64 \pm 2.70$   |
| Zn | $19.1 \pm 19.1$ | $158 \pm 96.5$    | $64.3 \pm 21.1$ | $3.75 \pm 3.13$ | $52.0 \pm 17.2$   |
| Pb | $1.41 \pm 0.72$ | $32.5 \pm 20.8$   | $14.4 \pm 8.5$  | $0.60 \pm 0.36$ | $5.69 \pm 4.58$   |
| Cd | $0.85 \pm 0.52$ | $1.04 \pm 0.66$   | $0.73 \pm 0.58$ | $0.15 \pm 0.08$ | $0.48 \pm 0.22$   |
| Ni | $0.71 \pm 0.36$ | $6.09 \pm 2.71$   | $11.1 \pm 6.1$  | $2.86 \pm 1.77$ | $10.4 \pm 4.8$    |
| V  | $7.20 \pm 3.98$ | $17.4 \pm 9.0$    | $54.6 \pm 16.0$ | $5.90 \pm 1.64$ | $93.7 \pm 88.7$   |
| As | <dl*            | $0.68 \pm 0.66$   | $0.06 \pm 0.10$ | <dl             | $0.11 \pm 0.14$   |
| Hg | <dl             | $0.020 \pm 0.012$ | <dl             | <dl             | $0.098 \pm 0.067$ |

\* below the detection limit

Cu: Copper is a very important element, which could influence the metabolism of the human body and it is also a nutritional element for living beings. But if the intake is too much, it will cause toxicity. The largest Cu content in both types of sediment was extracted in the third stage of extraction (moderately reducible step), in which the partial dissolution of crystalline Fe oxides occurs. For the Tisa sediments, a significant of Cu was extracted in the third and second and slightly less in the fifth extraction fraction. In the Pančevo sediments, Cu was significantly extracted in the third and fifth stage of extraction. Generally, Cu was bound in more mobile fractions in the Tisa River sediments in relation to the sediments from Pančevo. This distribution by the fractions is the result of intensive interactions that occur between the river water and river sediments and the changing environmental conditions (pH, *Eh*) in the Tisa samples with respect to the interactions between the groundwater and alluvial sediment. In addition, this distribution indicates the likely existence of anthropogenic sources of Cu in the Tisa sediments, which is consistent with results (Prusty et al., 1994) that binding of Cu with carbonate minerals and oxides of iron and manganese indicates contamination of the river system from basic (primary) mining. Under reducing conditions, decomposition of Fe and Mn oxides results in the subsequent remobilization of  $\text{Fe}^{3+}$  and  $\text{Mn}^{4+}$  in the aquatic system.

Zn: Most of Zn from the Tisa sediment was extracted in the second extraction fraction (more than 50 %), then in the third and fifth phases of extraction, while from the Pančevo sediments, more than 50 % of the Zn content was extracted in the fifth phase of the extraction, and some in the third and second extraction stages. This distribution is consistent with a common association of this element in the soil, such as association with Fe oxides and Mn, Al and clay minerals. It can be concluded that in the Tisa River sediments, Zn is significantly bound to more mobile fractions in relation to the Pančevo sediment. Fe and Mn oxides are of great importance in binding Zn, and the mobile fractions of these oxides are relevant Zn substrates in the Tisa sediments. Hydrous oxides of manganese and iron are the well known "sinks" in the surface environment for heavy metals. In addition, this distribution, which is consistent with the results of other authors for polluted river systems (Prusty et al., 1994), indicates the presence of anthropogenic sources of the elements in the Tisa sediments.

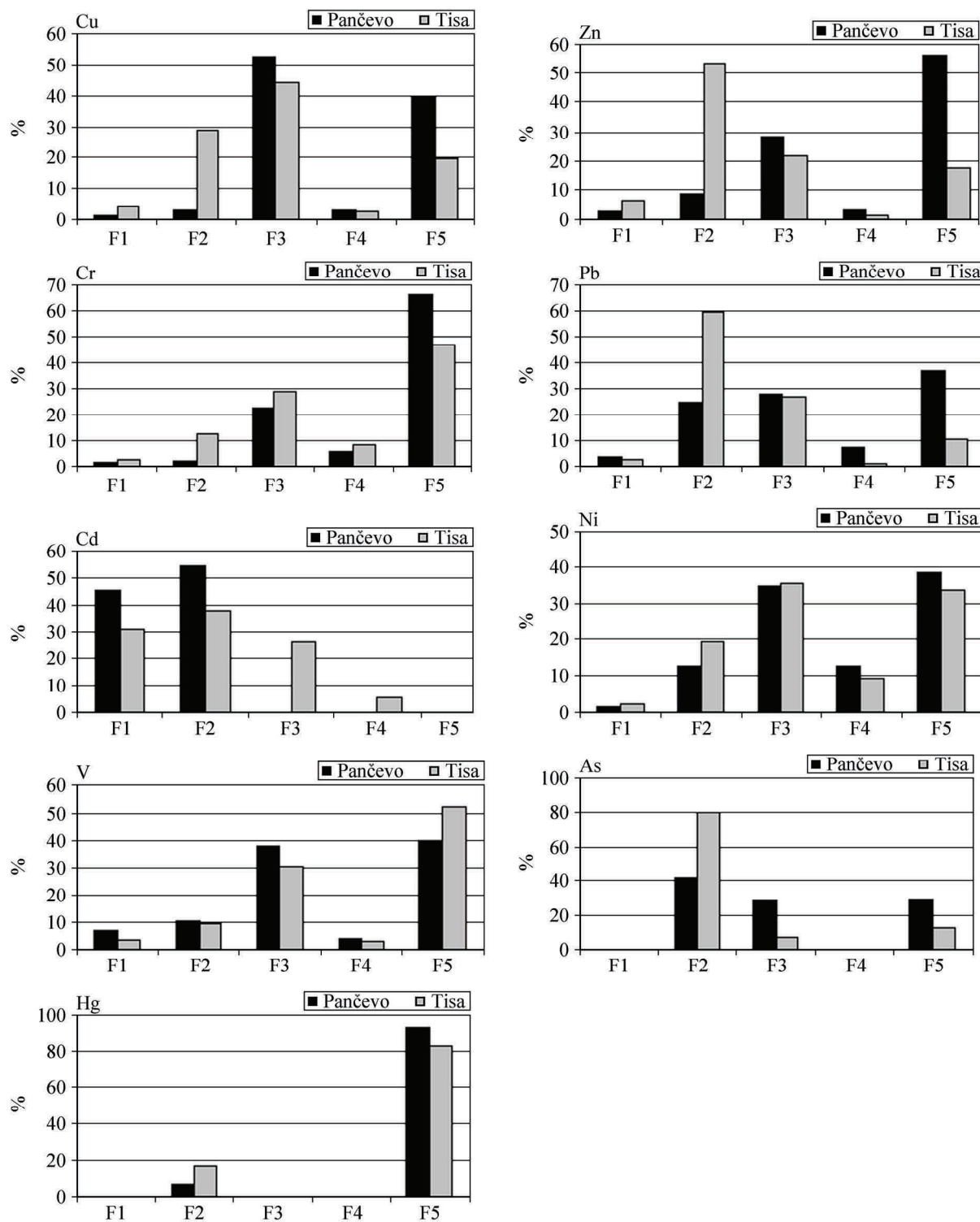


**Fig. 2** The distribution of trace element content by fraction of the sequential extraction. Explanation: along the x-axis are shown fraction of extraction (numbered from F1 to F5); along the y-axis is shown the contents of extracted element, expressed in % (The percentage element distribution by fractions was calculated as the average content of the extracted element in each fraction with respect to the total content of the extracted element).

Cr: The largest percentage of Cr was extracted in the third and the fifth extraction fraction (Fe oxides, partially crystallized and crystallized), while in the other fractions, lower amounts of this element were extracted. Part of the Cr is bound in the second and fourth phase, while the content of exchangeable Cr was negligible. This distribution is consistent with data from the literature (Kabata-Pendias and Pendias, 1989) that showed that most of Cr in soil is in the

form of  $\text{Cr}^{3+}$  which enters into the structure of minerals and forms different  $\text{Cr}^{3+}$ - and  $\text{Fe}^{3+}$ - oxides. Over 60 % of Cr in the sediments from Pančevo was extracted in the fifth stage and over the 40% in the Tisa sediment. This distribution suggests the importance of the oxide and silicates for chromium binding, as well as significant geochemical origin of chromium in the investigated sediments. The relative content of a metal in the residual fraction can be used as a measure of the contribution of natural sources, and also of the degree of contamination of the investigated sediment, with a higher percentage indicative of lower levels of pollution.

**Table 3** Distribution by fractions in the Pančevo sediment ( $\text{mg kg}^{-1}$ )

|    | F1 fraction     | F2 fraction       | F3 fraction     | F4 fraction     | F5 fraction       |
|----|-----------------|-------------------|-----------------|-----------------|-------------------|
| Cu | $0.29 \pm 0.19$ | $0.50 \pm 1.09$   | $8.80 \pm 6.83$ | $0.48 \pm 0.58$ | $6.68 \pm 11.48$  |
| Cr | $0.26 \pm 0.14$ | $0.31 \pm 0.18$   | $2.88 \pm 1.54$ | $0.74 \pm 0.30$ | $8.32 \pm 5.06$   |
| Zn | $1.52 \pm 5.05$ | $4.86 \pm 11.46$  | $16.2 \pm 11.4$ | $1.76 \pm 2.74$ | $31.4 \pm 20.1$   |
| Pb | $0.43 \pm 0.23$ | $2.90 \pm 8.23$   | $3.25 \pm 2.12$ | $0.80 \pm 0.87$ | $4.27 \pm 4.00$   |
| Cd | $0.05 \pm 0.03$ | $0.06 \pm 0.03$   | $0.61 \pm 0.16$ | $0.07 \pm 0.01$ | $0.28 \pm 0.11$   |
| Ni | $0.31 \pm 0.14$ | $2.61 \pm 2.08$   | $7.32 \pm 3.78$ | $2.63 \pm 2.32$ | $8.04 \pm 4.81$   |
| V  | $6.63 \pm 4.19$ | $9.88 \pm 10.22$  | $35.3 \pm 14.2$ | $4.18 \pm 2.52$ | $37.4 \pm 36.2$   |
| As | <dl*            | $0.10 \pm 0.25$   | $0.07 \pm 0.11$ | <dl             | $0.07 \pm 0.10$   |
| Hg | <dl             | $0.004 \pm 0.003$ | <dl             | <dl             | $0.057 \pm 0.064$ |

\* below the detection limit

Pb: Most of the Pb was extracted in the second, third and fifth extraction fractions, and a lower amount in the fourth and sparingly in the first fraction. The distribution of Pb by fractions was different in the investigated sediments. In the Tisa sediments, most important was the binding of Pb in the mobile fractions (about 60 % in the second and 20 % in the third fraction), which indicates that Pb is bound to amorphous and partially crystallized Fe and Mn oxides, as well as carbonate. This distribution is consistent with data from the literature (de Andrade Passos et al., 2010). The obtained results indicate that Pb can easily be mobilized from the sediments with changing conditions in the external environment. This distribution is characteristic of the lake and river sediments. In the Pančevo sediments, most of the Pb was related to the fifth phase (crystalline Fe oxides and silicates), then the third and second (oxide and carbonate fractions), which indicates that Pb was significantly bound in the less mobile fractions. These distributions indicate a significant anthropogenic origin of Pb in the investigated sediments, especially in the Tisa sediments. Lead should be managed seriously for large quantity and high percentage of reactive fractions. In addition, the distribution may indicate to the possibility of contamination in the recent past in respect to the time of sampling.

Cd: The largest part of Cd in the Pančevo sediments was extracted in the first and second fraction. In the Tisa sediments, Cd was dominantly extracted in the first and second, and some in the third and fourth fraction. This distribution by fractions is often characteristic for Cd in lake and river sediments (most of the cadmium was bound in exchangeable positions, carbonate fractions and oxides of iron and manganese). This indicates the great mobility of Cd in the Tisa and Pančevo sediments and that cadmium was very active. The present data are consistent with other studies which found that the greatest part of the total cadmium content in the sediments existed in the easily soluble fractions (Vasile and Vlădescu, 2010). Although the mean total amount of cadmium in the sediments was lower than that of other metals, the amount poured into water should be managed. As the amounts increase, the active fractions would be easily released, and would then influence the environment and human beings through the food chain. In addition, there is a possibility of the existence of significant anthropogenic sources of Cd in the investigated sediments, which is especially important for the Tisa sediments, due to the higher content of extracted elements in the Tisa sediment, in respect to the alluvial sediment of Pančevo.

Ni: A quite uniform distribution of Ni by extraction stages was found in both types of sediments, with the maximal amounts extracted in the third, fifth and second fractions. This indicates that oxides (amorphous, partially crystallized and crystallized oxides, especially Fe oxides) and silicates are the most important for Ni binding in the investigated sediments. Small differences existed in the extracted contents in the second and fifth fractions; a higher amount of the element was extracted in the second fraction in the Tisa sediments with respect to the Pančevo alluvial sediments and, a slightly higher percentage content of Ni was extracted in the fifth fraction from the sediment samples from Pančevo. The obtained results show that content of extracted Ni in the residual fraction is much higher than in the non-residual fraction, indicating the Ni originates mainly from crystal material. This result is in accordance with results of de Andrade Passos et al. (2010), which showed that Ni was more associated with the inert fraction, which reduced its solubility and rendered it immobile under natural conditions. The low percentage active fraction was an advantage, to control the pollution in this area. It should also be noted, that unlike the other elements, some percentage of Ni was extracted in the fourth extraction fraction, which means that Ni was also bound to organic substances in the Tisa and Pančevo sediments. The organic fraction released in the oxidizable is not considered very mobile or available since it is thought to be associated with the stable high molecular weight humic substances that release small amounts of metals in a slow manner.

V: Vanadium is a ubiquitous trace metal in the environment, which is an essential trace element for living organisms, but the excessive content is harmful to human beings, animals, and plants. Since that the toxicity, bioavailability, and transport properties of V are highly dependent upon its chemical form, method of sequential extraction is used for extraction of this element. The most significant amounts of V were extracted in the third and fifth fraction, while the amounts extracted in other fractions were below 10 %. It is important to emphasize that, unlike the other elements, V was extracted in the more mobile fractions (1–3) from the Pančevo sediment with respect to the Tisa River sediment. From the Tisa sediment, V was more extracted in the fifth fraction. This indicates that on the Pančevo locality, V has a slightly greater mobility and that there is a significant anthropogenic source of this element. Since the alluvial sediment was sampled near the Pančevo refinery and Petrochemical Complex, this distribution of vanadium may indicate on the existence of contamination with crude oil, since V is often used as tracer of crude oil pollution in various environments (Okay et al., 2008).

As: The dominant content of As from the Tisa sediment was extracted in the second extraction fraction, while a smaller percentage was extracted in the third and fifth fractions. In the alluvial sediments from Pančevo, a fairly consistent content of the element was extracted in all three fractions, with a slightly higher content in the second fraction. This distribution indicates that As is significantly present in the form carbonates, while a part of the As is in the form of oxides. The carbonate nature of As is a consequence of the alkaline reaction of most of the land in Vojvodina. In addition, a significant presence of  $\text{CaCO}_3$  in the soils of Vojvodina was evidenced (Kastori, 1993; Kostic, 2001). It is known that in alkaline soils rich in limestone, As is mainly present in the form of  $\text{Ca}_3(\text{AsO}_4)_2$  (Ferguson, 1990).

Hg: Mercury is one of the most toxic metals and it is listed as a priority pollutant by international agencies. The most important extraction of Hg occurred in the fifth fraction, over 80 %, for both types of sediment, indicating a strong association between Hg and Fe crystalline oxides. These results are consistent with the results of Sánchez et al., (2005), in which it was shown that the highest percentage of Hg from soil was extracted with 6 M HCl (82 %). The high percentage of Hg extracted with 6 M HCl can be explained by strong binding capacity of crystalline Fe oxyhydroxide and dissolution of metacinnabar ( $\text{HgS}$ ) in 6M HCl, which was shown in the literature (Sánchez et al., 2005). Mercury in the fifth fraction suggests that it would be present in the mineral particles, material does not participate in early diagenesis. Some Hg was also extracted in the second fraction, with higher rates in the sediments from Pančevo with respect to the Tisa sediment, which may indicate the importance of carbonate as an Hg substrate in alluvial sediments. The content of extracted Hg in other fractions was negligible, indicating that Hg is not readily available in the examined sediments.

Chemical fractionation differentiates metals of natural origin from those derived from anthropogenic sources. Anthropogenic metals are predominantly found in the most labile sediment fractions, which are vulnerable to small changes in environmental conditions, such as those caused by human activity (de Andrade Passos et al., 2010). The high mobility of Cu, Zn, Pb and Cd in sediments of the Tisa River is based on their common origin from recent mining accidents (January and March, 2000, the Baia Mare and Baia Borsa Accidents in Romania) and mining runoff during the period of industrial development in the Tisa River region. The upper Tisa River, flowing through Hungary has been subjected to severe metal pollution due to mining activities and major industrial complexes in Romania, near the border of Romania and Hungary. An investigation of the Tisa River sediment in Hungary (Nguyen et al. 2009) showed the existence of contamination in the Tisa sediment (contamination with Cu, Zn, Pb, and Cd), which is in accordance with the obtained results for Tisa sediment in Serbia. These elements are the most important elements in environmental pollution. In addition, Bird et al. (2003) and Bird et al. (2010) showed that 19–75 % of Cd and Zn in river channel sediments (Tisa and Mureş catchments, northwestern Romania and eastern Hungary) were present in the "exchangeable" sedimentary phase and the authors pointed out that the Cd and Zn pollution was associated with metal mining activities. The presence of Cd and V in the non-residual fractions in the Pančevo alluvial sediment indicates that these elements mainly originated from anthropogenic sources. The distribution of V may indicate the existence of contamination with crude oil, since the investigated area is near the Pančevo Oil Refinery and Petrochemical Complex.

Fe and Mn oxides are of great importance as a sink for most of the elements (Cu, Zn, Cr, Pb, Ni, V, and As). Elements that are retained in this form may be released from sediment, if there is a change of oxidation state of Fe and Mn and could be a long-term source of contamination.

### 3.1 The distribution of elements by fractions at the sampling sites

The results of the distribution of elements at the sampling sites are given in Fig. 3 (Tisa sediment) and Fig. 4 (Pančevo alluvial sediment). The obtained results show the different distributions of elements, mainly Cu, Zn and Pb in the sediments of the Tisa River and in the sediments of the tributaries and pools. In the Tisa sediment, it can be observed larger content of extracted elements from surface sediment in respect to the buried sediments and sediments from tributaries, primarily, Zn and Cu (first and second fractions), and Zn, Cu and Cd (second fraction). From the buried sediments of the Tisa River, the largest percentage of the elements were extracted in the third fraction, while for elements from tributaries sediments, significant content were extracted in the fifth fraction. Increased content of investigated elements extracted in more mobile fractions, primarily Cu, Zn, and V (sediment sample labeled as 11, International Journal of Sediment Research, Vol. 28, No. 2, 2013, pp. 234–245

surface sediment, 90 km, Tisa), Zn, and Pb (sediment sample 5, surface sediment, 40 km, Tisa), and V, Pb, Cu, and Zn (sediment sample 7, surface sediment, 60 km, Tisa,) indicate on the existence of local sources of metal contamination on this localities.

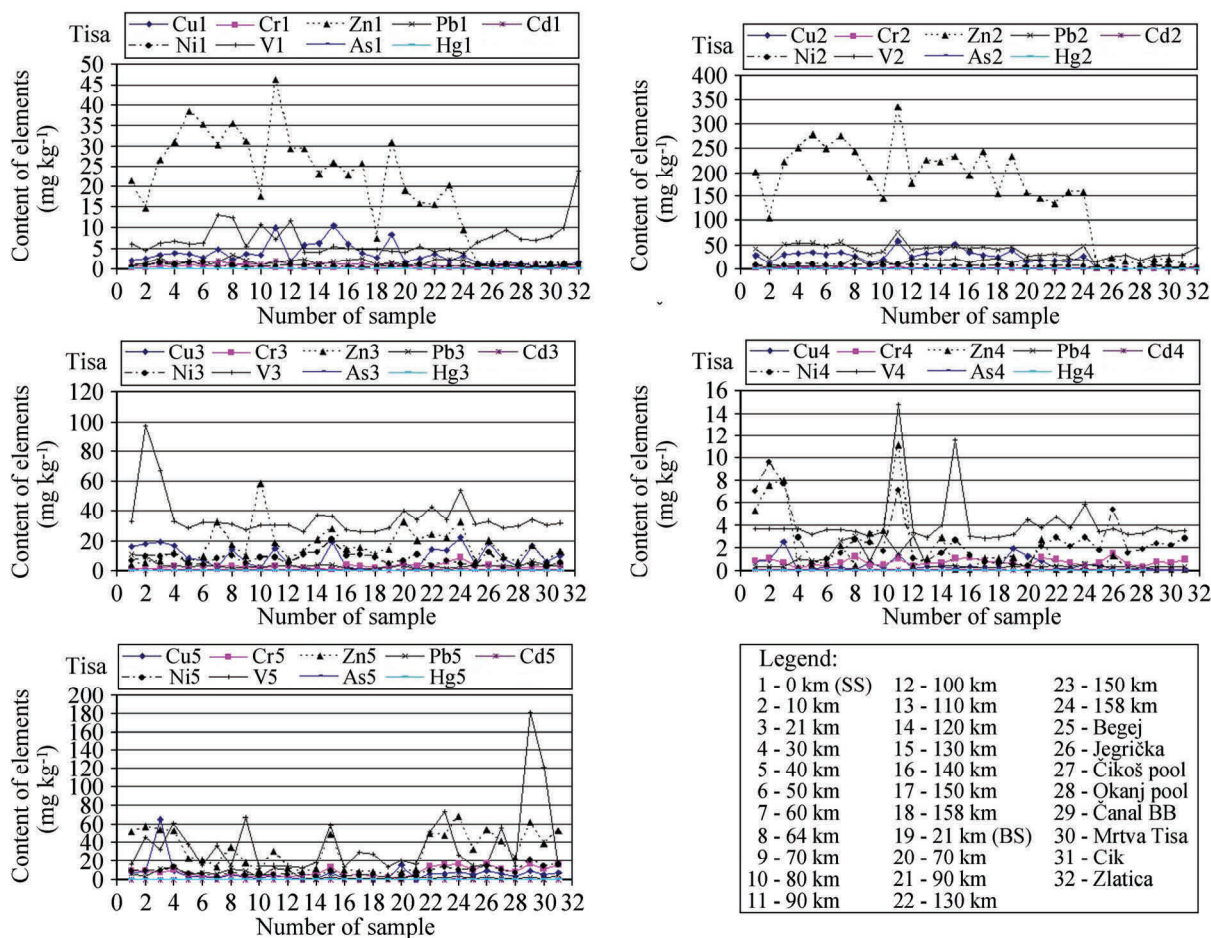


Fig. 3 The distribution of elements by fractions at the different sampling sites (Tisa River sediments)

Generally, the presence of extracted elements (especially Cu, Zn, Pb) in the more mobile fraction of the Tisa sediment in relation to the Tisa tributaries sediment indicates the existence of anthropogenic sources of these elements in the Tisa River watershed. In relation to the contents of the extracted elements from Pančevo sediment, the larger content of vanadium was extracted in relation to other elements. Also, it can be observed an increased content of vanadium in the samples that are closer to the end of the channel, i.e. samples from Petrohemija locality, which may be a consequence of vanadium origin from crude oil, since that investigated area is close to the refinery. Increased content of Zn at the site labeled as 10 (S4/1.0), indicating the presence of local sources of zinc contamination. Significant extraction of Pb in drill-hole located nearest the refinery (samples marked as 1-S1/1.0 and 2-S1/2.4), mainly in second fraction, indicated on the influence of the refinery on Pb content.

### 3.2 Risk assessment code

The results of the risk assessment codes, with values given as percentages of the F1 fraction for the nine trace elements are illustrated in Fig. 5. In general, the sediments show: no risk (for As and Hg), low risk (for Cu, Zn, Cr, Pb, Ni and V), medium risk (for Cd in the Tisa river sediment) and high risk (for Cd in the alluvial sediment from Pančevo) to local environment. The total content of cadmium is low, but its mean total percentage of active fractions is very high, therefore, its input also must be managed meticulously. This suggests that small variations in the environmental conditions could increase the availability of Cd. Due to the toxicity and availability of Cd, this element could pose serious problems to the ecosystem.

### 3.3 Contamination factors

The individual contamination factors ( $C_f$ ) for Cu, Cr, Zn, Pb, Cd, Ni, and V were calculated. These factors are defined as the sum of heavy metal concentrations in the mobile phases (non-residual phases) of the sample divided by the



residual phase content [ $C_f = \sum (\text{step } 1+2+3+4)/\text{residual}$ , step 5]. The lower  $C_f$  values, the higher the relative metal retention (Jamali et al., 2007). The obtained results (Table 4) showed that the relative metal retention was not the same for all of elements. For the Tisa sediment, Pb, Cd, Zn, and Cu presented high values of individual contamination factors, and for sediments from Pančevo, Cd presented high values of contamination factor. It can be concluded that Cr, Ni, and V have a high the relative metal retention in respect to other elements for both types of sediments.

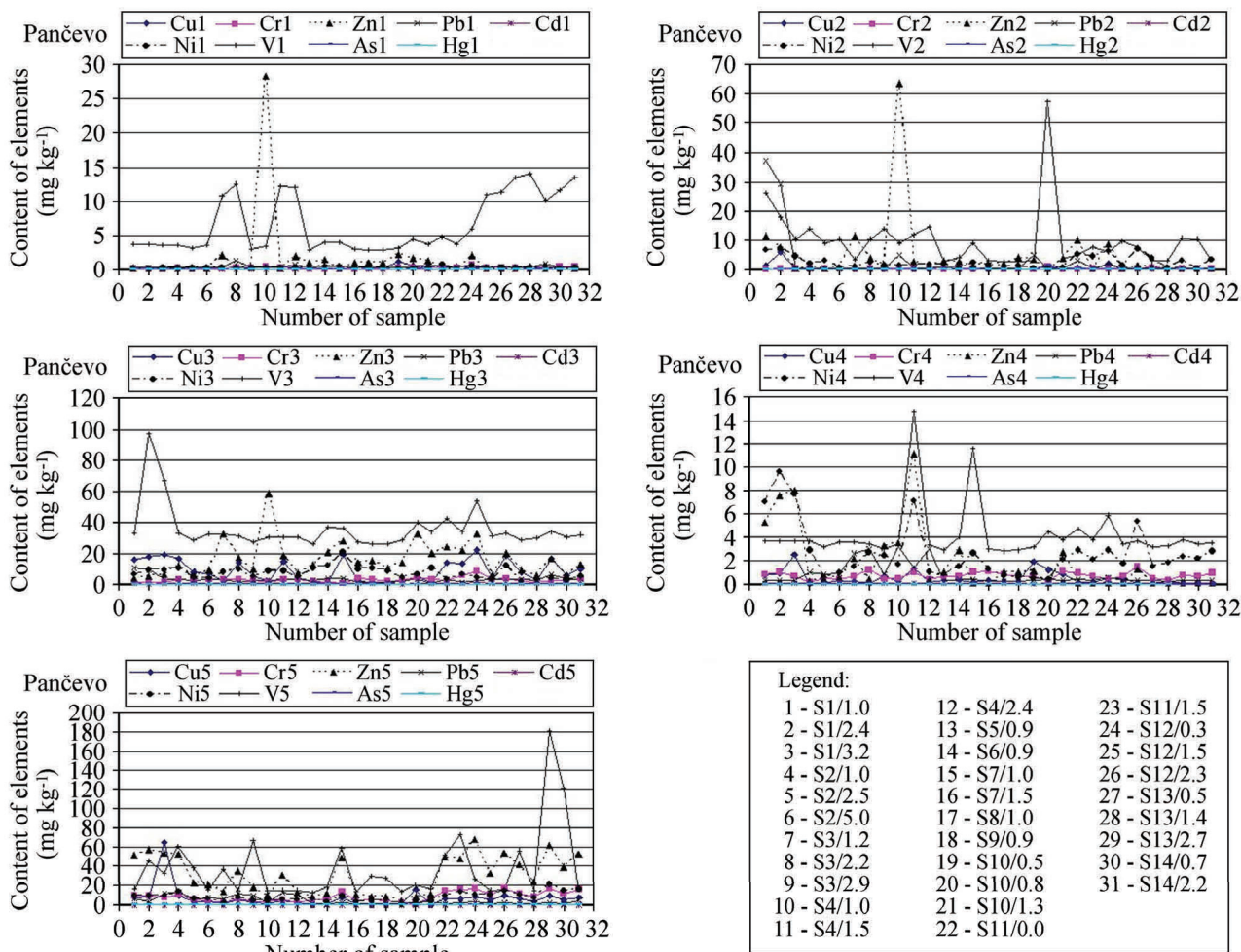


Fig. 4 The distribution of elements by fractions at the different sampling sites (Danube alluvial formation, Pančevo)

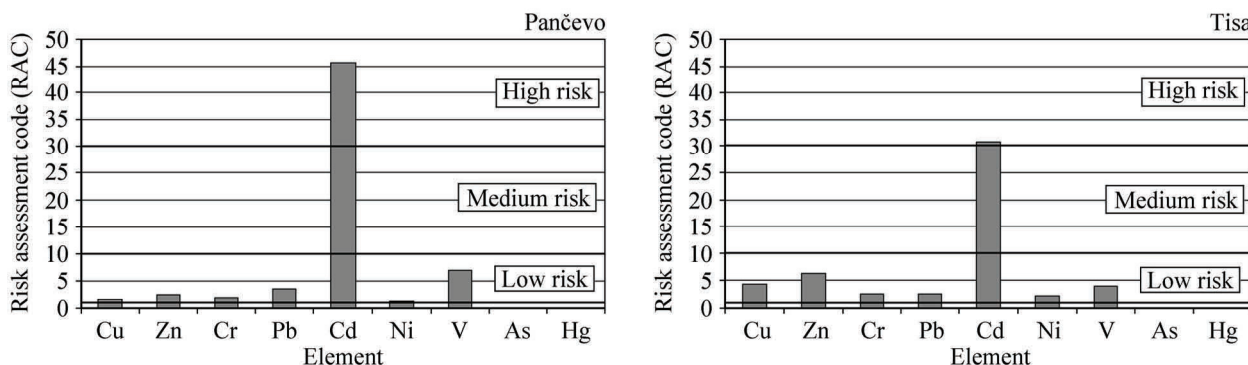


Fig. 5 Risk assessment codes (RAC) for Cu, Zn, Cr, Pb, Cd, Ni, V, As and Hg in the Tisa River sediments and Canal Sediments (Danube alluvial formation, Pančevo)

#### 4 Conclusions

Sequential extraction can be used as a valuable tool to provide information on the mobility, bioavailability and potential toxicity of trace elements in the environment. In this study, five-step sequential extraction procedure was used to fractionate Cd, As, Hg, Cu, Zn, Cr, Pb, Ni and V in the investigated river and canal sediments.



**Table 4** Contaminated factor for each element in investigated sediment

| Element | Contamination factor ( $C_f$ ) |         |
|---------|--------------------------------|---------|
|         | Tisa                           | Pančevo |
| Cu      | 4.06                           | 1.51    |
| Cr      | 1.14                           | 0.50    |
| Zn      | 4.71                           | 0.78    |
| Pb      | 8.60                           | 1.73    |
| Cd      | 5.77                           | 2.82    |
| Ni      | 2.00                           | 1.60    |
| V       | 0.91                           | 1.50    |

From the results of sequential extraction, it can be concluded that the elements presented different distributions in the sediment fractions. The studied elements were present in higher amounts in the residual fraction than non-residual fractions in the Pančevo alluvial sediment, except for Cd and V, indicating that they arise mainly from crystal material. Chromium and nickel were mainly present in the inert fraction, being of detrital and lattice origin and their concentration can be taken as a measure of the contribution by natural sources. The distribution of vanadium in the Pančevo alluvial sediments could be used as indicator for input from anthropogenic sources. Analyses of the sediments showed that Hg preferentially was associated with the crystalline Fe oxides and sulphides. The high mobility of Cu, Zn, Pb, and Cd in sediments of the Tisa River is based on their common origin from mining accidents, and these elements are therefore readily available to aquatic organisms. Obtained results indicate that As is mainly in the form of carbonates and oxides in investigated sediments. The reducible fraction principally contained Cu, Zn, Cr, Pb, Ni, V, and As, due to their strong interaction with oxides and hydroxides of Fe and Mn, and release of these elements from this matrix would most likely be affected by the redox potential and pH status.

The results of sequential extraction were corroborated by the results of risk assessment for selected elements and suggest that high mobility of Cu, Zn, Pb and Cd in Tisa river sediments may be an indicator for the existence of significant anthropogenic sources of these elements. Obtained results demonstrate the high ecological risk and need of an environmental monitoring, supporting the development of an efficient strategy to reduce local pollution and contamination of investigated system.

#### Acknowledgements

This research was supported by the Ministry of Science of the Republic of Serbia, Grant No 172001. The authors are grateful to Prof. Dr. Predrag Polić for guidance throughout this research.

#### References

- de Andrade Passos E., Alves J. C., dos Santos I.S., Alves J. P. H., Garcia C. A. B., and Costa C. S. 2010, Assessment of trace metals contamination in estuarine sediments using a sequential extraction technique and principal component analysis. *Microchemical Journal*, 96, pp. 50–57.
- Acosta J. A., Martínez-Martínez S., Faz A., and Arocena J. 2011, Accumulations of major and trace elements in particle size fractions of soils on eight different parent materials. *Geoderma*, 161, pp. 30–42.
- Baig J. A., Kazi T. G., Ariain M. B., Shah A. Q., Sarfraz R. A., Afridi H. I., Kandhro G. A., and Khan S. 2009, Arsenic fractionation in sediments of different origing using BCR sequential and Single extraction methods. *Journal of Hazardous Materials*, 167, pp. 745–751.
- Bird G., Brewer P. A., Macklin M. G., Balteanu D., Driga B., Serban M., Zaharia S. 2003, The solid-state partitioning of contaminant metals and As in river channel sediments of the mining affected Tisa drainage basin, northwestern Romania and eastern Hungary. *Applied Geochemistry*, 18, pp. 1583–1595.
- Bird G., Brewer P. A., and Macklin M. G. 2010, Management of the Danube drainage basin: Implications of contaminant-metal dispersal for the implementation of the EU water Framework Directive. *The International Journal of River Basin Management*, Vol. 8, No. 1, pp. 63–78.
- Bourennane H., Douay F., Sterckeman T., Villanneau E., Ciesielski H., King D., and Baize D. 2010, Mapping of anthropogenic trace elements inputs in agricultural topsoil from Northern France using enrichment factors. *Geoderma*, 157, pp. 165–174.
- Devesa-Rey R., Díaz-Fierros F., and Barral M.T. 2010, Trace metals in river bed sediments: An assessment of their partitioning and bioavailability by using multivariate exploratory analysis. *Journal of Environmental Management*, 91, pp. 2471–2477.
- Ferguson J. E. 1990, *The heavy elements: Chemistry, environmental impact and health effects*. Pergamon Press Oxford.
- Jain, C.K., 2004, Metal fractionation study on bed sediments of River Yamuna, India. *Water Research*, 38, pp. 569–578.
- Jamali M. K., Kazi T. K., Afridi H. I., Arain M. B., Jalbani N., and Memon A. R. 2007, Speciation study of heavy metals in untreated domestic wastewater sludge by time saving BCR sequential extraction method. *Journal of Environmental Science and Health Part A*, 42, pp. 649–659.
- Kabata-Pendias A. and Pendias H. 1989, *Trace elements in soils and plants*. Mir, Moskva.
- Kastori R. 1993, Heavy metals and pesticides in soil: heavy metals and pesticides in soils of Vojvodina. Faculty of Agriculture, Novi Sad.

- Kostic N. 2001, Distribution and Chemical Speciation of some Heavy Metals in Soils of Vojvodina and Central Serbia. Proceedings of the 10<sup>th</sup> Congress of Yugoslav Soil Sci. Soc., CD copy by Soil Sciences Institute, Belgrade.
- Laszlo F., Csanyi B., and Literathy P. 2000, Cyanide and heavy metals accidental pollution in the Tisza river basin: Consequences on water quality monitoring and assessment. Monitoring Tailor-Made III International workshop on information for sustainable water management. Nunspeet, The Netherlands.
- Lin C. E., Chen C. T., Kao C. M., Hong A., and Wu C. Y. 2011, Development of the sediment and water quality management strategies for the Salt-water River, Taiwan. *Marine Pollution Bulletin*, 63, pp. 528–534.
- Nguyen H. L., Braun M., Szaloki I., Baeyens W., Van Grieken V., and Leermakers M. 2009, Tracing the Metal Pollution History of the Tisza River Through the Analysis of a Sediment Depth Profile. *Water, Air, and Soil Pollution*, 200, pp. 119–132.
- Okay O. S., Pekey H., Morkoç E., Başak S., and Baykal B. 2008, Metals in the surface sediments of Istanbul Strait (Turkey). *Journal of Environmental Science and Health, Part A* 43, pp. 1725–1734.
- Perin G., Craboledda L., Lucchese M., Cirillo R., Dotta L., Zanette M. L., and Orio A. A. 1985, Heavy metal speciation in the sediments of Northern Adriatic Sea—a new approach for environmental toxicity determination. In: Lekkas TD, editor. *Heavy metal in the environment*, 2, pp. 45–46.
- Planojević I., Teodorović I., Bartova K., Tubić A., Jurca T., Kope W., Machat J., Blaha L., and Kovačević R. 2011, Wastewater canal Vojlovica, industrial complex Pančevo, Serbia – preliminary ecotoxicological assessment of contaminated sediment. *Journal of the Serbian Chemical Society*, Vol. 76, No. 3, pp. 459–478.
- Polić P. and Pfindt P. 1992, Iron and manganese oxides as dominant nickel substrates in the Novi Beograd aquifer. *Journal of the Serbian Chemical Society*, Vol. 57, No. 10, pp. 697–703.
- Prusty B. G., Sahu K. C., and Godgul G. 1994, Metal contamination due to mining and milling activities at the Zawar zinc mine, Rajasthan, India 1. Contamination of stream sediments. *Chemical Geology*, 112, pp. 275–292.
- Reimann C. and Filmozer P. 1999, Normal and lognormal data distribution in geochemistry: Death of a myth. Consequences for the statistical treatment of geochemical and environmental data. *Environmental Geology*, Vol. 39, No. 9, pp. 1001–1014.
- Relić D., Đorđević D., Sakan S., Anđelković I., Miletić S., and Đuričić J. 2011, Aqua regia extracted metals in sediments from the industrial area and surroundings of Pančevo, Serbia. *Journal of Hazardous Materials*, 186, pp. 1893–1901.
- Relić D., Đorđević D., Popović A., and Blagojević T. 2005, Speciations of trace metals in the Danube alluvial sediments within an oil refinery. *Environment International*, 31, pp. 661–669.
- Rodríguez L., Ruiz E., Alonso-Azcárate J., and Rincón J. 2009, Heavy metal distribution and chemical speciation in tailings and soils around a Pb-Zn mine in Spain. *Journal of Environmental Management*, 90, pp. 1106–1116.
- Sakan S., Gržetić I., and Đorđević D. 2007, Distribution and Fractionation of Heavy Metals in the Tisza (Tisza) River Sediments. *Environmental Science and Pollution Research*, Vol. 14, No. 4, pp. 229–236.
- Sánchez D. M., Quejido A. J., Fernández M., Hernández C., Schmid T., Millán R., González M., Alde M., Martín R., and Morante R. 2005, Mercury and trace element fractionation in Almaden soils by application of different sequential extraction procedure. *Analytical and Bioanalytical Chemistry*, 381, pp. 1507–1513.
- Schoer J. and Eggersgluess D. 1982, Chemical Forms of Heavy Metals in Sediments and Suspended Matter of Weser, Elbe and Ems Rivers. SCOPE/UNEP Sonderband, Heft 52, Hamburg, pp. 667–685.
- Shikazano N., Tatewaki K., Mohiuddin K. M., Nakano T., and Zakir H. M. 2012, Sources, spatial variation, and speciation of heavy metals in sediments of the Tamagawa River in Central Japan. *Environmental Geochemistry and Health*, 34, pp. 13–26.
- Sultan K. and Shazili N. A. 2010, Geochemical baselines of major, minor and trace elements in the tropical sediments of the Terengganu River basin, Malaysia. *International Journal of Sediment Research*, 25, pp. 340–354.
- Varejão E. V. V., Bellato C. R., Fontes M. P. F., and Mello J. W. V. 2010, Arsenic and trace metals in river water and sediments from the southeast portion of the Iron Quadrangle, Brazil. *Environmental Monitoring and Assessment*, doi: 10.1007/s10661-010-1361-3.
- Varol M. 2011, Assessment of heavy metal contamination in sediments of the Tigris River (Turkey) using pollution indices and multivariate statistical techniques. *Journal of Hazardous Materials*, 195, pp. 355–364.
- Varol M. and Şen B. 2012, Assessment of nutrient and heavy metal contamination in surface water and sediments of the upper Tigris River, Turkey. *Catena*, 92, pp. 1–10.
- Vasile G. D. and Vlădescu L. 2010, Cadmium partition in river sediments from an area affected by mining activities. *Environmental Monitoring and Assessment*, 167, pp. 349–357.
- Wong C. S. C., Li X., and Thornton I. 2006, Urban environmental geochemistry of trace metals. *Environmental Pollution*, 142, pp. 1–16.
- Yi Y., Wang Z., Zhang K., Yu G., and Duan X. 2008, Sediment pollution and its effect on fish through food chain in the Yangtze River. *International Journal of Sediment Research*, 23, pp. 338–347.



## Non-Elastic Processes in Atom Rydberg-Atom Collisions: Review of State of Art and Problems

A. A. Mihajlov<sup>1</sup>, V. A. Srećković<sup>1,\*</sup>, Lj. M. Ignjatović<sup>1</sup>,  
A. N. Klyucharev<sup>2</sup>, M. S. Dimitrijević<sup>3,4,5</sup> & N. M. Sakan<sup>1</sup>

<sup>1</sup>*Institute of Physics, University of Belgrade, P.O. Box 57, 11001, Belgrade, Serbia.*

<sup>2</sup>*Department of Physics, St-Petersburg University, Ulianovskaya 1, 198904 St. Petersburg, Petrodvorets, Russia.*

<sup>3</sup>*Astronomical Observatory, Volgina 7, 11060 Belgrade 74, Serbia.*

<sup>4</sup>*Observatoire de Paris, 92195 Meudon Cedex, France.*

<sup>5</sup>*IHS Techno Experts, Batajnički put 23, 11080 Zemun, Serbia.*

\**e-mail: sreckovicvladimir@gmail.com*

Received 19 June 2015; accepted 16 October 2015

DOI: 10.1007/s12036-015-9364-7

**Abstract.** In our previous research, it has been demonstrated that inelastic processes in atom Rydberg-atom collisions, such as chemi-ionization and  $(n-n')$  mixing, should be considered together. Here we will review the present state-of-the-art and the actual problems. In this context, we will consider the influence of the  $(n-n')$ -mixing during a symmetric atom Rydberg-atom collision processes on the intensity of chemi-ionization process. It will be taken into account  $H(1s) + H^*(n)$  collisional systems, where the principal quantum number is  $n \gg 1$ . It will be demonstrated that the inclusion of  $(n-n')$  mixing in the calculation, influences significantly on the values of chemi-ionization rate coefficients, particularly in the lower part of the block of the Rydberg states. Different possible channels of the  $(n-n')$ -mixing influence on chemi-ionization rate coefficients will be demonstrated. The possibility of interpretation of the  $(n-n')$ -mixing influence will be considered on the basis of two existing methods for describing the inelastic processes in symmetrical atom Rydberg-atom collisions.

**Key words.** Atomic and molecular processes—plasmas—spectral line profiles.

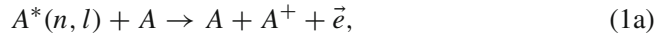
### 1. Introduction

Exploring and improving the new calculation possibilities and simulation techniques, attracted extensive attention in the chemi-ionization and  $(n-n')$ -mixing processes

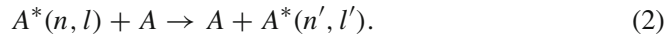
in atom Rydberg-atom collisions, which resulted in numerous papers dedicated to this problem in various research fields like astrophysics, plasma physics, chemistry (see for example, Bohr *et al.* 2012; Barklem 2007; Mihajlov *et al.* 2007a; Ryabtsev *et al.* 2005).

Two groups of inelastic processes in slow atom Rydberg-atom collisions will be considered in this paper:

*The chemi-ionization processes,*



*The processes of  $(n-n')$ -mixing,*



Here  $A$  and  $A^*(n, l)$  denote atom in the ground and in the highly excited (Rydberg) state with the given principal and orbital quantum numbers  $n$  and  $l$ ,  $A^+$  and  $\vec{e}$  are atomic ion in the ground state and free electron, while  $A_2^+$  denotes the molecular ion in the ground state.

The processes (1) and (2), illustrated in Figures 1(a) and 1(b), were examined and discussed in the literature for a long time (see Mihajlov & Janev 1981; Janev *et al.* 1987). These processes are conditioned by the dipole resonant mechanism which was described in detail in Mihajlov *et al.* (2012). Significant contribution of processes (1) and (2) in modeling of solar atmosphere is shown in Mihajlov *et al.* (2011a, 2011b) Barklem (2007), Mashonkina (2009, 2010), while the papers of Mihajlov *et al.* (2003) and Srećković *et al.* (2013) are devoted to the influence of these processes on the kinetic of helium-rich star atmospheres. Another important contribution is that the presented results suggest that these processes, due to their influence on free electron density and excited state populations in the atmospheres of M red dwarfs, should also influence the atomic spectral line shapes (see e.g. Mihajlov *et al.* 2007b).

In spite of the fact that processes (1) and (2) are caused by the same mechanism, they are considered separately up to now. The main aim of this work is to determine the influence of processes (2) on the processes of chemi-ionization (1a) and (1b). Namely, already from Fig. 1(b) one can notice the following: in the case when the considered atomic collision proceed in accordance with the excited molecular term  $U_2(R)$ , before it enters in the zone where the chemi-ionization processes (1a) and (1b) occur, the system  $A^*(n, l) + A$  passes through the zone where the processes (2) with  $n' > n$  take place.

First, the way the inclusion of process (2) in the procedure of calculation of rate coefficients of the chemi-ionization processes (1a) and (1b) will be described. For this purpose their values will be determined under the conditions characteristic for the solar photosphere in the case  $A = \text{H}(1s)$  and compared with the rate coefficients of the same chemi-ionization processes, determined in Mihajlov *et al.* (2011a), but without inclusion of  $(n-n')$ -mixing processes. We draw attention to the fact that, as a difference from this previous article, chemi-ionization rate coefficients are here without the simplification of the expression for Gaunt factor, connected with the photo-ionization cross sections for the transitions of Rydberg electron  $\varepsilon(n, l) \rightarrow \varepsilon(k)$ . Besides, here, as a difference from Mihajlov *et al.* (2011a), the average chemi-ionization rate coefficient for a given  $n$  is obtained as a result of

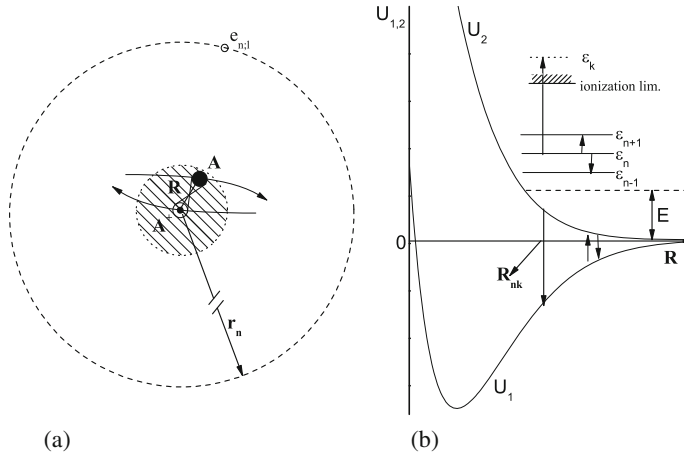


**Figure 1.** (a) Schematic illustration of  $A^*(n, l) + A$  collision within the domain of internuclear distances  $R \ll r_{n,l}$ , where  $r_{n,l} \sim n^2$  is the characteristic radius of Rydberg atom  $A^*(n, l)$ . (b) Schematic illustration of the simultaneous resonant transitions of the outer electron from the initial bound to the final state and the sub-system  $A^+ + A$  from initial excited to the final ground electronic state. If the outer electron becomes free ( $\epsilon_k > 0$ ) the processes (1) occur, while if the outer electron remains in the bound state ( $\epsilon_{n'} < 0$ ) the processes (2) occur.

the corresponding averaging of partial chemi-ionization rate coefficients for every  $l$  where  $0 \leq l \leq n - 1$ .

Atomic units will be used throughout the paper.

## 2. Theory

### 2.1 General formulas

Let  $K_{1a}(n, l; T)$  and  $K_{1b}(n, l; T)$  are rate coefficients of processes (1a) and (1b), separately determined for a given  $n, l$  and  $T$ , where  $T$  is the temperature of the considered plasma, and  $K_1(n, l; T)$  is the total rate coefficient of processes (1a) and (1b) together, namely  $K_1(n, l; T) = K_{1a}(n, l; T) + K_{1b}(n, l; T)$ .

Because of further applications, we will then determine the average total rate coefficient

$$K_{1;n}(T) = \frac{1}{n^2} \cdot \sum_{l=0}^{n-1} (2l + 1) \cdot K_1(n, l; T), \quad (3)$$

and average rate coefficient of associative ionization  $K_{1b;n}(T)$ ,

$$K_{1b;n}(T) = \frac{1}{n^2} \cdot \sum_{l=0}^{n-1} (2l + 1) \cdot K_{1b}(n, l; T). \quad (4)$$

Partial rate coefficients  $K_1(n, l; T)$  and  $K_{1b}(n, l; T)$  are determined on the basis of standard expressions

$$K_1(n, l; T) = \int_{E_{n,i}}^{\infty} \sigma_1(n, l; E) \left( \frac{2E}{\mu_{\text{red}}} \right)^{1/2} f_T(E) dE, \quad (5)$$

$$K_{1b}(n, l; T) = \int_{E_{n;i}}^{\infty} \sigma_{1b}(n, l; E) \left( \frac{2E}{\mu_{\text{red}}} \right)^{1/2} f_T(E) dE, \quad (6)$$

where  $E$  is the impact energy,  $\sigma_1(n, l; E)$  and  $\sigma_{1b}(n, l; E)$  are the corresponding cross sections,  $\mu_{\text{red}}$  is the reduced mass of the subsystem  $\text{H}(1s)+\text{H}^+$ , and  $f_T(E)$  is the Maxwell distribution function:  $f_T(E) = \exp(-E/kT)\sqrt{E}$ . Parameter  $E_{n;i}$  is given here with the relation  $E_{n;i} = U_2(R_{n;i})$ , where  $R_{n;i}$  is the upper limit of the chemi-ionization zone which is the root of the equation  $U_{12} = 1/2n^2$ .

The mentioned cross sections are determined here within the semi-classical approximation, with the help of the standard expressions

$$\begin{aligned} \sigma_1(n, l; E) &= 2\pi \int_0^{\rho_{1;\text{max}}} P_1(n, l; \rho; E) \rho d\rho, \\ \sigma_{1b}(n, l; E) &= 2\pi \int_0^{\rho_{1b;\text{max}}} P_{1b}(n, l; \rho; E) \rho d\rho, \end{aligned} \quad (7)$$

where  $\rho$  is the impact parameter,  $\rho_{1;\text{max}}$  and  $\rho_{1b;\text{max}}$  are the corresponding maximal values of this parameter, and  $P_1(n, l; \rho; E)$  and  $P_{1b}(n, l; \rho; E)$  are the total probability of chemi-ionization and the probability of associative ionization, respectively determined for the given values of  $n$ ,  $l$ ,  $\rho$  and  $E$ . We will determine these probabilities in the form

$$P_1(n, l; \rho; E) = \frac{1}{2} \cdot p_{\text{keep}}(n, l; \rho; E) \cdot p_{i;1}(n, l; \rho; E), \quad (8)$$

$$P_{1b}(n, l; \rho; E) = \frac{1}{2} \cdot p_{\text{keep}}(n, l; \rho; E) \cdot p_{i;1b}(n, l; \rho; E), \quad (9)$$

where  $1/2$  is the probability that the subsystem  $\text{H}(1s)+\text{H}^+$  develops in accordance with the term  $U_2(R)$ ,  $p_{\text{keep}}(n, l; \rho; E)$  the probability that in the domain of values of  $R$  where the processes (2) with  $n' > n$  are possible, the state of this subsystem is held on, i.e. the excited electronic state with the energy  $U_2(R)$ , while  $p_{i;1}(n, l; \rho; E)$  and  $p_{i;1b}(n, l; \rho; E)$  are the corresponding ionization probabilities determined under the condition that subsystem  $\text{H}(1s) + \text{H}^+$  enters into the ionization zone with probability equal to 1.

## 2.2 Probability of ionization decay

As in the previous papers, probabilities  $p_{i;1}(n, l; \rho; E)$  and  $p_{i;1b}(n, l; \rho; E)$  are determined here within the quasi-static decay approximation. Since these probabilities are determined in a similar way as in the previous works of Mihajlov *et al.* (2007a) and Mihajlov *et al.* (2011a), here they are taken in the form

$$\begin{aligned} p_{i;1}(n, l; \rho; E) &= 1.0 - \exp(-2q_{i;1}), \\ p_{i;1b}(n, l; \rho; E) &= \exp(-q_{i;2}) \cdot [1.0 - \exp(-2q_{i;as})], \end{aligned} \quad (10)$$

where the quantities  $q_{i;1}$ ,  $q_{i;2}$  and  $q_{i;as}$  are given as

$$q_{i;as} = q_{i;1} - q_{i;2}, \quad q_{i;1} = \int_{R_0}^{R_{n;i}} \frac{W_i(n, l; R)}{v_{\text{rad}}(E, \rho; R)} dR,$$

$$q_{i;2} = \int_{R_{1b;\text{max}}}^{R_{n;i}} \frac{W_i(n, l; R)}{v_{\text{rad}}(E, \rho; R)} dR. \quad (11)$$

The rate coefficient of ionization decay  $W_i(n, l; R)$  and radial ion-atom velocity  $v_{\text{rad}}(E, \rho; R)$  are given by the expressions

$$W_i(n, l; R) = \frac{1}{2\pi} \cdot c \cdot U_{12}^3(R) \cdot D_{12}^2(R) \cdot \sigma_{\text{ph},i}(n, l, \varepsilon_{\text{ph}}),$$

$$v_{\text{rad}}(E, \rho; R) = \left( \frac{2}{\mu_{\text{red}}} \left[ E - U_2(R) - \frac{E\rho^2}{R^2} \right] \right)^{1/2}, \quad (12)$$

where  $c$  is the speed of light,  $D_{12} = |\langle 1 | \hat{d}_{m,i} | 2 \rangle|$  is the molecular-ion dipole matrix element,  $\sigma_{\text{ph},i}(n, l, \varepsilon_{\text{ph}})$  is the cross section for photoionization of excited hydrogen atom  $\text{H}^*(n, l)$  by a photon with energy  $\varepsilon_{\text{ph}} = U_{12}(R)$ , and  $U_{12}(R) = U_2(R) - U_1(R)$ .

In the expression for dipole matrix element  $\hat{d}$  denotes the operator of ion dipole momentum  $H_2^+$  and  $|1\rangle$  and  $|2\rangle$  are the ground and first excited state of this ion.

In equation (11),  $R_0$  is denoted by the lower limit of the domain  $R$  which is reached during the collision with a given  $\rho$  and  $E$ , and with  $R_{1b;\text{min}}$ , the upper limit of the domain  $R$  where only the process of associative ionization (1b) is possible. Consequently, parameters  $R_0$  represents the roots of the equation:  $U_2(R) = E \cdot (1 - \rho^2/R^2)$  and  $R_{1b;\text{max}}$  is the root of the equation  $U_{12}(R) = E$ . Let us draw our attention to where it is assumed in expressions (10) and (11) that  $R_{1b;\text{max}} < R_{n;i}$ . In the case of  $R_{1b;\text{max}} > R_{n;i}$  we have that the quantity  $q_{i;2} = 0$  and  $q_{i;as} = q_{i;1}$ .

We draw our attention that already at this point there exist a difference compared to previous works concerning the chemi-ionization processes in stellar atmospheres (Mihajlov *et al.* 2007a, 2011a). Namely, in the mentioned works, the chemi-ionization rate coefficients were determined with the averaged ionization decay rate, obtained by averaging partial rates over the whole shell with a given  $n$ . This gives possibility to use the average over shell Kramers photo-ionization cross-section adjusted with the help of approximate Gaunt factor. As a difference, the rate coefficients  $K_1(n, l; T)$  and  $K_{1b}(n, l; T)$  were determined here on the basis of equations (5) and (6) with the help of partial cross sections for photo-ionization, determined here on the basis of exact expressions from Sobelman (1979).

### 2.3 Probability of pre-ionization decay

From equations (8) and (9) one can notice that the basic difference, in comparison with previous papers, represents taking into account of the effect of decay of the initial electronic state of the considered atom Rydberg-atom system, due to the possibility of execution of excitation processes (2) with  $n' > n$ . This one is taken into account by the introduction of probability of maintenance of this state  $p_{\text{keep}}(n, l; \rho; E)$ . One determines this probability on the basis of the modified



version of approximate method described in Mihajlov *et al.* (2004) dedicated to the  $(n - n')$ -mixing processes. Let us remind that the essence of this method is that, at a given  $n$ , each block of Rydberg states from  $n' = n + p_1$  to  $n' = n + p_2$  is 'spreading' in a part of 'quasicontinuum' limited by values  $n + p_1 - \delta_n$  and  $n + p_2 + 1 - \delta_n$ , where the parameters  $\delta_n$  are determined from the condition of maintainance of total number of states and total oscillator strengths for transitions from initial state of Rydberg electron to all states of the separated block. The mentioned modification has been conditioned with the fact that in the just mentioned work, an average rate of decay of the initial state of system connected with the transition of Rydberg electron from the state with the given  $n$  in states with  $n' = n + p$ , where  $p \geq 1$ , was determined while we must consider transitions of Rydberg electron from the state  $|n, l\rangle$  to the states  $|n + p, l - 1\rangle$  and  $|n + p, l + 1\rangle$ . In accordance, it is considered here that the preionization zone form the domain of internuclear distances such that  $R_{n;i} < R < R_{n;n+1-\delta_n}$ , where  $\delta_n = 0.5 \cdot [1 - (1/3) \cdot O(1/n)]$ , and domains  $R$  corresponding to the mentioned transitions with  $p = 1, 2, 3 \dots$  make intervals  $(R_{n;n+2-\delta_n}, R_{n;n+1-\delta_n})$ ,  $(R_{n;n+3-\delta_n}, R_{n;n+2-\delta_n})$  and  $(R_{n;n+4-\delta_n}, R_{n;n+3-\delta_n})$ . The limits of these domains  $R_{n;n+p-\delta_n}$  are roots of the equations:  $U_{12}(R) = 0.5 \cdot [1/n^2 - 1/(n + p - \delta_n)^2]$ .

In this work, the transitions with  $1 \leq p \leq 5$  are taken into account. Consequently, the probability  $p_{\text{keep}}(n, l; \rho; E)$  could be represented as

$$p_{\text{keep}}(n, l; \rho; E) = \prod_{p=1}^5 p_{p;\text{keep}}(n, l; \rho; E), \quad (13)$$

where  $p_{p;\text{keep}}(n, l; \rho; E)$  is the probability of the maintenance of the initial state of the system within the interval  $(R_{n;n+p+1-\delta_n}, R_{n;n+p-\delta_n})$ .

Since the mechanism of the pre-ionization decay is the same as in the case of the ionization one, we take immediately that probabilities  $p_{p;\text{keep}}(n, l; \rho; E)$  are given by the relations

$$p_{p;\text{keep}}(n, l; \rho; E) = \exp(-x_p),$$

$$x_p = \int_{R_{n;n+p+1-\delta_n}}^{R_p} \frac{w_{n;n+p}(n, l; R)}{\nu_{\text{rad}}(E, \rho, R)}, \quad (14)$$

where the decay rate  $w_{n;n+p}(n, l; R)$  is conditioned by the dipole mechanism within the interval  $(R_{n;n+p+1-\delta_n}, R_{n;n+p-\delta_n})$ .

The upper limit  $R_p$  is given by

$$R_p = \begin{cases} R_{n;n+p-\delta_n}, R_{n;n+p-\delta_n} \leq R_{up;\text{mix}}(E, \rho) \\ R_{up;\text{mix}}(E, \rho), R_{n;n+p-\delta_n} > R_{up;\text{mix}}(E, \rho) \geq R_{n;n+p} \end{cases} \quad (15)$$

where  $R_{n;n+p}$  is the resonant distance of the process (2) for a given  $n - n' = n + p$ , determined as the root of the equation

$$U_{12}(R) = \frac{1}{2} \cdot \left[ \frac{1}{n^2} - \frac{1}{(n + p)^2} \right]. \quad (16)$$

The parameter  $R_{up;\text{mix}}(E, \rho)$  is separately discussed in Appendix 4. Let us draw attention that in the case when  $R_{up;\text{mix}}(E, \rho) < R_{n;n+p}$ , it is considered that

$p_{p;\text{keep}}(n, l; \rho; E) = 0$ . Thus the decay rate  $w_{n;n+p}(n, l; R)$  is given by the relation

$$w_{n;n+p}(n, l; R) = \frac{2\pi}{3} \cdot U_{12}^4(R_{n;n+p}) \cdot \tilde{n}^3 \cdot D_{12}^2 \cdot r_{n,l;n+p}^2, \\ \tilde{n} = n \cdot [1 - 2n^2 \cdot U_{12}(R)]^{-1/2}, \quad (17)$$

where  $r_{n,l;n+p}^2 = |\langle n, l | \hat{d}_{at} | n, l - 1 \rangle|^2 + |\langle n, l | \hat{d}_{at} | n, l + 1 \rangle|^2$ ,  $\hat{d}_{at}$  is the operator of the dipole moment of hydrogen atom, and  $|n, l\rangle$ ,  $|n, l - 1\rangle$  and  $|n, l + 1\rangle$  denote the corresponding states of Rydberg electrons.

### 3. Results and discussion

It follows from the above presented material that the total rate coefficients of the processes (1a) and (1b) together, and rate coefficients for the associative ionization (1b), i.e.  $K_{1;n}(T)$  and  $K_{1b;n}(T)$  are determined on the basis of equations (3)–(17). Let us draw attention that, strictly speaking, chemi-ionization processes (1a) and (1b) can be described on the basis of dipole resonant mechanism only in the case of the state with  $n \geq 5$ , for which the potential curves of the system  $\text{H}^*(n, l) + \text{H}(1s)$  lie above the potential curve of the system  $\text{H}^+ + \text{H}^-(1s^2)$ , where  $\text{H}^-(1s^2)$  is a stable negative hydrogen ion. However, it can be shown that the points of the intersection of potential curves of the system  $\text{H}^*(n, l) + \text{H}(1s)$  with  $n = 2, 3$  and  $4$  with the potential curve of the system  $\text{H}^+ + \text{H}^-(1s^2)$  are located on the internuclear distances, which are several times larger than the average atomic radius  $\text{H}^*(n, l)$  so that the existence of these intersections can not significantly affect the values of the corresponding rate coefficients of the processes (1a) and (1b). Consequently the applicability of the dipole resonance mechanism for the states with  $n < 5$  depends to what degree it may be regarded as fulfilled condition  $R_{n;n+1} \ll r_{n;l}$ , where  $r_{n;l}$  is the mean radius of the corresponding orbit of the outer electron. One notices that from this aspect, the dipole resonant mechanism can not be applied in the case of  $n = 2$ , while in the case of the states  $n = 3$  and  $4$  the application of this mechanism can be completely justified.

Total values of the rate coefficients of chemi-ionization processes  $K_{1;n}(T)$  within the range  $3 \leq n \leq 15$  are presented in Table 1. Bearing in mind the main application (of the results obtained here), on the photosphere and lower chromosphere of the Sun, calculations of these rate coefficients were performed for temperatures  $4000 \text{ K} \leq T \leq 10000 \text{ K}$ . The processes (1b) are characterized in this paper via the corresponding branch coefficient  $X_{1b;n}(T)$  given as

$$X_{1b;n}(T) = \frac{K_{1b;n}}{K_{1;n}}. \quad (18)$$

Values of coefficients  $X_{1b;n}(T)$  for the same  $n$  and  $T$  are presented in Table 2. In accordance with the above, rate coefficients are determined by summing the probability of the decay of the initial state of the collisional system in preionization zone with Rydberg electron transitions from state  $|n\rangle$  to state  $|n + p\rangle$ , where  $1 \leq p \leq 5$ .

In order to demonstrate significance of the presented calculation, we will compare the chemi-ionization rate coefficients  $K_{i;n}(T)$  with the corresponding rate coefficients  $K_{i;n}^*(T)$  from Mihajlov *et al.* (2011a). Let us note that the coefficients

**Table 1.** Calculated values of the coefficient  $K_{1;n}(T)(\text{cm}^3 \text{ s}^{-1})$  as a function of  $n$  and  $T$ .

| $T$   | $n$      |          |          |          |          |          |          |          |          |          |          |          |          |  |  |
|-------|----------|----------|----------|----------|----------|----------|----------|----------|----------|----------|----------|----------|----------|--|--|
|       | 3        | 4        | 5        | 6        | 7        | 8        | 9        | 10       | 11       | 12       | 13       | 14       | 15       |  |  |
| 4000  | 7.17E-12 | 1.54E-10 | 3.58E-10 | 4.28E-10 | 3.98E-10 | 3.30E-10 | 2.61E-10 | 2.06E-10 | 1.63E-10 | 1.28E-10 | 1.02E-10 | 8.14E-11 | 6.62E-11 |  |  |
| 4250  | 9.01E-12 | 1.63E-10 | 3.88E-10 | 4.52E-10 | 4.15E-10 | 3.42E-10 | 2.69E-10 | 2.11E-10 | 1.66E-10 | 1.31E-10 | 1.04E-10 | 8.28E-11 | 6.72E-11 |  |  |
| 4500  | 1.11E-11 | 1.72E-10 | 4.16E-10 | 4.76E-10 | 4.32E-10 | 3.53E-10 | 2.76E-10 | 2.16E-10 | 1.70E-10 | 1.33E-10 | 1.06E-10 | 8.40E-11 | 6.81E-11 |  |  |
| 4750  | 1.33E-11 | 1.83E-10 | 4.43E-10 | 4.98E-10 | 4.48E-10 | 3.63E-10 | 2.83E-10 | 2.20E-10 | 1.73E-10 | 1.35E-10 | 1.07E-10 | 8.51E-11 | 6.89E-11 |  |  |
| 5000  | 1.53E-11 | 1.96E-10 | 4.71E-10 | 5.20E-10 | 4.63E-10 | 3.72E-10 | 2.89E-10 | 2.24E-10 | 1.76E-10 | 1.38E-10 | 1.09E-10 | 8.62E-11 | 6.97E-11 |  |  |
| 5250  | 1.73E-11 | 2.12E-10 | 4.98E-10 | 5.42E-10 | 4.77E-10 | 3.81E-10 | 2.95E-10 | 2.28E-10 | 1.78E-10 | 1.40E-10 | 1.10E-10 | 8.73E-11 | 7.05E-11 |  |  |
| 5500  | 1.96E-11 | 2.31E-10 | 5.26E-10 | 5.63E-10 | 4.90E-10 | 3.89E-10 | 3.01E-10 | 2.31E-10 | 1.80E-10 | 1.41E-10 | 1.11E-10 | 8.84E-11 | 7.12E-11 |  |  |
| 5750  | 2.30E-11 | 2.51E-10 | 5.53E-10 | 5.83E-10 | 5.03E-10 | 3.96E-10 | 3.06E-10 | 2.35E-10 | 1.82E-10 | 1.43E-10 | 1.13E-10 | 8.94E-11 | 7.19E-11 |  |  |
| 6000  | 2.81E-11 | 2.71E-10 | 5.79E-10 | 6.03E-10 | 5.15E-10 | 4.04E-10 | 3.11E-10 | 2.38E-10 | 1.84E-10 | 1.44E-10 | 1.14E-10 | 9.03E-11 | 7.25E-11 |  |  |
| 6250  | 3.53E-11 | 2.91E-10 | 6.03E-10 | 6.21E-10 | 5.26E-10 | 4.11E-10 | 3.16E-10 | 2.41E-10 | 1.86E-10 | 1.46E-10 | 1.15E-10 | 9.12E-11 | 7.30E-11 |  |  |
| 6500  | 4.37E-11 | 3.11E-10 | 6.26E-10 | 6.39E-10 | 5.37E-10 | 4.17E-10 | 3.20E-10 | 2.44E-10 | 1.88E-10 | 1.47E-10 | 1.16E-10 | 9.19E-11 | 7.36E-11 |  |  |
| 7000  | 6.01E-11 | 3.50E-10 | 6.70E-10 | 6.72E-10 | 5.59E-10 | 4.30E-10 | 3.28E-10 | 2.50E-10 | 1.92E-10 | 1.49E-10 | 1.18E-10 | 9.33E-11 | 7.46E-11 |  |  |
| 7500  | 7.08E-11 | 3.90E-10 | 7.13E-10 | 7.03E-10 | 5.80E-10 | 4.43E-10 | 3.36E-10 | 2.55E-10 | 1.95E-10 | 1.51E-10 | 1.20E-10 | 9.46E-11 | 7.57E-11 |  |  |
| 8000  | 7.91E-11 | 4.31E-10 | 7.54E-10 | 7.31E-10 | 5.99E-10 | 4.55E-10 | 3.44E-10 | 2.60E-10 | 1.98E-10 | 1.54E-10 | 1.21E-10 | 9.57E-11 | 7.68E-11 |  |  |
| 8500  | 8.91E-11 | 4.71E-10 | 7.93E-10 | 7.57E-10 | 6.14E-10 | 4.65E-10 | 3.51E-10 | 2.64E-10 | 2.01E-10 | 1.56E-10 | 1.22E-10 | 9.66E-11 | 7.75E-11 |  |  |
| 9000  | 9.91E-11 | 5.13E-10 | 8.27E-10 | 7.82E-10 | 6.27E-10 | 4.74E-10 | 3.56E-10 | 2.68E-10 | 2.04E-10 | 1.58E-10 | 1.23E-10 | 9.74E-11 | 7.81E-11 |  |  |
| 9500  | 1.06E-10 | 5.56E-10 | 8.57E-10 | 8.06E-10 | 6.40E-10 | 4.82E-10 | 3.61E-10 | 2.72E-10 | 2.06E-10 | 1.59E-10 | 1.25E-10 | 9.82E-11 | 7.86E-11 |  |  |
| 10000 | 1.07E-10 | 6.03E-10 | 8.82E-10 | 8.30E-10 | 6.55E-10 | 4.90E-10 | 3.66E-10 | 2.75E-10 | 2.08E-10 | 1.61E-10 | 1.26E-10 | 9.91E-11 | 7.93E-11 |  |  |

$K_{i;n}^*(T)$  are obtained in the same way as the coefficients  $K_{i;n}(T)$  by taking  $p_{\text{keep}}(n, l; \rho; E) = 0$ , where  $p_{\text{keep}}(n, l; \rho; E)$  is the total probability of the preionization decay given by equations (13)–(17). All the mentioned quantities are presented in Fig. 2 for the case of  $T = 5000$  K. Note that in relation to the previous work of Mihajlov *et al.* (2011a), in this figure are presented not only the total rate coefficients, determined on the basis of dipole resonance mechanism for  $3 \leq n \leq 8$  but also rate coefficients are determined on the basis of data from Janev *et al.* (1987) for  $n = 3$  and 4, and from

**Table 2.** Calculated values of the branch coefficient  $X_{1b;n}$  as a function of  $n$  and  $T$ .

| $T$   | $n$   |       |       |       |       |       |       |       |       |       |       |       |       |
|-------|-------|-------|-------|-------|-------|-------|-------|-------|-------|-------|-------|-------|-------|
|       | 3     | 4     | 5     | 6     | 7     | 8     | 9     | 10    | 11    | 12    | 13    | 14    | 15    |
| 4000  | 0.684 | 0.608 | 0.458 | 0.365 | 0.306 | 0.243 | 0.218 | 0.208 | 0.201 | 0.186 | 0.169 | 0.154 | 0.137 |
| 4250  | 0.607 | 0.563 | 0.437 | 0.346 | 0.284 | 0.232 | 0.211 | 0.202 | 0.195 | 0.178 | 0.160 | 0.143 | 0.129 |
| 4500  | 0.543 | 0.519 | 0.421 | 0.329 | 0.265 | 0.222 | 0.206 | 0.198 | 0.189 | 0.170 | 0.152 | 0.132 | 0.122 |
| 4750  | 0.497 | 0.475 | 0.407 | 0.314 | 0.248 | 0.213 | 0.201 | 0.194 | 0.184 | 0.162 | 0.144 | 0.122 | 0.114 |
| 5000  | 0.467 | 0.431 | 0.395 | 0.301 | 0.232 | 0.205 | 0.197 | 0.190 | 0.180 | 0.155 | 0.137 | 0.112 | 0.108 |
| 5250  | 0.473 | 0.427 | 0.370 | 0.284 | 0.223 | 0.201 | 0.193 | 0.185 | 0.172 | 0.146 | 0.130 | 0.109 | 0.104 |
| 5500  | 0.467 | 0.419 | 0.347 | 0.269 | 0.215 | 0.197 | 0.189 | 0.181 | 0.164 | 0.137 | 0.123 | 0.107 | 0.101 |
| 5750  | 0.442 | 0.411 | 0.328 | 0.254 | 0.208 | 0.193 | 0.186 | 0.177 | 0.157 | 0.128 | 0.116 | 0.104 | 0.098 |
| 6000  | 0.397 | 0.403 | 0.310 | 0.242 | 0.201 | 0.190 | 0.183 | 0.173 | 0.150 | 0.119 | 0.110 | 0.101 | 0.095 |
| 6250  | 0.349 | 0.380 | 0.294 | 0.229 | 0.197 | 0.187 | 0.179 | 0.166 | 0.142 | 0.116 | 0.107 | 0.099 | 0.092 |
| 6500  | 0.308 | 0.360 | 0.279 | 0.218 | 0.194 | 0.184 | 0.175 | 0.159 | 0.134 | 0.113 | 0.104 | 0.096 | 0.089 |
| 7000  | 0.263 | 0.327 | 0.254 | 0.198 | 0.187 | 0.178 | 0.169 | 0.146 | 0.118 | 0.106 | 0.098 | 0.092 | 0.083 |
| 7500  | 0.223 | 0.292 | 0.234 | 0.190 | 0.180 | 0.172 | 0.157 | 0.133 | 0.112 | 0.101 | 0.093 | 0.086 | 0.078 |
| 8000  | 0.199 | 0.263 | 0.216 | 0.183 | 0.173 | 0.167 | 0.146 | 0.120 | 0.105 | 0.096 | 0.087 | 0.081 | 0.073 |
| 8500  | 0.198 | 0.243 | 0.194 | 0.178 | 0.169 | 0.161 | 0.134 | 0.112 | 0.100 | 0.092 | 0.083 | 0.075 | 0.070 |
| 9000  | 0.198 | 0.225 | 0.175 | 0.173 | 0.165 | 0.156 | 0.123 | 0.105 | 0.095 | 0.087 | 0.080 | 0.069 | 0.067 |
| 9500  | 0.201 | 0.210 | 0.164 | 0.167 | 0.161 | 0.142 | 0.116 | 0.099 | 0.091 | 0.084 | 0.075 | 0.067 | 0.065 |
| 10000 | 0.218 | 0.196 | 0.155 | 0.161 | 0.156 | 0.129 | 0.109 | 0.095 | 0.087 | 0.081 | 0.071 | 0.066 | 0.063 |

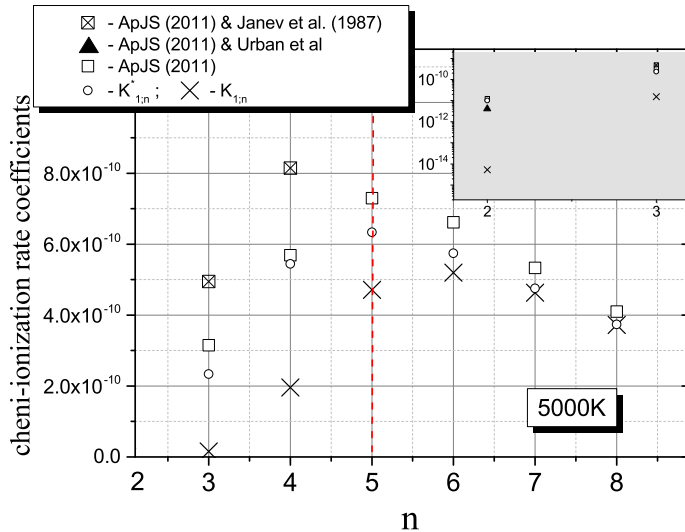


**Figure 2.** Comparison of the calculated values of rate coefficients of the chemi-ionization processes (1a) and (1b) with the data from Mihajlov *et al.* (2011a).

Urbain *et al.* (1991) for  $n = 2$ . One can notice from this figure that there are noticeable differences between the values of the rate coefficients determined in Mihajlov *et al.* (2011a) and values  $K_{i;n}^*(T)$ , while the differences in relation to the rate coefficients  $K_{i;n}(T)$  are very large for  $n \leq 6$  and decreases quickly with the increase of  $n$  in  $n > 6$ .

In previous works (Mihajlov *et al.* 2003, 2007b) related to the photosphere of a  $M$  red dwarf with temperature near to 4000 K, it has been shown that on populations of hydrogenic Rydberg states in this photosphere as well as on its other characteristics, the chemi-ionization processes (1a) and (1b) influence strongly with  $4 \leq n \leq 8$ . It is clear that because of this, it is indispensable to take into account the changes of rate coefficients of these processes, which, in accordance with our results, are particularly large for  $n \leq 6$ . From the material presented here, further investigation of the properties of decay of the initial state of the collisional system  $H^*(n, l) + H(1s)$  in the pre-ionization zone is of great importance.

Additionally, results obtained here suggest that the rate coefficients of the chemi-ionization processes (1a) and (1b) could be affected by other channels of influence of the processes (2). Here we have in view the processes of  $(n-n')$  mixing taking place in two or more steps.

#### 4. Conclusions

In this work, it is shown that the processes of  $(n-n')$ -mixing (equation (2)) influence considerably the rates of chemi-ionization processes (1a) and (1b). Calculations, which characterize this influence on the quantitative level have been performed. As one can see from figure 2, inclusion of the  $(n-n')$  mixing processes reduce the chemi-ionization rate coefficients. The obtained results are finalized in tabular form, where the values of total constants for rates of the processes (1a) and (1b) together, and rates for the process of associative ionization (1b) are presented. The tables cover the range of values, of the principal quantum number of Rydberg states of the hydrogen atom, from  $n = 3$  to  $n = 15$  and the temperature range from  $T = 4000$  K to  $T = 10000$  K, so that they can be directly applied in connection with the modeling of photosphere and lower chromosphere of the Sun. Moreover, investigation of the influence of  $(n-n')$ -mixing processes on the chemi-ionization processes taking into account  $(n-n')$  mixing processes which occur in two or more steps have been discussed.

#### Acknowledgements

The authors are thankful to the Ministry of Education, Science and Technological Development of the Republic of Serbia for the support of this work through projects 176002, III44002 and 171014.

#### Appendix

The characteristic length  $R_{up;mix}$  is defined here as the upper limit of the domain  $R$  where at a given  $E$  and  $\rho$ , we can consider that the inner electron is in the subsystem  $H^+ + H(1s)$  and that is sufficiently delocalized, so that this subsystem could be

treated as a quasi-molecular complex. As a qualitative characteristics of the mentioned delocalization, one takes here the probability of resonant charge exchange  $P_{c.exc}(R; E; \rho)$  in the subsystem  $H^+ + H(1s)$  as a function of  $R$  at a given  $\rho$  and  $E$ . As a basis for this, is taken the theory of the process:  $H^+ + H(1s) \rightarrow H(1s) + H^+$  developed in Firsov (1951) and Bates & Boyd (1962). From this theory it follows that

$$P_{c.exc}(R; E; \rho) = \sin^2(\varphi(R; E; \rho)), \quad (A1)$$

where the phase  $\varphi(R; E; \rho)$  is given by the relation

$$\varphi(R; E; \rho) = \frac{1}{2} \int_R^\infty \frac{U_{12}(R')}{v_{rad}(R', \rho, E)} dR', \quad (A2)$$

which can be used in the considered case since  $P_{c.exc}(R; E; \rho)$  becomes noticeably different from zero only deeply inside the orbit of the Rydberg electron at a given  $n$ . On the basis of the data from Firsov (1951) and Bates & Boyd (1962), it can be considered that in the case when  $P_{c.exc}(R; E; \rho)$  reaches the value of  $1/2\pi$ , the corresponding  $R$  may be considered as the upper limit of the charge exchange zone at a given  $\rho$  and  $E$ , and consequently, as the upper limit of domain with a sufficient degree of delocalization of electron in the subsystem  $H^+ + H(1s)$ . Thus, the parameter  $R_{up;mix}$  is determined here as the root of the equation

$$\sin^2(\varphi(R; E; \rho)) = \frac{1}{2\pi}, \quad (A3)$$

where  $\varphi(R; E; \rho)$  is given by equation (A2) under condition that this root is in the domain of monotonical increase of the left side of equation (A3).

The behavior of phase  $\varphi(R; E; \rho)$  is illustrated in Table 3, where its values for  $E = E_{n;i}$ ,  $\rho = 0$  and  $R = R_{n;n+1}$  within the range  $3 \leq n \leq 15$  are shown. Of course, these data should be treated as qualitative ones since equations (A1) and (A2) have strict sense in the case  $E \gg U_{12}(R)$  while in our case, this condition is fulfilled only for  $n > 7$ .

**Table 3.** Calculated values of the parameters which characterize pre-ionization zone. Phase  $\varphi(R_{n,n+1}, E_{n;i}; \rho = 0)$  is given by equation (A2).

| $n$ | $R_{ni}$ | $E_{n;i} = U2(Rn; i)$ | $R_{n,n+1}$ | $\varphi(R_{n,n+1}, E_{n;i}; \rho = 0)$ | $P_{c.exc}(\varphi(R_{n,n+1}, E_{n;i}; \rho = 0))$ |
|-----|----------|-----------------------|-------------|---|--|
| 3   | 4.79     | 0.02738               | 5.839       | 1.840                                   | 0.92929  |
| 4   | 5.52     | 0.01431               | 6.777       | 1.143                                   | 0.82824  |
| 5   | 6.08     | 0.00871               | 7.497       | 0.782                                   | 0.49618  |
| 6   | 6.52     | 0.00581               | 8.087       | 0.567                                   | 0.28891  |
| 7   | 6.89     | 0.00413               | 8.580       | 0.433                                   | 0.17619  |
| 8   | 7.21     | 0.00306               | 9.010       | 0.341                                   | 0.11201  |
| 9   | 7.49     | 0.00234               | 9.380       | 0.278                                   | 0.07544  |
| 10  | 7.73     | 0.00183               | 9.725       | 0.229                                   | 0.05167  |
| 11  | 7.95     | 0.00146               | 10.035      | 0.193                                   | 0.03667  |
| 12  | 8.16     | 0.00119               | 10.317      | 0.165                                   | 0.02691  |
| 13  | 8.34     | 0.00098               | 10.551      | 0.146                                   | 0.02108  |
| 14  | 8.51     | 0.00081               | 10.839      | 0.122                                   | 0.01489  |
| 15  | 8.66     | 0.00068               | 11.002      | 0.114                                   | 0.01297  |

## References

- Barklem, P. S. 2007, *A&A*, **466**, 327.
- Bates, D. R., Boyd, A. H. 1962, *Proceedings of the Physical Society*, **80**, 1301.
- Bohr, A., Blickle, A., Paolini, S., Ohlinger, L., Forrey, R. C. 2012, *Phys. Rev. A*, **85**, 042710.
- Firsov, O. B. 1951, *Zh. Eksp. Teor. Fiz.*, **21**, 1001.
- Janev, R. K., Langer, W. D., Evans, K. 1987, *Springer Series on Atoms and Plasmas*, Springer, Berlin, pp. 1987.
- Mashonkina, L. 2009, *Physica Scripta Volume T*, **134**, 014004.
- Mashonkina, L. 2010, *EAS Publications Series*, **43**, 79.
- Mihajlov, A. A., Janev, R. K. 1981, *J. Phys. B: At. Mol. Opt. Phys.*, **14**, 1639.
- Mihajlov, A. A., Ignjatović, L. M., Srećković, V. A., Dimitrijević, M. S. 2011a, *ApJS*, **193**, 2.
- Mihajlov, A. A., Ignjatović, L. M., Srećković, V. A., Dimitrijević, M. S. 2011b, *Baltic Astronomy*, **20**, 566.
- Mihajlov, A. A., Srećković, V. A., Ignjatović, L. M., Klyucharev, A. N. 2012, *J. Cluster Science*, **23**(1), 47.
- Mihajlov, A. A., Ignjatović, L. M., Sakan, N. M., Dimitrijević, M. S. 2007a, *A&A*, **469**, 749.
- Mihajlov, A. A., Jevremović, D., Hauschildt, P. et al. 2007b, *A&A*, **471**, 671.
- Mihajlov, A. A., Ignjatovic, L. M., Djuric, Z., Ljepojevic, N. N. 2004, *J. Phys. B: Atomic Molecular Physics*, **37**, 4493.
- Mihajlov, A. A., Jevremović, D., Hauschildt, P. et al. 2003, *A&A*, **403**, 787.
- Ryabtsev, I. I., Tretyakov, D. B., Beterov, I. I. et al. 2005, *J. Phys. B: Atomic Molecular Physics*, **38**, 17.
- Sobelman, I. I. 1979, *Springer Series in Chemical Physics*, Springer, Berlin, pp. 1979.
- Srećković, V. A., Mihajlov, A. A., Ignjatović, L. M., Dimitrijević, M. S. 2013, *A&A*, **552**, A33.
- Urbain, X., Cornet, A., Brouillard, F., Giusti-Suzor, A. 1991, *Phys. Rev. Lett.*, **66**, 1685.



## Inverse Bremsstrahlung in Astrophysical Plasmas: The Absorption Coefficients and Gaunt Factors

A. A. Mihajlov, V. A. Srećković\* & N. M. Sakan

*Institute of Physics, University of Belgrade, P.O. Box 57, 11001, Belgrade, Serbia.*

\**e-mail: sreckovicvladimir@gmail.com*

Received 19 June 2015; accepted 4 September 2015

DOI: 10.1007/s12036-015-9350-0

**Abstract.** The electron–ion inverse Bremsstrahlung is considered here as a factor of the influence on the opacity of the different stellar atmospheres and other astrophysical plasmas. It is shown that this process can be successfully described in the frames of cut-off Coulomb potential model within the regions of the electron densities and temperatures. The relevant quantum mechanical method of the calculation of the corresponding spectral coefficient processes is described and discussed. The results obtained for the plasmas with the electron densities from  $10^{14} \text{ cm}^{-3}$  to  $2 \cdot 10^{19} \text{ cm}^{-3}$  and temperatures from  $5 \cdot 10^3 \text{ K}$  to  $3 \cdot 10^4 \text{ K}$  in the wavelength region  $100 \text{ nm} < \lambda < 3000 \text{ nm}$  are presented. Also, these results can be of interest for different laboratory plasmas.

*Key words.* Atomic and molecular processes—plasmas—spectral lines.

### 1. Introduction

Since the Bremsstrahlung process is inevitable in the case of plasma spectroscopy, until now the entire literature was devoted to the subject (see e.g. Berger 1956; Karzas & Latter 1961; D’yachkov 1990; Hazak *et al.* 2002; van Hoof *et al.* 2014; Armstrong *et al.* 2014).

It could be seen in the literature that most of the papers are devoted to the determination of the Gaunt factor for the inverse Bremsstrahlung process. The reason behind this approach lies in the exact relation for the direct Bremsstrahlung process differential cross section (Sommerfeld 1953). This automatically led to the possibility of the exact term for the  $\sigma_{i,b}^{(\text{ex})}(E, \varepsilon_{\text{ph}})$  cross section, where  $E$  is the free electron initial energy,  $\varepsilon_{\text{ph}}$  the absorbed photon energy, for the inverse Bremsstrahlung considered here. In relation with this, although mentioned exact term for  $\sigma_{i,b}^{(\text{ex})}(E, \varepsilon_{\text{ph}})$  relates, strictly speaking, to the case of scattering of the free electron onto the Coulomb potential, it is important to mention that it could be applied onto any diluted enough

plasma (e.g. plasma with considerably small density). The fact that the practical applicability of this term was rather complex led to difficulties in its application. However, for the same process, a simple and widely used quasi classical, Kramer's cross section  $\sigma_{i.b.}^{q.c.}(E, \varepsilon_{ph})$  was known and used in practice. The meaningful idea of presenting  $\sigma_{i.b.}^{(ex)}(E, \varepsilon_{ph})$  in the form

$$\sigma_{i.b.}^{(ex)}(E, \varepsilon_{ph}) = \sigma_{i.b.}^{q.c.}(E, \varepsilon_{ph}) \cdot g_{i.b.}(E, \varepsilon_{ph}), \quad (1)$$

was derived. Here  $g_{i.b.}(E, \varepsilon_{ph})$  is the adequate Gaunt factor. A further step was to yield simple approximations for this quantity.

We mention that, in the general case, both cross sections as well as Gaunt factors are functions not only of  $E, \varepsilon_{ph}$ , but also of the positively charged center on which the free electrons scatter, e.g.  $ze$ , where  $e$  is the modulus of the electron charge and  $z > 0$ . However, only the singly charged plasma should be considered in this manuscript, taking  $z = 1$  in the entire space.

Since, in the case of plasma, adequate absorption coefficient is governed by the inverse Bremsstrahlung process, the natural transition towards the averaged values of the plasma parameters occurs. Such an averaged value is an implicit function of the plasma electron and ion concentration, and explicitly depends on plasma temperature  $T$  as well as absorbed photon wavelength  $\lambda$ . Here, the exact coefficients are denoted by  $k_{i.b.}^{(ex)}(\lambda, T; Ne, Ni)$  and  $k_{i.b.}^{q.c.}(\lambda, T; Ne, Ni)$ , where  $Ne$  is free electron density, and  $Ni$  is the positive ion density.

Accordingly, those coefficients are connected with the relation

$$k_{i.b.}^{(ex)}(\lambda, T; Ne, Ni) = k_{i.b.}^{q.c.}(\lambda, T; Ne, Ni) \cdot G_{i.b.}(\lambda, T), \quad (2)$$

where  $G_{i.b.}(\lambda, T)$  is the sought Gaunt factor. The determination of such averaged Gaunt factor as a function of  $\lambda$  and  $T$  was the object of investigation in majority of the previous papers devoted to the inverse Bremsstrahlung process. This is illustrated in Figure 1, where the behavior of the Gaunt factor  $G_{i.b.}(\lambda, T)$  is shown on the base of the results obtained in several earlier papers (Berger 1956; Karzas & Latter 1961; D'yachkov 1990; van Hoof et al. 2014).

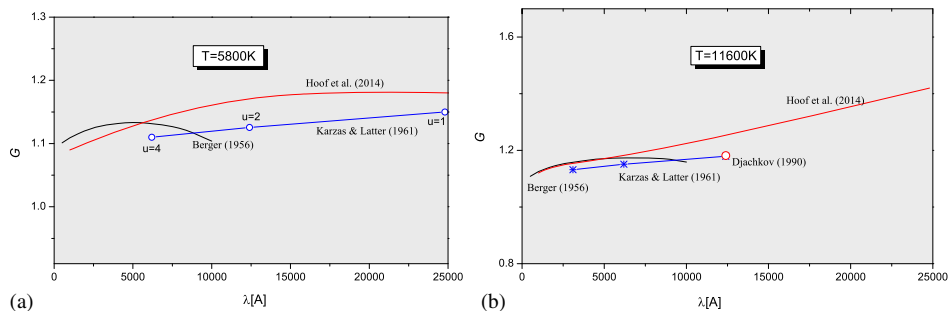


**Figure 1.** (a) Data for Gaunt factor from Berger (1956), Karzas & Latter (1961), D'yachkov (1990) and van Hoof et al. (2014) as a function of  $\lambda$  for  $T = 5800$  K; (b) Same as in Figure 1(a) but for  $T = 11600$  K.

It is clear that the application of the approximate relations, strictly applicable only on the case of diluted plasma, would lead to erroneous error in the case of plasma of higher densities, e.g. non-ideal plasma. The yielding of the applicable relations for the higher density plasma is related with the determination of the adequate coefficient  $\sigma_{i.b.}^{(ex)}$ . It represents a separate problem, and because of this, relatively small amount of published papers were devoted to the determination of the  $\sigma_{i.b.}^{(ex)}$  applicable to the higher density plasma (see Hazak *et al.* 2002; Armstrong *et al.* 2014).

Since the objective of this work is exactly the determination of the absorption coefficient  $k_{i.b.}^{(ex)}(\lambda, T; Ne, Ni)$  and Gaunt factor  $G_{i.b.}(\lambda, T)$  applicable on the case of higher densities plasma, at this point it is necessary to make an observation on the method of their determination in the previous papers in the case of the mentioned dense plasma. Namely, the electron–ion scattering is treated there as a scattering of the electron onto the adequate Yukawa or Debye–Hückel potential. However, in Mihajlov *et al.* (1986), as well as in Mihajlov *et al.* (2011a, b) the fact that Debye–Hückel potential cannot be used for the description of the electron scattering in the case of dense plasma was taken into account. As a reminder, it should be mentioned that the Debye–Hückel potential is defined as a potential of the observed ion and its entire surrounding as a function of the distance from the ion, and as such could be used only for the determination of its average potential energy in the observed plasma. Because of this, in the papers of Mihajlov *et al.* (1986) and Mihajlov *et al.* (2011a, b), a model potential was applied, specially adopted for the description of the electron scattering onto the ion inside the plasma. Here the cut-off Coulomb potential, described by the relations

$$U_{\text{cut}}(r) = \begin{cases} -\frac{e^2}{r} + \frac{e^2}{r_c}, & 0 < r \leq r_c, \\ 0, & r_c < r \end{cases} \quad (3)$$

is pointed out. Here  $r_c$  is the cut-off radius, and  $-e^2/r_c$  is the average potential energy of the electron in the considered plasma. Let us note that such a potential, which was introduced in the considerations in Suchy (1964) in connection with the transport plasma processes was investigated in detail in Mihajlov *et al.* (1986). Here we will show that in the case of non-ideal plasmas this potential could be successfully applied also for determination of spectral coefficients for the electron–ion inverse Bremsstrahlung processes.

## 2. Theory

Since the potential equation (3) is one of the finite radius for determination of the cross section  $\sigma_{i.b.}^{(ex)}$  for the inverse Bremsstrahlung process, we can use the standard expressions from Sobelman (1979), namely

$$\sigma_{i.b.}^{(ex)}(E; E') = \frac{8\pi^4}{3} \frac{\hbar e^2 k}{q^2} \sum_{l'=l\pm 1} l_{\max} |\hat{D}_{E,l;E'l'}|^2, \quad (4)$$

$$\hat{D}_{E,l;E'l'} = \int_0^\infty P_{E'l'}(r) \cdot r \cdot P_{E,l}(r) dr,$$

where  $r$  is the distance from the beginning of the coordinate system,  $P_{E;l}(r)$  is the solution of the radial Schrodinger equation

$$\frac{d^2 P_{E;l}(r)}{dr^2} + \left[ \frac{2m}{\hbar^2} (E - U_{\text{cut}}(r)) - \frac{l(l+1)}{r^2} \right] P_{E;l}(r) = 0, \quad (5)$$

and  $U_{\text{cut}}(r)$  is the cut-off Coulomb potential given by equation (3).

Let us note that because of the well known properties of the free electron wave functions, the direct calculation of the dipole matrix element  $\hat{D}_{E;l;E'l'}$  is practically impossible until now.

However, cut-off Coulomb potential model gives the possibility of direct determination of the cross section for the inverse Bremsstrahlung process without any additional approximations. For that purpose it is enough to use in equation (4) the matrix element of the gradient of the potential energy instead of the dipole matrix element Sobelman (1979) given by

$$|\hat{D}(r)_{ab}|^2 = \frac{\hbar^4}{m^2 (E_a - E_b)^4} |\nabla U_{ab}|^2, \quad (6)$$

$$\nabla_r U_{ab} = \int_0^{r_{\text{cut}}} P_b(r) \cdot \nabla_r U(r) \cdot P_a(r) dr. \quad (7)$$

Namely, in the case of the cut-off potential (3) in the last expression, integration over  $r$  is carried out only in the interval from 0 to  $r_{\text{cut}}$ .

The given method enabled the fast and reliable calculation of the discussed cross section and, consequentially, the corresponding spectral absorption coefficient.

Here, it is common to use a dimensionless coupling parameter, the plasma non-ideality coefficient  $\Gamma$ , that characterizes the physical properties of the plasma. It is of special importance to describe dense, non-ideal plasmas, as the ones considered in this paper. The parameter  $\Gamma = e^2/(akT)$  as such characterizes the potential energy of interaction at average distance between particles  $a = (3/4\pi n_e)^{1/3}$  in comparison with the thermal energy. The well-known Brueckner parameter  $r_s = a/a_B$  is the ratio of the Wigner–Seitz radii to the Bohr radius.

In connection with this, we considered here plasma with the electron densities from  $10^{14} \text{ cm}^{-3}$  to  $2 \cdot 10^{19} \text{ cm}^{-3}$  and temperatures from  $5 \cdot 10^3 \text{ K}$  to  $3 \cdot 10^4 \text{ K}$ , where the corresponding coupling parameter  $\Gamma \leq 1.3$ . For such plasmas, in accordance with Mihajlov et al. (1993) and Adamyan et al. (1994), we have that the value of the chemical potential for electron component (treated as appropriate electron gas on the positive charged background) is practically equal to the value which is obtained in the classical case. This means that the distribution function for electrons may be taken as appropriate Maxwell's function. In accordance with this, we will look for  $\kappa_{i.b.}^{(\text{ex})}$  in the form

$$\begin{aligned} \kappa_{i.b.}^{(\text{ex})}(\varepsilon_\lambda; N_e, T) = & N_i N_e \cdot \int_0^\infty \sigma_{i.b.}^{(\text{ex})}(E; E') v \\ & \cdot f_T(v) \cdot 4\pi v^2 dv \cdot \left( 1 - \exp \left[ -\frac{\hbar\omega}{kT} \right] \right), \end{aligned} \quad (8)$$

where  $f_T(v)$  is the corresponding Maxwell-ova distribution function for a given temperature  $T$ , and the expression in parentheses was introduced in order to take into account the effect of stimulated emission. On the other hand, quasi classical Kramer's  $k_{i.b.}^{q.c.}(\lambda, T; Ne, Ni)$  is given by the known expression (see e.g. Sobelman 1979), namely

$$k_{i.b.}^{q.c.}(\lambda, T; Ne, Ni) = N_i N_e \cdot \frac{16\pi^{5/2} \sqrt{2} e^6}{3\sqrt{3} cm^{3/2} \varepsilon_{ph}^3} \frac{\hbar^2}{(kT)^{1/2}} \left( 1 - \exp \left[ -\frac{\hbar\omega}{kT} \right] \right), \quad (9)$$

where  $\varepsilon_{ph} = 2\pi \hbar c / \lambda$ . According to this, averaged Gaunt factor  $G_{i.b.}(\lambda, T)$  is determined here from equation (2), where  $k_{i.b.}^{(ex)}(\lambda, T; Ne, Ni)$  and  $k_{i.b.}^{q.c.}(\lambda, T; Ne, Ni)$  are given by equations (8) and (9).

### 3. Results and discussion

In this work, the calculations of the Gaunt factor  $G_{i.b.}(\lambda, T)$  was carried out for the electron densities in the range from  $10^{14} \text{ cm}^{-3}$  to  $2 \cdot 10^{19} \text{ cm}^{-3}$  and temperatures from  $5 \cdot 10^3 \text{ K}$  to  $3 \cdot 10^4 \text{ K}$ , where the coupling parameter is  $0.01 \leq \Gamma \leq 1.3$ . The observed wavelengths cover the region  $100 \text{ nm} < \lambda < 3000 \text{ nm}$ . The important quantity for the process of the light plasma interactions is critical plasma density. This quantity plays an important role because the critical plasma density is the free electron density at which the absorption tends to be the maximum  $n_c = 1.113 \cdot 10^{21} (1/\lambda_{\mu m})^2 \text{ cm}^{-3}$ . Absorption occurs at densities less than the critical density (where the plasma frequency  $\omega_p = (4\pi n_e e^2 / m)^{1/2}$  equals the optical frequency). In connection with the investigation of inverse Bremsstrahlung processes in different stellar atmospheres (for e.g. solar and different dwarf atmospheres) in the range of the investigated wavelengths  $100 \text{ nm} \leq \lambda \leq 3000 \text{ nm}$ , the critical electron densities lie in the region of densities between  $\sim 10^{20} \text{ cm}^{-3}$  and  $10^{23} \text{ cm}^{-3}$ .

Here the obtained results are illustrated in Figures 2, 3 and 4. Figure 2 illustrates the behavior of the Gaunt factor  $G_{i.b.}(\lambda, T)$  for the electron concentrations

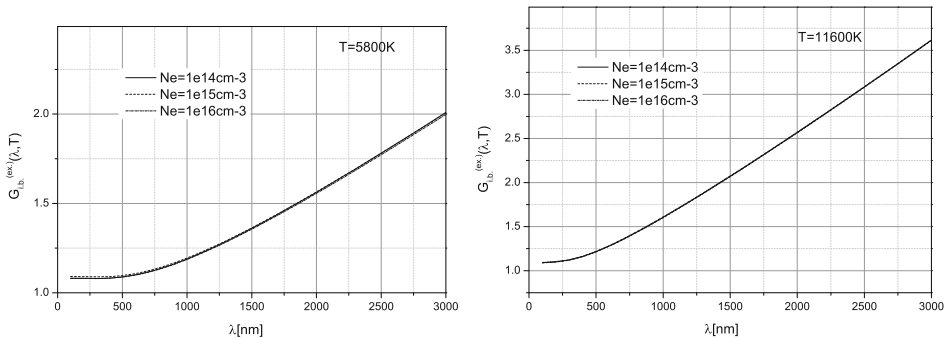


**Figure 2.** (a) Behavior of the Gaunt factor  $G_{i.b.}^{(ex.)}(\lambda, T)$  for temperature  $T = 5800 \text{ K}$  and electron concentration  $Ne = 10^{14} \text{ cm}^{-3}$ ,  $10^{15} \text{ cm}^{-3}$  and  $10^{16} \text{ cm}^{-3}$ , (b) Same as in Figure 2(a) but for  $T = 11600 \text{ K}$ .

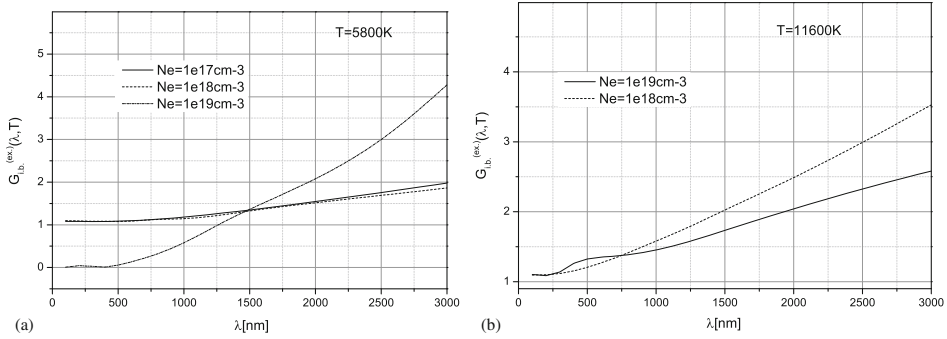


**Figure 3.** (a) Behavior of the Gaunt factor  $G_{i,b}^{(ex.)}(\lambda, T)$  for temperature  $T = 5800$  K and  $N_e = 10^{17} \text{ cm}^{-3}$ ,  $10^{18} \text{ cm}^{-3}$  and  $10^{19} \text{ cm}^{-3}$ . (b) Calculated values  $G_{i,b}^{(ex.)}(\lambda, T)$  at  $T = 11600$  K for  $10^{18} \text{ cm}^{-3}$  and  $10^{19} \text{ cm}^{-3}$ .

$10^{14} \text{ cm}^{-3}$ ,  $10^{15} \text{ cm}^{-3}$  and  $10^{16} \text{ cm}^{-3}$  and temperatures 5800 K and 11600 K, and Fig. 3 illustrates the electron concentrations  $10^{17} \text{ cm}^{-3}$ ,  $10^{18} \text{ cm}^{-3}$  and  $10^{19} \text{ cm}^{-3}$  in the same temperature range as in Figure 2. Figure 4 illustrates the dynamics of the Gaunt factor change with the increase of the electron concentrations from  $10^{18} \text{ cm}^{-3}$  up to  $10^{19} \text{ cm}^{-3}$  in the case of  $T = 11600$  K. Let it be noted that each of the figures shows a Gaunt factor behavior determined for the same temperature also, as in the case of an ideal plasma. It enables the estimate of the differences, bearing in mind the electron–ion influence on the inverse Bremsstrahlung in the case of non-ideal plasma. Our attention should be focused on the fact that the dependence of the Gaunt factor  $G_{i,b}^{(ex.)}(\lambda, T)$  on the electron density is governed by the dependence of the screening radius  $r_{\text{cut}}$  in equation (3) on the same electron density.

The data shown in Figure 5 enables the comparison of the results obtained here with the results of electron–ion inverse Bremsstrahlung processes in the case of

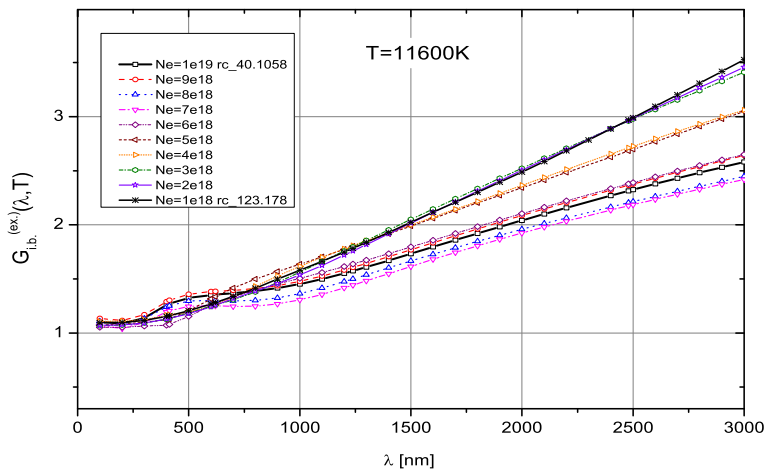


**Figure 4.** Dynamics of the Gaunt factor change with increase of the electron density from  $N_e = 10^{18} \text{ cm}^{-3}$  to  $10^{19} \text{ cm}^{-3}$  in the case of temperature  $T = 11600$  K.

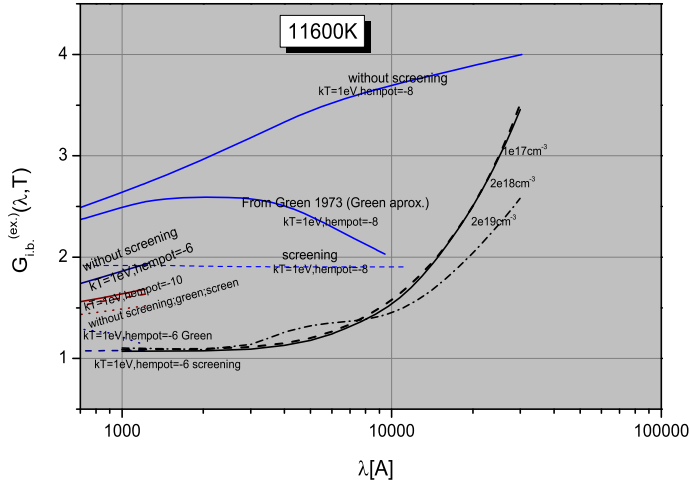


**Figure 5.** The behavior of the mean Gaunt factor for few cases that differ in the values of the chemical potential of electronic components ( $\mu_{e1}$ ), i.e. concentration of free electrons at  $T = 11600$  K (Armstrong *et al.* 2014), together with our corresponding data (solid, dashed and dotted black lines).

non-ideal plasma by other authors. This figure shows the behavior of the averaged Gaunt factor  $G_{i,b.}(\lambda, T)$  determined in Armstrong *et al.* (2014) for  $T = 11600$  K in several cases of different chemical potential of the electron component ( $\mu_{e1}$ ), that implies different electron concentrations also. The following cases are considered:  $\mu_{e1} = -10, -8, -6$ . The same figure also shows the behavior of the Gaunt factor  $G_{i,b.}^{(ex.)}(\lambda, T)$  determined for the corresponding region of electron concentration and temperature. The differences of the obtained results and those from Armstrong *et al.* (2014) are evident in the figure and expected. It is clear that these differences are affected by the principal differences in the way of describing the electron–ion scattering in the rest of the plasma.

#### 4. Conclusion

The exact quantum mechanical method presented here could be used to obtain the spectral coefficients for inverse Bremsstrahlung process for the broad class of weakly non-ideal plasmas as well as for plasma of higher non-ideality. It is expected that the cut-off Coulomb potential model results are more accurate in comparison with other methods, which is so far used for cases of non-ideal plasma. Certainly, this method can be of interest in connection with the investigation of inverse Bremsstrahlung processes in different stellar atmospheres. Also, these results can be of interest for different high energy laboratory plasma research.

#### Acknowledgements

The authors are thankful to the Ministry of Education, Science and Technological Development of the Republic of Serbia for the support of this work under the projects 176002, III44002 and 171014.



**References**

- Adamyany, V. M., Djuric, Z., Ermolaev, A. M., Mihajlov, A. A., Tkachenko, I. M. 1994, *J. Phys. D*, **27**, 927.
- Armstrong, G. S. J., Colgan, J., Kilcrease, D. P., Magee, N. H. 2014, *High Energy Density Phys.*, **10**, 61.
- Berger, J. M. 1956, *ApJ*, **124**, 550.
- D'yachkov, L. G. 1990, *J. Phys. B At. Mol. Phys.*, **23**, L429.
- Hazak, G., Metzler, N., Klapisch, M., Gardner, J. 2002, *Phys. Plasmas (1994-present)*, **9**, 345, doi: [10.1063/1.1408913](https://doi.org/10.1063/1.1408913).
- Karzas, W. J., Latter, R. 1961, *ApJS*, **6**, 167.
- Mihajlov, A. A., Djordjević, D., Vučić, S., Kraeft, W. D., Luft, M. 1986, *Contrib. Plasma Phys.*, **26(1)**, 19–35.
- Mihajlov, A. A., Ermolaev, A. M., Djuric, Z., Ignjatovic, L. 1993, *J. Phys. D*, **26**, 1041.
- Mihajlov, A. A., Sakan, N. M., Srećković, V. A., Vitel, Y. 2011a, *J. Phys. A Math. Gen.*, **44**, 095502.
- Mihajlov, A. A., Sakan, N. M., Srećković, V. A., Vitel, Y. 2011b, *Balt. Astron.*, **20**, 604.
- Sobelman, I. I. 1979, Springer Series in Chemical Physics, Springer, Berlin.
- Sommerfeld, Arnold 1953, *Atombau und Spektrallinien*, 2 Bnde (vol. 2).
- Suchy, K. 1964, *Beitr. Plasma Phys.*, **4**, 71.
- van Hoof, P. A. M., Williams, R. J. R., Volk, K. *et al.* 2014, *MNRAS*, **444**, 420.

# SOFTWARE/HARDWARE DESIGN OF DECISION-MAKING CONTROLLERS FOR OBJECT NAVIGATION IN HORIZONTAL PLANE

*Mohammed Amine Boulahlib, Momcilo Milinovic, Mourad Bendjaballah, Olivera Jeremic, Nenad Sakan*

Original scientific paper

The paper aims to research the orientation possibilities of an object in the horizontal plane, from its start course into a required orientating recourse, by using simplified navigation methods. The object's directed motion uses controlling powering impulses, variable distributed in time, during constrained motion time. Three logical decision-making methods are designed for calculating the best maneuvering trajectory with minimal error on the target. Computing the powering impulses, their execution instances, as well as their types, are ensured by the methods and presented in the paper. The developed controlling methods are: a modified multiple shooting method, a new control law, called in this paper, current error orientation, as well as a fuzzy logic method. These methods are designed as decision-making software implemented in an electronic hardware as a predefined programmable controller. This provides pre-programmable orientation of the object at the very beginning of course motion, towards a targeted point settled out of initial direction. The controlling methods use optimal diversification of full elapsed determining time to execute, in sequences, appropriate types and number of powering impulses. Simulation tests of the methods, as well as the designed hardware, are also presented in this paper as a contribution to the development researches of horizontal motion control.

**Keywords:** *fuzzy logic controller; guidance laws; programmable motion; shooting method; software/hardware set up*

## Dizajn softvera/hardvera kontrolera za donošenje odluke pri navigaciji objekta u horizontalnoj ravnini

Izvorni znanstveni članak

Cilj rada je istražiti mogućnosti orijentacije objekta u horizontalnoj ravnini, počevši od njegovog početnog kursa u zahtjevani rakurs, koristeći pojednostavljene metode navigacije. Usmjeravanje gibanja objekta koristi kontrolirane pogonske impulse neravnomjerno distribuirane u ograničenom vremenskom intervalu gibanja. Dizajnirane su tri metode logičkog odlučivanja za izračunavanje najbolje putanje, čije su greške na cilju minimalne. Računanje pogonskih impulsa, njihovih izvršnih instanci kao i tipova, prezentirani su u ovom radu. Razvijene kontrolne mjere su: modificirana višestruka shooting metoda, odnosno novi zakon upravljanja kako je nazvan u ovom radu, trenutna orijentacijska greška, kao i metoda fuzzy logike. Metode su projektirane kao softver za donošenje odluke implementiran u elektronski hardver kao predefimirani programabilni kontroler. To daje preliminarno programiranje usmjeravanja objekta na samom početku kursa gibanja prema ciljnoj točki smještenoj van početnog pravca. Metodama se optimiziraju raspodijele ukupno determiniranog vremena radi realiziranja odgovarajućih tipova i broja pogonskih impulsa u sekvencama. Simulacijski testovi ovih metoda, kao i projektirani hardver, također su prezentirani u radu kao doprinos razvojnog istraživanju upravljanja horizontalnim gibanjem.

**Ključne riječi:** *fuzzy logički kontroler; programabilna gibanja; shooting metoda; softver/hardver oprema; zakoni vođenja*

## 1 Introduction

Controlled objects in the horizontal plane have been the subject of research in tremendous number of papers over the last decades. The studied controlled objects are mainly wheeled mobile robots and vehicles. Their control presents a serious challenge as it brings laterally all the problems that can be faced in control theory. Various approaches to their control are offered in literature. There are approaches that do not aim to imitate the human behaviour but simply use the well-known control forms. These are time-varying controllers, typically known by low convergence speed [1, 2], or time-invariant controllers, with discontinuities, usually characterized by exponential convergence speed [3, 4]. The approaches to multi-level controllers consist of two levels: the lower one is presented by the classical proportional, integral and differential (PID) laws of control [5], while the higher-sophisticated level, mainly targets an imitation of human behaviour, with a goal to avoid constraints imposed by the environments [6, 7], or with an appropriate selection of the desired robot trajectory [8]. The present research paper considers the navigation problem of a new subject of control, referred as an optimal orientated motion of an object, executed by powering impulses (henceforth impulses), in a horizontal plane, from its start course into a required recourse, orientated to a target point. The object's motion has the next specifications: a rigid constrain of full motion time, only one-way possibility of

maneuver and a limited number of impulses. These specifications are interpreted by the mathematical model but lead to development of new approaches for the object's control.

The paper presents three new applications of controlling approaches: numerical controlling algorithm presented by a Modified Multiple Shooting method (henceforth MMS), time-invariant controller, called in this paper Current Error Orientation (henceforth CEO), as well as fuzzy logic method (henceforth FLC), basically developed as requirement to imitate human behaviour, presented in papers [9, 10]. The goal of these controlling methods is to evaluate the best navigating-maneuvering trajectory to the target point from the initial course, by making decision on the types and sequence of impulses' execution. Derived simulations, supported by numerous optimizing examples with and without presence of perturbations, are discussed further in this paper. The controlling methods are implemented on a software/hardware experimental platform designed for simulating types and execution sequences of the impulses, calculated by the mentioned methods. The research results given in this paper are a new contribution in controlling process, for object's simplified navigation, based on their sequent orientation during elapsed time instants, programmed previously, as designed requirements, to move from starting to the targeting point.

## 2 Mathematical model of the object motion

It is supposed that the object’s motion is achieved in the horizontal plane and constrained by invariant full time  $\tau$  and same initial distance-to-target with and without maneuver D (Fig. 1a). This motion consists of two phases, first is a straight line phase with constant velocity without any external controlling inputs, whereas the second one is a controlled orientating phase. First phase’ course and its radial displacement, before orientating the object are given by equations of motion, in the polar coordinate system, respectively as,

$$\varphi^{(1)} = \varphi_0, \rho^{(1)} = V_0^{(1)}t \tag{1}$$

where  $\varphi_0$  is the initial course and  $V_0^{(1)}$  is the initial object’s velocity in the 1<sup>st</sup> phase.

Straight-line phase is presented in Fig. 1a as the trajectory from A to B with a required duration of  $\tau^{(1)} = \tau \times \tau^*$ , where  $\tau^* = \tau^{(1)} / \tau$  is the relative time factor.

Initial distance-to-target D is presented in Fig. 1a as the distance from A to C (with maneuver) which is equal to the distance from A to C’ (without maneuver). The distance D is given as;

$$D = V_0^{(1)}\tau \tag{2}$$

The second orientating phase is mainly defined by two parameters, one is the relative time factor  $\tau^*$  and the other is turning course angle  $\Delta\varphi$  (Fig. 1a). This phase is divided into (N) sub-phases noted as (i+1) for  $i = 1, 2, \dots, N$ , after the achievement of the first phase. The phase duration is  $\tau^{(2)} = \tau - \tau^{(1)}$  along recourse line (BC) (Fig. 1b).

It is supposed that the initial horizontal velocity is known at the moment of maneuvering and that for each of the sub-phases the horizontal velocity is generally expressed as

$$\vec{V}_0^{(i+1)} = \vec{V}_1^{(i)} + \vec{U}^{(i+1)} = \vec{V}_0^{(i)} + \vec{U}^{(i+1)} \tag{3}$$

where  $\vec{V}_0^{(i+1)}$  and  $\vec{V}_0^{(i)}$  are the initial velocity vectors in the sub-phases (i) and (i+1) respectively, whereas  $\vec{U}^{(i+1)}$  represents the orientating velocity vector. It has to be noted that the initial and final velocity vectors in any sub-phases are the same ( $\vec{V}_1^{(i)} = \vec{V}_0^{(i)}$ ).

Initial course and radial distance for each sub-phase (i+1) correspond to their achieved homologues in the previous sub-phase i (Fig. 1b) as,

$$\rho_0^{(i+1)} = \rho_1^{(i)} \text{ and } \varphi_0^{(i+1)} = \varphi_1^{(i)} \tag{4}$$

In this paper, the initial values of the radial unit vector  $\vec{\lambda}_0^{(i+1)}$  as well as the turning unit vector  $\vec{\mu}_0^{(i+1)}$  in the particular phase (i + 1) are respectively equal to their homologues  $\vec{\lambda}_0^{(i)}$  and  $\vec{\mu}_0^{(i)}$  at the end of the previous phase (i) (Fig. 1b), as

$$\vec{\lambda}_0^{(i+1)} = \vec{\lambda}_1^{(i)} \text{ and } \vec{\mu}_0^{(i+1)} = \vec{\mu}_1^{(i)} \tag{5}$$

If the duration of a sub-phase is  $\tau^{(2)}$ , starting at the maneuver beginning B and achieving at target point C, the turning motion has only one sub-phase. This case is considered as mono-phase and its turning distance and time are invariant values in the above model.

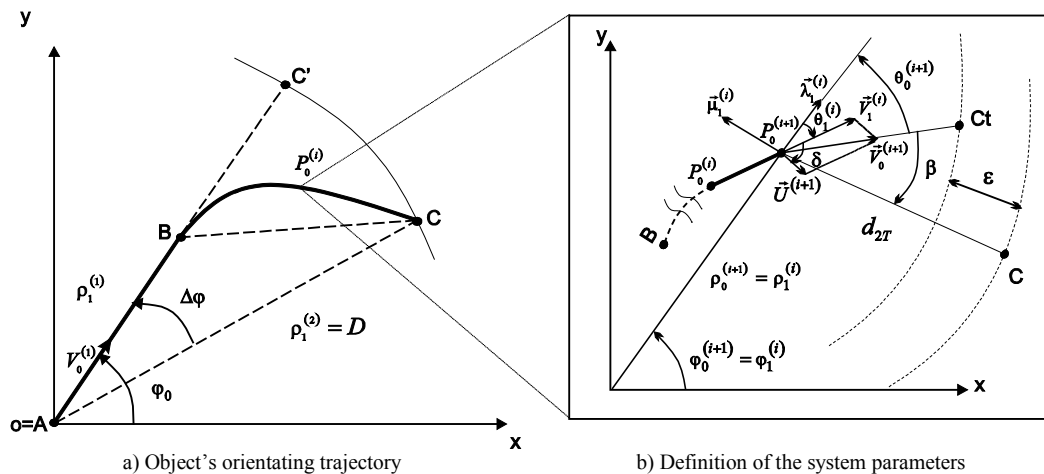


Figure 1 Controlled object trajectory and parameters

Mono-phase turning motion requires higher values of orientating velocity components for the maneuvering motion, while multi-phase turning is less restrictive and can be used to avoid the rigid motion conditions during the orientation. The mono-phase maneuvering path, along recourse line (B to C) (Fig.1-a) is considered as a referencing distance to test achieved maneuvering

recourses in sub-phases, and final motion errors to target C.

The orientating velocity  $\vec{U}^{(i+1)}$  in Eq. (3) is characterized by its magnitude  $U^{(i+1)}$  and direction  $(\nu + \theta_1^{(i)})$ , in the polar coordinate system (Fig. 1b), as;

$$\vec{U}^{(i+1)} = U^{(i+1)}[\cos(\nu + \theta_1^{(i)})\vec{\lambda}_0^{(i+1)} + \sin(\nu + \theta_1^{(i)})\vec{\mu}_0^{(i+1)}] \tag{6}$$

where  $\nu$  is the angle between  $\vec{U}^{(i+1)}$  and  $\vec{v}_0^{(i)}$ , while  $\theta_1^{(i)}$  is the final direction of  $\vec{v}_0^{(i)}$  in the sub-phase ( $i$ ). By scalar and vector optimization of the orientating velocity vector given in Eq. (6), three cases of impulses generating the orientating velocity are adopted to be used in simulation tests. They are the next;

- *Lateral impulse for turn-of motion* where the orientating velocity  $\vec{U}$  is characterized by a finite magnitude and a fixed angle  $\nu$  nearby  $80^\circ$ . This type of impulses, noted as  $\vec{U}_{Lat}$ , has two components: one is orthogonal to the object's velocity  $\vec{v}_0$ , which represents the only contribution to the turning motion and the major part of orientating velocity magnitude. The other one is longitudinal, as velocity addition along  $\vec{v}_0$  direction, to slightly adjust misses due to lateral motion path. The expression of object's velocity, in the ( $i+1$ ) sub-phase, in the polar coordinate system, is given by :

$$\vec{v}_0^{(i+1)} = \left[ V_1^{(i)} \cos(\theta_1^{(i)}) + U_{Lat} \cos(\nu + \theta_1^{(i)}) \right] \vec{\lambda}_0^{(i+1)} + \left[ V_1^{(i)} \sin(\theta_1^{(i)}) + U_{Lat} \sin(\nu + \theta_1^{(i)}) \right] \vec{\mu}_0^{(i+1)} \quad (7)$$

- *Longitudinal impulse for run motion* is a contribution to run-to-target motion. In this case the orientating velocity is noted as  $\vec{U}_{Lon}$ , and defined by a finite magnitude and a null angle  $\nu$ . This impulse role is to correct the missed distance-to-target made by elapsed constrained time to move object to the targeted point C. The expression of  $\vec{v}_0^{(i+1)}$  is shown as:

$$\vec{v}_0^{(i+1)} = \left[ (V_1^{(i)} + U_{Lon}) \cos(\theta_1^{(i)}) \right] \vec{\lambda}_0^{(i+1)} + \left[ (V_1^{(i)} + U_{Lon}) \sin(\theta_1^{(i)}) \right] \vec{\mu}_0^{(i+1)} \quad (8)$$

- *No impulses*, this type motion is the most common where the object continues its movement in the same direction with its same velocity magnitude. In this case, the magnitude of the orientating velocity vector is to equal zero, for that the object's velocity is expressed as;

$$\vec{v}_0^{(i+1)} = \left[ V_1^{(i)} \cos(\theta_1^{(i)}) \right] \vec{\lambda}_0^{(i+1)} + \left[ V_1^{(i)} \sin(\theta_1^{(i)}) \right] \vec{\mu}_0^{(i+1)} \quad (9)$$

The types of the impulses are abbreviated in the following text as Lat, Lon and Ni for lateral, longitudinal and no impulse respectively. By determining the types of the impulses in every sub-phase, the maneuvering phase may be adjusted and corrected in both misses by distance-to-target and by direction.

Orientating velocities,  $\vec{U}_{Lat}$  and  $\vec{U}_{Lon}$  in this manuscript, are previously defined by determined time profiled values, starting from 0 to  $U_{max}$  during a short elapsed instants  $\Delta\tau$ . Different logic controllers are tested to select the best impulse execution sequences to make software base, which provides minimal errors in the maneuver powered by impulses.

### 3 Definition of the controlling methods

Three methods are proposed and implemented to optimize the sequent turning trajectories toward the target, by calculating the instants of activation and the types of impulses. The idea is to divide the maneuvering phase time  $\tau_2$  into  $N$  intervals of  $\Delta t$ , then respectively apply one of the following decision-making methods to activate one of impulse types, by Eq. (7), (8) and (9), at each interval beginning from 1 to  $N$ . The goal is to calculate sub-trajectories for each interval, so that the trajectory to the target C is the connection of the  $N$  sub-trajectories. The methods that solve the problem are given in the following paragraphs.

#### 3.1 Modified multiple shooting method

The classical single shooting method is a numerical method widely used for solving two-point boundary value problems (BVP), these are mainly differential equations with initial and final values of the solution prescribed, as given in [11]. This method takes its name from varying the initial slope to suggest the trajectory of an object "shot" from the initial point. That initial slope is sought which results in the trajectory "hitting" the target or the final value, reported by [12]. The controlled object's motion phase can be considered as a kind of BVP where the initial and final values are the start-maneuvering point B and the target C respectively. Taking into consideration the specifications of the system, the variation of the initial slope is limited to the mentioned three types of impulses (Lat, Lon and Ni) as determined by Eq. (7), (8) and (9). The controlling method has to evaluate the trajectory between the boundary points B and C.

The modified multiple shooting method (MMS) uses the time decomposition of the problem, together with additional matching conditions at the time interfaces as used in the original direct multiple shooting [13]. Precisely, the time domain is divided into ( $N$ ) intervals  $\Delta t = [t^{i-1}, t^i]$  for  $i = 1, 2, \dots, N$ , where  $\tau^{(2)} = [t^0, t^N]$  and;

$$\tau^{(1)} = t^0 < t^1 < \dots < t^N = \tau \quad (10)$$

The novelty is that the MMS instead of introducing artificial initial values for each time interval, applies three single shots before selecting the best one. The best shot selection is based on an optimality criterion presented by the minimal temporary final error to the target.

$$E_i(I_i, t_{i-1}) = \sqrt{(x_T - x_f^{(i+1)})^2 + (y_T - y_f^{(i+1)})^2} \quad (11)$$

where  $I_i$  is the impulse type selected for the sub-phase ( $i+1$ ) and applied at  $t_{i-1}$ . The parameters  $(x_T, y_T)$  are the target's coordinates while  $(x_f^{(i+1)}, y_f^{(i+1)})$  are the temporary final object's coordinates calculated with the remaining time  $t_{2go} = \tau_2 - (i-1)\Delta t$  based on the impulse type by Eqs. (7), (8) and (9). The temporary final object's coordinates are given as

$$\begin{cases} x_f^{(i+1)} = \rho_1^{(i)} \cos(\varphi_1^{(i)}) + (V_0^{(i+1)} t_{2go}) \cos(\varphi_1^{(i)} + \theta_0^{(i+1)}) \\ y_f^{(i+1)} = \rho_1^{(i)} \sin(\varphi_1^{(i)}) + (V_0^{(i+1)} t_{2go}) \sin(\varphi_1^{(i)} + \theta_0^{(i+1)}) \end{cases} \quad (12)$$

It is important to emphasize that the  $E_N(I_N, t_{N-1})$  represents the final error distance to the target, noted in the following text as  $Err_{df}$ .

The MMS presented above aims to evaluate the optimal trajectory between the boundary points B and C that minimizes the cost functional  $J$  of the temporary final errors to the target given as;

$$\min J = \sum_{k=1}^N [E_k(I_k, t_{k-1})]^2 \quad (13)$$

The outputs of the MMS are the types of impulses applied at the instances  $t_{k-1}$  that generate the optimal trajectory. Making the MMS into practice, for instance, for the  $j^{th}$  interval start between 1 to  $N$ , the algorithm computes the trajectories with the remaining time, after the three shots. The closest shot to the target is selected as the best shot. The trajectory induced by the best shot is then adopted for the  $j^{th}$  interval and its final values are used as initial values for determination of the best shot for the  $(j+1)^{th}$  interval. The optimal couple data resulted in this method is used to evaluate the other methods.

### 3.2 Current error orientation method

The maneuvering object's motion, in this section, is treated as a controlled navigation between start-orientating point B and the target C, taking into consideration the above mentioned specifications of the system. Based on these facts, a logical decision-making controller is designed to ensure minimal error to the target for this type of systems. In this paper, a new time-invariant controller, called Current Error Orientation controller (CEO), is designed and its structure is showed in Fig. 2.

The designed two-input-one-output CEO controller uses as inputs: the error  $E_1(t)$  that marks the disparity between the desired angle  $\beta_c$  and the angle  $\beta(t)$ , and the error  $E_2(t)$  which represents the difference between the desired current error  $\varepsilon_c$  and the actual current error  $\varepsilon(t)$  where  $\beta(t)$  represents the angle between the object's velocity vector  $\vec{v}^{(i)}(t)$  and the current line-to-target  $(P_0^{(i+1)}C)$  (Fig. 1-b), while the current error  $\varepsilon(t)$  is defined as the difference between the remaining distance to the target  $d_{2T}$  and the distance to go  $d_{2go}$ ,  $(P_0^{(i+1)}Ct)$  (Fig. 1b), in the motion direction calculated by  $\vec{v}^{(i)}(t)$  and the remaining motion time  $t_{2go}$  as,

$$\varepsilon(t) = d_{2T} - d_{2go} = d_{2T} - V^{(i)} t_{2go} \quad (14)$$

The mathematical expressions of  $E_1(t)$  and  $E_2(t)$  are given by Eq. (15) and Eq. (16) respectively.

$$E_1(t) = \beta_c - \beta(t) \quad (15)$$

$$E_2(t) = \varepsilon_c - \varepsilon(t) \quad (16)$$

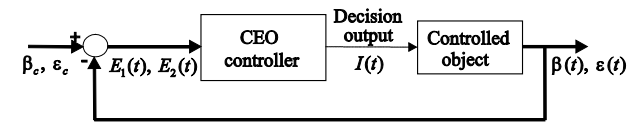


Figure 2 Structure and input/output definition of CEO method

The CEO controller output is the decision  $I(t)$  on the type of the impulse to be used (Lat, Lon and Ni). The output  $I(t)$  follows a designed time-invariant law given by Eq. (17).

$$I(t) = \begin{cases} Lat & E_1(t) > 0 \\ Lon & E_1(t) \leq 0 \text{ and } E_2(t) > 0 \\ Ni & otherwise \end{cases} \quad (17)$$

The CEO controller given by Eq. (17) regulates the object's direction  $\beta(t)$  towards the target, interpreted by  $E_1(t)$ , by means of lateral impulses (Lat). After achieving the desired direction  $\beta(t)$ , the CEO controller implicitly adjusts the final error by controlling their current value  $\varepsilon(t)$ , represented by  $E_2(t)$ , by executing the longitudinal impulses (Lon). In case of reaching both desired direction  $\beta(t)$  and current error  $\varepsilon(t)$ , the controller makes the decision of no impulse use (Ni), which corresponds to the third type. These logical decisions are generated for each instance  $t$  during the maneuvering phase.

The choice of the set-points or the desired inputs is crucial for the reason that it affects directly the work of CEO controller. This choice has to fit the system requirements and specifications. In this application, the choice of  $\beta_c$  and  $\varepsilon_c$  was  $\beta_c \in [2.1^\circ, 2.6^\circ]$  and  $\varepsilon_c = 25$  m, which corresponds to the desired requirement for a one-way maneuver.

### 3.3 Fuzzy logic method

The maneuvering The schematic structure of the decision-making Fuzzy Logic Controller (FLC) is shown in Fig. 3, where FLC is used for controlling the object's lateral motion powered by impulses. FLC is designed, in this present application, to make decisions on the type of impulses to be executed in each time interval. This impulse sequence is made to ensure minimal error for each pre-defined angle  $\Delta\varphi$  and relative factor  $\bar{T}$  of maneuver.

Membership functions are used by fuzzy logic to define the degree to which crisp physical input values belong to terms in a linguistic variable set. Generally, FLCs are mainly composed of three basic components, which are the fuzzification block, fuzzy inference engine (rule base), and defuzzification block, reported by [14]. The essence of any FLC is the fuzzy inference engine which includes both the decision-making logic and knowledge base. The fuzzification block converts each crisp input information into fuzzy values. The knowledge base comprises a database with necessary linguistic variables as a set of rules, while decision-making logic is used to decide how the fuzzy logic operations are performed. The fuzzy inference engine determines the outputs, as fuzzy values, of each fuzzy IF-THEN rule.

These fuzzy values (outputs) are converted into crispy values in the defuzzification block.

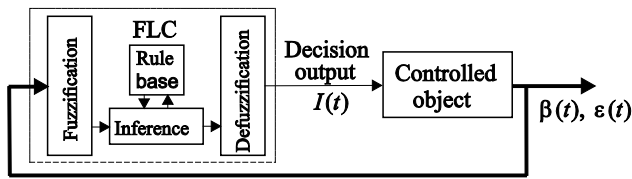


Figure 3 Structure of fuzzy logic method

The FLC designed in this paper is a two-input-one-output controller. The inputs to the FLC are the angle  $\beta(t)$  and the current error  $\varepsilon(t)$  from the CEO method (Fig. 1b). Both inputs are defined on a universe of discourse with three membership functions, for  $\alpha(t)$  (Small, Medium and

Large) and for  $Err_{logo}(t)$  (Negative, Zero and Positive) or abbreviated as (S, M and L) and (N, Z and P) respectively.

The output of the FLC is the decision  $I(t)$  on the impulse type to be executed at the start of a particular time interval. Accordingly the output is attributed to three membership functions (Lateral, Longitudinal and No impulse), or abbreviated as (Lat, Lon and Ni).

The trapezoidal shaped membership functions are used to fuzzify the input variables while triangular shaped ones are used for output variable. The membership boundaries are shown in Fig.4 and their coefficients  $\beta_i, i = 1, \dots, 7, \varepsilon_i, i = 1, \dots, 6, I_i, i = 1, 2, 3$  and  $w$  are given in Tab. 1.

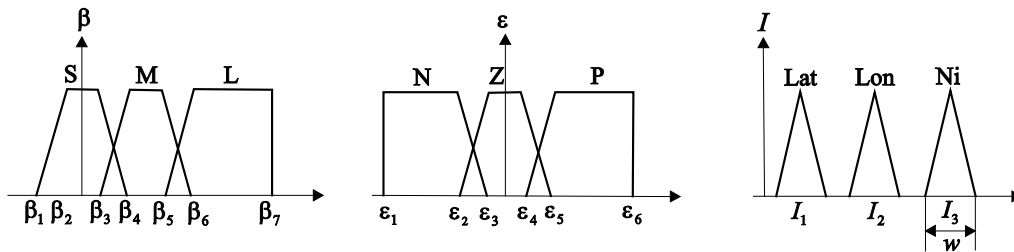


Figure 4 Definition of membership function for input and output variables

Table 1 FLC membership boundaries

|             |                  |                 |                 |                 |             |              |            |                  |                  |
|-------------|------------------|-----------------|-----------------|-----------------|-------------|--------------|------------|------------------|------------------|
| Coefficient | $\beta_1$        | $\beta_2$       | $\beta_3$       | $\beta_4$       | $\beta_5$   | $\beta_6$    | $\beta_7$  | $\varepsilon_1$  | $\varepsilon_2$  |
| Value       | $-7^\circ$       | $-6,2^\circ$    | $2,36^\circ$    | $2,64^\circ$    | $3,1^\circ$ | $3,82^\circ$ | $70^\circ$ | $-2E3 \text{ m}$ | $-150 \text{ m}$ |
| Coefficient | $\varepsilon_3$  | $\varepsilon_4$ | $\varepsilon_5$ | $\varepsilon_6$ | $I_1$       | $I_2$        | $I_3$      | $w$              | -                |
| Value       | $-100 \text{ m}$ | $100 \text{ m}$ | $150 \text{ m}$ | $4E3 \text{ m}$ | $0$         | $10$         | $20$       | $8$              | -                |

Fuzzy rules given in Tab. 2 are defined basing on the following points:

- Impulses' use causes changes in direction and magnitude of the object's velocity vector depending on their types. Lateral impulses must be used to correct the direction of the velocity vector towards the target;
- In case of a good orientation of controlled object's velocity vector toward the target, the magnitude of controlled object's velocity vector rises with the increase in current error  $\varepsilon(t)$ ;
- When the orientation of the controlled object's velocity vector toward the target reaches nearby zero, the need of executing lateral impulses decreases, to respect the requirements for a one-way maneuver.

Table 2 Fuzzy rules set

|       |            |                  |        |
|-------|------------|------------------|--------|
| Rules | $\beta(t)$ | $\varepsilon(t)$ | $I(t)$ |
| 1     | -          | N                | Ni     |
| 2     | L          | -                | Lat    |
| 3     | M          | P                | Lon    |
| 4     | M          | Z                | Lat    |
| 5     | S          | P                | Lon    |
| 6     | S          | Z                | Ni     |

The fuzzy inference system presented in this paper is a Mamdani type [10]. Defuzzification method used in this paper is Mean of Maximum (henceforth MoM). The defuzzified value is defined as the mean of all values of the universe of discourse, having maximal membership grades, derived by [15], given by Eq. (18) as;

$$I(t) = \frac{\sum_{j=1}^L c_j}{L} \tag{18}$$

where  $I(t)$  is the MoM,  $c_j$  is the point at which the memberships function is maximum, and  $L$  is the number of times the output distribution reaches the maximum level.

#### 4 Simulation and discussion

To research the ability of the proposed methods to generate maneuvering trajectories with minimal final error, a number of simulations are realized using the above mathematical model. The maneuvers are executed by three types of powering impulses, namely lateral impulses (*Lat*) that generate lateral velocities  $U_{Lat} = 21.8 \text{ m/s}$  with optimal angle  $\nu = 82^\circ$  and longitudinal impulses (*Lon*)  $U_{Lon} = 20.0 \text{ m/s}$  along the object's direction of motion, as well as no impulse (*Ni*) where the controlling velocity is  $U_{Ni} = 00.0 \text{ m/s}$ . The impulses' execution duration and the sampling time were  $300 \text{ ms}$  and  $\Delta t = 320 \text{ m}$ , respectively. For the present study, the target C is situated on a radial distance  $D = 36697 \text{ m}$  from the initial location of the object. It is assumed that the object's initial velocity  $V_0^{(1)} = 423 \text{ m/s}$  while the full motion time is fixed as  $\tau = 86.97 \text{ s}$ . To select the final error, the simulation is



repeated for each chosen relative time factor  $\tau^* \in [0.5, 0.8]$  and desired turning course angle  $\Delta\varphi \in [8^\circ, 18^\circ]$ . The simulation results are presented in the Tab. 3. The final error distance to the target  $Err_{df}$  is achieved by appropriate number and types of the powering impulses, presented in Tab. 3 as (Lat/Lon) for lateral and longitudinal impulses respectively. The relative time factor  $\tau^*$  which gives the minimum  $Err_{df}$  for each  $\Delta\varphi \in [8^\circ, 18^\circ]$  is also shown in Tab. 3.

The comparative analysis shows that the results obtained for all the three methods are overall acceptable. Comparing the results by methods, one can conclude that

all methods give approximately close  $Err_{df}$  for each desired couple of maneuvering courses  $\Delta\varphi$  and time factor  $\tau^*$ . The greatest difference in  $Err_{df}$  is observed for the couple  $\Delta\varphi = 9^\circ$  and  $\tau^* = 0.8$ , where it is equal to 113.2 m, whereas the lowest is witnessed for the couple  $\Delta\varphi = 8^\circ$  and  $\tau^* = 0.75$ , where it is about 1.66 m. This variation in  $Err_{df}$  between methods is due to the differences in the order, and execution instants and the type of impulses calculated by the stated methods.

These simulations are presented for ideal case regardless of all perturbations or mathematical model errors.

**Table 3** Simulation results for the decision-making methods

| $\Delta\varphi$ (°) | $\tau^*$ | MMS method |     |                | CEO method |     |                | Fuzzy logic method |     |                |
|---------------------|----------|------------|-----|----------------|------------|-----|----------------|--------------------|-----|----------------|
|                     |          | Lat        | Lon | $Err_{df}$ (m) | Lat        | Lon | $Err_{df}$ (m) | Lat                | Lon | $Err_{df}$ (m) |
| 8                   | 0,75     | 12         | 1   | 54,24          | 12         | 1   | 56,9           | 12                 | 1   | 55,13          |
| 9                   | 0,80     | 17         | 4   | 147,5          | 18         | 4   | 34,3           | 17                 | 3   | 124,55         |
| 10                  | 0,75     | 15         | 3   | 43,21          | 15         | 2   | 45,06          | 15                 | 2   | 39,94          |
| 11                  | 0,75     | 16         | 3   | 51,03          | 16         | 3   | 51,03          | 16                 | 3   | 59,9           |
| 12                  | 0,75     | 18         | 4   | 106,65         | 19         | 4   | 75,26          | 18                 | 4   | 127,81         |
| 13                  | 0,75     | 19         | 5   | 115,49         | 20         | 5   | 75,75          | 19                 | 5   | 116,15         |
| 14                  | 0,70     | 17         | 3   | 168,7          | 17         | 3   | 170,49         | 17                 | 3   | 168,28         |
| 15                  | 0,50     | 11         | 0   | 114,28         | 11         | 0   | 119,19         | 11                 | 0   | 138,66         |
| 16                  | 0,50     | 12         | 0   | 28,84          | 12         | 0   | 30,42          | 12                 | 0   | 48,07          |
| 17                  | 0,50     | 13         | 1   | 97,32          | 13         | 0   | 64,29          | 13                 | 0   | 64,29          |
| 18                  | 0,50     | 13         | 1   | 210,08         | 14         | 0   | 168,05         | 14                 | 0   | 168,05         |

In this sense of meaning, errors  $Err_{df}$  presented in Tab. 3 are assumed to be systematic errors (bias). In order to determine the sensitivity of the system due to errors in the model, arbitrary perturbations are added to the system's parameters in each sampling interval. For the reason that the object's velocity is the essence of the mathematical model, the perturbations are expected and chosen to be added to its magnitude as  $\Delta V^{(i)} \in [-5, +5] ms^{-1}$ , which represents around 25% of orientating velocity magnitude, as well as to its direction as  $\Delta\theta_i \in [-0.25^\circ, +0.25^\circ]$ . To simulate the effectiveness of the three methods in perturbation presence, the case of  $\Delta\varphi = 8^\circ$  and  $\tau^* = 0.75$  is selected. The perturbation will be equally added for the three methods in each sampling interval in the maneuvering phase. The simulation is repeated ( $n$ ) times and the final errors for the three methods obtained in this study follow the normal distributions law. Their resulting parameters are shown in Tab. 4 as the average final errors,  $\overline{Err_{df}}$ , and the standard deviation  $\sigma$  as well as minimal and maximal error distances  $(Err_{df})_{min}$  and  $(Err_{df})_{max}$  values.

**Table 4** Simulation results in perturbation presence

|     | $\overline{Err_{df}}$ (m) | $\sigma$ (m) | $(Err_{df})_{min}$ (m) | $(Err_{df})_{max}$ (m) |
|-----|---------------------------|--------------|------------------------|------------------------|
| MMS | 183,98                    | 147,85       | 5,48                   | 534,6                  |
| CEO | 178,45                    | 151,78       | 1,76                   | 577,1                  |
| FLC | 177,06                    | 150,27       | 0,43                   | 546,5                  |

#### 4 Hardware design and impulse sequences simulation by the implemented decision-making methods

The static simulation test is realized by software/hardware designed assembly shown in Fig.5. The electronic controller is linked with led diodes which simulate the impulses executions, both in type and instances. The required software control inputs are the desired turning angle  $\Delta\varphi \in [8^\circ, 18^\circ]$ , relative time factor  $\tau^*$  as well as one of the controlling methods stated above. The static impulse simulator turns on diodes in time sequences which are the results of the appropriate method given in Tab. 3 for optimal final error distance to the target. In addition to the desired pair  $\Delta\varphi$  and  $\tau^*$  given in Tab. 3, the operator has the possibility to choose the other desired pair for non-optimal final errors. The operator has to choose also the object angular rate (RPM) between a set of predefined ones. This visualization procedure corresponds to the ignition of powering impulses mounted on the controlled object in two rings. First is oriented toward  $82^\circ$  in lateral direction to simulate the lateral impulses work (Lat), whereas the second is mounted in a resulting  $0^\circ$  in axial direction that presents the longitudinal impulses (Lon) Fig. 6. The hardware is designed and programmed to switch on green lights on all the dual-color diodes in order to indicate the system readiness as well as the duration of the first phase  $\tau^{(1)}$ . To visualize the impulse execution instances and type, the microcontroller turns on red light on the appropriate diode depending on two requirements. First is the motion turning cycle given in Tab. 3, for desired pair of data and chosen controlling method. Second is the diode position on the controlled object ring which



corresponds to predefined chosen rpm (required in real motion). Turning on red light lasts  $\Delta t$  before switching on the mixed light to indicate that impulse is not further available for the turning and lasts all the remaining orientating time  $t_{2go}$ .

The electronic input consists of microcontroller unit, the Arduino board, capable of USB connection with the PC and an add-on board. As it could be seen from the block schematics of the hardware presented in Fig.5. The human machine interface based upon character LCD module, accompanied with the tactile switches for selecting the methods and desired pair  $\Delta\varphi$  and  $\tau^*$ . The external EPROM unit enables the storing capability and recalling of large data sets.

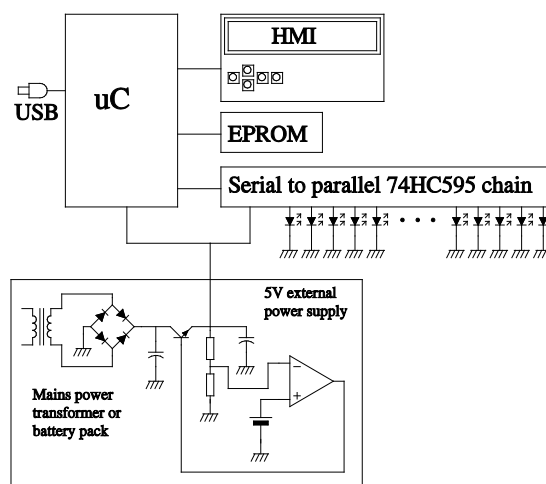


Figure 5 Software /hardware assembly

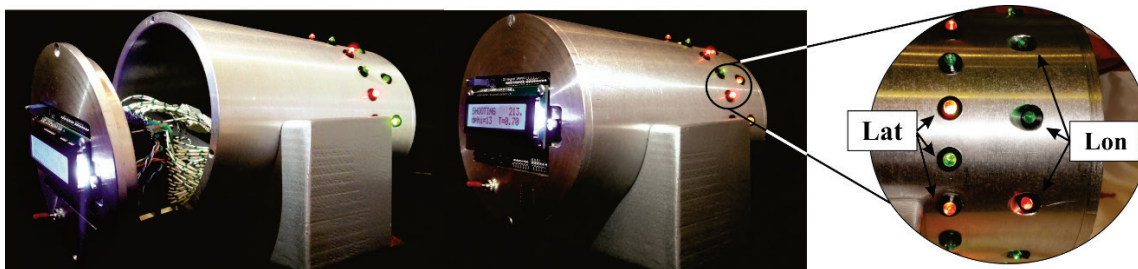


Figure 6 Experimental static simulator of impulses' execution sequences

The visualization process of the impulses' execution is accomplished by means of the 34 LED diodes, 22 for lateral impulses (Lat) and 12 liked simultaneously in 6 pairs for longitudinal impulses (Lon), which corresponds to the maximal number of impulses (Fig. 6). On the applied hardware, the 74HCT595 serial to parallel chain is powered by the external power supply. The diode current is limited by the anode resistor. Since the entire serial chain of 74HCT595 sets the output to the parallel register on strobe of the storage register clock signal (pin 12) all predefined states in serial register appear simultaneously on the output ports. The internal timer interrupt routine enables the precise timing of the visualized process, the 1ms time resolution was selected, and the mentioned hardware possesses the jitter smaller than 62 ns, while the delay is constant and repeatable. The hardware is produced as an add-on board for the Arduino Mega 2560.

## 5 Conclusion

The comparative analysis of the three decision-making methods, aimed for the maneuvering control of the object, shows promoting and closes results for all methods in presence of external perturbations. Each method has its specifications as the following:

- The modified multiple shooting approach, presented in this paper, combines the direct multiple shooting method and the single one. This constitutes a significant simplification of the maneuvering trajectory optimization and a numerical stability over single shooting methods. The MMS approach involves a minimum logic problem analysis, for that reason it is used as a reference for the preliminary estimation of the controlled objects' parameters. The

disadvantage of this approach is that it does not allow to explicitly including information about the solution into the problem solving procedure.

- The CEO method uses the classical controlling theory by applying a time-invariant controlling law for the multi-input-single-output system. This method presents mathematical solution for maneuvering but requires a further stability analysis before implementing it on a real system.
- The well-known fuzzy method (FLC) has proved its efficiency on numerous systems. It provides an explicitly incorporating knowledge about the solution into the problem by fuzzy rules set.

Further research is orientated on real testing of the designed software/hardware platform mounted on a real mobile system.

## Acknowledgements

This research is a part of the PhD applicant's research program and published by the support of the project III-47029MoESTD RS, funded in the year 2016.

## 6 References

- [1] Pomet, J. B. Explicit design of time-varying stabilizing control laws for a class of controllable systems without drift. // System and Control Letters, 18, (1992), 147-158. [https://doi.org/10.1016/0167-6911\(92\)90019-O](https://doi.org/10.1016/0167-6911(92)90019-O)
- [2] Murray, R. M.; Walsh, G.; Sastry, S. S. Stabilization and tracking for nonholonomic control systems using time-varying state feedback. // IFAC Nonlinear control systems design, (2014), 109-114.

- [3] Astolfi, A. Discontinuous control of the nonholonomic integrator. // *Modeling and Control of Mechanical Systems*, (1997), 293-309. [https://doi.org/10.1142/9781848160873\\_0019](https://doi.org/10.1142/9781848160873_0019)
- [4] Kim, B.; Tsiotras, P. Controllers for unicycle-type wheeled robots: Theoretical results and experimental validation. // *Robotics and Automation, IEEE Transactions on*, 18, 3(2002), 294-307. <https://doi.org/10.1109/TRA.2002.1019460>
- [5] Hernández-Guzmán, V. M.; Silva-Ortigoza, R.; Márquez-Sánchez, C. A PD path-tracking controller plus inner velocity loops for a wheeled mobile robot. // *Advanced Robotics*, 29, 16(2015), 1015-1029. <https://doi.org/10.1080/01691864.2015.1033459>
- [6] Wang, M.; Liu, J. N., Fuzzy logic-based real-time robot navigation in unknown environment with dead ends. // *Robotics and Autonomous Systems*, 56, 7(2008), 625-643. <https://doi.org/10.1016/j.robot.2007.10.002>
- [7] Yerubandi, V.; Reddy, Y. M.; Reddy, M. V. K. Navigation system for an autonomous robot using fuzzy logic. // *International Journal of Scientific and Research Publications*, 5, 2(2015).
- [8] Chwa, D. Fuzzy adaptive tracking control of wheeled mobile robots with state-dependent kinematic and dynamic disturbances. // *Fuzzy Systems, IEEE Transactions on*, 20(3), 587-593. (2012). <https://doi.org/10.1109/TFUZZ.2011.2176738>
- [9] Zadeh, L. A. Toward a theory of fuzzy information granulation and its centrality in human reasoning and fuzzy logic. // *Fuzzy sets and systems*, 90, 2(1997), 111-127. [https://doi.org/10.1016/S0165-0114\(97\)00077-8](https://doi.org/10.1016/S0165-0114(97)00077-8)
- [10] Mamdani, E. H. Advances in the linguistic synthesis of fuzzy controllers. // *International Journal of Man-Machine Studies*, 8, (1976), pp. 669-678. [https://doi.org/10.1016/S0020-7373\(76\)80028-4](https://doi.org/10.1016/S0020-7373(76)80028-4)
- [11] Keller, H. B. *Numerical Methods for Two-point Boundary Value Problems*. Dover, New York. (1992):
- [12] Bailey, P. B.; Shampine, L. F. Waltman, *Nonlinear Two Point Boundary Value Problems*; Press, New York, (1968)
- [13] Bock, H. G.; Plitt K. J. A multiple shooting algorithm for direct solution of optimal control problems. // *Proc. 9th IFAC World Congress Budapest*, Pergamon Press, (1984). [https://doi.org/10.1016/S1474-6670\(17\)61205-9](https://doi.org/10.1016/S1474-6670(17)61205-9)
- [14] Cox, E. Fuzzy fundamentals. // *IEEE Spectrum*, 29, 10(1992), 58-61. <https://doi.org/10.1109/6.158640>
- [15] Iancu, I. A. Mamdani type fuzzy logic controller. INTECH Open Access Publisher. (2012), 331-335, ISBN: 978-953-51-0396-7. <https://doi.org/10.5772/36321>

**Nenad Sakan, PhD, research associate**

University of Belgrade, Institute of Physics,  
Pregrevica 118, 11080, Zemun, Belgrade, Serbia  
E-mail: nsakan@ipb.ac.rs

#### Authors' addresses

**Mohammed Amine Boulahlib, PhD applicant**

Ministry of Defence of Algeria, PhD applicant at Military Academy, University of Defence, Belgrade  
Pavla Jurišića Šturma Street 33, 11000 Belgrade, Serbia  
E-mail: m.a.boulahlib@gmail.com

**Momcilo Milinovic, PhD, Full professor**

University of Belgrade, Faculty of Mechanical Engineering, Kraljice Marije 16, Beograd, Serbia  
E-mail: mmilinovic@mas.bg.ac.rs

**Mourad Bendjaballah, PhD applicant**

Ministry of Defence of Algeria, PhD applicant at Military Academy, University of Defence, Belgrade  
Pavla Jurišića Šturma Street, number 33, Belgrade, Serbia  
E-mail: mourad.bendjaballa@hotmail.com

**Olivera Jeremic, PhD, Associate Professor**

University of Belgrade, Faculty of Mechanical Engineering Kraljice Marije 16, Beograd, Serbia  
E-mail: ojeremic@mas.bg.ac.rs

# Free-Free Absorption in Solar Atmosphere<sup>1</sup>

M. S. Dimitrijević<sup>a, b, \*</sup>, V. A. Srećković<sup>c</sup>, N. M. Sakan<sup>c, \*\*</sup>, N. N. Bezuglov<sup>d</sup>, and A. N. Klyucharev<sup>d</sup>

<sup>a</sup>*Astronomical Observatory, Belgrade, 11060 Serbia*

<sup>b</sup>*Observatoire de Paris, Meudon Cedex, 92195 France*

<sup>c</sup>*Institute of Physics, University of Belgrade, Belgrade, 11001 Serbia*

<sup>d</sup>*St. Petersburg State University, St. Petersburg, 199034 Russia*

\**e-mail: mdimitrijevic@aob.rs*

\*\**e-mail: vlada.nsakan@ipb.ac.rs*

Received November 23, 2017

**Abstract**—The free-free i.e. electron-ion inverse “Bremsstrahlung” characteristics are determined for the case of the solar atmosphere as well as solar interior where such plasma characteristics as plasma density and temperature change in wide region. We demonstrate that determination of these characteristics such as the absorption coefficients and Gaunt factors can be successfully performed in the whole diapason of electron densities and temperatures which is relevant for the corresponding atmosphere model. The used quantum mechanical method of the calculation of the corresponding spectral absorption coefficient and Gaunt factor is described and discussed in details. The results are obtained for the case of a solar photosphere and solar interior model in the wavelength region  $10 \text{ nm} \leq \lambda \leq 3000 \text{ nm}$ . The range of the physical parameters covers the area important for plasma modeling from astrophysical standpoint (white dwarfs, central stars of planetary nebulae, etc). Also, these results can be of interest and use in investigation of different laboratory plasmas.

DOI: 10.1134/S0016793218080054

## 1. INTRODUCTION

Free-free i.e. Inverse Bremsstrahlung processes are important radiation mechanism in laboratory and astrophysical plasmas. Anyone interested in these processes must be fascinated by the amount of works about them (D’yachkov, 1990; Hazak et al., 2002; Grinenko and Gericke, 2009a; Mihajlov et al., 2015). For example, Grinenko and Gericke (2009b) stated that inverse bremsstrahlung is the dominant absorption mechanism for lasers with parameters typical for inertial confinement fusion. Plasma in inertial confinement fusion experiments has properties which are similar to the conditions in stellar interiors. Consequently, it is of interest to investigate the role of inverse bremsstrahlung in subphotospheric and deeper layers, and to examine its influence on radiative transfer through such layers. The contribution of inverse bremsstrahlung to the total absorption in stellar atmospheres is not crucial, but its contribution increases with density (i.e. when approaching the Sun interior), and for very dense plasmas it becomes dominant. These processes belong to the type of processes whose efficiency increases proportionally to the square of free-electron density. In addition to other factors that determine the importance of inverse bremsstrahlung, we should bear in mind the

existence of a physical area where inverse bremsstrahlung is dominant compared to other processes. The examples which demonstrate this can be found in the literature (Rozsnyai, 2001; Grinenko and Gericke, 2009b; Moll et al., 2012). In the theory of stellar interiors the free-free (i.e. Inverse Bremsstrahlung) contribution to the opacity is significant in parts of the star where details about the structure are of interest i.e. regions of energy generation at the edges of degenerate cores in red giants (see Iben (1968)).

The aim of this work is determination of the corresponding spectral absorption coefficients for inverse “Bremsstrahlung” process and the corresponding Gaunt factors for a broad class of weakly non-ideal plasmas, as well as for plasmas of higher non-ideality. It is shown that this process can be successfully described by cut-off Coulomb potential model within the range of the physical parameters which covers the area important for modeling astrophysical plasma (white dwarfs, solar atmospheres, etc.). The physical sense and the properties of a group screening parameters for two-component systems which are used in this paper are discussed in details in the previous papers (Mihajlov et al., 2009a, 2009b; Ignjatović et al., 2017).

<sup>1</sup> The article is published in the original.

## 2. THEORY

### 2.1. Electrostatic Screening Model

In the paper of Mihajlov et al. (2011a) the model of the inner plasma screening was applied for the first time in the investigation of the optical characteristics. The investigated processes are considered as a result of radiative transition in the whole system “electron-ion pair (atom) + the neighborhood”. However, as it is well known, many-body processes can sometimes be simplified by their transformation to the corresponding single-particle processes in an adequately chosen model potential.

In this screening model the potential energy of free electron  $U_{\text{scr}}(r)$  is strictly Coulomb:  $U_{\text{scr}}(r) = -e^2/r$  in the region  $r < r_{\text{cut}}$ , where  $r_{\text{cut}}$  is the corresponding cut-off radius, and  $U_{\text{scr}}(r) = \text{const} = U_{\text{cut}}$  in the region  $r > r_{\text{cut}}$ , where  $U_{\text{cut}}$  is equal to the average energy of the free electron in the considered system. In the further consideration we take  $U_{\text{cut}} = -e^2/r_{\text{cut}}$  as the zero of energy and describe such plasma by means just of the model cut-off potential given by Eq. (1), which is especially suitable for describing electron-ion scattering within plasma. This potential is given by

$$U(r) = \begin{cases} -\frac{e^2}{r} + \frac{e^2}{r_{\text{cut}}}, & 0 < r \leq r_{\text{cut}}, \\ 0, & r_{\text{cut}} < r \end{cases} \quad (1)$$

where  $r$  is the distance from the coordinate origin,  $r_{\text{cut}}$  is a parameter defined and determined further on in the text.

Certainly, we assume that the above described electrostatic screening model could be applicable in such a wide range of electron densities and temperatures that this allows to consider it as an almost universal model. For that very reason the cut-off potential Eq. (1) could also be considered as almost universal.

Let us note that in Mihajlov et al. (2011a,b) the universality of the screening model did not arise at all. However, in the case of the electron-ion inverse “Bremsstrahlung” process, which is possible in plasmas with enormous differences of the electron densities and temperature, the situation is opposite.

In order to complete the described model we have to determine the cut-off parameter  $r_{\text{cut}}$  and the energy parameter  $U_{\text{cut}}$  as functions of the electron density  $Ne$  and the temperature  $T$ . Here we will use the fact that these parameters can be determined using the data from Mihajlov et al. (2009a). Namely, the curve presented in figure 4 from Mihajlov et al. (2009a) shows the behaviour of the parameter  $a_{\text{cut}} = r_{\text{cut}}/r_e$  as a function of the ratio  $r_{s;i}/r_e$ , where  $r_e$  and the ion Wigner-Seitz radius  $r_{s;i}$  are given by relations

$$r_{s;i} = \left[ \frac{3}{4\pi N_i} \right]^{1/3}, \quad r_e = \left[ \frac{kT}{4\pi N_e e^2} \right]^{1/2}, \quad (2)$$

where  $N_i$  is the ion density. After that the cut-of radius  $r_{\text{cut}}$  is determined here as the function of  $N_e$ ,  $T$  by means of relations

$$r_{\text{cut}} = a_{\text{cut}} r_e, \quad (3)$$

where the parameter  $a_{\text{cut}}$  can be directly determined as a function of the ratio  $r_{s;i}/r_e$ .

### 2.2. The Cross Section

After an introduction of the potential Eq. (1) the procedure of determination of inverse bremsstrahlung characteristic such as the spectral absorption coefficients, Gaunt factors, is possible.

For the inverse “Bremsstrahlung” cross section  $\sigma_{i.b.}^{(ex)}$ , the standard expressions from Sobelman (1979) is used, since the potential Eq. (1) has the finite radius. Consequently:

$$\sigma_{i.b.}^{(ex)}(E; E') = \frac{8\pi^4 \hbar e^2 k}{3 q^2} \sum_{l'=l\pm 1} l_{\text{max}} |\hat{D}_{E,l;E'l'}|^2, \quad (4)$$

$$\hat{D}_{E,l;E'l'} = \int_0^{\infty} P_{E'l'}(r) r P_{E,l}(r) dr,$$

where the radial functions  $P_{E,l}(r)$  and  $P_{E'l'}(r)$  are the solutions of the radial Schrödinger equation

$$\frac{d^2 P_{E,l}(r)}{dr^2} + \left[ \frac{2m}{\hbar^2} (E - U(r)) - \frac{l(l+1)}{r^2} \right] P_{E,l}(r) = 0, \quad (5)$$

and  $U(r)$  is the cut-off Coulomb potential given by Eq. (1). The radial functions  $P_{E,l}(r)$  of all states which are possible in the potential  $U(r)$  are described and discussed in Mihajlov et al. (1986). As the next step, using the transformation characteristics of the matrix element of the solutions  $P_{E,l}(r)$  we will replace dipole matrix element  $\hat{D}_{E,l;E'l'}$  in Eq. (4) by the matrix element of the gradient of potential energy  $U(r)$ . This procedure is described by the expressions

$$|\hat{D}(r)_{E,l;E'l'}|^2 = \frac{\hbar^4}{m^2 (E - E')^4} |\nabla U_{E,l;E'l'}|^2, \quad (6)$$

$$\nabla_r U_{E,l;E'l'} = \int_0^{r_{\text{cut}}} P_{E,l}(r) \nabla_r U(r) P_{E'l'}(r) dr, \quad (7)$$

where  $U(r)$  is given by Eq. (1).

The transition from the dipole matrix element  $\hat{D}_{E,l;E'l'}$  to dipole matrix element  $\nabla_r U_{E,l;E'l'}$  in the case of  $U(r)$  which is given by Eq. (1) means a transition from determination of the quantity  $\hat{D}_{E,l;E'l'}$ , which can-

not be factually calculated, to determination of a quantity which can be calculated routinely. Namely, in the case of this potential the integral of two function of Coulomb continuum from 0 to  $\infty$  gets replaced by the integral of the same two functions, but from 0 to  $r_{\text{cut}}$ .

### 2.3. The Absorption Coefficients

On the bases of the used solar models of Fontenla et al. (2007) and Bahcall et al. (2006) we consider here plasmas with electron densities from  $10^{14}$  to  $\sim 10^{20}$   $\text{cm}^{-3}$  and temperatures from 6000 to 100000 K. In accordance with Adamyan et al. (1994), for such conditions we have that for the electron component, treated as appropriate electron gas on a positively charged background, the value of chemical potential is practically equal to the classical one, so that the distribution function for electrons is

Maxwellian  $f_T(v) = 4\pi(m/2\pi kT)^{3/2} v^2 e^{-mv^2/2kT}$ , for the given temperature  $T$ . Consequently:

$$\begin{aligned} & \kappa_{i.b.}^{(\text{ex})}(\varepsilon_\lambda; N_e, T) \\ &= N_e^2 \int_0^\infty \sigma_{i.b.}^{(\text{ex})}(E; E') v f_T(v) dv \left( 1 - \exp\left[-\frac{\hbar\omega}{kT}\right] \right), \end{aligned} \quad (8)$$

where the expression in parentheses takes into account the effect of stimulated emission. Additionally, the quasi classical Kramer's  $k_{i.b.}^{q.c.}(\lambda, T; Ne)$  we take (see e.g. Sobelman (1979)) as:

$$\begin{aligned} & k_{i.b.}^{q.c.}(\lambda, T; Ne) \\ &= N_e^2 \frac{16\pi^{5/2} \sqrt{2} e^6}{3\sqrt{3} cm^{3/2} \varepsilon_{ph}^3} \frac{\hbar^2}{(kT)^{1/2}} \left( 1 - \exp\left[-\frac{\hbar\omega}{kT}\right] \right), \end{aligned} \quad (9)$$

where  $\varepsilon_{ph} = 2\pi\hbar c/\lambda$ , and the averaged Gaunt factor  $G_{i.b.}(\lambda, T)$  is:

$$k_{i.b.}^{(\text{ex})}(\lambda, T; N_e) = k_{i.b.}^{q.c.}(\lambda, T; N_e) G_{i.b.}(\lambda, T), \quad (10)$$

where  $k_{i.b.}^{(\text{ex})}(\lambda, T; Ne)$  and  $k_{i.b.}^{q.c.}(\lambda, T; Ne)$  are given by Eqs. (8) and (9).

## 3. RESULTS AND DISCUSSION

The contribution of inverse bremsstrahlung to the total absorption in stellar atmospheres is not crucial, but its contribution increases with density (i.e. when approaching deeper in the Sun interior), and for very dense plasmas it becomes dominant. Consequently, it is of interest to investigate the role of inverse bremsstrahlung in subphotospheric and deeper layers, and to examine its influence on radiative transfer through such layers. In addition to other factors that determine the importance of inverse bremsstrahlung, we should bear in mind the existence of a physical area where inverse bremsstrahlung is dominant compared to other processes. Moreover, we expect a major contribution to inverse bremsstrahlung process in a dense highly

ionized plasma (see e.g. Fig. 3, the marked region of  $r$ ) in the process of transfer of radiation. Here we mean the high electron density and temperature that occur in the interior of the Sun which are in Fig. 3 presented as a function of radius (Standard Solar Models Bahcall et al. (2006)).

In Fig. 1 on left side is presented the behavior of the temperature  $T$  and  $N_e$  as a function of height  $h$  within the considered part of the solar atmosphere model of Fontenla et al. (2007). In Fig. 1 on right side is shown the surface plots of Gaunt factor as a function of wavelength and height  $h$  for the case of a solar atmosphere model from Fontenla et al. (2007). From this figure one can see that the values of the Gaunt factor strongly depend on the atmosphere parameters, mainly temperature, as well as on photon wavelengths.

In Fig. 2, are shown the plots of absorption coefficient of all considered absorption processes for the case of a solar atmosphere model from Fontenla et al. (2007) as a function of height for various values of wavelengths. Here  $h$  is the height of the considered layer with the respect to the chosen referent one. The corresponding plasma parameters are presented in Fig. 1 left panel. The electron-atom processes which

are treated sometimes as the  $\text{H}^-$  continuum, are represented here by their common plot which in these figures is marked by  $EA$  ( $\kappa_{EA}$ ). With  $IA$  i.e.  $\kappa_{ai}$  atom-ion symmetric and non-symmetric processes (Ignjatović et al. 2014; Srećković et al. 2014) are represented. From this figure one can see that the inverse ‘‘Bremsstrahlung’’ absorption coefficients are comparable with the concurrent ones especially in the region of higher electron density and temperature  $h \leq -70$  km (left part of Fig. 2). Consequently, we can conclude that influence of inverse ‘‘Bremsstrahlung’’ process increases with temperature, density as well as with increase of wavelength.

Figure 3 left panel present the electron density and temperature in the interior of the Sun as a function of radius for the Standard Solar Models (Bahcall et al., 2006). On the right panel is presented the surface plots of Gaunt factor as a function of wavelength and radius for the Standard Solar Model (Bahcall et al., 2006). The plots of absorption coefficients of considered absorption processes for the case of a Standard Solar Model (Bahcall et al., 2006) are presented in Fig. 4. From this figure one can see that the values of the Gaunt factor strongly depend on the plasma parameters, mainly temperature, as well as on photon wavelengths. The values of the absorption coefficients in Fig. 4 increase with density and temperature increment i.e. when the value of ratio  $r/R$  decreases from 1 to 0.98 (when approaching deeper in the Sun interior). This result confirmed the increase of importance of inverse bremsstrahlung process when we go deeper into the interior of the Sun.

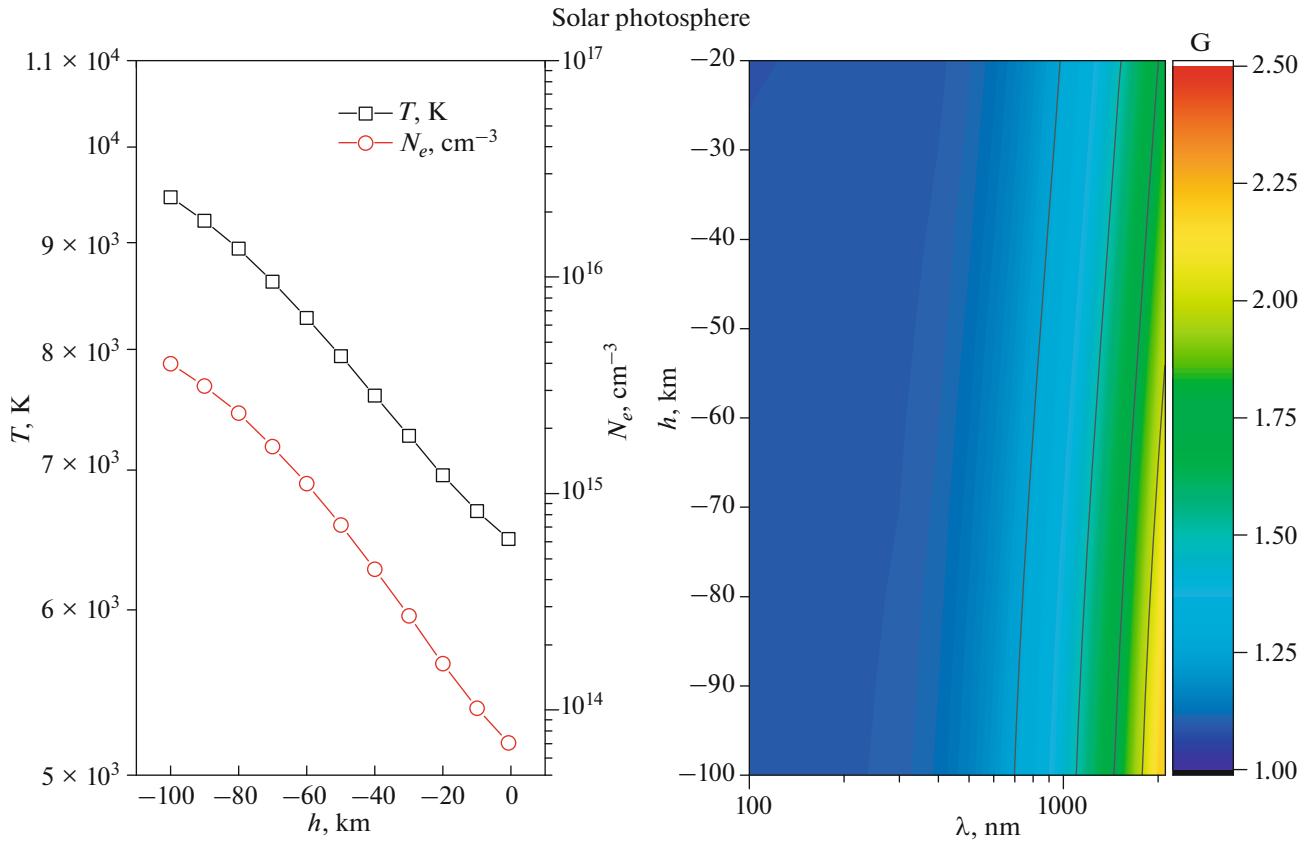


**Fig. 1.** Left side: the behavior of the temperature  $T$  and  $N_e$  as a function of height  $h$  within the considered part of the solar atmosphere model of Fontenla et al. (2007). Right side: the surface plots of Gaunt factor as a function of wavelength and height  $h$  for the case of a solar atmosphere model from Fontenla et al. (2007).

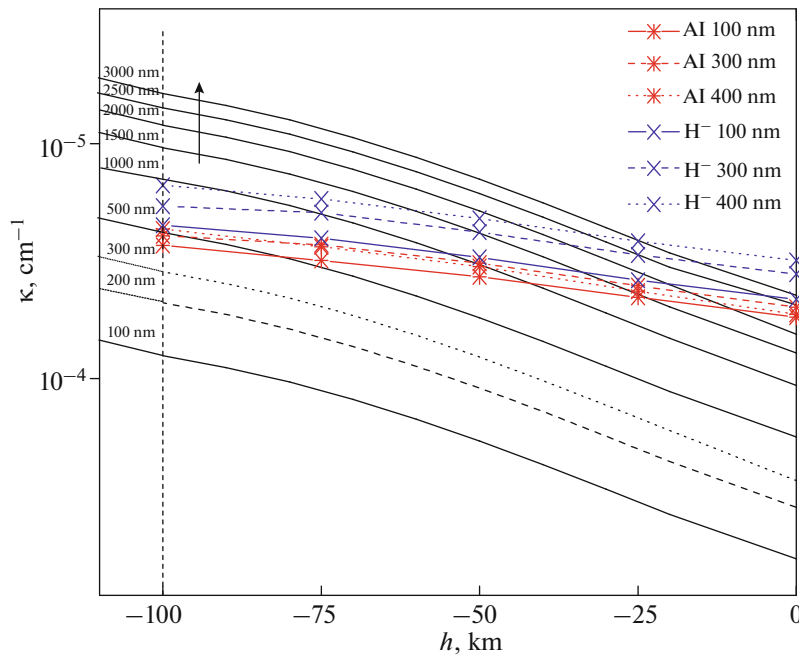


**Fig. 2.** The plots of absorption coefficients of considered absorption processes for the case of a solar atmosphere model from Fontenla et al. (2007). With black lines are denoted  $f$ -absorption processes i.e. inverse “Bremsstrahlung” absorption coefficients, with blue electron-atom i.e.  $\text{H}^-$  continuum and with red ion-atom absorption coefficients (Ignjatović et al. (2014); Srećković et al. (2014)). The extrapolated values are in the left shaded region in front of the dashed line.

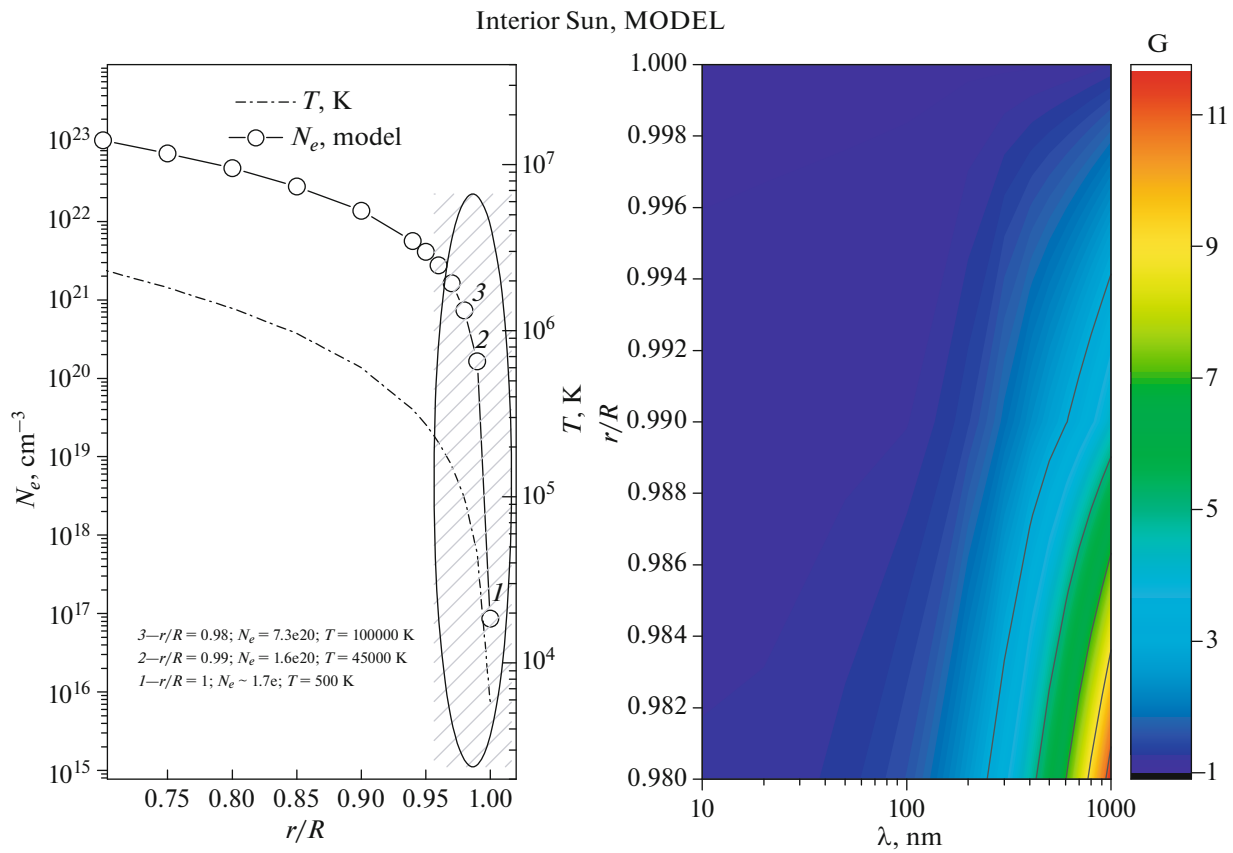


**Fig. 3.** Left: The electron density and temperature in the interior of the Sun as a function of radius for the Standard Solar Models (Bahcall et al., 2006). Right: the surface plots of Gaunt factors as a function of wavelength and radius for the investigated regions of solar interior.

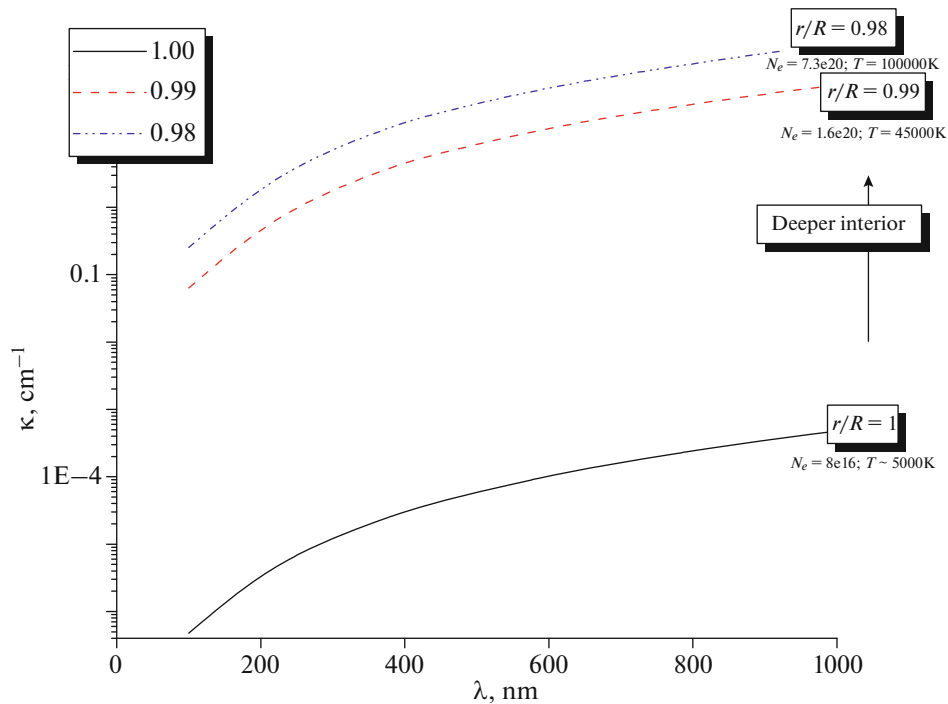


**Fig. 4.** The plots of absorption coefficients of considered absorption processes as a function of wavelength and radius in the investigated regions of solar interior (Standard Solar Model (Bahcall et al., 2006)).



The presented quantum-mechanical method is used to obtain the spectral coefficients for inverse “Bremsstrahlung” process and the corresponding Gaunt factors for a broad class of moderately non-ideal plasmas, as well as for plasmas of higher non-ideality. The range of the physical parameters covers the area important for plasma modeling from astrophysical standpoint (stellar atmospheres, central stars of planetary nebulae, etc.). The contribution of inverse bremsstrahlung to the total absorption in stellar atmospheres increases with density, and for very dense plasmas it becomes dominant. Finally, we are also able to notice that the data are highly sensitive to change of the temperature. Also, the data depend on the wavelength region i.e. absorption coefficients increase with increase of wavelength.

Further directions of development of the method would be determination of absorption coefficients and Gaunt factors for two-component systems (ions with an arbitrary charge  $Z$  and electron component) Mihajlov et al. (2009b) as well as for three-component systems (two kinds of ions with different charges and electron component) Ignjatović et al. (2017).

We acknowledge the contribution of late Dr. A.A. Mihajlov who participated in the discussions and the preparation of this paper. This work is partially supported by Ministry of Education, Science and Technological Development of the Republic of Serbia under the grants III 44002, and 176002.

## REFERENCES

- Adamyán, V.M., Djuric, Z., Ermolaev, A.M., Mihajlov, A.A., and Tkachenko, I.M., The RPA conductivity of fully ionized plasmas in a magnetic field, *J. Phys. D: Appl. Phys.*, 1994, vol. 27, no. 1, pp. 111–118.
- Bahcall, J.N., Serenelli, A.M., and Basu, S., 10,000 standard solar models: A Monte Carlo simulation, *Astrophys. J. Suppl. Ser.*, 2006, vol. 165, no. 1, pp. 400–431.
- D'yachkov, L.G., Simple formula for the average Gaunt factor, *J. Phys. B: At. Mol. Phys.*, 1990, vol. 23, no. 16, pp. L429–L432.
- Fontenla, J.M., Balasubramaniam, K.S., and Harder, J., Semiempirical models of the solar atmosphere. II. The quiet-Sun low chromosphere at moderate resolution, *Astrophys. J.*, 2007, vol. 667, no. 2, pp. 1243–1257.
- Grinenko, A. and Gericke, D.O., Dense plasma heating by inverse Bremsstrahlung, in *Central Laser Facility, Annual Report 2008/2009*, Didcot, Oxfordshire: Science and Technology Facilities Council, Rutherford Appleton Laboratory, Harwell Science and Innovation Campus, 2009a, p. 110.
- Grinenko, A. and Gericke, D.O., Nonlinear collisional absorption of laser light in dense strongly coupled plasmas, *Phys. Rev. Lett.*, 2009b, vol. 103, 065005.
- Hazak, G., Metzler, N., Klapisch, M., and Gardner, J., Inverse bremsstrahlung in cold dense plasmas, *Phys. Plasmas*, 1994, vol. 9, no. 1, pp. 345–357.
- Iben, I., Jr., Electron conduction in red giants, *Astrophys. J.*, 1968, vol. 154, pp. 557–580.
- Ignjatović, L.M., Mihajlov, A.A., Srećković, V.A., and Dimitrijević, M.S., The ion–atom absorption processes as one of the factors of the influence on the sunspot opacity, *Mon. Not. R. Astron. Soc.*, 2014, vol. 441, no. 2, pp. 1504–1512.
- Ignjatović, L.M., Srećković, V.A., and Dimitrijević, M.S., The screening characteristics of the dense astrophysical plasmas: The three-component systems, *Atoms*, 2017, vol. 5, no. 4, id 42.
- Mihajlov, A.A., Djordjević, D., Vučić, S., Kraeft, W.D., and Luft, M., Elastic scattering of electrons by a cut-off Coulomb potential at low energies, *Contrib. Plasma Phys.*, 1986, vol. 26, no. 1, pp. 19–35.
- Mihajlov, A.A., Vitel, Y., and Ignjatović, L.M., The new screening characteristics of strongly non-ideal and dusty plasmas. Part 2: Two-component systems, *High Temp.*, 2009a, vol. 47, no. 1, pp. 1–12.
- Mihajlov, A.A., Vitel, Y., and Ignjatović, L.M., The new screening characteristics of strongly non-ideal and dusty plasmas: Part 3: Properties and applications, *High Temp.*, 2009b, vol. 47, no. 2, pp. 147–157.
- Mihajlov, A.A., Sakan, N.M., Srećković, V.A., and Vitel, Y., Modeling of continuous absorption of electromagnetic radiation in dense partially ionized plasmas, *J. Phys. A: Math. Gen.*, 2011a, vol. 44, 095502.
- Mihajlov, A.A., Sakan, N.M., Srećković, V.A., and Vitel, Y., Modeling of the continuous absorption of electromagnetic radiation in dense hydrogen plasma, *Balt. Astron.*, 2011b, vol. 20, pp. 604–608.
- Mihajlov, A.A., Srećković, V.A., and Sakan, N.M., Inverse bremsstrahlung in astrophysical plasma, *J. Astrophys. Astron.*, 2015, vol. 36, pp. 635–642.
- Moll, M., Bornath, T., Schlanges, M., and Krainov, V.P., Inverse bremsstrahlung heating rate in atomic clusters irradiated by femtosecond laser pulses, *Phys. Plasmas*, 2012, vol. 19, 033303.
- Rozsnyai, B.F., Solar opacities, *J. Quant. Spec. Radiat. Transfer*, 2001, vol. 71, pp. 655–663.
- Sobelman, I.I., *Atomic Spectra and Radiative Transitions*, Berlin: Springer, 1979.
- Srećković, V.A., Mihajlov, A.A., Ignjatović, L.M., and Dimitrijević, M.S., Ion–atom radiative processes in the solar atmosphere: Quiet Sun and sunspots, *Adv. Space Res.*, 2014, vol. 54, no. 7, pp. 1264–1271.



НАЦЫЯНАЛЬНАЯ АКАДЭМІЯ  
НАВУК БЕЛАРУСІ

Дзяржаўная навуковая ўстанова  
«Інстытут фізікі імя Б. І. Сцяпанова  
Нацыянальнай акадэміі навук Беларусі»

Пр. Незалежнасці, 68, 220072, г. Мінск  
Тэл. (017) 284 17 55, факс (017) 284 08 79

E-mail: ifanbel@ifanbel.bas-net.by  
URL: <http://ifanbel.bas-net.by>

НАЦИОНАЛЬНАЯ АКАДЕМИЯ  
НАУК БЕЛАРУСИ

Государственное научное учреждение  
«Институт физики имени Б. И. Степанова  
Национальной академии наук Беларуси»

Пр. Независимости, 68, 220072, г. Минск  
Тел. (017) 284 17 55, факс (017) 284 08 79

E-mail: ifanbel@ifanbel.bas-net.by  
URL: <http://ifanbel.bas-net.by>

06.12.2021 № 101-01-17/1601

На № \_\_\_\_\_ ад \_\_\_\_\_

Dr. Nenad Sakan  
Institute of Physics,  
University of Belgrade,  
Pregrevica 118  
11080 Belgrade, Serbia  
Fax: +381 11 3162 190

05/11/2021

Dear Doctor **Nenad Sakan**,

It is a great pleasure of inviting you to participate in the XIII Belarusian-Serbian Symposium "Physics and Diagnostics of Laboratory and Astrophysical Plasmas" (PDP-13) which will be held in Minsk in September 13–17, 2021. Your work entitled « The introduction of more complex atoms in a cut-off Coulomb model potential, the Ar I model» has been accepted for invited lecture presentation at the PDP-13.

Programme of PDP-13 includes:

Arrival day – 12.12.2021;

Working days of PDP-13 – 13.12.2021-17.12.2021;

Departure day – 20.12.2021.

Registration fee is not provided.

We are looking forward to seeing you in Minsk, Belarus.

Sincerely yours,  
Deputy director of B.I. Stepanov  
Institute of Physics of the NAS of  
Belarus



I.S. Nikonchuk

**THE NATIONAL ACADEMY OF SCIENCES OF BELARUS  
B.I. STEPANOV INSTITUTE OF PHYSICS**

**PROCEEDINGS OF THE XIII BELARUSIAN-SERBIAN SYMPOSIUM  
"PHYSICS AND DIAGNOSTICS OF LABORATORY AND  
ASTROPHYSICAL PLASMAS" (PDP-13)**

**December 13–17, 2021, Minsk, Belarus**

**Edited by A.N. Chumakov, M.M. Kuraica and M.S. Usachonak**

**MINSK  
«Kovcheg»  
2021**



**НАЦИОНАЛЬНАЯ АКАДЕМИЯ НАУК БЕЛАРУСИ  
ИНСТИТУТ ФИЗИКИ ИМЕНИ Б.И.СТЕПАНОВА**

**ТРУДЫ XIII БЕЛОРУССКО-СЕРБСКОГО СИМПОЗИУМА  
"ФИЗИКА И ДИАГНОСТИКА ЛАБОРАТОРНОЙ И  
АСТРОФИЗИЧЕСКОЙ ПЛАЗМЫ" (ФДП-13)**

**13–17 декабря 2021 г., Минск, Беларусь**

**Под редакцией А.Н. Чумакова, М.М. Кураицы и М.С. Усачёнка**

**МИНСК  
«Ковчег»  
2021**

УДК 533.9 (043.2)  
ББК 22.3  
Т78

Под редакцией  
А.Н. Чумакова, М.М. Кураицы и М.С. Усачёнка

**ТРУДЫ XIII БЕЛОРУССКО-СЕРБСКОГО СИМПОЗИУМА  
Т78 "ФИЗИКА И ДИАГНОСТИКА ЛАБОРАТОРНОЙ И  
АСТРОФИЗИЧЕСКОЙ ПЛАЗМЫ" (ФДП-13) :** Минск, 13–17  
декабря 2021г. / Под ред. А.Н. Чумакова, М.М. Кураицы и  
М.С. Усачёнка. – Электрон. дан. – Минск : Ковчег, 2021. – 1 электрон.  
опт. флеш-карта (USB) ; 54 мм. – Систем. требования : IBM-  
совместимый PC ; 256 Мб RAM ; VGA ; Windows 2000 / xp / Vista ; USB  
разъём ; мышь. – Загл. с экрана.

ISBN 978-985-884-108-9.

Сборник трудов составлен по материалам докладов, представленных на XIII Белорусско-Сербском симпозиуме "Физика и диагностика лабораторной и астрофизической плазмы" (ФДП-13), 13–17 декабря 2021 года, г. Минск. Тематика включенных в сборник статей охватывает широкий круг вопросов, касающихся способов получения плазмы, методов ее диагностики и их применения для решения актуальных практических задач.

The Proceedings have been compiled from materials of reports presented at The XIII Belarusian-Serbian Symposium "Physics and Diagnostics of Laboratory and Astrophysical Plasmas" (PDP-13), December 13–17, 2021, Minsk. The scope of papers covers a wide range of topics concerning techniques of plasma generation, methods of plasma diagnostics, and their application in solving real-world challenges of the present day.

**УДК 533.9 (043.2)  
ББК 22.3**

**ISBN 978-985-884-108-9**

© B.I. Stepanov Institute of Physics, The  
National Academy of Sciences of Belarus, 2021

© Оформление. ООО «Ковчег», 2021

## **SYMPOSIUM ORGANIZERS**

The National Academy of Sciences of Belarus  
State Committee on Science and Technology of Belarus  
Ministry of Education of the Republic of Belarus  
Belarusian Republican Foundation for Fundamental Research  
B.I. Stepanov Institute of Physics of NAS of Belarus  
Institute of Heat and Mass Transfer of NAS of Belarus  
Belarusian State University  
A.N. Sevchenko Scientific-Research Institute of Applied Physical Problems

The papers in these Proceedings are presented by the individual authors. The views expressed are their own and do not necessarily represent the views of the Publishers or Sponsors. Whilst every effort has been made to ensure the accuracy of the information contained in this book, the Publisher or Sponsors cannot be held liable for any errors or omissions however caused.

PROCEEDINGS OF THE XIII BELARUSIAN-SERBIAN SYMPOSIUM  
"PHYSICS AND DIAGNOSTICS OF LABORATORY AND  
ASTROPHYSICAL PLASMAS" (PDP-13): December 13–17, 2021, Minsk,  
Belarus / Edited by A.N. Chumakov, M.M. Kuraica, M.S. Usachonak

All rights reserved.

No part of this publication may be reproduced, stored in a retrieval system, in any form or by any means, electronic, mechanical, photocopying, recording or otherwise, without the prior permission of the copyright owner.



## HONOUR COMMITTEE

**Chairman: S.Ya. Kilin** (Deputy Chairman of the Presidium of NAS of Belarus)

**S.S. Scherbakov** (Vice-Chairman of the State Committee on Science and Technology of Belarus)

**M.V. Bogdanovich** (Director of The B.I. Stepanov Institute of Physics of NAS of Belarus)

The Ambassador of Serbia in the Republic of Belarus

**S.V. Gaponenko** (Chairman of the Scientific Council of the Belarusian Republican Foundation for Fundamental Research)

**A.D. Korol** (Rector of the Belarusian State University)

**P.V. Kuchinsky** (Director of the A. N. Sevchenko Institute of Applied Physical Problems of Belarusian State University)

**O.G. Penyazkov** (General Director of the A.V. Luikov Heat and Mass Transfer Institute of NAS of Belarus)

**A.P. Voitovich, A.F. Chernyavskii, V.I. Arkhipenko, V.K. Goncharov, M.S. Dimitrijević, J. Purić, N. Konjević**

## PROGRAMME SCIENTIFIC COMMITTEE

**Co-Chairmen:** A.N. Chumakov (Belarus)  
M.M. Kuraica (Serbia)

**Vice-Chairmen:** L.V. Simonchik (Belarus)  
B. Obradović (Serbia)

**Scientific Secretary:** M.S. Usachonak (Belarus)

V.M. Astashynski (Belarus), M.V. Belkov (Belarus), N. Cvetanović (Serbia), I.I. Filatova (Belarus), K.V. Kozadaev (Belarus), M. Kuzmanović (Serbia), I.S. Nikanchuk (Belarus), L. Popović (Serbia), M.V. Puzyrov (Belarus), J. Savović (Serbia), A.S. Smetannikov (Belarus), I.P. Smyaglikov (Belarus), N.V. Tarasenko (Belarus), M. Trtica (Serbia).

## LOCAL COMMITTEE

**Chairmen:** L.V. Simonchik (Belarus)

**Vice-Chairmen:** M.V. Puzyrov (Belarus)

**Secretary:** V.A. Lyushkevich (Belarus)

N.A. Bosak, E.A. Ershov-Pavlov, S.V. Goncharik, A.V. Kazak, V.G. Kornev, A.A. Kirillov, V.V. Lychkovskiy, M.I. Nedelko, A.A. Nevar, N.N. Tarasenko, A.M. Vabishchevich.

## THE INTRODUCTION OF MORE COMPLEX ATOMS IN A CUT-OFF COULOMB MODEL POTENTIAL, THE AR I MODEL

Sakan Nenad M.<sup>1</sup> and Simić Zoran J.<sup>2</sup>

<sup>1</sup>Institute of Physics, University of Belgrade, PO Box 57, 11001 Belgrade, Serbia

<sup>2</sup>Astronomical Observatory, Volgina 7, 11060 Belgrade, Serbia

**Introduction.** Dense plasma is a object of interest in recent years [1]. Up until now the absorption coefficients of hydrogen plasma, were calculated within the frame of cut-off Coulomb potential model, for the wide area of electron densities and temperatures [2-9]. The optical parameters of hydrogen plasma of mid and moderately high non-ideality parameter are described successfully, thus enabling the modeling of optical properties [2,3], [5-9]. Governed by this results a effort has been made to introduce a extension of a model towards the more complex atoms. As a first goal the Ar atom model was used since the ionic core model potential for the Ar I was analyzed in [10]. As it was case with the hydrogen model here, the model potential for Ar is solvable in entire space and within entire energy spectrum, thus the yielded wave function solutions are a combination of a special functions. As it was proven a faster, and no less reliable, method of numerical integration using a Numerov integration is used. It posses a fast convergence and as such is preferred method for introduction of more complex atom and ion model potentials in consideration, the comparison and application is shown in [11].

**Theory remarks.** The collective phenomena of plasma that consists of many interacting particles, could be described as quantum mechanical system consists of a single emitter, and averaged plasma influence as whole. This approach is more applicable for the plasma of higher non-ideality, and it is easy to introduce additional processes within the considered model. The heart of modeling of plasma-emitter interaction and investigation of it's optical behavior is done by the introduction of adequate model potential, the one for Ar I is given by

$$V(r) = \begin{cases} -\frac{Z_l e^2}{4\pi\epsilon_0 r} & : r < r_0 \\ -\frac{e^2}{4\pi\epsilon_0 r} & : r_0 \leq r < r_c \\ 0 & : r \geq r_c \end{cases}, \quad Z_l = \begin{cases} 9.04 - l \frac{8.04}{3} & : l \leq 3 \\ 1 & : l > 3 \end{cases}, \quad r_0 = 1.7 a_0. \quad (1)$$

Here the  $a_0$  is the Bohr radius.

In such way the results yielded within the frame of this model method are purely quantum mechanical solutions for the considered plasma. All the optical properties are connected to each other, so the main goal of describing optical parameters of plasma is by the solving or the radial part of the Schrodinger equation,

$$\frac{-\hbar^2}{2m} \frac{1}{r^2} \frac{\partial}{\partial r} \left( r^2 \frac{\partial R_{nl}}{\partial r} \right) + \left[ V(r) + \frac{\hbar^2 l(l+1)}{2mr^2} \right] R_{nl}(r) = E_{nl} R_{nl}(r), \quad (2)$$

by the help of new function  $P(r)=r R(r)$  it gives an more easily solvable form

$$\frac{-\hbar^2}{2m} \frac{d^2}{dr^2} P_{nl}(r) + \left[ V(r) + \frac{\hbar^2 l(l+1)}{2mr^2} - E_{nl} \right] P_{nl}(r) = 0. \quad (3)$$

The eigenvalues  $E_{nl}$  and eigenvectors  $P_{nl}$  are needed to have a dipole matrix element  $\hat{D}(r; r_0; r_c; n_i l_i; n_f l_f) = \langle n_f l_f | r | n_i l_i \rangle$  determined, and further on the adequate cross-sections like  $\sigma_0(\omega = \omega_{fi}) \sim |\hat{D}(r; r_0; r_c; n_i l_i; n_f l_f)|^2$  for the bond-bond transitions.

**Results and discussion.** The goal of presented work is to prove that a Ar atom optical behavior in plasma could be described by the means of solving the Schrodinger equation (3) with the model potential (1), in the same way as it was a case with the hydrogen atom. Since, in contrast to the hydrogen model, there is not a adequate theoretical functions for the optical properties the only way was to compare the results to the hydrogen model ones, and to analyze a convergence of the wave functions towards the model of unperturbed argon atom in case of diminishing a plasma influence.

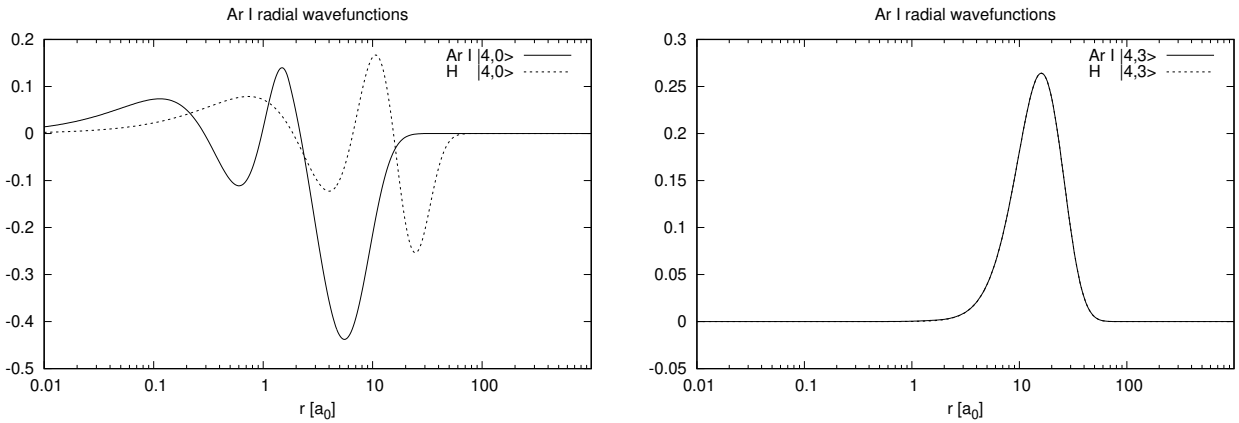


Figure 1. Comparison of hydrogen and Ar I wave functions.

As first, a pure comparison of argon radial wave functions with the hydrogen atom ones was made. It could be seen from the example on the Figure 1. that for the orbital quantum number small enough ( $l < 3$ ) where the ionic core has effect onto the potential (1), the wave function is bond more stiffer to the core than the hydrogen one, as expected.

On the Figure 2. the set of wave functions are given as a illustration of their behavior. And finally, the Figure 3. presents a result of the investigation of the behavior of the wave functions for the variety of cut-off radius  $r_c$  values that reflects the averaged plasma influence onto the emitter. For the presented calculation results a more complex potential is used

$$V^i(r) = V(r) + \langle E_{plas} \rangle = V(r) + \frac{e^2}{4\pi\epsilon_0 r_c}. \quad (4)$$

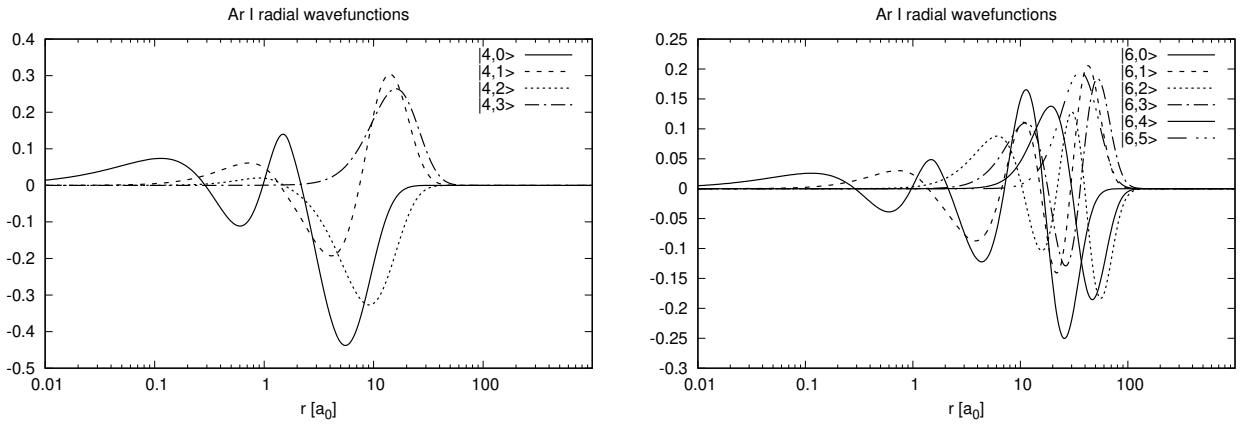


Figure 2. Example sets of Ar I wave functions.

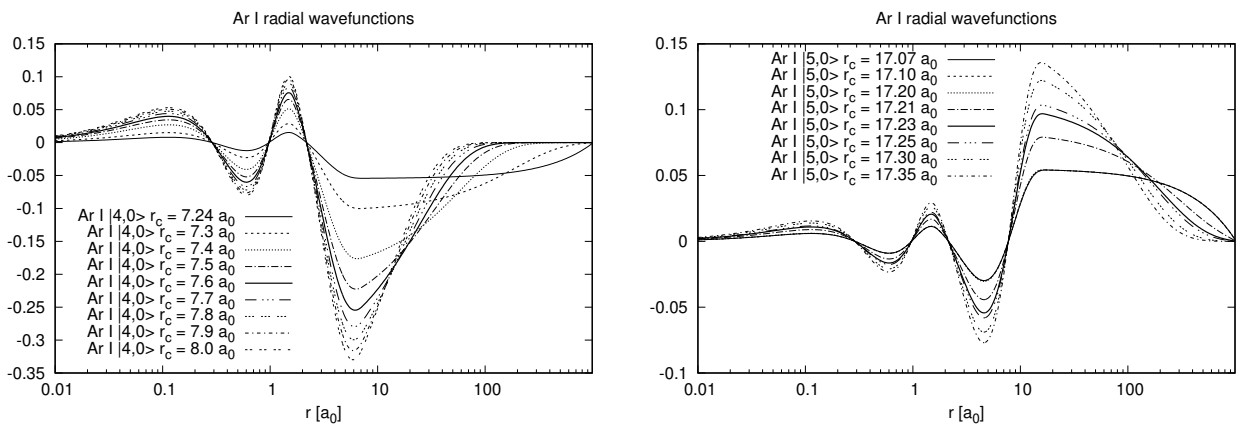


Figure 3. Plasma influence on Ar I wave functions and convergence towards unperturbed case.

As expected the convergence toward an unperturbed values is proven.

**Conclusion.** The presented results are leading us to conclusion that the cut-off Coulomb potential model is usable for the describing more complex atoms in plasma in general. The well behaved wave function convergences are more than encouraging for the using of the presented results in a modeling of the optical properties of plasma. The effort on connecting of optical and transport plasma parameter is to be done. The considered here Ar I as a emitter is expected to be used in near future in both single component and complex composition non-ideal plasma. The mid and higher non-ideality, that is a goal of model, has a influence on describing of stellar processes. Although the presented work is still in progress, the results could be used directly even in this early development phase.

**Acknowledgment.** Funding provided by the Institute of Physics Belgrade, through the grant by the Ministry of Education, Science, and Technological Development of the Republic of Serbia.

## Literature

1. **Fortov, V.E., Iakubov, I.T.** // The physics of non-ideal plasma / World Scientific, 1999.
2. **Mihajlov, A.A., Sakan, N.M., Srećković, V.A., Vitel, Y.** // Modeling of continuous absorption of electromagnetic radiation in dense partially ionized plasmas. *J. Phys. A* (2011), 44, 095502.
3. **Mihajlov, A.A., Ignjatović, L.M., Srećković, V.A., Dimitrijević, M.S., Metropoulos, A.** // The non-symmetric ion-atom radiative processes in the stellar atmospheres, *Mon. Not. R. Astron. Soc.* 2013, 431, 589–599.
4. **Mihajlov, A.A., Djordjević, D., Popović, M.M., Meyer, T., Luft, M., Kraeft, W.D.** // Determination of the Electrical Conductivity of a Plasma on the Basis of the Coulomb cut-off Potential Model., *Contrib. Plasma Phys.*, 1989, 29, 441–446.
5. **Ignjatović, L.M., Srećković, V.A., Dimitrijević, M.S.** // The Screening Characteristics of the Dense Astrophysical Plasmas: The Three-Component Systems., *Atoms*, 2017, 5, 42.
6. **Mihajlov, A.A., Sakan, N.M., Srećković, V.A., Vitel, Y.** // Modeling of the Continuous Absorption of Electromagnetic Radiation in Dense Hydrogen Plasma., *Balt. Astron.*, 2011, 20, 604–608.
7. **Mihajlov, A.A., Srećković, V.A., Sakan, N.M.** // Inverse Bremsstrahlung in Astrophysical Plasmas: The Absorption Coefficients and Gaunt Factors., *J. Astrophys. Astron.*, 2015, 36, 635–642.
8. **Sakan, N.M., Srećković, V.A., Mihajlov, A.A.** // The application of the cut-off Coulomb potential for the calculation of a continuous spectra of dense hydrogen plasma., *Mem. S. A. I. Suppl.*, 2005, 7, 221–224.
9. **Sakan, Nenad M. and Srećković, Vladimir A. and Simić, Zoran J. and Dimitrijević, Milan S.** // The Application of the Cut-Off Coulomb Model Potential for the Calculation of Bound-Bound State Transitions, *Atoms*, 2018, 6, 1, 4
10. **A. Mihajlov and D. Djordjević and M.M. Popović** // The inner charge defect method as an analog to the quantum defect method, *JQSRT*, 1980, 47-52, [https://doi.org/10.1016/0022-4073\(80\)90040-0](https://doi.org/10.1016/0022-4073(80)90040-0)
11. **Nenad M. Sakan, Zoran J. Simić, and Momchil Dechev** // The optical properties of Hydrogen plasma described in the frame of the fully quantum method based on a cut-off Coulomb model potential, 16th ESPM - European Solar Physics Meeting, 6-10 September 2021, online

## The Calculation of the Photo Absorption Processes in Dense Hydrogen Plasma with the Help of Cut-Off Coulomb Potential Model

This content has been downloaded from IOPscience. Please scroll down to see the full text.

2010 J. Phys.: Conf. Ser. 257 012036

(<http://iopscience.iop.org/1742-6596/257/1/012036>)

View [the table of contents for this issue](#), or go to the [journal homepage](#) for more

### Download details:

IP Address: 24.135.226.112

This content was downloaded on 23/10/2016 at 19:22

Please note that [terms and conditions apply](#).

You may also be interested in:

[Modeling of continuous absorption of EM radiation, dense partially ionized plasmas](#)

A A Mihajlov, N M Sakan, V A Srekovi et al.

[Formation and decay of the Rydberg states of multiply charged ions interacting with solid surfaces](#)

M A Mirkovi, N N Nedeljkovi and D K Božani

[On the calculation of resonances by means of analytic continuation in coupling constant](#)

J Horáek and I Paidarová

[Theory of below-threshold kinetic electron emission](#)

P Tiwald, Ch Lemell, G Wachter et al.

[The disk emission in the Broad Line Region of Active Galactic Nuclei](#)

Edi Bon, Luka Popovi, Nataša Gavrilovi et al.

[Helium-rich white dwarf atmospheres: the non-symmetric ion-atom absorption processes](#)

V A Srekovi, A A Mihajlov, Lj M Ignjatovi et al.

[Line profile variations in selected Seyfert galaxies](#)

W Kollatschny, M Zetzl and K Ulbrich

# The Calculation of the Photo Absorption Processes in Dense Hydrogen Plasma with the Help of Cut-Off Coulomb Potential Model

Nenad M. Sakan

Institute of Physics, Pregrevica 118, Zemun, Belgrade, Serbia

E-mail: nsakan@ipb.ac.rs

**Abstract.** Extensive work was done in the application of a cut-off Coulomb model on the description of the optical processes of the photo ionization and inverse bremsstrahlung. Presented work deals with a usage of a cut-off Coulomb model pseudo potential for the calculation of the optical absorption process in dense hydrogen plasma as a entirely quantum mechanical process. Although the mentioned processes are strongly influenced by the collective process in dense plasma, the used pseudo potential enables to model the described interaction with the plasma system as a binary process. There are several advantages of such approach; the existence of the exact analytical solutions for the wave functions in the described potential enables to eliminate one of the several sources of numerical error. Also, more complex processes of the interaction inside plasma could be considered, and they have been added in presented work. The work on description of such processes has been started. The collective phenomena of the plasma are here described as an additional shifting and broadening of a bond states levels. Furthermore, with the adding of mentioned broadening and additional shifting of the bond states as free external parameters the good agreement between the analyzed experimental data and our model solutions occurs. The method of determination of the cut-off radius was developed and applied in our considerations. The presented model is a good approach for the description of dense hydrogen plasma of moderate and high non-ideality. It presents an easily extendable model, in which is easy to introduce additional processes and effects.

## 1. Introduction

In this paper is studied a new model method of the describing of the continuous absorption of electromagnetic (EM) radiation in dense strongly ionized hydrogen plasma, caused by the atomic photo-ionization processes

$$E_{h\nu} + H^*(nl) \rightarrow H^+ + e_{\vec{q}}, \quad (1)$$

and electron-ion inverse "bremsstrahlung" processes

$$E_{h\nu} + e_{\vec{q}} + H^+ \rightarrow e_{\vec{q}'} + H^+, \quad (2)$$

where  $E_{h\nu}$  is the energy of the photon with the wavelength  $\lambda$ ,  $n$  and  $l$  - principal and orbital quantum numbers of hydrogen excited states,  $\vec{q}$  and  $\vec{q}'$  - the momentum of the free electron before and after scattering on the considered ion  $H^+$ .



While in weakly and moderately non-ideal plasma, this absorption is caused by the neutral atoms and electron-ion collision complex which interaction with the neighborhood can be neglected, as for example in Solar photosphere [5, 6], or described within the framework of a perturbation theory [18, 12, 13, 15, 16] in the dense strongly non-ideal plasma the situation is in principle different.

By now a lot of effort was aimed to the development of the quantum-statistical methods for the description of the thermodynamical and transport properties of dense strongly non-ideal plasma [9, 11, 8, 7, 10, 14] while the absorption processes was treated only for plasma with electron densities  $N_e < 10^{18} \text{cm}^{-3}$ , where the approximation of electron-atom and electron-ion binary collisions is still applicable. The area of really dense plasma with  $N_e > 10^{19} \text{cm}^{-3}$  was not systematically studied from the aspect of the bound-bound, bound-free and free-free absorption processes, excluding some efforts of semi-empirical describing of such processes [25, 26]. Because of that the development of a model method which describes the mentioned absorption process in dense strongly non-ideal plasma on a simple and physically acceptable way is the one of the actual tasks. Within this work as a landmark is taken the hydrogen plasma with the electron density  $N_e = 1.5 \cdot 10^{19} \text{cm}^{-3}$  and the temperature  $T = 23000 \text{K}$ , which was experimentally studied in [26]. The direct result of this work is a new model method for the determination of absorption coefficients  $\kappa_{bf}(\lambda)$  and  $\kappa_{ff}(\lambda)$ , characterizing the bound-free and free-free absorption processes (1) and (2) in the strongly non-ideal hydrogen plasma, which is based on a cut-off Coulomb pseudo-potentials, similar to the one used for the determination of the non-ideal plasma conductivity. The presented method is tested in the optical range of photon wavelengths  $350 \text{nm} \leq \lambda_{h\nu} \leq 550 \text{nm}$ .

## 2. Theory

### 2.1. The cut-off Coulomb potentials

The obvious way of simplification of principally many body processes of photo absorption transitions inside plasma was transformation to the corresponding transitions of the electron in an adequately chosen pseudo-potential, which replaces the considered ion and the rest of the system. In [22], in order to obtain the method of the describing of such process which would be practically applicable, generally non-local pseudo-potential in usual way was sought in the form of the corresponding local one-particle potential. As such potential was chosen one of model screening Coulomb potential, namely cut-off potential (4).

On the occasion of the choosing of the model potential it was taken into account the argumentation from the [22], which shows that often used model Debye-Hückel (DH) potential is not adequate for strongly non-ideal plasma. Let us draw attention that we here do not have in mind some undesirable properties of the DH potential [28, 27], but the way of the obtaining of that potential itself. Namely, in accordance with [19] the DH potential is the average electrostatic potential which is generated by the observed ion and all charged particles from its neighborhood, which are often treated as the screening cloud. Consequently, the electron, that is involved in scattering on the considered ion, also is the part of that cloud. In spite of this fact the DH potential, as it is known, is used often in weakly non-ideal plasma when the number  $n_D \gg 1$ , where  $n_D$  is the number of the electrons inside the sphere with the Debye radius  $r_D$ .

However, in the case of strongly non-ideal plasmas, when  $n_D \cong 1$ , as it is in the considered plasma, practically, the complete cloud is consisted of the free electron that is involved in scattering, and the DH potential could not be used any more. Contrary to that, in the case  $n_D \cong 1$  the application of the cut-off Coulomb potential, as it was noted in [22], is physically completely justified, since it automatically provides: just Coulomb behavior of the potential in the close vicinity of the considered ion; the lowering of the atom ionization potential caused by the influence of the neighborhood, which is equal to the average potential energy of a free electron in plasma; non Coulomb asymptotic of the wave function of a free electron.

All mentioned have caused that one of the considered here model cut-off Coulomb potentials has the form, which is shown, in the Fig. (1a), where  $e$  is the absolute value of electron charge,  $r$  - the distance from the origin of the chosen reference frame,  $r_c$  - corresponding screening radius, and the value  $U_p = -e^2/r_c$  has to be interpreted as the above mentioned the average potential energy of a free electron in plasma. Other model cut-off Coulomb potential is considered here because the fact that in the case of the first model the average potential energy of the electron in the region  $0 < r < r_c$ , for the difference of the region  $r_c < r < \infty$ , is not equal to the energy  $U_p$ , which is illustrated by Fig. (1 a). However, in the plasma the moving of the electron from the region occupied by the one ion to the region occupied by the nearest neighbor ion is realized in the potential with the maximal value (between the position of the mentioned ions), which is greater than average values of potential. Because of that the average potential energies of the electron in the region occupied by the one ion and in the rest of the plasma have to be equal to the average energy of the free electron in the whole system denoted here by  $U_p$ . One can see that this condition can be satisfied in the case of other cut-off Coulomb potential, which is shown in Fig. (1b), when the parameter  $k = 1/2$ . Namely, it can be shown that

$$\int_0^{(k+1)r_c} U(r)4\pi r^2 dr = U_p V = -\frac{e^2}{r_c} \cdot \frac{4\pi}{3} [(k+1)r_c]^3, \quad (3)$$

is only valid for  $k = 1/2$ , where  $V$  is the volume of sphere with radius  $r_c$ , which is determined on the basis of the result from [28].

In further consideration we will take the value  $-e^2/r_c$  as the zero of the energy. After that, the potentials shown in the Figs. (1a) and (1b) are transformed to the forms  $U_0(r; r_c)$  and  $U_k(r; r_c)$ , respectively, where

$$U_0(r; r_c) = \begin{cases} -\frac{e^2}{r} + \frac{e^2}{r_c} & : 0 < r \leq r_c, \\ 0 & : r_c < r, \end{cases} \quad (4)$$

$$U_k(r; r_c) = \begin{cases} -\frac{e^2}{r} + \frac{e^2}{r_c} & : 0 < r \leq (k+1)r_c, \\ 0 & : (k+1)r_c < r \end{cases}, \quad (5)$$

where  $U_0(r; r_c)$  is the same potential as in [22]. Because of the above mentioned, in the case of the potential  $U_k(r; r_c)$  we will consider that  $k = 1/2$ .

Let us denote that the form of the potential (5) is not caused by the presence of some new mechanism that increases the barrier in the region  $r > r_c$  for the electron in the complex  $(H^+ + e)_{nl}$  or  $(H^+ + e)_{\bar{q}}$ , but exclusively by the requirement for the satisfying of the condition (3).

## 2.2. The photo-ionization and inverse "bremsstrahlung" cross-sections

Since under the condition from [26] the considered wavelength  $\lambda \gg r_s$ , where  $r_s = (3/4\pi N_e)^{1/3}$  is the corresponding Wigner-Seitz radius, the dipole approximation in the case of considered processes is valid. According to that, the cross section for these bound-free and free-free absorption processes are given by the expressions from [24], namely

$$\sigma(nl; E') = \frac{4\pi^2 e^2 k}{3(2l+1)} \sum_{l'=l\pm 1} l_{max} \left( \int P_{nl} r P_{E'l'} dr \right)^2, \quad (6)$$

$$\sigma(E; E') = \frac{8\pi^4 \hbar e^2 k}{3 q^2} \sum_{l'=l\pm 1} l_{max} \left( \int P_{El} r P_{E'l'} dr \right)^2, \quad (7)$$

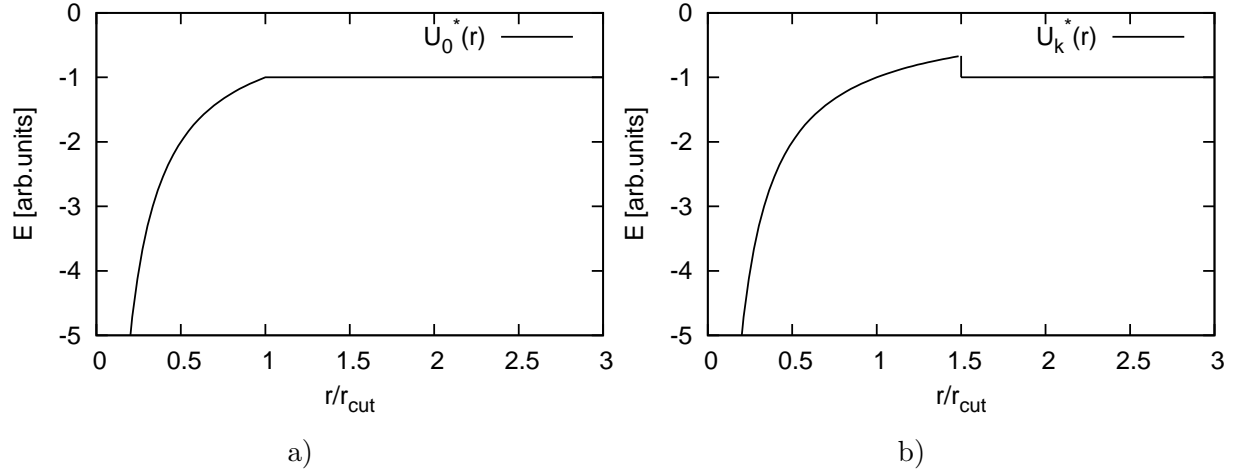


**Figure 1.** The behavior of the used potentials: **a)** - from (4), **b)** - from (5).

where  $k = \epsilon_\lambda/\hbar c$  is the momentum of the absorbed photon with the given  $\lambda$ ,  $E = \hbar^2 q^2/2m$  and  $E' = \hbar^2 q'^2/2m$  - the energies of the free electron,  $l_{max}$  - maximal value of  $l$  and  $l'$ ,  $m$  - the electron mass, and  $c$  - the light velocity. Here the radial wave function of the electron in the model potentials (4) and (5) with  $k = 0.5$  is denoted with  $P_{nl}/r$ , for the bound states with given  $n$  and  $l$ , and with  $P_{El}/r$  and  $P_{E'l'}/r$  for the free states with the given  $E$  and  $l$  or  $E'$  and  $l'$ . The functions  $P_{nl}$  and  $P_{El}$  are obtained in strict analytical form by the means of the expressions for the Whittaker, Coulomb, spherical Bessel, and modified Bessel functions.

In further calculations for the determination of the photo-ionization cross section  $\sigma(nl; E')$  is used Eq. 6, while in the case of inverse "bremsstrahlung" cross section  $\sigma(E; E')$  is used the expression which is obtained by means of the known relations [24], which connect the matrix elements of the  $j$ -th components ( $j = 1, 2, 3$ ) of the radius-vector  $\vec{r}$ , electron momentum  $\vec{p}$ , and gradient of the potential  $\vec{\nabla}U(\vec{r})$ , namely

$$\langle in|\vec{\nabla}_j U(\vec{r})|fin \rangle = \frac{i}{\hbar}(E_{in} - E_{fin}) \langle in|\vec{p}_j|fin \rangle, \quad (8)$$

$$\langle in|\vec{p}_j|fin \rangle = \frac{i}{\hbar} m (E_{in} - E_{fin}) \langle in|\vec{r}_j|fin \rangle, \quad (9)$$

where  $U(\vec{r})$  in the considered case is equal to  $U_0(r)$  or  $U(r; k)$ . Namely, from Eqs. (7), (8) and (9) it follows the expression

$$\sigma(E; E') = \frac{4\pi^4}{3} \frac{\hbar^6 e^2}{m^3 c E E_{\hbar\nu}^3} \sum_{\nu=l\pm 1}^{l_{max}} \left( \int_0^{(k+1)r_c} P_{El} \nabla_r U(r) P_{E'l'} dr \right)^2, \quad (10)$$

where  $E_{\hbar\nu} = E' - E$ , and with  $U(r) = U(r; k = 0) \equiv U_0(r)$  or  $U(r; k = 1/2)$ , which enables to use the shape of the potentials (4) and (5) and to avoid all difficulties connected with the calculation of the dipole matrix element in Eq. (7) in the whole region of space  $0 < r \leq \infty$ . Just Eq. (10) is used here for the calculation of the inverse "bremsstrahlung" cross-section  $\sigma(E; E')$ .

### 2.3. The partial and total absorption coefficients

The expressions (6) and (10) for the photo-ionization and inverse "bremsstrahlung" cross-sections enable the direct determination of the partial absorption coefficients, characterizing the bound-free and free-free absorption processes (1) and (2), given by the relations

$$\kappa_{bf}^{(0)}(\lambda; N_e, T) = \sum_{n=1}^{n_{max}} \sum_{l=0}^{n-1} N_{nl} \cdot \sigma(nl; E'), \quad (11)$$

$$\kappa_{ff}^{(0)}(\lambda; N_e, T) = N_i N_e \cdot \int_0^\infty \sigma(E; E') v f(v) dv, \quad (12)$$

where  $N_{nl}$  is the density of the atoms  $H^*$ , e.g. electron-ion pairs in the bound states with the given quantum numbers  $n$  and  $l$ ,  $T$  - the plasma temperature, and  $n_{max}$  - the principal quantum number of the last realizing bound state for the given  $N_e$  and  $T$ . However, while the expression (12) for the free-free absorption coefficient  $\kappa_{ff}^{(0)}(\lambda; N_e, T)$  should generate the purely acceptable results, the situation in connection with Eq. (11) is different. Namely, the results obtained by means of Eq. (11) should be similar to the ones for the diluted plasma (see for example [5]), since, contrary to the existing experimental results [26], the unique serious difference would ensue from the lowering of the photo-ionization limits for the realizing bound states for the value close to  $e^2/r_c$ .

The plasma-ion interaction at the considered densities is mainly of Stark type, and also it was made a transition from many particle model towards the two particle model. Because of that there should be included and additionally considered a shift and the broadening of a bond state levels, as a result of a many particle interactions. The mentioned shifts and broadenings are treated as the semi-empirical quantities, which appear as the external parameter of the theory. Here, the shift of  $(nl)$ -level is denoted by  $\Delta_{nl}^{sh}$ , and broadening by  $\Delta_{nl}^{br}$ . As it is usual we assume that the electron in atom  $H_{nl}^*$  in the plasma could be in the state with the energies which are dominantly grouped around the energy  $\varepsilon_{nl}^{max} = \varepsilon(nl) + \Delta_{nl}^{sh}$ , inside the interval  $(\varepsilon_{nl}^{max} - \Delta_{nl}^{br}/2, \varepsilon_{nl}^{max} + \Delta_{nl}^{br}/2)$ . Let  $P_{nl}(\varepsilon)$  is the probability density which characterizes the distribution of the energies of the mentioned state within the interval  $(\varepsilon_{nl}^{max} - \Delta_{nl}^{br}/2, \varepsilon_{nl}^{max} + \Delta_{nl}^{br}/2)$ , which satisfies the conditions

$$max\{P_{nl}(\varepsilon)\} = P(\varepsilon = \varepsilon_{nl}^{max}), \quad \int_{\varepsilon_{nl}^{max} - \Delta_{nl}^{br}/2}^{\varepsilon_{nl}^{max} + \Delta_{nl}^{br}/2} P_{nl}(\varepsilon) d\varepsilon = 1. \quad (13)$$

In accordance with above consideration, here we will characterize the bound-free and free-free processes by the photo-ionization and inverse "bremsstrahlung" partial absorption coefficients

$$\kappa_{bf}(\lambda; N_e, T) = \int_{\varepsilon_{nl}^{max} - \Delta_{nl}^{br}/2}^{\varepsilon_{nl}^{max} + \Delta_{nl}^{br}/2} P_{nl}(\varepsilon) \cdot \tilde{\kappa}_{bf}^{(0)}(\lambda; N_e, T; \varepsilon) d\varepsilon, \quad (14)$$

where  $\tilde{\kappa}_{bf}^{(0)}(\lambda; N_e, T; \varepsilon)$  is obtained from (6) and (11) by replacing free electron energy  $E'$  with  $\tilde{E}' = E' + (\varepsilon - \varepsilon_{nl})$ ,

$$\kappa_{ff}(\lambda; N_e, T) = \kappa_{ff}^{(0)}(\lambda; N_e, T), \quad (15)$$

where  $\kappa_{ff}^{(0)}(\lambda; N_e, T)$  is given by Eq. (12), as well as the corresponding total absorption coefficient

$$\kappa_{tot}(\lambda; N_e, T) = (\kappa_{ff}(\lambda; N_e, T) + \kappa_{bf}(\lambda; N_e, T)) \cdot \left[ 1 - \exp\left(-\frac{\epsilon\lambda}{kT}\right) \right], \quad (16)$$

where it is taken into account the influence of the stimulated emission.

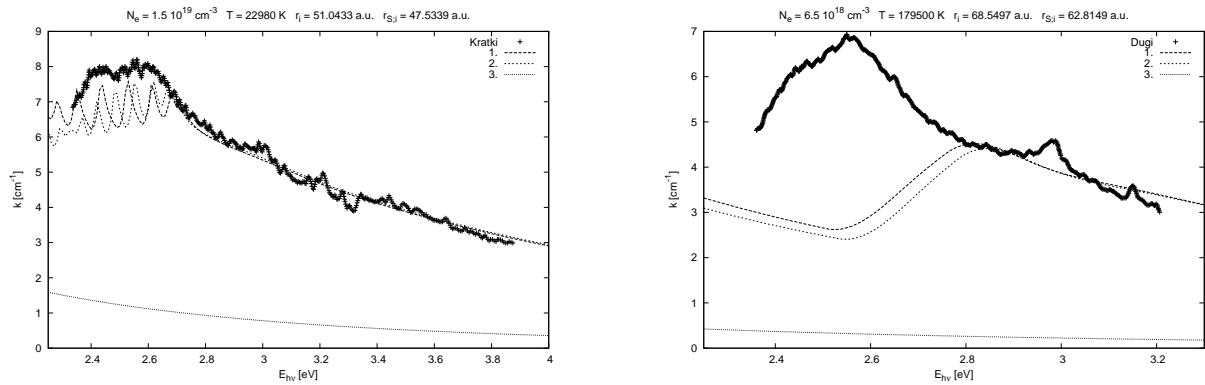


**Figure 2.** The calculated data for the potential (4), left figure The short pulse, comparison with the results in the case of the potential  $U_0$  with  $r_c = 44.964 a.u.$  Curve **1.** - model with changeable shift and broadening,  $\Delta E = 0.6 eV$  and  $\delta E = 1 eV$  for  $n = 2$ . Curve **2.** - model with constant shift and broadening, case  $\Delta E = 0,5 eV$  i  $\delta E = 0,75 eV$ . **3.** -  $\kappa_{ff}$ . The right figure, long pulse, comparison with the results in case of the potential  $U_0$  with  $r_c = 55.0523 a.u.$ . Curve **1.** - model with changeable shift and broadening  $\Delta E = 0.275 eV$  and  $\delta E = 0.25 eV$  for  $n = 2$ . Curve **2.** - model with constant shift and broadening, case  $\Delta E = 0.25 eV$  i  $\delta E = 0.25 eV$ , **3.** -  $\kappa_{ff}$ .

### 3. Results and discussion

In this paper the calculations of the total absorption coefficient  $\kappa_{tot}(\lambda; N_e, T)$  with the cut-off Coulomb potential (4) were made for the strongly non-ideal hydrogen plasma  $N_e = 1.5 \cdot 10^{19} cm^{-3}$  and  $T = 23000K$ , as well as  $N_e = 6.5 \cdot 10^{18} cm^{-3}$  and  $T = 18000K$  taken from [26].

After process of selection of adequate shift and broadening parameters and comparison with the experimental data, good agreement was found. The good agreement with the experimental data in area where only continuous absorption is present, e.g. at the energies  $E_{h\nu} \geq 2.8 eV$ , and the form of the total continuous absorption coefficient gives a space for bond-bond transition absorption.

Without further research on bond-bond transition within the frame of this model, there is not much to be said and analyzed for the model of broadening and shifting of bond state levels. Allthow, at this moment, it is just a parameter without further involvement into the processes behind it, it should be emphasized again that good agreement with experimental data exists.

### 4. Conclusion

Besides the fact that the presented model is still in process of development, a good agreement with the experimental data was shown.

There is a need to develop a model of bond-bond absorptions, which would enable the investigation of form of broadening and shifting of bond state levels. It would enable the studies of the broadening and shifting effects more in detail and develop a more concise model.

Also there is still a need for developing of both faster numerical procedures and code parallelism to improve speed and accuracy.

### Acknowledgments

The work presented in this progress report was done under the MNTRS project 141033.

### References

- [1] K. Suchy. *Beitz. Plasmaphysik*, 4:71, 1964.

- [2] C. Deutsch, M. M. Gombert, and H. Mino. *Phys. Letters*, 66A:381, 1978.
- [3] K. Gunther and R. Radtke. *Electric Properties of Weakly Nonideal Plasmas*. Akademie, Berlin, 1984.
- [4] W. Kraeft, D. Kremp, W. Ebeling, and G. Röpke. *Quantum Statistics of Charged Particle System*. Akademie-Verlag, Berlin, 1986.
- [5] D. Mihalas. *Stellar Atmospheres* W. H. Freeman, San Francisco 1978
- [6] A. A. Mihajlov and Lj. M. Ignjatović and N. M. Sakan and M. S. Dimitrijević *Astronomy and Astrophysics*, 437:1023-1025, 2007.
- [7] G. Rinker, *Phys.Rev.A*. 37 (1988) 1284, Technical Report No. LA-10608-MS, Los Alamos National Laboratory (1986), unpublished.
- [8] S. Ichimaru H. Iyetomi and S. Tanaka, *Phys. Rep.* 149 (1987) 91.
- [9] W. Ebeling, W. D. Kraeft, and D. Kremp, *Theory of bound states and Ionization Equilibrium in Plasmas and Solids*, Academia-Verlag, Berlin (1976).
- [10] V. E. Fortov and I. T. Iakubov, *Physics of Nonideal Plasma* Hemisphere, New York (1989).
- [11] W. D. Kraeft, D. Kremp, W. Ebeling, and G. Röpke *Quantum Statistics of Charged Particle Systems* Akademie-Verlag, Berlin, (1986).
- [12] I. M. Tkachenko and P. Fernández de Córdoba *Phys.Rev.E*. **57**, No.2, (1997) 2222-2229
- [13] H. Reinholz, Yu. Zaporozhetz, V. Mintsev, V. Fortov, I. Morozov, and G. Röpke, *Phys.Rev.E*. **68**, (2003) 036403-1-036403-10
- [14] V. M. Adamyan, Z. Djuric, A. A. Mihajlov, N. M. Sakan and I. M. Tkachenko *J.Phys.D*. **37** (2004) 1896-1903.
- [15] V. B. Mintsev and V. E. Fortov *J.Phys.A* **39** (2006) 4319-4327
- [16] Gabor J. Kalman, J. Martin Rommel and Krastan Blagoev *Strongly Coupled Coulomb Systems* Kluwer academic publishers
- [17] A. A. Mihajlov, D. Djordjevic, M. M. Popovic, T. Meyer, M. Luft, and W.D. Kraeft. *Contrib. Plasma Phys.*, 29(4/5):441, 1989.
- [18] G.A. Kobzev, I.T. Jakubov, and M.M. Popovich, editors. *Transport and Optical Properties of Non-Ideal Plasmas*. Plenum Press, New York, London, 1995.
- [19] P. Debye and E. Hückel; *Physikalische Z.*, 1923, vol. 24, p.185
- [20] A. A. Mihajlov, D. Djordjević, M. M. Popović, T. Meyer, M. Luft, and W. D. Kraeft. Determination of electrical conductivity of a plasma on the basis of the coulomb cut-off potential model. *Contrib. Plasma Phys.*, 29(4/5):441-446, 1989.
- [21] Mihajlov, A. A., Dimitrijević, D., Vučić, S., Djordjević, D., Luft, M., Kraeft, D., *Contrib Plasma Phys.* **26** (1986) 19
- [22] Mihajlov, A. A., Dimitrijević, D., Djordjević, D., Luft, M., Kraeft, D., *Contrib Plasma Phys.* **27** (1987) 1
- [23] W. D. Kraeft, M. Luft, and A. A. Mihajlov. Scattering properties and electrical conductivity for the coulomb cut-off potential. *Physica A*, 120:263-278, 1983.
- [24] I. I. Sobel'man *Atomic Spectra and Radiative Transitions*. Springer Verlag, Berlin, 1979.
- [25] Gavrilova, T. V.; Aver'yanov, V. P.; et.al. *Optics and Spectroscopy* **98**, Issue 5, pp/667-674
- [26] Y. Vitel, T. V. Gavrilova, L. G. D'yachkov and Yu.K. Kurilenkov. Spectra of dense pure hydrogen plasma in Balmer area *JQSRT*, 83 (2004): 387..405
- [27] A. A. Mihajlov, Y. Vitel and Lj. M. Ignjatović, The new screening characteristics of strongly non-ideal and dusty plasmas. Part 1: Single-Component Systems, *High Temperature*, 46, No. 6, 737-745, (2008)
- [28] A. A. Mihajlov, Y. Vitel and Lj. M. Ignjatović, The new screening characteristics of strongly non-ideal and dusty plasmas. Part 2: Two-Component Systems, *High Temperature*, 47, No.1, 5-16, (2009)
- [29] V. M. Adamyan, *private communication* 2008.

# The Contribution of the Absorption Processes to the Opacity of DB White Dwarf Atmospheres in UV and VUV Regions

Lj. M. Ignjatović, A. A. Mihajlov, A. Metropoulos, N. M. Sakan, and M. S. Dimitrijević

Citation: **1203**, 121 (2010); doi: 10.1063/1.3322343

View online: <http://dx.doi.org/10.1063/1.3322343>

View Table of Contents: <http://aip.scitation.org/toc/apc/1203/1>

Published by the [American Institute of Physics](#)

---

---



# The Contribution of the Absorption Processes to the Opacity of DB White Dwarf Atmospheres in UV and VUV Regions

Lj. M. Ignjatović<sup>a</sup>, A. A. Mihajlov<sup>a</sup>, A. Metropoulos<sup>b</sup>, N. M. Sakan<sup>a</sup>,  
and M. S. Dimitrijević<sup>c</sup>

<sup>a</sup> Institute of Physics, P. O. Box 57, 11001 Belgrade, Serbia

<sup>b</sup> Theoretical and Physical Chemistry Institute, NHRF, Athens, Greece

<sup>c</sup> Astronomical Observatory, Volgina 7, 11160 Belgrade 74, Serbia

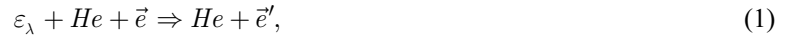
**Abstract.** The main aim of this work is to estimate the total contribution to the opacity of DB white dwarf atmosphere of the processes of the  $He_2^+$  molecular ion photo-dissociation and  $He + He^+$  collisional absorption charge exchange, and compare it with the contribution of  $He^-$ , and other relevant, radiative absorption processes included in standard models.

**Keywords:** atmospheres, radiative transfer, atomic processes, molecular processes.

**PACS:** 97.10.Ex, 95.30.Dr

## INTRODUCTION

Earlier, for the considered DB white dwarf atmospheres ( $T_{eff} = 12000$  K - 14000 K,  $\log g = 7 - 8$ ) as the main source of the continuous absorption was treated the  $He^-$  absorption process



where  $\varepsilon_\lambda$  is the energy of photon with the wavelength  $\lambda$ , and  $\vec{e}$  and  $\vec{e}'$  denotes the free electron before and after the collision with the  $He$  atom. Besides the  $He^-$  absorption process, usually included are the bound - free absorption processes, mentioned by [1] including the other relevant reaction channel



where  $He^*(n, L, S)$  is the helium atom in the excited state,  $n$  - the corresponding principal quantum number,  $L$  and  $S$  - quantum numbers of orbital momentum and spin. Continuous absorption opacity due to the processes of  $He_2^+$  molecular ion photo-dissociation



and  $He + He^+$  collisional absorption charge exchange



where  $He \equiv He(1s^2)$ ,  $He^+ \equiv He^+(1s)$  and  $He_2^+ \equiv He_2^+(X^2\Sigma_u^+)$ , were neglected in DB white dwarf atmosphere modeling up to the beginning of nineties. However, in [2] and [3], using DB white dwarf atmosphere models of [4], it was demonstrated that at least for  $T_{eff} < 16000$  K, these processes should contribute to the opacity in the optical region. In these papers the absorption coefficients for both (3) and (4) processes have been determined within the semiclassical (quasi-static) method developed by [5].

The results from [3], obtained for one Koester model ( $\log g = 8$  and  $T_{eff} = 12000$  K), already enabled a more real picture on the relative importance of  $He^-$  and  $He_2^+$  total absorption processes at least in the region  $\lambda \geq 300$  nm. From these results follows the crossing of the curves for  $He^-$  and  $He_2^+$  absorption coefficients. In the next paper [6] relative importance of  $He_2^+$  and other relevant absorption processes in the region  $\lambda \geq 200$  nm was examined for several Koester's models ( $T_{eff} = 12000$  K, 14000 K, 16000 K,  $\log g = 7, 8$ ; see [4]). It was shown that in all considered cases, the contribution to opacity of the processes of  $He_2^+$  molecular ion photo-dissociation and  $He + He^+$  collisional absorption charge exchange together, is close or at least comparable with the contribution of the  $He^-$  absorption processes (1) and the atomic absorption processes (2).

Here were performed the necessary calculations of absorption coefficients characterizing the processes (3) and (4). The determination of these coefficients was performed by the potential curves of molecular ion  $He_2^+$  in  $X^2\Sigma_u^+$ - and  $A^2\Sigma_g^+$ - states, as well as the corresponding dipole matrix element, which were precisely calculated during this research. These characteristics of  $He_2^+$  are here presented.

In order to determine the relative efficiency of the processes (3) and (4) in UV and VUV regions for particular DB white dwarf atmosphere layers, the corresponding absorption coefficients will be compared with the absorption coefficients which characterize the concurrent processes (1) and (2) for  $51 \text{ nm} \leq \lambda \leq 400 \text{ nm}$ . As the lower boundary of this region was taken  $\lambda = 51 \text{ nm}$  which is close to the  $He$  atom ionization boundary  $\lambda_{He} \cong 50.14 \text{ nm}$ , below which the photo-ionization of the  $He$  atom absolutely dominates in comparison with all other absorption processes.

Besides, here we will consider the hydrogen photo-ionization process



Although accordingly to [4] the ratio of hydrogen and helium abundances in the considered DB white dwarf atmospheres is  $1:10^5$ , our estimations showed that the process (5) could play certain role for  $\lambda < \lambda_H$ , where  $\lambda_H \cong 91.13 \text{ nm}$  is the  $H$  atom ionization boundary.

## CHARACTERISTICS OF PHOTO-DISSOCIATION AND ION-ATOM ABSORPTION PROCESSES

**The photo-dissociation cross-section.** The photo-dissociation process (3) is characterized here by the corresponding average cross-section  $\sigma_{phd}(\lambda, T)$ . This cross-section is defined by

$$\sigma_{phd}(\lambda, T) = \frac{\sum_J \sum_v g_{v,J} \cdot (2J+1) e^{-\frac{E_{v,J}}{kT}} \cdot \sigma_{v,J}(\lambda)}{\sum_J \sum_v g_{v,J} \cdot (2J+1) e^{-\frac{E_{v,J}}{kT}}}, \quad (6)$$

where  $v$  and  $J$  are the vibrational and rotational quantum numbers of the individual rovibrational states ( $v, J$ ) of the molecular ion  $He_2^+(X^2\Sigma_u^+)$ ,  $\sigma_{v,J}(\lambda)$  - the partial photo-dissociation cross-sections of these states,  $E_{v,J}$  and  $g_{v,J} \cdot (2J+1)$  - the corresponding energies with respect to the ground rovibrational state and statistical weights, while factor  $g_{v,J}$  describes the influence of the nuclear spin. Since for DB white dwarf atmospheres the temperatures  $T \geq 8000$  K are relevant, in further considerations we will take that  $g_{v,J} = 1$ .

Within the dipole approximation the partial cross-sections  $\sigma_{v,J}(\lambda)$  are given by the expressions

$$\sigma_{v,J}(\lambda) = \frac{8\pi^3}{3\lambda} \left[ \frac{J+1}{2J+1} |D_{E,J+1;v,J}|^2 + \frac{J}{2J+1} |D_{E,J-1;v,J}|^2 \right], \quad (7)$$

where  $D_{E,J+1;v,J}$  and  $D_{E,J-1;v,J}$  are the radial matrix elements given by the relations

$$D_{E,J;v,J'} = \langle \Psi_{2,E,J'}(R) | D_{12}(R) | \Psi_{1;v,J}(R) \rangle, \quad J = J' \pm 1, \quad (8)$$

$$D_{12}(R) = | \mathbf{D}_{12}(R) |, \quad \mathbf{D}_{12}(R) = \langle 1 | \mathbf{D}(R) | 2 \rangle, \quad (9)$$

where  $R$  is the internuclear distance,  $\mathbf{D}(R)$  - the operator of electron dipole momentum, and  $|1\rangle \equiv X^2\Sigma_u^+$  and  $|2\rangle \equiv A^2\Sigma_g^+$  - the ground and the first excited electronic states of the molecular ion  $He_2^+$  with the potential curves  $U_1(R)$  and  $U_2(R)$ , respectively. With  $\Psi_{1;v,J}(R)$  and  $\Psi_{2;E,J'}(R)$  are denoted the adiabatic nuclear radial wave functions of the bound state  $(v, J)$  in the potential  $U_1(R)$  and the continual state  $(E, J')$  in the potential  $U_2(R)$  respectively, with  $E = E_{v,J} + \varepsilon_\lambda$ . It is assumed that the wave functions  $\Psi_{1;v,J}(R)$  and  $\Psi_{2;E,J'}(R)$  satisfy the standard ortho-normalization conditions.

The calculations of the potential energies  $U_1(R)$  and  $U_2(R)$  and the matrix element  $D_{12}(R)$  were performed under  $D_{2h}$  symmetry using the MOLPRO package of programs [7]. They were performed at the multi-reference configuration interaction (MRCI) level using multi-configuration self-consistent field (MCSCF) orbitals with the cc-pv5z basis set of [8] and [9]. We started at the self-consistent field (SCF) level with the ground state electron configuration  $a_g^2 b_{1u}^1$ . The active space at the MCSCF step contained  $3a_g$  and  $3b_{1u}$  orbitals without any closed or core orbitals (all three electrons were involved). Obtained potential curves  $U_1(R)$  and  $U_2(R)$  are presented in Fig. 1a, and dipole matrix element  $D_{12}(R)$  - in Fig. 1b.

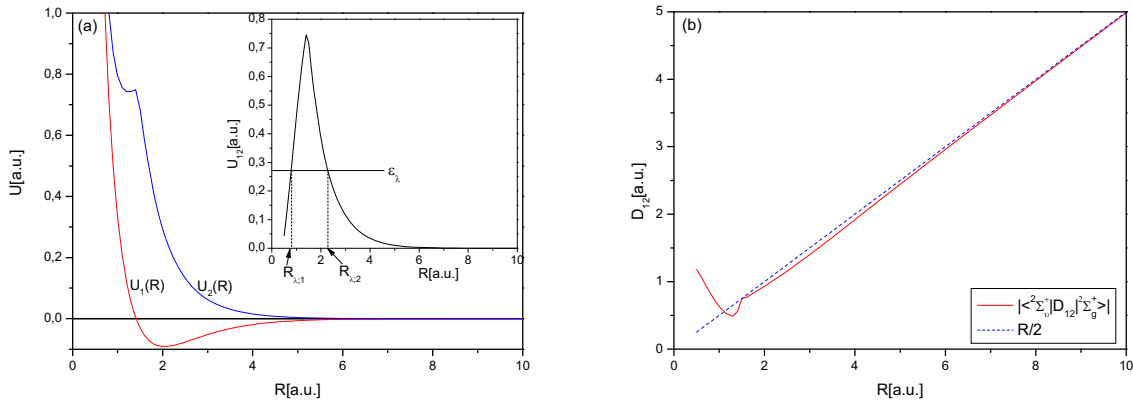


FIGURE 1. (a) The potential curves of the molecular ion  $He_2^+$ :  $U_1(R)$  ( $X^2\Sigma_u^+$ ), and  $U_2(R)$  ( $A^2\Sigma_g^+$ );  $U_{12}(R) = U_2(R) - U_1(R)$ ;  $R_{\lambda;1}$  and  $R_{\lambda;2}$  - two real roots of the equation  $U_{12}(R) = \varepsilon_\lambda$ ; (b) The matrix element  $D_{12}(R)$  for the transition between the electronic states  $X^2\Sigma_u^+$  and  $A^2\Sigma_g^+$  of the ion  $He_2^+$ .

**The partial absorption coefficients.** The efficiencies of the photo-dissociation process (3) and of the charge-exchange absorption process (4) are characterized separately by the partial spectral absorption coefficients  $\kappa_{ia}^{(a)}(\lambda) \equiv \kappa_{ia}^{(a)}(\lambda; T, N(He_2^+)) = \sigma_{phd}(\lambda, T)N(He_2^+)$  and  $\kappa_{ia}^{(b)}(\lambda) \equiv \kappa_{ia}^{(b)}(\lambda; T, N(He), N(He^+))$  where  $T$ ,  $N(He_2^+)$ ,  $N(He)$  and  $N(He^+)$  are the local temperature and the densities of  $He_2^+$  ( $X^2\Sigma_u^+$ ),  $He$  and  $He^+$  in the considered layer of the DB white dwarf atmosphere. Following our previous paper [10] and assuming the existence of LTE, we will take the photo-dissociation coefficient  $\kappa_{ia}^{(a)}(\lambda)$  in an equivalent form suitable for further considerations, namely

$$\kappa_{ia}^{(a)}(\lambda) = K_{ia}^{(a)}(\lambda, T)N(He)N(He^+), \quad (10)$$

$$K_{ia}^{(a)}(\lambda, T) = \sigma_{phd}(\lambda, T) \cdot \chi_{ia}(T); \quad \chi_{ia}(T) = \frac{N(He_2^+)}{N(He)N(He^+)}. \quad (11)$$

Here the photo-dissociation cross-section  $\sigma_{phd}(\lambda, T)$  is given by Eqs. (6)-(7), and the quantity  $\chi_{ia}$ , which contains the density  $N(He_2^+)$ , is determined from the law of mass action

$$\chi^{-1}(T) = \left( \frac{\mu k T}{2\pi \hbar^2} \right)^{\frac{3}{2}} \cdot \frac{g(He)g(H^+)}{\sum_J \sum_v g_{v,J} \cdot (2J+1)e^{-\frac{E_{v,J}}{kT}}} \cdot \exp\left(-\frac{D}{kT}\right), \quad (12)$$

where  $\mu$  and  $D$  are the reduced mass and the dissociation energy of the molecular ion  $He_2^+$ , and  $g(He) = 1$  and  $g(He^+) = 2$  - the statistical weights of the atom  $He$  and ion  $He^+$ . The charge-exchange absorption coefficient  $\kappa_{ia}^{(b)}(\lambda)$  is defined by

$$\kappa_{ia}^{(b)}(\lambda) = K_{ia}^{(b)}(\lambda, T)N(He)N(He^+), \quad (13)$$

where the coefficient  $K_{ia}^{(b)}(\lambda, T)$  is determined here by the semi-classical method developed in [5] on the basis of the quasi-static approximation [3,6,10]. Within this method, only the  $\lambda$  region where the equation

$$U_{12}(R) \equiv U_2(R) - U_1(R) = \varepsilon_\lambda \quad (14)$$

has real roots is considered. Consequently, in the helium case the quasi-static method is applicable in the region  $\lambda \geq 62$  nm where this equation has two real roots (see Fig. 1a),  $R_{\lambda;1}$  and  $R_{\lambda;2} > R_{\lambda;1}$ . In [6], where optical region of  $\lambda$  was treated, only the larger of these roots has been taken into account. However, in far UV and VUV regions both roots should be taken into account. Consequently, we will take here  $K_{ia}^{(b)}(\lambda, T)$  in the form

$$K_{ia}^{(b)}(\lambda, T) = 0.62 \cdot 10^{-42} \sum_{i=1}^2 \frac{\left[ \frac{2D_{\lambda;2}(R_{\lambda;i})}{eR_{\lambda;i}} \right]^2}{\gamma(R_{\lambda;i})} \left( \frac{R_{\lambda;i}}{a_0} \right)^4 \exp \left[ -\frac{U_1(R_{\lambda;i})}{kT} \right] \cdot \xi(R_{\lambda;i}) \quad (15)$$

$$\gamma(R_{\lambda;i}) = \left| \frac{d \ln \left[ \frac{U_{12}(R)}{2R_{\lambda;i}} \right]}{d(R/a_0)} \right|_{R=R_{\lambda;i}}, \quad \xi(R_{\lambda;i}) = \begin{cases} 1, & U_1(R_{\lambda;i}) \geq 0, \\ \frac{\Gamma\left(\frac{3}{2}; -\frac{U_1(R_{\lambda;i})}{kT}\right)}{\Gamma\left(\frac{3}{2}\right)}, & U_1(R_{\lambda;i}) < 0, \end{cases} \quad (16)$$

where  $e$  and  $a_0$  are the electron charge and the atomic unit of length, and  $K_{ia}^{(b)}(\lambda, T)$  is expressed in [ $\text{cm}^5$ ].

**The total absorption coefficient.** The efficiency of absorption processes (3) and (4) together is characterized by the total spectral absorption coefficient  $\kappa_{ia}(\lambda) \equiv \kappa_{ia}(\lambda; T, N(He), N(He^+))$  given by:  $\kappa_{ia}(\lambda) = \kappa_{ia}^{(a)}(\lambda) + \kappa_{ia}^{(b)}(\lambda)$ . Using Eqs. (10) and (13) for  $\kappa_{ia}^{(a)}(\lambda)$  and  $\kappa_{ia}^{(b)}(\lambda)$  we will take  $\kappa_{ia}(\lambda)$  in the form

$$\kappa_{ia}(\lambda) = K_{ia}(\lambda, T)N(He)N(He^+), \quad K_{ia}(\lambda, T) = K_{ia}^{(a)}(\lambda, T) + K_{ia}^{(b)}(\lambda, T), \quad (17)$$

where  $K_{ia}^{(a)}(\lambda, T)$  is given by Eq. (11), and  $K_{ia}^{(b)}(\lambda, T)$  - by Eq. (15). For the comparison of the efficiency of processes (3) and (4) with the efficiencies of the concurrent processes (1), (2) and (5) just the total absorption coefficients  $\kappa_{ia}(\lambda)$  and  $K_{ia}(\lambda, T)$  are needed.

The efficiency of processes (3) and (4) within DB white dwarf atmosphere is compared here with the efficiency of the concurrent absorption processes (1) and (2), which are characterized by the spectral absorption coefficients  $\kappa_{ea}(\lambda)$  and  $\kappa_{ei}(\lambda)$ , namely

$$\kappa_{ea}(\lambda) = K_{ea}(\lambda, T) \cdot N_e \cdot N(He), \quad \kappa_{ei}(\lambda) = K_{a;ei}(\lambda, T) \cdot N_e \cdot N(He^+), \quad (18)$$

$$K_{a;ei}(\lambda, T) = \sum_{n \geq 2, L, S} \sigma_{nLS}(\lambda) \cdot \chi_{nLS}(T) + K_{ei}(\lambda, T), \quad \chi_{nLS}(T) = \frac{N(He^*(n, L, S))}{N_e N(He^+)}. \quad (19)$$

where  $K_{ea}(\lambda, T)$  and  $K_{ei}(\lambda, T)$  are the rate coefficients which describe absorption by  $(e + He)$ - and  $(e + He^+)$ -collision systems. With  $N_e$  and  $N(He^*(n, L, S))$  are denoted the densities of the free electrons and the excited atoms  $He^*(n, L, S)$ , and with  $\sigma_{nLS}(\lambda)$  - corresponding excited atom photo-ionization cross-section. It was found that in all considered cases the absorption processes (2) play a minor role in comparison with the electron-atom process (1). This is a consequence of the fact that helium plasma in considered layers of DB white dwarf atmosphere is weakly ionized. The relative efficiency of the processes (3) and (4) with respect to processes (1) and (2) together is characterized by the parameter  $F_{He}(\lambda)$  defined by

$$F_{He}(\lambda) = \frac{\kappa_{ia}(\lambda)}{\kappa_{ea}(\lambda) + \kappa_{ei}(\lambda)} = \frac{K_{ia}(\lambda, T)[N(He^+)/N_e]}{K_{ea}(\lambda, T) + K_{ei}(\lambda, T)[N(He^+)/N(He)]}. \quad (20)$$

In calculations of  $F_{He}(\lambda)$  the coefficient  $K_{ea}(\lambda, T)$  was determined by means of the data from [11], and  $K_{a;ei}(\lambda, T)$  - by means of expressions from [12] for the partial photo-ionization cross-section  $\sigma_{nLS}(\lambda)$  and the free-free electron-ion absorption coefficient  $K_{ei}(\lambda, T)$ .

As in [3,6] the parameter  $F_{He}(\lambda)$  is treated as a function of  $\log \tau$ , where  $\tau$  is Rosseland optical depth of the considered atmosphere layer [13]. The values of  $\log \tau$  are taken from [4]. The behavior of  $F_{He}(\lambda; \log \tau)$  is illustrated in Fig. 2, for atmosphere of DB white dwarfs with  $T_{eff} = 12000$  K and  $\log \tau = 8$ . According to the expectations, the relative efficiency of absorption processes (3) and (4) in far UV and VUV regions was increased several times with respect to the optical region. The result is that the processes (3) and (4) in the region  $80 \text{ nm} \leq \lambda \leq 200 \text{ nm}$  dominate in comparison with the concurrent processes (1) and (2) in significant parts of DB white dwarf atmospheres (maximal values of  $F_{He} \approx 2.5$ ).

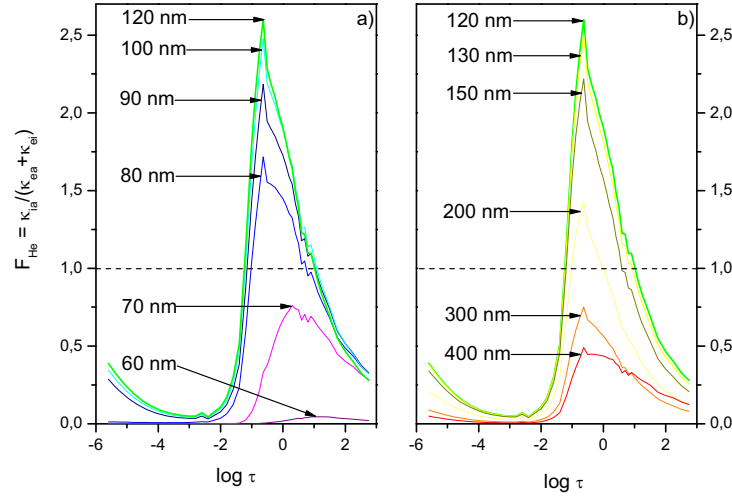


FIGURE 2. The quantity  $F_{He} = \kappa_{ia}/(\kappa_{ea} + \kappa_{ei})$  for DB white dwarf in the case  $\log g = 8$  and  $T_{eff} = 12000$  K.

Apart of that, the efficiency of the absorption processes (3) and (4) in the region  $\lambda_{He} < \lambda \leq \lambda_H$  is compared with the efficiency of the hydrogen photo-ionization process (1), which is characterized by the spectral absorption coefficient  $\kappa_H(\lambda) \equiv \kappa_H(\lambda; N(H))$  defined by  $\kappa_H(\lambda) = \sigma_{phi}(\lambda)N(H)$ , where  $N(H)$  is the local density of atom  $H$ , and  $\sigma_{phi}(\lambda)$  - the corresponding photo-ionization cross-section. Consequently, the relative efficiency of the processes (3) and (4) and (5) for  $\lambda \leq \lambda_H$  can be characterized by the parameter  $F_H(\lambda)$  defined by

$$F_H(\lambda) = \frac{\kappa_{ia}(\lambda)}{\kappa_H(\lambda)} = \frac{K_{ia}(\lambda, T)N(He^+)N(He)}{\sigma_{phi}(\lambda)N(H)}, \quad (21)$$

where the cross-section  $\sigma_{phi}(\lambda)$  is taken from [14]. It was found that the behavior of  $F_H(\lambda)$  in DB white dwarf atmospheres considered in [6] is qualitatively similar. Consequently, the behavior of  $F_H(\lambda)$  is illustrated only by Fig. 3 for the case  $T_{eff} = 12000$  K and  $\log g = 8$ . Namely, for each  $\lambda$  from this region there is a significant part of DB white dwarf atmosphere where the process (5) dominates comparing to the other absorption processes.

\*\*\*

Obtained results give possibility to estimate which absorption processes give the main contribution to the opacity in DB white dwarf atmospheres, in different spectral regions. So, from these results follows that the helium absorption processes (3) and (4) are dominant in the region  $70 \text{ nm} \leq \lambda \leq 200 \text{ nm}$ , while in the region  $\lambda > 200$  nm, the principal role have the  $He^-$  absorption processes (1). However, the absorption processes (3) and (4) deserve to be included not only in codes developed by e.g. [15], but also in other used for DB white dwarf research. Finally, it was shown that in the region  $\lambda_{He} < \lambda < 70 \text{ nm}$ , the hydrogen photo-ionization processes (5) take the dominant role in spite of the fact that the ratio of hydrogen and helium abundances in the considered DB white dwarf atmosphere is  $1 : 10^5$ .

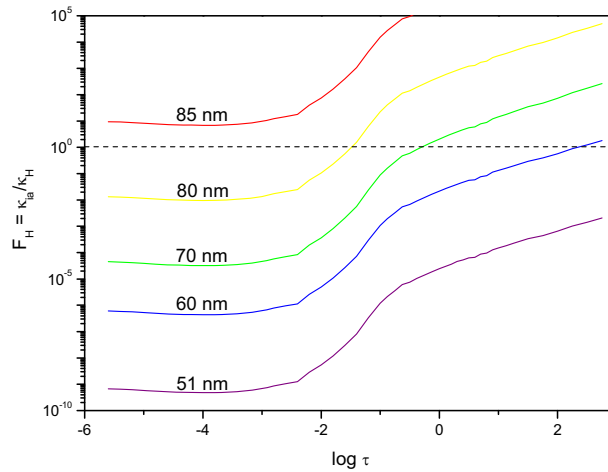


FIGURE 3. The quantity  $F_H = \kappa_{aa}/\kappa_H$  for DB white dwarf in the case  $\log g = 8$  and  $T_{eff} = 12000$  K.

## ACKNOWLEDGMENTS

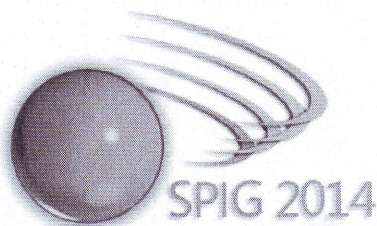
This work was supported by the Ministry of Science and Technological Development of Serbia as a part of the project "Radiation and transport properties of the non-ideal laboratory and ionospheric plasma" (Project number 141033) and "Influence of collisional processes in astrophysical plasma line shapes" (Project number 146001).

## REFERENCES

1. D. Koester, *MemSAIt*, (2008) (in press), arXiv 0812.0482.
2. A. A. Mihajlov and M. S. Dimitrijević, *Astr. Astrophys.* **256**, 305 (1992).
3. A. A. Mihajlov, M. S. Dimitrijević and Lj. M. Ignjatović, *Astr. Astrophys.* **287**, 1026 (1994).
4. D. Koester, *Astr. Astrophys. Suppl. Ser.* **39**, 401 (1980).
5. D. R. Bates, *Mon. Not. Royal Astron. Soc.* **112**, 40 (1952).
6. A. A. Mihajlov, M. S. Dimitrijević, Lj. M. Ignjatović and Z. Djurić, *Astrophys. J.* **454**, 420 (1995).
7. H.-J. Werner, P. J. Knowles., R. Lindh, F. R. Manby, M. Schütz et al., *MOLPRO*, Cardiff, UK (2006).
8. T. H. Dunning, *J. Chem. Phys.* **90**, 1007 (1989).
9. R. A. Kendall, T. H. Dunning and R. J. Harrison, *J. Chem. Phys.* **96**, 6769 (1992).
10. A. A. Mihajlov, Lj. M. Ignjatović, N. M. Sakan and M. S. Dimitrijević, *Astr. Astrophys.* **469**, 749 (2007).
11. W. B. Somerville, *Astrophys. J.* **141**, 811 (1965).
12. I. I. Sobel'man, *Atomic Spectra and Radiative Transitions*. Springer Verlag, Berlin, 1979.
13. D. Mihalas, *Stellar Atmospheres*. W.H. Freeman, San Francisco, 1978.
14. H. Bethe and E. Salpeter, *Quantum mechanics of one and two electron atoms*. Springer Verlag, 1957.
15. P. Bergeron, F. Wesemael and A. Beauchamp, *Publ. Astron. Soc. Pacific*, **107**, 1047 (1995).



K3



# 27<sup>th</sup> Summer School and International Symposium on the Physics of Ionized Gases

August 26-29, 2014, Belgrade, Serbia

## CONTRIBUTED PAPERS

&

ABSTRACTS OF INVITED LECTURES,  
TOPICAL INVITED LECTURES, PROGRESS  
REPORTS AND WORKSHOP LECTURES

Editors:

Dragana Marić

Aleksandar R. Milosavljević

Zoran Mijatović

Institute of Physics, Belgrade  
University of Belgrade



Institute of Physics, Belgrade  
University of Belgrade

Serbian Academy  
of Sciences and Arts



Serbian Academy  
of Sciences and Arts



**27<sup>th</sup> Summer School and International  
Symposium on the Physics of Ionized  
Gases**

August 26 – 29, 2014, Belgrade, Serbia

*Editors:*

Dragana Marić, Aleksandar R. Milosavljević and Zoran Mijatović

**SPIG 2014**

*Publishers:*

Institute of Physics, Belgrade  
Preobrazića 12, IV sprat  
11000 Belgrade, Serbia

**CONTRIBUTED PAPERS**

&

*Computer program:*

ABSTRACTS OF INVITED LECTURES,  
TOPICAL INVITED LECTURES, PROGRESS REPORTS  
AND WORKSHOP LECTURES

*Printed by:*

CICERO  
Belgrade

*Editors*

Dragana Marić, Aleksandar R. Milosavljević and  
Zoran Mijatović

*Number of copies:*

300

ISBN 978-86-7762-600-6

Institute of Physics, Belgrade  
University of Belgrade

Serbian Academy  
of Sciences and Art

All rights reserved. No part of this book may be reproduced, stored or transmitted in any manner without the written permission of the Publisher.

Belgrade, 2014



CONTRIBUTED PAPERS & ABSTRACTS OF INVITED  
LECTURES, TOPICAL INVITED LECTURES, PROGRESS  
REPORTS AND WORKSHOP LECTURES  
of the 27<sup>th</sup> Summer School and International Symposium on  
the Physics of Ionized Gases

August 26 – 29, 2014, Belgrade, Serbia

*Editors:*

Dragana Marić, Aleksandar R. Milosavljević and Zoran Mijatović

*Publishers:*

Institute of Physics, Belgrade  
Pregrevica 118, P. O. Box 68  
11080 Belgrade, Serbia

Klett izdavačka kuća d.o.o.  
Maršala Birjuzova 3-5, IV sprat  
11000 Belgrade

*Computer processing:*

Sanja D. Tošić, Nikola Škoro and Miloš Ranković

*Printed by*

**CICERO**  
Belgrade

*Number of copies*

300

ISBN 978-86-7762-600-6

©2014 by the Institute of Physics, Belgrade, Serbia and Klett izdavačka kuća d.o.o. All rights reserved. No part of this book may be reproduced, stored or transmitted in any manner without the written permission of the Publisher.



## INVERSE BREMSSTRAHLUNG ABSORPTION COEFFICIENTS FOR DENSE HYDROGEN PLASMA IN CUT-OFF COULOMB POTENTIAL MODEL

N. M. Sakan<sup>1</sup>, A. A. Mihajlov<sup>1</sup> and V. A. Srećković<sup>1</sup>

<sup>1</sup> *Institute of Physics, University of Belgrade,  
Pregrevica 118, Zemun, 11080 Belgrade, Serbia*

**Abstract.** The inverse Bremsstrahlung process play important role in modeling of continuous electromagnetic absorption in plasmas and as such should be investigated with more details. Here it is shown that this process can be successfully described in the frames of cut-off Coulomb potential model within the broad area of electron concentrations and temperatures. The corresponding quantum mechanical method of determination of the spectral coefficient for the considered processes is presented. The results discussed here are for the plasma with electron densities  $N_e \sim 10^{19} \text{cm}^{-3}$  and temperatures  $T \approx 2 \cdot 10^4 \text{K}$ . The calculation method is applied to wavelength region  $200 \text{nm} < \lambda < 500 \text{nm}$ . The presented results can be of interest for dense laboratory plasmas as well as for partially ionized layers of different stellar atmospheres.

### 1. INTRODUCTION

Recently, in [1] it was shown that so-called cut-off Coulomb potential could be successfully applied in the case of dense highly ionized plasmas for the description not only transport processes (see [2]) but also the relevant photo-ionization processes. Here we keep in mind the model potential which is described by the relations

$$U_{cut}(r) = \begin{cases} -\frac{e^2}{r} + \frac{e^2}{r_c} & : 0 < r \leq r_c \\ 0 & : r_c < r \end{cases} \quad (1)$$

where  $r_c$  is the cut-off radius, and  $-e^2/r_c$  - the average potential energy of the electron in the considered plasma. Let us note that such potential was introduced in the considerations in [3] investigated in detail in [4]. Here we will show that in case of highly ionized non-ideal plasmas this potential could be successfully applied also for determination of spectral coefficients for the electron-ion inverse Bremsstrahlung processes.



## 2. THEORY

Since the cut-off Coulomb potential has radial symmetry, the adequate wave functions of the free electron could be taken in form  $\Psi(r, \theta, \varphi) = (P_{nl}(r)/r) \cdot Y_{lm}(\theta, \varphi)$ , where  $P(r)$  is the solutions of the radial Schroedinger equation

$$\frac{d^2 P(r)}{dr^2} + \left[ \frac{2m}{\hbar^2} (E - U(r)) - \frac{l(l+1)}{r^2} \right] P(r) = 0. \quad (2)$$

Accordingly to [5] the cross section for the inverse Bremsstrahlung process is given by the relations

$$\sigma(E; E') = \frac{8\pi^4 \hbar e^2 k}{3 q^2} \sum_{l'=l\pm 1}^{l_{max}} |\hat{D}_{E,l;E'l'}|^2, \quad \hat{D}_{E,l;E'l'} = \int_0^\infty P_{E'l'} \cdot r \cdot P_{El} dr. \quad (3)$$

Because of the well known properties of the free electron wave functions the direct calculation of the dipole matrix element  $\hat{D}$  is very difficult and in practice, all until now, cross section was calculated with the help of approximate formulas (see e.g. [5]) based on the model of binary electron-ion interaction in the absence of any external perturbers. Because of that such approximations are valid only in cases of electron-ion plasmas that could be treated practically as ideal ones. Non-ideal plasmas were also discussed in literature (see e.g. [6], [7]), but only with the help of partial, and also approximative expressions. On the other hand, cut-off Coulomb potential model gives the possibility of direct determination of the cross section for the inverse Bremsstrahlung process without any additional approximations. Namely in the frames of presented model, with that purpose in mind, it is simple change from the dipole matrix element in Eq. 3 to the gradient of the potential energy ([5]) given by

$$|\hat{D}(r)_{ab}|^2 = \frac{\hbar^4}{m^2 (E_a - E_b)^4} |\nabla U_{ab}|^2, \quad (4)$$

$$\nabla_r U_{ab} = \int_0^{r_{cut}} P_b(r) \cdot \nabla_r U(r) \cdot P_a(r) dr. \quad (5)$$

The given method enabled the fast and reliable calculation of the discussed cross section and, consequentially, the corresponding spectral absorption coefficient which is given by

$$\kappa_{ff}(\varepsilon_\lambda; N_e, T) = N_i N_e \int_0^\infty \sigma(E; E') v f_T(v) dv \left( 1 - \exp \left[ -\frac{\hbar\omega}{kT} \right] \right), \quad (6)$$

where  $N_i$  and  $N_e$  are the ion and free electron densities, and  $f_T(v)$  - the Maxwell distribution (over electron speeds) with given temperature  $T$ .



It is obvious that this model could be used even in case  $r_{coul} \rightarrow \infty$ , i.e. in case of the Coulomb potential.

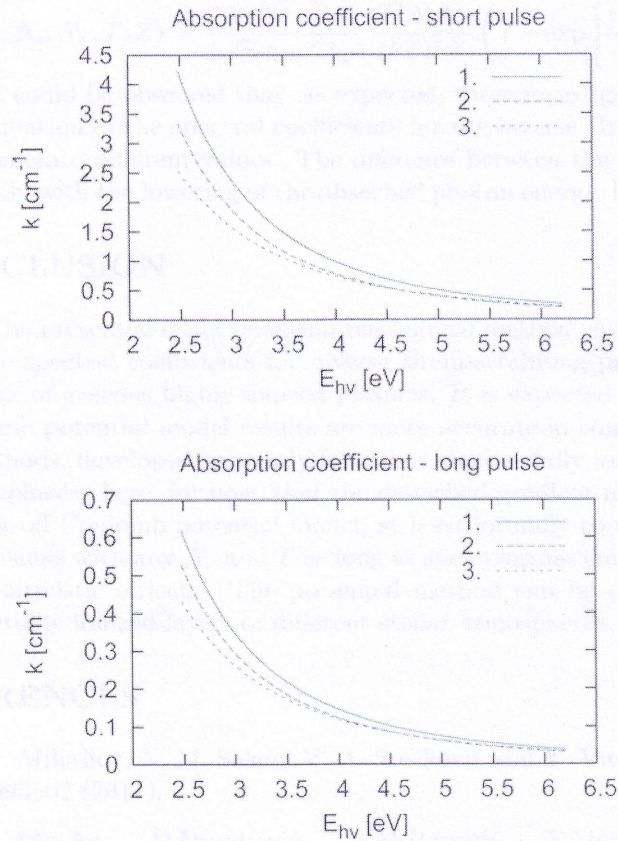


**Figure 1.** Absorption coefficient for the inverse Bremsstrahlung, **1.** - the gradient method - Coulomb potential, **2.** - the gradient method - cut-off Coulomb potential, **3.** - formula (7) from [5]. The presented data are calculated for the short and long pulse from [8].

### 3. RESULTS AND DISCUSSION

Here the described gradient method is applied for determination of the spectral coefficients for the inverse Bremsstrahlung process in two cases of non-ideal highly ionized hydrogen plasma [8] ( $N_e = 1.8 \cdot 10^{19} \text{cm}^{-3}$ ,  $T = 23650 \text{K}$  - short and  $N_e = 6.5 \cdot 10^{18} \text{cm}^{-3}$ ,  $T = 17960 \text{K}$  - long pulse) and considered later in [1]) in relation with photo-ionization processes. The results are presented on the Fig. 1. On this figures are presented also the



calculations of the same coefficients with the help of approximate expression from [5], namely

$$\kappa_{ff}^{Sob}(\varepsilon\lambda; N_i, N_e, T, Z) = \frac{16\pi^{5/2}\sqrt{2}e^6}{3\sqrt{3}chm^{3/2}\omega^3} \frac{Z^2 N_i N_e}{(kT)^{1/2}} \left(1 - \exp\left[-\frac{h\omega}{kT}\right]\right). \quad (7)$$

It could be observed that, as expected, three investigated methods of determination of the spectral coefficients for the inverse Bremsstrahlung process generate different values. The difference between the results grows significantly with the lowering of the absorbed photon energy, less than 4eV.

#### 4. CONCLUSION

The presented exact quantum mechanical method could be used to obtain the spectral coefficients for inverse Bremsstrahlung process for the broad class of gaseous highly ionized plasmas. It is expected that the cut-off Coulomb potential model results are more accurate in comparison with other methods, developed primarily for either ideal or fully ionized plasma. Let us emphasize here, for now, that the described gradient method, based on the cut-off Coulomb potential model, at least formally could be applied on the plasmas with any  $N_e$  and  $T$  as long as such plasmas could be treated as non-relativistic objects. The presented method can be of interest for dense partially ionized layers of different stellar atmospheres.

#### REFERENCES

- [1] A. A. Mihajlov, N. M. Sakan, V. A. Srećković and Y. Vitel, *J. Phys. A* 44, 095502 (2011).
- [2] A.A.Mihajlov, D.Djordjević, M.M.Popović, T.Meyer, M.Luft, W.D.Kraeft, *Contrib.Plas.Phys.* vol.29, no.415, p.441-446 (1989).
- [3] K. Suchy, *Beitr. Plasmaphys.* 4, 71 (1964).
- [4] A.A.Mihajlov, D.Djordjević, S.Vučić, W.D.Kraeft, M.Luft, *Contrib. Plasma Phys.* vol.26, no.1, p.19-35 (1986).
- [5] I. I. Sobel'man, *Atomic Spectra and Radiative Transitions*, Springer Verlag, Berlin, 1979.
- [6] V. E. Fortov, I. T. Iakubov, *Physics of Nonideal Plasma*, Hemisphere, New York, 1989.
- [7] G. Kobzev, I. Jakubov, M. Popovich (Eds.), *Transport and Optical Properties of Non-Ideal Plasmas*, Plen.Press, New York, London, 1995.
- [8] Y. Vitel, T. V. Gavrilova, L. G. D'yachkov, Y. Kurilenkov, *JQSRT* 83 387-405 (2004).



6<sup>th</sup> INTERNATIONAL SCIENTIFIC CONFERENCE

# OTEH 2014

ON DEFENSIVE TECHNOLOGIES



## PROCEEDINGS

Belgrade, 09 – 10 October 2014



**Publisher**

**The Military Technical Institute**  
Ratka Resanovića 1, 11030 Belgrade

**Publisher's Representative**

Doc. Col **Zoran Rajić**, PhD (Eng)

**Editor**

**Zoran Anastasijević**, PhD (Eng)

**Technical Editing**

Dragan Knežević  
Liljana Kojičin

**Graphic Editing**

Milica Dimitrijevic

Printing

300 copies

CIP - Каталогизacija u publikaciji  
Narodna biblioteka Srbije, Beograd

623.4/.7(082)(0.034.2)  
66.017/.018:623(082)(0.034.2)

INTERNATIONAL Scientific Conference on  
Defensive Technologies (6th ; 2014 ; Beograd)  
Proceedings [Elektronski izvor] / 6th  
International Scientific Conference on  
Defensive Technologies, OTEH 2014, Belgrade,  
09-10 October 2014 ; organized by Military  
Technical Institute, Belgrade ; [editor Zoran  
Anastasijević]. - Belgrade : The Military  
Technical Institute, 2014 (Beograd : The  
Military Technical Institute). - 1  
elektronski optički disk (CD-ROM) ; 12 cm

Sistemska zahteva: Nisu navedeni. - Nasl. sa  
naslovne strane dokumenta. - Tiraž 300. -  
Bibliografija uz svaki rad.

ISBN 978-86-81123-71-3

1. The Military Technical Institut  
(Belgrade)

a) Војна техника - Зборници b) Технички  
материјали - Зборници

COBISS.SR-ID 210344204



# 6<sup>th</sup> INTERNATIONAL SCIENTIFIC CONFERENCE

## ON DEFENSIVE TECHNOLOGIES



SUPPORTED BY

**Ministry of Defence**

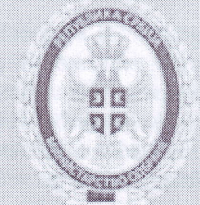
[www.mod.gov.rs](http://www.mod.gov.rs)



Organized by  
**MILITARY TECHNICAL INSTITUTE**  
1 Ratka Resanovića St., Belgrade 11000, SERBIA

[www.vti.mod.gov.rs](http://www.vti.mod.gov.rs)





## TEST SIMULATOR FOR THE DISCRETE MULTI-PARAMETRIC DECISION FLIGHT SYSTEM

STOJAN MARKOVIĆ

University of defense, Military academy, Belgrade, Serbia, [stmarkovic@yahoo.com](mailto:stmarkovic@yahoo.com)

MOMČILO MILINOVIĆ

Faculty of Mechanical Engineering, University of Belgrade, Serbia, [mmilinovic@mas.bg.ac.rs](mailto:mmilinovic@mas.bg.ac.rs)

NENAD SAKAN

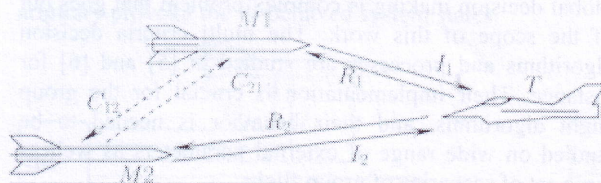
Institute of Physics, University of Belgrade, Serbia, [nsakan@ipb.ac.rs](mailto:nsakan@ipb.ac.rs)

**Abstract:** The system concept, decision making mathematical model and top level algorithm for multi-parametric singular system for the missile control and guidance is presented. As a part of the research, a software top level algorithm is yielded and experimentally tested and proven by the means of the hardware test system. The systems runs multi-parametric criteria decision functionality simultaneously and sequentially, on each of the flight and ground based objects, coupled by singular decision functions. The studied system present the set of controlled objects interconnected in the system capable of adopting to the external stimuli as well as internal conditions changes. Such simulation hardware serves as operational test of concept for the mentioned adoptable system of controlled coupled objects, interconnected in the decision making process in the simulation of real flight conditions as an add-on hardware to the real missile. The studied mathematical relations that provided model for the decision making process in the operational algorithms are visualized in the experiments, and a set of parameters of the well behaved model is presented.

**Keywords:** missile guidance, control system synthesis, decentralized control, decision making, singular system.

### 1. INTRODUCTION

Behavior of the interconnected groups of missiles and the analysis of the flight paths of missile group are opened problem with work in progress, see [1] and [2]. Although this subject is not published extensively this does not reflect the work that is actively going on in several technological advanced countries.



Picture 1: System concept

The goal of the work presented in this manuscript was to present the results of hardware co-simulation of the system of interconnected missiles in the real flight conditions, and by the means of such simulation to measure time constrains of missiles, as well as to yield a group decision making algorithm. Taking this on mind, the minimum set of two missiles is studied. This decision does not affect neither the top level algorithm of the system nor the test procedure. The analyzed interconnected system consists of two missiles, M1 and

M2, shown in picture 1, with data exchange communication channels  $C_{12}$  ad  $C_{21}$ .

By the usage of data exchange channels the data for the decision making as well as requests and commands are transferred between missile group. In such way two individual flight systems becomes a subsets of the newly developed system, e.g. they are treated as a subsystems of such set. Initial and final phase of the group of flight vehicles under control is behind the scope of this work.

The studied system consists of two subsystems, e.g. missiles M1 and M2. They react on external stimuli parameters, as well as commands transferred between M1 and M2. Their reaction is not known in detail, so the test procedure for the closed system as a black box is needed, the method for the analysis of such systems is described in detail in [3]. As a main stimuli parameter of the subsystem the reflected signals from the target T,  $R_1$  and  $R_2$  are simulated, and studied on the real system. Other parameters are not shown on figure for the simplicity of discussion. The algorithm of the system behavior is based onto the role change between subsystems. The two roles of each missile are leader and leaded one. Only one of the subsystems could be the leader at a time, and as such could command to the rest of the group members its role and request for their data also. During free flight phase the role exchange between subset members occurs. Action



taking place of each subsystem could be illumination of the target, presented in picture 1 as  $I_1$  and  $I_2$ , request for the change of role to the group leader, as well as data and request exchange between group members and command from the leader to the rest of the group. The leader missile illuminates the target and commands rest of group about their role change. All the missiles follow the reflected signal from the target and fly towards the predicted space point. The follower missile sends regular data packets with its intrinsic state to the leader, as well as possible request to the leader for the role change. The internal time constrains of each of the group members plays an important role in algorithm optimization.

In order of analyzing of real subsystem reactions on external stimuli parameters as well as internal time constraints of the subsystem the hardware co-simulation was constructed. Based on this the external hardware was capable of state visualization as well as limited possibility to change the external stimuli. It was adapted to the missile to visualize and stimulate the missile pair, and to test the system level algorithm.

The natural splitting of the decision process into three layer scheme is made. The stimulus, as a first, the decision making and data exchange as a second one and a reaction layer as a third one. In the order of analysis the first one is controlled, while the reaction of the subsystem is measurable from the intrinsic parameters as well as third, reaction layer. Some of the reaction layer states also reflect on the first layer as stimuli. The second, decision and data exchange, layer is studied in order to determine the best system algorithm as well as subsystems reaction and behavior in group conditions.

## 2. BASICS OF THE MATHEMATICAL MODEL

In order of explaining of the hardware co-simulation model only the basics of the used mathematical model is presented.

The analyzed system, consist of two missiles M1 and M2, that could take the role of leader or follower each, and change their role accordingly. Their reaction on the set of external stimuli, denoted here as  $x^1_1, \dots, x^1_N$  for M1 and  $x^2_1, \dots, x^2_N$  for M2, is studied. Based on this the reaction of the system occurs as a change of the internal system states  $i^1_1, \dots, i^1_M$  and  $i^2_1, \dots, i^2_M$ , as well as external states  $e^1_1, \dots, e^1_P$  and  $e^2_1, \dots, e^2_P$  for the M1 and M2 respectively.

Decision making algorithm, in general presents a multi criteria decision process, see [4]. The intrinsic parameters are yielded by the first decision making process,

$$D_1: \begin{cases} i^1_1 = \varphi_1(x^1_1, x^1_2, \dots, x^1_N, i^1_1, i^1_2, \dots, i^1_M) \\ \dots \\ i^1_G = \varphi_G(x^1_1, x^1_2, \dots, x^1_N, i^1_1, i^1_2, \dots, i^1_M) \end{cases} \quad (1)$$

Where  $\varphi_i$  is the  $i$ -th internal parameter decision function. The parameters  $i^j_k$  present the intrinsic parameters from the previous decision step, while index  $j$  covers all  $G$

members of the group. The intrinsic parameters are evaluated and compared to some base values and as a result a set of singular functions are led to digital logic that makes decisions based on their values.

The leader on the other hand, besides the intrinsic decision process has possibility to make a global decision concerning behavior of the system as a whole.

$$\Delta: \begin{cases} q_1 = \xi_1(i^1_1, i^1_2, \dots, i^1_G, i^2_1, i^2_2, \dots, i^2_G) \\ \dots \\ q_G = \xi_G(i^1_1, i^1_2, \dots, i^1_G, i^2_1, i^2_2, \dots, i^2_G) \end{cases} \quad (2)$$

Where  $\xi_i$  is the  $i$ -th internal parameter decision function. Each decision value of the decision process  $\Delta$  is a function of all intrinsic parameters of the entire group, e.g. for the group members 1 to  $G$ . Similarly parameters  $q$  are evaluated and compared to some base values and as a result a set of singular functions are led to digital logic that makes decisions based on their values. This decision has global effect on group as a system.

In studied case both decision processes (1) and (2) are implemented on each group member, and decision on activity of process (2) is the decision of the group member role, e.g. a leader or a follower missile.

Leader has decision making role, where it commands the states of the other members of the group based on its estimate. On the other hand all other group members have only possibility to obey commands from leader or to send a request for state change. Final decision on state change moment and selection of the next leader from the group members is based onto the entire parameter set analysis on the leader missile hardware. So the leader has several decision making processes, its intrinsic one and comparison of results of all group members, including itself, and adequate decision making on all group member states.

The behavior changing then influences only on possibility to decide on the basis of all group member states. Follower could request reevaluation of its role based on estimate of its state. The comparison of the states of subsystem as well as of entire system as a process of global decision making is complex problem that goes out of the scope of this work. The multi criteria decision algorithms and processes are studied in [5] and [6] for instance. Their implementation is crucial for the group flight algorithms, and their behavior is needed to be studied on wide range of external parameters as well as large set of scenarios of group flight.

## 3. RESULTS

The test results of the real missile system, consists of two missiles, are presented. The measurements were made with the help of micro controller unit that has role of visualization of states of missile as well as control of some of external parameters. Such measurements enabled the estimate of the time constrains, that the well behaved system should respect in order of maintain the control over each group member. The time diagram of such system is presented in picture 2.



ISSN 1986-8588

# SVAROG

NAUČNO-STRUČNI ČASOPIS ZA DRUŠTVENE I PRIRODNE NAUKE



**IZAZOVI RAZVOJA DO 2020. GODINE**  
**DEVELOPMENT CHALLENGES TO 2020**

**MEĐUNARODNA NAUČNA KONFERENCIJA**

- Tematski broj -

**nubl**   
NEZAVISNI UNIVERZITET BANJA LUKA  
BROJ 10, MAJ 2015 . GODINA



**IZDAVAČ:**  
Nezavisni univerzitet Banja Luka

**ZA IZDAVAČA:**  
Mr Goran KALINIĆ

**GLAVNI I ODGOVORNI UREDNIK:**  
Prof. dr sci Mliovčan MILUTINOVIĆ

**REDAKCIJA ČASOPISA:**

Prof. dr Žarko PAVIĆ (rektor NUBL); prof. dr Momčilo SAKAN (redovni profesor NUBL); prof. dr Slobodan ZUPLJANIN (prorektor NUBL-a); prof. dr Predrag KOVAČEVIĆ (dekan Pedagoškog fakulteta); doc. dr Vaso ARSENOVIĆ (dekan Ekonomskog fakulteta); prof. dr Mliovčan MILUTINOVIĆ (dekan Fakulteta za političke nauke); prof. mr Stjepko DIVLJAN (akademski slikar i doc. mr Jelena RUBIL (Fakultet liječničkih nauka); prof. dr Milenko KUNDAČINA (redovni profesor, NUBL); prof. dr Novak POPOVIĆ (Institut za političke studije Beograd, Srbija); prof. dr Vujko VUKMIRIĆ, emeritus (profesor ekonomije, Banjaluka); prof. dr Rađe BIOČANIN (redovni profesor ekologije); prof. dr Stjepan VASILJEVIĆ, emeritus (profesor ekonomije Univerzitet Subotica); prof. dr Božidar VELJKOVIĆ (Univerzitet Maribor); doc. dr Mladen MIROSAVLJEVIĆ (BLC Banjaluka); doc. dr Ostoja BARAŠIN (profesor sociologije, NUBL); prof. dr Mladenka BALABAN (profesor Bankarska akademija Beograd); doc. dr Dragan GOLJAN (profesor prava, NUBL); doc. dr Mliovčan MARTIĆ (profesor sociologije NUBL); doc. dr Saša CEKLIJA (profesor NUBL); doc. dr Slobodanka PAVLOVIĆ (dekan Ekološkog fakulteta); mr Ljiljana AULIĆ (viši asistent);

**SAVJET ČASOPISA:**

Akademik ANURS prof. dr Drago BRANKOVIĆ (Univerzitet u Banjoj Luci); akademik SANU prof. dr Jelena GUSKOVA (rukovodilac centra za istraživanje savremene balkanske krize pri Ruskoj akademiji, Rusija); akademik prof. dr Ljubiša S. ADAMOVIĆ (Florida Univerzitet SAD); prof. dr Lidija CEHULIĆ VUKADINOVIĆ (redovni profesor Fakulteta političkih znanosti Zagreb); prof. dr Zoran KALINIĆ, (predsjednik Upravnog odbora, NUBL); prof. Nebojša RADMANOVIĆ (Parlament BiH); prof. dr Đorđe MIKIĆ, emeritus (profesor istorije); prof. dr Bračo KOVAČEVIĆ (Univerzitet u Banjoj Luci); prof. dr Dragan KOKOVIĆ (Univerzitet Novi Sad); prof. dr Besim SPahić, (redovni profesor Univerzitet Sarajevo); akademik SAJIN prof. dr Olena Kovalenko EDUARDIVNA (Univerzitet Kijev, Ukrajina); prof. dr Milan MUALKOVSKI (Univerzitet Beograd); prof. dr Stevo PAŠALIĆ, (redovni profesor Univerzitet Istočno Sarajevo); prof. dr Milan AMBROŽ (Univerzitet Maribor, Slovenija); prof. dr Setedin SEHOVIĆ (Univerzitet Novi Pazar, Srbija); prof. dr Zdravko GLUŠIĆA (redovni profesor NUBL); prof. dr Željko KOVAČEVIĆ (profesor ekonomije); prof. dr Luka TODOROVIĆ (vanredni profesor NUBL); prof. dr Momčilo SAKAN (redovni profesor NUBL); prof. dr Zarko PAVIĆ (redovni profesor, NUBL) i prof. dr Mliovčan MILUTINOVIĆ (glavni i odgovorni urednik).

**ŠTAMPA:**

Grafič – Banja Luka

**ZA ŠTAMPARIJU:**  
Branislav IVANKOVIĆ

**UREDNIŠTVO I ADMINISTRACIJA:**

Veljka Mladenovića 12 E, Banja Luka, Republika Srpska, Bosna i Hercegovina  
Kontakti: telefon: +387 51 456 600, fax +387 51 456 602, e-mail: info@nubl.org  
WEB: www.svarog-nubl.com i www.nubl.org/svarog

**LEKTOR:**

Mr Igor SIMANOVIĆ

**PREVODILAC:**

Mr Čedomir KNEŽEVIĆ

**Tiraž: 400**

Rješenjem Ministarstva prosvjete i kulture Republike Srpske, br. 07.023/612-79/10 od 24.05.2010. godine, časopis je upisan u Registar javnih glasila pod brojem 597.

Radove objavljene u časopisu nije dozvoljeno preštamovati, bilo u cjelini, bilo u dijelovima, bez saglasnosti uredništva. Ocjene iznjete u člancima lični su stavovi autora i ne podliježu nužno mišljenju uredništva. Svi tekstovi u časopisu su recenzirani.



**Nezavisni univerzitet  
Banja Luka**

# S V A R O G

časopis za društvene i  
prirodne nauke

Tematski broj

**IZAZOVI RAZVOJA DO 2020. GODINE**

**DEVELOPMENT CHALLENGES TO 2020**

**ISSN 1986-8588**

**UDK 3+5**

**Br. 10.**

**Maj 2015. godine**



# MEDUNARODNA NAUČNA KONFERENCIJA

## IZAZOVI RAZVOJA DO 2020. GODINE

### ORGANIZACIONI ODBOR

1. Prof. dr Žarko Pavić, NUBL Banja Luka
2. Prof. dr Zoran Kalinić, NUBL Banja Luka
3. Prof. dr Slobodan S. Župljanin, NUBL Banja Luka
4. Prof. dr Milovan Milutinović, NUBL Banja Luka
5. Prof. dr Predrag Kovačević, NUBL Banja Luka
6. Prof. dr Dragomir Keserović, NUBL Banja Luka
7. Doc. dr Slobodanka Pavlović, NUBL Banja Luka
8. Doc. dr Vaso Arsenović, NUBL Banja Luka
9. Doc. dr Mirjana Stojanović – Trivanović, NUBL Banja Luka
10. Doc. dr Saša Čekrijić, NUBL Banja Luka
11. Doc. dr Maja Trifunović, NUBL Banja Luka
12. Mr Ljiljana Aulić, NUBL Banja Luka
13. Goran Kalinić, NUBL Banja Luka

### NAUČNI ODBOR

1. Akademik prof. dr Ljubisa Adamović – državni univerzitet Florida, California
2. Emeritus prof. dr Stevan Vasiljev – NUBL Banja Luka
3. Emeritus prof. dr Momčilo Sakan – NUBL Banja Luka
3. Prof. dr Zoltan Baračkai – Doctus Consulting Hungary, Madarska
4. Prof. dr Jolan Velencei – Budapest University of Tehnology and Economics, Madarska
5. Prof. dr Vujo Vukmirica – Univerzitet u Banjoj Luci
6. Akademik prof. dr Drago Branković – ANURS
7. Akademik prof. dr Jelena Guskova – SANU i ruska akademija nauka, Rusija
8. Akademik prof. dr Olena Kovalenko Eduardivna – SAIIIN, Ukrajina
9. Prof. dr Milian Ambrož – Slovenija
10. Prof. dr Tsvetan Kotcev – Evropski koledž, Sofja, Bugarska
11. Prof. dr Mirko Tripunovski – Univerzitet Union, Skoplje, Makedonija



12. Prof. dr Vladimir Marinković – Narodna skupština Republike Srbije, Srbija
13. Prof. dr Drago Cvijanović – Institut za ekonomiku poljoprivrede, Srbija
14. Prof. dr Ana Vovk Korže – Međunarodni centar za ekoremedijaciju, Slovenija
15. Prof. dr Hasan Hanic – Univerzitet Union, BBA, Beograd
16. Prof. dr Božidar Veljković, Univerzitet u Mariboru, Slovenija
17. Prof. dr Halid Makić, Biotehnički fakultet Univerziteta u Bihacu
18. Prof. dr Husein Muratović, Ekonomski fakultet Univerziteta u Bihacu
19. Prof. dr Milenko Brkić, Univerzitet Hercegovina, Mostar
20. Prof. dr Ibrahim Jusufrić, Internacionalni univerzitet Travnik
21. Prof. dr Nikola Špirić, Univerzitet u Banjoj Luci

## S A D R Ź A J

|  |         |
|--|---------|
| <b>PREDGOVOR</b> .....   | 11-18   |
| <b>Prof. dr Žarko Pavić, prof. dr Zoran Kalinić</b><br>ODRŽIVI RAZVOJ UNIVERZITETA .....   | 19-28   |
| <b>Prof. dr Zoltán Baraaskai, prof. dr Jolán Velencei</b><br>PAMETNI ILI UMI .....   | 29-32   |
| <b>Prof. dr sci Milovan Milutinović</b><br>POLITIČKA STABILNOST BOSNE I HERCEGOVINE<br>PREDUSLOV DRUŠTVENOG RAZVOJA .....  | 33-45   |
| <b>Prof. dr sci Luka V. Todorović</b><br>PODGREVANJE HLADNOG MIRA I GLOBALNA BEZBEDNOST .  | 46-64   |
| <b>Prof. dr Dragan M. Golijan, Radoslav Lavrić, Jelena Golijan</b><br>LTIČAJ LJUDSKIH PRAVA NA DRUŠTVENI RAZVOJ.....   | 65-74   |
| <b>Doc. dr Gordan Radić</b><br>GOSPODARSKA DIPLOMACIJA, DIPLOMACIJA BUDUĆNOSTI....   | 75-81   |
| <b>Dr Jelena Vukočić</b><br>BUDUĆNOST BOSNE I HERCEGOVINE U SVETLU<br>PROMENA NA MEĐUNARODNOJ POLITIČKOJ SCENI .....   | 82-93   |
| <b>Doc. dr sci Zoran Pejić</b><br>SIROMAŠTVO U BOSNI I HERCEGOVINI KAO<br>EKOLOŠKA PRIJETNJA I IZAZOV .....  | 94-103  |
| <b>Prof. dr Simeun D. Vilenđević, Jovo S. Vilenđević</b><br>MATERIJALNO RASLOJAVANJE KAO FAZA RAZVOJA .....  | 104-116 |
| <b>Prof. dr Željko Vojinović, dr Blaženka Pinuković Babicković</b><br>PERSPEKTIVE PENZIONOG SISTEMA KAO IZAZOV<br>STABILNOSTI DRUŠTVENOG I ŽIVOTNOG STANDARDA.....   | 117-127 |
| <b>Doc. dr Mira Ćuk</b><br>SOCIJALNA SIGURNOST KAO IZAZOV I FAKTOR<br>DRUŠTVENOG RAZVOJA U REPUBLICI SRPSKOJ .....   | 128-143 |
| <b>Prof. dr Mladenka Balaban</b><br>PREDUSLOVI ZA EKONOMSKI RAZVOJ SRBIJE .....  | 144-151 |
| <b>Doc. dr Mirjana Stojanović Trivanović, doc. dr Mihajlo Travar,</b><br>doc. dr Dijana Grahovac<br>INOVACIJE I NJIHOV ZNAČAJ ZA KONKURENTSKU POZICIJU U<br>BH PROIZVOĐAČA U USLOVIMA GLOBALNOG TRŽIŠTA..... | 152-163 |
| <b>Prof. dr Slobodan S. Župljanin</b><br>UPRAVLJANJE MALOPRODAJOM U REPUBLICI SRPSKOJ<br>DO 2020. GODINE .....   | 164-179 |
| <b>Doc. dr Vaso Arsenović</b><br>DRUŠTVENO-EKONOMSKI IZAZOVI RAZVOJA PRIMJENOM<br>PREKOGRANIČNIH MERDŽERA I AKVIZICIJA .....   | 180-195 |







1.2. Description of the sampling site and sampling

Cross border pollution indicates a need to determine the pollutants in the water and sediment in all the countries along the river's flow. Because of that, for this sake investigation 35 river sediment samples were taken from the main rivers in Serbia: the Danube (Black Sea watershed), the Sava (Danube watershed), the Tisa (Danube watershed), the Ibar (West Morava watershed), the Great Morava (Danube watershed), the West Morava (Great Morava watershed), the South Morava (Great Morava watershed), the Nišava (South Morava watershed), the Tamiš (Danube watershed), the Porečka River (Danube watershed), the Topčiderska River (Sava watershed), the Pek (Danube watershed) and the Toplica (South Morava watershed). For the larger river sampling was conducted at several locations (Figure 1 and Table 1).

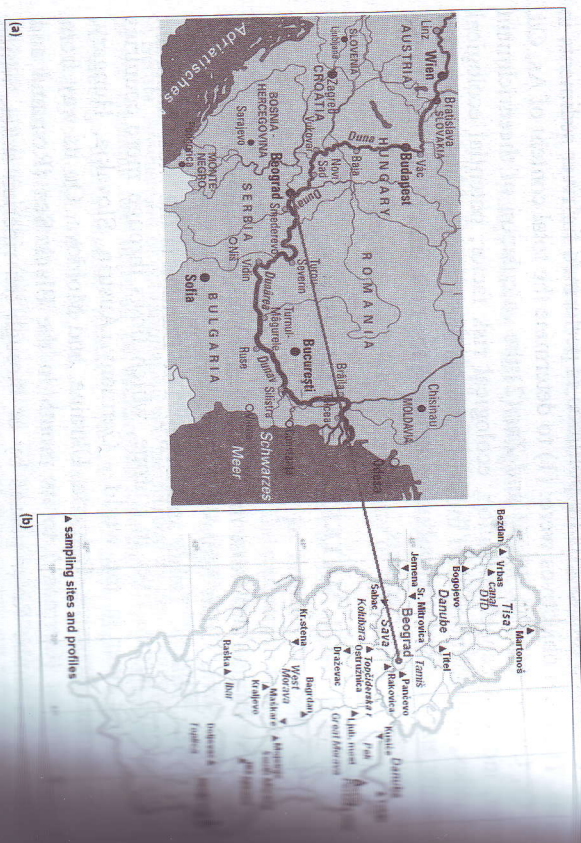


Figure 1 Danube watershed and sampling locations

The sediment samples were stored at 4°C in order to prevent changes in the chemical composition of the sediments. The contents of the macro-elements were determined in the granulometric fraction < 63 µm of bottom sediment samples ("grab" - the sample) after air drying for 4 days.

1.3. Analytical procedures and element analysis

In this paper, the total content of elements in the sediments was determined by digestion with very strong acids: HNO<sub>3</sub>+HCl+HF. After digestion was performed in a pressurised microwave oven (Ethos 1, Advanced Microwave Digestion System, Milestone, Italy) equipped with a 1000 W 10 microwave vessels (PTFE).

Table 1. Sampling locations

| River             | Watershed    | Sampling sites |
|-------------------|--------------|----------------|
| Danube            | Black Sea    | D1-D6          |
| Sava              | Danube       | S1-S4          |
| Tisa              | Danube       | T1-T9          |
| Ibar              | West Morava  | I1, I2         |
| Great Morava      | Danube       | V1, V2         |
| West Morava       | Great Morava | Z1, Z2         |
| South Morava      | Great Morava | JM             |
| Nišava            | South Morava | N1, N2         |
| Tamiš             | Danube       | Ta             |
| DTD canal         | Danube       | DT             |
| Topčiderska River | Sava         | Tr             |
| Porečka River     | Danube       | Pr             |
| Kolubara          | Sava         | Ko             |
| Pek               | Danube       | Pe             |
| Toplica           | South Morava | To             |

In this research, the following elements were determined in each sample: As, Cd, Co, Cr, Cu, Fe, Mn, Ni, Pb, V and Zn. The obtained results in this manuscript are expressed in mg kg<sup>-1</sup> dry sediment. The analytical procedure of the studied elements was realised with an atomic emission spectrometer with an inductively coupled plasma ICP-AES Duo (ThermoFisher, United Kingdom).

1.4. Assessment of sediment contamination

Various calculation methods for quantifying the degree of metal contamination in sediments have been put forward. In this paper, different indices were used to assess the degree of trace element contamination in river sediments in Serbia: Enrichment factor (EF), Index of geoaccumulation (Igeo), Potential risk factor (Er<sup>1</sup>), Potential ecological risk index (RI), and Pollution Index (PI<sub>1</sub>).

**Enrichment factor (EF):** A common approach to estimate how much contamination is impacted (naturally and anthropogenically) with heavy metal is to use the Enrichment Factor (EF) for metal concentrations above the unimpacted background levels. The EF of a heavy metal in sediment can be calculated using the following formula:

$$EF = (M_i)_{sample} / (M_i)_{background}$$



Y is the concentration of the proxy element. Although EF is not a function of time in its mathematical expression, it reflects the status and degree of sediment pollution.<sup>7</sup>

**Index of geoaccumulation ( $I_{geo}$ ):** Index of geoaccumulation ( $I_{geo}$ ) introduced by Müller<sup>8</sup>, has been used widely to evaluate the degree of metal contamination or pollution in terrestrial, aquatic and marine environments. The  $I_{geo}$  of an element in sediment can be calculated with the formula<sup>9</sup>:

$$I_{geo} = \log_2(C_{metal}/1.5 C_{metal(controls)})$$

where:

the heavy metal in the enriched sample

$C_{metal}$  is the concentration of the metal in the enriched sample or control sediment<sup>10</sup>

concentration of the metal in the unpolluted sample or control sediment<sup>10</sup>

to minimise the effect of the possible variations in the background control values, which may be attributed to lithogenic variations in sediment<sup>10</sup>

**Ecological risk factor ( $Er^j$ ):** An ecological risk factor is used quantitatively to express the potential ecological risk of a given contaminant suggested by Hakanson (1980). This factor can be calculated with the formula:

$$Er^j = T^j \cdot C^j$$

where:

$T^j$  is the toxic-response factor for a given substance (for Hg, Cd, As, Cr and Zn, they are 30, 10, 2 and 1 respectively; and 5 for Pb, Cu and Ni<sup>11</sup>, and  $C^j$  is the concentration factor.

**Ecological risk index (RI):** The potential ecological risk index (RI) is defined as the summation of the change occurred in metals with respect to the background values considering the toxicological factor. The mathematical relation of RI can be shown as:

$$RI = \sum (T_i \cdot x C_i / C_o)$$

where:

for a given substance,

content in the sediment and

background value of heavy metals.

<sup>7</sup> Ruzhong et al. 2010  
<sup>8</sup> Müller, 1979  
<sup>9</sup> Asadi and Abimbola, 2005; Mediola et. al 2008  
<sup>10</sup> Mediola et al. 2008

**Sakan Sanjya and another: ASSESSMENT OF POLLUTION WITH TOXIC...**

**Pollution load index (PLI):** Tomlinson et al.<sup>13</sup> introduced the concept of the PLI to assess metal pollution in sediment. The PLI for a single site is the  $n$ th root of the number ( $n$ ) of multiple contamination factors (CF) multiplied together:

$$PLI = (CF_1 \times CF_2 \times CF_3 \times \dots \times CF_n)^{1/n}$$

This empirical index provides a simple, comparative mean for assessing the level of heavy metal pollution.

### 1.5. Statistical analysis

Multivariate analysis was performed using principal component analysis (PCA). The statistical analyses were conducted by using SPSS 11.0 untransformed data set.

## 2. RESULTS AND DISCUSSION

### 2.1. Performance of the analytical procedure

The accuracy and precision of the obtained results were checked by analyzing sediment reference material (BCR standards, 143R and 146R). The results indicate a good agreement between the certified and analytical values. The recovery of elements being practically complete for most of them and the values were in the acceptable range (recovery: 80-120%)<sup>14</sup>. The precision is expressed as relative standard deviations. The relative standard deviations of means of duplicate measurement were less than 4% (from 0.03 to 3.80%) for all the measured elements.

### 2.2. Descriptive statistics of elements contents in sediments

Basic statistics (minimum and maximum, as well as the means and standard deviations) for the total contents of all the measured elements in the analyzed river sediments are shown in Table 2. The order of the total element content was Zn > Cu > Pb > Ni > Cr > V > Co > Cd > As (not taking account Fe and Mn). Some of heavy metals showed significant spatial variations, suggesting there is no uniform distribution of those heavy metals.

Table 2. Total contents of elements in different river sediments, this study (mg kg<sup>-1</sup>)

|    | As  | Cd   | Co   | Cr  | Cu   | Fe   | Mn  | Ni  | Pb  | V   | Zn   |
|----|-----|------|------|-----|------|------|-----|-----|-----|-----|------|
| 1  | 0.2 | 1.2  | 8.22 | 59. | 11.  | 2455 | 648 | 33. | 57. | 60. | 66.6 |
| 2  | 8   | 8    |      | 8   | 5    | 6    |     | 2   | 8   | 4   |      |
| 3  | 10. | 36.2 | 230  | 870 | 6280 | 368  | 274 | 318 | 149 | 109 |      |
| 4  | 5   |      |      | 0   | 8    |      |     |     |     | 5   |      |
| 5  | 14  | 4.8  | 21.9 | 113 | 78.  | 4417 | 139 | 77. | 132 | 111 | 353  |
| 6  | 2   | 2    | 7    | 5   | 7    | 9    | 8   |     |     |     |      |
| 7  | 14  | 2.0  | 6.63 | 41. | 141  | 7200 | 556 | 58. | 51. | 18. | 232  |
| 8  | 8   | 8    | 0    | 0   |      |      | 5   | 0   | 0   | 4   |      |
| 9  | 8   | 4.6  | 21.5 | 102 | 47.  | 4578 | 135 | 46. | 124 | 111 | 330  |
| 10 | 8   | 9    |      | 9   | 0    | 2    | 3   |     |     |     |      |

<sup>11</sup> Vanni et al. 2009



Contamination of the investigated river sediments with trace elements was assessed using: EF,  $I_{geo}$ , Er, RI, and PLI. Table 4 shows the grades of contamination and ecological risk based on the factors. On the base of the pollution load index, contamination of sediments can be classified as: pollution exists, when the PLI > 1, and no metal pollution exists, when the PLI < 1<sup>15</sup>.

The element content in the DTD canal (station in Vrbas) was as the background values for elements in this research because these significant anthropogenic sources of toxic elements at this locality. Sediment samples are similar to the other investigated river sediments geochemical characteristics and composition. Background elements in this research are (in  $mg\ kg^{-1}$ ): 1.28 (Cd), 11.5 (Cu), 8.22 (Co), 60.4 (Cr), 34.7 (Ni), 57.8 (Pb), 66.6 (Zn), 60.4 (V), 2455.6 (Fe) and 1.7  $mg\ kg^{-1}$ . For the background value of As, the content of the continental crust is 1.7  $mg\ kg^{-1}$ .

Table 3. Grades of Enrichment factor and Index of geoaccumulation.

| Enrichment factor (EF) |                    | Index of geoaccumulation ( $I_{geo}$ ) |                                |
|------------------------|--------------------|--|--------------------------------|
| Value                  | Pollution category | Value                                  | Pollution category             |
| EF < 1                 | No enrichment      | $I_{geo} < 0$                          | uncontaminated (background)    |
| $1 \leq EF \leq 3$     | Minor              | $0 \leq I_{geo} < 1$                   | unpolluted background          |
| $3 \leq EF \leq 5$     | Moderate           | $1 \leq I_{geo} < 2$                   | moderately polluted            |
| $5 \leq EF \leq 10$    | Moderately severe  | $2 \leq I_{geo} < 3$                   | moderately to heavily polluted |
| $10 \leq EF \leq 25$   | Severe             | $3 \leq I_{geo} < 4$                   | heavily polluted               |
| $25 \leq EF \leq 50$   | Very severe        | $4 \leq I_{geo} < 5$                   | heavily to extremely polluted  |
| EF > 50                | Extremely severe   | $I_{geo} \geq 5$                       | extremely polluted             |

The sediment normalization element is aluminum. This element is chosen because Al is a conservative element and a major constituent of minerals, and has been successfully used in previous investigations.

Table 4. Grades of Ecological risk factor and Ecological risk factor.

| Ecological risk factor ( $Er^i$ ) |               | Ecological risk index ( $RI$ ) |               |
|-----------------------------------|---------------|--------------------------------|---------------|
| Value                             | Risk category | Value                          | Risk category |
| Er < 40                           | Low           | RI < 150                       | Low           |
| $40 \leq Er < 80$                 | Moderate      | $150 \leq RI < 300$            | Moderate      |
| $80 \leq Er < 160$                | Considerable  | $300 \leq RI < 600$            | Considerable  |
| $160 \leq Er < 320$               | High          | RI ≥ 600                       | High          |
| Er ≥ 320                          | Very high     | /                              | /             |

<sup>15</sup> Varol 2011  
<sup>16</sup> Wedepohl 1995  
<sup>17</sup> Rubio et al. 2000

### Enrichment factor (EF)

The EF values were interpreted as suggested by Acevedo-Figueroa et al. (2003) (Table 3) and were calculated separately for all the sampling sites. In general, the order of the average EF values was Cu > Zn > Cd > Ni > Mn > Cr > As. According to the categories, these findings show that Cu, Zn and Cd enrichment was high. From the point of view of pollution, the EF of Cu in the river Pek (35.03) were the highest among the elements of the investigated sediments, suggesting significant pollution at this locality. There is also a significant anthropogenic contribution to the elements in the sediments, mainly from the Ibar (I1, I2), Morava (V1), West Morava (Z1) and Tisa (T7).

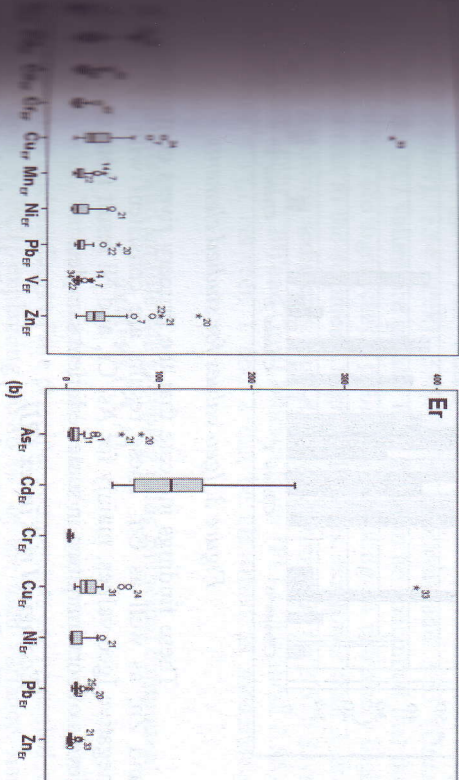


Figure 2. Values of EF (a) and Er (b) for studied elements.

### Ecological risk factor ( $Er^i$ )

The ecological risk assessment results are summarised in Figure 2b. The ecological risk factor for the individual element values varied among the studied elements in the sediments, as well as in different river results indicated that the river sediments posed a low to high potential ecological risk.

The potential ecological risk indices of Cr, Ni, Pb, Zn and As were calculated (except for arsenic at two locations in the Ibar River), which show a slight potential of ecological risk of these elements in the main river. Among the studied elements, Cd and Cu present a higher ecological risk than any other element because of their higher toxic coefficient. The ecological risk of Cd was over 80, indicating that Cd posed a moderate risk to local environment. The highest Er value is observed for Cu in the river sediment, which indicates a very high potential of ecological risk locally.



Müller (1979) proposed seven grades or classes based on increasing numerical value of the  $I_{geo}$  index (Table 3). The greatest number of samples belong to Class 1 (Figure 3), i.e. moderately polluted sediment (with As, Cd, Co, Cr, Cu, Fe, Mn, Ni, Pb, V). Class 2 (Cd, Cu, Zn, Cd and Pb in some samples), Class 3 (Cr, Ni, Pb) and the West Morava 1, and Zn in the Ibar 1 and Ibar 2 and Pek 1 largest  $I_{geo}$  value - 3.92 in sediment from the Pek River for Cu (highest pollution).

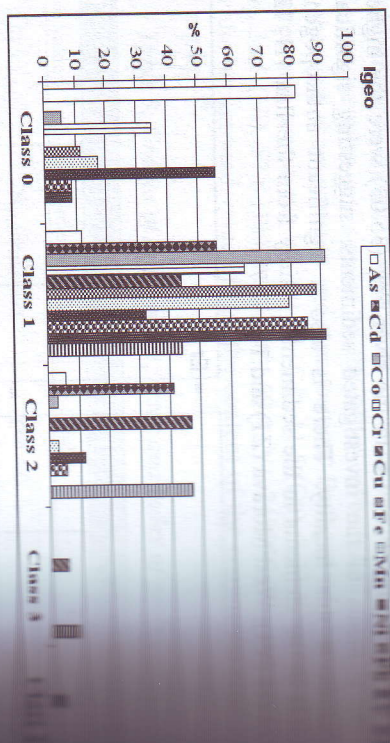


Figure 3.  $I_{geo}$  values for studied elements

These findings indicate that the primary rivers contribute As and Zn, as well as Cd. These results are consistent with the negative Igeo values, mainly for As, Cr, and Ni result from the low levels of contamination in some sediment samples.

**Ecological risk index (RI)**

The RI was calculated as the sum of all the calculated risk. The contamination categories on the basis of ecological risk are presented in Table 4 and Figure 4.

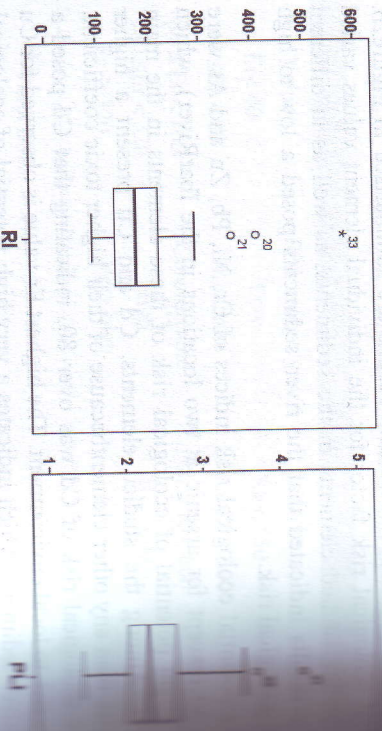


Figure 4. RI and PLI in river sediments

... suggesting that sediment samples from the river catchments of low and moderate ecological risk for the investigated elements. In three (two sediment samples from the Ibar and one from the Pek River) of 14 samples of sediments had RI values (from 300 to 600), which is a high ecological risk of heavy metals

The contribution percent of the individual element to the overall ecological risk revealed that the most toxic element, Cd, is the main contributor to the total potential ecological risk. Because Cd pollution, in this area, is the result of a long history of accumulation, there is a strong ecological risk to the ecosystem and the health of the residents in this region.

**Pollution load index (PLI)**

Figure 4 represents the PLI values of the studied elements. The PLI values ranged from 1.4 to 4.27 for the investigated sediments, suggesting that the sediments are moderately polluted. The highest PLI values were observed in the following order: 4.27 (Ibar), 3.66 (Pek), 3.49 (West Morava) and 3.33 (Great Morava). Since the PLI values are greater than 3, it can be concluded that the river systems are significantly polluted (indicating an extremely high content in the sediment). High PLI values, but lower than 3, are observed in the following sediments: Tisa River (PLI from 2.00 to 2.67); Sava River (PLI values about 2.20) and Great Morava River (PLI value about 2.86). Sediments with a PLI between 1 and 2 can be classified as moderately polluted.

**Factor elements and sample site grouping using principal component analysis (PCA)**

A PCA with Varimax normalised rotation was performed in this study. The scores and loadings of the principal components are presented in Table 5 and Figure 5. PC1, explaining 60.86 % of the total variance, has positive loadings for Fe, Mn, Co, Cr and V. PC2, explaining 15.67 % of the total variance, has strong loadings for As, Pb, Zn, Cd and Ni. PC3, explaining 10.58 % of the total variance, has a strong positive loading on Cu.

Table 5. Loadings of experimental variables

|    | PC1   | PC2   | PC3 |
|----|-------|-------|-----|
| As |       | 0.906 |     |
| Fe | 0.933 |       |     |
| Mn | 0.778 |       |     |
| Co | 0.933 |       |     |
| Cr | 0.862 |       |     |
| Pb | 0.590 | 0.720 |     |
| Zn |       | 0.774 |     |



|                       |        |        |        |
|-----------------------|--------|--------|--------|
| Ni                    | 0.579  | 0.610  | 0.601  |
| Cu                    |        |        | 0.601  |
| V                     | 0.911  |        |        |
| Eigenvalue            | 6.694  | 1.724  | 1.108  |
| % Total variance      | 60.855 | 15.669 | 10.532 |
| Cumulative % variance | 60.855 | 76.525 | 87.057 |

Obtained results indicate that elements with similar origins (Fe, V, Mn, Co and Cr; (2) Pb, Zn, Cd, As and Ni and (3) Cu. It is obvious that the sources of Cu are different from the other elements (R mode, p. 215-5a).

Fe, V, Mn, Co and Cr have a combined source and these elements are derived from lithogenic and anthropogenic sources. Iron is abundant in Earth's crust, though the pollution indicates the existence of anthropogenic sources of this element at some localities. Also, enrichment is observed in some of sediments. Cr is generally a sign of the paint and metal industry. V is greatly impacted by anthropogenic activities such as extraction, agricultural processes, and Co is mainly from anthropogenic sources such as paint, fertiliser or agrochemical industries. The low content of V, Fe, Mn, Co and Cr at the studied locality.

Pb, Zn, Cd, As and Ni are mainly derived from anthropogenic sources. The significant anthropogenic source of these elements is the Trepča mining complex in Serbia. Trepča mining complex is the source of lead and zinc. In addition to mining, anthropogenic sources of elements may be directly discharged from locally based sources such as industrial and urban discharges carrying metal and metallurgical waste. Contaminants mainly come from metallurgy and coal burning. Heavy pesticides containing As can also lead to an increase of As. Ni is mainly derived from anthropogenic activities, especially from industrial sources. Cu is derived from anthropogenic sources, most significantly from metallic wastewater discharges. The significant anthropogenic source is the open-pit mine in Majdanpek. Another source of Cu may be the discharges from industries, as well as agricultural activities.

Figure 5b displays isolated three groups of samples: 20 (V1), 22 (V1), 23 (V2) and 25 (Z2) - first group, 33 (Pe) - second group, and other sediment samples constitute the third group. These are the results of application of the PCA (Q mode). Sampling site 33 (Pek River) has the most polluted river sediments at the investigated localities. The contamination to the overall pollution is the most significant, compared to other sites in this sediment. In the group with sediments 20, 21, 23 and 25 is the sample with significant pollution compared to other moderately polluted studied sediments.

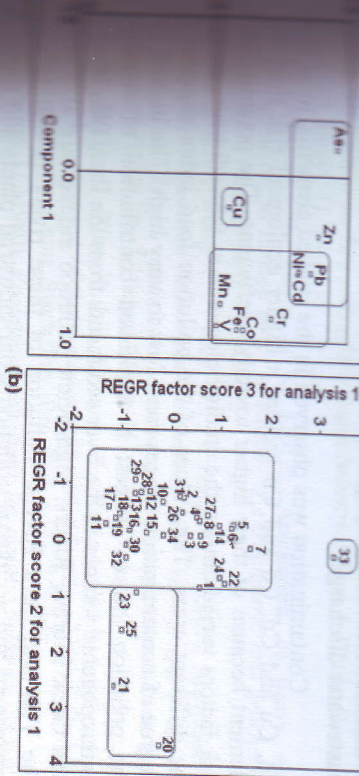


Figure 5. Results of PCA analysis.

The results in this manuscript indicate that the most polluted sites at the studied localities are sediments from the Ibar and Pek Rivers. In these two rivers, the Great Morava and West Morava are also significantly polluted river systems. Pollution of these rivers is mainly caused by industrial and accidental pollution from industrial plants and mines that are present in the basins of these rivers. One of the main industrial polluters of the Ibar River is the Trepča mining complex. This huge industrial mining site has been active since the year 2000, lead and zinc has been mined and smelted and the resulting waste has been discharged into the environment and continue polluting the Ibar River<sup>19</sup>.

The significant pollution with Cu of sediments from the Pek River is related to the Cu mining complex in Majdanpek. The copper ore extraction process produces large amounts of ore waste and flotation tailing ponds in the vicinity of Bor and Majdanpektowns. In addition to this pollution, the accidental pollution significantly affects the pollution of the Ibar River. The most serious incidents are the breaches of tailing dams at the Bor and Veliki Majdan causing direct and serious contamination of the Ibar River by heavy metals.

In general, the results obtained using multivariate statistical analysis are in agreement with the results obtained using the calculation of pollution indices of the same category have the same source of pollution and a degree of contamination. The applied methods can classify sediments from the investigated region according to the degree of pollution and to the main sources of toxic elements.

## CONCLUSION

The impact of trace element pollution on the quality of the river water in Serbia was evaluated using different pollution indices. The source of pollution carried out using multivariate analyses shows that: (1) Fe, V, Mn, Co and Cr are derived from lithogenic and anthropogenic sources, (2) Pb, As, and Ni are mainly derived from anthropogenic sources, and (3) Cu



Contamination was observed in the studied elements, most of Zn, Cu and Cd. Cd and Cu present a higher ecological risk than other element because of their higher toxicity coefficient. The potential risk factors varied among the studied elements in the sediments as well the different areas. The values of the pollution load index suggest the degree of contamination ranges from low to very high. The highest pollution indices suggest a significant contribution of elements of anthropogenic sources in the river sediments from the Ibar, Pele, West and Great Morava Rivers. Significant pollution indexes are also observed in the Tisa and Sava Rivers. Pollution of these rivers is mainly permanent and accidental pollution from industrial plants and mines located in the basins of these rivers. Significant influences are evident in mining complexes (mainly in Treпча and Majdanpek) on river contamination with toxic trace elements.

The above results confirmed the existence of pollution trace elements in the studied river sediments. The calculated pollution indices and the application of statistical methods are recognised as useful for the ecological risk assessment and the management of trace elements in

#### Acknowledgments

This study was supported by the Ministry of Education, Science and Technological Development of Serbia, Grant Nos. 172001 and 172002. In addition, we would like to thank the Republic Hydrometeorological Institute of Serbia for the sediment samples.

#### PROCENA ZAGADENJA REČNIH SEDIMENATA TOKOM PROMENLIVOSTI KLIMATSKIH USLOVA IZ OBLASTI VEŠTAČENJA IZ OBLASTI ELEMENTITIMA PRIMENOM FAKTORA KONTAMINACIJE I STATISTIČKIH METODA

Dr Sanja Sakan, dr Dragana Đorđević, doc. dr Nenad Sakan

**Apstrakt:** Da bi se mogao pratiti uticaj zagađenog rečnog sedimenta na životnu sredinu i zdravlje ljudi veoma su važne informacije o prisutnosti elemenata (geohemijski ili antropogeno), njihovoj varijabilnosti i ekološkom riziku. Istraživanje u ovom radu je sprovedeno na celovitom kvantifikovanju kontaminacije, kao i procene rizika od zagađenosti elementima (As, Cd, Co, Cr, Cu, Fe, Mn, Ni, Pb, V i Zn) u rečnim sedimentima. Procena kontaminacije je izvedena određivanjem definisanjefonskog sadržaja elemenata u sedimentu, kao i određivanjem kontaminacije. Rezultati primene statističkih metoda ukazuju na antropogeni izvor. Najviše kontaminirani rečni sistemi su Ibar, Pele, West and Velika Morava. Rezultati pokazuju da u slivovim ovih reka postoje uticaji teških metala, uglavnom industrija i rudarski baseni.

**Cljučne reči:** zagađenje, toksični elementi, rečni sedimenti, kontaminacije, statističke metode

#### REFERENCES

1. Acevedo-Figueroa, D., Jiménez, B.D., Rodríguez-Sierra, C.J. (2009): *Metals in sediments of two estuarine lagoons from Puerto Rico*. Pollut. 141, 336-342.

- Chahkhalam, M., Nema, A.K. (2012): Assessment of heavy metal contamination in Hindon River sediments: A chemometric and geochemical approach. *Chemosphere* 87, 945-953.
- Chang, C.Y., Wang, C.F., Mu, D.T., Chiang, H.L. (2009): Application of methods (sequential extraction procedures and high-pressure digestion method) to fly ash particles to determine the element constituents: a case study for BCR 176. *J. Hazard. Mater.* 163, 578-587.
- Choi, H., Bai, J., Xiao, R., Liu, P., Jiang, W., Wang, J. (2013): Levels, sources and risk assessment of trace elements in wetland soils of a typical shallow freshwater lake, China. *Stoch. Env. Res. Risk A* 27, 275-284.
- Hakanson, L. (1980): *Ecological risk index for aquatic pollution control, a sedimentological approach*. *Water Res.* 14, 975-1001.
- Kahle, I., Lee, H., Kim, G., Jun, T. (2011): Correlation assessment and monitoring of the potential pollutants in the surface sediments of Poyangchang River. *Int. J. Sedim. Res.* 26, 152-162.
- Kalantzi, I., Shinnied, T.M., Pergantis, S.A., Papageorgiou, N., Black, K.D., Karakassis, I. (2013): Heavy metals, trace elements and sediment geochemistry at four Mediterranean fish farms. *Sci. Total Environ.* 444, 128-137.
- Medelha, L.L., Domingues, M.C.D., Sandoval, M.R.G. (2008): *Environmental Assessment of and Active Tailings Pile in the State of Mexico (central Mexico)*. *Res. J Environ. Sci.* 2, 197-208.
- Müller, G. (1979): *Schwermetalle in den Sedimenten des Rheins-Veränderungen seit 1971*. *Umschau* 79, 778-783.
- Rank, J., Klemmensen, B. (2003/2004): *Environmental management in Kosovo*, Heavy metal emission from Treпча. TekSam (Institut for Miljio, Viteknology og Samfund).
- Rubio, B., Nombela, M.A., Vilas, F. (2000): *Geochemistry of major and trace elements in sediments of the Ria de Vigo (NW Spain): an assessment of metal pollution*. *Mar. Pollut. Bull.* 40, 968-980.
- Ruehling, L., Kun, S., Yueying, L., Yong, S. (2010): *Assessment of heavy metal pollution in estuarine surface sediments of Tangxi river in Chaohu Lake basin*. *Chinese Geogr. Sci.* 20, 9-17.
- Sakan, S.M., Đorđević, D.S., Dević, G., Relić, D., Anđelković, I., Đuričić, J. (2011): *A study of trace element contamination in river sediments in Serbia using microwave-assisted aqua regia digestion and multivariate statistical analysis*. *Microchem. J.* 99, 492-502.
- Tomlinson, D.C., Wilson, J.G., Harris, C.R., Jeffrey, D.W. (1980): *Problems in the assessment of heavy-metal levels in estuaries and the formation of a pollution index*. *Helgolander Mar. Res.* 33, 566-575.
- Vogel, M. (2011): *Assessment of heavy metal contamination in the sediments of the Tigris river (Turkey) using pollution indices and multivariate statistical techniques*. *J. Hazard. Mater.* 195, 355-364.
- Wetzeloh, K.H. (1995): The composition of the continental crust. *Geochim. Cosmochim. Ac.* 59, 1217-1232.
- Yang, Z., Wang, Y., Shen, Z., Niu, J., Tang, Z. (2009): *Distribution and geochemical characteristics of heavy metals in sediments from the mainstream, tributaries, and lakes of the Yangtze River catchment of Wuhan, China*. *J. Hazard. Mater.* 166, 1160-1194.





# 28<sup>th</sup> Summer School and International Symposium on the Physics of Ionized Gases

Aug. 29 - Sep. 2, 2016, Belgrade, Serbia

## CONTRIBUTED PAPERS

&

ABSTRACTS OF INVITED LECTURES,  
TOPICAL INVITED LECTURES, PROGRESS REPORTS  
AND WORKSHOP LECTURES

Editors:

Dragana Marić, Aleksandar Milosavljević,  
Bratislav Obradović and Goran Poparić



University of Belgrade,  
Faculty of Physics



Serbian Academy  
of Sciences and Arts

# BOND - BOUND STATE TRANSITIONS IN THE FRAME OF COULOMB CUT-OFF MODEL POTENTIAL

N. M. Sakan<sup>1</sup>, V. A. Srećković<sup>1</sup>, Lj. M. Ignjatović<sup>1</sup> and A. A. Mihajlov<sup>1</sup>

<sup>1</sup>*Institute of Physics, University of Belgrade, Pregrevica 118, Zemun,  
11000 Belgrade, Serbia*

**Abstract.** The cut-off Coulomb potential has proven itself as a model potential for the dense hydrogen plasma. It was tested and proven in calculation of the photo-ionization processes as well as inverse Bremsstrahlung processes of hydrogen atom in the photon wavelength region  $300 \text{ nm} < \lambda < 1000 \text{ nm}$ , with and without the influence of plasma. The further steps of improvement of the usage of model potential is carried out. Here are presented first test results of bond state transition modeling in the frame of cut-off Coulomb model potential. The presented results converge towards the theoretical values for plasma of small plasma coupling  $\Gamma$ , e.g. the plasma of small non-ideality. The investigated results are good indicator that the inclusion of the bond-bond radiation transitions could be well funded. It is expected that such approach would lead towards to the inclusion of bond state transition photo-absorption process within the frame of the presented Coulomb cut-off potential model.

## 1. INTRODUCTION

The cut-off Coulomb potential has been proven in modeling of continuous photo absorption of the dense plasma of moderate non-ideality, e.g. plasma coupling parameter  $\Gamma$  (see [1]), is comparable to or slightly greater than unity. Although the implementation of the cut-off Coulomb model potential is not entirely developed and performed, it's preliminary results were present in several papers [2, 3, 4, 5, 6, 7]. The usage of the mentioned model potential is in process of continuous development. As first step in extending of the model with additional processes is the bond state transition processes inclusion. The bond state transition processes is stated as most important goal in the development of the self containing model, capable of describing of optical as well as dynamical characteristics of dense hydrogen



plasma. The characteristics of the bond state transitions in plasma diagnostics is well known, almost mandatory method, [8]. The usage of the hydrogen lines as a probing method for the plasma characteristics are also well known and widely used in plasma of moderate and small non-ideality, [9].

As it was shown in [4], the extensive work was carried out in order to prove the model potential usage and to adopt the bond state level broadening models. Analysis of the results led to the conclusion to focus the research onto one of the potential models, e.g. the potential

$$U_0(r; r_{cut}) = \begin{cases} -\frac{e^2}{r} & 0 < r \leq r_{cut}, \\ 0 & r_{cut} < r, \end{cases} . \quad (1)$$

Here  $r_{cut}$  is a model parameter, cut-off radius, determining the boundary between the zone where there is influence of individual ion-electron interaction, and the other zone where only collective phenomena of average plasma influence exists.

In accordance with the previously mentioned the continuation of research of the presented approach is the inclusion of the the bound-bound photo absorption process using the same model potential.

The investigated process, the bound-bound photo absorption, in accordance with previously used notation, is denoted as

$$\varepsilon_\lambda + H^*(n_i, l_i) \rightarrow H^*(n_f, l_f), \quad (2)$$

and was not considered within the frame of the used model potential. Here  $n$  and  $l$  are the principal and the orbital quantum number of hydrogen-atom excited states, hydrogen atom in it's initial state  $|n_i, l_i\rangle$  is presented by  $H^*(n_i, l_i)$ , it's final state  $|n_f, l_f\rangle$  by  $H^*(n_f, l_f)$ , and  $\varepsilon_\lambda$  presents absorbed photon energy.

The dipole transitions are favorable ones in radiative transition for the plasma in area where the usage of this model is preferred, e.g. where there is a single electron in average, in specific plasma sphere,  $r_{cut}$ . In accordance with that, the behavior of the dipole matrix element is investigated here. It is given by

$$\hat{D}(r; r_{cut}; n_i, l_i; n_f, l_f) = \langle n_f, l_f | \mathbf{r} | n_i, l_i \rangle, \quad (3)$$

where the wave functions  $|n_i, l_i\rangle$  and  $|n_f, l_f\rangle$  are initial and final hydrogen wave functions.

## 2.RESULTS AND DISCUSSION

The investigation of the bond transitions in the frame of cut-off Coulomb potential has shown good behavior. As it could be shown on figure 1a and 1b, the oscillator strength values converge towards the theoretical ones for the hydrogen without plasma influence.

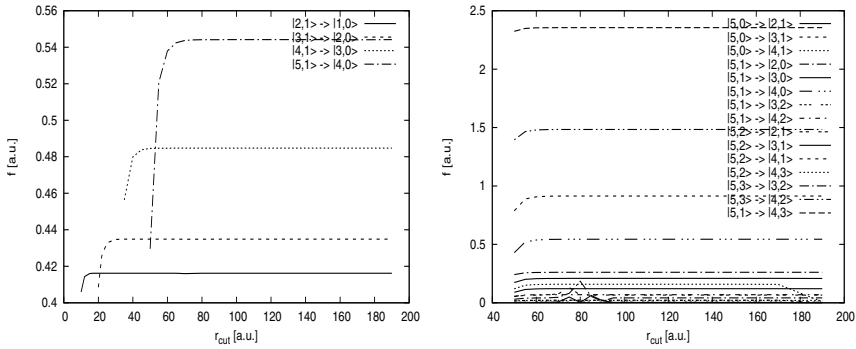


**Figure 1.** a) b)  
Convergence of the oscillator strength values.

### 3. CONCLUSION

From the results of the investigation of the behavior of bond level transitions in the frame of cut-off Coulomb potential model it is obvious that it is possible to include the bond transition processes. There is a need to investigate further, more in depth, the shown behavior in order to prove that there is no numerical artifacts within the shown results. Also there is a need to include the broadening of the bond states, as first to reproduce the results with models already shown in [4], and after to further investigate various models for broadening mechanisms.

The preliminary results has shown that there is a possibility of inclusion of the bond transitions in the frame of cut-off Coulomb potential method for the describing of optical properties of the dense hydrogen plasma. There is a need for further development of the model and extending it's usage on more complex atoms also.

### Acknowledgements

The authors are thankful to the Ministry of Education, Science and Technological Development of the Republic of Serbia for the support of this work within the projects 176002, 171014 and III44002.

### REFERENCES

- [1] V. E. Fortov, I. T. Iakubov, Physics of Nonideal Plasma, Hemisphere, New York, 1989.
- [2] Yu. N. Gnedin, A. A. Mihajlov, Lj. M. Ignjatovi, N. M. Sakan, V. A. Srekovi, M. Yu. Zakharov, N. N. Bezuglov, A. N. Kly-

- charev, *New Astronomy Reviews* 53, 710, (2009), pp 259-265, DOI: 10.1016/j.newar.2009.07.003,
- [3] Ignjatović, L. M., Mihajlov, A. A., Sakan, N. M., Dimitrijević, M. S., Metropoulos, A., *MNRAS*, 396, (2009) pp2201-2210, DOI: 10.1111/j.1365-2966.2009.14870.x
- [4] Nenad M Sakan, The Calculation of the Photo Absorption Processes in Dense Hydrogen Plasma with the Help of Cut-Off Coulomb Potential Model, *J.Phys.: Conference Series* 257, 1, (2010),012036, DOI: 10.1088/1742-6596/257/1/012036
- [5] A A Mihajlovn N M Sakann V A Sreković, Y Vitel, *J.Phys.A* 44, 9, (2011), 095502, DOI: 10.1088/1751-8113/44/9/095502
- [6] Mihajlov, A. A., Srećković, V. A., Sakan, N. M., *J.Astrophys.Astr.* 36 (2015), pp 635–642, DOI: 10.1007/s12036-015-9350-0
- [7] Mihajlov, A. A., Srećković, V. A., Ignjatović, Lj. M., Klyucharev, A. N., Dimitrijević, M. S., Sakan, N. M., *J.Astrophys.Astr.* 36, 4, (2015) pp 623–634, DOI: 10.1007/s12036-015-9364-7
- [8] Hans R. Griem, *Principles of Plasma Spectroscopy*, Cambridge University Press, 1997, ISBN: 9780511524578, DOI: 10.1017/CBO9780511524578
- [9] N. Konjević, M. Ivković, N. Sakan, *Spectrochimica Acta Part B: Atomic Spectroscopy*, 76, (2012), pp 16-26, DOI: 10.1016/j.sab.2012.06.026
- [10] I. I. Sobel'man, *Atomic Spectra and Radiative Transitions*, Springer Verlag, Berlin, 1979.



# 7th INTERNATIONAL SCIENTIFIC CONFERENCE ON DEFENSIVE TECHNOLOGIES OTEH 2016

Belgrade, Serbia, 6 – 7 October 2016



## STRATEGY IMPLEMENTATION OF DUAL-SEMI-ACTIVE RADAR HOMING GUIDANCE WITH COUPLING OF TANDEM GUIDED AND LEADING MISSILE OF AIR DEFENCE MISSILE SYSTEM ON REAL MANEUVERING TARGET

MARKOVIC STOJAN

University of defense, Military academy, Pavla Jurisica Sturma 33, 11000 Belgrade, Serbia, [stomarkovic@yahoo.com](mailto:stomarkovic@yahoo.com)

MILINOVIC MOMCILO

Faculty of Mechanical Engineering, University of Belgrade Kraljice Marije 16, 11120 Beograd 35, Serbia, [mmilinoVIC@mas.bg.ac.rs](mailto:mmilinoVIC@mas.bg.ac.rs)

NENAD SAKAN

Institute of Physics, University of Belgrade, Pregrevica 118, Zemun, 11080 Belgrade, Serbia, [nsakan972@gmail.com](mailto:nsakan972@gmail.com)

**Abstract:** The paper investigated the possibilities of newly formed dual system SARH (Semi-active radar homing) missiles SA-6 mid-range category, on standard manoeuvrable targets. The system was set up as a dual-cooperative guidance of the first launched (guided-slave) missile from second launched missile (leading-master), with a time delay of 3[s]. Angle position of target is measuring using two existing RHH, which together with additional illuminators on missiles, represent two active seekers, with a period of mutual scanning and with changing the roles-status of 1[s]. Also, missiles synchronously communicate between each other through free caudal antenna, when it is situation based on the smaller current error, determines the status of a missile. Proces of coupled guidance is modeled with specially designed program in MATLAB with appropriate adjustment AD, AL and effective radius of action Warhead. Missiles are guiding in calculated point of overtaking with classical method PN with changing the angle of launch SPLV, by changing the distance, altitude and speed targets and other given parameters of flight. Simulations were examined specific conditions and regimes of shooting with one or two missiles, the correlation results and made conclusions of the most efficient mode and optimal performances of dual system homing missiles AAD.

**Keywords:** slave and master missile guidance, control system simulation MATLAB, dual navigation missile, Semi Active Radar Homing, Proportional Navigation, Miss distance missile-target, Radar lighter

### 1. INTRODUCTION

Classical artillery, with multi tools, relies upon prediction trajectory of target in open loop control, with the help of Optica or radar devices for control, tracking and action, respectively fire control, primarli through LFT (Low Flying Target). In order to achieve the required the accuracy of the action, either by LFT as well as on the medium altitudes targets, used in missile systems AAD (Anti-Air Defence) that have automatic control closed loop for continous reading errors in order to provide meeting missile with the target and its translation in corrective maneuver, with additional required acceleration. Designing law of guidance, that the distance to the goal (ultimate corrent miss) decreases to the lowest possible value, in real world resulting in a final breach by objective, which compensates with the action of remote lighter missile. Representative and reliable way of guidance missile in terms middle range AAD is Semy Active Radar Homing wich provide that the source of radiation missile, which iluminates the target, located on the ground, both at the begining and below, in the next

phase of guidance, provides at the end reliable work or RHH (Radar Homing Head) missile.

Disidvantage of this system is that it binds to the resource on the ground and thereby prevents its engagement to launch and guidance other missiles upon targets in AS (Air-Space). Also, drawback of this system that he may warn opponents, respectively aircraft as a target, that is launched missiles on it and that the same guiding from the ground. Semi-active RHH has potential possibility to messasure the relative direction to the missile as well as angle speed LOS (Line of Sight) missile-target, but there is no possibility of measurment distance to target In this paper, missile has been analyzed with SARH way of guidance which has two rear tail antenna, operable to receive a facing direct signal illumination target, which carries a reference frequency, and thus enabling the measurementof Dopler frequency and estimate III MF (Mixed Frequency) however, the change of distance to target irrelevant and it has no need to be seperately "measured by". This channel is desirable, and his role is not to guide the missile, but to allow her to distinguish target from the cluster and interference signal and

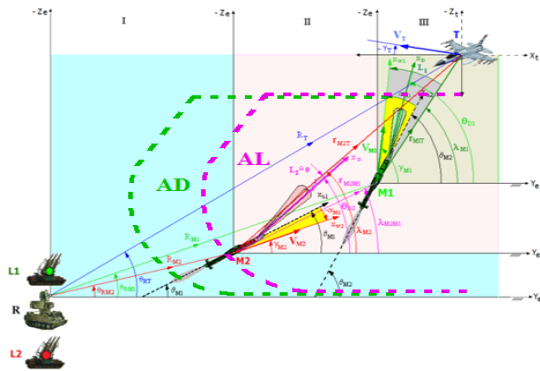


**Figure 1.** Starting kinematic show dual-cooperative homing two missiles on one target

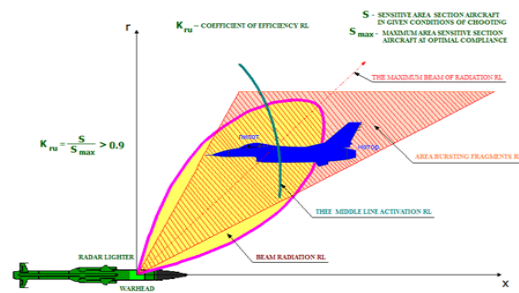


**Figure 2.** Area of bursting fragments WARHED and optimal position of antenna activation RL at the midline

CEW (Countermeasure Electronic Warfare) [5]. There is a second parallel channel, and that is angle grip and guidance upon target through the front and face of the antenna, regulated AOT (Automat Opertion target) who later become the dominant in missile guidance, and can be stored with the "services" of the other radar and optical devices (TOV-Television Optical Veiwfinder) in the AIR. Many yearsof observation AAD system, with completely pros and cons imposed the idea of specific researh methodes of fighting with modern targets in AS, with decreases the intence of probability of their hit and destruction, relative to the initial set requirements. Otherwise, effectively reducing and zeroing error homing missil, with increased range and speed of target, his CEW and maneuar, intensively thinkingin world in last ten years with the delopment of modern theories of guidance and applying the most modern mathematical and software tools.

$$P_{dualM1,M2} = 1 - (1 - P_{singlM}) \quad (1)$$

One of the ways, or strategies in real application and improving efficiency, probability of hitting and destruction of target (manufacturers information:  $p_{1M} = P_{singlM} = 0,80$  and  $p_{2M} = 0,96$ ) for MIG-19 with out considering CEW, of the existing system of mide-range, will be analyzed and exposed on the basis of the initial equation.

## 2. FORMULATION OF THE PROBLEM OF DUAL HOMING MISSILE

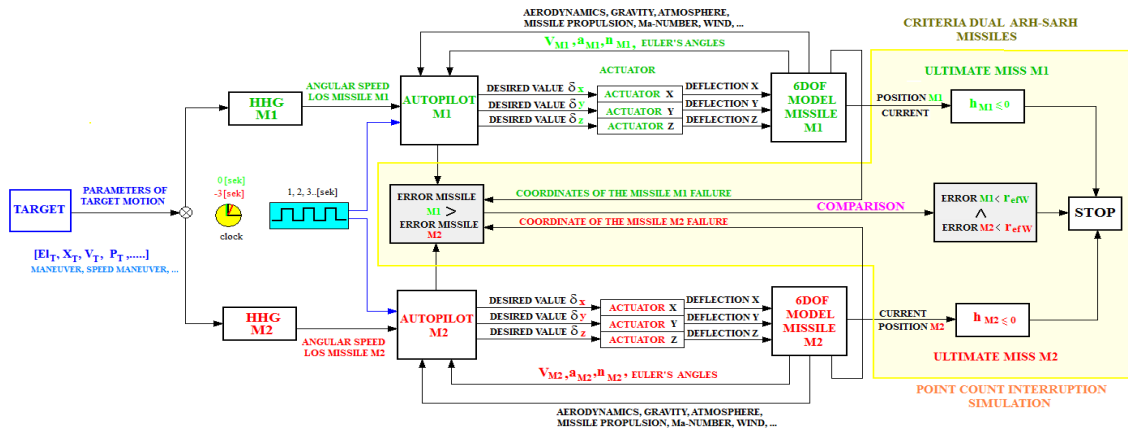
The initial phase of flight AAMS (Anti-Aircraft Missile System) is the command radio-guidance, whose realization in system initially begins on the launcher, before launching missiles, which continues to fly ballistic in POT (Point of OverTaking) with the accuracy of  $(+4[0])$ , and of itself doesn't see the target.

With the work off start phase of missile propulsion, achieves the necessary speed of missile, and at the same

With the work off start phase of missile propulsion, achieves the necessary speed of missile, and at the same time, protection of other missiles and resources, with the delay activation of RAMJET engine. After that stabilization of missile occur and follow-up of its stable and manageable flight, engagemnts, the already calculated point of overtaking, but now with the classical method PN (Proportional Navigation) with default AL (Area Launch) with their borders. This means that the part of radar-computer system on the ground did all the procedures provided for complex procedures (46 equations), actions and modes of work, from observations, expectations, appearance and allocation target in the launch zone, to give accurate coordinates and creating condotions for launch. It is calculated and the time entered reinforcement RL (Radar-Lighter) the 0.6[s] distance till encounter with target with a given AD (Area of Destruction) from near and far, uper and lower limit, dictated the height of target,dedad zone, its speed, parameter target and type of aircraft as a target, figure 1.

Second phase of flight missiles is marching mode of work when RAMJET propulsion engine is activated. Missile is included in the loop of guidance, ate target is still continuously illuminates CW illuminater with 1S91(RSSG-Radar Station Surveillance and Guidance), and at same time monitors TR (Tracking Radar) ie pulse radar. Necessary presence included continuous pulse transmitter RG (Radar Guidance 1S31) represents, with observation RS (Surveillance Radar 1S11) all the while guiding missile to hit and destruction of the target, great technical and tactical problem of hitting the target and same time surviving crew and resources. It shows practice and out dated system, which makes it inferior, in relation to the modern affensive resources from AS Also, possibility of hitting modern targets is drastically reduced, and to achieve the reguired real norms its necessary a far greater number consumption of missiles by one target (from 18 to 22 missiles) in a short period of time, wich is economically unsustainable and imposible in our conditions short period of time,





Picture 3. Starting conception strategies simulation of dual homing AAD missiles on one target

which is economically unsustainable and impossible in our conditions. So, exclusion RG from system and substitution on missile (placing additional illuminator on missiles) and modernization of the existing receivers (digitalization, silent in SST-Solide State Tehniques) in the existing RHH, with innovated roles of tail antenna. Missiles get divided but each other interchangeable roles (guided –

slave missile M1- that excels 3[s] and she is always in role that attack target and leading-master missile M2- with illuminates target T and flight behind guided M1 and support it) is the core cooperatively coupled homing two missiles to one target, figure 4[2].

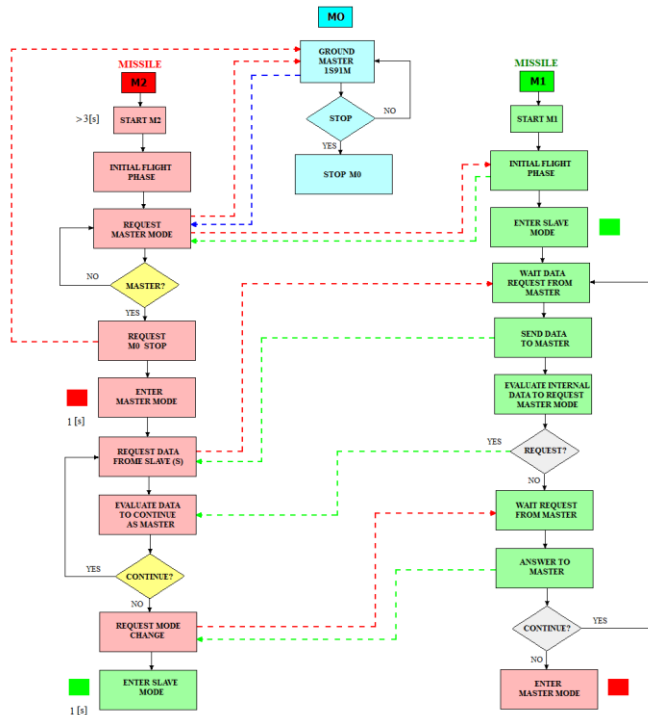


Figure 4. Proposal algorithm decision - making in tandem homing missiles

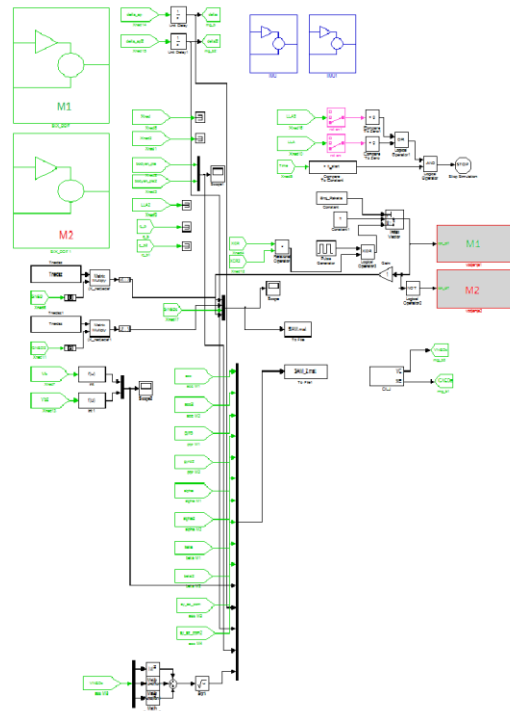


Figure 5. Matlab block scheme simulation

Missiles are changing roles changing the specified status, at defined intervals of time and thus obtaining SARH in the air, with all know pros and cons. Algorithm applied in strategy dual-coupled homing is shown in figure 4. It can be seen that guided missile M1 travels in PO (Point of Overtkong), optional guided missile M1, wich illuminates target, with criteriechange of roles of missiles. Algorithm decision, running parameters, wich are in accordance with the decisions

state (missiles), expressed as control functions of time in respective sequences, processed in [2], from the time of operation target to its cooperative destruction. Also, one of the condition that must be provided energy relation, expressed through the signal stenght transmitter from ground toward target and strenght signal of giving tail antenna from missile to target, according to eq.(2).

$$P_{illum.RAR} = P_{RSIOG} / (R_{RSIOG-Targ et} / r_{Missile-Targ et})^4 \quad (2)$$

Missiles fly based on criteria set current failures  $m$  (max - miss distance) and achieving the lowest end-flops in relation to the position and maneuver of the target in area. Starting pictures kinematics, as the basis of simulation, shown in figures 4 and 5.

Unfavorable position, with structural constraints and performance of missiles (max 4[s] flight toward as per predictable path) at one time for a second missile, that was with big fault, becomes a priority. So, there is a possibility of additional processing through GP (Generator of Searching) in Homing Head, respectively

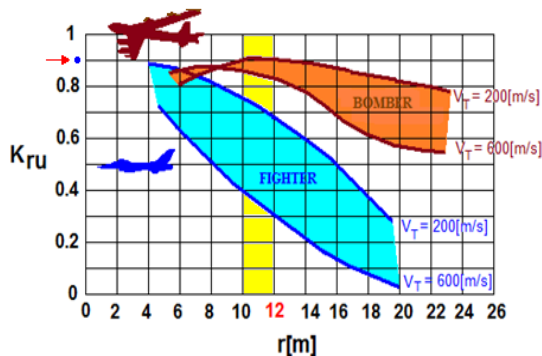


**Figure 6.** Dependence  $K_{ru}$  of speed targets (bomber, fighter) and failures of AADS missile

### 3. REALIZATION OF SIMULATION TANDEM DUAL COUPLED MISSILES

Conceptual scheme of simulation coupled guidance tandem missiles AAD, in software program MATLAB, has shown in picture 5.

We see that they are mathematically coupled two module 6.DOF missile, autopilot and executive actuators of missile. At the entrance, a module target formed and module of comparing errors of missile M1 relative to M2 i module of additional calculation, with respect to the effective radius of action  $W$  (Warhead). System has possibility to of giving the stroke duration (clock) roles of missiles (guided, leading), with the necessary delay missile launch M2 than 3 [s].

Matlab model simulation, picture 5, done on the basis of kinematic relations of picture 1, includes: model of gravity and shape of Earth, kinematics and law of guidance, dynamics and 6DOF, disruption and settings, aerodynamics (parameters and coefficients), missile launcher, geometry of missile, radar lighter i warhead, mass-propulsion-inertia characteristics, run the simulation with default parameters, reading file, select a time changes status of missile inding the closest point of the encounter and presentation of data and results (diagrams) given simulation.

In simulations, with solutions ballistic flight, active guidance and SARH mode, were used real parameters

additional grip (if target was lost for flight in "remembered" TP (Point of overtaking). Also, she has enough time and benignity of movement, so that in the area, guided missile its longitudinal axis and with angle of beam transmitter RL, placed in the optimal position parallel to the longitudinal axis of aircraft (decreases the tilt radiation pattern in relation to longitudinal axis with command changing antenna) for acyion remote radar lighter and destruction of target, figure 6.

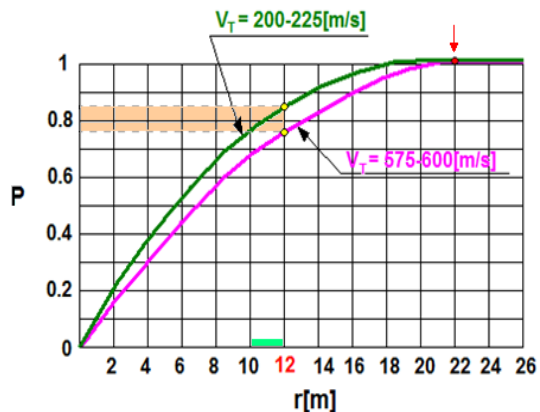


**Figure 7.** Integral law probability failure missile SA-6 at various speeds target less than 12[m] for a given probability - P

of missiles: navigation constant  $[N=3.5]$ , timing constant HHM  $[T_g = 004[s]]$ , memory Point of Overtaking the Target (POT) from Generator Search (GS) RHHM  $t_{memory} = [2,5-4[s]]$ , radius of efficient action warhead  $[r_{efw} = 25[m]]$ , time reinforcement RL  $[t_{earmRL} = 0,6D_{POT}]$ , coefficient effectiveness radar lighter  $K_{ru} > 0.90$ , figure 6, side overload  $[a_b=15[g]]$ , longitudinal overload  $[a_n=23[g]]$ , loss of guiding until meeting with starting maneuver of flight  $[t_{vgsmanevart} = 6-8 [s]]$ , clearance failure of missile  $[r_{pr} = 3-20[m]]$ .

### 4. SHOWING RESULTS MATLAB SIMULATION AND RESEARCH

Based on the collected data in the real world, setting model SARH as bistatic radar in the air (alternating shifts, giving - active radiation and reception-semi-active) obtained are the result of the launch of two tandem, the two missiles (guided and leading) on real targets (strategic bombers and attack fighter). Also, experiential data, which provides original rule shooting system, were amendments of the input data and parameters, on what basis are made numerous simulations using the Matlab 2R2011a, whose Simulink model custom-built analysis and set up for this type of missile, in figure 5. The results are shown in Table 1. First, it provides a case in shooting case of forced release of missiles with SPLV -1,2.

**Table 1.** Showing results of Matlab simulation for default parameters of target and and avariety of shooting modes and launching missiles AADS

| Serial number launching | REGIME AND TYPE OF LAUNCHING MISSILES   |  |    | SPECIFY PARAMETERS OF TARGET |                |              |               |                          |                 |                        |                           |   | INTRODUCTION OF PROGRAM STATUS              |                                  |                               | TARGET TYPE  | SHOW SIMULATION RESULTS |    |  |
|-------------------------|---|--|----|------------------------------|----------------|--------------|---------------|--------------------------|-----------------|------------------------|---------------------------|---|---|----------------------------------|-------------------------------|--|-------------------------|----|--|
|                         |   |  |    | ELEVA-TION [°]               | DI-STANCE [km] | HEI-GHT [km] | SPE-EED [m/s] | SPE-EED MANE-UVER [m/s²] | FREQ-UENCY [Hz] | LATE-RAL OVE-RLOAD [g] | PAR-AMETER P <sub>T</sub> | SHIFT OF MISSILES Δt <sub>shift</sub> [s] | POINT PARTING PP [s]                        | Coordi-nate - T - M1 - M2 [m]    | End misses target M1 - M2 [m] |  | REMARKS                 |    |  |
|                         |   |  |    | 4                            | 5              | 6            | 7             | 8                        | 9               | 10                     | 11                        | 12  | 13  | 14                               | 15                            |  | 16                      | 17 |  |
| 1                       | SHOOTING WITH 1 MISSILE RADIO-COMMANDE GUIDANCE EK12M 1 SPLV START -MARCH PHASE FORCEDLY LAU. | TO MEET BALLISTIC N=1 Tg=004[s]            | 25 | 65                           | 0.01           | 1.0          | 0             | 0                        | 0               | 0                      | 0                         | 0   | 178.99                                      | GROUND TARGET                    | 63210.06<br>47497.40          | 15713.99   | Δ=47.5[m]               |    |  |
| 2                       | SHOOTING WITH 1 MISSILE RADIO-COMMANDE GUIDANCE EK12M 1 SPLV START -MARCH PHASE               | TO MEET RCG + PN N=3.5 Tg=004[s]           | 25 | 35                           | 7              | 600          | 45            | 0.01*4<br>+2*π           | 8               | 0                      | 1                         | 30.71                                     | MODERN FIGHTER                              | 16571.00<br>16560.12<br>14887.79 | 11.28<br>2283.25              | Δ=5.5[m]   |                         |    |  |
| 3.1                     | SHOOTING WITH 1 MISSILE RADIO-COMMANDE GUIDANCE EK12M 1 SPLV START -MARCH PHASE               | OUTGOING RCG + PN N=3.5 Tg=004[s]          | 20 | 15                           | -3             | -350         | 45            | 0.01*4<br>+2*π           | 8               | 0                      | 1                         | 48.92                                     | MODERN FIGHTER                              | 31.125<br>27.466                 | 16.65.49                      | Δ=2.45[m]  |                         |    |  |
| 3.2                     | SHOOTING WITH 1 MISSILE RADIO-COMMANDE GUIDANCE EK12M 1 SPLV START -MARCH PHASE               | OUTGOING RCG + PN N=3.5 Tg=004[s]          | 20 | 15                           | -3             | -350         | 45            | 0.01*4<br>+2*π           | 8               | 0                      | 1                         | 55.22                                     | MODERN FIGHTER                              | 33329.45<br>29939.48<br>28936.74 | 1397.6<br>4399.88             | Δ=2.1[m]   |                         |    |  |
| 3.3                     | SHOOTING WITH 1 MISSILE RADIO-COMMANDE GUIDANCE EK12M 1 SPLV START -MARCH PHASE               | OUTGOING RCG + PN N=3.5 Tg=004[s]          | 20 | 15                           | -3             | -350         | 45            | 0.01*4<br>+2*π           | 8               | 0                      | 1                         | 41.48                                     | MODERN FIGHTER                              | 23519.4<br>23471.43              | 19.80                         | Δ=1.8[m]   |                         |    |  |
| 3.4                     | SHOOTING WITH 1 MISSILE RADIO-COMMANDE GUIDANCE EK12M 1 SPLV START -MARCH PHASE               | OUTGOING RCG + PN N=3.5 Tg=004[s]          | 20 | 15                           | -3             | -350         | 45            | 0.01*4<br>+2*π           | 8               | 0                      | 1                         | 41.64                                     | MODERN FIGHTER                              | 23575.4<br>23563.6<br>21743.3    | 11.84<br>1866.6               | Δ=1.8[m]   |                         |    |  |
| 4.1                     | DUAL-COUPLED SHOOTING WITH 2 MISSILES RCG+SARH AR EK12M 2SPLV                                 | PENDULUM RCG + PN N=3.5 Tg=004[s]          | 30 | 15                           | 3              | 150          | 10            | 0.1*4<br>+2*π            | 5               | 2                      | 1                         | 25.77                                     | HELICOPTER                                  | 14133<br>1422<br>12254           | 11.54<br>1881.65              | Δ=2.7[m]   |                         |    |  |
| 4.2                     | DUAL-COUPLED SHOOTING WITH 2 MISSILES RCG+SARH AR EK12M 2SPLV                                 | LOW-FLYING TARGET RCG + PN N=3.5 Tg=004[s] | 30 | 15                           | 0.02           | 115          | 10            | 0.1*4<br>+2*π            | 5               | 2                      | 1                         | 27.40                                     | (UAV) DRONE                                 | 14848<br>14837<br>13146          | 11.46<br>1747.68              | Δ=3.1[m]   |                         |    |  |
| 5.1                     | DUAL-COUPLED SHOOTING WITH 2 MISSILES RCG+SARH AR EK12M 2SPLV L1, L2                          | TO MEET RCG + PN N=3.5 Tg=004[s]           | 25 | 65                           | 7              | 600          | 45            | 0.001<br>+4*π            | 8               | 0                      | 1                         | 30.71                                     | MODERN FIGHTER                              | 16569.80<br>16559.82<br>14884.13 | 11.85<br>11.86<br>2034.33     | a) 11.85<br>b) 11.86<br>c) 20.84<br>d) 11.93<br>Δ=7.0[m] |                         |    |  |
| 5.2                     | DUAL-COUPLED SHOOTING WITH 2 MISSILES RCG+SARH AR EK12M 2SPLV L1, L2                          | TO MEET RCG + PN N=3.5 Tg=004[s]           | 25 | 65                           | 7              | 600          | 45            | 0.001*<br>+4*π           | 8               | 0                      | 1                         | 30.71                                     | MODERN FIGHTER                              | 10268.4<br>10258.6<br>8572.9     | 11.86<br>11.86<br>1904.8      | b) 11.86<br>Δ=7.0[m]                                     |                         |    |  |
| 6                       | DUAL-COUPLED SHOOTING WITH 2 MISSILES RCG+SARH AR EK12M 2SPLV                                 | OUTGOING RCG + PN N=3.5 Tg=004[s]          | 20 | 14                           | -3             | -250         | 45            | 0.01*2<br>+4*π           | 8               | 0                      | 1                         | 43.64                                     | MODERN FIGHTER                              | 24910<br>24898<br>23013          | 11.92<br>1904.1               | Δ=7.0[m]   |                         |    |  |
| 7                       | DUAL-COUPLED SHOOTING WITH 2 MISSILES RCG+SARH AS K-1M 2SPLV                                  | TO MEET RCG + PN N=3.5 Tg=004[s]           | 35 | 35                           | 12             | 550          | 45            | 0.01*2<br>+4*π           | 8               | 0                      | 1                         | 33.01                                     | MODERN FIGHTER                              | 16842.3<br>16831.8<br>14528.30   | 11.10<br>1904.06              | Δ=7.0[m]   |                         |    |  |
| 7                       | DUAL-COUPLED SHOOTING WITH 2 MISSILES RCG+SARH AS K-1M 2SPLV                                  | TO MEET RCG + PN N=3.5 Tg=004[s]           | 35 | 35                           | 12             | 550          | 45            | 0.01*2<br>+4*π           | 8               | 0                      | 1                         | 33.01                                     | MODERN FIGHTER                              | 16842.3<br>16831.8<br>14528.30   | 11.10<br>1904.06              | Δ=7.0[m]   |                         |    |  |
| 8                       | DUAL-COUPLED SHOOTING WITH 2 MISSILES RCG+SARH AR EK12M 2SPLV                                 | TO MEET RCG + PN N=3.5 Tg=004[s]           | 30 | 45                           | 10             | 440          | 0             | 0.01*2<br>+4*π           | 5               | 0                      | 1                         | 42.88                                     | CRITERION MANUFACTURE BOMBER                | 26131<br>26119<br>23332          | 11.12<br>1904.06              | Δ=7.0[m]   |                         |    |  |
| 9                       | DUAL-COUPLED SHOOTING WITH 2 MISSILES RCG+SARH AR EK12M 2SPLV                                 | TO MEET RCG + PN N=3.5 Tg=004[s]           | 25 | 35                           | 7              | 300          | 45            | 0.01*2<br>+4*π           | 8               | 0                      | 1                         | 39.57                                     | CRITERION MANUFACTURE ATTACK FIGHTER MIG-19 | 23128.70<br>23117.99<br>20946.75 | 11.07<br>1904.06              | Δ=7.0[m]   |                         |    |  |

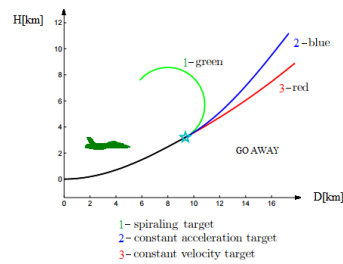
Then it examined individually shooting with one missile on modern target flying to meet in standardized height 7[km] and then dual shooting on target which are flow with zero radial velocity (helicopter) on 3[km]. Then engage targets outgoingm which is defined by the manufacturer in the development system (strategic bombers and attack fighter MIG-19).

It is taken case of shooting in the autonomous mode 2K12M and centralized (K-1M) management of fire from the upper-level. In the end results were compared for various modes of launching missiles (shooting with one missile and shooting with two coupled missiles, on different specific altitudes of 0.01-1[km], 3-7-12[km], and set speed targets in and check-out) as well as other parameters of the target (helicopter, drone, bomber, attack fighter, modern fighter- to meet and outgoing), testing time shift status missiles M1 and M2 and its impact on the ultimate failure, table 1.

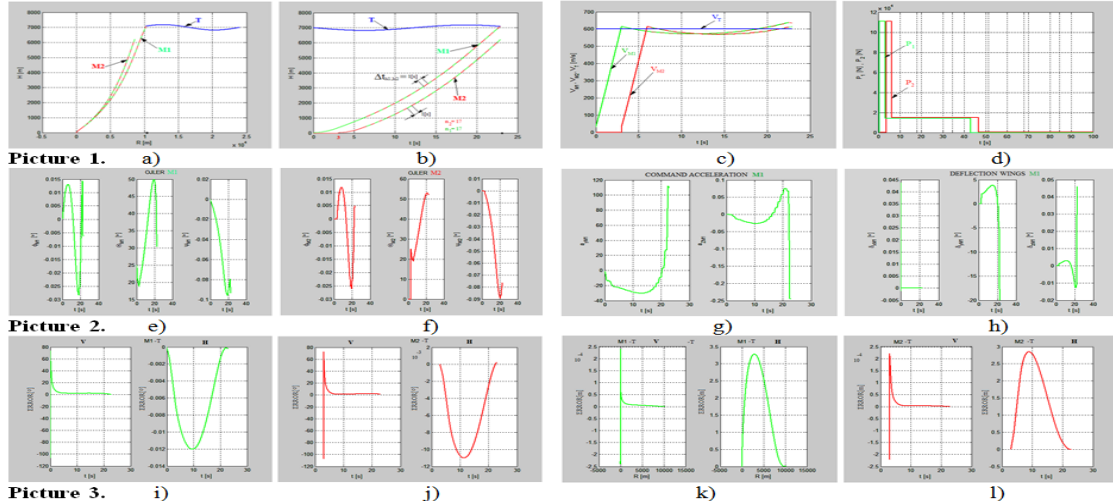
For that purpose given algorithm was used in pictures 3 and 4 for autonomous launching two coupled missiles with limited time simulation propulsion missile, with allow overload and parameters of target, etc. Used as real technical parameters of geometry missiles, its aerodynamic parameters, blend together in two coupled 6DOF dynamics model and and the kinematics associated with the module objective (uniform movement or maneuver as sinusoidal movement, or by changing the position and target vectors). In table 1, has shown results of simulation, for various modes of launching and variable of parameter target (elevation, distance, altitude, speed, maneuver, maneuver frequency, parameter). In the analysis was tested changed duration status of missile M1 and M2. For specific targets, criterion manufactures SA-6 missile system they were:

**Table 2.** Research optimal time simulation shift missiles M1,M2

| PARAMETERS<br>TARGET<br>(Table 1, ser.n.5.1) | ONE MISSILE             |                         | TWO MISSILES                                   |                         |                         |
|--|-------------------------|-------------------------|--|-------------------------|-------------------------|
|  | TO<br>MEET<br>md<br>[m] | GO<br>AWAY<br>md<br>[m] | SHIFT<br>MISSILES<br>$\Delta t_{M1,M2}$<br>[s] | TO<br>MEET<br>md<br>[m] | GO<br>AWAY<br>md<br>[m] |
| $E_{H_1} = 25$ [°]                           | 10.97                   | 11.85                   | 0.1  | 11.90                   |                         |
| $X_{C_1} = 25$ [km]                          |                         |                         | 0.5  | 11.95                   |                         |
| $H_t = 7$ [km]                               |                         |                         | 1  | 10.84                   | 11.28                   |
| $V_{C_1} = 600$ [m/s]                        |                         |                         | 2  | 11.97                   |                         |
| $V_{M_1} = 45$ [m/s]                         |                         |                         | 3  | 11.34                   |                         |
| $f_r = 0.01 \cdot 4 + 2 \cdot \pi$ [Hz]      |                         |                         | 4  | 11.85                   |                         |
| $R_{BRT} = 8$ [s]                            |                         |                         | 6  | 13.41                   |                         |
| $P_r = 0$ [km]                               |                         |                         | 8  | 16.81                   |                         |

**Figure 8.** Typical engagement geometry A-M**Figure 9.**

Starting conception strategies simulation of dual homing PVO missiles on one target:



strategic bombers and attack fighter, serial number 8. and 9. Tabele 1, was adopted as the optimal value time duration status of missile of  $t=1$  [s].

Appearance representative diagram of radiation, with two SPLV and tandem dual coupled AAD missiles, shown as a variable kinematic size and trajectory of target and missile, figure 9. Given failures PAAD missile, very well agree with a given dependence  $K_{ru} = f(r[m])$ , figure 6, referred to in [3], the original instructions – rules producer system. Pictures 1,2,3 show (a-l) the end results and given failures. Comparing the results, with the results of the launch of a single missile on same target, result in an improvement of about 3.9 -8.02 [%].

## 5. CONCLUSION

The obtained representative results show that the strategy of dual SARH, coupled guiding and leading missile, with optimal interval of time changed status of 1[s] improved around 8.02[%], for almost all targets and modes of shooting on average. Thereby were analyzed strict requirements, dictated by modern high performance targets (attack fighters) with curvilinear maneuver and in encounter and in leaving phase. Realistic performance of SA-6 were taken into account with from near and far boundary zone of launches and destruction, on various at different altitudes. It turned out that the results of the dual tandem rocket launching, the best solution for LF targets, the distance from the

launch 9[km], height 3[km], target speed 1,2[Ma], side overload of 8 [g] and with parameter 0[km]. The ultimate failure of the rocket is upgraded from 48.80[m] to 11.83[m], which is within the limits of efficient operations radar lighters, and it is 412[%], in relation to launch of a single missile on the same target. Due to the requirements set SA-6, which date from 55 years ago, use of dual launching of two missiles represent a good basis for observation and modification SAM in mid-range category. Further directions of research should be directed on expansion mutually coupled guidance on modern target with complex maneuver, improving the algorithm by the expanded method (PPN) and salvo launch of homing missiles SAM on one target.

## References

- [1] V.Shaferman, Y.Oshman., *Cooperative Interception in a Multi-Missile Engagement*, AIAA Guidance, Navigation and Control Conference, Chicago, Illinois, 2009.
- [2] S.Markovic, M.Milinovic, N.Sakan., *Test simulator for the discrete multi-parametric decision flight system*, OTEH-2014, Beograd, VTI.
- [3] UARJ PVO, *SSRP KUB-M –Teorija i Pravilo gađanja*, udbenik -122, VIZ Beograd, 1977.
- [4] MATLAB 2R2011a, Aerospace-modul, Simulink.
- [5] A.V.Bogdanov, V.A.Golubenko, J.A Gorešanić....., MO RF, Vojni univerzitet PVO, *Primena Doplerovske filtracije u višefunkcionim radiolokacionim kompleksima*, Moskva, 2001.





## The inverse bremsstrahlung absorption coefficients and Gaunt factors in astrophysical plasmas

This content has been downloaded from IOPscience. Please scroll down to see the full text.

2017 J. Phys.: Conf. Ser. 810 012059

(<http://iopscience.iop.org/1742-6596/810/1/012059>)

View [the table of contents for this issue](#), or go to the [journal homepage](#) for more

Download details:

IP Address: 80.82.77.83

This content was downloaded on 23/07/2017 at 13:16

Please note that [terms and conditions apply](#).

You may also be interested in:

[Intensity dependence of the inverse bremsstrahlung absorption coefficient in hot plasmas](#)

T P Hughes and M B Nicholson-Florence

[Multiphoton inverse bremsstrahlung](#)

H Brysk

[Pulsed Nd:YAG laser welding qualitative features](#)

J Sabbaghzadeh, S Dadras and M J Torkamany

[Measurements of the heat flux, inverse bremsstrahlung absorption and equilibration in an under-dense laser heated plasma](#)

A Dyson, A E Dangor, A K L Dymoke-Bradshaw et al.

[The effects of the use of different shielding gas mixtures in laser welding of metals](#)

M H Glowacki

[Vapor-plasma plume investigation during high-power fiber laser welding](#)

P Yu Shcheglov, A V Gumenyuk, I B Gornushkin et al.

[Space-dependent characterization of laser-induced plasma plume during fiber laser welding](#)

Xianfeng Xiao, Lijun Song, Wenjia Xiao et al.

[Study of the effect of low-power pulse laser on arc plasma and magnesium alloy target in hybrid welding by spectral diagnosis technique](#)

Liming Liu and Xinfeng Hao

[Analytical formulae for the inverse bremsstrahlung absorption coefficient](#)

J R Stallcop and K W Billman

# The inverse bremsstrahlung absorption coefficients and Gaunt factors in astrophysical plasmas

A A Mihajlov<sup>1</sup>, V A Srećković<sup>1</sup>, N M Sakan<sup>1</sup>, Lj M Ignjatović<sup>1</sup>,  
Z Simić<sup>2</sup> and M S Dimitrijević<sup>2,3,4</sup>

<sup>1</sup> University of Belgrade, Institute of Physics, P. O. Box 57, 11001 Belgrade, Serbia

<sup>2</sup> Astronomical Observatory, Volgina 7, 11160 Belgrade 74, Serbia

<sup>3</sup> IHIS-Technoexperts, Bežanijska 23, 11080 Zemun, Serbia

<sup>4</sup> Observatoire de Paris, 92195 Meudon Cedex, France

E-mail: mihajlov@ipb.ac.rs

**Abstract.** In this paper we present the method of determination of the electron-ion inverse Bremsstrahlung characteristics in order to cover the corresponding stellar atmosphere models. The used method is based on cut-off Coulomb model potential. It is shown that determination of these characteristics i.e. the absorption coefficients and Gaunt factors can be successfully performed in the region of electron densities from  $10^{13} \text{ cm}^{-3}$  to  $3 \cdot 10^{19} \text{ cm}^{-3}$  and temperatures from 3000 K to 50000 K within the wavelength region  $100 \text{ nm} \leq \lambda \leq 3000 \text{ nm}$ .

## 1. Introduction

After examining the existing literature about inverse "Bremsstrahlung" process [1, 2, 3, 4, 5], it could be seen that the most of presented papers are devoted to the determination of the corresponding Gaunt factor. Namely, the exact relation for the differential cross section for the direct "Bremsstrahlung" process exist for a long time [6]. This automatically led to the possibility of the exact term for the inverse "Bremsstrahlung" cross section  $\sigma_{i.b.}^{(ex)}(E, \varepsilon_{ph})$ , for the considered inverse "Bremsstrahlung". However, the practical applicability of mentioned strict relation was complex, which suggested the search of a practical ways for describing inverse "Bremsstrahlung". Therefore, it has been taken the simple and widely used quasi classical (Kramer's) cross section for the direct and inverse "Bremsstrahlung" process. The idea was to present exact  $\sigma_{i.b.}^{(ex)}(E, \varepsilon_{ph})$  in a form

$$\sigma_{i.b.}^{(ex)}(E, \varepsilon_{ph}) = \sigma_{i.b.}^{q.c.}(E, \varepsilon_{ph}) \cdot g_{i.b.}(E, \varepsilon_{ph}), \quad (1)$$

where  $g_{i.b.}(E, \varepsilon_{ph})$  is the adequate defined Gaunt factor. Because of that, further step was to find a simple approximations for the Gaunt factor  $g_{i.b.}(E, \varepsilon_{ph})$  in relation (1). The mentioned exact and approximated absorption coefficient are denoted with  $k_{i.b.}^{(ex)}(\lambda, T; N_e)$  and  $k_{i.b.}^{q.c.}(\lambda, T; N_e)$ , where  $N_e$  is free electron density. Here it is taken into account that in our case (single charged ions) the ion density is equal to electron density  $N_e$ . Consequently, these coefficients are connected with the relation

$$k_{i.b.}^{(ex)}(\lambda, T; N_e) = k_{i.b.}^{q.c.}(\lambda, T; N_e) \cdot G_{i.b.}(\lambda, T), \quad (2)$$

where  $G_{i.b.}(\lambda, T)$  is the required Gaunt factor. The determination of such averaged Gaunt factor as a function of  $\lambda$  and  $T$  was the object of investigation in the majority of previous papers devoted to the inverse "Bremsstrahlung" process (see e.g. [1, 2, 3, 4]).

In connection with the relations (1) and (2) it is needed to keep in mind the fact that exact terms for the inverse "Bremsstrahlung" process are determined in the case of scattering of the free electron onto the Coulomb potential. This means that mentioned exact terms are strictly applicable on the case of diluted plasma. It is clear that the same holds for all approximate relations which were obtained by now on the basis of these terms. From above mentioned it follows that all such relations become the unusable in the case of plasma of higher densities, e.g. non-ideal plasma. The aim of this work is to find such relations for  $\sigma_{i.b.}^{(ex)}(E, \varepsilon_{ph})$  which could be applicable in the case of different stellar atmospheres (with higher densities), where the values of the electron density changes from  $N_e \sim 10^{13} \text{ cm}^{-3}$  to  $N_e \sim 10^{20} \text{ cm}^{-3}$ .

## 2. Theory

This work is continuation of our previous investigation devoted to the examination of the opacity of the weakly and strongly ionized parts of the solar photospheres and lower chromospheres and different helium rich white dwarfs atmospheres [7, 8, 9, 10, 11, 12, 13]. The aim of this work is determination of such absorption coefficient  $k_{i.b.}^{(ex)}(\lambda, T; N_e)$  and Gaunt factor  $G_{i.b.}(\lambda, T)$  which could be applicable on the case of plasma with higher densities. Because of that, we applied a model potential, specially adopted for the description of the electron scattering onto the ion inside plasma i.e. cut-off Coulomb potential, described by the relations  $U_{cut}(r) = -\frac{e^2}{r} + \frac{e^2}{r_{cut}}$  if  $0 < r \leq r_{cut}$  and  $U_{cut}(r) = 0$ , if  $r_{cut} < r$ .

Here, we use the procedure of the determination of inverse Bremsstrahlung cross-section which is improved comparing to [12]. Using this improved procedure in this work were performed calculations of the corresponding Gaunt factor in the wide region of electron densities and temperature which can be used in connection with the different astrophysical and laboratory plasmas. Special calculations were made in order to determine free-free spectral absorption coefficients for the different stellar atmosphere models. Here we take  $\kappa_{i.b.}^{(ex)}$  in the form

$$\kappa_{i.b.}^{(ex)}(\varepsilon_\lambda; N_e, T) = N_e^2 \cdot \int_0^\infty \sigma_{i.b.}^{(ex)}(E; E') v \cdot f_T(v) \cdot 4\pi v^2 dv \cdot \left(1 - \exp\left[-\frac{\hbar\omega}{kT}\right]\right), \quad (3)$$

where  $f_T(v)$  is the corresponding Maxwellian distribution function for given temperature  $T$ . On the other hand quasi classical Kramer's  $k_{i.b.}^{q.c.}(\lambda, T; N_e)$  is given by the known expression

$$k_{i.b.}^{q.c.}(\lambda, T; N_e) = N_e^2 \cdot \frac{16\pi^{5/2}\sqrt{2}e^6}{3\sqrt{3}cm^{3/2}\varepsilon_{ph}^3} \frac{\hbar^2}{(kT)^{1/2}} \left(1 - \exp\left[-\frac{\hbar\omega}{kT}\right]\right), \quad (4)$$

where  $\varepsilon_{ph} = 2\pi\hbar c/\lambda$ . According to this, averaged Gaunt factor  $G_{i.b.}(\lambda, T)$  is determined here from Eq. (2), where  $k_{i.b.}^{(ex)}(\lambda, T; N_e)$  and  $k_{i.b.}^{q.c.}(\lambda, T; N_e)$  are given by Eqs. (3) and (4).

It is important that within this work the inverse "Bremsstrahlung" absorption coefficients  $\kappa_{i.b.}^{(ex)}(\varepsilon_\lambda; N_e, T)$  are determined by Eq. (3), where the spectral absorption cross section  $\sigma_{i.b.}^{(ex)}(E; E')$  is calculated using the improved procedure from [12], where all relevant quantities are determined strictly numerically without any additional approximation.

## 3. Results and discussion

The calculations of the Gaunt factor  $G_{i.b.}(\lambda, T)$  and absorption coefficients  $k_{i.b.}^{(ex)}(\lambda, T; N_e)$  were carried out for the electron densities in the range from  $1 \cdot 10^{13} \text{ cm}^{-3}$  to  $3 \cdot 10^{19} \text{ cm}^{-3}$  and temperatures from  $3 \cdot 10^3 \text{ K}$  to  $1 \cdot 10^5 \text{ K}$ , and the observed wavelength region  $100 \text{ nm} < \lambda < 3000 \text{ nm}$

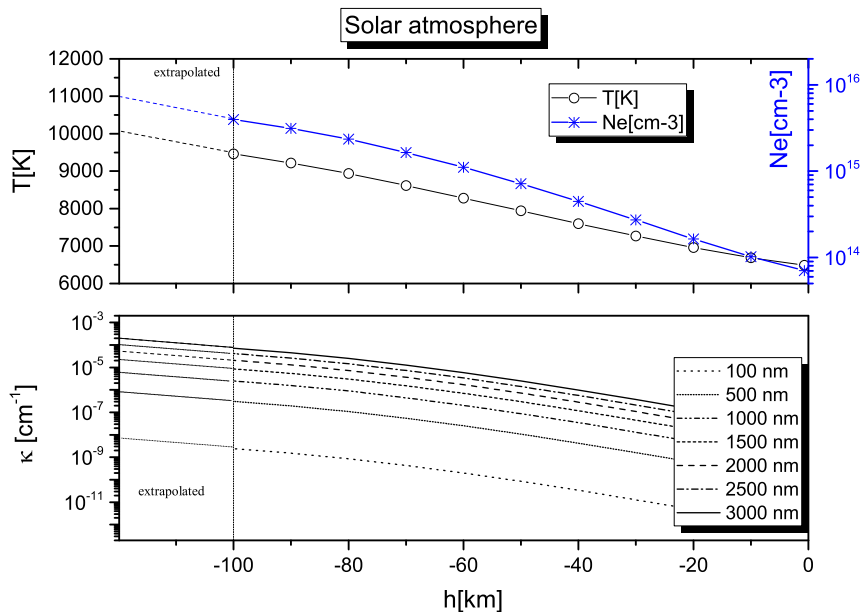


**Figure 1.** Upper panel: The behavior of  $T$  and  $N_e$  as a function of height within the considered part of the solar atmosphere model of [14]; lower panel: The absorption coefficient for inverse "Bremsstrahlung" processes within the considered part of the solar atmosphere model.

in order to cover the corresponding stellar atmosphere models. This is illustrated by Fig.1 which shows the behavior of the absorption coefficient for inverse "Bremsstrahlung" processes within the considered part of the solar atmosphere. Also the absorption coefficients for different DB white dwarf atmospheres were carried out. Here we highlight that the presented exact quantum mechanical method can be used to obtain the spectral coefficients for inverse "Bremsstrahlung" process for the broad class of plasma of higher non-ideality. We expect that the cut-off Coulomb potential model results are more accurate in comparison with other methods, which are so far used for cases of stellar plasma with higher non-ideality.

### Acknowledgments

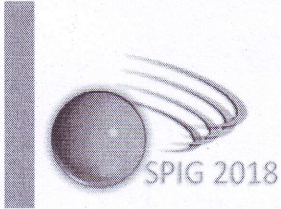
The authors are thankful to the Ministry of Education, Science and Technological Development of the Republic of Serbia for the support of this work within the projects 176002 and III4402.

### References

- [1] Berger J M 1956 *ApJ* **124** 550
- [2] Karzas W J, Latter R 1961 *ApJS* **6** 167
- [3] D'yachkov L G 1990 *J.Phys.B* **23** L429
- [4] van Hoof P A M, Williams R J R, Volk K, et al. 2014 *MNRAS* **444** 420
- [5] Armstrong G S J, Colgan J, Kilcrease D P, Magee N H 2014, *High Energy Density Physics* **10** 61
- [6] Sommerfeld A 1953, "Atombau und Spektrallinien", 2 Bnde (vol 2)
- [7] Mihajlov A A, Sakan N M, Srećković V A, Vitel Y 2011 *J.Phys. A* **44** 095502
- [8] Mihajlov A A, Sakan N M, Srećković V A, Vitel Y 2011 *Baltic Astronomy* **20** 604
- [9] Mihajlov A, Ignjatović L, Srećković V A, Dimitrijević M, Metropoulos A. 2013 *MNRAS* **431** 589
- [10] Ignjatović L M, Mihajlov A A, Srećković V A, Dimitrijević M S 2014 *MNRAS* **441** 1504
- [11] Ignjatović L M, Mihajlov A A, Srećković V A, Dimitrijević M S 2014 *MNRAS* **439** 2342
- [12] Mihajlov A A, Srećković V A, Sakan N M 2015 *Journal of Astrophysics and Astronomy* **36** 635
- [13] Srećković V A, Mihajlov A A, Ignjatović L M, Dimitrijević M S 2014 *Adv.Sp.Res.* **54** 1264
- [14] Fontenla J M, Balasubramaniam K S, Harder J 2007 *ApJ* **667** 1243



18



29<sup>th</sup> Summer School and  
International Symposium on  
the Physics of Ionized Gases

Aug. 28 - Sep. 1, 2018, Belgrade, Serbia

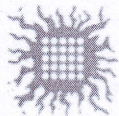
# CONTRIBUTED PAPERS

&

ABSTRACTS OF INVITED LECTURES,  
TOPICAL INVITED LECTURES, PROGRESS REPORTS  
AND WORKSHOP LECTURES

Editors:

Goran Poparić, Bratislav Obradović,  
Duško Borka and Milan Rajković



Vinča Institute of  
Nuclear Sciences



Serbian Academy  
of Sciences and Arts



**29<sup>th</sup> Summer School and International  
Symposium on the Physics of Ionized  
Gases**

August 28 – September 1, 2018, Belgrade, Serbia

**S P I G 2018**

*Editors:*  
Goran Poparić, Bratislav Obradović,  
Duško Borka and Milan Rajković

**CONTRIBUTED PAPERS**

*Publisher:*  
Vinča Institute of Nuclear Sciences  
University of Belgrade  
P.O. Box 5747, Belgrade, Serbia

**ABSTRACTS OF INVITED LECTURES,  
TOPICAL INVITED LECTURES, PROGRESS REPORTS  
AND WORKSHOP LECTURES**

*Computer processing:*  
Tajana Milovanović

*Editors*

*Printed by:*  
Scripta Interdiciplinaris  
Goran Poparić, Bratislav Obradović,  
Duško Borka and Milan Rajković

*Number of copies:*  
200

Vinča Institute of  
Nuclear Sciences

Serbian Academy  
of Sciences and Arts

All rights reserved. No part of this book may be reproduced, stored or transmitted in any manner without the written permission of the Publisher.

Belgrade, 2018



CONTRIBUTED PAPERS & ABSTRACTS OF INVITED  
LECTURES, TOPICAL INVITED LECTURES, PROGRESS  
REPORTS AND WORKSHOP LECTURES

of the 29<sup>th</sup> Summer School and International Symposium on  
the Physics of Ionized Gases

August 28 – September 1, 2018, Belgrade, Serbia

*Editors:*

Goran Poparić, Bratislav Obradović,  
Duško Borka and Milan Rajković

*Publisher:*

Vinča Institute of Nuclear Sciences,  
University of Belgrade,  
P.O. Box 522,  
11001 Belgrade, Serbia

*Computer processing:*

Tatjana Milovanov

*Printed by*

Skripta Internacional, Mike Alasa 54, Beograd

*Number of copies*

200

ISBN 978-86-7306-146-7

© 2018 by Vinča Institute of Nuclear Sciences, University of Belgrade

All rights reserved. No part of this book may be reproduced, stored or  
transmitted in any manner without the written permission of the Publisher.



## PHOTOABSORPTION CROSS SECTION OF A DENSE HYDROGEN PLASMA, MODEL METHOD

Nenad M. Sakan<sup>1\*</sup>, Vladimir A. Srećković<sup>1</sup>, Zoran J. Simić<sup>2</sup> and Milan  
S. Dimitrijević<sup>2,3</sup>

<sup>1</sup> *Institute of Physics, Belgrade University, Pregrevica 118, 11080 Zemun, Belgrade, Serbia* <sup>2</sup> *Astronomical Observatory, Volgina 7, 11060 Belgrade, Serbia* <sup>3</sup> *LERMA, Observatoire de Paris, UMR CNRS 8112, UPMC, 92195 Meudon Cedex, France.*

**Abstract.** Here are presented results of bound state transition modeling using the cut-off Coulomb model potential. The cut-off Coulomb potential has proven itself as a model potential for the dense hydrogen plasma. The main aim of our investigation include a further steps of improvement of the usage of model potential. The results deal with partially ionized dense hydrogen plasma. The presented results covers  $N_e = 6.5 \cdot 10^{18} \text{ cm}^{-3}$ ,  $T = 18000 \text{ K}$  and  $N_e = 1.5 \cdot 10^{19} \text{ cm}^{-3}$ ,  $T = 23000 \text{ K}$  where the comparison with the experimental data as well as with the theoretical values should take place. Since the model was successfully applied on continuous photoabsorption of dense hydrogen plasma in the broad area of temperatures and densities it is expected to combine both continuous and bound-bound photoabsorption within single quantum mechanical model with the same success.

### 1. INTRODUCTION

The problems of plasma opacity, energy transport and radiative transfer under moderate and strong non-ideality are of interest in theoretical and experimental research [1, 2, 3, 4]. The strong coupling and density effects in plasmas radiation were the subject of numerous experimental and theoretical studies in the last decades. In this paper we presented a new model way of describing atomic photo-absorption processes in dense strongly ionized hydrogen plasmas, which is based on the approximation of the cut-off Coulomb potential. By now this approximation has been used in order to describe transport properties of dense plasmas (see e.g. [1, 5, 6]), but it



was clear that it could be applied to some absorption processes in non-ideal plasmas too [3, 7, 8, 9]. More detailed explanation could be found in [10].

## 2. THEORY

### 2.1 The approximation of the cut-off Coulomb potential

Many body processes, namely:  $\varepsilon_\lambda + (H^+ + e)_i + S_{rest} \rightarrow (H^+ + e)_f + S'_{rest}$ , where  $S_{rest}$  and  $S'_{rest}$  denote the rest of the considered plasma are here considered simplified by the use of transformation to the corresponding single-particle processes in an adequately chosen model potential, for the detailed theory [10] should be considered.

As an adequate model potential for hydrogen plasma with such density we choose, as in [5, 3], the screening cut-off Coulomb potential, which satisfies above conditions, and is used in form

$$U_c(r) = \begin{cases} -\frac{e^2}{r} + \frac{e^2}{r_c}, & 0 < r \leq r_c, \\ 0, & r_c < r < \infty, \end{cases} \quad (1)$$

where the mean potential energy of an electron in the considered hydrogen plasma  $U_{p;c} = -e^2/r_c$  is used as a energy origin of the potential. Here  $e$  is the modulus of the electron charge,  $r$  - distance from the ion, and cut-off radius  $r_c$  - the characteristic screening length of the considered plasma.

It is important that the cut-off radius  $r_c$  can be determined as a given function of  $N_e$  and  $T$ , using two characteristic lengths,  $r_i = (k_B T / 4\pi N_i e^2)^{1/2}$  and  $r_{s;i} = (3N_i / 4\pi)^{1/3}$ , where  $N_i$  and  $r_{s;i}$  are the ion density and the corresponding Wigner-Seitz's radius and  $k_B$  - Boltzmann's constant. Namely, taking that  $N_i = N_e$  and  $r_c = a_{c;i} \cdot r_i$  we can directly determine the factor  $a_{c;i}$  as a function of ratio  $r_{s;i}/r_i$ , on the basis of the data about the mean potential energy of the electron in the single ionized plasma from [11]. The behavior of  $a_{c;i}$  in a wide region of values of  $r_{s;i}/r_i$  is presented in Fig. 1.

### 2.2 The calculated quantities

In accordance with that, the behavior of the dipole matrix element is investigated here. It is given by  $\hat{D}(r; r_c; n_i, l_i; n_f, l_f) = \langle n_f, l_f | \mathbf{r} | n_i, l_i \rangle$ , where the wave functions  $|n_i, l_i\rangle$  and  $|n_f, l_f\rangle$  are initial and final state wave functions obtained within the model of cut-off Coulomb potential.

The total absorption cross section of the line could be linked with the dipole moment directly with the help of relation

$$\sigma_0(\omega = \omega_{fi}) = \frac{1}{3} \frac{g_2}{g_1} \frac{\pi \omega_{fi}}{\varepsilon_0 \hbar c} \hat{D}(r; r_c; n_i, l_i; n_f, l_f)^2. \quad (2)$$

The total bound-bound absorption cross section for the "short" pulse from [12],  $N_e = 1.5 \cdot 10^{19} \text{ cm}^{-3}$ ,  $T = 23000 \text{ K}$  goes in the range



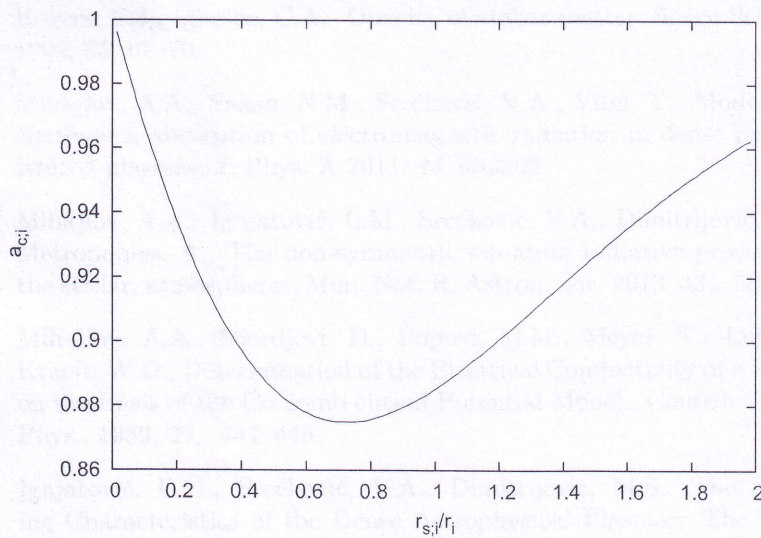


**Figure 1.** Behavior of the parameters  $a_{c,i} \equiv r_c/r_i$ , from [11], as the function of the ratio  $r_{s,i}/r_i$ , details on  $r_{s,i}$  and  $r_i$  are in the text.

from  $1,84 \cdot 10^{-7} \text{m}^2(\text{rad/s})^{-1}$  to  $1,72 \cdot 10^{-5} \text{m}^2(\text{rad/s})^{-1}$  . and for the "long" pulse,  $N_e = 6.5 \cdot 10^{18} \text{cm}^{-3}$ ,  $T = 18000 \text{K}$ , from  $1.99 \cdot 10^{-8} \text{m}^2(\text{rad/s})^{-1}$  to  $2.25 \cdot 10^{-5} \text{m}^2(\text{rad/s})^{-1}$  .

### 3. CONCLUSION

The presented results are step forward towards inclusion of the entire photo-absorption processes for hydrogen atom in plasma within the frame of the cut-off Coulomb potential model. One of the benefits of the presented results is a completely quantum mechanical solution for considered case, obtained from wave functions that are analytical and represented with the help of special functions, e.g. the influence of additional numerical source of errors is minimized as possible. The work on including model broadening process for each of energy levels, and inclusion in calculation is going on.

### REFERENCES

- [1] Fortov, V.E., Iakubov, I.T. The physics of non-ideal plasma; World Scientific, 1999.



- [2] Rogers, F.J., Iglesias, C.A. Opacity of stellar matter. *Space Sci. Rev.* 1998, 85, 61–70.
- [3] Mihajlov, A.A., Sakan, N.M., Srećković, V.A., Vitel, Y., Modeling of continuous absorption of electromagnetic radiation in dense partially ionized plasmas. *J. Phys. A* 2011, 44, 095502.
- [4] Mihajlov, A.A.; Ignjatović, L.M., Srećković, V.A., Dimitrijević, M.S., Metropoulos, A., The non-symmetric ion-atom radiative processes in the stellar, atmospheres, *Mon. Not. R. Astron. Soc.* 2013, 431, 589–599.
- [5] Mihajlov, A.A., Djordjevi, D., Popovi, M.M., Meyer, T., Luft, M., Kraeft, W.D., Determination of the Electrical Conductivity of a Plasma on the Basis of the Coulomb cut-off Potential Model., *Contrib. Plasma Phys.*, 1989, 29, 441–446.
- [6] Ignjatović, L.M., Srećković, V.A., Dimitrijević, M.S., The Screening Characteristics of the Dense Astrophysical Plasmas: The Three-Component Systems., *Atoms*, 2017, 5, 42.
- [7] Mihajlov, A.A., Sakan, N.M., Srećković, V.A., Vitel, Y., Modeling of the Continuous Absorption of Electromagnetic Radiation in Dense Hydrogen Plasma., *Balt. Astron.*, 2011, 20, 604–608.
- [8] Mihajlov, A.A., Srećković, V.A., Sakan, N.M., Inverse Bremsstrahlung in Astrophysical Plasmas: The Absorption Coefficients and Gaunt Factors., *J. Astrophys. Astron.*, 2015, 36, 635–642.
- [9] Sakan, N.M., Srećković, V.A., Mihajlov, A.A., The application of the cut-off Coulomb potential for the calculation of a continuous spectra of dense hydrogen plasma., *Mem. S. A. I. Suppl.*, 2005, 7, 221–224.
- [10] Sakan, Nenad M. and Srećković, Vladimir A. and Simi, Zoran J. and Dimitrijević, Milan S., The Application of the Cut-Off Coulomb Model Potential for the Calculation of Bound-Bound State Transitions, *Atoms*, 2018, 6, 1, 4
- [11] Mihajlov, A., Vitel, Y., Ignjatović, L.M., The new screening characteristics of strongly non-ideal and dusty plasmas. Part 3: Properties and applications., *High Temp.*, 2009, 47, 147–157.
- [12] Vitel, Y., Gavrilova, T., D'yachkov, L., Kurilenkov, Y.K., Spectra of dense pure hydrogen plasma in Balmer area., *J. Quant. Spectrosc. Radiat. Transf.*, 2004, 83, 387–405.

See discussions, stats, and author profiles for this publication at: <https://www.researchgate.net/publication/327239325>

# THE WORK ON INCLUSION OF THE BOUND-BOUND OPTICAL TRANSITION PROCESS WITHIN THE FRAME OF THE CUT-OFF COULOMB POTENTIAL MODEL – MAIN NUM....

Conference Paper · August 2018

CITATIONS

0

READS

22

4 authors:



**Nenad Sakan**

Institute of Physics Belgrade

45 PUBLICATIONS 233 CITATIONS

[SEE PROFILE](#)



**V. A. Srećković**

Institute of Physics Belgrade

113 PUBLICATIONS 287 CITATIONS

[SEE PROFILE](#)



**Zoran Simic**

Astronomska opservatorija

78 PUBLICATIONS 201 CITATIONS

[SEE PROFILE](#)



**Milan S. Dimitrijevic**

Astronomical Observatory Belgrade

1,125 PUBLICATIONS 3,657 CITATIONS

[SEE PROFILE](#)

Some of the authors of this publication are also working on these related projects:



Astronomy [View project](#)



History of Astronomy [View project](#)

The XII Symposium of Belarus and Serbia on  
Physics and Diagnostics of Laboratory and  
Astrophysical Plasmas

August 27-31, 2018, Belgrade, Serbia

# Proceedings

Eds. M. M. Kuraica, B. M. Obradović and N. Cvetanović

**Organized by:**  
Faculty of Physics,  
University of Belgrade  
Studentski Trg 12,  
Belgrade, Serbia



**Sponsored by:**  
Ministry of Education, Science  
and Technological Development  
of the Republic of Serbia



# THE WORK ON INCLUSION OF THE BOUND-BOUND OPTICAL TRANSITION PROCESS WITHIN THE FRAME OF THE CUT-OFF COULOMB POTENTIAL MODEL – MAIN NUMERICAL ERROR SOURCES

Nenad M. Sakan<sup>1</sup>, Vladimir A. Srećković<sup>1</sup>, Zoran J. Simić<sup>2</sup>  
and Milan S. Dimitrijević<sup>2,3</sup>

<sup>1</sup>*Institute of Physics, Belgrade University, Pregrevica 118, 11080 Zemun, Belgrade, Serbia*

<sup>2</sup>*Astronomical Observatory, Volgina 7, 11060 Belgrade, Serbia*

<sup>3</sup>*LERMA (Laboratoire d'Etudes du Rayonnement et de la Matière en Astrophysique et Atmosphères), Observatoire de Paris, UMR CNRS 8112, UPMC, 92195 Meudon CEDEX, France*

**Abstract.** In the process of inclusion of the bound-bound photo absorption processes within cut-off Coulomb potential model some of the numerical errors appeared. The analysis of the source of numerical errors led to conclusion about avoiding them and also led to the procedure for inclusion of more complex atom models.

## 1. INTRODUCTION

The strong coupling and density effects in plasmas radiation were the subject of numerous experimental and theoretical studies in the last decades. The description of a plasma behavior in a state of moderate and strong non-ideality is ongoing process, characteristics like plasma opacity, energy transport and radiative transfer are of interest in theoretical and experimental research since they are measurable quantities [1-4]. The implementing of all processes in the frame of the cut-off Coulomb potential model is work in progress, see for example [4,5], where more in depth analysis and further references could be found. Problems in such process are mostly related to the applied numerical solution procedure for the presented model, and some of them are successfully avoided. The presented work is a progress report on sought of sources of numerical errors and procedures to avoid them in the dense hydrogen plasma optical parameters description within the frame of cut-off Coulomb potential model.



## 2. THEORY

In the dense plasma, where strong coupling and collective effects are dominant, all the methods of description of plasma of small non-ideality are not either partially or completely applicable. One of the models used in description of the dense plasma behavior is the cut-off Coulomb potential model. The considered many body system could be reduced to the more easily describable model of a single ion inside plasma. The cut-off Coulomb potential model is complete quantum mechanical model of the dense plasma behavior, and since it posses the analytical solutions for the wave functions in the entire energy and radial region it is convenient for the calculations. The way of implementing the description of the optical properties of dense plasma in the frame of the mentioned model potential is to solve free-free cross section problem, and then to include bound-free, bound-bound absorption processes in dipole approximation.

The bound-bound absorption processes is considered here as a result of radiative transition in the whole system "electron-ion pair (atom) + the neighborhood", namely:

$$\varepsilon_i + (H^+ + e)_i + S_{rest} \rightarrow (H^+ + e)_f + S'_{rest}, \quad (1)$$

where  $S_{rest}$  and  $S'_{rest}$  denote the rest of the considered plasma. However, as it is well known, many-body processes can sometimes be simplified by their transformation to the corresponding single-particle processes in an adequately chosen model potential.

As an adequate model potential for hydrogen plasma with such density we choose, as in [6,7], the screening cut-off Coulomb potential, which satisfies above conditions, and can be presented in the form:

$$U(r; r_c) = \begin{cases} -\frac{e^2}{r}, & 0 < r \leq r_c, \\ U_{p;c}, & r_c < r < \infty, \end{cases}, \quad (2)$$

where the cut-off radius  $r_c$ , defined by the mean potential energy of an electron in the considered hydrogen plasma,  $U_{p;c} = -e^2 / r_c$ ,  $e$  is the modulus of the electron charge,  $r$  - distance from the ion, and cut-off radius  $r_c$  - the characteristic screening length of the considered plasma.

The mentioned potential is a strictly radial symmetric, and the solution for the wave functions and sought dipole moments and cross sections could be reduced to a radial part of wave function  $\psi(r) = R(r) / r$ .

Within the usage of the mentioned model, during a several years practice, the main source of numerical errors is determined as a procedure of bound state wave function determination. In the process of calculation of the wave functions for the mentioned radial wave function solutions, an appropriate



cut-off radius,  $r_c$ , is fixed, for the procedure for its determination please see some of the newer papers, e.g. [5]. After that, a procedure of determination of a bound state energy level and appropriate wave function took place. Since all of the energy and radius areas possess an adequate analytical function solution, the process of fitting of wave function is applied, e.g. the system of two equations are used, the equation of continuity and smoothness of the wave function. When such system of equations is solvable the appropriate energy level and wave function is reached.

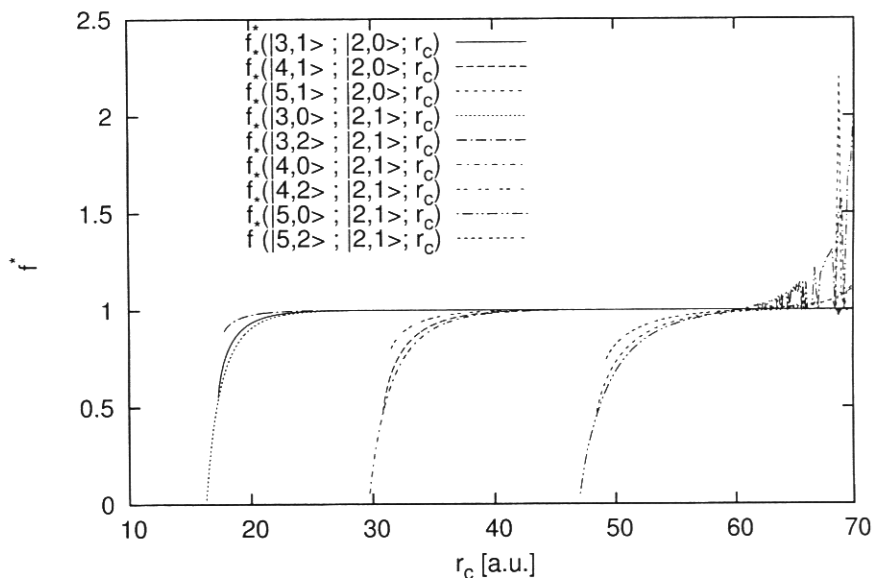


**Figure 1.** An example of a numerical “explosion” reflecting on the absorption oscillator strength for the bound-bound transitions,  $f^*$  is normalized on theoretical pure hydrogen values.

### 3. THE SOURCE OF PROBLEMS

As it was mentioned in the previous section, the continuity and smoothness of a wave function is sought as a root finding solution of a set of two special function equations. There are two problems laying within the process, the quality of the special function solution and the root finding itself. First of two problems was solved by the usage of a mathematical library, a GSL – gnu scientific library [8] had a best usable, most precise, solutions for the special functions. In this way, the first source of problem is avoided as good as possible. The second problem, the numerical root finding, has more severe reflection on the wave function itself. The sensitivity on the energy level step in root finding becomes more and more severe, the used Newton method for the root finding is capable of yielding a solution for the bound state energy with an almost entire

mantissa precision, but the sought wave function starts to possess a discontinuity in the first order derivative, it has not fulfill a smoothness condition. Fortunately, it appeared just for some of the wave functions in the area where the sought solution was not used in any of the analyzed plasma. When the convergence of the wave functions for the hydrogen model was analyzed, it was seen that the difference between our model solutions and the hydrogen model without plasma influence diminishes much faster than this problem occurs. An example of a numerical “explosion” is given in Figure 1 (on the right side of fig).

The behavior of the error in finding of the bound state energy levels and wave functions led to conclusion that the additional procedure for the smoothness of the wave function should be implemented. Furthermore, such a procedure implemented with a self-learning algorithm could be the way for implementing more complex atom models, where no theoretical wave functions exist for the atom without plasma influence.

#### 4. CONCLUSIONS

The determination of a main source of the numerical error in a procedure of cut-off Coulomb potential model bound state energy level and wave function determination had put a light not only on the method for avoiding of the unwanted numerical errors solution but also had shown a way of implementing such a procedure for the implementing of a more complex atom models.

#### Acknowledgements

This work is partially supported by our Ministry under the grant NO 176002.

#### REFERENCES

- [1] Fortov, V. E.; Iakubov, I. T. *The physics of non-ideal plasma*, (World Scientific, 1999).
- [2] Rogers, F. J., Iglesias, C. A. *Space Sci. Rev.*, **85**, p. 61–70 (1998).
- [3] Mihajlov, A. A., Sakan, N. M., Srećković, V. A., Vitel, Y. *J. Phys. A*, **44**, p. 095502 (2011).
- [4] Mihajlov, A. A., Ignjatović, L. M., Srećković, V. A., Dimitrijević, M. S., Metropoulos, A., *Mon. Not. R. Astron. Soc.*, **431**, p. 589–599 (2013)
- [5] Sakan N. M., Srećković V. A., Simić Z. J., Dimitrijević M. S. *Atoms.*, **6**(1), p. 4., (2018)
- [6] Mihajlov, A. A., Djordjević, D., Popović, M. M., Meyer, T., Luft, M., Kraeft, W. D., *Contrib. Plasma Phys.* **29**, pp. 441–446 (1989).
- [7] Mihajlov, A. A., Sakan, N. M., Srećković, V. A., Vitel, Y. , *Balt. Astron.*, **20**, pp. 604–608 (2011)
- [8] M. Galassi et al, *GNU Scientific Library Reference Manual* (3rd Ed.), ISBN 0954612078.



**30<sup>th</sup> Summer School and  
International Symposium on  
the Physics of Ionized Gases**

Šabac, Serbia,  
August 24 -28, 2020

**CONTRIBUTED PAPERS**

&

**ABSTRACTS of INVITED LECTURES,  
TOPICAL INVITED LECTURES and PROGRESS REPORTS**

**Editors:**

**Luka Č. Popović, Duško Borka,  
Dragana Ilić and Vladimir Srećković**



**БЕОГРАД  
2020**



**30<sup>th</sup> Summer School and  
International Symposium on  
the Physics of Ionized Gases**



August 24 – 28, 2020, Šabac, Serbia

# **S P I G 2020**

## **CONTRIBUTED PAPERS**

&

ABSTRACTS OF INVITED LECTURES,  
TOPICAL INVITED LECTURES AND  
PROGRESS REPORTS

*Editors*

Luka Č. Popović, Duško Borka,  
Dragana Ilić and Vladimir Srećković

Faculty of Mathematics  
(Department of Astronomy)  
Astronomical Observatory  
of Belgrade

Institute of Physics,  
University of Belgrade

Belgrade, 2020



**PUBLICATIONS OF THE ASTRONOMICAL OBSERVATORY OF BELGRADE**  
**FOUNDED IN 1947**

**EDITORIAL BOARD:**

Dr. Srdjan SAMUROVIĆ, Editor-in-Chief (Astronomical Observatory, Belgrade)

Dr. Rade PAVLOVIĆ (Astronomical Observatory, Belgrade)

Dr. Miroslav MIĆIĆ (Astronomical Observatory, Belgrade)

Dr. Branislav VUKOTIĆ (Astronomical Observatory, Belgrade)

All papers in this Publication are peer reviewed.

Published and copyright © by Astronomical Observatory, Volgina 7, 11060 Belgrade  
38, Serbia

Director of the Astronomical Observatory: Dr. Gojko Djurašević

Typesetting: Tatjana Milovanov

Internet address <http://www.aob.rs>

ISSN 0373-3742

ISBN 978-86-80019-94-9

Number of copies / tiraž : 250

Production: Skripta Internacional, Mike Alasa 54, Beograd

CIP - Каталогизација у публикацији - Народна библиотека Србије, Београд

537.56(082)

539.186.2(082)

539.121.7(082)

533.9(082)

**SUMMER School and International Symposium on the Physics of Ionized Gases (30 ; 2020 ; Šabac)**

Contributed papers & abstracts of invited lectures, topical invited lectures and progress reports / 30th Summer School and International Symposium on the Physics of Ionized Gases - SPIG 2020, August 24 - 28, 2020, Šabac, Serbia ; [organized by] Faculty of Mathematics (Department of Astronomy) [and] Institute of Physics, University of Belgrade [and] Astronomical Observatory of Belgrade ; editors Luka Č. Popović ... [et al.]. - Belgrade : Astronomical Observatory, 2020 (Beograd : Skripta Internacional). - 344 str. : ilustr. ; 24 cm. - (Публикације Астрономске опсерваторије у Београду, ISSN 0373-3742 ; св. 99 = Publications of the Astronomical Observatory of Belgrade ; no. 99)

Tiraž 250. - Str. 17-18: Preface / editors. - Bibliografija uz svaki rad. - Registar.

ISBN 978-86-80019-94-9

а) Јонизовани гасови -- Зборници б) Атоми -- Интеракција -- Зборници

в) Плазма -- Зборници

COBISS.SR-ID 18580233

# **SPIG 2020**

## **SCIENTIFIC COMMITTEE**

D. Borka (Co-chair), Serbia  
L. Č. Popović (Co-chair), Serbia

R. White, Australia  
J. Burgdörfer, Austria  
J. Cvetić, Serbia  
E. Danezis, Greece  
Z. Donko, Hungary  
V. Guerra, Portugal  
D. Ilić, Serbia  
M. Ivković, Serbia  
I. Mančev, Serbia  
D. Marić, Serbia  
N. J. Mason, UK  
A. Milosavljević, France  
K. Mima, Japan  
Z. Mišković, Canada  
L. Nahon, France  
B. Obradović, Serbia  
G. Poparić, Serbia  
P. Roncin, France  
I. Savić, Serbia  
Y. Serruys, France  
N. Simonović, Serbia  
M. Škorić, Japan  
M. Trtica, Serbia  
S. Tošić, Serbia

## **ADVISORY COMMITTEE**

D. Belić  
N. Bibić  
M. S. Dimitrijević  
S. Đurović  
N. Konjević  
M. M. Kuraica  
J. Labat  
G. Malović  
B. P. Marinković  
Z. Mijatović  
M. Milosavljević  
Z. Lj. Petrović  
L. Č. Popović  
J. Purić  
B. Stanić

## **ORGANIZING COMMITTEE**

D. Ilić (Co-chair)  
V. Srečković (Co-chair)  
J. Kovačević-Dojčinović (Co-secretary)  
N. Cvetanović (Co-secretary)  
J. Aleksić  
A. Kovačević  
S. Marčeta-Mandić  
A. Nina  
D. Onić  
S. Simić  
V. Zeković

## NUMEROV METHOD ANALYSIS WITH A GOAL OF APPLICATION OF COMPLEX PLASMA MODELS

NENAD M. SAKAN<sup>1</sup> and ZORAN SIMIĆ<sup>2</sup>

<sup>1</sup>*Institute of Physics Belgrade Pregrevica 118, Belgrade, Serbia*  
*E-mail nsakan@ipb.ac.rs*

<sup>2</sup>*Astronomical Observatory Volgina 7, P.O.Box 74 11060 Belgrade, Serbia*

**Abstract.** The dense plasma is a complex system, with its specifics in describing of related to more common plasma systems. It is proven that a Cut-off coulomb model potential had its advantages in describing of the hydrogen plasma of moderate up to the higher plasma non ideality. The need for introducing a more complex models of atom in plasma is needed. The further modification and development of a similar or more advanced model potentials is expected to produce a better and more applicable results. There is a need for fast and accurate enough method of their solution. In this paper the analysis of the logarithmic grid of Numerov method for solving a Hydrogen Coulomb potential is analyzed.

### 1. THEORY

Moderate and high density plasma is characterized by the strong inter particle forces, leading to the coupling of the charged species in plasma, see Fortov et al. 1989, Kobzev et al. 1995., Adamyan et al. 1994 and Adamyan et al. 2004 for example. In order to characterize a non ideality the parameter  $\Gamma$  is defined by

$$\Gamma = \frac{\langle E_{Coul} \rangle}{kT_e} = \frac{q_e^2}{4\pi\epsilon_0 kT_e} \sqrt[3]{\frac{4\pi n_e}{3}}, \quad (1)$$

for the plasma of temperature  $T_e$  and density  $n_e$ , note that in the local thermodynamical equilibrium an electron temperature and electron density could be used. Non ideality parameter itself presenting a ratio of Coulomb inter particle interaction in compare to average thermal energy of the plasma system. The  $\Gamma$  parameter for slightly and moderately non ideal plasma is within orders of 0.1 up to 10.

The plasma, as a collective phenomena, could be analyzed in a quantum mechanical approach, as a single particle which potentials is influenced by all the plasma species. The particle-plasma interaction is therefore described with the help of the pseudo potential. Having in mind that the closest neighbors reflect onto the mid range zone of the potential, where Coulomb potential weakness in comparison to their influence, while average plasma influence reflects as a constant potential level in a far field region. The cut-off Coulomb potential presents a good description of plasma influence in close vicinity of the analyzed particle, as well as in far field zone, so the

more complex forms of the pseudo potential is needed, see Mihajlov et al. 2011, Sakan 2010, Sakan et al. 2018 and Srećković et al. 2010. In general the potential of arbitrary form does not possess an analytical solution, so that numerical method for solution of a Schrödinger equation is needed.

In this paper an initial analysis of the stability of the numerical solution method took a place. As a main candidate the Numerov method with the logarithmic grid is selected.

### 1. 1. RADIAL PART OF THE SCHRÖDINGER EQUATION

In description of the plasma atom interaction a radial part of Schrödinger equation is used in order to calculate the radiative parameters of plasma

After introducing a new function  $R(r) = P(r)/r$  into the radial part of the Schrödinger equation, as well as the use of a modified potential  $\tilde{V}(r) = V(r) + (\hbar^2/2m)(l(l+1)/r^2)$ , simplifies the form of the radial part

$$-\frac{\hbar^2}{2m} \frac{d^2 P(r)}{dr^2} + \tilde{V}(r)P(r) = EP(r). \quad (2)$$

### 1. 2. NUMEROV METHOD FOR RADIAL SCHRÖDINGER EQUATION

The differential equation 2 is solvable with the help of Numerov method behind which a Taylor expansion of the differential equation is used. If the new function  $q(r) = \tilde{V}(r) - E$ , the differential equation takes the form  $P''(r) = q(r)P(r)$ . Having in mind that the Taylor expansion is valid for the linear mesh, e.g.  $r_i = i * h$ , where the notation  $P(r_i) \equiv P_i$  and  $q(r_i) \equiv q_i$  is used here. As it is known a solution for the radial function  $P_i$  is given by

$$P_{i+1} = \frac{12[2P_i - P_{i-1}] + h^2[10q_i P_i - q_{i-1} P_{i-1}]}{12 - h^2 q_{i+1}} - \frac{P_i^{(6)} h^6}{20(12 - h^2 q_{i+1})}, \quad (3)$$

where  $P_i^{(n)} \equiv \frac{d^n}{dr^n} P(r_i)$ . The first order differential is given by

$$P'_i = \frac{1}{12h} [P_{i-2} - 8P_{i-1} + 8P_{i+1} - P_{i+2}] - \frac{h}{60} [q_{i-2} P_{i-2} - 2q_{i-1} P_{i-1} + 2q_{i+1} P_{i+1} - q_{i+2} P_{i+2}] - \frac{11}{2520} P_i^{(7)} h^7. \quad (4)$$

More details about the application of the Numerov procedure from Noumerov 1924, and the application onto the radial Schrödinger equation could be seen in Paolo Giannozzi 2012/2013 and Havlová et al. 1984. It could be seen from the previous equations that an error of the Numerov method could be estimated easily and is well behaved in most of the radial part of the function space. In order to avoid the problems related to the accumulation of the numerical error as well as to adopt for a more realistic grid for the differential equation that has to be solved, a new variable is introduced,  $x = x(r)$ ,  $dx = x'(r)dr$ . For the logarithmic grid a function is given by

$$x(r) = \log\left(\frac{Zr}{a_0}\right), \quad \Delta x = \frac{a_0}{Zr} \delta r. \quad (5)$$

in order for system to be solvable by a Numerov method on a different grid  $x_i = x_0 + h * i$ . In a case of logarithmic grid a function  $y(x) = P(r(x))/\sqrt{r(x)}$  neutralizes the first

order differential and preserves a form of differential equation  $y''(x) = q(r(x))y(x)$ , solvable by a Numerov method.

## 2. TEST PROCEDURE AND RESULTS

The analysis is performed using the Coulomb potential, e.g. the solution are for the hydrogen atom without the influence of the plasma, since the stability is expected to be the same with more complex pseudo potentials and the Coulomb one have an analytical and known solutions.

Here we applied the Numerov procedure method that uses two separate solution, outward integration, from the smallest radius values to the end of the classical solution zone, and other, inward integration, from the largest values of the radius down to the joining point. The solution is possible only for some values of the energy levels, so the shooting method is applied in order to search for the values of the bond state energy.

As it is known, the convergence of the potential and physical meaning of the wave function led to asymptotic solutions used for the initial values of the numerical solution presented by

$$R(r)|_{r \rightarrow 0} \sim r^l, \quad P(r)|_{r \rightarrow 0} \sim r^{l+1}, \quad (6)$$

and for the large values of  $r$

$$R(r)|_{r \rightarrow \infty} \sim r^{n-1} \exp\left\{-\frac{Zr}{na_0}\right\}, \quad P(r)|_{r \rightarrow \infty} \sim r^n \exp\left\{-\frac{Zr}{na_0}\right\}. \quad (7)$$

In order to study a stability of the procedure of variation of a second initial value is involved. With the help of varying parameter  $\varepsilon$  the second bond value in both inward and outward integration is varied, mathematically could be presented as

$$F_0 = F_0, \quad F_1^{NEW} = k * F_1, \quad F_N = F_N, \quad F_{N-1}^{NEW} = k * F_{N-1}, \quad (8)$$

$$F \equiv [R(r), P(r)] \quad k = (1 + \varepsilon), \quad \varepsilon \in (-1, 1)$$

In this analysis a parameter  $\varepsilon$  took values  $[-0.1, -0.05, -0.01, -0.005, -0.001, 0, 0.001, 0.005, 0.01, 0.05, 0.1]$ . All of these parameter values, in exception of  $-0.1$ , that are smaller or equal to 0, led to the same energy values with the relative error smaller than  $10^{-5}$ . In the case of the smallest values for  $\varepsilon > 0$  the result yields a lower energy state, otherwise the numerical solution will be colapsed.

## 3. CONCLUSION

The preliminary test led a conclusion that the numerical integration method, particularly the Numerov type integration method with logarithm and  $1/r^3$  grid could be used for solving of model potential of dense hydrogen plasma, Havlová et al. 1984. In analyzed cases there is an exact mathematical form of the wave function. The analysis of the stability of the solution with the initial values on the Coulomb potential led us to conclusion that the model is also usable for cut-off Coulomb model potential. The method possesses fast convergence toward to a solution, and because of that is very applicable when using it in more complex analysis, as well as for coupling with molecular dynamics codes. Even more, it gave an opportunity to solve more complex



| $n$ | $l$ | $E_{calc}/E_H$ | $dE/E$     |
|-----|-----|----------------|------------|
| 1   | 0   | 0.9998168      | -0.0001832 |
| 2   | 0   | 0.9999084      | -0.0000916 |
|     | 1   | 1.0000000      | 0.0000000  |
| 3   | 0   | 0.9999387      | -0.0000613 |
|     | 1   | 1.0000000      | 0.0000000  |
|     | 2   | 1.0000000      | 0.0000000  |
| 4   | 0   | 0.9999442      | -0.0000458 |
|     | 1   | 1.0000000      | 0.0000000  |
|     | 2   | 1.0000000      | 0.0000000  |
|     | 3   | 1.0000000      | 0.0000000  |
| 5   | 0   | 0.9999632      | -0.0000368 |
|     | 1   | 1.0000000      | 0.0000000  |
|     | 2   | 1.0000000      | 0.0000000  |
|     | 3   | 1.0000000      | 0.0000000  |
|     | 4   | 1.0000000      | 0.0000000  |

Table 1: Calculated energy for the unmodified initial values.

model potential in order to describe different atoms in dense plasma. The further analysis is needed for development of a method for determination and avoid of numerical errors in solution, as well as to optimize a procedure for best mesh densities selection.

### References

- Adamyán, V. M., Djurić, Z., Ermolaev, A. M., Mihajlov, A. A., Tkachenko, I. M.: 1994, *J.Phys.D*, **27**, 111.
- Adamyán V. M., Djurić Z., Mihajlov, A. A., Sakan, N. M., Tkachenko, I. M.: 2004, *J.Phys.D.*, **37**, 1896.
- Fortov V. E., Iakubov I. T.: 1989, *Physics of Nonideal Plasma*, Hemisphere, New York
- Havlová, H., Smrčka, L.: 1984, *Czech J Phys* **34**, 961.
- Kobzev G., Jakubov I., Popovich M. (Eds.): 1995., *Transport and Optical Properties of Non-Ideal Plasmas*, Plenum Press, New York, London.
- Mihajlov, A. A., Sakan N. M., Srećković V. A., Vitel Y.: 2011, *Baltic Astron.* **20**, 604.
- Noumerov, B. V.: 1924, *MNRAS* **84**, 8., 592.
- Paolo Giannozzi: 2012/2013, lecture notes: *Numerical Methods in Quantum Mechanics*, Corso di Laurea Magistrale in Fisica Interateneo Trieste.
- Sakan, N. M.: 2010, *Journal of Physics: Conference Series*, **257**, 012036.
- Sakan, N.M., Srećković, V.A., Simić, Z.J., Dimitrijević, M.S.: 2018, *Atoms* **6**, 4.
- Srećković, V. A., Ignjatović, L. M., Mihajlov, A. A., Dimitrijević, M. S.: 2010, *MNRAS*, **406** 590.

FLOWING DISCHARGES IN  $Ar - H_2$  MIXTURES

N. M. Sakan<sup>(1)</sup>, M. Ivkovic<sup>(1)</sup>, J. D. Drake<sup>(2)</sup>, S. Popovic<sup>(3,\*)</sup>, L. Vuskovic<sup>(3)</sup>  
 Contacting author<sup>(3,\*)</sup>

<sup>(1)</sup> Institute of Physics, Belgrade, Serbia

<sup>(2)</sup> University of Iowa, Iowa City, IA, USA

<sup>(3)</sup> Old Dominion University, Norfolk, VA, USA

<sup>(\*)</sup> spopovic@odu.edu

A prospective unseeded hydrogen plasma-based high-Mach number fuel is a complex mixture of at minimum three initial species: noble gas ( $Ar$ ), hydrogen, and air. Noble gas is added in the mixture to reduce the penalty of ionization. However, the presence of hydrogen, nitrogen, and oxygen molecules leads to complex branching inter-radical chemistry, which may result in the decrease of the degree of ionization. These processes are poorly understood and their study is the primary motivation for the present work. Effects on plasma properties upon addition of hydrogen have been noted in many cases [1-4].

In this work we are comparing experimental results on the decrease of ionization in an  $Ar$  plasma with variable (1 – 10 %) addition of hydrogen in two flowing pulsed discharges – microwave cavity discharge operating in the initial pressure range from 0.1 to 10  $kPa$  (static pressure range from 0.5 to 50  $kPa$ ) and a pulsed dc discharge operating in the initial pressure range 1 to 10  $kPa$ , but at static pressure 20 to 400  $kPa$ . Apart from the pressure range, the two discharges differ in the degree of ionization, and departure from Saha equilibrium. Both discharges could serve as generic plasma sources for flowing combustion reactors, one at sub-atmospheric and other at super-atmospheric pressures serving as fuel reformation devices in renewable energy sources.

The initial question how addition of hydrogen in Argon plasma affects the discharge kinetics and parameters at sub-atmospheric and super-atmospheric pressures is addressed in this paper. Further addition of fuel components was planned and executed in the supersonic, low pressure version [1], but it is still in preparation for the high pressure version.

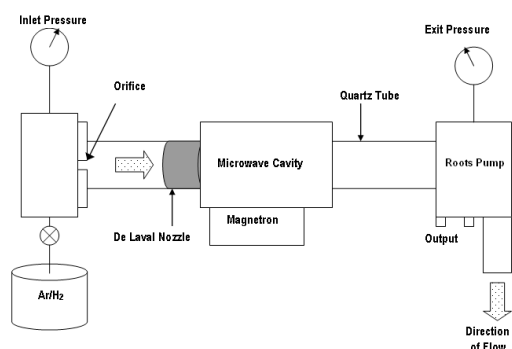


Fig. 1: Scheme of supersonic microwave discharge.

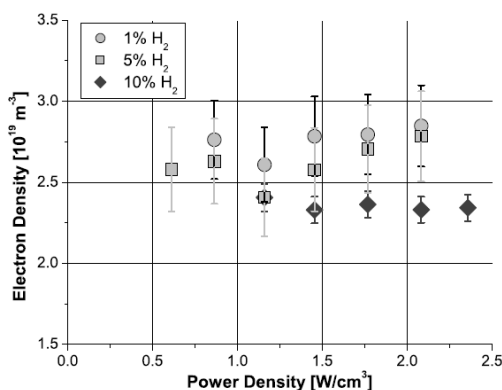


Fig. 2: Electron density drop in the cavity microwave discharge at 300  $Pa$ , with different initial amounts of  $H_2$  in the mixture. Statistical error is indicated.

The pulsed light source used for this study is laboratory made low pressure pulsed plasma source of specific design [5] with possibility to generate high electron number density helium plasma with  $N_e$  up to  $10^{24} m^{-3}$ . The schematic drawing of discharge tube, together with experimental setup is given in Fig. 3. The separation between tungsten electrodes (placed inside a quartz

tube with an inner diameter of 8 mm) was 8 cm. Each electrode has a 0.6 mm diameter central opening to enable interferometric and spectroscopic measurements along the axis of plasma column.

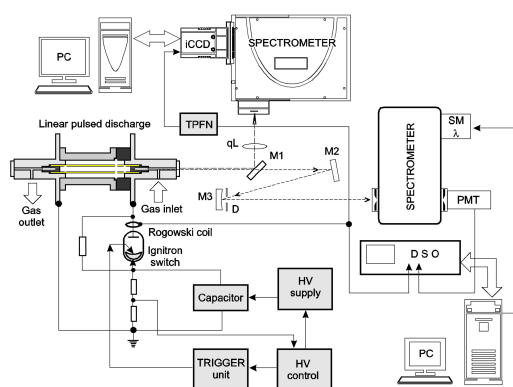


Fig. 3: Experimental setup

The discharge was driven by the low inductance  $15 \mu\text{F}$  capacitor charged in this experiment up to  $6 \text{ kV}$ . In order to decrease the circuit inductance three electric cables are coaxially connected with cathode. For data acquisition two different line shape recording systems were used. In the first one, see right hand side of Fig. 3, a  $1 : 1$  image of the plasma source is projected, by means of: flat  $M2$  and focusing  $M3$  mirror (diameter  $D = 50 \text{ mm}$  and focal length  $f = 100 \text{ cm}$ ), onto the entrance slit ( $15 \mu\text{m}$  wide and  $1 \text{ mm}$  vertical opening) of a  $1 \text{ m}$  monochromator (inverse linear dispersion  $0.833 \text{ nm/mm}$ ). Behind the exit slit ( $15 \mu\text{m}$ ) of the spectrometer thermoelectrically cooled photomultiplier (PMT) EMI 9813QB was mounted. The second data acquisition system is based on a  $0.3 \text{ m}$  Shamrock 303 spectrometer equipped with Andor ICCD camera DH724. A  $1 : 1$  image of the plasma source was projected on the  $10 \mu\text{m}$  entrance slit by means of an optional folding mirror  $M1$  and quartz focusing lens  $qL$  ( $D = 36 \text{ mm}$ ,  $f = 33.6 \text{ cm}$ ), see Figs. 1 and 2. The camera was synchronized with the trigger pulse forming network - TPFN activated by the pulse from the Rogowski coil.

Our primary aim is to determine the extent of ionization loss due to the addition of hydrogen and air in two discharges that are the closest by configuration to the anticipated plasma-assisted hydrogen combustion devices in high-Mach number gas flows. Additionally, we aim to use non-invasive, *in situ* diagnostic techniques to study the mechanisms of ionization loss and consequent decrease of active radicals needed for the enhancement of hydrogen oxidation.

## Reference

- [1] D. J. Drake, S. Popović, and L. Vušković, *J. Appl. Phys.*, **063305** (2008).
- [2] A. Bogaerts and R. Gijbels, *Spectrochim. Acta B* **57**, 1071 (2002).
- [3] C. V. Budtz-Jørgensen, P. Kringhøj, and J. Bøttiger, *Surf. Coat. Technol.* **116–119**, 938 (1999).
- [4] R. S. Mason, P. D. Miller, and I. P. Mortimer, *Phys. Rev. E*, **55**, 7462 (1997).
- [5] K. Grützmacher and U. Johannsen, *Spectral Line Shapes*, **Nova Science Publishers**

**THE MODELING OF THE CONTINUOUS ABSORPTION OF EM  
RADIATION IN HYDROGEN PLASMAS WITH ELECTRON  
DENSITIES ABOUT  $5 \cdot 10^{18} \text{ cm}^{-3}$  -  $1.5 \cdot 10^{19} \text{ cm}^{-3}$  AND  
TEMPERATURES ABOUT  $1.6 \cdot 10^4 \text{ K}$  -  $2.5 \cdot 10^4 \text{ K}$**

**A. A. Mihajlov<sup>1</sup>, N. M. Sakan<sup>1</sup>, V. A. Srećković<sup>1</sup> and Y. V. Vitel<sup>2</sup>**

<sup>1</sup>*Institute of Physics, Belgrade University, Pregrevica 118, Zemun,  
11080 Belgrade, Serbia*

<sup>2</sup>*UPMC Univ Paris 6, Laboratoire des Plasmas Denses,  
3 rue Galilée, 94200 Ivry sur Seine, France*

*E-mail: mihajlov@ipb.ac.rs*

In this work is examined a new modeling way of describing the continuous absorption of electromagnetic (EM) radiation in a dense partially ionized hydrogen plasma. It is shown that the obtained results give a possibility of calculating spectral absorption coefficients which characterize the relevant absorption processes in partially ionized hydrogen plasmas with electron densities about  $5 \cdot 10^{18} \text{ cm}^{-3}$  -  $1.5 \cdot 10^{19} \text{ cm}^{-3}$  and temperatures about  $1.6 \cdot 10^4 \text{ K}$  -  $2.5 \cdot 10^4 \text{ K}$ . The calculation method is applied to the wavelength region  $300 \text{ nm} < \lambda < 500 \text{ nm}$ . The presented results can be of interest for dense laboratory plasmas as well as for partially ionized layers of different hydrogen stellar atmospheres. Namely the plasma of the inner layers of solar atmosphere, as well as the plasmas of partially ionized layers of some other stellar atmospheres, for example some DA and DB white dwarfs.



**XVII NATIONAL CONFERENCE OF ASTRONOMERS OF SERBIA**  
Belgrade, 23-27 September 2014

**Scientific Organizing Committee:**

- S. Šegan (co-chair, Faculty of Mathematics, Belgrade)
- S. Ninković (co-chair, Astronomical Observatory, Belgrade)
- O. Atanacković (Faculty of Mathematics, Belgrade)
- S. Jankov (Astronomical Observatory, Belgrade)
- Z. Knežević (Astronomical Observatory, Belgrade)
- N. Pejović (Faculty of Mathematics, Belgrade)
- L. Č. Popović (Astronomical Observatory, Belgrade)
- D. Urošević (Faculty of Mathematics, Belgrade)
- S. Vidojević (IHIS Techno Experts, Belgrade)

**Local Organizing Committee:**

- A. Kovačević (co-chair, Faculty of Mathematics, Belgrade)
- B. Novaković (co-chair, Faculty of Mathematics, Belgrade)
- B. Arbutina (Faculty of Mathematics, Belgrade)
- A. Dobardžić (Faculty of Mathematics, Belgrade)
- D. Marčeta (Faculty of Mathematics, Belgrade)
- D. Onić (Faculty of Mathematics, Belgrade)
- M. Ž. Pavlović (Faculty of Mathematics, Belgrade)
- V. Radović (Faculty of Mathematics, Belgrade)
- M. Stojanović (Astronomical Observatory, Belgrade)
- M. M. Vučetić (Faculty of Mathematics, Belgrade)
- V. Vujčić (Astronomical Observatory, Belgrade)
- V. Zeković (Faculty of Mathematics, Belgrade)

Published by: Department of Astronomy, Faculty of Mathematics, Studentski trg 16,  
11000 Belgrade, Serbia and Astronomical Observatory, Volgina 7, 11060 Belgrade,  
Serbia

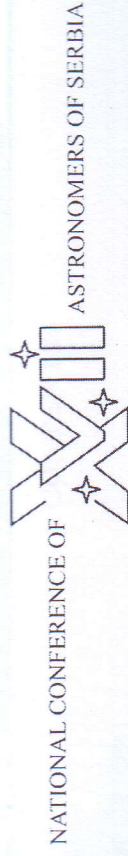
The publication of this issue is financially supported by the Ministry of Education,  
Science and Technological Development of the Republic of Serbia

Computer text design: T. Milovanov

ISBN 978-86-7589-098-0

Printed by: Kobdom, Vojvodjanska 41, Kovin

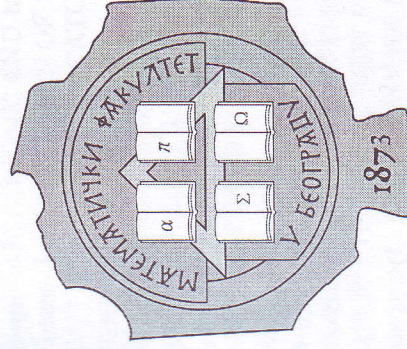
Number of copies: 170



**XVII NATIONAL CONFERENCE OF ASTRONOMERS OF SERBIA**  
Belgrade, 23 - 27 September 2014

**BOOK OF ABSTRACTS**

Eds. S. Šegan, S. Ninković, A. Kovačević and B. Novaković



Faculty of Mathematics

Astronomical Observatory

Belgrade 2014



СIP - Каталогизација у публикацији  
Народна библиотека Србије, Београд  
520/524(048)  
113/119(048)

NATIONAL Conference of Astronomers of Serbia  
(17 ; 2014 ; Београд)  
Book of Abstracts / XVIII National  
Conference of Astronomers of Serbia,  
Belgrade, 23 - 27 September 2014 ; eds. S.  
Šegan ... [et al.]. - Belgrade : Faculty of  
Mathematics, Department of Astronomy, 2014  
(Kovin : Kovidom). - 110 str. ; 24 cm

Tiraž 170. - Registrar.

ISBN 978-86-7589-098-0

а) Астрономија - Апстракти б) Астрофизика  
- Апстракти с) Космологија - Апстракти  
COBISS.SR-ID 209658124



PARTICIPATION OF SERBIA AT THE INTERNATIONAL  
OLYMPIAD IN ASTRONOMY AND ASTROPHYSICS  
IN 2012 AND 2013

S. Ninković<sup>1</sup>, S. Vidojević<sup>2</sup>, S. Anđelković<sup>3</sup>, F. Živanović<sup>4</sup>,  
V. Šarković<sup>3</sup>, S. Badža<sup>3</sup> and B. Simonović<sup>5</sup>

<sup>1</sup>Astronomical Observatory Belgrade, Volgina 7, P.O.Box 74 11060 Belgrade

<sup>2</sup>IHIS techno experts, Batajnički drum 23, 11080 Belgrade, Serbia

<sup>3</sup>Faculty of Physics, University of Belgrade, Studentski trg 16,  
11000 Belgrade, Serbia

<sup>4</sup>Faculty of Mathematics, University of Belgrade, Studentski trg 16,  
11000 Belgrade, Serbia

<sup>5</sup>Astronomical Society "Rudjer Bošković", Gornji grad 16,  
11000 Belgrade, Serbia

participation of contestants from Serbia at the VI International Olympiad in Astronomy and Astrophysics (IOAA) that took place in Brazil 2012, the VII IOAA took place in Greece 2013 and the Saint Petersburg Olympiad 2013 and 2014. One of the points examined in this poster. The poster will also discuss the position and preparation of contestants, volunteering done by the instructors, problems encountered and the contribution of the Mathematical High School grade. The poster will feature an in-depth review of the domestic competitions the teams for the international competitions were chosen, as well as a discussion of problems competitors were asked to solve. The international competitions, their organisation and the success of Serbian competitors will be analysed as well.

HF CHARACTERISTICS OF THE ASTROPHYSICAL PLASMAS

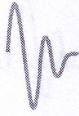
N. Sakan

*Institute of Physics, Pregrevnica 118, Zemun, 11000 Belgrade, Serbia*

*E-mail: nsakan@ipb.ac.rs*

The values of electrical conductivity of plasma of stars with a magnetic field or moving in the magnetic field of the other component in a binary system could be of significant interest, since they are useful for the study of thermal evolution of such objects, cooling, nuclear burning of accreted matter, and the investigation of their magnetic fields. So, on the basis of numerically calculated values for the dense plasma conductivity in an external HF electric field, we determine the HF characteristics of astrophysical plasmas under extreme conditions. The examined range of frequencies covers the IR, visible and near UV regions and consider electronic number density and temperature are in the ranges of  $10^{21} \leq N_e$  and  $20\,000 \leq T$ , respectively. The method developed here represents a powerful tool for research into white dwarfs with different atmospheric compositions (DA, DC etc.), and for investigation of some other stars (M-type red dwarfs, Sun etc.).





10<sup>th</sup> SCLSA  
Srebrno Jezero  
June 15-19, 2015  
Serbia

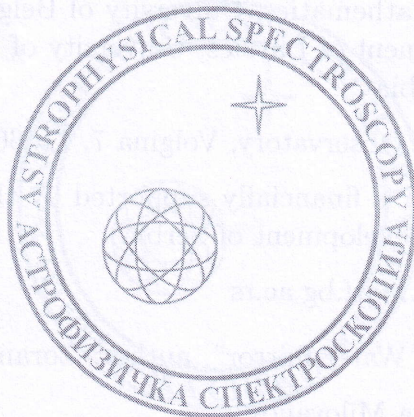


10<sup>th</sup> SCLSA  
Srebrno Jezero  
June 15-19, 2015  
Serbia

X SERBIAN CONFERENCE  
ON SPECTRAL LINE SHAPES IN ASTROPHYSICS

**BOOK OF ABSTRACTS**

Eds. Luka Č. Popović, Milan S. Dimitrijević and Saša Simić



Astronomical Observatory

Belgrade, 2015



# X SERBIAN CONFERENCE ON SPECTRAL LINE SHAPES IN ASTROPHYSICS

June 15-19, 2015, Srebrno jezero, Serbia

## Scientific Organizing Committee:

Luka Č. Popović (Serbia)  
Co-chairman

Milan S. Dimitrijević (Serbia)  
Co-chairman

Edward Baron (USA)

Nabil Ben Nessib (Saudi Arabia)

Emmanuel Danezis (Greece)

Peter Hauschildt (Germany)

Dragana Ilić (Serbia)

Darko Jevremović (Serbia)

Evencio Mediavilla (Spain)

Anatolij A. Mihajlov (Serbia)

Gillian Peach (United Kingdom)

Jagoš Purić (Serbia)

Sylvie Sahal-Bréchet (France)

Jack Sulentic (Spain)

Roland Stamm (France)

Aleksandar F. Zakharov (Russia)

## Local Organizing Committee:

Saša Simić  
Chairman

Edi Bon  
Secretary

Jovan Aleksić

Nataša Bon

Miodrag Dačić

Dragana Ilić

Andjelka Kovačević

Jelena Kovačević

Tanja Milovanov

Luka Č. Popović

Zoran Simić

Veljko Vujčić

Organized by: Astronomical Observatory Belgrade

Co-organizers: Faculty of Mathematics, University of Belgrade

Faculty of Sciences, Department of Physics, University of Kragujevac

Astronomical Society of Serbia

Published by: Astronomical Observatory, Volgina 7, 11060 Belgrade 38, Serbia

The publication of this issue is financially supported by the Ministry for Education,  
Science and Technological Development of Serbia

Website: <http://www.scslsa.matf.bg.ac.rs>

Picture on the back cover: "Water mirror", author: Zoran Simić

Computer text design: Tanja Milovanov

ISBN 978-86-80019-70-3

Printed by: Knjigovezačka radnja Kostić, ul. Radoja Domanovića 16,  
34000 Kragujevac

Number of copies: 100



**THE INVERSE BREMSSTRAHLUNG IN ASTROPHYSICAL  
PLASMAS: THE ABSORPTION COEFFICIENTS  
AND GAUNT FACTORS**

A. A. Mihajlov, N. M. Sakan and V. A. Srećković

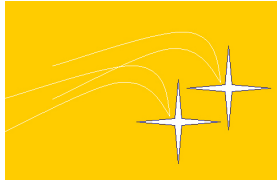
*Institute of Physics, Belgrade University, Pregrevica 118, Zemun,  
11080 Belgrade, Serbia*

*E-mail: nsakan@ipb.ac.rs*

The electron-ion inverse Bremsstrahlung is considered here as a factor of the influence on the opacity of the different stellar atmospheres and other astrophysical plasmas. It is shown that this process can be successfully described in the frames of cut-off Coulomb potential model within the regions of the electron densities and temperatures. The relevant quantum mechanical method of the calculation of the corresponding spectral coefficient processes is described and discussed. The results obtained for the plasmas with the electron densities from  $10^{14}\text{cm}^{-3}$  to  $10^{20}\text{cm}^{-3}$  and temperatures from  $5 \cdot 10^3\text{K}$  to  $3 \cdot 10^4\text{K}$  in the wavelength region  $200\text{nm} < \lambda < 500\text{nm}$  are presented. Also, these results can be of interest for different laboratory plasmas.





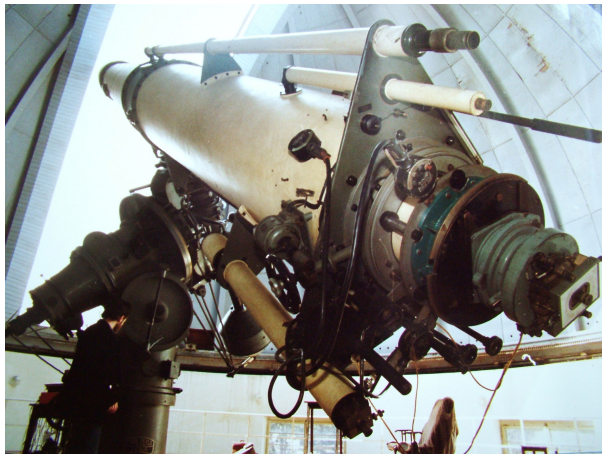


## **X SERBIAN-BULGARIAN ASTRONOMICAL CONFERENCE**

**May 30 - June 3, 2016, Belgrade, Serbia**

# **BOOK OF ABSTRACTS**

**Eds. Milan S. Dimitrijević and Milcho K. Tsvetkov**



**BELGRADE, 2016**



**INVERSE BREMSSTRAHLUNG CHARACTERISTICS IN DWARF  
ATMOSPHERES: THE ABSORPTION COEFFICIENTS  
AND GAUNT FACTORS**

**Anatolij A. Mihajlov<sup>1</sup>, Vladimir A. Srećković<sup>1</sup>, Nenad M. Sakan<sup>1</sup> and  
Milan S. Dimitrijević<sup>2,3,4</sup>**

<sup>1</sup>*University of Belgrade, Institute of Physics, P. O. Box 57, 11001, Serbia*

<sup>2</sup>*Astronomical Observatory, Volgina 7, 11160 Belgrade 74, Serbia*

<sup>3</sup>*IHIS-Technoexperts, Bežanijska 23, 11080 Zemun, Serbia*

<sup>4</sup>*Observatoire de Paris, 92195 Meudon Cedex, France*

E-mail: vlada@ipb.ac.rs

Here we determine the electron-ion inverse "Bremsstrahlung" characteristics for the case of the white dwarf atmospheres where such plasma characteristics as plasma density and temperature change in wide region. It is presented that determination of these characteristics i.e. the absorption coefficients and Gaunt factors can be successfully performed in the whole diapason of electron densities and temperatures which is relevant for the corresponding atmospheres.

The used quantum mechanical method of the calculation of the corresponding spectral absorption coefficient and Gaunt factor is described and discussed in details in the papers of Mihajlov *et al.* (2011, 2015).

The results are obtained for the DB White dwarf models (Koester 2015 private communication) in the wavelength region  $100 \text{ nm} < \lambda < 3000 \text{ nm}$  and presented in tabulated form. Also, these results can be of interest and use in investigation of different stellar and laboratory plasmas.

**References**

Mihajlov, A. A., Srećković, V. A., Sakan, N. M.: 2015, *Journal of Astrophysics and Astronomy*, **36**, 3.

Mihajlov, A. A., Sakan, N. M., Srećković, V. A.: 2011, *Balt. Astron.*, **20**, 604.

## HF ELECTRIC PROPERTIES OF THE ASTROPHYSICAL PLASMAS

Vladimir A. Srećković<sup>1</sup>, Anatolij A. Mihajlov<sup>1</sup>, Nenad M. Sakan<sup>1</sup>,  
Ljubinko M. Ignjatović<sup>1</sup>, Milan S. Dimitrijević<sup>2,3,4</sup>, Darko Jevremović<sup>2</sup> and  
Veljko Vujčić<sup>2</sup>

<sup>1</sup>University of Belgrade, Institute of Physics, P. O. Box 57, 11001, Serbia

<sup>2</sup>Astronomical Observatory, Volgina 7, 11160 Belgrade 74, Serbia

<sup>3</sup>IHIS-Technoexperts, Bežanijska 23, 11080 Zemun, Serbia

<sup>4</sup>Observatoire de Paris, 92195 Meudon Cedex, France

E-mail: vlada@ipb.ac.rs

Here we determine the HF characteristics of astrophysical plasmas on the basis of numerically calculated values for the dense plasma conductivity in an external HF electric field. The examined range of plasma frequencies covers the IR, visible and UV regions and consider electronic number density and temperature important for different stellar models.

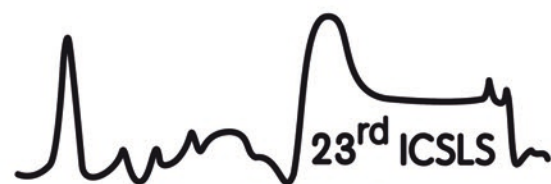
The results presented here are important for the investigation of atmosphere plasmas of astrophysical objects like white dwarfs with different atmospheric compositions (DA, DC etc.), and for investigation of some other stars (M-type red dwarfs, Sun etc.) as well as for laboratory plasma research (Srećković *et al.* 2010).

### References

Srećković, V. A., Ignjatović, Lj. M., Mihajlov, A. A., Dimitrijević, M. S: 2010, *MNRAS*, **406**, 590.



19 – 24 June 2016, Toruń, Poland



19 – 24 June 2016, Toruń, Poland



ALEKSANDER  
JABŁOŃSKI  
FOUNDATION



UNIWERSYTET  
MIKOŁAJA KOPERNIKA  
W TORUNIU



Ministry of Science  
and Higher Education  
Republic of Poland



Toruń

23rd International Conference on Spectral Line Shapes. June 19-24, 2016, Toruń, Poland



# 23<sup>rd</sup> INTERNATIONAL CONFERENCE

on Spectral Line Shapes

19-24 June, 2016, Toruń, Poland

## The inverse bremsstrahlung absorption coefficients and Gaunt factors in astrophysical plasmas

A A Mihajlov<sup>1</sup>, V A Srećković<sup>1</sup>, N M Sakan<sup>1</sup>, M S Dimitrijević<sup>2,3,4</sup> and Z Simić<sup>2</sup>

<sup>1</sup> Institute of physics, Univesity of Belgrade, P.O. Box 57, 11001, Belgrade, Serbia

<sup>2</sup> Astronomical Observatory, Volgina 7, 11060 Belgrade 74, Serbia

<sup>3</sup> Observatoire de Paris, 92195 Meudon Cedex, France

<sup>4</sup> IHIS Techno experts, Batajnički put 23, 11080 Zemun, Serbia

In this paper we will presents the method of determination of the electron-ion inverse "Bremsstrahlung" characteristics in the stellar atmospheres where the plasma characteristics are changing in a wide diapa-son. It is shown that determination of these optical characteristics i.e. the absorption coefficients and Gaunt factors can be successfully performed in the whole region of electron densities and temperatures which is relevant for stellar atmospheres. The used method is based on cut-off Coulomb model potential which was used by now for the describing of some spectral characteristics of plasma [1,2]. The relevant quantum mechanical method of the calculation of the corresponding spectral absorption coefficient and Gaunt factor is described and discussed.

The results obtained for plasmas with the electron densities from  $10^{14} \text{ cm}^{-3}$  to  $10^{19} \text{ cm}^{-3}$  and tempera-tures from 3000 K to 50000 K within the wavelength region  $100 \text{ nm} < \lambda < 3000 \text{ nm}$  are presented. These results can be of interest and use in the investigation of different laboratory plasmas.

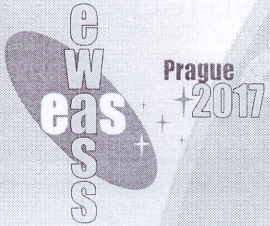
### References:

- [1] Mihajlov A A, Sakan N M, Srećković V A and Vitel Y 2011 Journal of Physics A Mathematical General **44** 095502
- [2] Mihajlov A A, Sakan N M, Srećković V A and Vitel Y 2011 Baltic Astronomy **20** 604



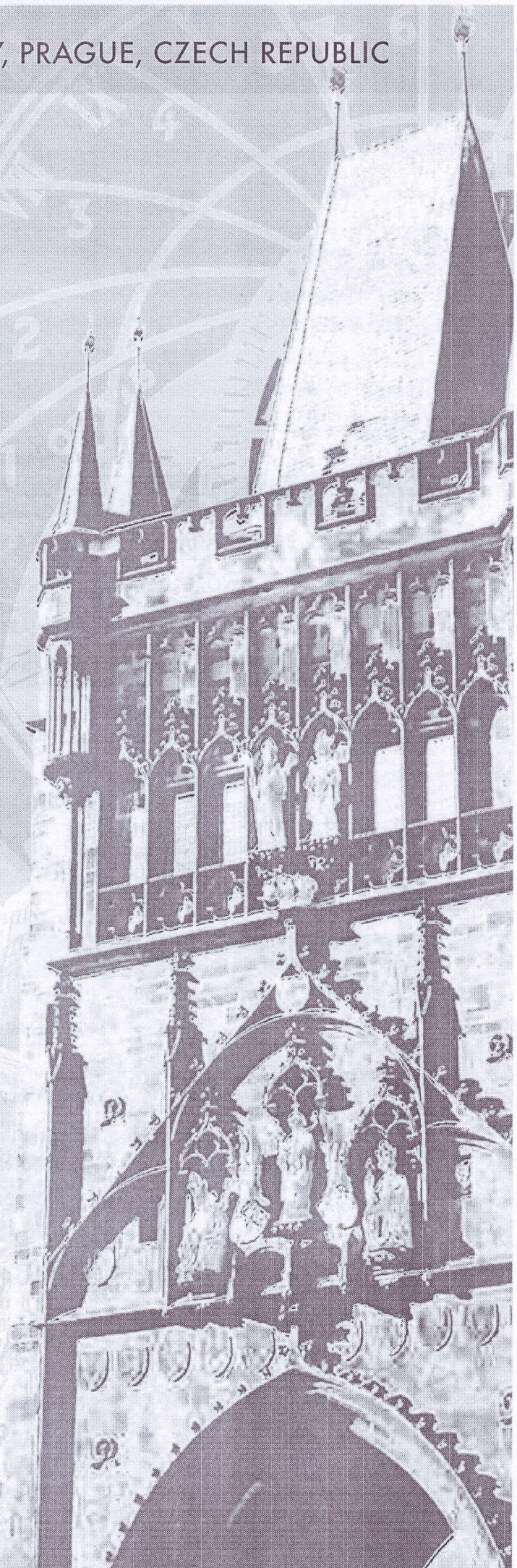
17

26 - 30 JUNE 2017, PRAGUE, CZECH REPUBLIC



# PROGRAMME

EUROPEAN WEEK OF ASTRONOMY AND SPACE SCIENCE





# SS05- Energy release and radiation in partially ionized plasma of solar and stellar atmospheres

## Room 345

|             |   |
|-------------|---|
| 09:00-09:40 | Flare heating in stellar chromospheres <b>Hugh Hudson</b>   |
| 09:40-10:00 | The temporal behaviour of MHD waves in a partially ionized prominence-like plasma: Effect of heating and cooling <b>José Luis Ballester</b> |
| 10:00-10:20 | On the Generation and Propagation of Alfvén Waves in the Lower Solar Atmosphere <b>Yuriy Tsap</b>   |
| 10:20-10:30 | <b>Short poster presentations</b>   |
| 10:30-11:00 | <b>COFFEE BREAK</b>   |
| 11:00-11:30 | <b>PLENARY 2 - GUILLEM ANGLADA-ESCUDE</b>   |
| 11:30-12:00 | <b>PLENARY 3 - ANTHONY G.A. BROWN</b>   |
| 12:00-12:30 | <b>TYCHO BRAHE PRIZE - BERNARD DELABRE</b>  |
| 12:30-14:00 | <b>LUNCH</b>  |
| 14:00-14:40 | Partially ionized atmospheric gases in cloud-forming, ultra-cool, low-mass stars <b>Christiane Helling</b>                                  |
| 14:40-15:00 | Ultracool stars: magnetic loop heating, electron acceleration and radio emission <b>Alexander Stepanov</b>                                  |
| 15:00-15:20 | STELLAR ACTIVITY IN SELECTED BINARY SYSTEMS WITH KEPLER PHOTOMETRY <b>Derviş Ersin Tokbay</b>   |
| 15:20-15:30 | <b>Short poster presentations</b>   |
| 15:30-16:00 | <b>COFFEE BREAK</b>   |
| 16:00-16:40 | Recent advances in millimeter to far-infrared solar physics <b>Jean Pierre Raulin</b>   |
| 16:40-17:00 | Observing capabilities of the European Solar Telescope <b>Jan Jurcak</b>  |
| 17:00-17:15 | Electric energy accumulation model for solar flares <b>Valery Krivodubskij</b>  |
| 17:15-17:30 | Free-free absorption coefficients in solar atmosphere <b>Milan S. Dimitrijević</b>  |
| 17:30-18:30 | <b>ERC FUNDING OPPORTUNITIES - ANDREAS KEIL</b>   |



XI SERBIAN CONFERENCE  
ON SPECTRAL LINE SHAPES IN ASTROPHYSICS

# BOOK OF ABSTRACTS

Eds. Luka Č. Popović, Andjelka Kovačević and Saša Simić



Astronomical Observatory  
Belgrade, 2017



**XI SERBIAN CONFERENCE ON SPECTRAL LINE SHAPES  
IN ASTROPHYSICS**

August 21-25, 2017, Šabac, Serbia

**Scientific Organizing Committee:**

Luka Č. Popović (Serbia)  
Chairman

Edward Baron (USA)  
Emmanuel Danezis (Greece)  
Milan S. Dimitrijević (Serbia)  
Peter Hauschildt (Germany)  
Dragana Ilić (Serbia)  
Darko Jevremović (Serbia)  
Erencio Mediavilla (Spain)  
Gillian Peach (United Kingdom)  
Jagoš Purić (Serbia)  
Sylvie Sahal-Bréchet (France)  
Jack Sulentic (Spain)  
Evgeny Stambulchik (Israel)  
Roland Stamm (France)  
Aleksander F. Zakharov (Russia)

**Local Organizing Committee:**

Andjelka Kovačević  
Co-chairperson  
Saša Simić  
Co-chairman

Nataša Bon  
Co-vicechairperson  
Jelena Kovačević-Dojčinović  
Co-vicechairperson

Edi Bon  
Dragana Ilić  
Maša Lakićević  
Sladjana Marčeta Mandić  
Tanja Milovanov  
Aleksandra Nina  
Djordje Savić  
Vladimir Srećković

Organized by: Astronomical Observatory Belgrade

Co-organizer: Faculty of Mathematics, University of Belgrade

Published by: Astronomical Observatory, Volgina 7, 11060 Belgrade 38, Serbia

The publication of this issue is financially supported by the Ministry for Education, Science and Technological Development of Serbia

Website: <http://www.scslsa.matf.bg.ac.rs>

Cover image design: Sladjana Marčeta Mandić

Computer text design: Tanja Milovanov

ISBN 978-86-80019-82-6

Printed by: Demo Group doo, Jaračkih žrtava 22/11/II, 15000 Šabac

Number of copies: 100



XI SERBIAN CONFERENCE  
ON SPECTRAL LINE SHAPES IN ASTROPHYSICS

# BOOK OF ABSTRACTS

Eds. Luka Č. Popović, Andjelka Kovačević and Saša Simić



Astronomical Observatory  
Belgrade, 2017



**THE APPLICATION OF THE CUT-OFF COULOMB MODEL  
POTENTIAL FOR THE CALCULATION OF BOUND - BOUND  
STATE TRANSITIONS**

N. M. Sakan<sup>1</sup>, V. A. Srećković<sup>1</sup>, Z. Simić<sup>2</sup>, and M. S. Dimitrijević<sup>2,3</sup>

<sup>1</sup>*Institute of Physics, Pregrevica 118, 11080 Zemun, Belgrade, Serbia*

<sup>2</sup>*Astronomical Observatory, Volgina 7, 11060 Belgrade 38, Serbia*

<sup>3</sup>*LERMA, Observatoire de Paris, UMR CNRS 8112, UPMC,  
92195 Meudon Cedex, France*

*E-mail: nsakan@ipb.ac.rs, vlada@ipb.ac.rs, zsimic@aob.rs, mdimitrijevic@aob.rs*

In this contribution we present results of bound state transition modeling using the cut-off Coulomb model potential. The cut-off Coulomb potential has proven itself as a model potential for the dense hydrogen plasma (see Mihajlov et al. 2011,2015). The main aim of our investigation include a further steps of improvement of the usage of model potential. The presented results cover a wide region of the plasma electron densities and temperatures. Such plasmas are of interest from both the laboratory and the astrophysical aspect. Here, we keep in mind the plasma of the inner layers of the solar atmosphere, as well as of partially ionized layers of other stellar atmospheres, for example the atmospheres of DA and DB white dwarfs with effective temperatures between 10 000 K and 25 000 K (Srećković et al. 2014). It is expected that such approach would lead towards the inclusion of bound state transition photo-absorption process within the frame of the presented Coulomb cut-off potential model.

**References**

- Mihajlov, A. A., Sakan, N. M., Srećković, V. A., Vitel, Y.: 2011, *J. Phys. A*, **9**, 095502.  
Mihajlov, A. A., Srećković, V. A., Sakan, N. M.: 2015, *J. Astrophys. Astr.*, **36**, 635-642.  
Srećković, V. A., Mihajlov, A. A., Ignjatović, L. M. and Dimitrijević, M. S.: 2014, *JPCS*, **565**, 012022.



THE CROSS SECTIONS AND THE RATE COEFFICIENTS  
OF THE FREE-FREE ABSORPTION PROCESSES  
IN STELLAR ATMOSPHERES

V. A. Srećković<sup>1</sup>, M. S. Dimitrijević<sup>2,3</sup>, Z. Simić<sup>2</sup> and N. M. Sakan<sup>1</sup>

<sup>1</sup>*Institute of Physics, Pregrevica 118, 11080 Zemun, Belgrade, Serbia*

<sup>2</sup>*Astronomical Observatory, Volgina 7, 11060 Belgrade, Serbia*

<sup>3</sup>*LERMA, Observatoire de Paris, UMR CNRS 8112, UPMC,  
92195 Meudon Cedex, France*

*E-mail: vlada@ipb.ac.rs, mdimitrijevic@aob.rs, nsakan@ipb.ac.rs*

The contribution of free-free electron-ion processes to the total absorption in stellar atmospheres increases with density, and for very dense plasmas it becomes dominant. Consequently, it is of interest to investigate the role of such processes in deeper layers, and to examine its influence on radiative transfer through such layers. In this contribution we present the free-free i.e. electron-ion characteristics for the case of the various models of stellar atmospheres where such plasma characteristics as plasma density and temperature change in wide region. It is shown that determination of these characteristics such as the cross-sections and the rate coefficients can be successfully performed in the whole diapason of electron densities and temperatures which is relevant for the corresponding non-ideal, dense astrophysical plasma. The Cut-off form of Coulomb potential is used to approximate the shielding effect in order to derive the cross-sections and the rate coefficients. We used quantum mechanical method of the calculation of the investigated characteristics (see Mihajlov et al. 2015). The results are obtained for the DB White dwarf models (Koester 2015 private communication) and for the solar model of Vernazza et al. (1981) in the wavelength region  $10 \text{ nm} < \lambda < 3000 \text{ nm}$ . Also, these results can be of interest and use in investigation of different laboratory non-ideal, dense plasmas.

References

- Mihajlov, A. A., Srećković, V. A., Sakan, N. M.: 2015, *J. Astrophys. Astr.*, **36**, 635-642.  
Vernazza, J., Avrett, E., Loser, R.: 1981, *ApJS*, **45**, 635.



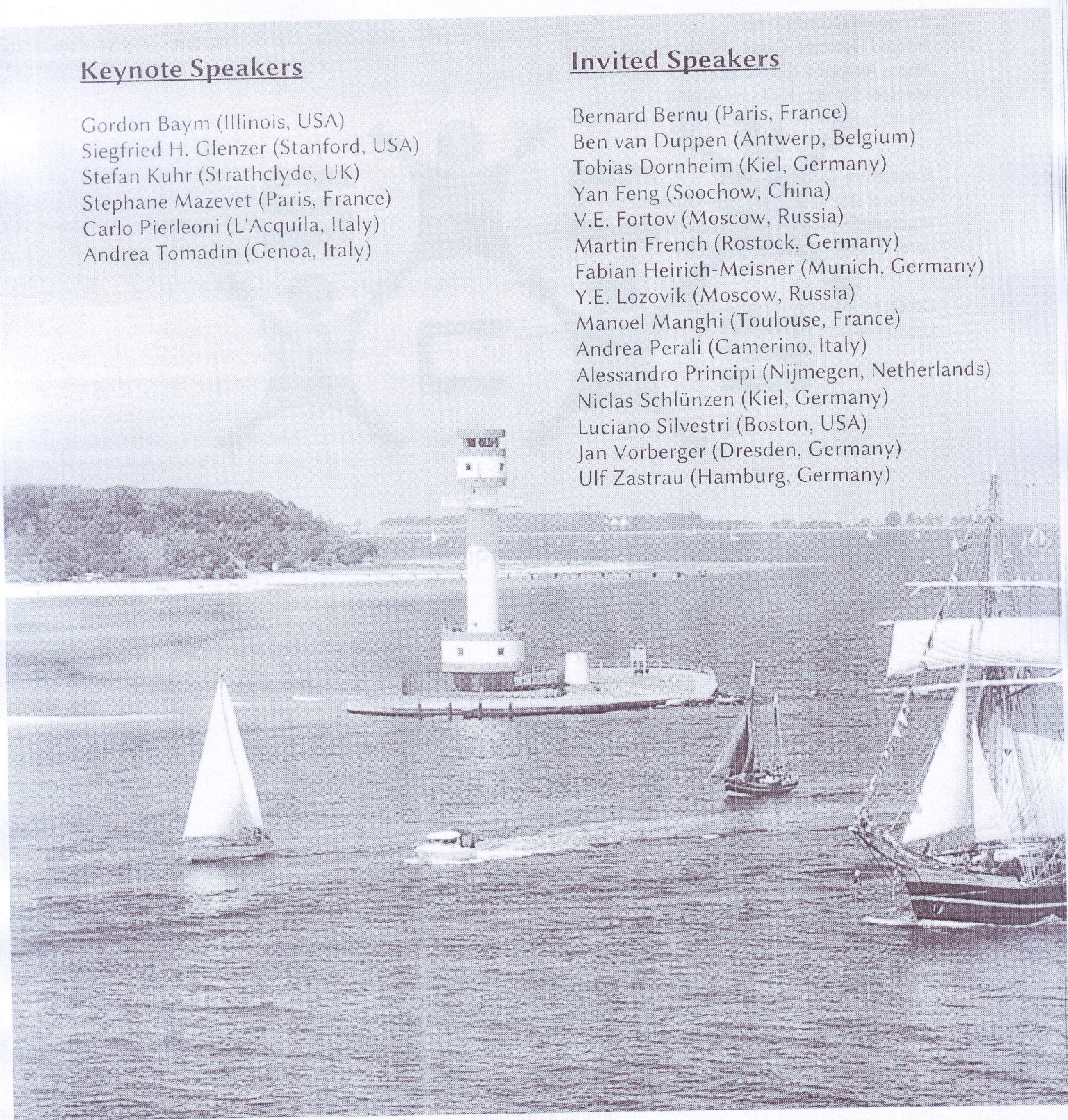
# International Conference Strongly Coupled Coulomb Systems 30 July – 4 August 2017, Kiel

## Keynote Speakers

Gordon Baym (Illinois, USA)  
Siegfried H. Glenzer (Stanford, USA)  
Stefan Kuhr (Strathclyde, UK)  
Stephane Mazevet (Paris, France)  
Carlo Pierleoni (L'Acquila, Italy)  
Andrea Tomadin (Genoa, Italy)

## Invited Speakers

Bernard Bernu (Paris, France)  
Ben van Duppen (Antwerp, Belgium)  
Tobias Dornheim (Kiel, Germany)  
Yan Feng (Soochow, China)  
V.E. Fortov (Moscow, Russia)  
Martin French (Rostock, Germany)  
Fabian Heirich-Meisner (Munich, Germany)  
Y.E. Lozovik (Moscow, Russia)  
Manoel Manghi (Toulouse, France)  
Andrea Perali (Camerino, Italy)  
Alessandro Principi (Nijmegen, Netherlands)  
Niclas Schlünzen (Kiel, Germany)  
Luciano Silvestri (Boston, USA)  
Jan Vorberger (Dresden, Germany)  
Ulf Zastra (Hamburg, Germany)



Local Organizing Committee SCCS 2017

Michael Bonitz, Patrick Ludwig & Zhandos Moldabekov  
e-mail: [sccs2017@physik.uni-kiel.de](mailto:sccs2017@physik.uni-kiel.de)



<http://www.uni-kiel.de/sccs2017>



### **Local Organizing Committee of SCCS 2017**

Michael Bonitz, Chair (Kiel University)

Patrick Ludwig (Kiel University)

Zhandos Moldabekov (Kiel University)

### **Program Committee**

Ronald Redmer, Chair (Rostock University)

Angel Alastuey (École Normale Supérieure de Lyon)

Michael Bonitz (Kiel University)

David Neilson (Università degli studi di Camerino)

### **Executive Committee**

Michael Bonitz, Chair (Kiel University)

Vladimir Fortov (Russian Academy of Sciences)

John Goree (University of Iowa)

### **Chair of International Advisory Board**

David Neilson (Università degli studi di Camerino)

### **Sponsors**

German Science Foundation (DFG)

Kiel Nano, Surface and Interface Science (KiNSIS)

WE Heraeus Travel Grant

Springer Science + Business Media

ShareLaTeX.com

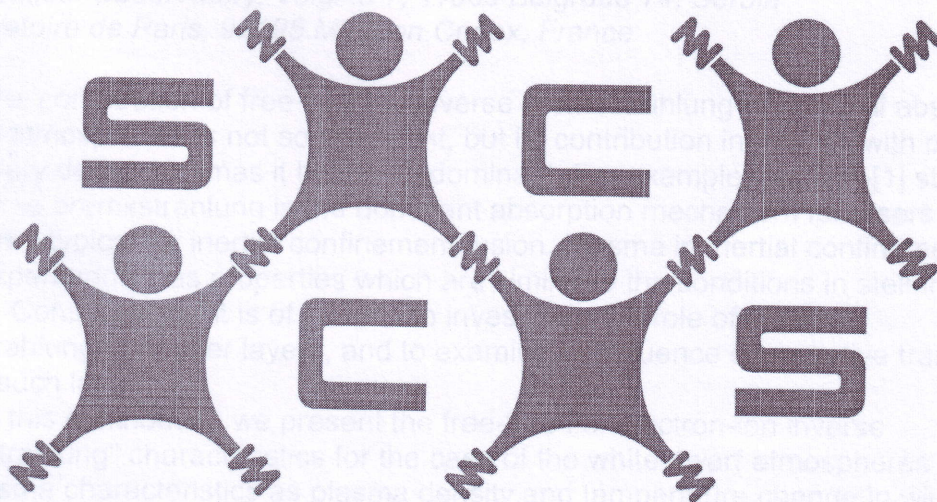
ADDITIVE Software



# Free-free absorption coefficients in white dwarf atmosphere

N.M. Sakan<sup>1</sup>, V.A. Srecković<sup>1</sup>, Z. Simić<sup>2</sup>, M.S. Dimitrijević<sup>3</sup>

<sup>1</sup>University of Belgrade, Institute of Physics, P. O. Box 57, 11001, Serbe  
<sup>2</sup>Astronomical Observatory, Vojvota 7, 11060 Belgrade 74, Serbia  
<sup>3</sup>Observatoire de Paris, 91190 Bruny-la-forêt, France



STRONGLY COUPLED COULOMB SYSTEMS

## FINAL PROGRAM & BOOK OF ABSTRACTS

Kiel, July 30–August 4, 2017  
Wissenschaftszentrum Kiel



## Free-free absorption coefficients in white dwarf atmosphere

N.M.Sakan<sup>\*1</sup>, V.A.Srećković<sup>1</sup>, Z.Simić<sup>2</sup>, M.S.Dimitrijević<sup>2,3</sup>

<sup>1</sup> University of Belgrade, Institute of Physics, P. O. Box 57, 11001, Serbia

<sup>2</sup> Astronomical Observatory, Volgina 7, 11060 Belgrade 74, Serbia

<sup>3</sup> Observatoire de Paris, 92195 Meudon Cedex, France

The contribution of free-free i.e. inverse bremsstrahlung to the total absorption in stellar atmospheres is not so important, but its contribution increases with density, and for very dense plasmas it becomes dominant. For example, authors [1] stated that inverse bremsstrahlung is the dominant absorption mechanism for lasers with parameters typical for inertial confinement fusion. Plasma in inertial confinement fusion experiments has properties which are similar to the conditions in stellar interiors. Consequently, it is of interest to investigate the role of inverse bremsstrahlung in deeper layers, and to examine its influence on radiative transfer through such layers.

In this contribution we present the free-free i.e. electron-ion inverse "Bremsstrahlung" characteristics for the case of the white dwarf atmospheres where such plasma characteristics as plasma density and temperature change in wide region. It is shown that determination of these characteristics such as the absorption coefficients and Gaunt factors can be successfully performed in the whole diapason of electron densities and temperatures which is relevant for the corresponding non-ideal, dense plasma of white dwarf atmospheres.

The Cut-off form of Coulomb potential is used to approximate the shielding effect in order to derive the absorption coefficients. The used quantum mechanical method of the calculation of the investigated characteristics is described and discussed in details in the papers of Mihajlov et al. [2,3]. The results are obtained for the DB White dwarf models (Koester 2015 private communication) in the wavelength region  $100 \text{ nm} < \lambda < 3000 \text{ nm}$ . The range of the physical parameters covers the area important for plasma modeling from astrophysical standpoint (white dwarfs, central stars of planetary nebulae, etc). Also, these results can be of interest and use in investigation of different laboratory non-ideal, dense plasmas.

[1] A. Grinenko, D.O. Gericke, Dense plasma heating by inverse Bremsstrahlung, in: Central Laser Facility, Annual Report 2008/2009, Science and Technology Facilities Council, Rutherford Appleton Laboratory, Harwell Science and Innovation Campus, Oxfordshire, p.110. (2009)

[2] A.A. Mihajlov, V.A. Srećković, N.M. Sakan, Journal of Astrophysics and Astronomy **3**, 36 (2015)

[3] A.A.Mihajlov, N.M Sakan, V. A. Srećković, Balt. Astron. **20**, 604 (2011)

\* email: nsakan@ipb.ac.rs



## HF electric properties of the astrophysical plasmas under extreme conditions

V.A.Srećković<sup>1</sup>, N.M.Sakan<sup>\*1</sup>, Z.Simić<sup>2</sup>, Lj.M. Ignjatović<sup>1</sup>, M.S.Dimitrijević<sup>2,3</sup>

<sup>1</sup> University of Belgrade, Institute of Physics, P. O. Box 57, 11001, Serbia

<sup>2</sup> Astronomical Observatory, Volgina 7, 11060 Belgrade 74, Serbia

<sup>3</sup> Observatoire de Paris, 92195 Meudon Cedex, France

For further investigation of strongly correlated plasma physics, the investigations of its electronic properties remains an ongoing problem. For example theoretical calculations and measurements of reflectivity are important because of its possible use as diagnostic tool in the physics of high-density energy [1].

Here we determine the HF characteristics of astrophysical, dense, non-ideal plasmas on the basis of numerically calculated values for the dense plasma conductivity in an external HF electric field. The examined range of plasma frequencies covers the IR, visible and UV regions and consider electronic number density and temperature important for different stellar models.

These results, can be applied in the experiments of high pressure discharge, shock waves etc., where strongly non-ideal plasmas, including extremely dense plasmas, are created. Also the results presented here are important for investigation of atmosphere plasmas of astrophysical objects like white dwarfs with different atmospheric compositions (DA, DC etc.), and for investigation of some other stars (M-type red dwarfs, Sun etc.) as well as for laboratory plasma research (see e.g. [2,3]).

[1] V. E. Fortov, *Extreme States of Matter: on Earth and in the Cosmos* (Springer Science & Business Media, 2010)

[2] V. A. Srećković, Lj. M. Ignjatović, A. A. Mihajlov, M. S. Dimitrijević, *MNRAS* **406**, 590 (2010)

[3] V. A. Srećković, Lj. M. Ignjatović, A. A. Mihajlov, and M. S. Dimitrijević, *Publ. Astron. Obs. Belgrade* **89**, 383 (2010)

---

\* email: nsakan@ipb.ac.rs



RUSSIAN ACADEMY OF SCIENCES / JOINT INSTITUTE FOR HIGH TEMPERATURES RAS /  
INSTITUTE OF PROBLEMS OF CHEMICAL PHYSICS RAS / KABARDINO-BALKARIAN STATE UNIVERSITY

# BOOK OF ABSTRACTS

MOSCOW & CHERNOGOLOVKA & NALCHIK, 2019



**XXXIV  
INTERNATIONAL  
CONFERENCE  
ON INTERACTION  
OF INTENSE ENERGY FLUXES  
WITH MATTER**

MARCH 1-6, 2019  
ELBRUS, KABARDINO-BALKARIA, RUSSIA





The book consists of abstracts of plenary lectures, oral reports and posters presented at the XXXIV International Conference on Interaction of Intense Energy Fluxes with Matter (1–6 March 2019, Elbrus, Kabardino-Balkaria, Russia). The presentations deal with the contemporary investigations in the field of physics of extreme states of matter. The conference topics are as follows: interaction of intense laser, x-ray and microwave radiation, powerful ion and electron beams with matter; techniques of intense energy fluxes generation; experimental methods of diagnostics of ultrafast processes; shock waves, detonation and combustion physics; equations of state and constitutive equations for matter at high pressures and temperatures; methods of mathematical modeling in physics of extreme states of matter; high-energy astrophysics; low-temperature plasma physics; physical issues of power engineering and technology aspects.

The conference is supported by the Russian Academy of Sciences.

Edited by Fortov V.E., Karamurзов B.S., Khishchenko K.V., Sultanov V.G., Kadatskiy M.A., Andreev N.E., Dyachkov L.G., Efremov V.P., Iosilevskiy I.L., Kanel G.I., Levashov P.R., Mintsev V.B., Savintsev A.P., Shakh-ray D.V., Shpatakovskaya G.V., Son E.E., Stegailov V.V.

**ISBN 978-5-6040595-9-3**

# Comparison of megaampere channel temperature value measured by different methods at its maximal contraction in high density gas

Bogomaz A A<sup>1</sup>, Pinchuk M E<sup>1,®</sup>, Budin A V<sup>1</sup>, Leks A G<sup>1</sup> and Sakan N M<sup>2</sup>

<sup>1</sup> Institute for Electrophysics and Electrical Power of the Russian Academy of Sciences, Dvortsovaya Naberezhnaya 18, Saint-Petersburg 191186, Russia



<sup>2</sup> Institute of Physics, Belgrade University, Pregrevica 118, Zemun, Belgrade 11080, Serbia

® pinchme@mail.ru

Comparison of discharge channel temperature in high density hydrogen with current amplitude of  $\sim 1$  MA at initial gas pressure of 5–7 MPa, determined by various methods, was done under stage of its maximal contraction. In the first case determination of the temperature value of 72–73 eV was made by intensity of soft x-ray radiation from the channel for experiments with current amplitude of 1.1–1.5 MA [1]. The estimation of the temperature on the basis of the data received by magnetic probe method and specified electric characteristics of the channel was of  $\approx 140$  eV for experiment with initial gas pressure of 5 MPa at current amplitude of 0.93 MA. The temperature determination by the last procedure had small accuracy caused by the limitation of the magnetic probe technique in determination of the channel contraction ratio [2] and some assumptions for nearelectrode voltage drops calculations by this way [3]. Apparently, the channel temperature in stage of maximal contraction is of  $\sim 100$  eV.

- [1] Bogomaz A A, Pinchuk M E, Budin A V, Leks A G, Kurakina N K, Pozubenkov A A and Kumkova I I 2019 *J. Phys.: Conf. Ser.* **1147** 012102
- [2] Bogomaz A A, Pinchuk M E, Budin A V, Leks A G, Leont'ev V V, Pozubenkov A A and Kurakina N K 2016 *J. Phys.: Conf. Ser.* **774** 012186
- [3] Bogomaz A A, Pinchuk M E, Budin A V, Leks A G, Leontev V V and Pozubenkov A A 2018 *J. Phys.: Conf. Ser.* **946** 012138

# 16th European Solar Physics Meeting

 Sep 6, 2021, 9:00 AM → Sep 10, 2021, 5:00 PM Europe/Rome  
 Online

**Description** The European Solar Physics Meetings (ESPM) are organised every three years by the board of the [European Solar Physics Division](#) (ESPD), a joint division of the [European Physical Society](#) (EPS) and the [European Astronomical Society](#) (EAS). The meetings bring together a large number of from Europe and beyond, who are active in the theoretical and observational study of solar phenomena.

The 16th European Solar Physics Meeting (ESPM-16), originally planned for 2020, took place as a virtual online meeting in **6-10 September 2021**, with free registration for all participants.

You can access the posters and presentation materials uploaded by the authors in the [meeting timetable](#).


## Confirmed invited speakers

- Axel Brandenburg (SE)
- Lakshmi Pradeep Chitta (DE)
- Sanja Danilovic (SE)
- Louise Harra (CH)
- Andrew Hillier (UK)
- Natasha Jeffrey (UK)
- Laurene Jouve (FR)
- Larisa Kashapova (RU)
- Ioannis Kontogiannis (DE)
- Simone Landi (IT)
- Eric Priest (UK, ESPD senior prize winner 2020)
- Marco Velli (US)

## Important dates

- **1 April 2021**. Registration and abstract submission open.
- **1 June 2021**. Deadline for abstract submission.
- **1 August 2021**. Deadline for registration.
- **6-10 September 2021**. Meeting.



 Special\_issue\_Desc...

## Participants

|   |                         |   |                            |   |                          |   |                                |   |                            |   |                     |
|---|-------------------------|---|----------------------------|---|--------------------------|---|--------------------------------|---|----------------------------|---|---------------------|
| A   | Aabha Monga             | A   | Aalaa Samy                 | A   | Aaron Peat               | A | Aarti Fulara                   | A   | Abdulaziz Alharbi          | A | ABDULRAHMAN ALBIDAH |
| A   | Abhinav Prasad          | A   | Abhishek Rajhans           | A   | Abril Sahade             | A | Ada Ortiz Carbonell            | A   | Aditi Bhatnagar            |   |                     |
| A   | Adriana María Gulisano  | A   | Adur Pastor Yabar          | A   | Agata Chuchra            | A | Agnieszka Ruminska             | A   | Ahmad Alharbi              |   |                     |
| A   | Akie Moritsuka          | A   | Alberto Vasquez            | A   | Alejandro J. P. Aparicio | A | Alejandro Miguel Moreno Vacas  |   |                            |   |                     |
| A   | Alejandro Reina Conde   | A   | Alena Zemanova             | A   | Alessandro Bemporad      | A | Alexander Getling              |  | Alexander Hillaris         |   |                     |
| A   | Alexander James         | A   | Alexander Kutsenko         | A   | Alexander Nindos         | A | Alexander Pietrow              | A   | Alexander Stepanov         |   |                     |
| A   | Alexander Warmuth       | A   | Alexandr Afanasiev         | A   | Alexandros Adamis        | A | Alexandros Koukras             | A   | Amanda Stricklan           |   |                     |
| A   | Ana Belén Griñón Marín  | A   | Ana Cadavid                | A   | Anamaria Navarro Noguera | A | Ananya Rawat                   | A   | Anastasiya Zhukova         |   |                     |
| A   | Andrea Diercke          | A   | Andrea Francesco Battaglia | A   | Andrea Perdomo           | A | Andreas Wagner                 | A   | Andrei Afanasev            |   |                     |
| A   | Andrei Chelpanov        | A   | Andrei Plotnikov           | A   | Andrei Zhukov            | A | Andrew Hillier                 | A   | Andrzej Fludra             |   |                     |
| A   | Andrés Asensio Ramos    | A   | Andy S.H. To               | A   | Anett Elek               | A | Angela Yulieth Bautista Sierra | A   | Anik De Groof              |   |                     |
| A   | Anna Khlystova          | A   | Anna Kępa                  | A   | Anthony Yeates           | A | Antoine Doliou                 | A   | Antonino Petralia          |   |                     |
| A   | Antonio Esteban Niemela |  | Anwasha Maharana           | A   | Arghyadeep Paul          | A | Arkadiusz Berlicki             | A   | Arpit Shrivastav           |   |                     |
| A   | Arturs Vrublevskis      | A   | Arun Awasthi               | A   | Astrid Veronig           | A | Atul Mohan                     | A   | Avijeet Prasad             | A | Axel Brandenburg    |
| A   | Azaymi Siu              | B   | Barbara Perri              | B   | Barbara Sylwester        | B | Bartosz Dabrowski              | B   | Beatrice Popescu Braileanu |   |                     |
| B   | Belén Coronado Granados | B   | Ben Alterman               | B   | Ben Snow                 | B | Bernadett Belucz               | B   | Bernhard Fleck             |   |                     |
| B   | Bernhard Hofer          | B   | Bibhuti Kumar Jha          |  | Bidya Binay Karak        | B | Bin Zhuang                     | B   | BISWAJIT MONDAL            |   |                     |
| B   | Björn Löptien           |  | Brandon Panos              | B   | Brigitte Schmieder       | B | Błażej Kuźma                   | C   | Callan Noble               | C | Camilla Scolini     |
| C   | Camille Lorfing         | C   | Carlos Jose Diaz Baso      | C   | Carlos Larrodera         | C | Carolina Robustini             | C   | Catherine Fischer          |   |                     |
|  | Catia Grimani           | C   | Cecilia Mac Cormack        | C   | Chaitanya Prasad Sishtla | C | Chandrashekhhar Kalugodu       | C   | Chen Xing                  |   |                     |
| C   | Christian Baumgartner   | C   | Christian Vocks            | C   | Christoph Kuckein        | C | Christopher Prior              | C   | Ciara Maguire              |   |                     |
| C   | Cis Verbeeck            | C   | Clara Froment              | C   | Clementina Sasso         | C | Conrad Schwanitz               | C   | Cosima Breu                |   |                     |

|   |   |  |   |  |
|---|---|--|---|--|
|  Costas Alissandrakis   |  Costas Bouratzis   |  Cristina Mandrini   |  D. Shaun Bloomfield  |  Dan Kisman  |
|  Dana-Camelia Talpeanu   |  Daniel Clarkson   |  Daniel Müller  |  Daniel Nóbrega-Siverio  |  Daniel Price   |
|  Daniel Seaton   |  Daniele Calchetti   |  Daniele Spadaro  |  Daniele Telloni   |  Dario Del Moro   |
|  David Berghmans   |  David Brooks  |  David Long   |  David MacTaggart  |  David Martínez Gómez   |
|  David Millar  |  David Orozco Suarez   |  David Pontin   |  David Stansby   |  Deborah Baker  |
|  Devojyoti Kansabanik  |  DIBYA KIRTI MISHRA  |  Diego Lloveras   |   Diego Prado Barroso |  Dipali Burud   |
|  Dipankar Banerjee   |  Divya Oberoi  |  Dmitrii Kolotkov   |  Dorcas Oseni  |  Dorota Przepiórka  |
|  Dusan Vukadinovic   |  Eduard Kontar   |  Eino Valtonen  |   Ekaterina Dineva    |  Eleanna Asvestari  |
|  Elena Dzfíćáková  |  Elena García Broock   |  Elena Khomenko   |  Elena Kupriyanova   |  Elena Orlando  |
|  Eleni Lavasa  |  Elke D'Huys   |  Emanuele Papini  |  Emilia Kilpua   |  Eric Buchlin   |
|  Etienne Pariat  |  Evangelia Samara  |  Evgeniia Volchok   |  Ewan Dickson  |  Fabiana Ferrente   |
|  Fabio Reale   |   Fabio Riva              |  Fan Zhang  |  Federica Chiappetta   |  Federica Frassati  |
|  Fedor Vybornov  |  Fernando Carcaboso  |  Fernando Moreno-Insertis   |  Faisal Asiri  |  Flavio Calvo   |
|  Florentino Sánchez Bajo   |  Florian Koller  |  Francesca Zuccarello   |  Francesco Berrilli  |  Francesco Pecora   |
|   francesco pegoraro          |   Francesco Pegoraro      |  Frank Schulz   |  Frederic Schuller   |  Frederik Clemmensen  |
|  Frédéric Auchère  |  Gabriel Pelouze   |   Gaetano Zimbardo                 |  Galina Chikunova  |  Galina Motorina  |
|  Georgia Tsiropoula  |  Georgina Graham   |  Georgios Chintzoglou   |  GERRY DOYLE   |  Gherardo Valori  |
|  Gianluca Napoletano   |  Giorgio Viavattene  |  Giovanni Lapenta   |  Girjesh Gupta   |  Giulia Murtas  |
|  Giuliana Russano  |  Giulio Del Zanna  |  Giuseppe Emanuele Capuano  |  Giuseppe Nisticò  |  |
|  Giuseppina Carnevale  |  Giuseppina Nigro  |   Gordon Julian Koehn              |  GUILLEM CASTELLÓ  |  haitang I  |
|  Hamish Reid  |  Hana Meszarosova   |  Hardi Peter   |  Hariharan Krishnan   |  Harry Callingham  |
|   Hechao Chen             |  Helen Mason   |  Hema Kharayat  |  Henrik Eklund   |  Hugh Hudson  |
|  Iain Hannah   |  Iliaria Ermolli   |  Immanuel Christopher Jebaraj   |  Ineke De Moortel  |  Ioannis Dakanalis  |
|  Ioannis Kontogiannis  |  Irene Tovar Hernández   |   Irina Bakunina               |  Irina Bilenko   |  Istvan Ballai  |
|  Ivan Dorotović  |  Ivan Yakovkin   |  Ivica Skokić   |  Iñigo Arregui   |  Jack Reid  |
|  Jacques Gustin  |  Jaime de la Cruz Rodriguez  |  Jamie Gorman   |  Jan Benáček   |  Jan Gieseler   |
|  Jan Janssens  |  Jan Jurcak  |  Jan Rybak  |  Jana Kasparova  |  Janusz Sylwester   |
|  Jaroslav Urbář  |  Jasmina Magdalenic  |  Jayant Joshi   |  Jean-Marie Malherbe   |  |
|  Jeffersson Andres Agudelo Rueda   |  Jenny Marcela Rodríguez Gómez   |  Jens Pomoell   |  Jiajia Liu  |  Jie Hong   |
|  Jie Jiang   |  Jinge Zhang   |  Joe Scalisi  |  Johan Muhamad   |  Johannes Tschernitz  |
|  Jonas Saqri   |  Jonas Sinjan  |  Jonas Zbinden  |  Jorge Amaya   |  Joris Hermans  |
|  Jose Carlos del Toro Iniesta  |   Jose Luis Ballester |  José Manuel Vaquero  |  José Roberto Canivete Cuissa  |  |
|   João M. da Silva Santos |  Juan Camilo Guevara Gomez   |  Juan Manuel Borrero  |  Juan Pablo Maldonado  |  |
|  Juie Shetye   |  Julia Thalmann  |  Julius Koza  |  Juraj Loricik   |  Jörn Warnecke  |
|   Kamil Bicz              |  Kamlesh Bora  |  Karin Dissauer   |  Karl-Ludwig Klein   |  Katarzyna Mikula   |
|  Ke Yu   |  Kevin Reardon   |  Kilian Krikova   |  Konstantinos Karamelas  |  Korsos Marianna  |
|  Kostadinka Koleva   |  Kostas Moraitis   |  Kostas Tziotziou   |  Krishna Prasad Sayamanthula   |  Kristopher Cooper  |
|  Krzysztof Barczynski  |  Krzysztof Radziszewski  |  Lakshitha Nama   |  Lakshmi Pradeep Chitta  |  |
|  Larisa Kashapova  |  Larisza Krista  |  Laura Bercic   |  Laura Hayes   |  Laura Rodríguez-García   |
|  Laurene Jouve   |  Laurent Dolla   |  Lekshmi Biji   |  Li Feng   |  Liam Edwards   |
|  Lidia van Driel-Gesztelyi   |  Ilijia Liu  |  Lingfang Wang  |  Lisa-Marie Zessner  |   Louise Harra |
|  Luc Rouppe van der Voort  |  Luca Giovannelli  |  Lucia Abbo   |  Lucia Kleint  |  Luciano Rodriguez  |
|  Lucie Green   |  Luis Eduardo Vieira   |  Maciej Zapiór  |  Madhurjya Changmai  |  Mahir Pirgulyev  |
|  Malcolm Druett  |  Malte Bröse   |  manjunath hegde  |  Manolis Georgoulis  |  Manuel Collados  |
|  Manuel Luna   |  Manuela Temmer  |  Marco Marongiu   |  Marco Romoli  |  Marco Stangalini   |
|  Marek Stęślicki   |  Margit Haberreiter  |   Maria Guadalupe Barrios Sazo |  Maria Kazachenko  |  Maria Loukitcheva  |



|   |                              |   |                       |   |                                 |   |                                 |   |                             |   |                    |
|---|------------------------------|---|-----------------------|---|---------------------------------|---|---------------------------------|---|-----------------------------|---|--------------------|
| M | Maria Madjarska              | M | Mariana Cécere        | M | Mariano Poisson                 | M | Mariarita Murabito              | M | Marie Dominique             |   |                    |
| M | Marilena Mierla              | M | Marina Battaglia      | M | Markus Roth                     | M | Marta García Rivas              | M | Martin Reiss                | M | Maryam Saberi      |
| M | Mateja Dumbovic              | M | Matheus Kriginsky     | M | Mats Carlsson                   | M | Mats Ola Sand                   | M | Matteo Cantoresi            |   |                    |
| M | Matthew Lennard              | M | Max McMurdo           | M | Małgorzata Pietras              | M | Michalina Litwicka              | M | Michaël Geeraerts           |   |                    |
| M | Michele Fabi                 | M | michele piana         | M | Mihalis Mathioudakis            | M | Mijie Shi                       | M | Mikhail Modestov            | M | Mikolaj Szydlarski |
| M | Mirko Piersanti              | M | Moa Skan              | M | Mohamed Nedal                   |   | Mohammad Sadeghi                | M | Momchil Dechev              |   |                    |
| M | Morgan Stores                | N | Nancy Narang          | N | Nasrin Talebpour Sheshvan       | N | Nataliia Meshalkina             | N | Nataliia Shchukina          |   |                    |
| N | Natasha Jeffrey              | N | Neda Dadashi          | N | Nenad Sakan                     | N | Nicola Plutino                  | N | Nicolas Fuller              | N | Nicolas Labrosse   |
| N | Nicolas Poirier              | N | Nicole VILMER         | N | Nikola Veselinović              | N | Nikola Vitas                    | N | Nikolay Topchilo            |   |                    |
| N | Nikolina Milanovic           | N | Nina Dresing          | N | Nitin Vashishtha                | N | Nitin Yadav                     | N | Nived Vilangot Nhalil       |   |                    |
| N | Noemi Kinga Zsamberger       | N | Norbert Magyar        | O | Olena Podladchikova             | O | Olga Andreeva                   | O | Olga Golubchina             |   |                    |
| O | Olga Kutsenko                | O | Olga Panasenco        | O | Olga Sheiner                    | O | Oliver Rice                     | O | Oskar Steiner               | P | Paolo Massa        |
| P | Paolo Pagano                 | P | Paolo Romano          | P | Patrick Antolin                 | P | Patrick Ondratschek             | P | Paul Geyer                  | P | Paul Rajaguru      |
| P | Paulo Simões                 |   | Pavol Schwartz        | P | PAWAN KUMAR                     | P | Pearse Murphy                   | P | Peter Duchlev               | P | Peter Hunana       |
| P | Peter Wyper                  | P | Petr Heinzl           | P | Petr Jelínek                    | P | Philipp Löschl                  | P | Philippe-A. Bourdin         |   |                    |
| P | Pradeep Kumar Kayshap        | P | Prantika Bhowmik      | P | Prateek Mayank                  | P | Priyank Srivastava              | Q | Quentin Noraz               |   |                    |
| R | Radostin Simitev             | R | Raffaele Reda         | R | Raffaello Foldes                | R | Rahul Yadav                     | R | Rajab Ismayilli             |   |                    |
| R | Rajees Uthayasegaram         | R | Ramada Sukarnadji     | R | Rami Vainio                     | R | Ramon Oliver                    | R | Ranadeep Sarkar             |   |                    |
| R | Raveena Khan                 | R | Ravindra Desai        | R | Rebecca Robinson                | R | Reetika Joshi                   | R | Regina Biktimirova          |   |                    |
| R | Renzo Ramelli                | R | Ricardo Gafeira       | R | Richard Morton                  | R | Rita Ventura                    | R | Ritesh Patel                | R | Rob Rutten         |
| R | Robbe Vansintjan             | R | Robert Cameron        | R | Robert Jarolim                  | R | Robert Kavanagh                 | R | Robert Sych                 | R | Robert Walsh       |
| R | Roberta Morosin              | R | Roberto Bruno         | R | Roberto Soler                   | R | Robertus Erdelyi                | R | Roger Dufresne              | R | Rohit Sharma       |
| R | Rolf Schlichenmaier          | R | Roman Brajša          | R | Rony Keppens                    | R | Rositsa Miteva                  | R | Rossana De Marco            | R | Rui Liu            |
| R | Rui Pinto                    | R | Runbin Luo            | R | Russell Howard                  | R | Ryan Campbell                   | R | Ryan French                 | R | Ryan Milligan      |
| S | Sabrina Bechet               | S | Sabrina Guastavino    | S | Sahel Dey                       | S | Saida Milena Diaz Castillo      | S | Salvatore Luigi Guglielmino |   |                    |
| S | Salvatore Mancuso            | S | Sami Solanki          | S | Samrat Sen                      | S | Samridhi Sankar Maity           | S | Sanchita Pal                |   |                    |
| S | Sangeetha Chitrapadi Rajaram | S | Sanja Danilovic       | S | Sanjay Kumar                    | S | Santiago Vargas Domínguez       | S | Sara Mulas                  |   |                    |
| S | Sarah Paterson               | S | Sargam Mulay          | S | SATABDWA MAJUMDAR               |   | SATYAM AGARWAL                  | S | sean bruinsma               |   |                    |
| S | Sebastián Castellanos Durán  | S | Seray Sahin           | S | Serena Maria Lezzi              | S | Sergei Shestov                  | S | Sergey Anfinogentov         |   |                    |
|   | Sergio Dasso                 | S | Sergio Díaz Suárez    | S | Sergio Javier González Manrique | S | Sergio Toledo-Redondo           |   |                             |   |                    |
| S | shadi mohseni                | S | Shahin Jafarzadeh     | S | Shantanu Jain                   | S | Shanwlee Sow Mondal             | S | Shaonwita Pal               |   |                    |
| S | Shaun McLaughlin             | S | Shilpi Bhunia         | S | Siegfried Gonzi                 | S | Silja Pohjolainen               | S | Simeon Asenovski            |   |                    |
| S | Simon Cloutier               | S | Simon Good            | S | Simone Landi                    | S | Smitha Narayanamurthy           | S | Sneha Pandit                |   |                    |
| S | Sofia Carla Spago            | S | Sofya Belov           | S | Sondre Vik Furuseth             | S | Sonja Ježič                     | S | Sophie Masson               | S | Sophie Musset      |
| S | Sotiris Stamkos              |   | Soumyaranjan Dash     | S | Souvik Bose                     | S | Sowmya Krishnamurthy            | S | SPIROS PATSOURAKOS          |   |                    |
| S | Spyros Armatas               | S | Stanislav Gunár       | S | Stavro L. Ivanovski             | S | Stefaan Poedts                  | S | Stefan Hofmeister           |   |                    |
| S | Stefan Purkhart              | S | Stephan G. Heinemann  | S | Stephane Regnier                | S | Stephanie Yardley               | S | Sudip Mandal                |   |                    |
| S | Supriya Hebbur Dayananda     | S | Surajit Mondal        | S | Susan Samwel                    | S | Susanna Parenti                 | S | Sushree S Nayak             |   |                    |
| S | Suzana S. A. Silva           |   | Sven Wedemeyer        | S | Szabolcs Soós                   | T | Talwinder Singh                 | T | Tatiana Podladchikova       |   |                    |
| T | Tatyana Kaltman              | T | Teimuraz Zaqarashvili | T | Teodora Mihailescu              | T | Thanassis Katsiyannis           |   |                             |   |                    |
| T | Theodosios Chatzistergos     | T | Thomas Chen           | T | Thomas Hackman                  | T | Thomas Howson                   | T | Thomas Neukirch             |   |                    |
| T | Thomas Prevenslik            | T | Thomas Rees-Crockford | T | Thore Espedal Moe               | T | Théo Pellegrin                  | T | Tiago Pereira               |   |                    |
| T | Tim Duckenfield              | T | Timo Laitinen         | T | Tinatin Baratashvili            | T | Tingyu Gou                      | T | Tishtrya Mehta              | T | Tobias Felipe      |
| T | Tom Van Doorselaere          | T | Tomasz Mrozek         | T | Tomin James                     | U | Upasna Baweja                   | U | Urszula Bak-Steslicka       |   |                    |
| V | Valentina Abramenko          | V | Valentina Penza       | V | Valeria Quintero Ortega         | V | Valeria Sieyra                  | V | Valeriia Liakh              |   |                    |
| V | Valery NAGNIBEDA             | V | Valery Nakariakov     | V | Vartika Pandey                  | V | Vasco Manuel de Jorge Henriques |   |                             |   |                    |

of disturbances, associated with typical solar corona energy fluctuations, to generate these types of modes. We found that confined energy deposition excites slow modes, while global perturbations, capable of instantly modifying the loop temperature, excite fast sausage modes.

**Speaker:** Mariana Cécere (Instituto de Astronomía Teórica y Experimental (CONICET/UNC))

 ESPM\_Poster\_Cece...

9:13 AM

### Stability of solar atmospheric structures harboring standing slow waves: an analytical model in a compressible plasma 13m

In the context of the solar coronal heating problem, one possible explanation for the high coronal temperature is the release of energy by magnetohydrodynamic (MHD) waves. The energy transfer is believed to be possible, among others, by the development of the Kelvin-Helmholtz instability (KHI) in coronal loops. Our aim is to determine if standing slow waves in solar atmospheric structures such as coronal loops, and also prominence threads, sunspots, and pores, can trigger the KHI due to the oscillating shear flow at the structure's boundary. We used linearized nonstationary MHD to work out an analytical model in a cartesian reference frame. The model describes a compressible plasma near a discontinuous interface separating two regions of homogeneous plasma, each harboring an oscillating velocity field with a constant amplitude which is parallel to the background magnetic field and aligned with the interface. The obtained analytical results were then used to determine the stability of said interface, both in coronal and photospheric conditions. We find that the stability of the interface is determined by a Mathieu equation. In function of the parameters of this equation, the interface can either be stable or unstable. For coronal as well as photospheric conditions, we find that the interface is stable with respect to the KHI. Theoretically, it can, however, be unstable with respect to a parametric resonance instability, although it seems physically unlikely. We conclude that, in this simplified setup, a standing slow wave does not trigger the KHI without the involvement of additional physical processes.

**Speaker:** Michaël Geeraerts

 ESPM\_conference\_...

9:26 AM

### Public version of Mancha: a non-ideal MHD code for realistic simulations of the solar atmosphere. 13m

The MANCHA code development was started in 2006 to study wave dynamics in sunspots at the Instituto de Astrofísica de Canarias. Since then it has gradually been upgraded by adding new physics and improved programming techniques. The code can be used for a large variety of problems from linear wave propagation and classical hydrodynamic instabilities to highly realistic simulations of convection-driven solar and stellar atmosphere.

The code solves the MHD equations including nonlinear terms for the ambipolar and Hall diffusion, the Ohm's heating and the Biermann battery.

The radiative energy exchange is implemented by the short-characteristics method.

The equation of state is either ideal (computed on the fly) or realistic (interpolated from pre-computed lookup tables provided by the user).

The code uses uniform Cartesian grid with spatial discretization up to 6th order; the Runge-Kutta scheme is used for the time integration.

A super-time-stepping technique is implemented to overcome timestep limitation due to diffusion processes.

Hyper-diffusion and filtering are available to stabilize the high-frequency numerical noise.

A perfectly-matched-layer is implemented as an optional non-reflecting boundary condition.

MANCHA is written in Fortran and parallelized with MPI, including parallel I/O using the HDF library.

In order to solve a new problem, users will need to find their own optimal set of parameters in an input control file.

In the case of non-periodic boundaries, users are expected to create their own boundary condition module.

A set of samples together with the manual provide basic instructions on how to do that.

**Speaker:** Mikhail Modestov (Instituto de Astrofísica de Canarias)

 ESPM\_MANCHA.pdf


9:39 AM

### The optical properties of Hydrogen plasma described in the frame of the fully quantum method based on a cut-off Coulomb model potential 13m

The absorption coefficients of hydrogen plasma, calculated within the frame of cut-off Coulomb potential model, for the wide area of electron densities and temperatures observed within the solar atmosphere are presented here. The optical parameter of hydrogen plasma of mid and moderately high nonideality parameter could be described successfully, thus enabling the modeling of optical properties, especially the calculation of plasma opacity. The model was proven in both convergence towards normal condition, ideal plasma case, as well as with the help of analysis of the experimental data and further theoretical consideration. The model potential is solvable in entire space and within entire energy spectrum, thus the yielded wave function solutions are a combination of a special functions. The special form of the cut-off Coulomb potential, possesses an unique feature that enables the precise, fully quantum method of calculation of inverse Bremsstrahlung effect. Although the presented method development is still a work in progress the possibility of unifying a mode for both transport and optical properties of plasma within same model is an attractive direction for it's further development.

**Speaker:** Dr Nenad Sakan (Institute of Physics Belgrade)

 poster\_ESPM-16\_ns...

 Poster\_pres\_ns\_zs...

9:52 AM

### MHD wave propagation in asymmetric solar waveguides 13m

We present our findings on MHD wave propagation and instabilities in asymmetric Cartesian waveguide models. Generalising the classical slab models this way, thanks to the introduction of various sources of asymmetry (background density, magnetic field or flow speed) allows us to more precisely investigate several important features in the richly structured solar atmosphere. By developing solar magneto-seismologic methods from these analytical models, we can provide an efficient tool for obtaining further information about the solar plasma from observations. We offer further detail on the types and parameters of MHD waves expected to propagate and be observable in a number of multi-layered systems of the solar atmosphere (such as e.g. magnetic bright points or light walls) with new, high-resolution technology.

**Speaker:** Ms Noémi Kinga Zsámberger

10:05 AM

### From highly-collisional to collisionless fluid models 13m

The atmosphere of the sun represents a complex physical environment where two traditional classes of fluid theories come to interplay. While the solar chromosphere is typically modeled with fluid models derived under the highly-collisional assumption, whereas the collisional frequencies in the solar corona can become so small, that collisionless fluid models seem to be more appropriate. We briefly overview these two distinct classes of fluid theories and discuss the major differences

# The optical properties of Hydrogen plasma described in the frame of the fully quantum method based on a cut-off Coulomb model potential

Nenad M. Sakan<sup>1\*</sup>, Zoran J. Simić<sup>2</sup>, and Momchil Dechev<sup>3</sup>

<sup>1</sup> Institute of Physics, Belgrade University, Pregrevica 118, 11080 Zemun, Belgrade, Serbia

<sup>2</sup> Astronomical Observatory, Volgina 7, 11060 Belgrade, Serbia

<sup>3</sup> Institute of Astronomy and National Astronomical Observatory, Bulgarian Academy of Sciences, 72, Tsarigradsko chaussee Blvd. Sofia, Bulgaria

nsakan@ipb.ac.rs

## Abstract

The absorption coefficients of hydrogen plasma, calculated within the frame of cut-off Coulomb potential model, for the wide area of electron densities and temperatures observed within the solar atmosphere are presented here. The optical parameter of hydrogen plasma of mid and moderately high nonideality parameter could be described successfully, thus enabling the modeling of optical properties, especially the calculation of plasma opacity. The model was proven in both convergence towards normal condition, ideal plasma case, as well as with the help of analysis of the experimental data and further theoretical consideration. The model potential is solvable in entire space and within entire energy spectrum, thus the yielded wave function solutions are a combination of a special functions. The special form of the cut-off Coulomb potential, possesses an unique feature that enables the precise, fully quantum method of calculation of inverse Bremsstrahlung effect. Although the presented method development is still a work in progress the possibility of unifying a mode for both transport and optical properties of plasma within same model is an attractive direction for its further development

## 1. Introduction

In the theoretical models of Solar plasma a problems of plasma opacity, energy transport as well as radiative transfer under moderate and strong non-ideality are of strong interest, for the deeper analysis of the subject referre to [1, 2, 3, 4]. The strong coupling and density effects in plasma radiation were the subject of numerous experimental and theoretical studies in the last decades. The presented quantum way of describing atomic photo-absorption processes in dense strongly ionized hydrogen plasma is based on the approximation of the cut-off Coulomb potential. By now this approximation has been used in order to describe transport properties of dense plasma (see e.g. [1, 5, 6]), but it was clear that it could be applied to some absorption processes in non-ideal plasmas too [3, 7, 8, 9]. More detailed explanation could be find in [10].

## 2. Theory

### 2.1 The approximation of the cut-off Coulomb potential

Many body processes could be described by the use of transformation to the corresponding single-particle processes in an adequately chosen model potential, for the detailed theory [10] should be considered.

As an adequate model potential for hydrogen plasma of higher density, for instance referre to [5, 3], the screening cut-off Coulomb potential, that satisfies above conditions, and is used here is in form

$$U_c(r) = \begin{cases} -\frac{e^2}{r} + \frac{e^2}{r_c}, & 0 < r \leq r_c, \\ 0, & r_c < r < \infty, \end{cases} \quad (1)$$

where the mean potential energy of an electron in the considered hydrogen plasma  $U_c = -e^2/r_c$  is used as a energy origin of the potential. Here  $e$

is the modulus of the electron charge,  $r$  - distance from the ion, and cut-off radius  $r_c$  - the characteristic screening length of the considered plasma.

The cut-off radius  $r_c$  can be determined, see details in [11]. The code that calculates the characteristic screening length of considered plasma uses  $N_e$  and  $T$ , and is given at <https://github.com/nsakan972/ESPM-16.git>, it is open sourced and free for use.

### 2.2 The calculated quantities

In accordance with previously mentioned theory the behavior of the dipole matrix element is investigated. It is given by  $\hat{D}(r; r_c; n_i, l_i; n_f, l_f) = \langle n_f, l_f | \mathbf{r} | n_i, l_i \rangle$ , where  $|n_i, l_i\rangle$  and  $|n_f, l_f\rangle$  are initial and final state wave functions obtained within the model of cut-off Coulomb potential. So all the photon emission and absorption parameters are related with the dipole matrix element. A essential calculation for this is the solving of the radial part of Schrödinger equation, e.g. finding of energy level values as well as the radial parts of the wave functions. The radial part,  $R_{n,l;r_c}(r)$  presented as  $\chi(r) = rR(r)$  for the selected level  $n=3$  and  $l=0$  could be seen on Figure 1. Please note that in the strong local plasma field a wave functions differ significantly from Coulomb case and as such reflect on all parameters and further calculated values.

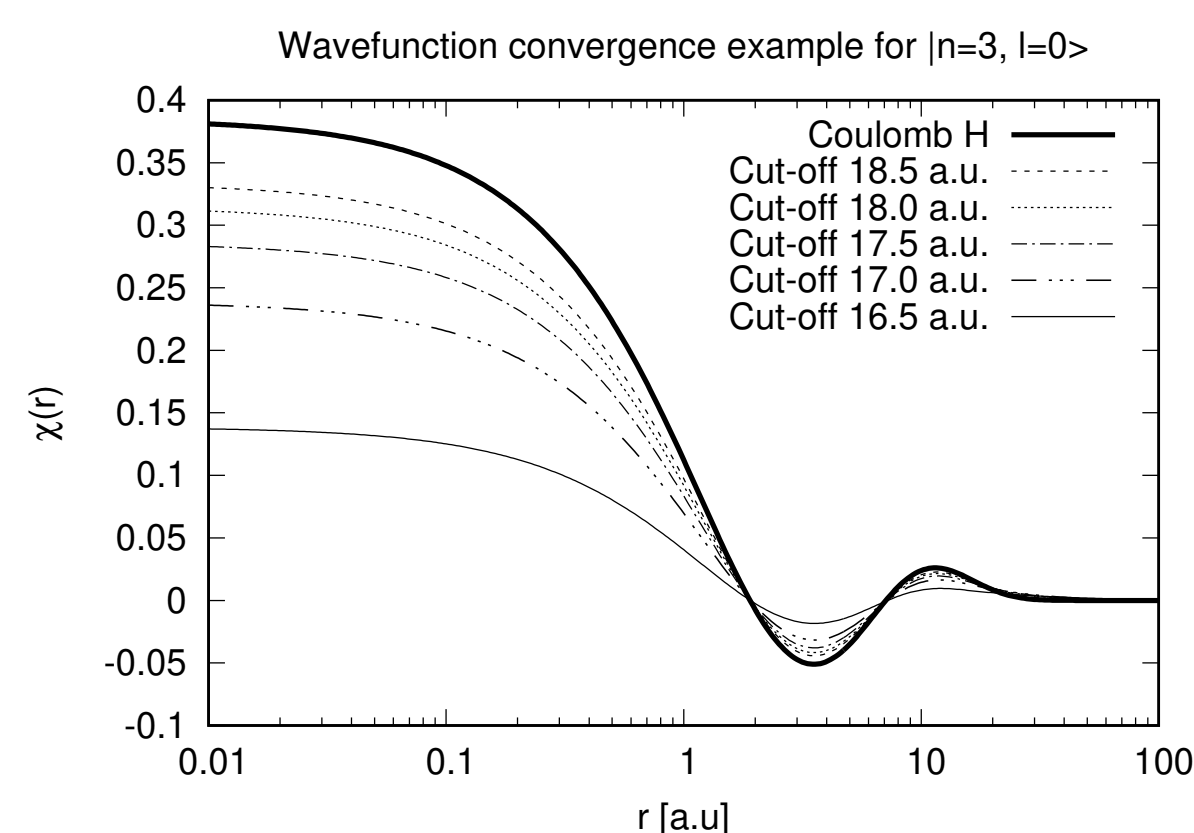


**Figure 1.** The plasma influence onto the form of wave function. Please note that  $\chi(r) = rR(r)$ , where  $R(r)$  is a radial part of wave function.

For instance the total absorption cross section is proportional to the dipole matrix element

$$\sigma_0(\omega = \omega_{fi}) \sim \left| \hat{D}(r; r_c; n_i, l_i; n_f, l_f) \right|^2, \quad (2)$$

and so any change of the wave function reflects on both dipole matrix element as well as total cross section symmetrically.

The test set of dipole matrix elements for the hydrogen atom in plasma calculated for the variety of cut-off radius,  $r_c$ , values is available at <https://github.com/nsakan972/ESPM-16.git>.

## 3. Conclusion

The presented work is a continuation of the previously developed modeling with for the photoionization and inverse Bremsstrahlung proceses of hydrogen plasma, and the goal is to include bond-bond processes within same model. All of previously calculated data is also usable in modeling of Solar plasma processes.

In order to model a behaviour of the plasma optical characteristics the used potential is a good approximation for the modeling of plasma interaction in a large area of densities and temperatures,

details in [10]. A strong plasma influence onto the optical parameters is observed where the plasma interaction energy is close to observed level energy value, e.g. when this level starts to appear, as illustrated in figure. The work on using a more complex potentials is going on. We have tested a numerical method of wave function solution, and as a first step the Ar atom modeled is introduced, and initial values are in a expected range. As a second effect, a more detailed plasma-emitter interaction could be modeled. For both experimental praxis as well as Sun processes modeling an introduction of He atom and ion model is must, and as such could determine the further research.

## References

- [1] Fortov, V.E., Iakubov, I.T. The physics of non-ideal plasma; World Scientific, 1999.
- [2] Rogers, F.J., Iglesias, C.A. Opacity of stellar matter. Space Sci. Rev. 1998, 85, 61–70.
- [3] Mihajlov, A.A., Sakan, N.M., Srećković, V.A., Vitel, Y., Modeling of continuous absorption of electromagnetic radiation in dense partially ionized plasmas. J. Phys. A 2011, 44, 095502.
- [4] Mihajlov, A.A.; Ignjatović, L.M., Srećković, V.A., Dimitrijević, M.S., Metropoulos, A., The non-symmetric ion-atom radiative processes in the stellar, atmospheres, Mon. Not. R. Astron. Soc. 2013, 431, 589–599.
- [5] Mihajlov, A.A., Djordjević, D., Popović, M.M., Meyer, T., Luft, M., Kraeft, W.D., Determination of the Electrical Conductivity of a Plasma on the Basis of the Coulomb cut-off Potential Model., Contrib. Plasma Phys., 1989, 29, 441–446.
- [6] Ignjatović, L.M., Srećković, V.A., Dimitrijević, M.S., The Screening Characteristics of the Dense Astrophysical Plasmas: The Three-Component Systems., Atoms, 2017, 5, 42.
- [7] Mihajlov, A.A., Sakan, N.M., Srećković, V.A., Vitel, Y., Modeling of the Continuous Absorption of Electromagnetic Radiation in Dense Hydrogen Plasma., Balt. Astron., 2011, 20, 604–608.
- [8] Mihajlov, A.A., Srećković, V.A., Sakan, N.M., Inverse Bremsstrahlung in Astrophysical Plasmas: The Absorption Coefficients and Gaunt Factors., J. Astrophys. Astron., 2015, 36, 635–642.
- [9] Sakan, N.M., Srećković, V.A., Mihajlov, A.A., The application of the cut-off Coulomb potential for the calculation of a continuous spectra of dense hydrogen plasma., Mem. S. A. I. Suppl., 2005, 7, 221–224.
- [10] Sakan, Nenad M. and Srećković, Vladimir A. and Simić, Zoran J. and Dimitrijević, Milan S., The Application of the Cut-Off Coulomb Model Potential for the Calculation of Bound-Bound State Transitions, Atoms, 2018, 6, 1, 4
- [11] Mihajlov, A., Vitel, Y., Ignjatović, L.M., The new screening characteristics of strongly non-ideal and dusty plasmas. Part 3: Properties and applications., High Temp., 2009, 47, 147–157.
- [12] Vitel, Y., Gavrilova, T., D'yachkov, L., Kurilenkov, Y.K., Spectra of dense pure hydrogen plasma in Balmer area., J. Quant. Spectrosc. Radiat. Transf., 2004, 83, 387–405.

## HF CHARACTERISTICS OF THE ASTROPHYSICAL PLASMAS

A. A. MIHAJLOV, N. M. SAKAN and V. A. SREĆKOVIĆ

*Institute of Physics, University of Belgrade, PO Box 57, 11000 Belgrade, Serbia*  
*E-mail: vlada@bg.ac.rs*

**Abstract.** The values of electrical conductivity of plasma of stars with a magnetic field or moving in the magnetic field of the other component in a binary system could be of significant interest, since they are useful for the study of thermal evolution of such objects, cooling, nuclear burning of accreted matter, and the investigation of their magnetic fields. So, on the basis of numerically calculated values for the dense plasma conductivity in an external HF electric field, we determine the HF characteristics of astrophysical plasmas under extreme conditions. The examined range of frequencies covers the IR, visible and near UV regions and consider electronic number density and temperature are in the ranges of  $10^{21}\text{cm}^{-3} \leq Ne$  and  $20\,000 \leq T$ , respectively. The method developed here represents a powerful tool for research into white dwarfs with different atmospheric compositions (DA, DC etc.), and for investigation of some other stars (M-type red dwarfs, Sun etc.).

### 1. INTRODUCTION

In this paper a highly ionized plasma in a homogenous and monochromatic external electric field  $\vec{E}(t) = \vec{E}_0 \exp\{-i\omega t\}$  is considered. According to Sreckovic et al. (2010) and Sakan et al. (2007), the dynamic electric conductivity of a strongly coupled plasma  $\sigma(\omega) = \sigma_{Re}(\omega) + i\sigma_{Im}(\omega)$  is represented by the expressions:

$$\sigma(\omega) = \frac{4e^2}{3m} \int_0^\infty \tau(E) \left[ -\frac{dw(E)}{dE} \right] \rho(E) E dE, \quad (1)$$

$$\sigma_{Re}(\omega) = \frac{4e^2}{3m} \int_0^\infty \frac{\tau(E)}{1 + (\omega\tau(E))^2} \left[ -\frac{dw(E)}{dE} \right] \rho(E) E dE, \quad (2)$$

$$\sigma_{Im}(\omega) = \frac{4e^2}{3m} \int_0^\infty \frac{\omega\tau^2(E)}{1 + (\omega\tau(E))^2} \left[ -\frac{dw(E)}{dE} \right] \rho(E) E dE, \quad (3)$$

where  $\rho(E)$  is the density of electron states in the energy space and  $w(E)$  is the Fermi-Dirac distribution function,  $\tau(E)$  is the relaxation time

$$\tau(E) = \frac{\tau(E)}{1 - i\omega\tau(E)}, \quad (4)$$

$\tau(E)$  being the 'static' relaxation time. The method of determination of  $\tau(E)$  is described in the previous papers (Adamyany et al. (2006), Tkachenko et al. (2006) and Sreckovic et al. (2010a,b)) in detail.



Other HF plasma characteristics can be expressed in terms of the quantities  $\sigma_{Re}(\omega)$  and  $\sigma_{Im}(\omega)$ .

Thus the plasma dielectric permeability is

$$\varepsilon(\omega) = 1 + i \frac{4\pi}{\omega} \sigma(\omega) = \varepsilon_{Re}(\omega) + i\varepsilon_{Im}(\omega), \quad (5)$$

where  $\varepsilon_{Re}(\omega)$  and  $\varepsilon_{Im}(\omega)$  are given as

$$\varepsilon_{Re}(\omega) = 1 - \frac{4\pi}{\omega} \sigma_{Im}(\omega), \quad \varepsilon_{Im}(\omega) = \frac{4\pi}{\omega} \sigma_{Re}(\omega). \quad (6)$$

The coefficients of refraction,  $n(\omega)$ , and reflection,  $R(\omega)$ , are determined as

$$n(\omega) = \sqrt{\varepsilon(\omega)} = n_{Re}(\omega) + in_{Im}(\omega), \quad (7)$$

$$R(\omega) = \left| \frac{n(\omega) - 1}{n(\omega) + 1} \right|^2 \quad (8)$$

where, bearing in mind that

$$|\varepsilon(\omega)| = \sqrt{\varepsilon_{Re}^2(\omega) + \varepsilon_{Im}^2(\omega)}, \quad (9)$$

the real and imaginary part of refractivity,  $n_{Re}(\omega)$  and  $n_{Im}(\omega)$ , are given by

$$n_{Re}(\omega) = \sqrt{\frac{1}{2}(|\varepsilon(\omega)| + \varepsilon_{Re}(\omega))}, \quad n_{Im}(\omega) = \sqrt{\frac{1}{2}(|\varepsilon(\omega)| - \varepsilon_{Re}(\omega))}. \quad (10)$$

From here the equation for the plasma reflectivity could be expressed as

$$R(\omega) = \left\{ \frac{1 + |\varepsilon(\omega)| - \sqrt{2}\sqrt{|\varepsilon(\omega)| + \varepsilon_{Re}(\omega)}}{1 + |\varepsilon(\omega)| + \sqrt{2}\sqrt{|\varepsilon(\omega)| + \varepsilon_{Re}(\omega)}} \right\}^{1/2} \quad (11)$$

The other parameter of interest is the penetration depth of electromagnetic radiation into plasma,  $\Delta(\omega)$ . This quantity is just the skin-layer width determined as the inverse imaginary part of the electromagnetic field wave number

$$\Delta(\omega) = \frac{c}{\omega n_{Im}(\omega)}. \quad (12)$$

where  $c$  is the speed of light.

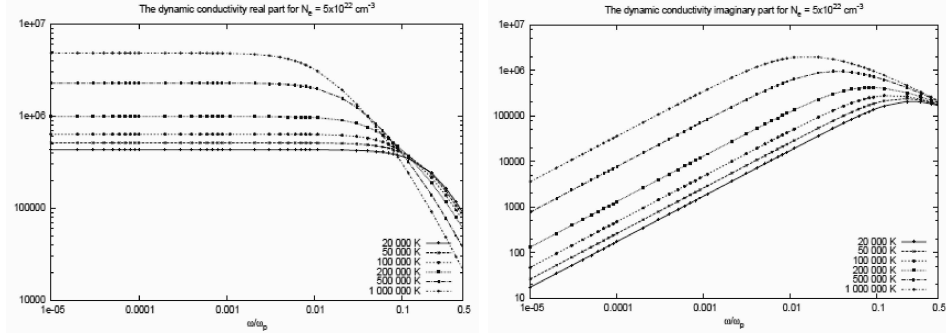


Figure 1: The dynamic conductivity real  $\sigma_{Re}(\omega)$  and imaginary part  $\sigma_{Im}(\omega)$  for  $N_e = 5 \cdot 10^{22} \text{ cm}^{-3}$  and  $20,000\text{K} < T < 100,000\text{K}$ .

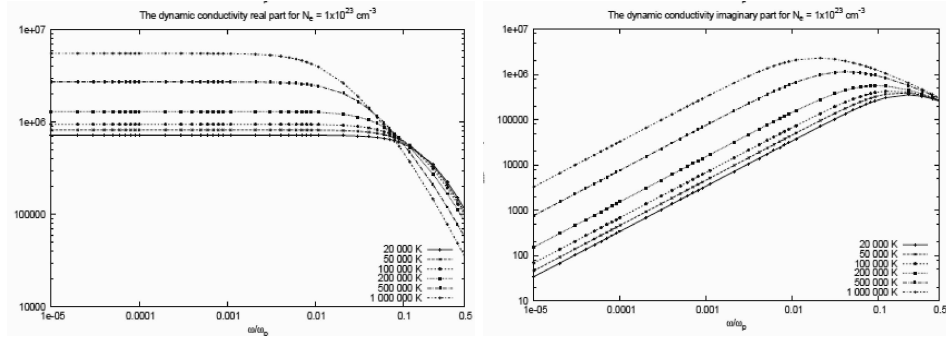


Figure 2: The dynamic conductivity real  $\sigma_{Re}(\omega)$  and imaginary part  $\sigma_{Im}(\omega)$  for  $N_e = 1 \cdot 10^{23} \text{ cm}^{-3}$  and  $20,000\text{K} < T < 100,000\text{K}$ .

## 2. RESULTS AND DISCUSSION

We here continue our previous investigations of plasma static electrical conductivity which are of interest for DB white dwarf atmospheres (see Sreckovic et al. (2010)b,c and Sreckovic et al. (2012)). So, in accordance with the aim of this work, we calculated HF plasma characteristics for wide plasma conditions in order to apply our results to the atmospheres of different stellar types.

Figures 1-3 illustrate the behavior of the HF conductivity for various plasma conditions which gives possibility to calculate other transport properties. Figures 1-3, demonstrate the regular behavior of  $\sigma_{Re}(\omega)$ , i.e. the convergence to the corresponding values of  $\sigma_0(n_e, T)$  when  $\omega \rightarrow 0$ , and the existence of the interval of variation of  $\omega$  where  $\sigma_{Re}(\omega)$  is practically constant. We observe the tendency of this interval to decrease when temperature  $T$  increases. Similarly, Figures 1-3, demonstrate a regular behavior of  $\sigma_{Im}(\omega)$ , i.e. the convergence to zero when  $\omega \rightarrow 0$ , and the presence of a maximum in the interval  $0 < \omega < 0.5\omega_p$ .

The method developed in this paper represents a powerful tool for research white dwarfs with different atmospheric compositions (DA, DC etc.), and some other stars (M-type red dwarfs, Sun etc.). Finally, the presented method provides a basis for

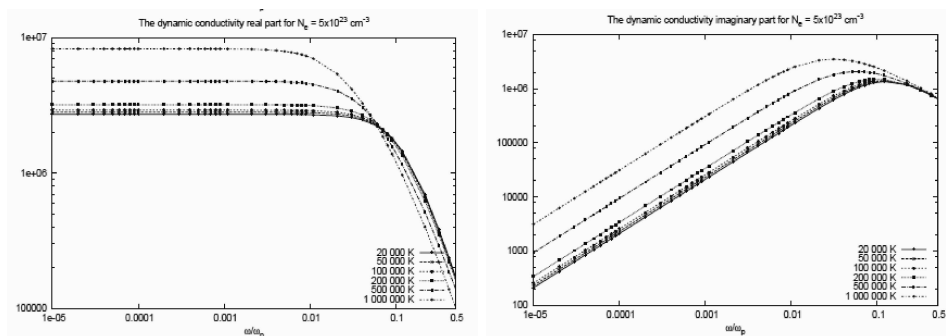


Figure 3: The dynamic conductivity real  $\sigma_{Re}(\omega)$  and imaginary part  $\sigma_{Im}(\omega)$  for  $N_e = 5 \cdot 10^{23} \text{ cm}^{-3}$  and  $20000\text{K} < T < 100000\text{K}$ .

the development of methods to describe other transport characteristics which are important for the study of all mentioned astrophysical objects, such as the electronic thermo-conductivity in the stellar atmosphere layers with large electron density, and electrical conductivity in the presence of strong magnetic fields.

### Acknowledgement

The authors are grateful to the Ministry of Education, Science and Technological Development of the Republic of Serbia for the support of this work within the projects 176002, III4402 and 171014.

### References

- Adamyany, V. M., Grubor, D., Mihajlov, A. A., Sakan, N. M., Srećković, V. A., Tkachenko, I. M.: 2006, *J. Phys. A*, **39**, 4401-4405.
- Sakan, N. M., Sreckovic, V. A., Adamyan, V. M., Tkachenko, I. M., Mihajlov, A. A.: 2007, *Publications de l'Observatoire Astronomique de Beograd*, **82**, 171.
- Srećković, V. A., Adamyan, V. M., Ignjatović, Lj. M., Mihajlov, A. A.: 2010, *Phys. Lett. A*, **374**, 754-760.
- Srećković, V. A., Ignjatović, Lj. M., Mihajlov, A. A., Dimitrijević, M. S.: 2010, *MNRAS*, **406**, 590-596.
- Srećković, V. A., Ignjatović, Lj. M., Mihajlov, A. A., Dimitrijević, M. S.: 2010 *American Institute of Physics Conference Series*, **1273**, 432-435.
- Srećković, V. A., Ignjatović, Lj. M., Mihajlov, A. A. & Dimitrijević, M. S.: 2012, *PASRB*, **11**, 331.
- Tkachenko, I. M., Adamyan, V. M., Mihajlov, A. A., Sakan, N. M., Šulić, D. M., Srećković, V. A.: 2006, *J. Phys. A*, **39**, 4693-4697.

Article

# The Application of the Cut-Off Coulomb Model Potential for the Calculation of Bound-Bound State Transitions

Nenad M. Sakan <sup>1,\*</sup> , Vladimir A. Srećković <sup>1</sup> , Zoran J. Simić <sup>2</sup>  
and Milan S. Dimitrijević <sup>2,3</sup> 

<sup>1</sup> Institute of Physics, Belgrade University, Pregrevica 118, 11080 Zemun, Belgrade, Serbia; vlada@ipb.ac.rs

<sup>2</sup> Astronomical Observatory, Volgina 7, 11060 Belgrade, Serbia; zsimic@aob.rs (Z.J.S.);  
mdimitrijevic@aob.rs (M.S.D.)

<sup>3</sup> LERMA (Laboratoire d'Etudes du Rayonnement et de la Matière en Astrophysique et Atmosphères),  
Observatoire de Paris, UMR CNRS 8112, UPMC, 92195 Meudon CEDEX, France

\* Correspondence: nsakan@ipb.ac.rs

Received: 9 September 2017; Accepted: 8 January 2018; Published: 12 January 2018

**Abstract:** In this contribution, we present results of bound state transition modeling using the cut-off Coulomb model potential. The cut-off Coulomb potential has proven itself as a model potential for the dense hydrogen plasma. The main aim of our investigation include further steps of improvement of the usage of model potential. The results deal with partially ionized dense hydrogen plasma. The presented results covers  $N_e = 6.5 \times 10^{18} \text{ cm}^{-3}$ ,  $T = 18,000 \text{ K}$  and  $N_e = 1.5 \times 10^{19} \text{ cm}^{-3}$ ,  $T = 23,000 \text{ K}$ , where the comparison with the experimental data should take place, and the theoretical values for comparison. Since the model was successfully applied on continuous photoabsorption of dense hydrogen plasma in the broad area of temperatures and densities, it is expected to combine both continuous and bound-bound photoabsorption within single quantum mechanical model with the same success.

**Keywords:** atomic processes; radiative transfer; Sun: atmosphere; Sun: photosphere; stars: atmospheres; white dwarfs

## 1. Introduction

The problems of plasma opacity, energy transport and radiative transfer under moderate and strong non-ideality are of interest in theoretical and experimental research [1–4]. The strong coupling and density effects in plasma radiation were the subject of numerous experimental and theoretical studies in the last decades. Here, we keep in mind the plasma of the inner layers of the solar atmosphere, as well as of partially ionized layers of other stellar atmospheres—for example, the atmospheres of DA white dwarfs with effective temperatures between 4500 K and 30,000 K.

In this paper, we presented a new model way of describing atomic photo-absorption processes in dense, strongly ionized hydrogen plasmas, which is based on the approximation of the cut-off Coulomb potential. By now, this approximation has been used in order to describe transport properties of dense plasmas (e.g., [1,5,6]), but it was clear that it could be applied to some absorption processes in non-ideal plasmas too [3,7–9]. This topic itself, and the search for more consistent models of screening and more realistic potentials in plasmas is still continuing and is very real (e.g., [10–13] and references therein).

The neutral hydrogen acts as an absorber in plasma, and its concentration determination is essential in order to calculate the absorption coefficients. The neutral hydrogen concentration from experimental data from [14] is used, and, since the result presented here is in the area where the Saha equation is valid, the neutral concentrations using the Saha equation with the ionization potential



correction is possible. Since this is related to the further step, bound level broadening mechanism, the procedure was not elaborated here. In addition, the emitter, neutral hydrogen, interacts with other plasma species such as electrons and ions. In such a way, the theoretical hydrogen plasma model results as well as NIST database values act as a limiting case for verification of solutions, in the case when plasma influence is small or diminishes, e.g.,  $r_c \rightarrow \infty$  in later case.

In order to calculate the total absorption coefficient, the same broadening mechanism for the bound state levels should be applied. Up until now, the continuous absorption processes were calculated with the help of parametric broadening for the bound-free absorption [7]. The broadening processes play a more important role in bound-bound processes, and, as such, the more realistic theoretical model of broadening of bound state levels or a result of adequate molecular dynamics (MD) simulations should be used. Only in such a case could the total absorption coefficients, obtained within the same broadening model, be compared with real experimental data. This work is in progress.

A first step in extending of the model with additional processes is the bound state transition processes inclusion. The bound state transition processes are stated as the most important goal in the development of the self containing model, capable of describing optical as well as dynamical characteristics of dense hydrogen plasma. The characteristics of the bound state transitions in plasma diagnostics are well known, an almost mandatory method [15]. The usage of the hydrogen lines as a probing method for the plasma characteristics is also well known and widely used in plasmas of moderate and small non-ideality [16]. In accordance with that previously mentioned, the continuation of research of the presented approach is the inclusion of the bound-bound photo absorption process using the same model potential. The investigated process is the bound-bound i.e., photo absorption processes:

$$\epsilon_\lambda + H^*(n_i, l_i) \rightarrow H^*(n_f, l_f), \tag{1}$$

where  $n$  and  $l$  are the principal and the orbital quantum number of hydrogen-atom excited states, hydrogen atom in its initial state  $|n_i, l_i\rangle$  is presented by  $H^*(n_i, l_i)$ , its final state  $|n_f, l_f\rangle$  by  $H^*(n_f, l_f)$ , and  $\epsilon_\lambda$  presents absorbed photon energy.

## 2. Theory

### 2.1. The Approximation of the Cut-Off Coulomb Potential

The absorption processes (1) in astrophysical plasma are considered here as a result of radiative transition in the whole system “electron–ion pair (atom) + the neighborhood”, namely:  $\epsilon_\lambda + (H^+ + e)_i + S_{rest} \rightarrow (H^+ + e)_f + S'_{rest}$ , where  $S_{rest}$  and  $S'_{rest}$  denote the rest of the considered plasma. However, as it is well known, many-body processes can sometimes be simplified by their transformation to the corresponding single-particle processes in an adequately chosen model potential.

As an adequate model potential for hydrogen plasma with such density, we choose, as in [3,5], the screening cut-off Coulomb potential, which satisfies above conditions, and can be presented in the form:

$$U(r; r_c) = \begin{cases} -\frac{e^2}{r}, & 0 < r \leq r_c, \\ U_{p;c}, & r_c < r < \infty, \end{cases} \tag{2}$$

where the cut-off radius  $r_c$  is defined by relation (3), as it is illustrated by Figure 1a. Here,  $e$  is the modulus of the electron charge,  $r$ —distance from the ion, and cut-off radius  $r_c$ —the characteristic screening length of the considered plasma. Namely, within this model, it is assumed that quantity

$$U_{p;c} = -\frac{e^2}{r_c} \tag{3}$$

is the mean potential energy of an electron in the considered hydrogen plasma.

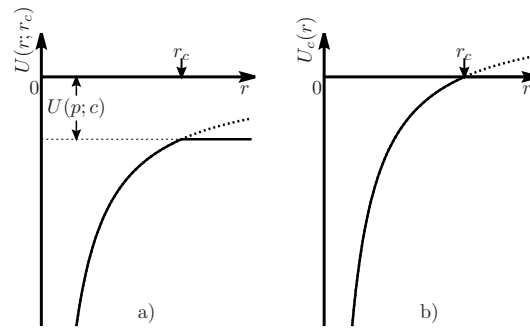


**Figure 1.** Behaviour of the potentials  $U(r; r_c)$  and  $U_c(r)$ , where  $r_c$  is the cut-off parameter. In (a) the potential goes to the mean potential energy of an electron in the considered hydrogen plasma  $U_{p;c}$ , and in (b), the value of  $U_{p;c}$  is taken as zero energy, i.e.,  $U_c = U(r; r_c) - U_{p;c}$ , in the more applicable form used here.

As in [3,5,8], we will take the value  $U_{p;c}$  as the zero of energy. After that, the potential Equation (2) is transformed to the form

$$U_c(r) = \begin{cases} -\frac{e^2}{r} + \frac{e^2}{r_c}, & 0 < r \leq r_c, \\ 0, & r_c < r < \infty, \end{cases} \quad (4)$$

which is illustrated by Figure 1b. Here,  $e$  is the modulus of the electron charge,  $r$ —distance from the ion, and cut-off radius  $r_c$ —the characteristic screening length of the considered plasma.

It is important that the cut-off radius  $r_c$  can be determined as a given function of  $N_e$  and  $T$ , using two characteristic lengths:

$$r_i = \left( \frac{k_B T}{4\pi N_i e^2} \right)^{1/2} \quad r_{s;i} = \left( \frac{3}{4\pi N_i} \right)^{1/3}, \quad (5)$$

namely, taking that  $N_i = N_e$  and  $r_c = a_{c;i} \cdot r_i$  we can directly determine the factor  $a_{c;i}$  as a function of ratio  $r_{s;i}/r_i$ , on the basis of the data about the mean potential energy of the electron in the single ionized plasma from [12]. The behavior of  $a_{c;i}$  in a wide region of values of  $r_{s;i}/r_i$  is presented in Figure 2.

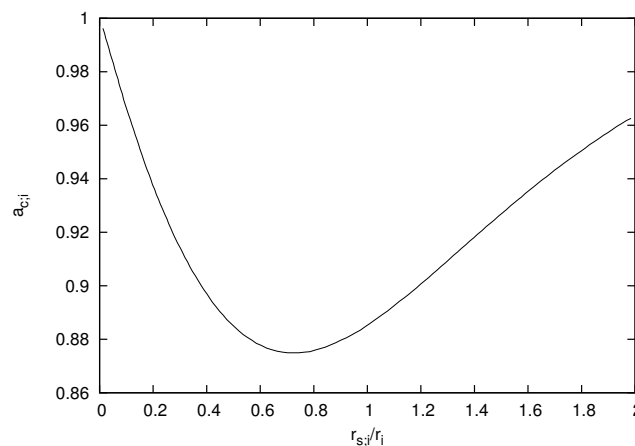


**Figure 2.** Behavior of the parameters  $a_{c;i} \equiv r_c/r_i$  as the function of the ratio  $r_{s;i}/r_i$ , where  $r_i$  is given by Equation (5) and  $r_{s;i}$  is the ion Wigner–Seitz radius for the considered electron-ion plasma (5). The presented curve is obtained on the basis of data presented in [12].

## 2.2. The Calculated Quantities

In accordance with that, the behavior of the dipole matrix element is investigated here. It is given by

$$\hat{D}(r; r_c; n_i, l_i; n_f, l_f) = \langle n_f, l_f | \mathbf{r} | n_i, l_i \rangle, \quad (6)$$

where the wave functions  $|n_i, l_i\rangle$  and  $|n_f, l_f\rangle$  are initial and final state wave functions obtained within the model of cut-off Coulomb potential, for the calculations of the plasma characteristics, or the theoretical hydrogen ones in order to additionally check the model.

For the calculation of oscillator strength, we use expressions from [17–19]

$$f(n_f, l_f; n_i, l_i; r_c) = \frac{1}{3} \frac{\nu}{Ry} \left[ \frac{\max(l_f, l_i)}{2l_f + 1} \right] \hat{D}(r; r_c; n_i, l_i; n_f, l_f)^2, \quad (7)$$

where  $Ry$  is the Rydberg constant, in the same units as the frequency  $\nu$  of the transition  $(n, l) \rightarrow (n', l')$ . The calculated data are presented in Table 1.

Our future plan is to include broadening processes and make it possible to directly compare data with the experimental ones (e.g., the data from [14]). In continuation, some of the bound-bound theoretical aspects are shown.

The total absorption cross section of the line could be linked with the dipole moment directly with the help of relation

$$\sigma_0(\omega = \omega_{fi}) = \frac{1}{3} \frac{g_2}{g_1} \frac{\pi \omega_{fi}}{\varepsilon_0 \hbar c} \hat{D}(r; r_c; n_i, l_i; n_f, l_f)^2. \quad (8)$$

It should be noted that the absorption line profile is needed in order to apply the obtained results to the absorption calculations:

$$\sigma(\omega) = \sigma_0(\omega = \omega_{fi}) g(\omega, \omega_{fi}). \quad (9)$$

Here,  $g(\omega, \omega_{fi})$  is the spectral line profile and could be obtained, for instance, as a result of a molecular dynamics (MD) simulations [20–22] or as a result of theoretical modeling and spectral line data [23–27]. The lineshape is normalized to unity area, e.g.,

$$\int_{-\infty}^{\infty} g(\omega) d\omega = 1. \quad (10)$$

The line profile is a convolution of the broadening of the initial and final state energy levels, e.g.,

$$g(\omega) = g_i(\omega) * g_f(\omega). \quad (11)$$

Here,  $g_i$  and  $g_f$  are energy level broadening shapes of the initial and final states.

From here, the absorption coefficient could be calculated

$$k(\omega) = N_i \int_f \int_i g_i(\omega) g_f(\omega) \sigma_0. \quad (12)$$

Here,  $N_i$  is the concentration of hydrogen in initial level  $|n_i, l_i\rangle$ . The broadening of the levels should be considered separately in order to use the same broadening profiles for the calculation of the bound-free transition continuous photo absorption.

There are a few steps to be carried out, and the first to be taken into account is to use a parametric level and line broadening model. The second one is to use a theoretical model for spectral line broadening and try to deconvolve level broadening values, and the final step should be the usage of the MD code [20–22]. A candidate for the coupling of the MD code is LAMMPS, which is capable of simulating a large scale molecular dynamics simulations, and it also could include particular interaction potential as well as all relevant processes of interest not included in the initial code as

an additional module. The broadening parameters could be calculated from average energy and particle distributions and their temporal distributions, or, as an iterative procedure, a more real plasma potential could be obtained [20,21,28,29]. In the former case, the solutions would not necessary to be described as a set of analytical functions. Since there are more steps, we did not elaborate on the ideas until we obtained some initial results.

**Table 1.** The oscillator strength values for the “short”,  $N_e = 1.5 \times 10^{19} \text{ cm}^{-3}$ ,  $T = 23,000 \text{ K}$ , and “long” pulse,  $N_e = 6.5 \times 10^{18} \text{ cm}^{-3}$ ,  $T = 18,000 \text{ K}$ , from [14], as well as a theoretical hydrogen case calculated by code from [18], and NIST spectral database values [30].

| $ n_i, l_i\rangle$ | $ n_f, l_f\rangle$ | Short Pulse<br>$f(n_f, l_f; n_i, l_i; r_c)$ | Long Pulse<br>$f(n_f, l_f; n_i, l_i; r_c)$ | Theory<br>$f(n_f, l_f; n_i, l_i)$ | NIST<br>$f(n_f, l_f; n_i, l_i)$ |
|--------------------|--------------------|---|--|-----------------------------------|---------------------------------|
| 1,0>               | 2,1>               | 0.416197                                    | 0.416197                                   | 0.416200                          | 0.416400                        |
| 1,0>               | 3,1>               | 0.079102                                    | 0.079102                                   | 0.079101                          | 0.079120                        |
| 1,0>               | 4,1>               | 0.028923                                    | 0.028991                                   | 0.028991                          | 0.029010                        |
| 1,0>               | 5,1>               |   | 0.013728                                   | 0.013938                          | 0.013950                        |
| 2,0>               | 3,1>               | 0.434865                                    | 0.434865                                   | 0.434870                          | 0.435100                        |
| 2,0>               | 4,1>               | 0.102533                                    | 0.102756                                   | 0.102760                          | 0.102800                        |
| 2,0>               | 5,1>               |   | 0.041425                                   | 0.041930                          | 0.041950                        |
| 2,1>               | 3,0>               | 0.013589                                    | 0.013589                                   | 0.013590                          | 0.013600                        |
| 2,1>               | 3,2>               | 0.695785                                    | 0.695785                                   | 0.695780                          | 0.696100                        |
| 2,1>               | 4,0>               | 0.003035                                    | 0.003045                                   | 0.003045                          | 0.003046                        |
| 2,1>               | 4,2>               | 0.121659                                    | 0.121795                                   | 0.121800                          | 0.102800                        |
| 2,1>               | 5,0>               |   | 0.001191                                   | 0.001213                          | 0.001214                        |
| 2,1>               | 5,2>               |   | 0.043962                                   | 0.044371                          | 0.044400                        |
| 3,0>               | 4,1>               | 0.483750                                    | 0.484708                                   | 0.484710                          | 0.484900                        |
| 3,0>               | 5,1>               |   | 0.119310                                   | 0.121020                          | 0.121100                        |
| 3,1>               | 4,0>               | 0.032165                                    | 0.032250                                   | 0.032250                          | 0.032280                        |
| 3,1>               | 4,2>               | 0.617675                                    | 0.618282                                   | 0.618290                          | 0.618600                        |
| 3,1>               | 5,0>               |   | 0.007299                                   | 0.007428                          | 0.007433                        |
| 3,1>               | 5,2>               |   | 0.138013                                   | 0.139230                          | 0.139300                        |
| 3,2>               | 4,1>               | 0.010971                                    | 0.010992                                   | 0.010992                          | 0.011000                        |
| 3,2>               | 4,3>               | 1.017260                                    | 1.017520                                   | 1.017500                          | 1.018000                        |
| 3,2>               | 5,1>               |   | 0.002180                                   | 0.002210                          | 0.002211                        |
| 3,2>               | 5,3>               |   | 0.156046                                   | 0.156640                          | 0.156700                        |
| 4,0>               | 5,1>               |   | 0.537527                                   | 0.544150                          | 0.544400                        |
| 4,1>               | 5,0>               |   | 0.052123                                   | 0.052907                          | 0.052940                        |
| 4,1>               | 5,2>               |   | 0.604678                                   | 0.609290                          | 0.609700                        |
| 4,2>               | 5,1>               |   | 0.027498                                   | 0.027822                          | 0.027840                        |
| 4,2>               | 5,3>               |   | 0.887328                                   | 0.890250                          | 0.890600                        |
| 4,3>               | 5,2>               |   | 0.008809                                   | 0.008871                          | 0.008877                        |
| 4,3>               | 5,4>               |   | 1.344790                                   | 1.345800                          | 1.346000                        |

### 3. Results and Discussion

The convergence toward theoretical values for hydrogen is examined and proven for the bound-bound transitions that could appear in the investigated area of electron concentrations and temperatures, [31]. Since the initial results have proven that the model potential could be used for the bound-bound state transition calculations, further investigation was completed.

The next step towards the application of the model results is a calculation of the oscillator strength values for the plasma parameters denoted as “short”, with  $N_e = 1.5 \times 10^{19} \text{ cm}^{-3}$ ,  $T = 23,000 \text{ K}$  and “long” pulse, with  $N_e = 6.5 \times 10^{18} \text{ cm}^{-3}$ ,  $T = 18,000 \text{ K}$  from [14]. The radius  $r_i$ , given by Equation (5), Wigner–Seitz and cut-off radius as well as atom concentrations given by the Saha equation are  $r_i = 51.0655 \text{ a.u.}$ ,  $r_{sji} = 47.5339 \text{ a.u.}$ ,  $r_c = 44.9907 \text{ a.u.}$ ,  $N_a = 1.9 \times 10^{19} \text{ cm}^{-3}$  for short and  $r_i = 68.6260 \text{ a.u.}$ ,  $r_{sji} = 62.8149 \text{ a.u.}$ ,  $r_c = 60.4062 \text{ a.u.}$ ,  $N_a = 3.4 \times 10^{19} \text{ cm}^{-3}$  for long pulse.



The essential quality of the presented approach is that the values are calculated with the help of wave functions that are obtained as a completely analytical solution in the frame of the presented model. The influence of the numerical procedure is minimized, and, as a consequence, the possibility of introducing the numerical artifacts into the solution is also minimized.

Since the convergence towards the theoretical, unperturbed Coulomb potential is investigated in [31], and the results of the presented calculations converge uniformly towards theoretical values, it is expected that the presented model could obtain good data in a wider variety of plasma parameters than shown here.

There is a need to introduce the broadening mechanism for the energy levels in the presented approach. There is a possibility to couple the presented model calculations with the MD code in order to obtain a consistent model for the broadening of the bound levels. Those results influence the bound-free and bound-bound absorption profiles and are essential for the hydrogen plasma optical properties calculation in the frame of the cut-off Coulomb potential model approach.

#### 4. Conclusions

The presented results are a step forward towards inclusion of the entire photo-absorption processes for hydrogen atoms in plasma within the frame of the cut-off Coulomb potential model. One of the benefits of the presented results is a completely quantum mechanical solution for the cut-off Coulomb model potential, obtained from wave functions that are analytical and represented with the help of special functions, e.g., the influence of additional numerical source of errors is minimized as much as possible. Along with this, the solutions converge towards theoretical pure Coulomb potential ones as the cut-off radius converges to infinity, e.g., the influence of plasma diminishes. Further steps in application of the presented results, the inclusion of the bound-bound transition processes within the continuous absorption model, as well as its application in the analysis of the spectral absorption processes is to be carried out. In order to make such calculations, it is needed to include the models for the bound state level broadening. Our plan is to present the results obtained during this investigation in a database that can be accessed directly through <http://servo.aob.rs> as a web service, similar to the existing databases [26,27,32].

**Acknowledgments:** The authors are thankful to the Ministry of Education, Science and Technological Development of the Republic of Serbia for the support of this work within the projects 176002 and III44002. We acknowledge the contribution of the late Dr A. A. Mihajlov, who participated in the initial discussions and preparation of this paper

**Author Contributions:** N. M. S. have adopted the cut-off Coulomb potential model for the optical plasma characteristics; N. M. S. developed the code and performed the calculations; M. S. D., Z. J. S. and V. A. S. analysed the data; N. M. S., V. A. S. and M. S. D. wrote the paper; M. S. D., V. A. S. and Z. J. S. have edited the paper.

**Conflicts of Interest:** The authors declare no conflict of interest.

#### References

1. Fortov, V.E.; Iakubov, I.T. *The Physics of Non-Ideal Plasma*; World Scientific: Singapore, 1999.
2. Rogers, F.J.; Iglesias, C.A. Opacity of stellar matter. *Space Sci. Rev.* **1998**, *85*, 61–70. [[CrossRef](#)]
3. Mihajlov, A.A.; Sakan, N.M.; Srećković, V.A.; Vitel, Y. Modeling of continuous absorption of electromagnetic radiation in dense partially ionized plasmas. *J. Phys. A* **2011**, *44*, 095502. [[CrossRef](#)]
4. Mihajlov, A.A.; Ignjatović, L.M.; Srećković, V.A.; Dimitrijević, M.S.; Metropoulos, A. The non-symmetric ion-atom radiative processes in the stellar atmospheres. *Mon. Not. R. Astron. Soc.* **2013**, *431*, 589–599. [[CrossRef](#)]
5. Mihajlov, A.A.; Djordjević, D.; Popović, M.M.; Meyer, T.; Luft, M.; Kraeft, W.D. Determination of the Electrical Conductivity of a Plasma on the Basis of the Coulomb cut-off Potential Model. *Contrib. Plasma Phys.* **1989**, *29*, 441–446. [[CrossRef](#)]
6. Ignjatović, L.M.; Srećković, V.A.; Dimitrijević, M.S. The Screening Characteristics of the Dense Astrophysical Plasmas: The Three-Component Systems. *Atoms* **2017**, *5*, 42. [[CrossRef](#)]

7. Mihajlov, A.A.; Sakan, N.M.; Srećković, V.A.; Vitel, Y. Modeling of the Continuous Absorption of Electromagnetic Radiation in Dense Hydrogen Plasma. *Balt. Astron.* **2011**, *20*, 604–608. [CrossRef]
8. Mihajlov, A.A.; Srećković, V.A.; Sakan, N.M. Inverse Bremsstrahlung in Astrophysical Plasmas: The Absorption Coefficients and Gaunt Factors. *J. Astrophys. Astron.* **2015**, *36*, 635–642. [CrossRef]
9. Sakan, N.M.; Srećković, V.A.; Mihajlov, A.A. The application of the cut-off Coulomb potential for the calculation of a continuous spectra of dense hydrogen plasma. *Mem. Soc. Astron. Ital. Suppl.* **2005**, *7*, 221–224.
10. Mihajlov, A.A.; Vitel, Y.; Ignjatović, L.M. The new screening characteristics of strongly non-ideal and dusty plasmas. Part 1: Single-component systems. *High Temp.* **2008**, *46*, 737–745. [CrossRef]
11. Mihajlov, A.A.; Vitel, Y.; Ignjatović, L.M. The new screening characteristics of strongly non-ideal and dusty plasmas. Part 2: Two-component systems. *High Temp.* **2009**, *47*, 1–12. [CrossRef]
12. Mihajlov, A.; Vitel, Y.; Ignjatović, L.M. The new screening characteristics of strongly non-ideal and dusty plasmas. Part 3: Properties and applications. *High Temp.* **2009**, *47*, 147–157. [CrossRef]
13. Demura, A. Physical models of plasma microfield. *Int. J. Spectrosc.* **2009**, *2010*, 671073. [CrossRef]
14. Vitel, Y.; Gavrilova, T.; D'yachkov, L.; Kurilenkov, Y.K. Spectra of dense pure hydrogen plasma in Balmer area. *J. Quant. Spectrosc. Radiat. Transf.* **2004**, *83*, 387–405. [CrossRef]
15. Griem, H.R. *Principles of Plasma Spectroscopy*; Cambridge University Press: Cambridge, UK, 2005; Volume 2.
16. Konjević, N.; Ivković, M.; Sakan, N. Hydrogen Balmer lines for low electron number density plasma diagnostics. *Spectrochim. Acta B* **2012**, *76*, 16–26. [CrossRef]
17. Sobelman, I.I. Atomic spectra and radiative transitions. In *Springer Series in Chemical Physics*; Springer: Berlin, Germany, 1979.
18. Hoang-Binh, D. A program to compute exact hydrogenic radial integrals, oscillator strengths, and Einstein coefficients, for principal quantum numbers up to  $n \approx 1000$ . *Comput. Phys. Commun.* **2005**, *166*, 191–196. [CrossRef]
19. Hilborn, R.C. Einstein coefficients, cross sections,  $f$  values, dipole moments, and all that. *Am. J. Phys.* **1982**, *50*, 982–986. [CrossRef]
20. Stambulchik, E.; Maron, Y. Plasma line broadening and computer simulations: A mini-review. *High Energ. Dens. Phys.* **2010**, *6*, 9–14. [CrossRef]
21. Stambulchik, E.; Fisher, D.; Maron, Y.; Griem, H.; Alexiou, S. Correlation effects and their influence on line broadening in plasmas: Application to  $H_{\alpha}$ . *High Energ. Dens. Phys.* **2007**, *3*, 272–277. [CrossRef]
22. Talin, B.; Dufour, E.; Calisti, A.; Gigosos, M.A.; Gonzalez, M.A.; Gaztelurrutia, T.D.R.; Dufty, J.W. Molecular dynamics simulation for modeling plasma spectroscopy. *J. Phys. A* **2003**, *36*, 6049. [CrossRef]
23. Ferri, S.; Calisti, A.; Mossé, C.; Rosato, J.; Talin, B.; Alexiou, S.; Gigosos, M.A.; González, M.A.; González-Herrero, D.; Lara, N.; et al. Ion Dynamics Effect on Stark-Broadened Line Shapes: A Cross-Comparison of Various Models. *Atoms* **2014**, *2*, 299–318. [CrossRef]
24. Calisti, A.; Demura, A.V.; Gigosos, M.A.; González-Herrero, D.; Iglesias, C.A.; Lisitsa, V.S.; Stambulchik, E. Influence of microfield directionality on line shapes. *Atoms* **2014**, *2*, 259–276. [CrossRef]
25. Alexiou, S.; Dimitrijević, M.S.; Sahal-Brechot, S.; Stambulchik, E.; Duan, B.; González-Herrero, D.; Gigosos, M.A. The second workshop on lineshape code comparison: Isolated lines. *Atoms* **2014**, *2*, 157–177. [CrossRef]
26. Marinković, B.P.; Jevremović, D.; Srećković, V.A.; Vujčić, V.; Ignjatović, L.M.; Dimitrijević, M.S.; Mason, N.J. BEAMDB and MolD—Databases for atomic and molecular collisional and radiative processes: Belgrade nodes of VAMDC. *Eur. Phys. J. D* **2017**, *71*, 158. [CrossRef]
27. Srećković, V.A.; Ignjatović, L.M.; Jevremović, D.; Vujčić, V.; Dimitrijević, M.S. Radiative and Collisional Molecular Data and Virtual Laboratory Astrophysics. *Atoms* **2017**, *5*, 31. [CrossRef]
28. Sadykova, S.; Ebeling, W.; Valuev, I.; Sokolov, I. Electric Microfield Distributions in Li + Plasma With Account of the Ion Structure. *Contrib. Plasma Phys.* **2009**, *49*, 76–89. [CrossRef]
29. Calisti, A.; Ferri, S.; Mossé, C.; Talin, B.; Gigosos, M.; González, M. Microfields in hot dense hydrogen plasmas. *High Energ. Dens. Phys.* **2011**, *7*, 197–202. [CrossRef]
30. Kramida, A.; Ralchenko, Y.; Reader, J.; NIST ASD Team. *NIST Atomic Spectra Database (Ver. 5.5)*; National Institute of Standards and Technology: Gaithersburg, MD, USA, 2017. Available online: <https://physics.nist.gov/asd> (accessed on 30 October 2017).

31. Sakan, N.M. The Calculation of the Photo Absorption Processes in Dense Hydrogen Plasma with the Help of Cut-Off Coulomb Potential Model. *J. Phys. Conf. Ser.* **2010**, *257*, 012036. [[CrossRef](#)]
32. Sahal-Bréchet, S.; Dimitrijević, M.; Moreau, N.; Nessib, N.B. The STARK-B database VAMDC node: A repository for spectral line broadening and shifts due to collisions with charged particles. *Phys. Scr.* **2015**, *90*, 054008. [[CrossRef](#)]



© 2018 by the authors. Licensee MDPI, Basel, Switzerland. This article is an open access article distributed under the terms and conditions of the Creative Commons Attribution (CC BY) license (<http://creativecommons.org/licenses/by/4.0/>).